

Editors  
R G Shulman  
and  
D L Rothman



# Brain Energetics & Neuronal Activity

Applications to fMRI and Medicine

 WILEY

# **Brain Energetics and Neuronal Activity**



# **Brain Energetics and Neuronal Activity**

## **Applications to fMRI and Medicine**

*Editors*

**R G Shulman and D L Rothman**

*Yale University School of Medicine  
New Haven, Connecticut, USA*



John Wiley & Sons, Ltd

Copyright © 2004

John Wiley & Sons Ltd, The Atrium, Southern Gate, Chichester,  
West Sussex PO19 8SQ, England

Telephone (+44) 1243 779777

Email (for orders and customer service enquiries): [cs-books@wiley.co.uk](mailto:cs-books@wiley.co.uk)  
Visit our Home Page on [www.wileyeurope.com](http://www.wileyeurope.com) or [www.wiley.com](http://www.wiley.com)

All Rights Reserved. No part of this publication may be reproduced, stored in a retrieval system or transmitted in any form or by any means, electronic, mechanical, photocopying, recording, scanning or otherwise, except under the terms of the Copyright, Designs and Patents Act 1988 or under the terms of a licence issued by the Copyright Licensing Agency Ltd, 90 Tottenham Court Road, London W1T 4LP, UK, without the permission in writing of the Publisher. Requests to the Publisher should be addressed to the Permissions Department, John Wiley & Sons Ltd, The Atrium, Southern Gate, Chichester, West Sussex PO19 8SQ, England, or emailed to [permreq@wiley.co.uk](mailto:permreq@wiley.co.uk), or faxed to (+44) 1243 770620.

This publication is designed to provide accurate and authoritative information in regard to the subject matter covered. It is sold on the understanding that the Publisher is not engaged in rendering professional services. If professional advice or other expert assistance is required, the services of a competent professional should be sought.

#### ***Other Wiley Editorial Offices***

John Wiley & Sons Inc., 111 River Street, Hoboken, NJ 07030, USA

Jossey-Bass, 989 Market Street, San Francisco, CA 94103-1741, USA

Wiley-VCH Verlag GmbH, Boschstr. 12, D-69469 Weinheim, Germany

John Wiley & Sons Australia Ltd, 33 Park Road, Milton, Queensland 4064, Australia

John Wiley & Sons (Asia) Pte Ltd, 2 Clementi Loop #02-01, Jin Xing Distripark, Singapore 129809

John Wiley & Sons Canada Ltd, 22 Worcester Road, Etobicoke, Ontario, Canada M9W 1L1

Wiley also publishes its books in a variety of electronic formats. Some content that appears in print may not be available in electronic books.

#### ***Library of Congress Cataloging-in-Publication Data***

Brain energetics and neuronal activity : applications to fMRI and medicine / editors, R. G. Shulman and D. L. Rothman.

p. ; cm.

Includes bibliographical references and index.

ISBN 0-470-84720-4 (cloth : alk. paper)

1. Brain—Metabolism. 2. Energy metabolism. 3.

Brain—Pathophysiology. 4. Brain—Magnetic resonance imaging.

[DNLM: 1. Brain—metabolism. 2. Magnetic Resonance Imaging—methods.

3. Brain Diseases—physiopathology. 4. Energy Metabolism. 5.

Neurons—metabolism. 6. Synaptic Transmission. WL 141 B8114 2004] I.

Shulman, R. G. (Robert Gerson) II. Rothman, D. L. (Douglas L.)

QP376 .B699 2004

612.8'2—dc22

#### ***British Library Cataloguing in Publication Data***

A catalogue record for this book is available from the British Library

ISBN 0-470-84720-4

Typeset in 10/12pt Times by Laserwords Private Limited, Chennai, India

Printed and bound in Great Britain by Antony Rowe Ltd, Chippenham, Wiltshire

This book is printed on acid-free paper responsibly manufactured from sustainable forestry

in which at least two trees are planted for each one used for paper production.

# Contents

Contributors	vii
Foreword	ix
<i>Section A: Background</i>	1
1 Introduction Douglas L. Rothman and Robert G. Shulman	3
2 Energy Metabolism in Neural Tissues <i>in vivo</i> at Rest and in Functionally Altered States Louis Sokoloff	11
3 Techniques—MRS, fMRI, $^{13}\text{C}$ NMR, Indirect Detection of $^{13}\text{C}$ Robin de Graaf	31
4 Metabolic Modeling Analysis of Brain Metabolism Graeme Mason	53
<i>Section B: Neuroenergetics and Activity</i>	73
5 Cerebral Energetics and Neurotransmitter Fluxes Nicola R. Sibson	75
6 NMR Studies of the Metabolism and Energetics of GABA Neurotransmitter Pathways Kevin L. Behar and Douglas L. Rothman	99
7 Neural Energy Consumption and the Representation of Mental Events Simon B. Laughlin and David Attwell	111
8 Imaging Cerebral Metabolic Rate of Oxygen Consumption (CMRO <sub>2</sub> ) using $^{17}\text{O}$ NMR Approach at Ultrahigh Field Wei Chen, Xiao-Hong Zhu and Kamil Ugurbil	125
9 Deriving Changes in CMRO <sub>2</sub> from Calibrated fMRI Fahmeed Hyder	147
10 Relationship between CMRO <sub>2</sub> and Neuronal Activity Fahmeed Hyder and Hal Blumenfeld	173

<i>Section C: Clinical Beginnings</i>	195
11 NMR Studies of Bioenergetic Impairment in Human Epilepsy Hoby P. Hetherington, Jullie W. Pan and Dennis D. Spencer	197
12 MRS Studies of the Role of Altered Glutamate and GABA Neurotransmitter Metabolism in the Pathophysiology of Epilepsy Ognen A. C. Petroff and Dennis D. Spencer	215
13 The Role of Altered Energetics of Neurotransmitter Systems in Psychiatric Disease Graeme F. Mason	239
<i>Section D: Brain and Mind</i>	257
14 Long-term Memory: Do Incremental Signals Reflect Engagement of Cognitive Processes? Jed A. Meltzer and R. Todd Constable	259
15 Using fMRI to Study the Mind and Brain Bruce E. Wexler	279
16 Brain and Mind: an NMR Perspective Robert G. Shulman and Fahmeed Hyder	295
17 The Role of the NMR Baseline Signal in the Study of Consciousness: the Restless Brain Robert G. Shulman	311
Index	315

# Contributors

David Attwell  
Department of Physiology  
University College London  
Gower Street  
London, WC1E 6BT, UK

Kevin L. Behar  
Department of Psychiatry  
Yale University School of Medicine  
MR Center  
P.O. Box 208043  
New Haven, CT 06520-8043, USA  
kevin.behar@yale.edu

Hal Blumenfeld  
Department of Neurology and Neurobiology  
Yale University School of Medicine  
P.O. Box 208018  
New Haven, CT 06510, USA  
hal.blumenfeld@yale.edu

Wei Chen  
Center for Magnetic Resonance Research  
Department of Radiology  
University of Minnesota Medical School  
2021 6th Street SE  
Minneapolis, MN 55455, USA  
tel: 612-625-8814  
wei@cmrr.umn.edu

Robert Todd Constable  
Department of Diagnostic Radiology  
Yale University School of Medicine  
P.O. Box 208042  
New Haven, CT 06520-8042, USA  
todd.constable@yale.edu

Robin de Graaf  
Department of Diagnostic Radiology  
Yale University School of Medicine  
MR Center  
P.O. Box 208043  
New Haven, CT 06520-8043, USA  
robin.degraaf@yale.edu

Susan Fitzpatrick  
James S. McDonnell Foundation  
1034 South Brentwood Blvd, Suite 1850  
St. Louis, MO 63117, USA  
susan@jsmf.org

Hoby Hetherington  
Departments of Radiology, Physiology  
and Biophysics  
Albert Einstein College of Medicine  
Jack and Pearl Resnick Campus  
1300 Morris Park Avenue  
Bronx, NY 10461, USA  
hhether@aecom.yu.edu

Fahmeed Hyder  
Departments of Diagnostic Radiology and Biomedical Engineering  
Yale University School of Medicine  
MR Center  
P.O. Box 208043  
New Haven, CT 06510, USA  
fahmeed.hyder@yale.edu

Simon B. Laughlin  
Department of Zoology  
University of Cambridge  
Downing Street  
Cambridge, CB2 3EJ, UK  
s1104@cam.ac.uk

Graeme Mason  
Department of Psychiatry  
Yale University School of Medicine  
MR Center  
P.O. Box 208043  
New Haven, CT 06520-8043, USA  
graeme.mason@yale.edu

Jed A. Meltzer  
Department of Diagnostic Radiology  
Yale University School of Medicine  
MR Center  
P.O. Box 208042  
New Haven, CT 06520-8042, USA

Jullie W. Pan  
Departments of Neurology and Neuroscience  
Albert Einstein College of Medicine  
Jack and Pearl Resnick Campus  
1300 Morris Park Avenue  
Bronx, NY 10461, USA  
jpan@aecon.yu.edu

Ognen A.C. Petroff  
Yale University School of Medicine  
Department of Neurology  
P.O. Box 208018  
New Haven, CT 06520-8018, USA  
ognen.petroff@yale.edu

Douglas L. Rothman  
Department of Diagnostic Radiology  
Yale University School of Medicine  
MR Center  
P.O. Box 208043  
New Haven, CT 06520-8043, USA  
douglas.rothman@yale.edu

Robert G. Shulman  
Yale University School of Medicine  
MR Center  
P.O. Box 208043  
New Haven, CT 06520-8043, USA  
robert.shulman@yale.edu

Nicola Sibson  
Experimental Neuroimaging Group  
Department of Biochemistry  
University of Oxford  
South Parks Road  
Oxford, OX1 3QU, UK  
niki@bioch.ox.ac.uk

Louis Sokoloff  
National Institute of Mental Health  
National Institutes of Health  
Bethesda, MD 20892, USA  
louis@shiloh.nimh.nih.gov

Dennis D. Spencer  
Department of Neurosurgery  
Yale University School of Medicine  
333 Cedar Street  
P.O. Box 208082  
New Haven, CT 08520-8082, USA

Kamil Ugurbil  
Center for Magnetic Resonance Research  
Department of Radiology  
University of Minnesota Medical School  
2021 6th St. SE  
Minneapolis, MN 55455, USA

Bruce E. Wexler  
Yale University School of Medicine  
Department of Psychiatry  
P.O. Box 208068  
New Haven, CT 06520-8068, USA  
bruce.wexler@yale.edu

Xiao-Hong Zhu  
Center for Magnetic Resonance Research  
Department of Radiology  
University of Minnesota Medical School  
2021 6th St. SE  
Minneapolis, MN 55455, USA

# Foreword

My experiences over the past 30 years have led me to the realization that there are two kinds of researchers in the biological sciences: those who almost immediately recognize the centrality of metabolism to a full understanding of biological function and those who do not. The latter group always seems to represent a larger proportion of biological scientists, so that the focus of biological research tends to drift from studying metabolism into various phenomenological directions, until one realizes, as one inevitably does, that metabolism, particularly the metabolism of cellular energy production, what is often termed ‘intermediary metabolism’ is the key to inter-level analysis of biological systems. Metabolism provides the bridge from the genetic to the cellular and from the cellular to the organismic. Sooner or later, therefore, the hard search for truth comes back to addressing and unraveling the complexities of intermediary metabolism and abandoning the quest for a ‘magic bullet’. This return to a focus on metabolism is becoming unavoidable for scientists studying the influence of gene expression patterns on biological function. Likewise, as the chapters in this book document, cognitive neuroscientists searching for an understanding of the mechanisms by which neuronal assemblies process information can not avoid acquiring a deeper awareness of brain energy and intermediary metabolism. Brain structure – function relationships can only be clearly seen through a metabolic lens.

As I neared completion of my doctoral research in the Laboratory of Cerebral Metabolism at Cornell University Medical College in 1984, I confronted the metabolism versus non-metabolism dichotomy head on. Although devoted to studying brain energy metabolism, my mentors advised me to forsake such studies and become more ‘molecular’ if I intended to have a viable research career. They had my best interests at heart; in their eyes, the era of traditional metabolic neurochemistry was on the wane. The classic approach of using metabolic encephalopathies (including ischemia, hypoxia, and hypoglycemia) to probe how perturbations in cerebral oxidative energy metabolism altered conscious states (e.g. lethargy, stupor, and coma) was becoming passé. To be fair, my advisors were not entirely incorrect. The general emphasis in neurochemical studies in the 1970s and 1980s concentrated on detailing how the supply of glucose and oxygen for energy metabolism supported neuronal function. The key observation (not yet made but described fully in this volume) needed to advance the field was the critical link between the need to sustain the high rate of energy metabolism and its driving force – glutamate neurotransmitter turnover.

Luckily, the solution to my career dilemma revealed itself while I browsed in the library. Serendipity, that often unacknowledged contributor to careers and discoveries, led me to one of the most important books I have ever read: *Biological Applications of Magnetic Resonance* edited by R.G. Shulman (1979 Academic Press New York, San Francisco and London). Shulman’s volume profiled several directions of research using nuclear magnetic resonance (NMR) spectroscopy to study metabolic reactions *in vivo*. It was immediately apparent to me that this approach, if applied to the brain, might be able to discover the Holy Grail of neurochemistry – the ability to monitor the metabolic correlates of neural information processing. *In vivo* NMR spectroscopy, because of its ability to monitor energy metabolism in the intact brain, *in vivo*, in real time, provided a novel approach for investigating the all-important tight coupling of cerebral metabolism and neuronal function. Not surprisingly, Bob Shulman’s laboratory at Yale University was

already actively pursuing this line of research – and soon after provided me a new intellectual home. NMR spectroscopy breathed renewed life into the pursuit of what remains a somewhat elusive goal – unraveling the complex inter-relationships among cerebral function, cerebral structure, and cerebral metabolism.

How closely the traditional tools of neurochemistry can monitor changes in the concentrations of intermediary and energy metabolites and accurately mirror real time *in vivo* levels is hampered by the unique dependence of brain function on blood flow and cerebral metabolism as thoroughly documented in the chapter by Sokoloff. The few seconds of hypoxia, ischemia, or hypoglycemia inflicted during the time between obtaining brain tissue for study and doing the study unavoidably alters the concentrations of energy metabolites and destroys the functional cyto-architecture. During the 1970s a significant percentage of neurochemists' research efforts were directed toward developing ingenious methods to minimize experimental post-mortem changes of intermediary and energy metabolite concentrations. Researchers pursued every strategy to freeze the metabolite levels by limiting the effects of ischemia and hypoxia so as to mirror the *in vivo* concentrations present at the experimental time of interest. Techniques such as *in situ* freezing preserved the structural integrity of the brain tissue, but risked uneven rates of inactivation of metabolic processes, particularly for deeper brain structures. The 'brain blowing' technique introduced by Bud Veech, a rather extreme apparatus using air pressure to extrude the brain from the cranium, provided shorter extraction and freezing times, but destroyed the anatomy. What was needed, if the field was to progress, were methods that could monitor blood flow and metabolism linked to normal cognitive and behavioral states in the intact brain, *in vivo*, in real time.

The development of the 2-deoxyglucose (2-DG) autoradiography technique in the laboratory of Louis Sokoloff in the 1970s offered neurochemists the ability to measure regional rates of glucose utilization in animal models and to begin to link metabolism with physiology in the absence of induced pathology. Soon thereafter, positron emission tomography made possible, for the first time, measurement of regional cerebral metabolic rates for glucose (FDG-PET) and oxygen (O-18 PET) in human subjects in real time as they engaged in behavioral tasks.

For studies correlating regional changes in cerebral metabolism with regional changes in neural activity, 2-DG autoradiography and PET have some limitations. The analysis of 2-DG autobiographic data occurs in brain slices, post-mortem. Each individual animal in an experimental design provides data on cerebral metabolic rates for many different brain regions but for only a single time point. Human PET studies provide measurements of cerebral metabolism with excellent temporal series and spatial resolution, but the short-lived radio-isotope labeled compounds needed to conduct the experiments limited research opportunities. Furthermore, the need for intravenous injections of radio-isotopes limited the subject pool and essentially eliminated the possibility of pursuing certain types of studies, such as those involving healthy children. Additionally, 2-DG autoradiography and FDG-PET are not identical in every aspect, somewhat complicating comparisons between human and animal studies. *In vivo* NMR spectroscopy offered an alternative approach which allowed direct comparison of animal models with human subjects and was also not dependent on the use of radioactive tracers.

As the development of *in vivo* NMR spectroscopic techniques for metabolic measurements was rapidly progressing, other applications of MR physics allowed scientists to obtain remarkably detailed anatomical images of the intact, living, human body. The brain images produced by magnetic resonance imaging (MRI) were particularly stunning; they revealed the 3-D complexity of the brain at a degree of resolution far surpassing that of contemporaneous imaging devices such as CAT scans. In the late 1980s, the physics of MRS and MRI led to the discovery of what could, arguably, be considered one of the 20th century's most powerful advances in the ability to monitor brain activity in the intact subject. In 1990 Seiji Ogawa and colleagues at Bell Laboratories published the first study using BOLD MRI, often referred to in the literature as functional magnetic resonance imaging or fMRI, to monitor ongoing brain activity related to ongoing behavior.

The ability to use PET and fMRI measurements to localize cognitive processes within a particular volume of neural tissue is based on the assumption that functional neuronal activity, and therefore metabolism, increase when a region is involved in the neural computations that implement a cognitive task. The functional neuronal activities involved in the communication of information between neurons include neurotransmitter synthesis, packaging, and release followed by the subsequent generation of action potentials. As explained above, the energy required for these and other brain processes is provided almost exclusively by oxidative glucose metabolism. Regions of increased functional energetic demand are identified by the corresponding increase in glucose metabolism, or the coupled parameters of the cerebral metabolic rate for oxygen (CMRO<sub>2</sub>) and the cerebral blood flow rate (CBF). Depending on the radio-labeled tracer used, PET can measure glucose consumption, oxygen utilization, or CBF. Interpreting the fMRI BOLD signal changes is somewhat more complicated because BOLD is sensitive to both CMRO<sub>2</sub> and CBF.

The cognitive neuroscience community quickly embraced BOLD fMRI despite the pitfalls of equating changes in a signal comprising several complex physiological parameters to changes in neuronal 'activity'. Cognitive neuroscience emerged as a unique academic discipline in the late 1980s from the deliberate efforts of scientists interested in identifying the neural correlates of cognition by integrating the experimental and theoretical traditions of cognitive psychology, systems and computational neuroscience, linguistics, and philosophy. BOLD fMRI seemed ideally suited for pursuing cognitive neuroscience's stated goals. Cognitive neuroscientists' enthusiasm for fMRI studies led to a rapid and exponential growth in institutional MR centers. These centers concentrated their resources on developing methods for marrying psychological studies to functional imaging. Unfortunately, their lack of interest in pursuing metabolic or mechanistic research meant there was not a corresponding commitment to nurturing brain research with *in vivo* NMR spectroscopy.

The lack of an appreciation by many cognitive neuroscientists (particularly those entering the field primarily trained as psychologists or systems neuroscientists) of the centrality of energetics to understanding how information is processed in the brain has resulted in a cognitive neuroscience that acts as though there has not been a century of effort expended on unraveling the mechanisms coupling metabolism, blood flow, and function in the brain. Cognitive neuroscientists interpreting changes in the BOLD signal as direct measurements of the neural correlates of human cognition and behavior without understanding the energetic and metabolic correlates of neural activity stand on theoretically shaky ground. It is the energetic and metabolic correlates of neuronal information processing that are coupled to the hemodynamic signals.

There are several important questions integral to the understanding of the neural basis of cognition that cannot be answered with functional imaging studies but that can be investigated with MR spectroscopy. Functional neuroimaging studies proceed from an assumption that the observed signal changes reflect neuronal activity, even though other cell types, most notably astrocytes, are known to be important contributors to overall brain energy metabolism and neurotransmitter function. Pierre Magistretti and his colleagues have published a series of papers identifying the astrocyte as the primary site of cerebral glucose consumption. Magistretti has proposed that astrocytic glucose uptake is mechanistically coupled to neuronal energy requirements via non-oxidative glycolysis to provide energy for removing glutamate, an excitatory neurotransmitter released by the nerve terminals, from the synaptic cleft. The lactate produced as a result of the incomplete oxidation of glucose is then transported from the astrocyte to the neuron as a substrate for oxidative energy metabolism. The chapter by Sibson summarizes the *in vivo* MRS results from rat and human brain detailing the flux from glucose to glutamate that support and extend Magistretti's findings. <sup>13</sup>C NMR spectroscopic studies have shown that the rate of astrocytic glutamate uptake increases with glucose metabolism at a close to 1:1 stoichiometry.

*In vivo* MRS findings offer insights into the underlying nature of the BOLD signal. This statement does not imply that MRS research should be embraced *merely* because it offers the hope of 'quantitating' BOLD. Rather, as is made clear by several chapters in this volume, MRS functional neuro-energetic studies offer

cognitive neuroscientists the ability to pursue an entirely new level of analysis of brain function. The series of PNAS papers by Hyder *et al.*, described in detail in this volume, provides a biological underpinning for theoretical models of unconscious and conscious information process such as that proposed recently by Stan Dehaene and Jean Pierre Changeux. Slowly but surely, cognitive neuroscience is becoming aware that the small physiological differences detected by BOLD imaging are the mere tip of an iceberg. Functionally, the high rate of ongoing neuronal activity, representing close to 80 % of total cerebral energy metabolism, may be of greater interest. *In vivo* MRS studies, together with fMRI, allow us to build an integrated science of brain/behavior by bridging from cognition to cerebral oxidative energy metabolism and by linking neuronal information processing with glutamate neurotransmitter function.

It is rare to discover a single volume that both summarizes and celebrates decades of biological research while also pointing out a path to the future. In 20 years I have come across only two. Not surprisingly, they both emphasize that we cannot understand biological function without understanding metabolism and both are edited by Bob Shulman.

*Susan Fitzpatrick*  
September 2003

<http://anestit.unipa.it/reference/bibliography/snacc/Metab3.html>

## **Section A**

### Background



# 1

## Introduction

**Douglas L. Rothman and Robert G. Shulman**

*Yale University School of Medicine, MR Center, P.O. Box 208043, New Haven,  
CT 06520-8043, USA*

---

1.1	Background	5
1.2	Energy and Neurotransmission	6
1.3	Clinical Beginnings	7
1.4	Brain and Mind	8

---

This book illustrates and celebrates recent NMR investigations of brain, identifying its molecular constituents and following their metabolic activities *in vivo*. This physical, spectroscopic method is anchored in its two origins – its present technical methods descended from Bloch and his colleagues and its present metabolic information derivable from the simple, beautiful NMR experiments on water of Bloembergen, Purcell and Pound. Water continues as an endlessly fascinating material and in the present volume plays the central role in MRI and fMRI experiments. From the beginning NMR studies have depended upon interaction between atomic nuclei and their chemical environment and have been valuable reporters of these environments. These interactions have been readily interpreted because of two simplifying characteristics of the NMR phenomena. First spin  $\frac{1}{2}$  nuclei of the common elements, e.g. hydrogen, carbon and phosphorus, interact very weakly with their environment relative to the strong forces they can experience in available laboratory magnetic fields. Accordingly environmental interactions affecting chemical shifts, multiplet structure and relaxation times, being weak compared to these Zeman interactions, are perturbations and as such are readily and quantitatively evaluated. The second simplifying property that allows reliable information about the nuclei's surroundings is that NMR phenomena, in contrast to most spectroscopic methods, take place in the ground electronic state, and thereby provide a well-established basis for interpreting the perturbations by the molecular environment. As a quantitatively understandable measure of molecules and their interactions NMR has grown continually in these years. It has become a prime method

for the study of matter – in chemistry, condensed matter physics, geology, biochemistry and in all studies of materials.

Studies of brain metabolism are playing a growing role in neuroscience. Cerebral metabolic pathways date back to the exciting beginnings of physiological chemistry, when Charles Sherrington proposed that ‘the blood supply of any part of the cerebral tissue is varied in accordance with the activity of the chemical changes which underlie the functional activation’. Activities of brain were then to be explained by the same criterion that physiologists were using in exploring the chemical basis of muscle and heart. Methods for measuring cerebral inputs of glucose and oxygen that have been developed since 1950 have established the basic dependence of cerebral energetics upon the oxidation of glucose. Cerebral blood flow has been measured by similar methods so that neurophysiology has shown that blood flow follows energy consumption and thereby links brain chemistry with the organism.

In more recent years non-invasive methods of nuclear magnetic resonance and positron emission tomography (PET) have played increasingly important roles in brain studies. Magnetic resonance imaging (MRI) has revealed cerebral anatomy with great specificity and has helped to localize the more chemical findings of PET, functional magnetic resonance imaging (fMRI), and magnetic resonance spectroscopy (MRS). These metabolic methods have now been developed to the point that their findings contribute substantially to brain science.

This book describes recent contributions of magnetic resonance methods to studies of brain energetics and function. The value of magnetic resonance, particularly MRI, has been evident from its first human applications. High-resolution non-invasive images moved clinical studies into a better-informed era. A little more than a decade after, fMRI made parallel advances in the localization of stimulated brain activity. MRS, particularly in measurements by  $^{13}\text{C}$ -label flow, has provided information relating brain metabolism and neurotransmitter flows. The contributions of  $^{13}\text{C}$  MRS to brain studies form the unifying theme underlying this book. The insights into metabolism, provided by MRS and PET, have depended to some extent upon the great powers of MRI and fMRI while, in turn, they have led to some re-interpretation of these imaging methods. Together these magnetic resonance methods have opened new understandings of brain function and now offer new directions for research.

Although in retrospect a smooth research path can be traced through the past decades leading to a metabolic model of brain function, nonetheless certain obstacles to research planning unique to the brain had to be overcome. The very nature of the work done by the brain was not as obvious as in other organs. Muscle work was readily defined and measured as force through a distance. Nor did muscle power expenditures, easily measured as the rate of work, present any conceptual difficulties. The chemical basis of cerebral work, like the analogous work done by the heart, is now being expressed by the studies presented in this book, in similar terms, as molecules and ions pumped across gradients by ATP. We have obtained this analogous definition and quantitation of brainwork from the experimental (Sibson) and theoretical (Laughlin) research described in Chapters 5 and 7.

However, these very recent results had to overcome paradigmatic ideas about the unimportance of energy for brainwork that had been formed on the basis of very few studies. Until recently the generally accepted belief in the field, from a comparison with the squid axon, considered only  $\sim 1\%$  of brain energy production to be devoted to neuronal firing. Only when the multi-synapses of the mammalian brain were specifically included did calculations support the MRS results that nearly all the brain energy was devoted to neuronal firing. The negligible role assumed for cerebral energetics had been reinforced by the suggestion that stimulated brain activity was supported by non-oxidative glycolysis despite the main energy source being the oxidation of glucose. The recent stoichiometries showing efficient use of glucose oxidation for energy had to overcome these widespread views.

Perhaps the more strongly held obstacles came from residual phenomenological dualism. It was difficult to realize that the thinking process of mind required work, based upon the hydrolysis of ATP, just as

a muscle did work when lifting weights. This traditional difficulty in formulating brainwork slowed the efforts to calculate such work energetically. But that relationship has now been quantified as described in the following pages, and provides a sturdy foundation for the study of the more complex aspects of brain. As this understanding advances it leads to consideration of the interactions between these aspects of neuroscience with the broad field of psychology. To what extent does modern psychology further our understanding of neurophysiology or, conversely, in what way does the understanding gained about brain activity and energetics advance psychological conceptualization? Functional imaging of brain localizes brain activity non-invasively and quickly – but how does this methodology illuminate our understanding of brain activity? And how does understanding energy consumption help to expand the scope of functional imaging? Finally, underlying all these questions, how does brain energy metabolism relates to neuroscience, the study of brain components, structure and action at the cellular and molecular level?

Out of the broad fields that are presently actively studying the functioning brain, the studies reviewed here have focused upon a simple concept, namely brain energy consumption and neuronal activity are chemical processes. Brain activity is not merely powered by chemical reactions – that activity, in fact, consists of chemical reactions. Brain energetics compares the production and use of energy, usually mediated through ATP, in which glucose is metabolized. Neuronal activity is the sum of chemical reactions by which information is processed. This activity we show can be profitably followed by measurements, *in vivo*, of the rates of chemical reactions. Chemical reactions *in vivo* do not occur in isolation, as they do in a test tube. *In vivo* all reactions are linked to others and the linked reactions form a network that is conveniently defined as metabolism. In the brain the chemical reactions of ion fluxes across membrane, neurotransmitter processing and the electrical actions of neuronal spiking are all coupled to energy consumption and the control of metabolism.

The unique perspective of this book derives from the ability to measure cerebral metabolic fluxes, in the living human and animal brains, by *in vivo* NMR methods. These quantitative assessments of metabolite concentrations and rates of reaction, *in vivo*, provide the unique, strong data set, that has allowed metabolism, studied this way, to provide a platform for novel insights into biological function.

## 1.1. BACKGROUND

The first four chapters provide background information of a historical and technical nature. The NMR studies of the brain, which form the core of this book are discussed in the early chapters. NMR methods, magnetic resonance spectroscopy (MRS) have measured *in vivo* concentrations and kinetics of molecular metabolites. These small molecules, e.g. glutamate, glutamine, lactate, glucose, etc., are studied as the components of energetic and neurotransmitter pathways. The early physiological studies of cerebral glucose and oxygen uptake established the chemical basis of brain energetics, showing that glucose oxidation is the main energy source, have been summarized by Lou Sokoloff, *a pioneer of this field*, in Chapter 2. Dr. Sokoloff's development of the deoxyglucose tracer extended these studies, which originally were primarily based on arterial venous difference measurements, to high resolution mapping of brain functional activity based upon glucose uptake and flow. This deoxyglucose mapping remains the gold standard to which more recent non-invasive modalities such as fMRI are compared. In addition these studies also formed the basis for the development of PET studies of human glucose metabolism using the deoxyglucose tracer. A key finding in these studies, the understanding that glucose oxidation provides the brain energy, was re-inforced and confirmed *in vivo* by  $^{13}\text{C}$  MRS measurements of the flux from labeled substrates particularly  $1-^{13}\text{C}$  glucose, through the (tricarboxylic acid) TCA cycle. Numerical values of the cerebral metabolic rate of oxygen consumption obtained from these MRS measures of TCA cycle flux agreed with the results from the deoxyglucose autoradiography and PET methods in animals and humans respectively.

Chapter 3 by Robin de Graaf introduces NMR methods used in the book. NMR of cerebral metabolism obtains quantitative measurements by combining the regional specificity of imaging methods with the

chemical identification and quantitation of metabolites which has been developed extensively by high resolution NMR. The description is at a simple level, suitable for anyone who has taken (and remembers some of) a course in organic chemistry. From this base more advanced methods used in MRS studies are developed and are referred to throughout the other reports.

Since the core of quantitation lies in hypothesizing and evaluating a model of *in vivo* fluxes, this subject is reviewed in Chapter 4 by Graeme Mason. ‘Modeling’ of data is used in a very positive way in these studies, in that the ‘model’ represents bundled hypotheses about the *in vivo* reaction pathways. As such the models serve to evaluate fluxes from data but also serve to test the hypothesis about the parameter being evaluated. In a particularly simple application, a model predicts that the value of a particular flux must be the same (within experimental error) when that flux is measured in different, independent experiments. Values of rates obtained by modeling the data depend upon statistical fits of the model to the data. A simplified, yet informative description of such calculation forms a central feature of this chapter.

## 1.2. ENERGY AND NEUROTRANSMISSION

Section B includes descriptions of the experimental and theoretical determinations of *in vivo* metabolic rates, energy consumption in the form of oxygen usage and neuronal work done by neurotransmission and spike activity. A key novel finding of this work is that energy consumption is coupled to the release of the neurotransmitter glutamate upon neuronal firing and its subsequent recycling through glutamine. This flux was proposed in the 1970s and was established as the major pathway by the  $^{13}\text{C}$  experiments. In Chapter 5 by Nicola Sibson, studies are described in which  $^{13}\text{C}$ -labeled glucose and other labeled precursors are followed into glutamate and glutamine pools in human and animal brains by *in vivo*  $^{13}\text{C}$  MRS. The rate of label appearance in glutamate has provided a measure of the tricarboxylic acid cycle flux  $V_{\text{TCA}}$ , which is a direct measure of neuronal energy consumption. The flux into the glutamine pool, measured in the same experiment by *in vivo*  $^{13}\text{C}$  MRS, is used to quantitate the rate of glutamate neurotransmitter release and recycling. The quantitation shows that there is a one-to-one change of glutamate neurotransmitter flux with neuronal glucose oxidation, i.e. for each additional molecule of glutamate released as a neurotransmitter there is one molecule of glucose oxidized in neurons. This stoichiometry allows changes in the cerebral rate of energy consumption to be converted directly into change of neuronal signaling, and provides key information for understanding the energetic and molecular mechanisms which couple glutamate neurotransmission to energy consumption. The proposal linking the *in vivo* results to the cellular findings of Magistretti and coworkers that astroglial glutamate uptake depends on glycolytic ATP are described. It provides a chemical measure of neuronal activity, which has previously been undefined, and in conformity with the message of this book, shows that the rate of neuronal activity is defined by the flux through a metabolic pathway.

These total fluxes of glutamate to glutamine neurotransmitter cycling reflect the sum of glutamate and GABA neurotransmitter flow. GABA is the most abundant inhibitory neurotransmitter in the cortex. Chapter 6, by Kevin Behar and Douglas Rothman, shows how GABA neurotransmitter release and cycling can be distinguished from the total glutamate to glutamine cycling. The contributions of GABA to the total glutamate plus GABA neurotransmitter cycling flux has been shown to be significant. The chapter describes how the use of other labeled substrates, in particular labeled acetate, allows this distinction to be made, and sets the stage for future studies to understand the relationship between inhibitory and excitatory neurotransmission and energetics, as well as subcellular metabolic compartmentation of GABA synthesis.

In Chapter 7, Laughlan and Attwell review their energy budget for glutamate neurotransmitter cycling. Taking literature values for the different steps in the pathway of neuronal firing with glutamate release and cycling they have broken the energy requirements into different steps. Most of this energy is consumed in pumping the neuronal ion gradients after firing with approximately equal energies devoted to pre- and post-synaptic pumping. As expected the energy requirements for the chemical steps of glutamate release and

conversion to glutamine and recycling back into the glutamate vesicles is small compared to the neuronal energy requirements. Assuming the glutamate concentration of vesicles, the efficiency of neuronal firing and based on a firing rate of 4 Hz, they find reasonable agreement with the observation by  $^{13}\text{C}$  MRS that a large majority of the energy is devoted to neuronal activity and only  $\sim 20\%$  is devoted to non-functional neuronal energy needs commonly called housekeeping. Their energy budget provides a valuable framework for relating energy consumption, measured by  $^{13}\text{C}$  MRS methods to detailed energetic sub-processes. It also provides a framework for studies combining MRS and MRI with inhibitors of specific energetic sub-processes to test the understanding of the energetic basis of function in detail.

The next two chapters present very recent NMR methods for measuring the basic neuroenergetic parameter,  $\text{CMR}_{\text{O}_2}$ . High magnetic fields have increased NMR sensitivity so that direct  $^{17}\text{O}$  NMR experiments can determine the rate of oxygen consumption by following the label flow to  $\text{H}_2^{17}\text{O}$ , as shown in Chapter 8 by Wei Chen. These quite direct measurements of oxygen usage are a substantial advance in sensitivity over previous  $^1\text{H}$ NMR methods using indirect detection of  $\text{H}_2^{17}\text{O}$  relaxation times. Furthermore they have potentially similar spatial and temporal resolution as PET  $\text{CMR}_{\text{O}_2}$  measurements, with the advantages of more accurate quantitation and the ability to perform multiple repeated studies due to the absence of radioactive isotope. Careful studies of this direct measurement of  $\text{CMR}_{\text{O}_2}$  have elucidated the methodology of similar PET measurements.

The BOLD fMRI, is known to depend upon complex interactions of NMR relaxation times,  $\text{CMR}_{\text{O}_2}$ , CBF and Cerebral Blood Volume (CBV). In Chapter 9, Hyder describes his method of determining  $\Delta\text{CMR}_{\text{O}_2}$  from BOLD measurements. This required associated measurements of  $\Delta\text{CBF}$  by a spin tagging imaging experiment, of  $\Delta\text{CBV}$  by the use of iron contrast reagents and of the spin-spin relaxation times. Values of  $\Delta\text{CMR}_{\text{O}_2}$  agreed with values obtained by an indirect  $^1\text{H}$ NMR detection of the  $^{13}\text{C}$  turnover of glutamate. The high resolution results of this method, giving increments of  $\Delta\text{CMR}_{\text{O}_2}$  can, by connections to absolute CBF – spin tagging results, be converted to absolute values. Values of  $\Delta\text{CMR}_{\text{O}_2}$  obtained this way are compared with the values measured by the flows of  $^{13}\text{C}$ -labeled glucose in the same experiments. This calibration brings together functional imaging and metabolic energetics. In place of the phenomenological connections offered by other investigators between functional imaging signals and arbitrarily selected variables, this calibration relates the fMRI signal mechanistically to a meaningful neurophysiological parameter. Once  $\text{CMR}_{\text{O}_2}$  is derived from the BOLD signal in this way, the relationships between energy and neuronal activity established throughout the earlier chapters become available with the temporal and spatial resolutions of the calibrated BOLD measurement. This connection forms the basis of interpreting the BOLD effect in later chapters. Both of these newer methods of determining  $\text{CMR}_{\text{O}_2}$  are shown to agree with classical methods of oxygen consumption with significant advantages over earlier methods.

In Chapter 10 single electrode recordings of neuronal firing rates are regionally coordinated with values of  $\text{CMR}_{\text{O}_2}$  obtained from calibrated BOLD measurements. Neuronal firing rates, or spiking, are for many the ‘gold standard’ of neuronal activity. To measure these rates, individual neurons are identified in the rat somatosensory cortex, located during forepaw stimulation by BOLD experiments, and their firing rates followed through changes in depth of anesthesia and during sensory stimulation. The ensemble of neurons, followed in this way, correlates deployments of the neuronal population with the total energetics. Changes during the stimulation are shown to involve the majority of neurons in the voxels, rather than a selected few. Implications of these results for neuronal function are explored here, and in several of the subsequent chapters.

### 1.3. CLINICAL BEGINNINGS

Applications of magnetic resonance results to epilepsy and the psychiatric diseases clearly indicate directions for future study. Mesial temporal lobe epilepsy, one of the most common and debilitating forms, has

been shown by these measurements in conjunction with PET and microdialysis to be a disease in which the energetics and the glutamate neurotransmitter cycling have been impaired. In Chapter 12, Petroff and Spencer describe applications of  $^{13}\text{C}$  MRS to the glutamate glutamine cycling in the hippocampus. They show that the degree of neuronal loss/damage in the hippocampus correlates well with the degree of impairment. A model is proposed in which astroglial metabolic impairments lead to reduced glutamate uptake, explaining the elevated extracellular glutamate (and resultant hyperexcitability) during even the quiescent interictal periods between seizures.

The concentration of NAA is shown by Hetherington *et al.* in Chapter 11 to depend upon the energetic state of the mitochondria NAA decreases, reflecting a decrease in mitochondrial energetics, are proposed to be accompanied by more rapid release of glutamate. The flux from neurons is measurable by  $^{13}\text{C}$  MRS. Combining the results from this two pronged study of temporal lobe epilepsy we see that (1) the epileptic focus has lower NAA; (2) this reflects decreased mitochondrial energetics which (3) leads to a more rapid release of glutamate, thereby suggesting a cause for the (4) high concentrations of extracellular glutamate previously observed. An additional mechanism that presumably contributes to the high glutamate levels is seen in (5) the decreased rate of glutamate neurotransmitter cycling in the epileptogenic focus. Clearly these novel, sturdy *in vivo* insights offer interventional opportunities for preventing epileptic seizures.

From another direction the concentration of GABA has been shown to correlate quantitatively with the mood of normal subjects. The variation of GABA levels during alcoholism and in the subsequent withdrawal period has promise for understanding features of addiction. In the more daunting problems of depression and schizophrenia, preliminary results of neurotransmitter activity give promising correlations. The approach from magnetic resonance as from so many directions is mainly confined to phenomenological correlations. The problem faced by magnetic resonance in studying mental illness resembles that of other physical methods, immersed as they all are in the cyclical problem of having to define the problem while studying it. The definite information about the depressed condition reported by Graeme Mason in Chapter 11 provides an exciting starting point for future studies.

## 1.4. BRAIN AND MIND

Several implications of the metabolic studies for the planning and interpretations of fMRI experiments are proposed in the book. The interpretations of fMRI experiments in light of these results are discussed in this section. The metabolic results are presented in six chapters of Section B and interpreted in Chapter 16. They emphasize that the differencing methods used in fMRI experiments, measure changes in neuronal activity between the baseline and stimulated conditions. fMRI by discarding the baseline activity neglects the majority of neuronal activity which has been measured in Chapters 5 and 10 where it was shown to participate in the brain's response to the stimulus. One implication for the usual functional imaging signal is that, while increases or decreases of signal show activity changes in the region, still the absence of changes does not mean the absence of activity. Furthermore the magnitude of the change, being dependent upon the baseline activity, does not measure the magnitude of brain activity during the task.

Chapter 14 applies some of these concepts to survey and evaluate fMRI studies of declarative memory in humans. The conventional differencing method has been employed in the experiments surveyed and information about the pathways of memories reviewed to show how differencing, if used carefully, can illuminate mental processes. It is suggested that the absence of incremental signals in the hippocampus during traditional memory tasks arises from the high baseline activities, in accordance with the  $^{13}\text{C}$  MRS results. The wide variety of enriched memory tasks that can provoke incremental fMRI signals are examined closely in the search of a unifying conceptual basis.

Chapter 15 reviews selective fMRI results to explore the accomplishments and limitations of localizing activations. Beyond the static mapping of brain responses this chapter investigates effects of the changing

nature of the response, of the task and of the subject upon the meaningfulness of the results. Chapter 16 considers the consequences of the present metabolic findings for the investigation of complex brain activities including subjectivity. It emphasizes how the quantitative description of baseline neuronal activity, reached in the early chapters, should not be ignored by any psychology of mind. In the resting awake state, there is a high level of cortical energy consumption dedicated to neuronal signaling. It is suggested that the high baseline activity is caused by wide neuronal connections which support consciousness. These results describe a brain that accommodates and is intrinsically dependent upon subjective experience. The metabolic findings of highly active baseline activities are proposed to provide boundary conditions for a view of mind in which subjectivity and consciousness are not neglected.

The last chapter summarizes conclusions reached in the book, and suggests possible future directions.



# 2

## Energy Metabolism in Neural Tissues *in vivo* at Rest and in Functionally Altered States

**Louis Sokoloff**

*Laboratory of Cerebral Metabolism, National Institute of Mental Health, National Institutes of Health, Bethesda, MD 20892, USA*

---

2.1 Introduction	11
2.2 Local Cerebral energy Metabolism	13
2.3 Biochemical Mechanisms of Functional Activation of Energy Metabolism at the Tissue Level	17
2.4 Localization of Functionally Activated Energy Metabolism at the Tissue Level	19
2.5 Cellular Localization of Functional Activation of Energy Metabolism	24
2.5.1 Effects of Increased Extracellular K <sup>+</sup> and Intracellular Na <sup>+</sup> Concentrations	24
2.5.2 Effects of Glutamate on Glucose Utilization in Astroglia	25
2.6 Summary	27

---

### 2.1. INTRODUCTION

The biochemical pathways of energy metabolism in brain are in most respects like those of other tissues, but special conditions peculiar to the central nervous system produce obstacles to studies of intermediary metabolism of the brain *in vivo*. For example, the blood-brain barrier restricts the exchange of substrates and products between brain and blood, and, consequently, biochemical reactions normally operating within the brain tissues are often not detectable with traditional *in vivo* methods based on exchange of substrates and metabolites between the blood and brain. *In vitro* studies best serve to identify pathways of intermediary

metabolism, biochemical mechanisms, and potential rather than actual performance, but valid identification of the ultimate substrates and products of cerebral energy metabolism and their rates of utilization and production under conditions of normal brain function can be obtained only *in vivo*.

The first definitive studies of cerebral energy metabolism *in vivo* began with the development of the nitrous oxide method by Kety and Schmidt (1948). This method made it possible to determine the rates of cerebral blood flow (CBF) and oxygen consumption (CMRO<sub>2</sub>). Originally designed for use in man it was also applicable in animals, and, furthermore, it could be used in the unanesthetized state, a particularly important requirement to study the normal functioning brain. The method was based on the indirect Fick principle which states that, when a chemically inert tracer (i.e. one that is neither consumed nor produced by a given tissue) is introduced into the circulation, the rate of change in its content in any tissue is equal to the difference between the rates at which it is brought to that tissue in the arterial blood and removed from it in the venous blood. The method originally employed low concentrations of nitrous oxide as the tracer but was subsequently adapted for use with inert radioactive gases, e.g., <sup>85</sup>Kr, <sup>79</sup>Kr, and <sup>133</sup>Xe. Inasmuch as application of the Fick principle requires sampling of both arterial and representative cerebral venous blood for determination of their tracer concentrations, cerebral arteriovenous differences for a variety of substrates and products of cerebral metabolism could also be measured and their rates of utilization or production by the brain calculated as the product of these arteriovenous differences and CBF.

Numerous studies with this method established that cerebral energy metabolism is extraordinarily active in the unanesthetized state (Clarke and Sokoloff, 1999). For example, in normal, conscious, young adult men the brain comprises only about 2% of total body weight, but it alone consumes about 20% of the total resting body oxygen consumption. Studies with the method also established that glucose is not only an essential but normally the almost exclusive substrate for the brain's energy metabolism. Under normal conditions the brain utilizes glucose in almost stoichiometric amounts with the oxygen required for the complete oxidation of glucose to CO<sub>2</sub> and H<sub>2</sub>O (Table 2.1). For complete stoichiometry 6 mol of O<sub>2</sub> are consumed and 6 mol of CO<sub>2</sub> produced per mole of glucose utilized, i.e., a molar ratio (O<sub>2</sub>/glucose ratio) of 6.0; the respiratory quotient (R.Q.) (ratio of CO<sub>2</sub> production to O<sub>2</sub> consumption) is then 1.0. Under normal conditions cerebral glucose utilization (CMR<sub>glc</sub>) not only accounts for all the O<sub>2</sub> consumed, but exceeds the rate for complete stoichiometry with CMRO<sub>2</sub> by about 20%, and the measured O<sub>2</sub>/glucose ratio is about 5.5 (Table 2.1). In ketotic states, such as those due to starvation, fat-feeding, diabetes, etc., the blood levels of the ketone bodies, D-β-hydroxybutyrate and acetoacetate, are elevated, and these can substitute partly but not completely for glucose as the substrate for the brain's

**Table 2.1.** Rates of and relationship between cerebral oxygen consumption and glucose utilization in normal, conscious, young adult men

Function	Rate
O <sub>2</sub> consumption (μmol/100 g of tissue/min)	156
Glucose utilization (mmol/100 g of tissue/min)	31
O <sub>2</sub> /glucose ratio (mol/mol)	5.5
Glucose equivalent of O <sub>2</sub> consumption (μmol/100 g tissue/min) (assuming 6 mol O <sub>2</sub> per mol of glucose)	26
Excess of total glucose utilized above glucose oxidized (mmol/100 g of tissue/min)	5
CO <sub>2</sub> production (μmol/100 g of tissue/min)	156
Cerebral respiratory quotient (R.Q.)	0.97

oxidative metabolism (Owen *et al.*, 1967; Krebs *et al.*, 1971); in such cases the O<sub>2</sub>/glucose ratio rises above 6.0.

Numerous studies with the nitrous oxide method and its derivatives demonstrated that cerebral energy metabolism declines in parallel with reduced levels of consciousness. For example, CMRO<sub>2</sub> was moderately lower in conditions in which the sensorium was impaired but not to the level of unconsciousness, e.g., diabetic acidosis, moderate hypoglycemia, cerebral arteriosclerosis, etc., and markedly depressed in conditions with complete unconsciousness or coma, e.g., general anesthesia, diabetic coma, insulin coma, hepatic coma, and cerebral ischemia due to increased intracranial pressure caused by brain tumors (Kety, 1950; Clarke and Sokoloff, 1999). All these were, however, pathological conditions in which energy metabolism was probably reduced due to disrupted intracellular biochemical processes, insufficient substrate supply, or lesser demand for energy because of pathologically depressed neuronal functional activity. In physiological and pharmacological states with obviously altered mental functions, not necessarily altered levels of consciousness, such as in schizophrenia, LSD intoxication, mild alcoholic inebriation, sedation, mental exercise during solving of arithmetic problems, etc., no changes in CMRO<sub>2</sub> were found. The failure of the nitrous oxide method to detect a relationship between energy metabolic rate and functional activity in the brain was undoubtedly due to the fact that it measured only average rates of oxygen and glucose utilization in the brain as a whole and not in the specific regions of the brain where the functional activities were localized.

## 2.2. LOCAL CEREBRAL ENERGY METABOLISM

The capability to determine local rates of energy metabolism in specific regions of the brain *in vivo* first became available with development of the 2-[<sup>14</sup>C]deoxyglucose ([<sup>14</sup>C]DG) method (Sokoloff *et al.*, 1977). This method measures local rates of glucose utilization simultaneously in all regions of the nervous system. Furthermore, it is fully applicable to unanesthetized animals, thus avoiding the complications of alterations of neural functions and metabolism by anesthetic agents. Because of the close to stoichiometric relationship between oxygen and glucose utilization in brain, glucose utilization is generally as good a measure of cerebral energy metabolism as oxygen consumption. 2-[<sup>14</sup>C]Deoxyglucose (2-[<sup>14</sup>C]DG) was used because it is an analog of glucose with which it competes for blood–brain transport into the brain and for phosphorylation by hexokinase to their hexose-6-phosphate derivatives. Unlike glucose-6-phosphate, however, which is very rapidly metabolized further via the glycolytic and tricarboxylic pathways ultimately to H<sub>2</sub>O and CO<sub>2</sub>, 2-[<sup>14</sup>C]DG-6-phosphate can be metabolized to some extent to 2-[<sup>14</sup>C]DG-1-phosphate, 2-[<sup>14</sup>C]DG-1-6-phosphate, and <sup>14</sup>C-labeled glycogen, but all the products of 2-[<sup>14</sup>C]DG phosphorylation remain trapped in the cells. Consequently, all the labeled products of 2-[<sup>14</sup>C]DG phosphorylation accumulate with time and are retained within the cells with negligible loss for considerable lengths of time. From a kinetic analysis of the behavior of glucose and tracer concentrations of 2-[<sup>14</sup>C]DG in brain an operational equation was derived with which to compute the local rates of CMR<sub>glc</sub> from the measured times courses of arterial plasma glucose and 2-[<sup>14</sup>C]DG concentrations and the local tissue isotope concentration at the end of the experimental period, usually 30–45 min. Local <sup>14</sup>C concentrations in identifiable anatomical structures throughout the brain are determined by the use of quantitative autoradiography (Figure 2.1), a technique originally developed for measurement of local cerebral blood flow in animals with chemically inert, diffusible radioactive tracers (Landau *et al.*, 1955; Freygang and Sokoloff, 1958). The autoradiographs obtained with the 2-[<sup>14</sup>C]DG method can be converted by computerized image-processing techniques into color-coded quantitative images of the brain in which local rates of CMR<sub>glc</sub> are encoded in the color scale. These processed autoradiographic images provide, therefore, the means to visualize local rates of glucose utilization throughout the brain exactly where they occur with a spatial resolution of 100–200  $\mu$ m (Smith, 1983a).

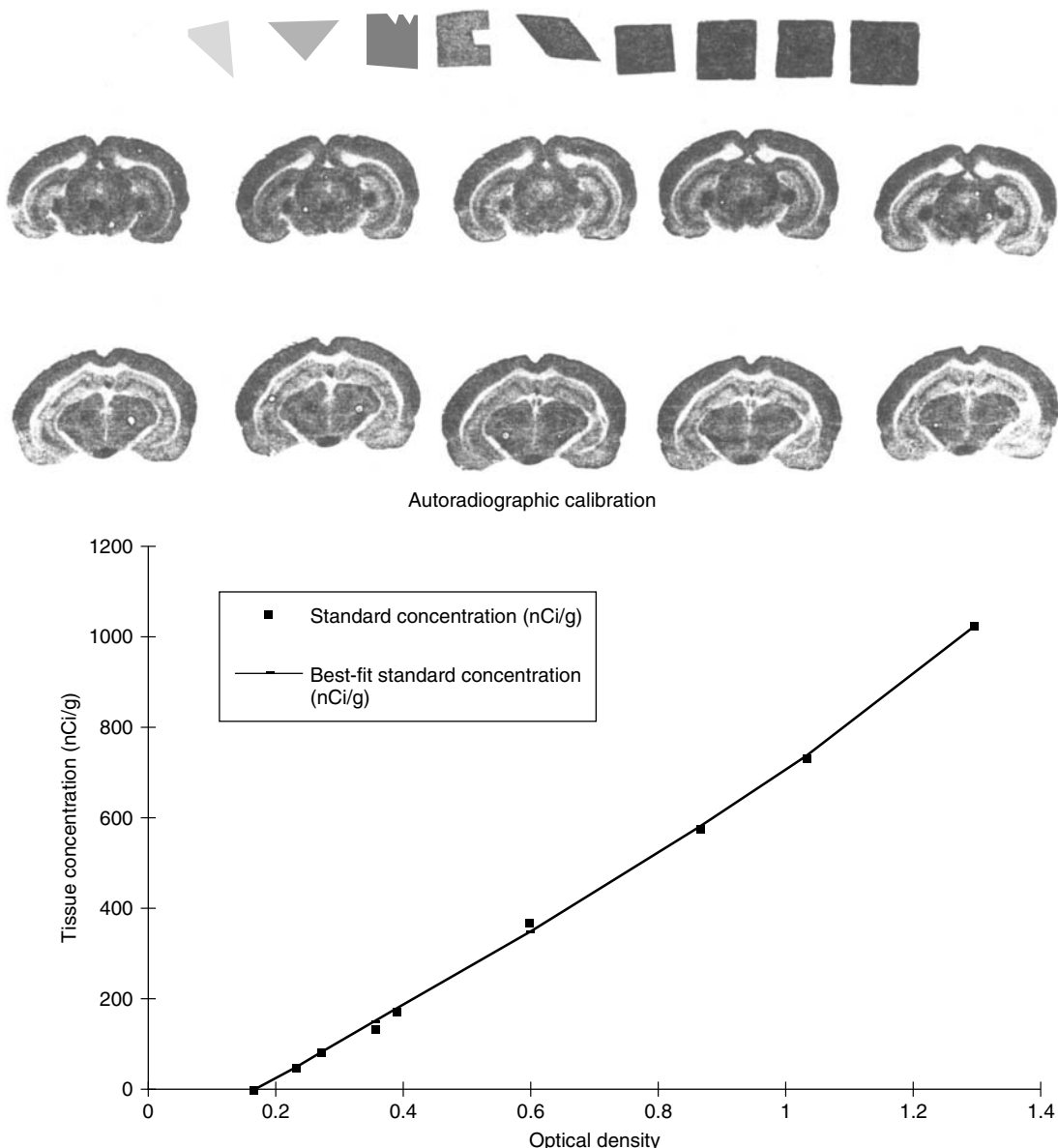


**Figure 2.1.**  $[^{14}\text{C}]$ DG autoradiographs of conscious rat brain and of calibrated  $[^{14}\text{C}]$ methylmethacrylate standards as well as the calibration curve between optical density and tissue  $^{14}\text{C}$  concentrations derived from densitometry of the standards.

Autoradiography is, of course, not applicable to man. To adapt the  $[^{14}\text{C}]$ DG method for use in man it was necessary to introduce a  $\gamma$ -emitting radioactive label into 2-deoxyglucose to allow external detection of the tracer. This was done by attaching  $^{18}\text{F}$  to the carbon in the 2-carbon position of 2-deoxyglucose to produce 2- $[^{18}\text{F}]$ fluoro-2-deoxy-D-glucose ( $^{18}\text{FDG}$ ), and the local tissue concentrations of label were determined by external scintillation counting with a single photon emission scanner in place of autoradiography (Reivich

*et al.*, 1979).  $^{18}\text{F}$  is a positron emitter, and the  $^{18}\text{FDG}$  method was subsequently adapted further for use with positron emission tomography (PET) (Phelps *et al.*, 1979). PET provides better accuracy and spatial resolution than single photon detection although its spatial resolution in the mm range is still at least an order of magnitude below the 100–200  $\mu\text{m}$  of the autoradiographic [ $^{14}\text{C}$ ]DG method.

Applications of the [ $^{14}\text{C}$ ]DG and  $^{18}\text{FDG}$  methods in both animals and man showed that  $\text{CMR}_{\text{glc}}$  varies widely in the various structures of the brain. It is much higher in gray matter than in white matter and is generally reduced by anesthesia (Table 2.2) (Sokoloff *et al.*, 1977). It was also clearly established that neuronal functional activation stimulates energy metabolism in neural tissues just as it does in other tissues (Sokoloff, 1981). The magnitude of the increases in glucose utilization is quantitatively related to the intensity of functional activation. For example, retinal stimulation by randomly timed light flashes raises local  $\text{CMR}_{\text{glc}}$  in proportion to the logarithm of the light intensity in those structures of the brain that receive direct projections from the retina (Figure 2.2). (Miyaoka *et al.*, 1979; Sokoloff, 1981). Electrical stimulation of the cervical sympathetic trunk or sciatic nerve increases  $\text{CMR}_{\text{glc}}$  linearly with spike frequency in the

**Table 2.2.** Local rates of cerebral glucose utilization in rats in the conscious state and under light thiopental anesthesia (means  $\pm$  SEM)

Structure	Conscious (6)	Anesthetized (8)	% Effect
<i>Gray Matter</i>			
Visual Cortex	111 $\pm$ 5	64 $\pm$ 3	-42
Auditory Cortex	157 $\pm$ 5	81 $\pm$ 3	-48
Parietal Cortex	107 $\pm$ 3	65 $\pm$ 2	-39
Sensory-motor Cortex	118 $\pm$ 3	67 $\pm$ 2	-43
Lateral Geniculate Nucleus	92 $\pm$ 2	53 $\pm$ 3	-42
Medial Geniculate Nucleus	126 $\pm$ 6	63 $\pm$ 3	-50
Thalamus: Lateral Nucleus	108 $\pm$ 3	58 $\pm$ 2	-46
Thalamus: Ventral Nucleus	98 $\pm$ 3	55 $\pm$ 1	-44
Hypothalamus	63 $\pm$ 3	43 $\pm$ 2	-32
Caudate-Putamen	111 $\pm$ 4	72 $\pm$ 3	-35
Hippocampus: Ammon's Horn	79 $\pm$ 1	56 $\pm$ 1	-29
Amygdala	56 $\pm$ 4	41 $\pm$ 2	-27
Cochlear Nucleus	124 $\pm$ 7	79 $\pm$ 5	-36
Nuclei of Lateral Lemniscus	114 $\pm$ 7	75 $\pm$ 4	-34
Inferior Colliculi	198 $\pm$ 7	131 $\pm$ 8	-34
Superior Colliculi	99 $\pm$ 3	59 $\pm$ 7	-40
Superior Olivary Nucleus	141 $\pm$ 5	104 $\pm$ 7	-26
Vestibular Nucleus	133 $\pm$ 4	81 $\pm$ 4	-39
Pontine Gray Matter	69 $\pm$ 3	46 $\pm$ 3	-33
Cerebellar Cortex	66 $\pm$ 2	44 $\pm$ 2	-33
Cerebellar Nuclei	106 $\pm$ 4	75 $\pm$ 4	-29
<i>White Matter</i>			
Corpus Callosum	42 $\pm$ 2	30 $\pm$ 2	-29
Genu of Corpus Callosum	35 $\pm$ 5	30 $\pm$ 2	-14
Internal Capsule	35 $\pm$ 5	29 $\pm$ 2	-17
Cerebellar White Matter	38 $\pm$ 2	29 $\pm$ 2	-24

Note: The effects of anesthesia were statistically significant in every structure ( $p < 0.05$ ).  
From Sokoloff *et al.* (1977).

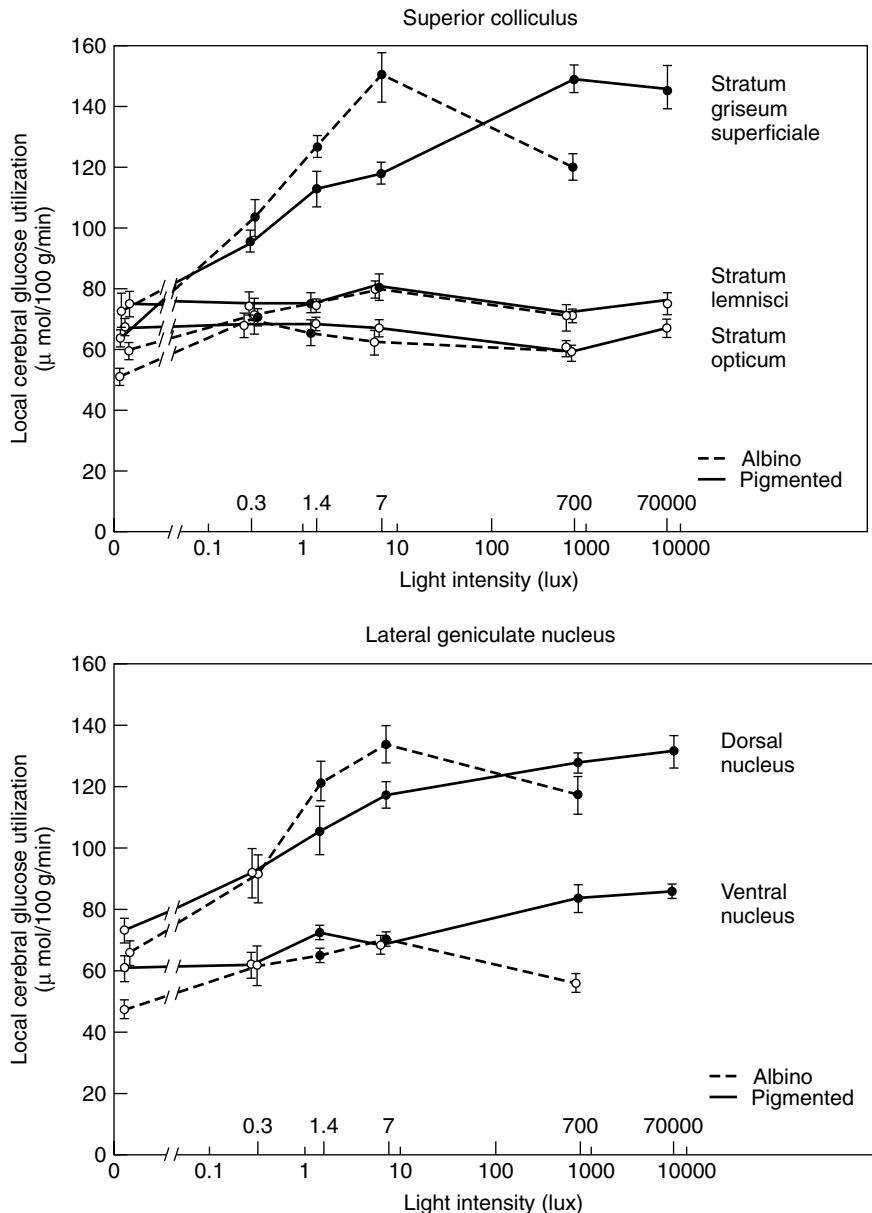


**Figure 2.2.** Rates of glucose utilization as a function of intensity of retinal illumination with randomly timed light flashes in various layers of superior colliculus and lateral geniculate nucleus of dark adapted albino and pigmented rats. From Miyaoka *et al.* (1979).

superior cervical ganglion (Yarowsky *et al.*, 1983) and dorsal horn of the lumbar spinal cord, respectively (Figure 2.3) (Kadekaro *et al.*, 1985). The glucose consumed per action potential can be determined from the slope of the straight line and equals 0.4 nmol/g of tissue per spike in the superior cervical ganglion and 0.6 nmol/g per spike in the dorsal horn of the lumbar spinal cord (Figure 2.3).

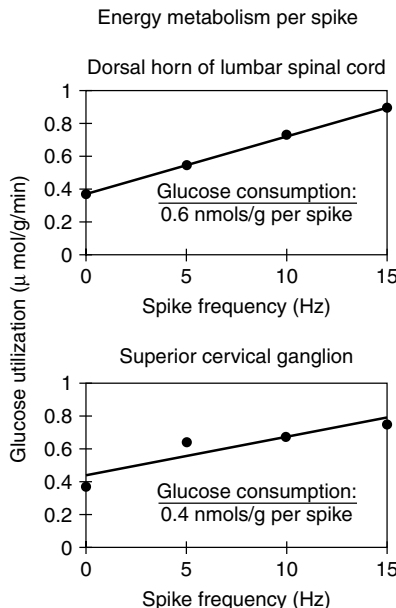


**Figure 2.3.** Relationship between frequency of action potentials and glucose utilization in dorsal horn of lumbar spinal cord and in superior cervical ganglion during electrical stimulation of sciatic nerve or cervical sympathetic trunk at different frequencies, respectively. Derived from data of Kadekaro *et al.* (1985) (top) and Yarowsky *et al.* (1983) (bottom).

### 2.3. BIOCHEMICAL MECHANISMS OF FUNCTIONAL ACTIVATION OF ENERGY METABOLISM AT THE TISSUE LEVEL

Muscles move or support masses against gravitational forces; the heart pumps blood against a pressure head; and kidneys transport water and solutes against concentration and osmotic gradients. These functions involve clearly definable physical work that requires expenditure of energy. It was less obvious what energy-requiring work nervous tissues do when functionally activated. Inasmuch as  $\text{CMR}_{\text{glc}}$  increases more or less linearly with spike frequency (Figure 2.3), it was reasonable to presume that the increased energy metabolism was somehow related to the generation, propagation, and conduction of action potentials. Action potentials result from the opening of ion channels that lead to increased  $\text{Na}^+$  influx and  $\text{K}^+$  efflux in neurons; they do not themselves directly consume energy but draw upon the potential energy stored in the membrane potentials. As spike frequencies increase, there are greater ion displacements and larger rises in intracellular  $\text{Na}^+$  ( $[\text{Na}^+]_i$ ) and extracellular  $\text{K}^+$  ( $[\text{K}^+]_o$ ) concentrations and, therefore, the need for more electrogenic  $\text{Na}^+$ ,  $\text{K}^+$ -ATPase activity to restore the ionic gradients across the membranes to their resting levels. This enzyme catalyzes the coupled transport of  $\text{Na}^+$  out of and  $\text{K}^+$  into the cells and consumes one molecule of ATP for every three  $\text{Na}^+$  ion exported and two  $\text{K}^+$  ions imported. Increased ATPase activity lowers intracellular ATP and raises ADP, AMP, phosphate acceptor, and inorganic phosphate concentrations, intracellular changes that stimulate glycolysis and electron transport and, therefore, energy metabolism. Many of the conditions of functional activation in which the  $^{14}\text{C}]\text{DG}$  method revealed local increases in  $\text{CMR}_{\text{glc}}$  have, in fact, been shown to be associated with elevated  $[\text{K}^+]_o$  in the activated tissues, and increasing  $[\text{K}^+]_o$  *in vivo* by applying  $\text{K}^+$  directly to the cerebral cortex, a treatment known to depolarize cell membranes and to cause spreading cortical depression, which itself raises  $[\text{K}^+]_o$  even further, profoundly stimulates cerebral cortical glucose utilization (Figure 2.4) (Shinohara *et al.*, 1979).

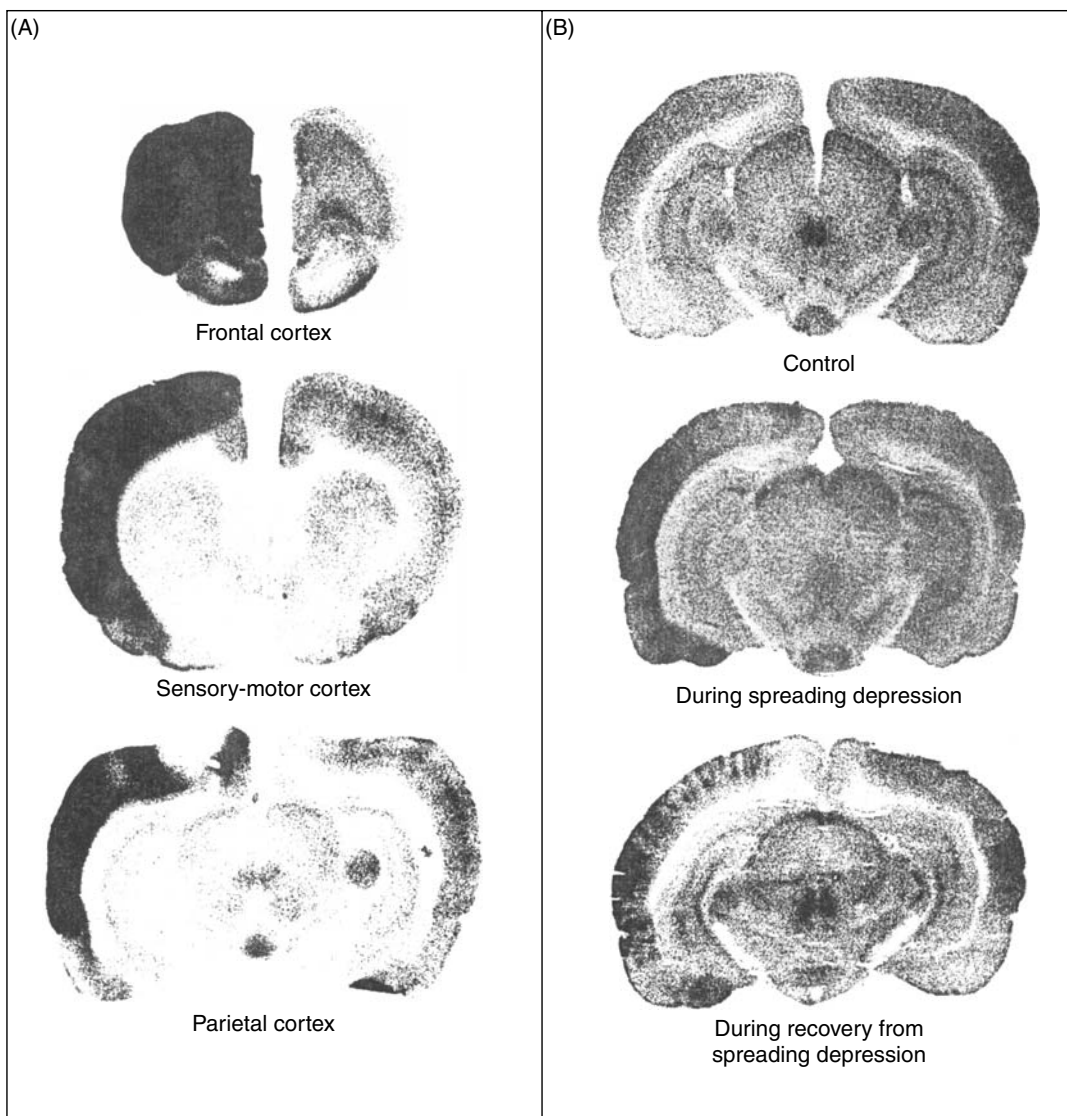


**Figure 2.4.**  $[^{14}\text{C}]$ Deoxyglucose autoradiographs showing changes in local  $\text{CMR}_{\text{glc}}$  during  $\text{K}^+$ -induced spreading cortical depression and during recovery in the rat; greater optical densities indicate higher  $\text{CMR}_{\text{glc}}$ . In all cases the experimental side on the left was treated with topically applied KCl, and the control side on the right was similarly treated with equivalent concentrations of NaCl. (A) Autoradiographs of brain sections at various levels of cerebral cortex from conscious rat in which spreading cortical depression was produced and sustained on left side by 5 M KCl applied to surface of intact dura over parietal cortex every 15–20 min; right side treated comparably with NaCl. (B) Autoradiographs of brain sections at level of parietal cortex from three rats under barbiturate anesthesia. Top section is from normal, anesthetized rat; middle section is from similarly anesthetized rat in which 80 mM KCl in artificial cerebrospinal fluid was repeatedly applied directly to the surface of the left parietal cortex; bottom section is from similarly anesthetized rat studied immediately after return of cortical DC potential to normal after a single wave of spreading depression induced by a single application of 80 mM KCl to the parieto-occipital cortex of the left side. From Shinohara *et al.* (1979).

**Table 2.3.** Influence of sodium pump activity and neurosecretion on [<sup>14</sup>C]deoxyglucose uptake in posterior pituitary *in vitro*<sup>a</sup>

Condition	[ <sup>14</sup> C]Deoxyglucose uptake (Cpm/100 µg protein/15 min)
<b>A. Dependence on activation of sodium pump</b>	Electrical stimulation
Controls (4)	988 ± 19
+ Electrical stimulation at 10 Hz (4)	1272 ± 57 <sup>b</sup>
+ Electrical stimulation at 10 Hz + 10 µM ouabain (4)	1018 ± 51 <sup>c</sup>
<b>B. Dependence on activation of sodium pump</b>	Opening Na <sup>+</sup> channels
Controls (14)	1381 ± 50
+60 µM veratridine (14)	1891 ± 85 <sup>b</sup>
+6 µM tetrodotoxin (9)	1209 ± 84 <sup>c</sup>
+60 µM veratridine + 6 µM tetrodotoxin (8)	1551 ± 72 <sup>c</sup>
+10 µM ouabain (4)	1318 ± 57 <sup>c</sup>
+60 µM veratridine + 10 µM ouabain (4)	1218 ± 120 <sup>c</sup>
<b>C. Independence from activation of secretion (Ca<sup>2+</sup>-free medium)</b>	
Controls (in Ca <sup>2+</sup> -free medium) (6)	1142 ± 38
+60 µM veratridine (in Ca <sup>2+</sup> -free medium) (6)	1681 ± 78 <sup>b</sup>

<sup>a</sup> The values represent means ± SEM of results obtained in number of experiments indicated in parentheses.

<sup>b</sup> Indicates statistically significant difference from controls ( $p < 0.001$ ).

<sup>c</sup> Indicates no statistical significant difference from controls. From Mata *et al.* (1980).

The possibility that activation of Na<sup>+</sup>, K<sup>+</sup>-ATPase activity by membrane-depolarizing stimulation mediates the coupling of energy metabolism to functional activity was examined directly in studies in which the rat neurohypophysis was electrically stimulated *in vitro* under conditions known to stimulate its secretion of vasopressin (Mata *et al.*, 1980). Such electrical stimulation raised [<sup>14</sup>C]DG phosphorylation, indicating increased glucose utilization, and this stimulation was completely blocked by addition of ouabain, a specific inhibitor of Na<sup>+</sup>, K<sup>+</sup>-ATPase (Table 2.3). Addition of veratridine, an agent that depolarizes cell membranes by opening voltage-dependent Na<sup>+</sup> channels and allows Na<sup>+</sup> entry into the cells, also markedly stimulated [<sup>14</sup>C]DG phosphorylation, and this stimulation too was eliminated by ouabain, as well as by tetrodotoxin, a known blocker of voltage-dependent Na<sup>+</sup> channels (Table 2.3). The stimulation of [<sup>14</sup>C]DG phosphorylation was not related to increased vasopressin secretion; the neurohypophysis *in vitro* cannot be stimulated to secrete hormone in Ca<sup>++</sup>-free medium, but even in such a medium veratridine stimulated [<sup>14</sup>C]DG phosphorylation (Table 2.3).

It appears then that the extra energy metabolism associated with electrical and functional activation in neural tissue is not used directly in the generation and propagation of action potentials. The energy is used rather to restore ionic gradients and resting membrane potentials that are partially degraded by the action potentials and also to some extent for other processes associated with or secondary to action potentials, such as neurotransmitter release, reuptake, and metabolism, exocytosis, endocytosis, etc.

## 2.4. LOCALIZATION OF FUNCTIONALLY ACTIVATED ENERGY METABOLISM AT THE TISSUE LEVEL

Traditional electrophysiology focuses largely on electrical recordings from neurons, and it was, therefore, originally assumed that the increases in local CMR<sub>glc</sub> associated with functional activation observed with the [<sup>14</sup>C]DG method were primarily in perikarya. Careful comparisons between the autoradiographs produced by the [<sup>14</sup>C]DG method and the stained brain sections from which they were prepared did not, however,

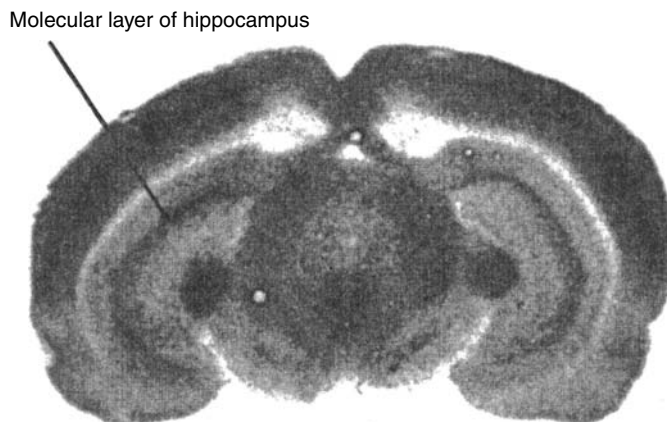


**Figure 2.5.**  $[^{14}\text{C}]$ Deoxyglucose autoradiograph of normal, conscious rat brain. Greater optical density reflects greater  $\text{CMR}_{\text{glc}}$ . Note high rate in molecular layer of hippocampus.

support this assumption. In the autoradiographs higher rates of glucose utilization are reflected in increasing darkness in the films (Figure 2.1). It was noted in the autoradiographs that the most metabolically active region in the hippocampus, which was at first thought to represent the cell-rich pyramidal cell layer, was actually the molecular layer, a region predominantly rich in synapses and poor in cell bodies (Figure 2.5).

In the striate cortex of the normal monkey  $\text{CMR}_{\text{glc}}$  is highest in a sub-layer of Layer IV that is not particularly rich in cellular elements; it is the layer where axonal terminals of the afferent geniculocalcarine pathway synapse with dendrites of neurons situated in other laminae of the visual cortex (Figure 2.6A, C) (Kennedy *et al.*, 1976). It is in this neuropil-rich layer that  $\text{CMR}_{\text{glc}}$  is most reduced when visual input is interrupted (Figure 2.6B).

The hypothalamo-neurohypophyseal pathway originates in cell bodies in the supraoptic and paraventricular nuclei in the hypothalamus and terminates in the neurohypophysis, 40 % of which consists of axonal terminals of the afferent tract (Nordmann, 1977). Osmotic stimulation by salt-loading is known to activate this pathway to stimulate vasopressin release from the neurohypophysis. Salt-loading was found also to stimulate local  $\text{CMR}_{\text{glc}}$  markedly in the neurohypophysis but to have no apparent effect on  $\text{CMR}_{\text{glc}}$  in the supraoptic and paraventricular nuclei (Figure 2.7) (Schwartz *et al.*, 1979). In contrast, hypotension produced by  $\alpha$ -adrenergic blockade with phenoxybenzamine or hemorrhage was found to stimulate local  $\text{CMR}_{\text{glc}}$  markedly in both these nuclei (Figure 2.7). The difference is that osmotic stimulation acts directly on the cell bodies to activate the hypothalamo-neurohypophyseal pathway whereas hypotension exerts its effects on the cell bodies in these nuclei indirectly via afferent inputs from the nucleus tractus solitarius in the brain stem that are part of the neural pathways of the baroreceptor reflexes. Results such as these suggested that *it is mainly the energy metabolism in regions rich in neuropil and synapses and not cell bodies that is linked to functional activity*.

To compare directly the effects of functional activation on local  $\text{CMR}_{\text{glc}}$  in perikarya and nerve terminals simultaneously in the same pathway, Kadekaro *et al.* (1985) stimulated the sciatic nerve at different frequencies and examined the effects on  $\text{CMR}_{\text{glc}}$  in both the dorsal root ganglia and the dorsal horn of corresponding segments of the lumbar spinal cord. The advantage of this system is that the body of the dorsal root ganglion contains perikarya devoid of neural processes, thus allowing examination of cell bodies free of nerve terminals simultaneously with the nerve terminals of the same pathway in the dorsal horn of the spinal cord. The results confirmed that it is  $\text{CMR}_{\text{glc}}$  in the region of the nerve terminals and not in the cell bodies that is linked to the functional activity. Glucose utilization increased linearly with the

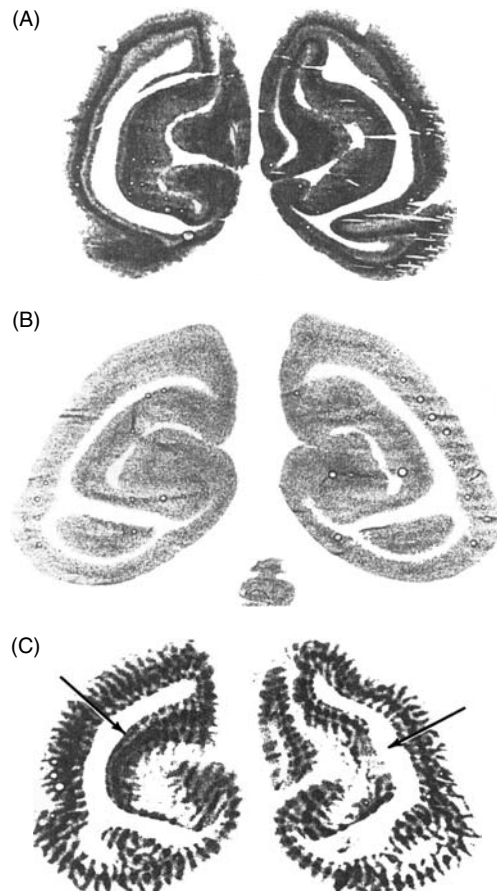


**Figure 2.6.**  $[^{14}\text{C}]$ Deoxyglucose autoradiographs demonstrating effects of bilateral and monocular visual occlusion on local  $\text{CMR}_{\text{glc}}$  in striate cortex of conscious monkey. Greater optical density indicates greater  $\text{CMR}_{\text{glc}}$ . (A) Striate cortex from animal with both eyes open. Note heterogeneity in laminae; the darkest lamina corresponds to Layer IV. (B) Striate cortex from monkey with both eyes patched. Note general reduction in density and almost complete disappearance of laminar heterogeneity, especially in Layer IV. (C) Striate cortex from animal with only right eye patched. Left half of autoradiograph corresponds to left hemisphere contralateral to occluded eye. Note alternating dark and light columns traversing the full thickness of the striate cortex which represent the ocular dominance columns. The dark bands represent the columns for the open eye; the light bands represent the columns for the patched eye and demonstrate the reduced glucose utilization resulting from reduced visual input. The arrows point to regions of bilateral asymmetry; these are the loci of representation of the blind spots of the visual fields. From Kennedy *et al.* (1976).

increasing frequency of stimulation of the sciatic nerve in the dorsal horn of the lumbar spinal cord, but it did not budge from its baseline levels in the cell bodies of the same pathway in the dorsal root ganglia (Figure 2.8). The lack of a metabolic response to electrical stimulation in the perikarya in the dorsal root ganglion may be surprising, but there is evidence that the soma membrane of neurons is not very excitable and not very productive of action potentials because of a relative paucity of voltage-gated  $\text{Na}^+$  channels. Smith (1983b), using patch clamp electrodes, obtained evidence that soma and dendrites of spinal cord neurons and soma of dorsal root ganglion cells cultured *in vitro* do not generate action potentials. Freygang

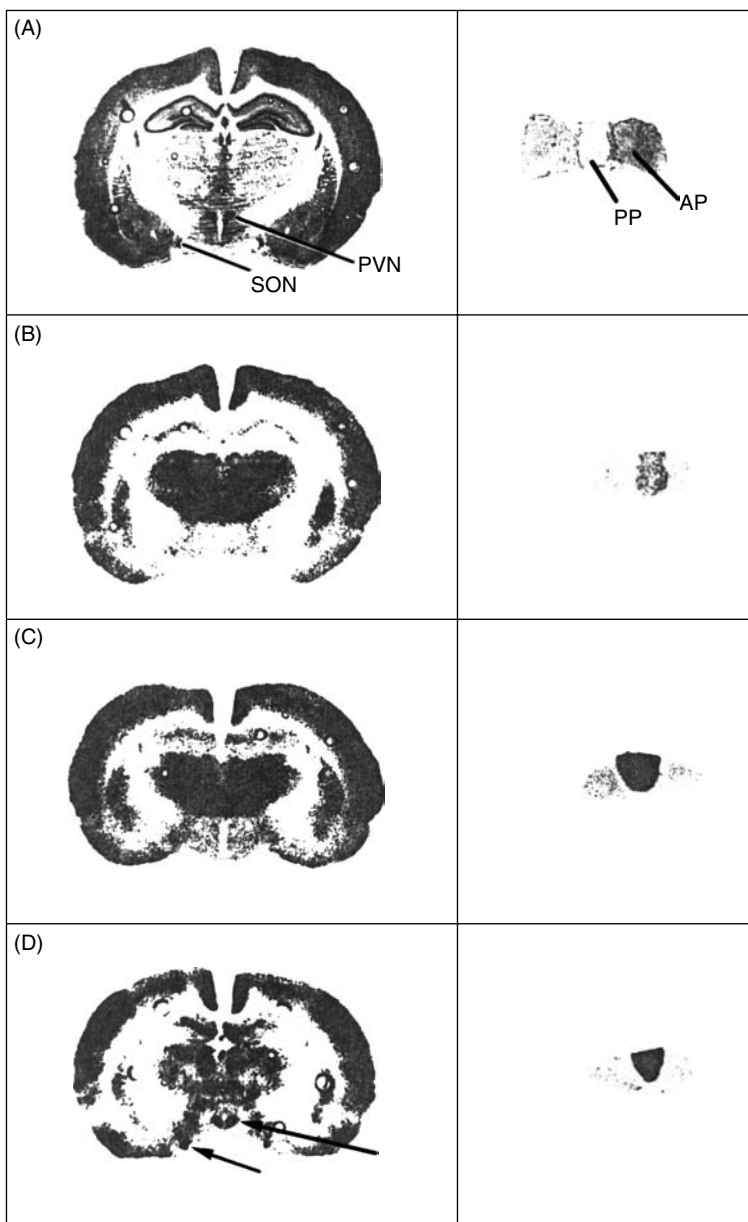


**Figure 2.7.** Effects of activation of hypothalamo-neurohypophyseal pathway by salt-loading or hypotension on local cerebral glucose utilization in the conscious rat. (A) Histological sections of brain stained with cresyl violet (Nissl) and pituitary stained with toluidine blue demonstrating positions of supraoptic nucleus (SON), paraventricular nucleus (PVN), posterior pituitary (PP), and anterior pituitary (AP). (B)  $[^{14}\text{C}]$ Deoxyglucose autoradiographs of brain and pituitary from normal control rat drinking only water. (C)  $[^{14}\text{C}]$ Deoxyglucose autoradiographs from rat given 2 % (w/v) NaCl in drinking water for 5 days. Note selective marked increase in density in posterior hypophysis, indicating increased glucose utilization. (D)  $[^{14}\text{C}]$ Deoxyglucose autoradiographs from rat made hypotensive by administration of 20 mg/kg of phenoxybenzamine 45–60 min prior to administration of the  $[^{14}\text{C}]$ deoxyglucose. Note selective increases in labeling of supraoptic and paraventricular nuclei and posterior pituitary. From Schwartz *et al.* (1979).

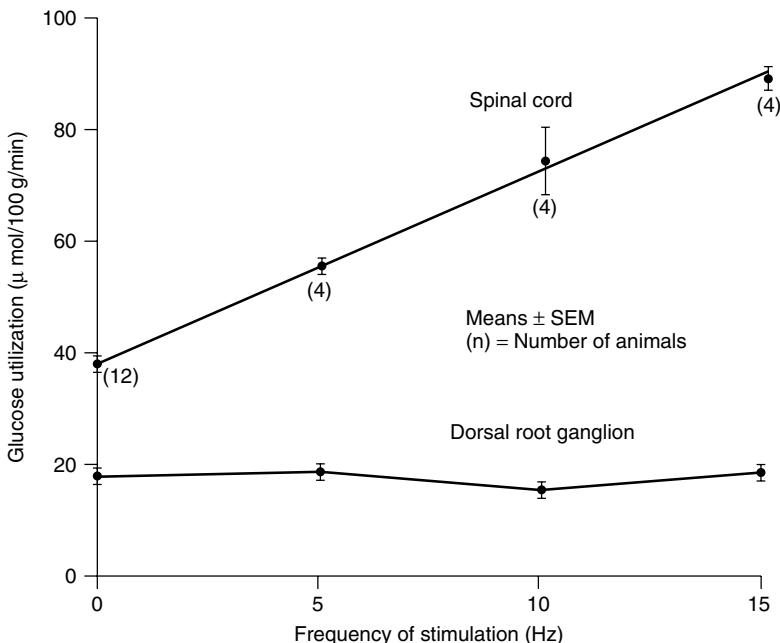


**Figure 2.8.** Frequency-dependent effects of electrical stimulation of sciatic nerve on local  $\text{CMR}_{\text{glc}}$  in dorsal root ganglion and dorsal horn of lumbar spinal cord. Error bars represent SEM. From Kadekaro *et al.* (1985).

(1958) and Freygang and Frank (1959) had previously concluded from analyses of extracellular potentials recorded from single spinal motor neurons and single neurons in the lateral geniculate nucleus that the soma-dendritic membrane can be driven synaptically to produce post-synaptic potentials but not propagating action potentials. Conduction through the cell body is mainly by electrotonic conduction rather than by action potentials. If action potentials do indeed mediate the coupling of energy metabolism to functional activity but are absent in the perikarya, then increased glucose metabolism due to functional activation is not to be expected in the perikarya. Some energy metabolism does, of course, proceed in cell bodies even at rest, but it is probably used more for vegetative, biosynthetic, and transport processes needed to maintain cellular structural and functional integrity rather than for processes directly related to functional activity. Some energy-consuming processes within the cell bodies that are related to intracellular signal transduction must also be activated by functional activation, but apparently their requirements are too small to be detected in the overall energy consumption of the cell.

The finding that rates of energy metabolism are linked to spike frequency in the terminal zones of the afferent pathways in the neuropil and not in cell bodies in the pathway should help to resolve questions about metabolic responses associated with functional excitation and inhibition. Glucose utilization has sometimes been observed to increase in structures in which electrophysiological evidence indicated inhibition of neuronal activity, thus raising questions whether active inhibition required energy just like excitation. It appears, however, that it is the spike activity in the afferent nerve terminals that correlates with the energy consumption, and this activity is the same whether the terminals are releasing excitatory or inhibitory neurotransmitters. The energy metabolism of the post-synaptic cell bodies, whether activated or inhibited, is not significantly altered, and to determine which has occurred, it is necessary to look downstream at the next synapses in the projection zones of those neurons. Glucose utilization is depressed in the projection zones of inhibited neurons and increased in the projection zones of excited neurons.

## 2.5. CELLULAR LOCALIZATION OF FUNCTIONAL ACTIVATION OF ENERGY METABOLISM

The neuropil, in which functionally activated energy metabolism is localized, contains not only neuronal elements, e.g., axonal terminals, dendritic processes, and synapses, but astrocytic processes as well. Because stimulation of local  $\text{CMR}_{\text{glc}}$  is linked to  $\text{Na}^+$ ,  $\text{K}^+$ -ATPase activity and the frequency of action potentials which are associated with increased  $\text{Na}^+$  influx and  $\text{K}^+$  efflux, some of the increased energy metabolism must be used to restore the ionic gradients in the neuronal elements where the action potentials are produced. Astrocytic processes envelop the synapses and could also be involved in the metabolic response. Astrocytes are believed to regulate  $[\text{K}^+]_{\text{o}}$  either by passive diffusion (Orkand *et al.*, 1966; Medzhradsky *et al.*, 1971) and/or active transport (Henn *et al.*, 1972) following increases in  $[\text{K}^+]_{\text{o}}$ , resulting from neuronal excitation (Hertz, 1977; Erecinska and Silver, 1994), and studies with tissue slices (Yarowsky *et al.*, 1986; Badar-Goffer *et al.*, 1992) or cultured cells (Cummins *et al.*, 1979a; Cummins *et al.*, 1979b; Brookes and Yarowsky, 1985; Hertz and Peng, 1992; Peng *et al.*, 1994) have indicated that energy is consumed in the process. The spatial resolution of the autoradiographic  $[^{14}\text{C}]DG$  method is limited to 100–200  $\mu\text{m}$  (Smith, 1983a) which is inadequate to identify the specific cellular or subcellular elements in neuropil that contribute to the increases in  $\text{CMR}_{\text{glc}}$  during functional activation.

### 2.5.1. Effects of Increased Extracellular $\text{K}^+$ and Intracellular $\text{Na}^+$ Concentrations

To approach this question, studies have been carried out *in vitro* with cells in culture. Changes in the extracellular medium expected to result from increased spike activity *in vivo* were simulated *in vitro*, and their effects on glucose metabolism of cultured neurons and astroglia examined. Spike activity in axonal terminals leads to increased extracellular  $\text{K}^+$  and intracellular  $\text{Na}^+$  concentrations and release of neurotransmitters. Therefore, the effects of elevated  $[\text{K}^+]_{\text{o}}$ ,  $[\text{Na}^+]_{\text{i}}$ , and the extracellular concentration of glutamate, the most prevalent excitatory neurotransmitter in brain, on  $[^{14}\text{C}]DG$  phosphorylation to  $[^{14}\text{C}]DG$ -6-phosphate, a measure of glucose utilization, were examined in cultured neurons and astroglia (Takahashi *et al.*, 1995).

Increasing  $[\text{K}^+]_{\text{o}}$  in the range of 5.4–56 mM stimulated  $[^{14}\text{C}]DG$  phosphorylation in both neuronal and mixed neuronal-astroglial cultures (Figure 2.9) (Takahashi *et al.*, 1995), and these increases were prevented by ouabain, implicating  $\text{Na}^+$ ,  $\text{K}^+$ -ATPase in the mechanism of the effect. Raising  $[\text{K}^+]_{\text{o}}$  in the same range had no such effect in the cultured astroglia. In fact, the highest levels of  $[\text{K}^+]_{\text{o}}$  examined tended to inhibit  $[^{14}\text{C}]DG$  phosphorylation in astroglia (Figure 2.9). On the other hand, promoting  $\text{Na}^+$  entry into the cells and increasing  $[\text{Na}^+]_{\text{i}}$  either by opening membrane voltage-gated  $\text{Na}^+$  channels with veratridine or by adding the  $\text{Na}^+$  ionophore monensin markedly stimulated  $[^{14}\text{C}]DG$  phosphorylation in astroglia, but only if  $\text{Na}^+$  were present in the extracellular medium (Figure 2.10) (Brookes and Yarowsky, 1985; Takahashi *et al.*, 1995). Tetrodotoxin, which blocks voltage-dependent  $\text{Na}^+$  channels, did not alter baseline rates of  $[^{14}\text{C}]DG$  phosphorylation in astroglia, and, as expected, prevented the stimulation by veratridine and had no effect on the stimulation by monensin (Figure 2.10). Inhibiting  $\text{Na}^+$ ,  $\text{K}^+$ -ATPase activity with ouabain lowered the basal rate of  $[^{14}\text{C}]DG$  phosphorylation, completely blocked the stimulation by veratridine, and partially suppressed the stimulation by monensin (Figure 2.10). The absence of a tetrodotoxin effect on the monensin stimulation can be explained by the fact that monensin-induced  $\text{Na}^+$  entry is not through voltage-dependent  $\text{Na}^+$  channels and is, therefore, insensitive to blockade by tetrodotoxin. The less than complete blockade of the monensin stimulation by ouabain can also be explained by the fact that monensin is a  $\text{Na}^+/\text{H}^+$  exchanger that exchanges extracellular  $\text{Na}^+$  for intracellular  $\text{H}^+$ . It, therefore, raises  $\text{Na}^+$  and lowers  $\text{H}^+$  concentrations in the cells, both ionic changes that can enhance glucose metabolism, the

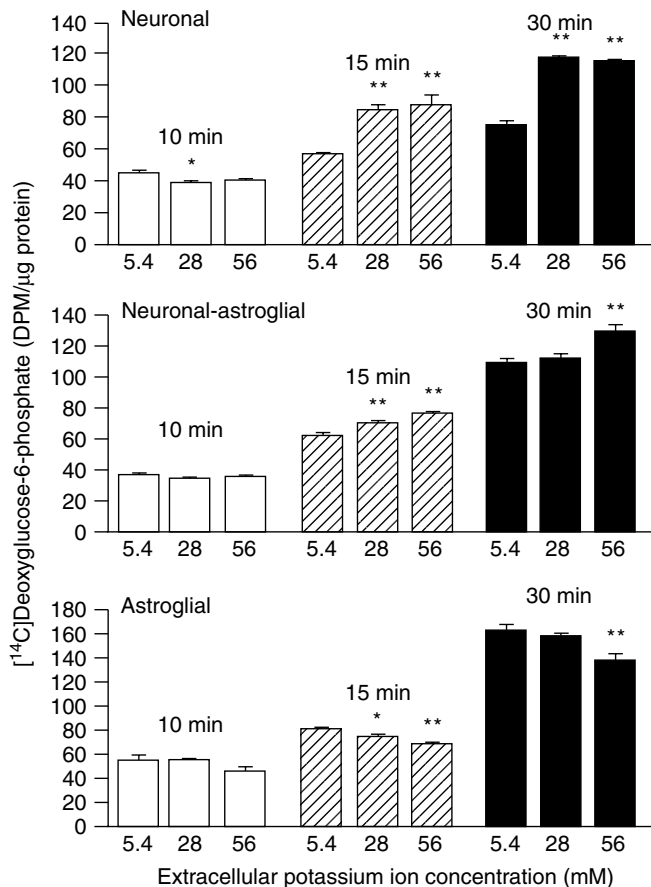


**Figure 2.9.** Effects of  $[K^+]_o$  on rates of  $[^{14}C]DG$  phosphorylation in cultured neurons, mixed neuronal-astroglia cultures, and astroglia cultures. Values are means  $\pm$  SEM obtained from quadruplicate wells. Numbers above bars indicate duration of incubation. \* $p < 0.05$ , \*\* $p < 0.01$  compared to the 5.4 mM  $[K^+]_o$  (Dunnett's test for multiple comparisons). Representative of at least three such experiments for each condition. From Takahashi *et al.* (1995).

former by ouabain-sensitive stimulation of  $Na^+, K^+$ -ATPase activity, and the latter by ouabain-insensitive stimulation of phosphofructokinase activity due to increased intracellular pH.

### 2.5.2. Effects of Glutamate on Glucose Utilization in Astroglia

Glutamate, the most prevalent excitatory neurotransmitter in the brain, is toxic to neurons, and must, therefore, be rapidly cleared from the extracellular space when it is released at glutamatergic synapses. Astrocytes, which have processes that envelop the synapses, carry out this function. They take up the glutamate from the extracellular space and convert it to glutamine, both steps that involve the consumption of energy. Addition of glutamate to the medium stimulates glucose utilization by astroglial cultures (Pellerin and Magistretti, 1994; Takahashi *et al.*, 1995). This stimulation is  $Na^+$  dependent, ouabain sensitive, unaffected by tetrodotoxin, and insensitive to NMDA and non-NMDA glutamate receptor antagonists (Figure 2.11). DL-Threo- $\beta$ -hydroxyaspartate, which competes with glutamate for uptake by

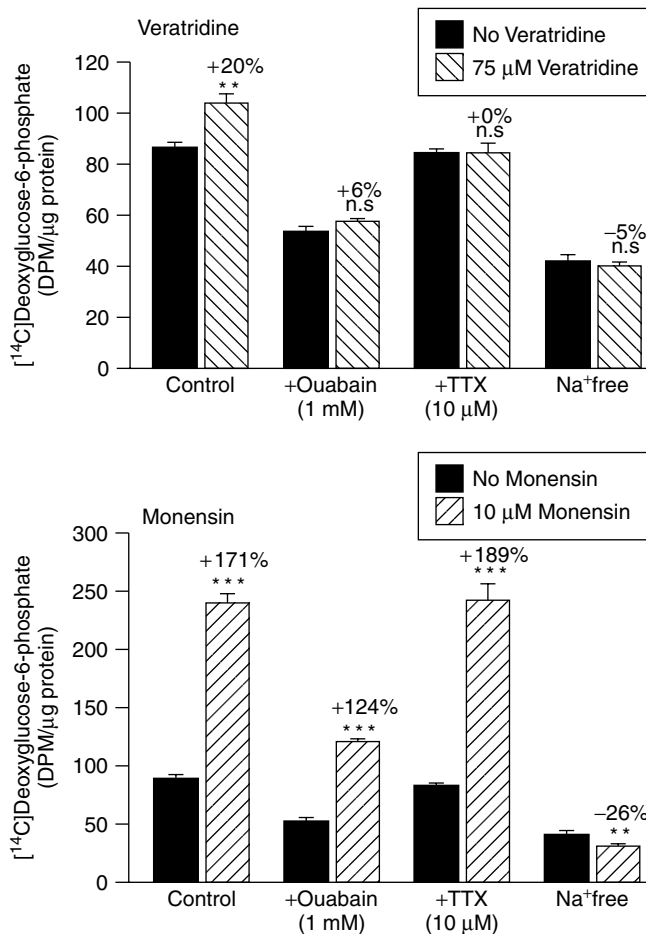


**Figure 2.10.** Effects of veratridine (upper) and monensin (lower) on  $[^{14}\text{C}]$ DG phosphorylation in astroglia (21-day old culture, no dbcAMP) and the effects of ouabain, tetrodotoxin (TTX), and  $\text{Na}^+$ -free medium on the veratridine and monensin effects. Values are means  $\pm$  SEM obtained from measurements of quadruplicate wells in three experiments. Numbers above bars indicate percent difference from each control. Representative of in three different astroglial preparations. \*\* $p < 0.01$ ; \*\*\* $p < 0.001$ ; n.s., not statistically significant from each control (grouped  $t$  test). From Takahashi *et al.* (1995).

the  $\text{Na}^+$ /glutamate co-transport system (Flott and Seifert, 1991), itself stimulates glucose utilization, and glutamate no longer stimulates in its presence. The hydroxyaspartate stimulation is also blocked by ouabain, absent in  $\text{Na}^+$ -free medium, and unaffected by tetrodotoxin and inhibitors of NMDA or non-NMDA receptors. These results show that the glutamate stimulation of glucose utilization by astroglia does not involve NMDA and non-NMDA glutamate receptors or voltage-dependent  $\text{Na}^+$  channels in the astroglia. It is due instead to the activation of  $\text{Na}^+$ ,  $\text{K}^+$ -ATPase activity by the increase in  $[\text{Na}^+]$ <sub>i</sub> that results from the coupled uptake of  $\text{Na}^+$  with glutamate into the astroglia. This uptake is mediated by a  $\text{Na}^+$ /glutamate co-transporter that co-transports 2–3  $\text{Na}^+$  ions with each glutamate molecule. In addition, much of the glutamate taken up by the astroglia is converted by glutamine synthetase to glutamine, a reaction consuming one ATP molecule for each molecule of glutamine formed. Inasmuch as it takes one molecule of ATP to pump out

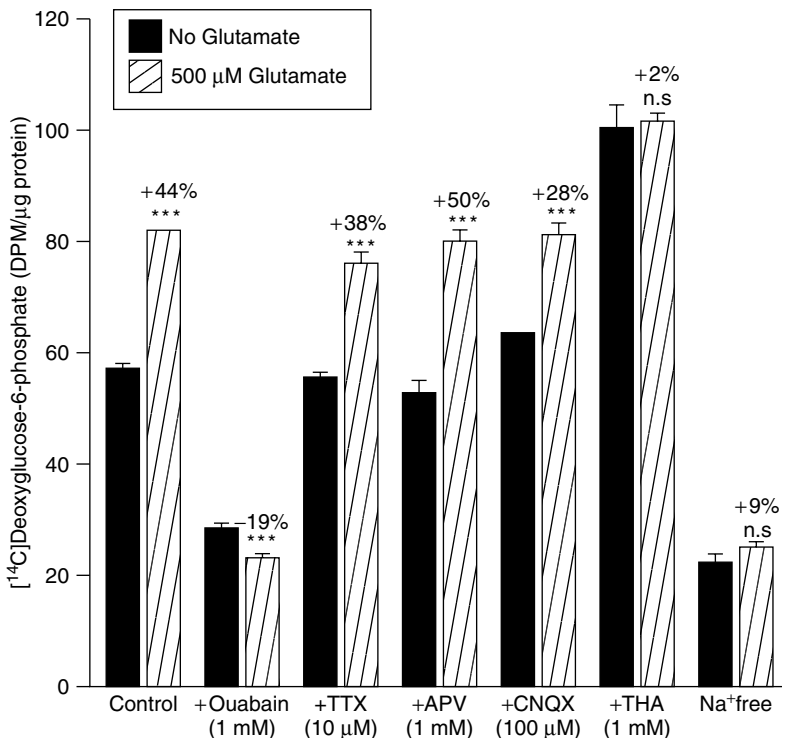


**Figure 2.11.** Effects of glutamate on  $[^{14}\text{C}]$ DG phosphorylation in astroglia and the effects of DL-2-amino-5-phosphonovaleric acid (APV), CNQX, ouabain, tetrodotoxin (TTX), DL-threo- $\beta$ -hydroxyaspartic acid (THA), and  $\text{Na}^+$ -free medium on the glutamate effects. Values are means  $\pm$  SEM obtained from quadruplicate wells, in three experiments, each with a different astroglial preparation. Numbers above bars indicate percent differences from each control. \*\*\*  $p < 0.001$ ; n.s., not statistically significant, from each control group (grouped  $t$  test). From Takahashi *et al.* (1995). Similar results were reported by Pellerin and Magistretti (1994).

the 2–3  $\text{Na}^+$  ions co-transported inward with each molecule of glutamate taken up, and one molecule of ATP is consumed in converting the molecule to glutamine, it appears that the net gain of two molecules of ATP from the glycolysis of one molecule of glucose is consumed in the processing of one molecule of glutamate by astroglia.

## 2.6. SUMMARY

The main energy-consuming work of functionally activated neural tissues is related to the generation and propagation of action potentials and the disposition of the neurotransmitter molecules that are released at the synapses. Normally, the energy required by neural tissues is almost entirely derived from glucose metabolism which increases almost linearly with spike frequency when tissue is functionally activated. Spikes result from  $\text{Na}^+$  influx and  $\text{K}^+$  efflux in the neuronal elements where they are generated, and the greater the spike frequency the greater the ionic displacements. Increased extracellular  $\text{K}^+$  and intracellular  $\text{Na}^+$  concentrations stimulate  $\text{Na}^+$ ,  $\text{K}^+$ -ATPase activity to restore the ionic gradients to their normal resting levels, and energy metabolism is then increased to resynthesize the ATP consumed in that process.

Functional activation of glucose utilization is essentially confined to neuropil which contains axonal, dendritic, and astrocytic processes. Obviously, some of the increased energy metabolism must occur in the

axonal terminals and dendrites where the spikes are generated. Functional activation of energy metabolism is not seen in perikarya, presumably because they have few voltage-dependent  $\text{Na}^+$  channels and, therefore, generate few if any action potentials.

Astrocytes contribute to the increased energy metabolism in neuropil during functional activation, but by other mechanisms. Astrocytic membranes can be depolarized by increased  $[\text{K}^+]_{\text{i}}$ , but they do not produce action potentials that would allow the  $\text{Na}^+$  influx into the cells needed to stimulate  $\text{Na}^+$ ,  $\text{K}^+$ -ATPase activity. Action potentials in axonal terminals, however, are associated with release of neurotransmitters. Glutamate is the most prevalent excitatory neurotransmitter in brain, but it is also a neurotoxin, and its extracellular concentration must be kept low by astrocytic reuptake via  $\text{Na}^+$ -dependent glutamate transporters that transport 2–3  $\text{Na}^+$  ions with each glutamate molecule into the cell. The increased  $[\text{Na}^+]_{\text{i}}$  then results in stimulation of  $\text{Na}^+$ ,  $\text{K}^+$ -ATPase activity and energy metabolism. In addition, glutamate taken up by astroglia is converted there to glutamine, an energy-requiring reaction that also consumes ATP.

Astrocytic processes surround the capillaries that bring glucose to the brain, and some if not all the glucose must traverse them before reaching the neurons. Evidence has been accumulating that astrocytes first metabolize glucose to lactate which they then export to the neurons for oxidation to  $\text{CO}_2$  and  $\text{H}_2\text{O}$  (Magistretti and Pellerin, 1996; Tsacopoulos and Magistretti, 1996). This would mean that glucose metabolism is compartmentalized between astroglia and neuronal elements, glycolysis in the astroglia and oxidation of the lactate/pyruvate products by the neurons. Glycolysis yields two molecules of ATP and two molecules of pyruvate/lactate per molecule of glucose glycolyzed. The two molecules of ATP produced in the astroglia are then consumed in the processing of each molecule of glutamate, suggesting that there may be a close quantitative relationship between glucose consumption and glutamate processing in the astroglia (Sibson *et al.*, 1998). The oxidation of the two molecules of pyruvate/lactate produced from glycolysis of one molecule of glucose leads to the generation of 36 additional molecules of ATP which is consumed mainly for the restoration of the ionic gradients and the membrane potentials degraded by the action potentials.

## REFERENCES

Badar-Goffer, R. S., Ben-Yoseph, O., Bachelard, H. S., and Morris, P. G. 1992. Neuronal–glial metabolism under depolarizing conditions. A  $^{13}\text{C}$ -n.m.r. study. *Biochem. J.* **282**: 225–230.

Brookes, N., and Yarowsky, P. J. 1985. Determinants of deoxyglucose uptake in cultured astrocytes: the role of the sodium pump. *J. Neurochem.* **44**: 473–479.

Clarke, D. D., and Sokoloff, L. 1999. Circulation and energy metabolism of the brain. In: Siegel, G., Agranoff, B., Albers, R. W., and Fisher, S. (Eds): *Basic Neurochemistry: Molecular, Cellular, and Medical Aspects*, 6th edn, Chapter 31. Lippincott-Raven, Philadelphia, PA, pp. 637–669.

Cummins, C. J., Glover, R. A., and Sellinger, O. Z. 1979a. Neuronal cues regulate uptake in cultured astrocytes. *Brain Res.* **170**: 190–193.

Cummins, C. J., Glover, R. A., and Sellinger, O. Z. 1979b. Astroglial uptake is modulated by extracellular  $\text{K}^+$ . *J. Neurochem.* **33**: 779–785.

Erecinska, M., and Silver, I. A. 1994. Metabolism and role of glutamate in mammalian brain. *Prog. Neurobiol.* **43**: 37–71.

Flott, B., and Seifert, W. 1991. Characterization of glutamate uptake in astrocyte primary cultures from rat brain. *Glia* **4**: 293–304.

Freygang, W. H., Jr. 1958. An analysis of extracellular potentials from single neurons in the lateral geniculate nucleus of the cat. *J. Gen. Physiol.* **41**: 543–564.

Freygang, W. H., Jr. and Frank, K. 1959. Extracellular potentials from single spinal motoneurones. *J. Gen. Physiol.* **42**: 749–760.

Freygang, W. H., Jr. and Sokoloff, L. 1958. Quantitative measurements of regional circulation in the central nervous system by the use of a radioactive inert gas. *Adv. Biol. Med. Phys.* **6**: 263–279.

Henn, F. A., Haljamäe, H., and Hamberger, A. 1972. Glial cell function: active control of extracellular  $\text{K}^+$  concentration. *Brain Res.* **43**: 437–443.

Hertz, L. 1977. Drug-induced alterations of ion distribution at the cellular level of the central nervous system. *Pharmacol. Rev.* **29**: 35–65.

Hertz, L., and Peng, L. 1992. Energy metabolism at the cellular level of the CNS. *Can. J. Physiol. Pharmacol.* **70** (Suppl.): S145–S157.

Kadekaro, M., Crane, A. M., and Sokoloff, L. 1985. Differential effects of electrical stimulation of sciatic nerve on metabolic activity in spinal cord and dorsal root ganglion in the rat. *Proc. Natl. Acad. Sci., USA* **82**: 6010–6013.

Kennedy, C., Des Rosiers, M. H., Sakurada, O., Shinohara, M., Reivich, M., Jehle, J. W., and Sokoloff, L. 1976. Metabolic mapping of the primary visual system of the monkey by means of the autoradiographic [<sup>14</sup>C]deoxyglucose technique. *Proc. Natl. Acad. Sci. USA* **73**: 4230–4234.

Kety, S. S. 1950. Circulation and metabolism of the human brain in health and disease. *Am. J. Med.* **8**: 205–217.

Kety, S. S., and Schmidt, C. F. 1948. The nitrous oxide method for the quantitative determination of cerebral blood flow in man: Theory, procedure, and normal values. *J. Clin. Invest.* **27**: 476–483.

Krebs, H. A., Williamson, D. H., Bates, M. W., and Hawkins, R. A. 1971. The role of ketone bodies in caloric homeostasis. *Adv. Enzyme Regul.* **9**: 387–409.

Landau, W. M., Freygang, W. H., Rowland, L. P., Sokoloff, L., and Kety, S. S. 1955. The local circulation of the living brain; values in the unanesthetized and anesthetized cat. *Trans. Am. Neurol. Assoc.* **80**: 125–129.

Magistretti, P. J., and Pellerin, L. 1996. Cellular bases of brain energy metabolism and their relevance to functional brain imaging: Evidence for a prominent role of astrocytes. *Cerebral Cortex* **6**: 50–61.

Mata, M., Fink, D. J., Gainer, H., Smith, C. B., Davidsen, L., Savaki, H., Schwartz, W. J., and Sokoloff, L. 1980. Activity-dependent energy metabolism in rat posterior pituitary primarily reflects sodium pump activity. *J. Neurochem.* **34**: 213–215.

Medzhradsky, F., Nandhasri, P. S., Idoyaga-Vargas, V., and Sellinger, O. Z. 1971. A comparison of ATPase activity of the glial cell fraction and the neuronal perikaryal fraction isolated in bulk from rat cerebral cortex. *J. Neurochem.* **18**: 1599–1603.

Myaoka, M., Shinohara, M., Batipps, M., Pettigrew, K. D., Kennedy, C., and Sokoloff, L. 1979. The relationship between the intensity of the stimulus and the metabolic response in the visual system of the rat. In: Cerebral Blood Flow and Metabolism. Gotoh, F., Nagai, H., and Tazaki, Y. (Eds). Hidejimi Seihanjo, Tokyo (Also, *Acta Neurol. Scand.*, Suppl. 72, **60**: 16–17).

Nordmann, J. J. 1977. Ultrastructural morphometry of the rat neurohypophysis. *J. Anat.* **123**: 213–218.

Orkand, R. K., Nicholls, J. G., and Kuffler, S. W. 1966. Effect of nerve impulses on the membrane potential of glial cells in the central nervous system of amphibia. *J. Neurophysiol.* **29**: 788–806.

Owen, O. E., Moran, A. P., Kemp, H. G., Sullivan, J. M., Herrera, M. G., and Cahill, G. F. 1967. Brain metabolism during fasting. *J. Clin. Invest.* **46**: 1589–1595.

Pellerin, L., and Magistretti, P. J. 1994. Glutamate uptake into astrocytes stimulates aerobic glycolysis: A mechanism coupling neuronal activity to glucose utilization. *Proc. Natl. Acad. Sci. USA* **91**: 10625–10629.

Peng, L., Zhang, X., and Hertz, L. 1994. High extracellular potassium concentrations stimulate oxidative metabolism in a glutamatergic neuronal culture and glycolysis in cultured astrocytes but have no stimulatory effect in a GABAergic neuronal culture. *Brain Res.* **663**: 168–172.

Phelps, M. E., Huang, S. C., Hoffman, E. J., Selin, C., Sokoloff, L., and Kuhl, D. E. 1979. Tomographic measurement of local cerebral glucose metabolic rate in humans with (F-18)2-fluoro-2-deoxy-d-glucose: validation of method. *Ann. Neurol.* **6**: 371–388.

Reivich, M., Kuhl, D., Wolf, A., Greenberg, J., Phelps, M., Ido, T., Cassella, V., Fowler, J., Hoffman, E., Alavi, A., Som, P., and Sokoloff, L. 1979. The [<sup>18</sup>F]fluoro-deoxyglucose method for the measurement of local cerebral glucose utilization in man. *Circulation Res.* **44**: 127–137.

Schwartz, W. J., Smith, C. B., Davidsen, L., Savaki, H., Sokoloff, L., Mata, M., Fink, D. J., and Gainer, H. 1979. Metabolic mapping of functional activity in the hypothalamo. *Science* **205**: 723–725.

Shinohara, M., Dollinger, B., Brown, G., Rapoport, S., and Sokoloff, L. 1979. Cerebral glucose utilization: Local changes during and after recovery from spreading cortical depression. *Science* **203**: 188–19.

Sibson, N. R., Dhankhar, A., Mason, G. F., Rothman, D. L., Behar, K. L., and Shulman, R. G. 1998. *Proc. Natl. Acad. Sci. USA* **95**: 316–321.

Smith, C. B. 1983a. Localization of activity-associated changes in metabolism of the central nervous system with the deoxyglucose method: Prospects for cellular resolution. In: Barker, J. L., and McKelvy, J. F. (Eds): *Current Methods in Cellular Neurobiology*, Vol. I, *Anatomical Techniques*. Wiley, New York, pp. 269–317.

Smith, T. G., Jr. 1983b. Sites of action potential generation in cultured neurons. *Brain Res.* **288**: 381–383.

Sokoloff, L. 1981. Localization of functional activity in the central nervous system by measurement of glucose utilization with radioactive deoxyglucose. *J. Cereb. Blood Flow Metab.* **1**: 7–36.

Sokoloff, L., Reivich, M., Kennedy, C., Des Rosiers, M. H., Patlak, C. S., Pettigrew, K. D., Sakurada, O., and Shinozaki, M. 1977. The [ $^{14}\text{C}$ ]deoxyglucose method for the measurement of local cerebral glucose utilization: Theory, procedure, and normal values in the conscious and anesthetized albino rat. *J. Neurochem.* **28**: 897–916.

Takahashi, S., Driscoll, B. F., Law, M. J., and Sokoloff, L. 1995. Role of sodium and potassium in regulation of glucose metabolism in cultured astroglia. *Proc. Natl Acad. Sci. USA* **92**: 4616–4620.

Tsacopoulos, M., and Magistretti, P. 1996. Metabolic coupling between glia and neurons. *J. Neurosci.* **16**: 877–885.

Yarowsky, P., Boyne, A. F., Wierwille, R., and Brookes, N. 1986. Effect of monensin on deoxyglucose uptake in cultured astrocytes: energy metabolism is coupled to sodium entry. *J. Neurosci.* **6**: 859–866.

Yarowsky, P., Kadekaro, M., and Sokoloff, L. 1983. Frequency-dependent activation of glucose utilization in the superior cervical ganglion by electrical stimulation of cervical sympathetic trunk. *Proc. Natl Acad. Sci. USA* **80**: 4179–4183.

# 3

## Techniques—MRS, fMRI, $^{13}\text{C}$ NMR, Indirect Detection of $^{13}\text{C}$

**Robin de Graaf**

*Department of Diagnostic Radiology, Yale University School of Medicine, MR Center, P.O. Box 208043, New Haven, CT 06520-8043, USA*

---

3.1	Introduction	31
3.2	<i>In vivo</i> NMR Spectroscopy	33
3.2.1	Proton NMR	33
3.2.2	Phosphorus NMR	34
3.2.3	Carbon-13 NMR	37
3.3	Elementary Experimental Techniques	39
3.3.1	Spatial Localization	39
3.3.2	Shimming	40
3.3.3	Water Suppression	42
3.3.4	Signal Quantification	43
3.4	Advanced Experimental Techniques	45
3.4.1	Introduction to Spectral Editing	45
3.4.2	Homonuclear Spectral Editing	46
3.4.3	Heteronuclear Spectral Editing	49

---

### 3.1. INTRODUCTION

Nuclear magnetic resonance (NMR) is based on the magnetic properties of nuclei. When placed in a (strong) external magnetic field, the nuclei can be observed by the absorption and emission of electromagnetic radiation. Purcell, Torrey and Pound (1) at MIT, Cambridge and Bloch, Hansen and Packard (2) at Stanford

simultaneously, but independently, discovered NMR in 1945. In 1952 Bloch and Purcell shared the Nobel prize for physics in recognition of their pioneering achievements (1–4). At this stage, NMR was purely an experiment for physicists to determine the nuclear magnetic moments of nuclei. NMR could only develop to one of the most versatile forms of spectroscopy after the discovery that nuclei within the same molecule absorb energy at different resonance frequencies. These so-called chemical shift effects, which are directly related to the chemical environment of the nuclei, were first observed in 1949 by Proctor and Yu (5), and independently by Dickinson (6).

During the first two decades, NMR spectra were recorded in a continuous wave mode in which either the magnetic field strength or the radio frequency was swept through the spectral area of interest, whilst keeping the other fixed. In 1966, NMR was revolutionized by Ernst and Anderson (7) who introduced pulsed NMR in combination with Fourier transformation, leading to greatly enhanced sensitivity and increased versatility (e.g. multi-pulse experiments). Pulsed or Fourier transform NMR is at the heart of all modern NMR experiments.

The induced energy level difference of nuclei in an external magnetic field is very small when compared to the thermal energy, so that the energy levels are almost equally populated. As a result the absorption of photons (electromagnetic quanta) is very low, making NMR a very insensitive technique when compared to other forms of spectroscopy. However, as a consequence of the minimal perturbation of the spins by the external magnetic field, NMR is also a noninvasive and nondestructive technique, ideally suited for *in vivo* measurements. In fact, by observing the water signal from his own finger, Bloch was the first to use NMR on a living system. Soon after the discovery of NMR, others showed the possibility of NMR to study living objects. In 1950, Shaw and Elsken (8) used proton NMR to investigate the water content of vegetable material. Odebold and Lindstrom (9) obtained proton NMR signals from a number of mammalian preparations in 1955. Continued interest in defining and explaining the properties of water in biological tissues led to the promising report of Damadian in 1971 (10) that NMR properties (relaxation times) of malignant tumorous tissues significantly differ from normal tissue, suggesting that (proton) NMR may have diagnostic value. In the early 1970s, the first high resolution NMR experiments on intact living systems were reported. Moon and Richards (11) used  $^{31}\text{P}$  NMR on intact red blood cells and showed how the intracellular pH can be determined from chemical shift differences. In 1974, Hoult *et al.* (12) reported the first study of  $^{31}\text{P}$  NMR on intact, excised rat hindleg skeletal muscle. Four years later, the first  $^{31}\text{P}$  NMR studies on excised and *in vivo* mammalian brain were performed by Chance *et al.* (13) and improved with surface coil detection by Ackerman *et al.* (14) in 1980. Technical difficulties, such as water suppression, delayed the application of  $^1\text{H}$  MRS to the study of brain metabolism. The first *in vivo*  $^1\text{H}$  MRS spectrum from rat brain was obtained by Behar *et al.* (15) in 1983 at Yale University. Two years earlier the same group also performed the first *in vivo*  $^{13}\text{C}$  MRS study on rat brain (16).

Around the same time that reports on *in vivo* NMR spectroscopy appeared, Lauterbur (17) and somewhat later Mansfield (18) described the first reports on a major constituent of modern NMR, namely *in vivo* NMR imaging or magnetic resonance imaging (MRI). By applying position dependent magnetic fields in addition to the static magnetic field, they were able to reconstruct the spatial distribution of the spins in the form of an image. *In vivo* NMR spectroscopy or magnetic resonance spectroscopy (MRS) and MRI have evolved from relatively simple one- or two-RF pulse sequences to complex techniques involving spatial localization, water and lipid suppression and spectral editing for MRS and time-varying magnetic field gradients, ultrafast and multi-parametric acquisition schemes for MRI.

Apart from MRI and MRS, there are many other tools available to study the anatomy, dynamics and metabolism of intact living tissues. For example, X-ray and computed tomography (CT) can provide high-resolution structural images, whereas others, including positron emission tomography (PET) and single photon emission computed tomography (SPECT) give rise to relatively low-resolution functional

images. MRI has been shown to provide both high-resolution, high-contrast morphological images and high-resolution functional data. Furthermore, NMR does not require the use of ionizing radiation, making MRI a completely noninvasive and nondestructive imaging modality. The major advantage of *in vivo* NMR spectroscopy over the other mentioned modalities is, besides the noninvasive character, the excellent chemical specificity as expressed in the chemical shift and  $J$  coupling constants. This allows the study of specific metabolites and metabolic pathways, thereby offering an unique tool to study *in vivo* metabolism.

This chapter will give a brief introduction to *in vivo* NMR spectroscopy with an emphasis on spectral appearance and experimental techniques. It does not represent a complete review, for which the interested reader is referred to the literature (19). It is assumed that the reader is familiar with the basic concepts of (organic) NMR spectroscopy.

## 3.2. IN VIVO NMR SPECTROSCOPY

### 3.2.1. Proton NMR

The proton nucleus is, besides the low abundance hydrogen isotope tritium, the most sensitive nucleus for NMR, both in terms of intrinsic NMR sensitivity (high gyromagnetic ratio) and high natural abundance (>99.9 %). Since nearly all metabolites contain protons, *in vivo*  $^1\text{H}$  MRS is, in principle, a powerful technique to observe, identify and quantify a large number of biologically important metabolites in intact tissue.

However, the application of  $^1\text{H}$  MRS to intact tissues *in vivo* is challenging for a number of reasons. Firstly, the water resonance is several orders of magnitude larger than the low-concentration metabolites, making metabolite detection difficult and ambiguous. Therefore, water suppression is a prerequisite for meaningful *in vivo*  $^1\text{H}$  MRS studies. More details on water suppression are given in Section 3.3.2. Secondly, the chemical shift range of *in vivo*  $^1\text{H}$  NMR spectra is narrow, spanning approximately 5 ppm (for nonexchangeable protons). This causes a large number of metabolite resonances to overlap, making their detection and quantification difficult. Thirdly, even though the proton nucleus is the most sensitive for NMR studies, (*in vivo*) NMR is in general a very insensitive technique, making the detection of low-concentration metabolites a compromise between time resolution and signal-to-noise ratio.

#### 3.2.1.1. Identification of resonances

The sensitivity of *in vivo* proton NMR typically limits the detection to compounds with a concentration higher than  $\sim 0.5$  mM. Despite this inherent limitation, an *in vivo*  $^1\text{H}$  NMR spectrum still holds many resonances from a wide range of different metabolites. Figure 3.1 shows a typical *in vivo*  $^1\text{H}$  NMR spectrum obtained from rat brain at 7 T. The dominating resonances are from the  $\text{N}(\text{CH}_3)_3$  group of total choline (Cho,  $\sim 3.22$  ppm) which consists mainly of phosphoryl choline and glycerophosphoryl choline; the  $\text{CH}_3$  group of total creatine (tCr, 3.03 ppm), consisting of creatine and phosphocreatine; and the  $\text{CH}_3$  groups of the combined *N*-acetyl resonances, mainly consisting of *N*-acetyl aspartate (NAA, 2.01 ppm) with a smaller contribution from *N*-acetylaspartyl glutamate (NAAG, 2.04 ppm). In many clinical examinations performed at longer echo times, only the resonances from Cho, tCr and NAA are observed. However, in short TE spectra (Figure 3.1) many additional NMR resonances can be observed (Table 3.1), in particular *myo*-inositol (mI) and glutamate (Glu). Even though these metabolites are present at similar concentrations as NAA (Table 3.1), they are less frequently observed since they are split into many smaller resonances due to scalar coupling interactions (see Section 3.4.1). Besides the high concentration metabolites, a typical short TE spectrum from brain holds information on alanine (Ala), aspartate (Asp),  $\gamma$ -aminobutyric acid (GABA), glucose (Glc), glutamine (Gln), glycine (Gly), lactate (Lac), *scyllo*-inositol (sI) and taurine (Tau). Typically the metabolite resonances are superimposed on a intense baseline arising from macromolecules (20, 21).

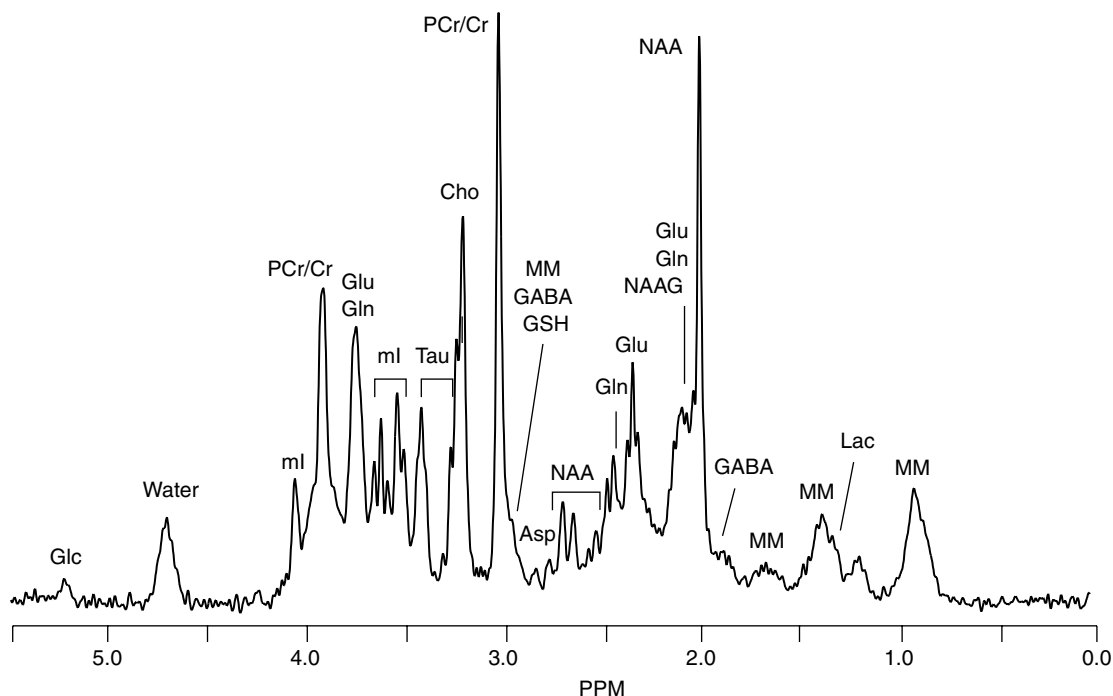


**Figure 3.1.** Proton NMR spectrum from rat brain *in vivo* (100  $\mu$ l, STEAM localization,  $TR = 4000$  ms,  $TE = 8$  ms,  $TM = 25$  ms,  $NEX = 128$ ). Abbreviations are given for aspartate (Asp), choline-containing compounds (Cho), creatine (Cr),  $\gamma$ -aminobutyric acid (GABA), glucose (Glc), glutamate (Glu), glutamine (Gln), macromolecules (MM), *myo*-inositol (ml), *N*-acetylaspartate (NAA), *N*-acetylaspartyl glutamate (NAAG), lactate (Lac), phosphocreatine (PCr) and taurine (Tau).

A detailed discussion on the biological function and significance of the detected metabolites will be given in the following chapters. Table 3.1 gives a short overview of the known functions of the detected metabolites. The interested reader can find additional information in (19, 22).

### 3.2.2. Phosphorus NMR

The success of *in vivo* proton NMR spectroscopy in routine (clinical) MR is only matched by phosphorus NMR. The relatively high sensitivity of phosphorus NMR (circa 7 % of protons), together with a 100 % natural abundance allows the acquisition of high-quality spectra within minutes. Furthermore, the chemical shift dispersion of the phosphates found *in vivo* is relatively large ( $\sim 30$  ppm), resulting in excellent spectral resolution even at low (clinical) magnetic field strengths. Phosphorus NMR is very useful because with simple NMR methods it is capable of detecting all metabolites that play key roles in tissue energy metabolism. Furthermore, biologically relevant parameters such as intracellular pH may be indirectly deduced.

#### 3.2.2.1. Identification of resonances

A typical *in vivo* phosphorus NMR spectrum holds a limited number of resonances (Figure 3.2). The exact chemical shift position of almost all resonances is sensitive to physiological parameters such as intracellular pH and ionic (magnesium) strength. By convention, the phosphocreatine resonance is used as

**Table 3.1.** Proton chemical shifts, concentration range and biological function or methodological significance for low molecular weight brain metabolites<sup>a,b</sup>

Compound	$^1\text{H}$ shift (ppm)	Resonance	Concentration range (mmol/kg <sub>ww</sub> )	Function/significance <sup>c</sup>
Acetate	1.90	$^2\text{CH}_3$	0.4–0.8	Substrate of glial metabolism
<i>N</i> -Acetyl aspartate	2.01	$^2\text{CH}_3$	7.9–16.6	Neuronal marker
	4.38, 2.67, 2.48	$^2\text{CH}_3, ^3\text{CH}_2, ^3\text{CH}_2$		Osmolite
<i>N</i> -Acetylaspartyl glutamate	2.04	$^2\text{CH}_3$	0.6–2.7	Involved in excitatory neurotransmission
Alanine	3.77, 1.47	$^2\text{CH}, ^3\text{CH}_3$	0.2–1.4	Meningioma marker
$\gamma$ -Aminobutyric acid	3.01, 1.89, 2.28	$^2\text{CH}_2, ^3\text{CH}_2, ^4\text{CH}_2$	1.3–1.9	Inhibitory neurotransmitter
Aspartate	3.89, 2.80, 2.65	$^2\text{CH}, ^3\text{CH}_2, ^3\text{CH}_2$	1.0–1.4	Excitatory neurotransmitter
Choline (total)	3.19, 4.05, 3.50	$\text{N}(\text{CH}_3)_3, ^1\text{CH}_2, ^2\text{CH}_2$	0.9–2.5	Membrane constituent
Creatine	3.03, 3.91	$\text{N}(\text{CH}_3), ^2\text{CH}_2$	5.1–10.6	Part of energy metabolism
Glucose	5.22, 4.63	$^1\text{CH}(\alpha, \beta)$	1.0	Substrate of energy metabolism
	3.52, 3.23, 3.70, 3.47	$^2\text{CH}(\alpha, \beta), ^3\text{CH}(\alpha, \beta)$		
	3.40, 3.39, 3.82, 3.45	$^4\text{CH}(\alpha, \beta), ^5\text{CH}(\alpha, \beta)$		
	3.83, 3.88, 3.75, 3.71	$^6\text{CH}(\alpha, \beta), ^6\text{CH}(\alpha, \beta)$		
Glutamate	3.74, 2.04, 2.12	$^2\text{CH}, ^3\text{CH}_2, ^3\text{CH}_2$	6.0–12.5	Excitatory neurotransmitter
	2.34, 2.35	$^4\text{CH}_2, ^4\text{CH}_2$		Intermediary metabolite
Glutamine	3.76, 2.13, 2.11	$^2\text{CH}, ^3\text{CH}_2, ^3\text{CH}_2$	3.0–5.8	Ammonia detoxification
	2.43, 2.45	$^4\text{CH}_2, ^4\text{CH}_2$		Intermediary metabolite
Glutathione <sup>d</sup>	3.77	Glycine moiety	2.0	Antioxidant
	4.56, 2.93, 2.97	Cysteine moiety		Storage of cysteine
	3.77, 2.16, 2.15	Glutamate moiety		
	2.51, 2.56			
Glycerophosphoryl choline	3.61, 3.67	$^1\text{CH}_2$ (glycerol)	1.0	Membrane constituent
	3.90, 3.87, 3.95	$^2\text{CH}, ^3\text{CH}_2$ (glycerol)		
	4.31, 3.66	$^7\text{CH}_2, ^8\text{CH}_2$ (choline)		
	3.21	$\text{N}(\text{CH}_3)_3$		
Glycine	3.55	$^2\text{CH}_2$	0.4–1.0	Inhibitory neurotransmitter
<i>myo</i> -Inositol	3.52, 4.05, 3.52	$^1\text{CH}, ^2\text{CH}, ^3\text{CH}$	3.8–8.1	Osmolyte
	3.61, 3.27, 3.61	$^4\text{CH}, ^5\text{CH}, ^6\text{CH}$		Glial marker
<i>scyllo</i> -Inositol	3.34	$^{1–6}\text{CH}$	0.3–0.6	Unknown
Lactate	4.10, 1.31	$^2\text{CH}, ^3\text{CH}_3$	0.3–0.8	End product of anaerobic glycolysis
Phosphocreatine	3.03, 3.93	$\text{N}(\text{CH}_3), ^2\text{CH}_2$	3.2–5.5	Part of energy metabolism
Phosphoryl choline	3.21, 4.28, 3.64	$\text{N}(\text{CH}_3)_3, ^1\text{CH}_2, ^2\text{CH}_2$	0.6	Membrane constituent
Phosphoryl ethanolamine	3.98, 3.22	$^1\text{CH}_2, ^2\text{CH}_2$	1.1–1.5	Membrane constituent
Taurine	3.42, 3.25	$^1\text{CH}_2, ^2\text{CH}_2$	0.9–1.5	Osmoregulator, neuromodulator
Threonine	3.58, 4.25, 1.32	$^2\text{CH}, ^3\text{CH}, ^4\text{CH}_3$	0.3	Unknown
Valine	3.60, 2.26	$^2\text{CH}, ^3\text{CH}$	0.1	Protein synthesis
	1.03, 0.98	$^4\text{CH}_3, ^4\text{CH}_3$		

<sup>a</sup> Chemical shifts are reported relative to the singlet resonance of 2,2-dimethyl-2-silapentane-5-sulfonate (DSS, also known as TSP) at 0.00 ppm. Water-exchangeable amide protons are not included.

<sup>b</sup> The absolute concentration ranges were adapted from Govindaraju *et al.*

<sup>c</sup> The function of many metabolites is only partially known and is the subject of ongoing research.

<sup>d</sup> *In vivo* glutathione is almost completely present in the reduced GSH form.

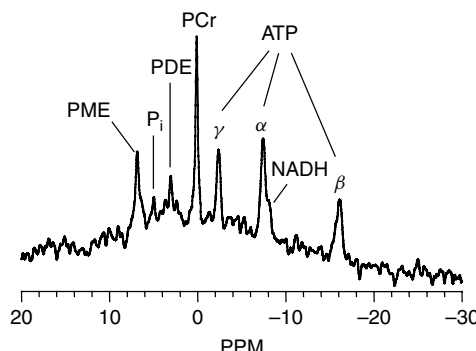


**Figure 3.2.** Phosphorus NMR spectrum from rat brain *in vivo* (300  $\mu$ l, ISIS localization,  $TR = 6000$  ms,  $NEX = 128$ ). Abbreviations are given for adenosine triphosphate (ATP), inorganic phosphate ( $P_i$ ), nicotinamide adenine dinucleotide (NADH), phosphocreatine (PCr), phospho-diesters (PDE) and phospho-monoesters (PME).

**Table 3.2.** Phosphorus chemical shifts for low molecular weight metabolites<sup>a</sup>

Compound	$^{31}\text{P}$ chemical shift (ppm)
Adenosine monophosphate (AMP)	6.33
Adenosine diphosphate (ADP)	
$\alpha$	-7.05
$\beta$	-3.09
Adenosine triphosphate (ATP)	
$\alpha$	-7.52
$\beta$	-16.26
$\gamma$	-2.48
Dihydroxyacetone phosphate	7.56
Fructose-6-phosphate	6.64
Glucose-1-phosphate	5.15
Glucose-6-phosphate	7.20
Glycerol-1-phosphate	7.02
Glycerol-3-phosphorylcholine	2.76
Glycerol-3-phosphorylethanolamino	3.20
Inorganic phosphate	5.02
Nicotinamide adenine dinucleotide (NADH)	-8.30
Phosphocreatine	0.00
Phosphoenolpyruvate	2.06
Phosphorylcholine	5.88

<sup>a</sup> Chemical shifts are reported relative to phosphocreatine at 0.00 ppm at pH 7.2 (fully complexed with magnesium).

an internal chemical shift reference and has been assigned a chemical shift of 0.00 ppm. At a pH of 7.2, with full magnesium complexation, the resonance of adenosine triphosphate (ATP) appear at -7.52 ppm ( $\alpha$ ), -16.26 ppm ( $\beta$ ) and -2.48 ppm ( $\gamma$ ). The resonance of inorganic phosphate appears at 5.02 ppm. Under favorable, high-sensitivity conditions phosphorus NMR spectra can also hold resonances from phospho-mono-esters and di-esters. Table 3.2 summarizes the chemical shifts of the most commonly observed  $^{31}\text{P}$ -containing metabolites.

### 3.2.2.2. Intracellular pH

The chemical shift of many phosphorus containing compounds is dependent on a number of physiological parameters, in particular intracellular pH and magnesium concentration. The cause of this phenomenon can be found in the fact that protonation (or complexation with magnesium) of a compound changes the chemical environment of nearby nuclei and hence changes the chemical shift of those nuclei. When the chemical exchange between the protonated and unprotonated forms is slow, the two forms will have two separate resonance frequencies with the resonance amplitudes indicating the relative amounts of the two forms. However, for most compounds observed with phosphorus NMR, the chemical exchange is fast relative to the NMR time scale and only a single, average resonance is observed. The resonance frequency is now indicative of the relative amounts of protonated and unprotonated form, and hence the pH, and can be described by a modified Henderson–Hasselbach relationship according to

$$\text{pH} = \text{p}K_{\text{A}} + \log \left( \frac{\delta - \delta_{\text{HA}}}{\delta_{\text{A}} - \delta} \right) \quad (3.1)$$

where  $\delta$  is the observed chemical shift,  $\delta_{\text{A}}$  and  $\delta_{\text{HA}}$  the chemical shifts of the unprotonated and protonated forms of compound A and  $\text{p}K_{\text{A}}$  the logarithm of the equilibrium constant for the acid–base equilibrium between HA and A.

Even though almost all resonances in  $^{31}\text{P}$  NMR spectra have a pH dependence, the resonance of inorganic phosphate is most commonly used for several reasons. Its  $\text{p}K$  is in the physiological range ( $\text{p}K = 6.77$ ), it is readily observed in most tissues (with muscle being a possible exception) and it has a large dependence on pH. Following similar arguments as outlined for intracellular pH, the free magnesium concentration can be deduced from the chemical shifts of ATP.

### 3.2.2.3. Creatine kinase

The application of magnetization transfer to phosphorus NMR has allowed the non-invasive measurement of the creatine kinase (CK) reaction



The most generally accepted function of the CK/PCr system is that of ‘temporal energy buffering’, i.e. during a high workload the levels of ATP remain constant through the conversion of PCr (which is present at relatively high concentrations) to ATP. Other, more controversial functions include that of an ‘energy transport system’ and preventing the inactivation of ATPases by maintaining low intracellular ADP levels. The technique of magnetization transfer allows the determination of the absolute flux through the CK enzyme by following the fate of labeled (i.e. saturated or inverted) magnetization from either PCr or  $\gamma$ -ATP. The forward flux, from PCr to ATP is a relatively straightforward measurement. However, the measurement of the reverse flux is complicated by ATP hydrolysis reactions by enzymes other than CK. However, proper modifications of the magnetization transfer experiment (i.e. multiple saturations) do allow the correct measurement of the reverse flux (23). It is generally assumed that in skeletal muscle, heart and brain the creatine kinase catalyzed reactions are near or at equilibrium. Under this assumption, the intracellular ADP concentration can be calculated from Equation (3.2) if the equilibrium constant, intracellular metabolite (ATP, PCr, Cr) concentrations and pH are known.

## 3.2.3. Carbon-13 NMR

Phosphorus and proton NMR spectroscopy have been successfully employed in a range of (clinical) *in vivo* NMR studies. Nevertheless, both nuclei have inherent limitations. Phosphorus NMR spectrum are normally

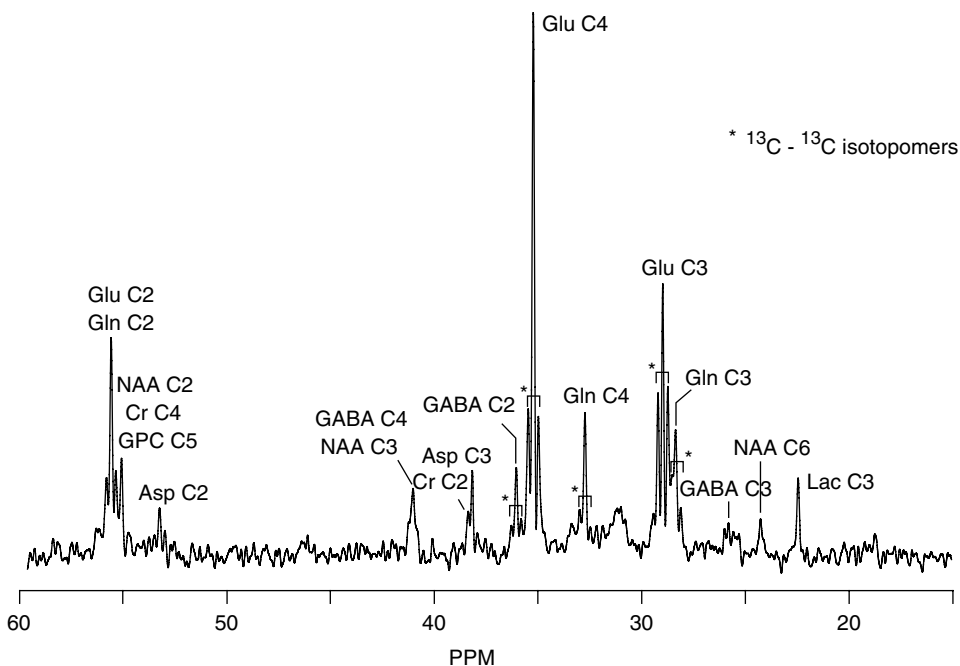


**Figure 3.3.** Carbon-13 NMR spectrum from rat brain *in vivo* (500  $\mu$ l, ISIS localization with polarization transfer,  $TR = 4000$  ms,  $NEX = 512$ ), averaged between 60 and 90 min following the intravenous infusion of [1, 6- $^{13}\text{C}_2$ ]-glucose. Abbreviations are defined in the legend of Figure 3.1. GPC = glycerophosphoryl choline.

characterized by a limited number of metabolites, while proton NMR is technically more challenging (e.g. water suppression) and suffers from an inherently poor spectral resolution.

Carbon-13 NMR can offer complementary information to that obtained with phosphorus and proton NMR. Since (almost) all biologically relevant metabolites contain carbon, carbon-13 NMR is in principle capable of detecting many metabolites. Furthermore, the chemical shift dispersion extends over 200 ppm. However, the common carbon-12 isotope is not NMR active. Carbon-13 does have a magnetic moment, but is only present at a 1.1 % natural abundance. This, in combination with the low gyromagnetic ratio, makes carbon-13 NMR an inherently insensitive technique. Furthermore, strong heteronuclear scalar coupling interactions complicate the spectra and further reduce the sensitivity, such that double-resonance techniques (and hence additional, nonstandard hardware) must be employed to remove the effects of heteronuclear scalar coupling. Nevertheless, natural abundance carbon-13 NMR has been used to detect a wide range of metabolites, with a special emphasis on glycogen at 100.5 ppm. The low natural abundance of carbon-13 can be transformed into an advantage in that  $^{13}\text{C}$ -enriched precursors can be infused to study metabolic pathways with little background interference from endogenous metabolites. Figure 3.3 shows a carbon-13 NMR spectrum from rat brain, 60 to 90 min after intravenous infusion of [1, 6- $^{13}\text{C}_2$ ]-glucose. The  $^{13}\text{C}$  label has been transferred from [1, 6- $^{13}\text{C}_2$ ]-glucose to [4- $^{13}\text{C}$ ]-glutamate (34.2 ppm) by the action of the glycolytic pathway and the TCA cycle. The excitatory neurotransmitter glutamate is released into the synaptic cleft by exocytosis, interacts with post-synaptic receptors after which it is taken up by nearby astrocytes. There the glutamate is converted to glutamine, leading to the formation of [4- $^{13}\text{C}$ ]-glutamine (31.7 ppm). Other metabolic pathways lead to the labeling of [2- $^{13}\text{C}$ ]-GABA (35.2 ppm) and a range of other metabolites (chemical shifts are reported in Table 3.3). Using a mathematical model of compartmentalized

**Table 3.3.** Carbon-13 chemical shifts for low molecular weight metabolites<sup>a</sup>

Compound	$^{13}\text{C}$ chemical shift (ppm)					
	C1	C2	C3	C4	C5	C6
Acetate	182.6	24.5				
Alanine	176.6	51.5	17.1			
Aspartate	175.1	53.0	37.4	178.4		
Citrate	179.7	46.8	76.0	82.8		
Creatine	175.4	37.8	158.0	54.7		
Ethanol	17.9	58.4				
$\gamma$ -Aminobutyric acid (GABA)	182.3	35.2	24.6	40.2		
Glycerol	63.6	73.3	63.6			
$\beta$ -Hydroxybutyrate	181.2	47.6	66.8	22.9		
$\alpha$ -D-Glucose	92.7	72.1	73.5	70.4	72.1	61.4
$\beta$ -D-Glucose	96.6	79.9	76.5	70.4	76.5	61.4
Glutamate	175.3	55.5	27.8	34.2	182.0	
Glutamine	174.8	55.0	27.1	31.7	178.4	
Glutathione (GSH, reduced)	56.6	55.1	44.3	32.2	27.1	26.6
Glycerophosphorylcholine	62.9	71.5	66.8	60.3	54.8	
Glycine	173.3	42.5				
Glycogen	100.5	72.0	74.0	78.1	72.1	61.4
Lactate	183.3	69.3	21.0			
<i>myo</i> -Inositol	73.3	73.1	73.3	71.9	75.1	71.9
<i>N</i> -Acetyl aspartate	179.7	54.0	40.3	179.7	174.3	22.8
Phosphorylethanolamine	61.9	41.6				
Taurine	48.4	36.2				

<sup>a</sup> Chemical shifts are reported relative to the singlet resonance of 2,2-dimethyl-2-silapentane-5-sulfonate (DSS, also known as TSP) at 0.00 ppm.

brain energy metabolism, the formation of [4- $^{13}\text{C}$ ]-glutamate, [2- $^{13}\text{C}$ ]-GABA and [4- $^{13}\text{C}$ ]-glutamine can provide quantitative flux information about the glutamatergic and GABAergic neuronal TCA cycles and the glutamate/GABA–glutamine neurotransmitter cycles between neurons and astrocytes. Metabolic modeling will be discussed in detail in Chapter 4. Besides the TCA cycle and related anaerobic pathways,  $^{13}\text{C}$  NMR studies have been reported for a wide variety of other metabolic pathways, including gluconeogenesis (24, 25) and the synthesis and degradation of glycogen (26).

### 3.3. ELEMENTARY EXPERIMENTAL TECHNIQUES

#### 3.3.1. Spatial Localization

One of the most striking differences between high-resolution liquid-state NMR and *in vivo* NMR is that biological samples can be highly inhomogeneous in terms of metabolic composition as well as ( $B_0$  and  $B_1$ ) magnetic field strengths and relaxation and diffusion parameters. Figure 3.4(B) shows a  $^1\text{H}$  NMR spectrum of rat brain obtained with surface coil localization. The surface coil, as placed on top of the rat head, provides an inherent degree of spatial localization, limiting the sensitive volume to large parts of the brain with smaller contributions from skin, skull and muscle (Figure 3.4(A)). The  $^1\text{H}$  NMR spectrum is characterized by two main signals arising from water (at  $\sim$ 4.7 ppm) and methyl and methylene protons of fat and lipids (at  $\sim$ 1.5 ppm). The resonance lines are generally very broad due to the inhomogeneous magnetic field over the sensitive volume of the surface coil.

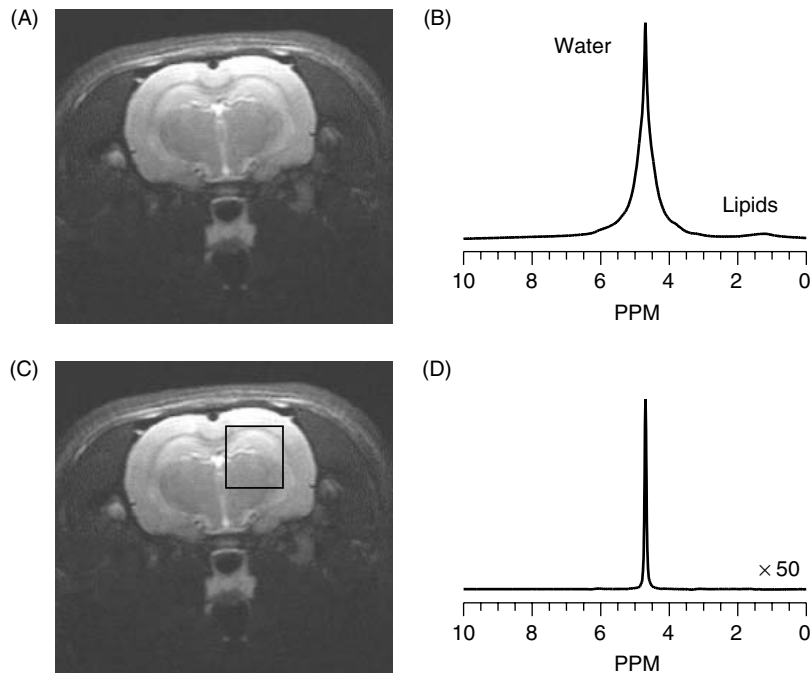


**Figure 3.4.** Effects of spatial localization. (A) Anatomical MR image of rat brain *in vivo* and (B) the corresponding proton NMR spectrum from the entire sensitive volume of the surface coil, which was placed on top of the rat. (D) Proton NMR spectrum from the localized volume as indicated in (C). Resonances from extracranial lipids are absent and the narrow water resonance line indicates the higher magnetic field homogeneity of the volume of interest.

For an adequate tissue characterization it is essential to employ a more robust spatial localization technique such that the origin of the NMR signal is accurately known without contamination from other spatial positions. In the case of the brain as shown in Figure 3.4, this means that NMR signals from extracranial tissue should be eliminated and the localized volume should be placed in homogeneous brain structures, if possible. In most applications, spatial localization is achieved by applying a frequency-selective RF pulse in the presence of a magnetic field gradient. The gradient makes the Larmor frequency linearly dependent on spatial position. Since the RF pulse only affects a selective range of frequencies, the combination results in the excitation (or refocusing/inversion) of a spatial slice. Three-dimensional localization is achieved by selecting the cubic intersection of three orthogonal slices. Figure 3.4(D) shows the  $^1\text{H}$  NMR spectrum as acquired from a localized (cubic) volume as indicated on the image of Figure 3.4(C). The methyl and methylene protons from (extracranial) fats and lipids no longer contribute to the spectrum, leaving the water resonance and low-intensity resonances (not visible in Figure 3.4) from cerebral metabolites. Due to the decreased volume of interest, the main magnetic field homogeneity is substantially improved, leading to narrower resonance lines and hence an improved spectral resolution. Single-volume spatial localization can be achieved with many different NMR sequences, of which ISIS (27), STEAM (28, 29) and PRESS (30) are most commonly used.

### 3.3.2. Shimming

NMR spectroscopy applications place stringent requirements on the magnetic field homogeneity. For example, most resonances observed with  $^1\text{H}$  NMR spectroscopy resonate within a range of several ppm. In

order to distinguish different chemical compounds it is therefore crucial to reduce the magnetic field inhomogeneities to a small fraction of this chemical shift dispersion. Even though spatial localization inherently improves the magnetic field homogeneity (see Section 3.3.1), this is often not sufficient and the technique of shimming is applied to improve the magnetic field homogeneity. Shimming is the process of canceling the magnetic field inhomogeneities with additional spatially dependent (but exactly defined) magnetic fields. Most NMR systems are equipped with shim coils that generate magnetic fields describing a particular order of spherical harmonics. Most NMR systems are equipped with at least eight shim coils, describing all first and second order spherical harmonics that can be used to cancel magnetic field inhomogeneities that vary linearly and quadratically with spatial position. Figure 3.5 shows a typical example of the spectral resolution and sensitivity enhancement achievable with shimming. The optimization of the magnetic field homogeneity used to be an iterative, time-consuming and user-dependent process susceptible to local minima of

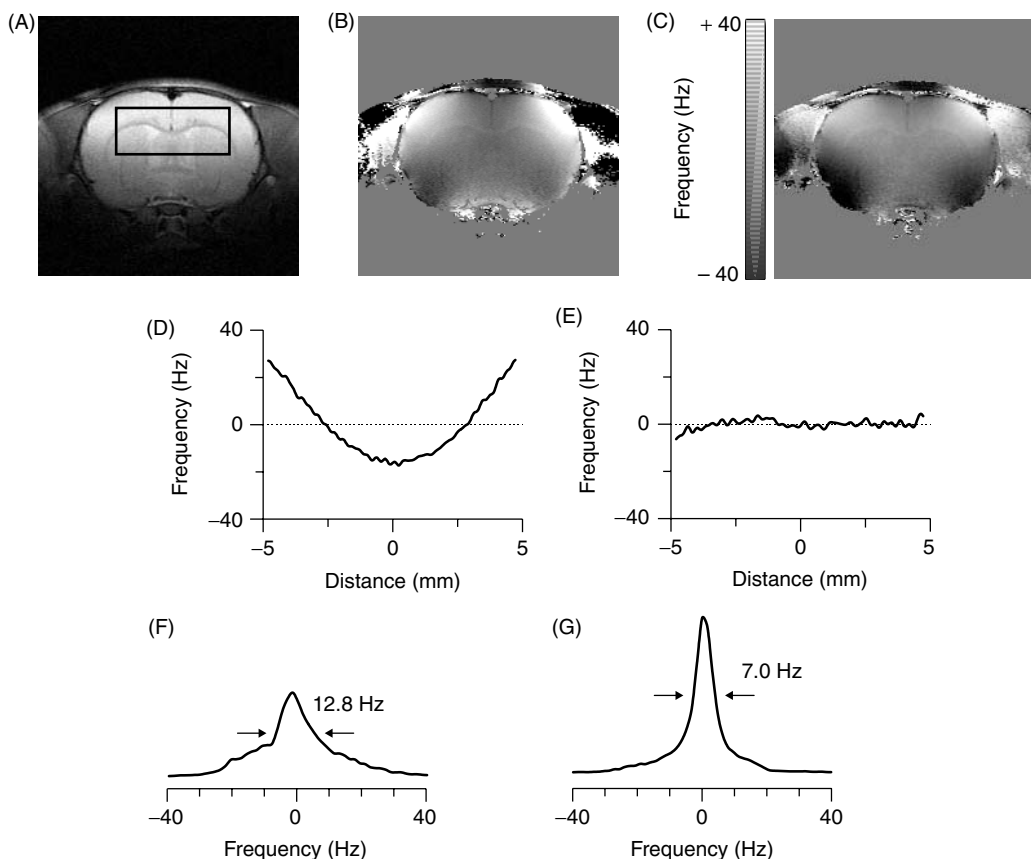


**Figure 3.5.** Effects of optimizing the magnetic field homogeneity. (A) Anatomical MR image of rat brain *in vivo*, indicating the rectangular volume of interest (VOI). (B, C) Two-dimensional images ('phase maps'), (D, E) one-dimensional traces of the magnetic field homogeneity and (F, G) NMR spectra of water from the VOI before (B, D, F) and after (C, E, G) optimization of the magnetic field homogeneity over the VOI with all first- and second-order shims. The one-dimensional traces (D, E) were extracted from (B, C) in the middle and along the long axis of the VOI. Note that an improved homogeneity within the VOI often leads to a reduced homogeneity outside the VOI (e.g. compare the somatosensory cortex/corpus callosum and caudate putamen areas in (B) and (C)).

suboptimal shim settings. Currently, a variety of noniterative and user-independent phase mapping techniques exist that can determine the optimal shim settings quantitatively within minutes (31, 32).

### 3.3.3. Water Suppression

One of the main problems encountered during *in vivo*  $^1\text{H}$  MRS studies is the large dynamic range of the resonances. The water signal is typically  $\sim 10^{+3}$ – $10^{+4}$  times stronger than the metabolite resonances (Figures 3.6(A) and (B)). Although a 16-bit analog-to-digital (ADC) converter should be able to adequately digitize the low metabolite resonances, the large water signal may also distort the baseline and introduce spurious sidebands (Figure 3.6(B)). For most  $^1\text{H}$  MRS applications the water signal needs to be suppressed, without disturbing the metabolite resonances. The suppression of a particular resonance in a NMR spectrum requires a difference in a property between the molecule of interest and the interfering compound (e.g. water). This property need not to be a magnetic one, but it must be reflected in an NMR observable parameter. Thus, besides differences in chemical shift, scalar coupling and  $T_1$  and  $T_2$  relaxation, properties such as diffusion and exchange can also be exploited. Although there is no universal technique, there are some criteria by which the existing water suppression methods can be evaluated. These criteria include (1) degree of suppression, (2) insensitivity to RF imperfections (inhomogeneities), (3) ease of phasing the spectra, (4) minimum attainable repetition and echo times, (5) insensitivity to relaxation effects, (6) perturbation of other resonances and (7) degree of distortion of resonances near or at the water frequency.

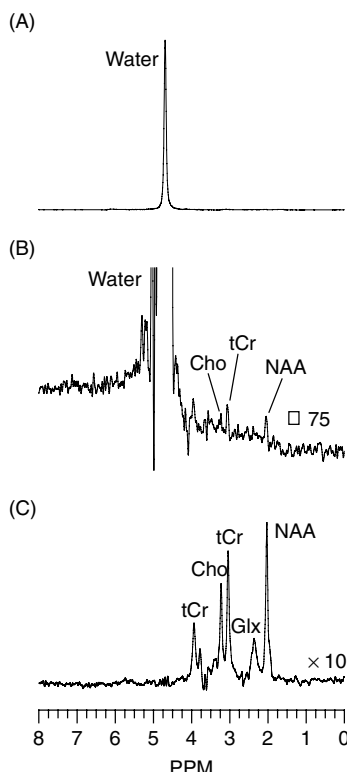


**Figure 3.6.** Effects of water suppression. (A) Localized proton NMR spectrum from rat brain *in vivo* without water suppression and (C) with CHESS water suppression. (B) Identical to (A) with an expanded vertical scale.

The existing water suppression techniques can be divided in four groups, namely (1) methods that employ frequency-selective excitation and/or refocusing (33–36) or (2) utilize differences in relaxation and diffusion parameters (37–39), (3) spectral editing methods such as polarization transfer (39) and (4) other methods, including software-based water peak elimination. The first group of water suppression techniques is currently most popular and, as a prominent example, the method of CHEmical Shift Selective (CHESS) water suppression (33) will be briefly discussed here. CHESS consists of a frequency-selective excitation pulse for the water followed by a magnetic field gradient. Therefore, the water is excited onto the transverse plane, where it will be destroyed (dephased) by the magnetic field gradient, while the metabolite resonances reside along the longitudinal axis. Next, the metabolites can be excited onto the transverse plane and be detected (Figure 3.6(C)). The CHESS pulse sequence element may be repeated a number of times to improve the water suppression. Several related techniques exist, which, for example, do not excite the water (e.g. binomial RF pulses (36)), do not refocus the water (e.g. MEGA (34)) or which saturate the water resonance (e.g. presaturation). CHESS, and all other water suppression techniques have to make compromises between the criteria mentioned above.

### 3.3.4. Signal Quantification

NMR is, in principle, a quantitative technique and as such NMR spectra can be used to derive absolute concentrations of metabolites in animal and human tissues. This originates from the fact that the total integrated area under a resonance in an NMR spectrum (or the first data point of a FID) is proportional to the longitudinal thermal equilibrium magnetization vector, which in turn is directly related to the number of spins in the sample and hence to the concentration of that particular compound.

However, in practice the derivation of absolute concentrations by MRS is not straightforward, since many additional factors can influence the metabolite resonance area. These factors can include  $T_1$  and  $T_2$  relaxation, diffusion, exchange, (partial) NMR invisibility, spectral overlap of resonances and the choice of an internal or external concentration reference. The literature on signal quantification by NMR is extensive (e.g. see (19) for reviews), but can essentially be simplified to a three-step process. First, one has to ensure that the integrated resonance area is directly proportional to the longitudinal thermal equilibrium magnetization. In many cases this can be achieved by proper experimental design. For example, an NMR spectrum acquired with a short repetition time and a long echo time will be heavily  $T_1$  and  $T_2$  weighted and the resonance areas will therefore not be representative of the thermal equilibrium magnetization. For this particular example this can be avoided by performing the experiment with a long repetition time (equal to five times the longest  $T_1$  relaxation time) and a short echo time (ideally an echo time of zero). In other cases, one may be able to derive a correction factor, whereas in the case of (partial) NMR invisibility due to excessive line widths, the quantification process will always underestimate the actual concentration. The second step is to determine the integrated resonance area. For *in vivo* MRS applications this is not a trivial exercise, since many resonances are (partially) overlapping, have a complex scalar coupling splitting pattern or are superimposed on an intense baseline. For these reasons, simple integration is normally not feasible and one has to resort to more complicated time- or frequency-domain fitting algorithms. After many years of development, two methods appear to crystallize as best suited for *in vivo* NMR spectroscopy. VARPOR (40) and related techniques appear to be well suited for fitting of relatively few resonances, such as those observed in  $^{31}\text{P}$  NMR spectra. This time-domain algorithm is flexible for varying chemical shifts and scalar couplings, can readily avoid problems associated with intense baselines and is now routinely used (41, 42). LCmodel (43–45) is becoming the method of choice for more complex resonances, such as those observed in short echo-time  $^1\text{H}$  NMR spectra. The LCmodel algorithm approximates the *in vivo* NMR spectrum as a linear combination of *in vitro* model solution spectra. Since all resonances of a given compound, e.g. glutamate, are fitted simultaneously the great complexity of the glutamate NMR spectrum actually helps the convergence. Figure 3.7 shows a typical example of resonance quantification of a short

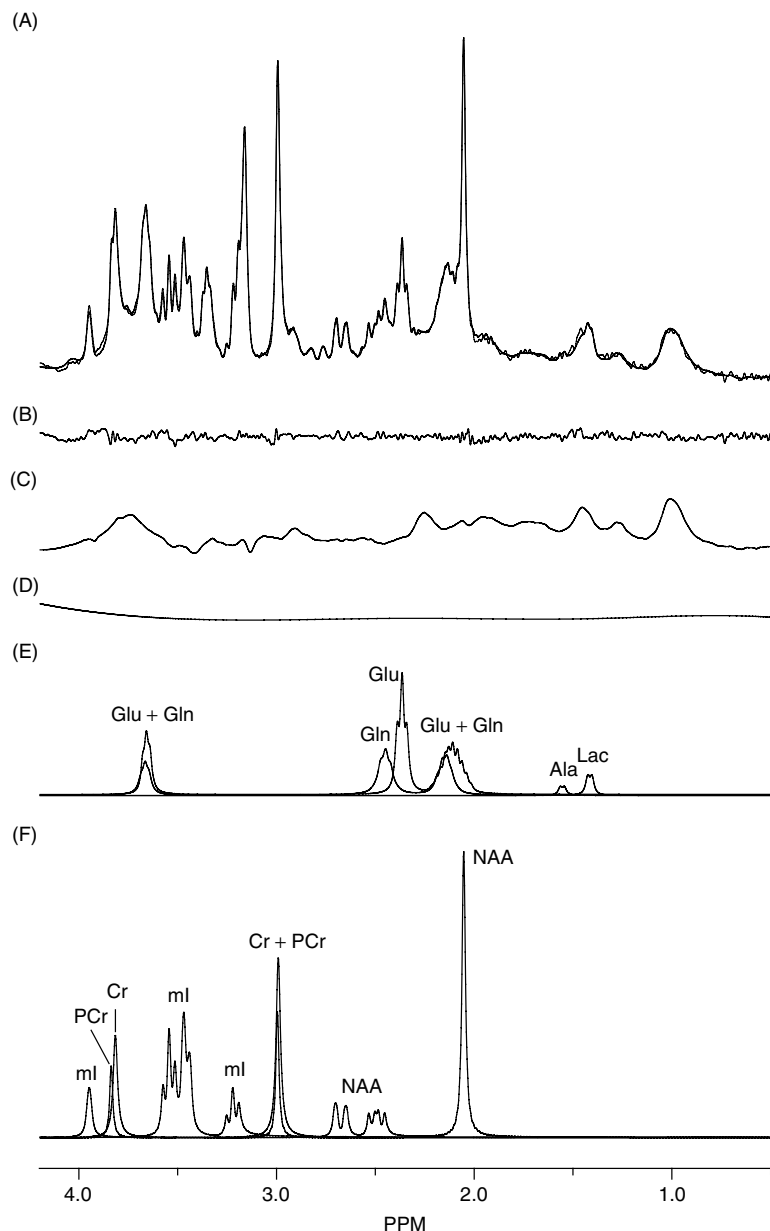


**Figure 3.7.** Spectral quantification of proton NMR spectra with LCmodel. (A) Experimental proton NMR spectra acquired from rat brain *in vivo* (100 ml, STEAM localization,  $TR = 4000$  ms,  $TE = 8$  ms,  $TM = 25$  ms,  $NEX = 128$ ) overlaid with the fitted NMR spectrum calculated by the LCmodel algorithm. (B) Difference between the calculated and measured spectra in (A). (C) Experimentally measured macromolecule baseline (double inversion recovery with  $TR = 6000$  ms,  $T1I = 1950$  ms,  $T12 = 550$  ms) as included in the LCmodel algorithm. (D) Additional cubic spline baseline required for an optimal spectral fit. Note that the macromolecule spectrum in (C) accounts for the majority of spectral baseline. (E, F) NMR spectra of individual compounds as extracted from the LCmodel fit shown in (A) for (E) alanine (Ala), glutamate (Glu), glutamine (Gln) and lactate (Lac) and (F) *myo*-inositol (mI), total creatine (sum of creatine (Cr) and phosphocreatine (PCr)) and *N*-acetyl aspartate (NAA).

echo-time  $^1\text{H}$  NMR spectrum by the LCmodel algorithm. The final step in the quantification process is the conversion of relative resonance areas into absolute metabolite concentrations. This is normally done by comparing the metabolite resonance area with that of an internal or external reference compound of known concentration. The advantage of an external concentration reference is that the concentration is exactly known. However, this approach will introduce uncertainties about differences in coil loading and coil sensitivity between the metabolites and the concentration reference. The advantages of an internal concentration reference are exactly opposite, i.e. exact concentration must be assumed, but the metabolite and reference compound are acquired in an identical manner. In most recent applications, an internal concentration reference is used. Total creatine (sum of creatine and phosphorylated creatine) or water are commonly used.

## 3.4. ADVANCED EXPERIMENTAL TECHNIQUES

### 3.4.1. Introduction to Spectral Editing

A significant number of compounds cannot be unambiguously detected by (direct) *in vivo*  $^1\text{H}$  NMR spectroscopy due to severe spectral overlap of resonances. The most commonly encountered examples of overlapping resonances *in vivo* are, lactate (and alanine) and lipids at  $\sim 1.3$  ppm, glutamate, glutamine, aspartate, *N*-acetyl aspartate and GABA between 1.9 and 2.4 ppm, GABA and total creatine at  $\sim 3.0$  ppm, and glucose and a wide range of other resonances between 3 and 4 ppm. There are several options to eliminate the overlapping resonances in order to unambiguously detect the metabolite of interest. Spectral editing techniques are the most straightforward methods to achieve this goal *in vivo*. Spectral editing may include all techniques that can simplify an NMR spectrum in order to limit the detection to specific metabolites. According to this general definition, spectral editing includes water suppression, spatial localization, use of shift reagents, selective excitation/refocusing and techniques utilizing differences in  $T_1$  and  $T_2$  relaxation, diffusion and magnetization transfer characteristics. However, to follow conventions of the (*in vivo*) NMR community, spectral editing is often restricted to those techniques which utilize the scalar coupling between spins to discriminate coupled from uncoupled spins. Two-dimensional (correlation) NMR spectroscopy can then be seen as the ultimate spectral editing technique, making no assumptions about the spin systems under investigations. The (one-dimensional) spectral editing techniques are generally more sensitive and less susceptible to motion, but require assumptions in order to selectively detect a given spin system.

#### 3.4.1.1. Intermezzo : Scalar coupling

A rigorous description of NMR requires the involvement of quantum mechanics and this is especially true for scalar-coupled spin systems. However, the interested reader is referred to excellent textbooks dealing with the quantum mechanics of NMR (46, 47). Here we will proceed with more intuitive and qualitative arguments to explain scalar coupling and formulate a number of practical rules that will allow one to understand the principle of the experiments described in the next section.

At first sight an NMR spectrum is completely characterized by the resonance frequencies and relative amplitudes originating from the nuclei under investigation. However, closer inspection reveals that most resonances are split into several smaller lines. This phenomenon of spin–spin or scalar coupling originates from the fact that nuclei with magnetic moments can influence each other, not only directly through space (dipolar coupling) but also through electrons in chemical bonds (scalar coupling). Even though dipolar interactions are the main mechanism for relaxation in a liquid, there is no net interaction between nuclei since rapid molecular tumbling averages the dipolar interactions to zero. However, interactions through chemical bonds do not average to zero and give rise to the phenomenon of scalar (or  $J$ ) coupling.

In order to understand scalar coupling, consider the interaction between a proton and a carbon-13 nucleus (e.g. in [1-<sup>13</sup>C]-glucose). For the proton there are two distinct states in which the magnetic moment of the scalar coupled <sup>13</sup>C nucleus is either parallel or anti-parallel to the external magnetic field. The proton ‘senses’ these different states which are conveyed through the electron spin in the covalent <sup>1</sup>H-<sup>13</sup>C chemical bond. As a result the energy levels of the proton will degenerate, leading to two frequencies separated by the scalar coupling constant  $J$ . The same situation arises for the <sup>13</sup>C nucleus that senses two different orientations for the proton and also splits into two resonances at slightly different frequencies. When there are more than two nuclei involved (as in a H<sub>3</sub><sup>13</sup>C methyl group) the resonances split in a binomial pattern. For example, the <sup>13</sup>C nucleus splits into two resonances due to the first proton. Each resonance splits again due to the second proton and again due to the third proton, finally appearing as four resonances, each separated by the scalar coupling constant at relative intensities of 1:3:3:1 (a so-called quartet). The protons only experience a single <sup>13</sup>C nucleus and therefore only split once into a doublet of relative intensity 1:1. Note that equivalent protons do not split among themselves due to magnetic equivalence rules. Further note that these splitting rules are only valid in the weak coupling approximation when the frequency difference between the resonances (e.g. <sup>1</sup>H and <sup>13</sup>C) is much larger than the scalar coupling constant. All heteronuclear scalar couplings are weak couplings, while most of the homonuclear scalar couplings (especially in proton NMR) are in the strong coupling limit. A noticeable exception is lactic acid, which is represented by a doublet resonance at 1.31 ppm and a quartet resonance at 4.10 ppm, even at low magnetic field strengths.

### 3.4.2. Homonuclear Spectral Editing

Homonuclear spectral editing is aimed at spectral simplification by utilizing the homonuclear (commonly the proton–proton) scalar coupling to selectively detect or eliminate NMR resonances. The scalar coupling is utilized in a so-called Hahn spin-echo sequence, which is characterized by six distinct periods/operations (Figure 3.8(A)). Following a recovery delay ( $TR$ ) in which the longitudinal magnetization is restored after any previous perturbations, the magnetization is excited onto the transverse plane by a 90° excitation pulse. During a time period  $TE/2$ , the transverse magnetization evolves under the influence of chemical shift, magnetic field inhomogeneities,  $T_2$  relaxation and scalar coupling. The 180° refocusing pulse inverts the acquired phase evolution due to chemical shift and magnetic field inhomogeneities, which will be perfectly refocused after the second  $TE/2$  delay at the start of the signal detection period. However, the effects of  $T_2$  relaxation and scalar coupling are not refocused by the 180° pulse and lead to echo-time ( $TE$ ) dependent signal loss and phase evolution, respectively. A complete description of the phase evolution due to scalar coupling (‘ $J$  evolution’) is beyond the scope of this chapter, but Figures 3.8(B) and (C) summarize the evolution of two important spin systems *in vivo*, namely lactic acid and  $\gamma$ -aminobutyric acid (GABA). It follows that the integrated transverse magnetization for the lactate methyl protons is described by a sinusoidal modulation. At  $TE = 1/J$  the lactate doublet (1.31 ppm) will be inverted relative to uncoupled spins (like water), while at  $TE = 1/2J$  the resonance appears as an antiphase doublet, with zero integrated intensity. GABA-H4, which is scalar coupled to two protons of GABA-H3, appears as a triplet at 3.01 ppm and will therefore have a more complicated  $J$ -coupling modulation. The inner resonance of GABA-4 does not modulate as a function of  $TE$  and essentially behaves as an uncoupled spin. The outer resonances have a sinusoidal modulation and are completely inverted at  $TE = 1/2J$ . Uncoupled spin systems do not have scalar coupling modulation and decrease exponentially with increasing echo time. This difference is utilized in spectral editing to differentiate between scalar-coupled and uncoupled spin systems.

One additional tool is required to achieve homonuclear spectral editing, namely frequency-selective RF pulses. An RF pulse that selectively refocuses one spin in a scalar-coupled multi-spin system effectively inhibits  $J$  evolution, such that only  $T_2$  relaxation affects the signal intensity as a function of the echo time  $TE$  (Figure 3.8). The results in Figure 3.8 indicate that the simplest form of homonuclear spectral

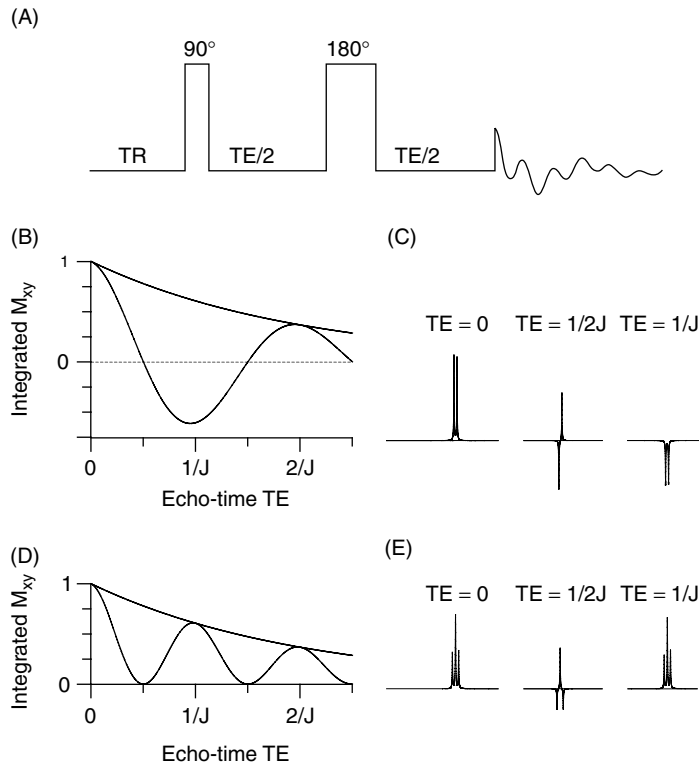


**Figure 3.8.** Effects of scalar coupling. (A) Generalized spin-echo sequence with a total echo time of  $TE$ . (B) Integrated transverse magnetization for noncoupled spins (exponential) and a scalar-coupled two-spin system (cosinoidal). (C) Spectral appearance for a scalar-coupled two-spin system at echo times  $TE$  of  $0$ ,  $1/2J$  and  $1/J$ . Note that the spectrum at  $TE = 1/2J$  is phase corrected by  $90^\circ$  relative to the other spectra. (D) Integrated transverse magnetization for noncoupled spins (exponential) and the A spin in a scalar-coupled three-spin  $\text{AX}_2$  system (e.g. GABA-H4 and H2). (E) Spectral appearance at echo times  $TE$  of  $0$ ,  $1/2J$  and  $1/J$ . When performing a selective spin-echo, the integrated transverse magnetization for a scalar-coupled spin system will be identical to noncoupled spins.

editing, namely  $J$  difference editing (48, 49), comes down to the acquisition of two experiments. In the first experiment a nonselective spin-echo is employed, leading to  $J$  evolution of the spin system of interest. At a total  $TE$  of  $1/2J$ , the outer resonances of GABA-H2 and GABA-H4 are inverted. In the second experiment a frequency-selective spin-echo is executed, with a refocusing pulse that is selective for GABA-H2 and GABA-H4 (but not for GABA-H3). As a result, the  $J$  evolution of GABA is inhibited leading to positive resonances for GABA-H2 and GABA-H4. Spectral editing is achieved by subtracting the two data sets from each other. The (uncoupled) resonances from other metabolites are refocused by either refocusing pulse and will therefore appear identical in both experiments. Subtraction of the two data sets will therefore lead to a cancellation of the unwanted resonances. The outer resonances of GABA-H2 and GABA-H4 modulate between the two experiments and will therefore survive the subtraction, forming the edited signal. The inner resonance of GABA-H2 and GABA-H4 behaves as an uncoupled spin system and is lost in the subtraction process.

The theoretical implementation of homonuclear  $J$  difference editing depicted in Figure 3.8 has to be extended with spatial localization and water suppression techniques for applications *in vivo*. Figure 3.9

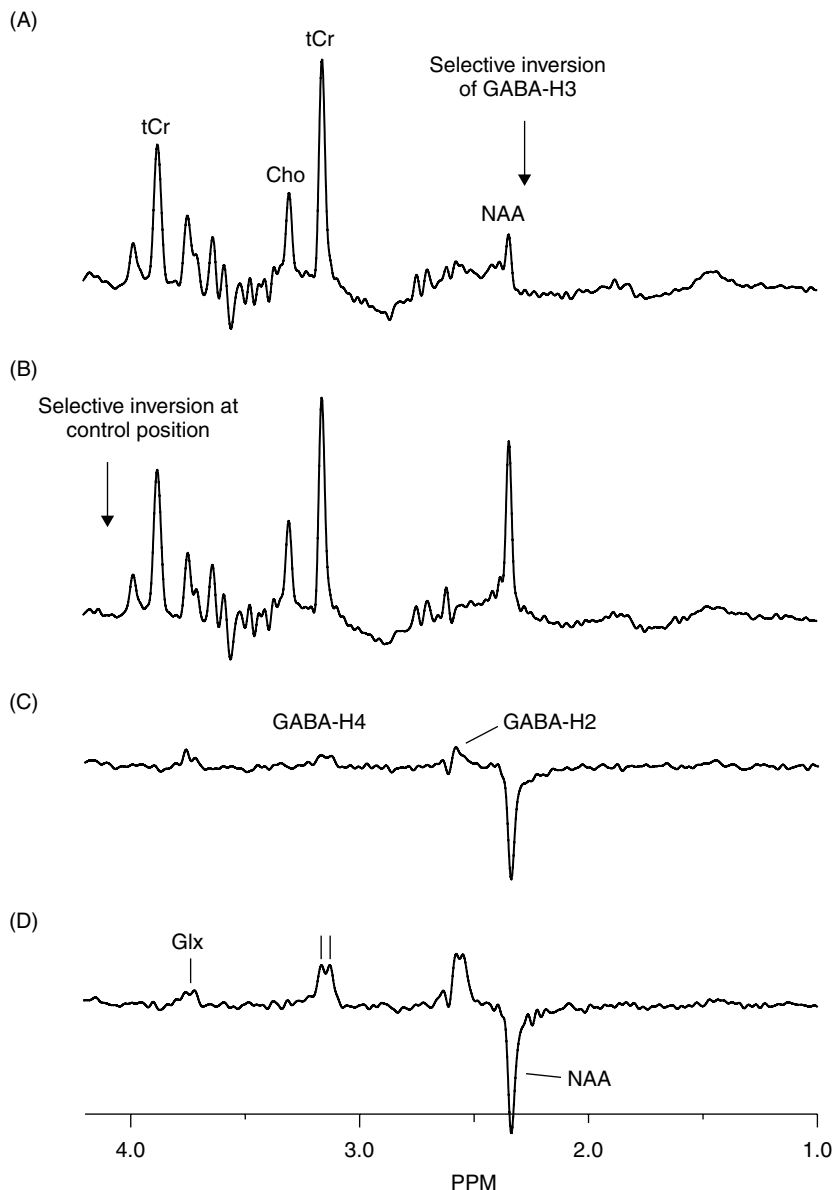


**Figure 3.9.** Homonuclear  $J$  difference spectral editing of GABA on rat brain *in vivo*. (A, B) Proton NMR spectra (160 ml,  $TR = 3000$  ms,  $TE = 68$  ms,  $NEX = 128$ ) obtained (A) with selective refocusing of GABA-H3 (inhibiting  $J$  evolution) and (B) with selective refocusing at a control position. (C) Difference between (A) and (B), showing editing resonances from GABA-H4 and GABA-H2 as well as a co-edited resonance from total glutamate (sum of glutamate and glutamine) and an inverted resonance from NAA due to the finite bandwidth of the selective refocusing pulse. (D) Edited GABA spectrum acquired 2 h following inhibition of the GABA degradation pathway by vigabatrin. Note the splitting of the edited GABA-H4 resonance, indicating a minimal contribution from macromolecules.

shows a typical *in vivo* result for GABA editing on rat brain. Besides  $J$  difference editing, homonuclear spectral editing includes a wide range of techniques, utilizing different manipulations of the scalar coupling and  $J$  evolution (see (19) for review). Each spectral editing technique has unique characteristics in terms of sensitivity, ease of use, motion, suppression of unwanted resonances and sensitivity to system imperfections. As a rough guideline,  $J$  difference editing is close to optimal for stationary objects such as the brain. For more demanding applications, other techniques may be more optimal.

### 3.4.3. Heteronuclear Spectral Editing

In analogy to homonuclear spectral editing (Section 3.4.2), heteronuclear spectral editing is aimed at the simplification of NMR spectra by selectively detecting NMR resonances based on the absence or presence of heteronuclear scalar coupling. The principle of heteronuclear  $J$  difference editing, or POCE (Proton-Observed, Carbon-Edited) NMR spectroscopy (50), is analogous to the homonuclear version with some practical exceptions. Since the heteronuclear  $J$  coupling is often much larger than homonuclear  $J$  coupling constants ( $J_{1\text{H}13\text{C}} = 120\text{--}180\text{ Hz}$  versus  $J_{1\text{H}1\text{H}} = 1\text{--}15\text{ Hz}$ ), the optimal echo time  $1/J$  is much shorter (normally  $TE \sim 7\text{--}9\text{ ms}$ ). Furthermore, since protons can form only a single covalent bond, heteronuclear scalar coupling always lead to the simplest splitting, i.e. a doublet. A doublet can be edited with 100 %

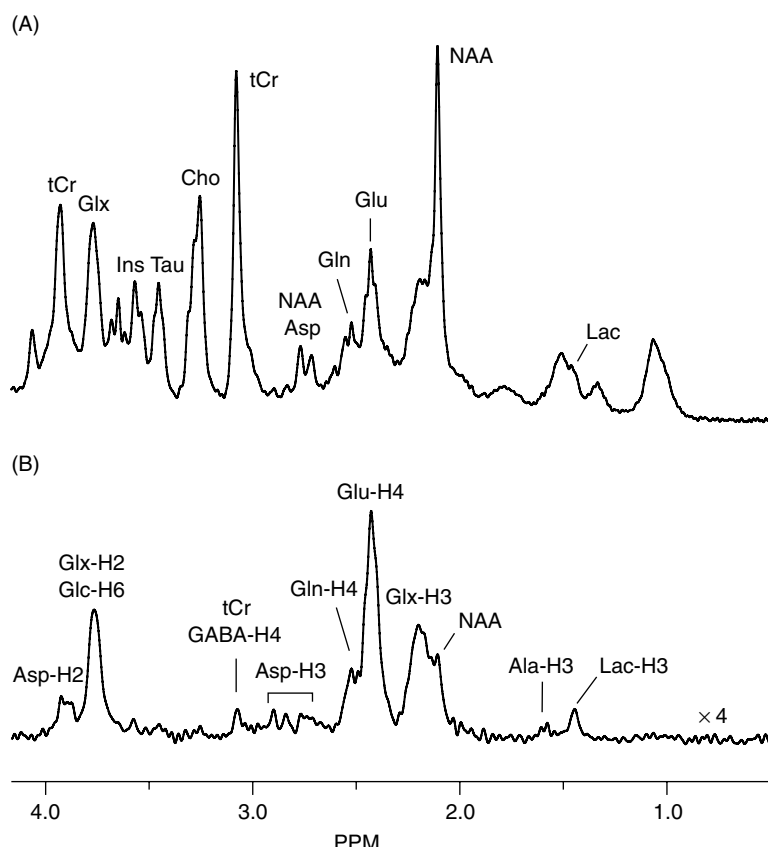


**Figure 3.10.** (A) Nondited and (B) edited  $^1\text{H}-[^{13}\text{C}]$  NMR spectra from rat brain *in vivo* as averaged from a  $100\text{ }\mu\text{l}$  volume over 25 min between 85 and 110 min following the onset of intravenous  $[1,6\text{-}^{13}\text{C}_2]\text{-glucose}$  infusion.

efficiency, unlike other more complicated splitting patterns. Heteronuclear editing also requires selective RF pulses, but the large difference in resonance frequency between protons (300 MHz at 7 T) and for instance carbon-13 (75 MHz at 7 T) ensures that any RF pulse applied to one nucleus is automatically selective for the other nucleus. Besides some additional technical challenges, such as decoupling, heteronuclear editing is identical to homonuclear editing. Two experiments are required, with and without a (selective) RF pulse on the carbon-13 channel. Subtracting the two data sets give the proton NMR resonances from spins that are coupled to carbon-13 spins, while the sum gives the spins that are not scalar coupled (i.e. are bound to a carbon-12 nucleus). The fractional enrichment of any metabolite can be calculated directly from the ratio ( ${}^1\text{H}-[{}^{13}\text{C}]$ / ${}^1\text{H}-[{}^{12}\text{C} + {}^{13}\text{C}]$ ). The fractional enrichment, in combination with the absolute concentration, form the basis of metabolic modeling and interpretation of  ${}^{13}\text{C}$  turnover data, as will be described in detail in several of the following chapters. Figure 3.10 shows a typical example of a  ${}^1\text{H}-[{}^{13}\text{C}]$ -NMR spectrum obtained from rat brain between 60 and 80 min following the infusion of [1, 6- ${}^{13}\text{C}_2$ ]-glucose.

## REFERENCES

1. Purcell EM, Torrey HC, Pound RV, Resonance absorption by nuclear magnetic moments in a solid. *Phys Rev* 1946; **69**: 37–38
2. Bloch F, Hansen WW, Packard ME, Nuclear induction. *Phys Rev* 1946; **69**: 127
3. Bloch F, Nuclear induction. *Phys Rev* 1946; **70**: 460–473
4. Bloch F, Hansen WW, Packard ME, The nuclear induction experiment. *Phys Rev* 1946; **70**: 474–485
5. Proctor WG, Yu FC, The dependence of a nuclear magnetic resonance frequency upon chemical compound. *Phys Rev* 1950; **77**
6. Dickinson WC, Dependence of the F19 nuclear resonance position on chemical compound. *Phys Rev* 1950; **77**: 736
7. Ernst RR, Anderson WA, Applications of Fourier transform spectroscopy to magnetic resonance. *Rev Sci Instrum* 1966; **37**: 93–102
8. Shaw TM, Elsken RH, Nuclear magnetic resonance absorption in hygroscopic materials. *J Chem Phys* 1950; **18**: 1113–1114
9. Odebold E, Lindstrom G, Some preliminary observations on the proton magnetic resonance in biological samples. *Acta Radiol* 1955; **43**: 469–476
10. Damadian R, Tumor detection by nuclear magnetic resonance. *Science* 1971; **171**: 1151–1153
11. Moon RB, Richards JH, Determination of intracellular pH by  ${}^{31}\text{P}$  magnetic resonance. *J Biol Chem* 1973; **248**: 7276–7278
12. Hoult DI, Busby SJ, Gadian DG, Radda GK, Richards RE, Seeley PJ, Observation of tissue metabolites using  ${}^{31}\text{P}$  nuclear magnetic resonance. *Nature* 1974; **252**: 285–7
13. Chance B, Nakase Y, Bond M, Leigh JS, Jr., McDonald G, Detection of  ${}^{31}\text{P}$  nuclear magnetic resonance signals in brain by *in vivo* and freeze-trapped assays. *Proc Natl Acad Sci U S A* 1978; **75**: 4925–9
14. Ackerman JJ, Grove TH, Wong GG, Gadian DG, Radda GK, Mapping of metabolites in whole animals by  ${}^{31}\text{P}$  NMR using surface coils. *Nature* 1980; **283**: 167–70
15. Behar KL, den Hollander JA, Stromski ME, Ogino T, Shulman RG, Petroff OA, Prichard JW, High-resolution  ${}^1\text{H}$  nuclear magnetic resonance study of cerebral hypoxia *in vivo*. *Proc Natl Acad Sci U S A* 1983; **80**: 4945–8
16. Alger JR, Sillerud LO, Behar KL, Gillies RJ, Shulman RG, Gordon RE, Shae D, Hanley PE, *In vivo* carbon-13 nuclear magnetic resonance studies of mammals. *Science* 1981; **214**: 660–2
17. Lauterbur PC, Image formation by induced local interactions: examples employing nuclear magnetic resonance. *Nature* 1973; **242**: 190–191
18. Mansfield P, Multiplanar image formation using NMR spin echoes. *J Phys C: Solid State Phys* 1977; **10**: L55–L58
19. de Graaf RA, *In vivo NMR Spectroscopy. Principles and Techniques*. 1998, Chichester: Wiley.
20. Behar KL, Ogino T, Characterization of macromolecule resonances in the  ${}^1\text{H}$  NMR spectrum of rat brain. *Magn Reson Med* 1993; **30**: 38–44

21. Behar KL, Rothman DL, Spencer DD, Petroff OA, Analysis of macromolecule resonances in  $^1\text{H}$  NMR spectra of human brain. *Magn Reson Med* 1994; **32**: 294–302
22. Govindaraju V, Young K, Maudsley AA, Proton NMR chemical shifts and coupling constants for brain metabolites. *NMR Biomed* 2000; **13**: 129–53
23. Ugurbil K, Magnetization transfer measurements of individual rate constants in the presence of multiple reactions. *J Magn Reson* 1985; **64**: 207–219
24. Cohen SM, Ogawa S, Shulman RG,  $^{13}\text{C}$  NMR studies of gluconeogenesis in rat liver cells: utilization of labeled glycerol by cells from euthyroid and hyperthyroid rats. *Proc Natl Acad Sci U S A* 1979; **76**: 1603–9
25. Stromski ME, Arias-Mendoza F, Alger JR, Shulman RG, Hepatic gluconeogenesis from alanine:  $^{13}\text{C}$  nuclear magnetic resonance methodology for *in vivo* studies. *Magn Reson Med* 1986; **3**: 24–32
26. Sillerud LO, Shulman RG, Structure and metabolism of mammalian liver glycogen monitored by carbon-13 nuclear magnetic resonance. *Biochemistry* 1983; **22**: 1087–94
27. Ordidge RJ, Connelly A, Lohman JA, Image-selected *in vivo* spectroscopy (ISIS). A new technique for spatially selective NMR spectroscopy. *J Magn Reson* 1986; **66**: 283–294
28. Frahm J, Merboldt KD, Hanicke W, Localized proton spectroscopy using stimulated echoes. *J Magn Reson* 1987; **72**: 502–508
29. Granot J, Selected volume excitation using stimulated echoes (VEST). Application to spatially localized spectroscopy and imaging. *J Magn Reson* 1986; **70**: 488–492
30. Bottomley PA, Spatial localization in NMR spectroscopy *in vivo*. *Ann N Y Acad Sci* 1987; **508**: 333–348
31. Shen J, Rothman DL, Hetherington HP, Pan JW, Linear projection method for automatic slice shimming. *Magn Reson Med* 1999; **42**: 1082–8
32. Gruetter R, Automatic, localized *in vivo* adjustment of all first- and second-order shim coils. *Magn Reson Med* 1993; **29**: 804–11
33. Haase A, Frahm J, Hanicke W, Matthaei D,  $^1\text{H}$  NMR chemical shift selective (CHESS) imaging. *Phys Med Biol* 1985; **30**: 341–344
34. Mescher M, Tannus A, O’Neil Johnson M, Garwood M, Solvent suppression using selective echo dephasing. *J Magn Reson A* 1996; **123**: 226–229
35. de Graaf RA, Nicolay K, Adiabatic water suppression using frequency selective excitation. *Magn Reson Med* 1998; **40**: 690–6
36. Hore PJ, Solvent suppression in Fourier transform nuclear magnetic resonance. *J Magn Reson* 1983; **55**: 283–300
37. Patt SL, Sykes BD, Water eliminated Fourier transform NMR spectroscopy. *J Chem Phys* 1972; **56**: 3182–3184
38. van Zijl PCM, Moonen CTW, Complete water suppression for solutions of large molecules based on diffusional differences between solute and solvent (DRYCLEAN). *J Magn Reson* 1990; **87**: 18–25
39. van Zijl PCM, Moonen CTW, Solvent suppression for *in vivo* magnetic resonance spectroscopy. In *NMR Basic Principles and Progress*, Diehl, P, Fluck, E, Gunther, H, Kosfeld, RSeelig, J (Eds). 1992, Berlin: Springer-Verlag, pp. 67–108.
40. van der Veen JW, de Beer R, Luyten PR, van Ormondt D, Accurate quantification of *in vivo*  $^{31}\text{P}$  NMR signals using the variable projection method and prior knowledge. *Magn Reson Med* 1988; **6**: 92–8
41. Maintz D, Heindel W, Kugel H, Jaeger R, Lackner KJ, Phosphorus-31 MR spectroscopy of normal adult human brain and brain tumours. *NMR Biomed* 2002; **15**: 18–27
42. van den Boogaart A, Howe FA, Rodrigues LM, Stubbs M, Griffiths JR, *In vivo*  $^{31}\text{P}$  MRS: absolute concentrations, signal-to-noise and prior knowledge. *NMR Biomed* 1995; **8**: 87–93
43. de Graaf AA, Bovee WM, Improved quantification of *in vivo*  $^1\text{H}$  NMR spectra by optimization of signal acquisition and processing and by incorporation of prior knowledge into the spectral fitting. *Magn Reson Med* 1990; **15**: 305–19
44. Provencher SW, Estimation of metabolite concentrations from localized *in vivo* proton NMR spectra. *Magn Reson Med* 1993; **30**: 672–9
45. Pfeuffer J, Tkac I, Provencher SW, Gruetter R, Toward an *in vivo* neurochemical profile: quantification of 18 metabolites in short-echo-time ( $^1\text{H}$ ) NMR spectra of the rat brain. *J Magn Reson* 1999; **141**: 104–20
46. Slichter CP, *Principles of Magnetic Resonance*. 1990, Berlin: Springer-Verlag.
47. Ernst RR, Bodenhausen G, Wokaun A, *Principles of Nuclear Magnetic Resonance in One and Two Dimensions*. 1987, Oxford: Clarendon Press.

48. Rothman DL, Behar KL, Hetherington HP, Shulman RG, Homonuclear  $^1\text{H}$  double-resonance difference spectroscopy of the rat brain *in vivo*. *Proc Natl Acad Sci U S A* 1984; **81**: 6330–4
49. Rothman DL, Petroff OA, Behar KL, Mattson RH, Localized  $^1\text{H}$  NMR measurements of gamma-aminobutyric acid in human brain *in vivo*. *Proc Natl Acad Sci U S A* 1993; **90**: 5662–6
50. Rothman DL, Behar KL, Hetherington HP, den Hollander JA, Bendall MR, Petroff OA, Shulman RG,  $^1\text{H}$ -Observe/ $^{13}\text{C}$ -decouple spectroscopic measurements of lactate and glutamate in the rat brain *in vivo*. *Proc Natl Acad Sci U S A* 1985; **82**: 1633–7

# 4

## Metabolic Modeling Analysis of Brain Metabolism

**Graeme Mason**

*Department of Psychiatry, Yale University School of Medicine, MR Center, P.O. Box 208043, New Haven, CT 06520-8043, USA*

---

4.1	Introduction	54
4.2	Basic Elements of a Metabolic Model for $^{13}\text{C}$ NMR Studies	57
4.2.1	Metabolic Pools	57
4.2.2	Sources of Substrates Supplied to the System	59
4.2.3	Rates of Metabolic Pathways	59
4.2.4	Combination Pools	59
4.2.5	Targets	60
4.3	Uniting the Elements to Create a Model	60
4.3.1	Mass and Isotope Balance Equations	60
4.3.2	Constraints upon a Model	61
4.3.3	Simplifications of a Model	61
4.3.4	Isotopomer Analysis in a Model	61
4.4	Mechanics of Fitting Data	62
4.4.1	Least-squares Fitting	62
4.4.2	Numerical Fitting Algorithms	63
4.4.3	Effects of Scatter	64
4.4.4	Information Content in a $^{13}\text{C}$ -Labeling Experiment	66
4.5	Conclusion	69

---

## 4.1. INTRODUCTION

Mathematical modeling of brain metabolism to interpret isotopic labeling data was pioneered by van den Berg and Garfinkel, who developed multi-compartmental models of brain metabolism that explained what were apparent paradoxes of  $^{14}\text{C}$  biochemical labeling studies performed with radioisotopes (Van den Berg and Garfinkel 1971; Van den Berg *et al.*, 1970). A limitation of the  $^{14}\text{C}$  methodology is that it requires sacrificing animals and chemical extraction of the brain to obtain data. Today, NMR spectroscopy has allowed isotopic labeling measurements of  $^{13}\text{C}$  and other nuclei to be performed *in vivo* (Beckmann *et al.*, 1991; Behar *et al.*, 1986; Bluml *et al.*, 2001a; Bluml *et al.*, 2001b; Fitzpatrick *et al.*, 1990; Gruetter *et al.*, 1994; Gruetter *et al.*, 2001; Künnecke *et al.*, 1993; Moreno *et al.*, 2001a; Moreno *et al.*, 2001b; Rothman *et al.*, 1992), *in vitro* (Sillerud *et al.*, 1981; Sonnewald *et al.*, 1991; Sonnewald *et al.*, 1996; Szczepaniak *et al.*, 1996; Waagepetersen *et al.*, 2000), in perfused organs (Lewandowski *et al.*, 1997; Yu *et al.*, 1995), and in brain slices (Badar-Goffer *et al.*, 1990; Badar-Goffer *et al.*, 1992). *In vivo* MRS is less sensitive than  $^{14}\text{C}$  methods, but has the advantages of allowing many more time points in turnover curves and can be applied to human studies.

The major fuel for brain metabolism is glucose with monocarboxylic acids such as acetate,  $\beta$ -hydroxybutyrate, and lactate acting as minor but significant fuel sources. As described in detail in Chapters 5 and 6 there are two major cell types in the brain, neurons and glia. Neurons transmit electrical impulses and communicate with each other by release of chemicals called neurotransmitters. Glia surround the neurons and maintain a stable extracellular environment as well as providing the neurons with key substrates. There are many types of neurons, usually classified based upon morphology and the primary neurotransmitter they release. In the cerebral cortex over 90 % of the neurons and synapses are from glutamatergic and GABAergic neurons (Shephard, 1994). Although multi-compartment models are vulnerable to multiple solutions, in the brain the modeling is simplified by the presence of key synthetic enzymes and metabolite pools in specific cell types. For example glutamine is only synthesized in glial cells, GABA is only synthesized in GABAergic neurons, and brain glutamate is primarily in glutamatergic neurons. To a first order these metabolite pools may be considered as reflecting cell specific metabolism, and each of the pools modeled separately. More sophisticated analysis allows the metabolic interactions between these cell types to be calculated (Rothman *et al.*, 2003). A further simplification in the modeling is that, to a resolution on the order of  $200\text{ }\mu\text{m}$ , most of the cerebral cortex has its own arterial blood supply (see Chapter 8). Therefore, across the cortex, there is not the gradation of plasma substrate levels that complicates the modeling of hepatic and muscle metabolism.

In this review we focus on the modeling of neuronal glucose metabolism, in particular the neuronal TCA cycle and, secondarily, the glutamine cycle. As described extensively in other chapters, the glutamate/glutamine cycle is a metabolic pathway shared between neurons and glia. In this pathway glutamate released by the neuron as a neurotransmitter is taken up by surrounding glial cells and converted to glutamine. Glutamine is not neuroactive and is released by the glia for uptake by the neurons to replace lost glutamate. Figure 4.1 shows the metabolic interactions of glutamate metabolism between glia and neurons. Measurement of the glutamate/glutamine cycle is of particular interest because it is a direct measurement of glutamate neurotransmission, which is the major excitatory neurotransmitter pathway in the cerebral cortex. Neuronal glucose oxidation by the TCA cycle is the main source of energy for the brain, and impairment of the TCA cycle is a symptom of several neurological and psychiatric diseases. *In vivo* NMR has the unique ability to measure both of these critical pathways simultaneously and noninvasively.

In this chapter we focus on the principles for using mathematical modeling of dynamic and steady-state isotopic labeling to derive rates of brain metabolism, and some of the issues which are unique to modeling MRS data. The intention is primarily pedagogical, and readers are referred to other chapters in this book for current thinking on brain metabolism. Because glucose is the most common substrate used experimentally, we focus on the use of  $[1-^{13}\text{C}]$ glucose as an isotopic precursor. Figure 4.2 shows a

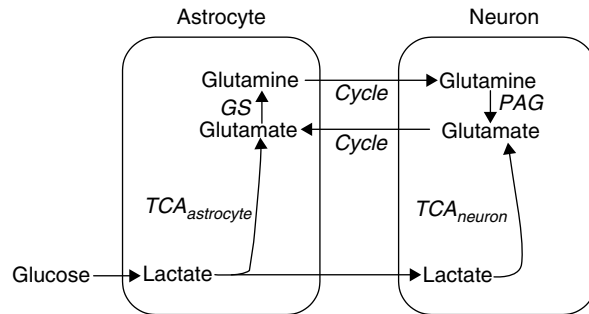


**Figure 4.1.** Schematic representation of the glutamate/glutamine cycle between neurons and glia. The diagram shows a two-compartment model of brain metabolism between glutamate-releasing (glutamatergic) neurons and surrounding astrocyte cells. Glutamate is released from the neuron through the dumping of the contents of synaptic vesicles upon depolarization. Released neurotransmitter glutamate is transported from the synaptic cleft by surrounding glial end processes, in a process that is driven by the glial sodium gradients. Once in the glia glutamate is converted to glutamine by glutamine synthetase (GS). Glutamine is released by the astrocyte, transported into the neuron, and converted to glutamate by phosphate-activated glutaminase (PAG), which completes the cycle.

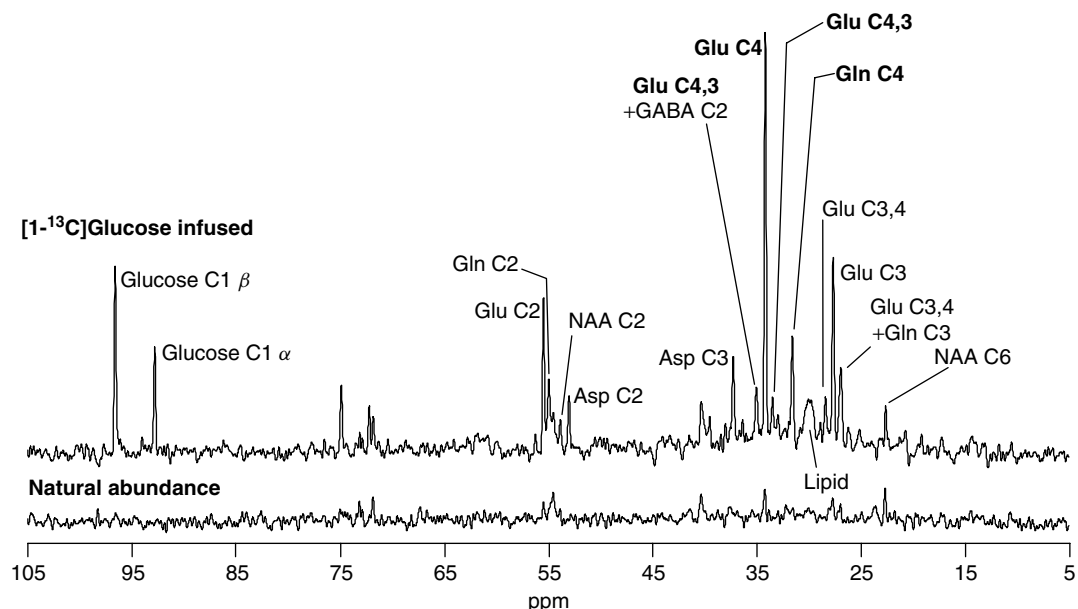


**Figure 4.2.** <sup>13</sup>C MRS spectrum in the occipital/parietal lobe at 2.1 T. The figure shows a 45 min accumulation <sup>13</sup>C MRS spectrum obtained at 2.1 T approximately 60 min after the start of a 1-<sup>13</sup>C glucose infusion. The spectrum was obtained from a 144 ml volume centered on the midline in the occipital/parietal lobe. Labeled resonances include the C2, C3, and C4 positions of glutamate, glutamine, aspartate, and GABA and the C3 position of lactate. The localization of the synthetic enzymes and pools of GABA and glutamine to GABAergic neurons and glia, respectively, and the localization of the majority of the glutamate pool to glutamatergic neurons, allows the relative rates of glucose oxidation in these cell types to be determined from the flow of <sup>13</sup>C label into these pools (Rothman *et al.*, 2003). Figure from Mason *et al.*, 2003.

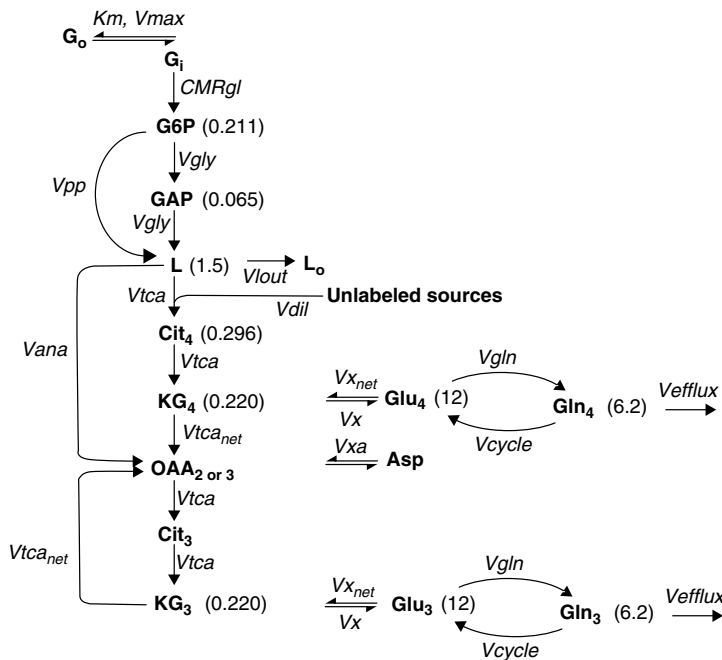


**Figure 4.3.** Schematic representation of flow of  $^{13}\text{C}$  from glucose through glutamate to glutamine in a simplified one-compartment model. This model is the initial model used to fit dynamic time courses of brain isotopic labeling data. It is simplified from the neuronal/glial interactions shown in Figure 4.1 by not modeling internal glial metabolism. Provided that the amount of glial glutamate is small, this model provides an accurate description of neuronal metabolism when glutamine labeling, which is the main input to the neuron from the glial cells, is measured. The concentrations of each metabolite are given in parentheses next to the pool name, in units of mmol/kg. Glucose in the plasma ( $\text{G}_0$ ) and the brain ( $\text{G}_i$ ) are in exchange at rates  $V_{\text{in}}$  and  $V_{\text{out}}$ ; these rates vary with plasma glucose concentration but can be predicted with Michaelis–Menten kinetics. The  $^{13}\text{C}$  label flows at the rate  $\text{CMR}_{\text{gl}}$  through glucose-6-phosphate and fructose-6-phosphate, which are assumed to be in isotopic equilibrium and are therefore added to form a single pool (G6P). The pentose phosphate pathway removes label from G6P at the rate  $V_{\text{pp}}[0.03V_{\text{gly}}]$  (Hawkins *et al.*, 1985; Mason *et al.*, 1992b). The  $^{13}\text{C}$  label continues through glycolysis, passing through all of the intermediates from fructose-1,6-bisphosphate to phosphoenolpyruvate; these intermediates are assumed to be in isotopic equilibrium and are therefore added to form a single pool (GAP). The  $^{13}\text{C}$  arrives at pyruvate and through exchange labels lactate; lactate and pyruvate are assumed to be in isotopic equilibrium and are therefore added to form a single pool (L). This pool is in exchange with plasma pyruvate and lactate ( $\text{L}_0$ ) at the rates  $V_{\text{in}}$  [0.05 mmol/kg/min (Pardridge and Oldendorf, 1977)] and  $V_{\text{out}}$  [0.085 mmol/kg/min; calculated from Pardridge and Oldendorf (1977) and intracerebral lactate concentrations reported by Hawkins and Mans (1983)]. The  $^{13}\text{C}$  enters the TCA cycle and labels citrate and isocitrate at carbon 4; these pools are assumed to be in isotopic equilibrium and are added to form a single pool (Cit<sub>4</sub>). At  $\alpha$ -KG and glutamate C4, the  $^{13}\text{C}$  label exchanges between the mitochondrial and cytosolic pools of each; these exchanges are reduced to a single exchange between two grouped pools (KG<sub>4</sub> and Glu<sub>4</sub>). Glutamate is released from the neuron, taken into the astrocyte, and converted to glutamine at the rate  $V_{\text{gln}}$  [0.08–0.5 mmol/kg/min (Sibson *et al.*, 1998) and calculated from Dzubow and Garfinkel (1970)], labeling the C4 of glutamine (Gln<sub>4</sub>). The  $^{13}\text{C}$  label continues through the TCA cycle to oxaloacetate, which then exchanges with aspartate (Asp); the TCA cycle intermediates between  $\alpha$ -KG and glutamate C4 are assumed to be in isotopic equilibrium and are added to form a single pool (OAA). The  $^{13}\text{C}$  label enters its second and all subsequent turns of the cycle at the lumped citrate pool (Cit<sub>3</sub>), so called because the  $^{13}\text{C}$  now flows to the C3 of  $\alpha$ -KG (KG<sub>3</sub>), glutamate (Glu<sub>3</sub>), and glutamine (Gln<sub>3</sub>).  $^{13}\text{C}$  flow diverges at L at the pyruvate carboxylase rate  $V_{\text{pc}}$  [0.10  $V_{\text{tca}}$  (Berl *et al.*, 1962)].  $V_{\text{efflux}}$  is equal to  $V_{\text{pc}}$ , which maintains the balance of mass in the TCA cycle. This figure was adapted from Mason *et al.* (1992b). Reproduced by permission of Lippincott, Williams and Wilkins.

$^{13}\text{C}$  NMR spectrum obtained from the human brain after intravenous infusion of  $[1-^{13}\text{C}]$ glucose. The key metabolites involved in glutamate metabolism, which are glutamate, glutamine, and  $\gamma$ -aminobutyric acid (GABA), are heavily labeled. By fitting the *in vivo* labeling curves with multi-compartment metabolic model, key metabolic rates can be calculated, including the rate of neuronal glucose metabolism, and the glutamate/glutamine cycle.

Figure 4.3 shows a schematic diagram of a model of  $^{13}\text{C}$  labeling from  $[1-^{13}\text{C}]$ glucose based on Figure 4.1, which will be referred to in the rest of this review. The caption to the figure describes the model in detail. This model is focused on neuronal metabolism in glutamatergic cells. However, it takes into account neuronal/glial interactions by treating glial glutamine labeling as an input. Although simplified relative to the models that we and other groups are currently using, we will use this one-compartment model to explain the concepts and procedures involved in the modeling analysis. Extensions to two and three compartments are described in Chapters 5 and 6 and the following references (Gruetter *et al.*, 2001; Mason *et al.*, 2001; Rothman *et al.*, 2003; Sibson *et al.*, 2001).

## 4.2. BASIC ELEMENTS OF A METABOLIC MODEL FOR $^{13}\text{C}$ NMR STUDIES

A metabolic modeling analysis of isotopic turnover data requires several basic elements: metabolic pools, sources of substrates supplied to the system, rates of metabolic pathways, and for fitting, one needs the target data that have been measured experimentally. Some models also require the calculation of *combination pools*, which will be defined in this section of the chapter. With these five basic elements, it is possible to generate equations that express any scenario of mass and isotopic flow among metabolic pools and adjust them to obtain the closest approximation to real life.

### 4.2.1. Metabolic Pools

Metabolic pools are characterized by four components. They are the initial concentration, the position of isotopic labeling that results from a particular flow or combination of flows, the inflows, and the outflows. The initial concentration is required because it controls the percent enrichment of the pool.

Although consumption of a molecule degrades the entire chemical at the same rate through the same pathways, the carbon that is supplied to a molecule can be derived from different sources and paths. For example, in Figure 4.3, glutamate is used to synthesize glutamine or  $\alpha$ -ketoglutarate. However, an examination of the individual atoms of glutamate shows that the C4 must come from carbon derived from acetyl-CoA, and the C3 may come from anaplerotic fueling of the C2 of oxaloacetate, or from carbon that originated in the C3 position of glutamate itself. In fact, each of the carbon positions of glutamate has a different set of sources. So, the C4 of glutamate and each of the other glutamate carbon positions function as distinct metabolic pools that happen to have the same rates of degradation by virtue of their residing in the same chemical but usually are not labeled by the same pathways. Investigators may also analyze the combinations of  $^{13}\text{C}$ -labeling that can occur at multiple carbon positions within a molecule, and each of those combinations can be modeled as additional, distinct metabolic pools (Figure 4.3).

The inflows and outflows are simply rates of transfer of mass and isotope into and out of the metabolic pool. The flows can be of many types, including absolute rates, mass-dependent time constants of flow, source-dependent flows that are governed by Michaelis–Menten kinetics, or flows that introduce feedback or feedforward regulation. Whatever the type of flow, there come into play two key concepts, and which are *turnover* and *accumulation* (Figure 4.4), and carefully structured metabolic modeling becomes extremely important in the case of turnover.

When  $^{13}\text{C}$  arrives in a metabolite pool and replaces carbon that is leaving the pool, turnover has occurred. If the metabolite pool becomes labeled without an increase in concentration, then turnover has occurred. The

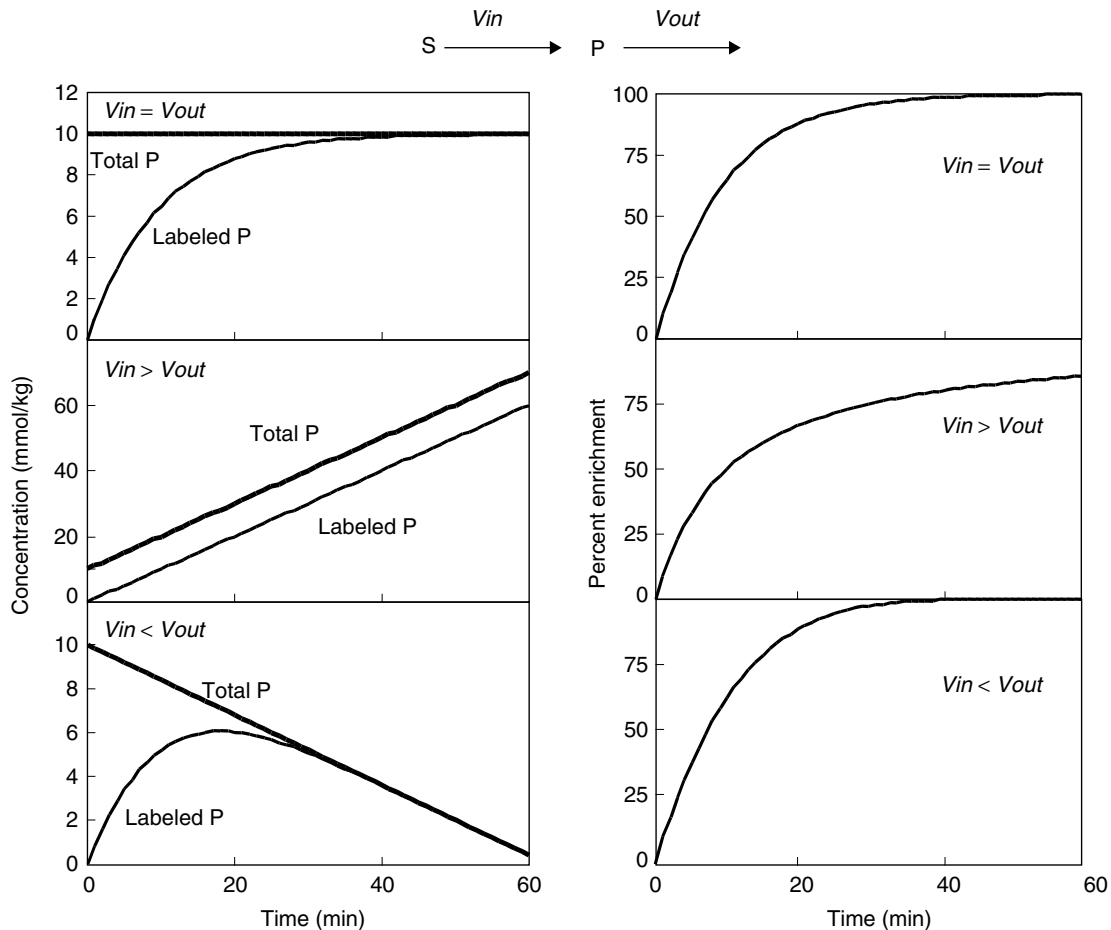


**Figure 4.4.** The effects of flow from a labeled substrate  $S$  into a product  $P$  at the respective rates  $V_{in}$  and  $V_{out}$ , for  $P = 10 \text{ mmol/kg}$ ,  $V_{in} = 1 \text{ mmol/kg/min}$ , and  $S$  is 100% enriched. Top pair: if  $V_{in} = V_{out}$ , the total amount of  $P$  is constant, and the amount of labeled  $P$  increases as a single-exponential function, as does the percent enrichment of  $P$ . Middle pair: if  $V_{in} > V_{out}$ , the total amount of  $P$  and labeled  $P$  increase linearly. In the example here,  $V_{out} = 0$ . The percent enrichment can no longer be described by a single-exponential function. Bottom pair: if  $V_{in} < V_{out}$ , the total amount of  $P$  decreases linearly. In this example,  $V_{out} = 1.14 \text{ mmol/kg/min}$ . The amount of labeled  $P$  increases as  $V_{in}$  supplies label and increases the percent enrichment of  $P$ , but as the total quantity of  $P$  decreases, so eventually must the quantity of labeled  $P$ . It is interesting to see that the percent enrichment actually rises slightly more quickly for  $V_{in} < V_{out}$ , and this is because the amount of  $P$  to enrich decreases, requiring less and less labeled substrate to reach 100% enrichment.

metabolite pool can decrease in level, still with the labeling described as turnover, but when the introduction of label occurs with an increase in total mass of the metabolite pool, the result is mass accumulation. Mass accumulation requires that the breakdown of the metabolite be slower than its synthesis. Referring to Figure 4.4, in a case of pure mass accumulation, the appearance of  $^{13}\text{C}$  label represents pure synthesis, and the mass and isotope balance equations would be

$$d[P]/dt = V_{in}$$

and

$$d[P^*]dt = ([S^*]/[S])V_{in}$$

One such case would be if the breakdown of lactate were completely blocked, and the rate of increase in  $^{13}\text{C}$ -lactate were measured. In that case of pure accumulation, the slope of the time-dependent increase in  $^{13}\text{C}$ -labeling of the product could be used directly for a simple, easy determination of its rate of synthesis (middle set of graphs of Figure 4.4).

In contrast, turnover requires more intense mathematics to interpret than does mass accumulation. While accumulation means that mass is being added to the observed pool, turnover means that the sample is being changed rather than simply increased, with at least some of the sample leaving and being replaced by new material. That requires some breakdown of the product. Pure turnover occurs for  $V_{in} \leq V_{out}$ . The determination of the metabolic rates under conditions of turnover is considerably more complicated than is the case for mass accumulation. The top and bottom panels of Figure 4.4 show the time courses of  $^{13}\text{C}$ -label accumulation and  $^{13}\text{C}$  percent enrichment for when turnover occurs under conditions of  $V_{in} = V_{out}$  and under conditions of net loss of P ( $V_{in} < V_{out}$ ).

#### 4.2.2. Sources of Substrates Supplied to the System

Isotopic labeling measurements are based on an initial condition in which there is less of an isotope in the system than is present in the substrate that will be injected into the system.  $^{13}\text{C}$ -labeling studies almost always begin with carbon having the 1.1 % of natural abundance, and that enrichment can be raised a little or a lot, depending on the experimental preparation and the pathways that are being evaluated. One common substrate, C1-labeled glucose, typically leads to labeling that is 15–30 % at the isotopic steady state *in vivo*, whereas C2-labeled glucose leads to labeling of only a few percent, because the pathways of entry are different.

A labeled substrate should be characterized as a function of time, beginning with the condition before the start of the labeled infusion and continuing through the time that the last metabolic measurements are acquired. The time course of labeling is used as a driver for the system of equations that will be used to simulate metabolism. For example, the rate of labeling of brain glucose is the rate of flow of  $^{13}\text{C}$ -glucose from the blood to the brain, which is governed by blood–brain transport of glucose and by the availability of  $^{13}\text{C}$ -glucose in the blood. Generally, the time courses of concentration and percent enrichment of any labeled substrates should be known for this measurement to be successful. In Figure 4.3, the C1 of glucose is labeled.

It is important to remember that many substrates may contribute carbon to the chemicals whose labeling is observed in a study. For example, ketone bodies, acetate, pyruvate, and lactate all provide carbon that flows to glutamate C4. During infusions of  $[1-^{13}\text{C}]$ glucose *in vivo*, the carbon from these alternative substrates remains unlabeled, but the substrates should still be included as sources of unlabeled carbon.

#### 4.2.3. Rates of Metabolic Pathways

For the neurochemicals to become labeled from the carbon substrates, the substrates and chemicals must be linked by rates of metabolic flow. Although it is also possible in principle to adjust the sizes of metabolic compartments (Lebon *et al.*, 2002), it is metabolic rates that are most often adjusted when fitting experimental data. The rates of flow can either be evaluated as absolute rates or as kinetic parameters that are used to calculate rates of flow, such as Michaelis–Menten  $K_m$  or  $V_{max}$  (Mason *et al.*, 1992a).

#### 4.2.4. Combination Pools

Although NMR spectroscopy is unrivaled in its chemical specificity, the specificity is not complete, especially for studies that are performed *in vivo*. Separate metabolic pools of the same chemical are often not

distinguished, and sometimes even different chemicals cannot be resolved from one another, and for this purpose, most models that are analyzed *in vivo* require the use of combination pools.

One example of the lack of differentiation of resonances from several metabolic pools is the compartmentation of glutamate among glutamatergic neurons, GABAergic neurons, and astroglia. Although distinct physical compartments exist for these pools of glutamate, there is currently no distinction among them as detected by NMR spectroscopy; what is observed is a *combination pool*. Therefore, to simulate observations of  $^{13}\text{C}$ -labeling, metabolic models require the labeling of each pool to be calculated separately and then summed to compute the kinetics of the combination pool of total glutamate. Fortunately, the glutamate pools in the GABAergic and glial compartments are small relative to glutamatergic neurons, so the rates of metabolism calculated are relatively unaffected by uncertainties about their pool sizes (Lebon *et al.* 2002; Rothman *et al.* 2003).

#### 4.2.5. Targets

A simulation of metabolism by itself can be a useful tool to test the consequences of ideas, but the simulation should always be done in the context of actual data. So, any model should be able to be compared to experimental observations, which are called *target data*.

A set of target data should include the time that corresponds to each NMR measurement and either a concentration or a percent enrichment of  $^{13}\text{C}$ -labeling of a particular carbon position. If the concentration of the observed metabolic pool changes with time, then the target data should also include the total concentration (labeled plus unlabeled) material as a function of time.

If  $^{13}\text{C}$ -labeling is measured by tissue extraction, then the time of a particular data point in the target set is the time at which the tissue was removed and metabolism halted by freezing, microwaving, or chemical means. If  $^{13}\text{C}$ -labeling is measured *in vivo*, the time of the data point should be the average of the time interval over which the signals were accumulated for the measurement. For example, in previously published studies of human brain metabolism, individual spectra were acquired every 5 min, so each time point corresponded to 2.5 min after the start of the acquisition.

### 4.3. UNITING THE ELEMENTS TO CREATE A MODEL

The metabolic pools, substrate drivers, and rates of metabolic pathways are combined to create a set of mass balance equations and a set of isotope balance equations, with one of each for every relevant labeling pattern of each metabolic pool that is in the model. The mass and isotope balance equations can then be solved in light of various constraints that are placed on the model by mass balance and *a priori* knowledge from other experiments.

#### 4.3.1. Mass and Isotope Balance Equations

The mass balance equations are a mathematical statement of how the total mass of a metabolic pool changes over time. A mass balance equation has the general form

$$\frac{dP}{dt} = V_{\text{in}} - V_{\text{out}} \quad (4.1)$$

where  $dP/dt$  is the rate of change of the metabolic pool,  $V_{\text{in}}$  is the rate of flow from the metabolite  $M$ , and  $V_{\text{out}}$  is the rate of flow out of the pool (Figure 4.4). At a metabolic steady state,  $V_{\text{in}} = V_{\text{out}}$ , and the mass of the pool  $P$  does not change with time.

The isotope balance equations show quantitatively how the isotopically labeled concentration of a metabolic pool changes over time, with the general form

$$\frac{dP^*}{dt} = \frac{M^*}{M} V_{\text{in}} - \frac{P^*}{P} V_{\text{out}} \quad (4.2)$$

where each  $M$  is the metabolic intermediate that provides mass for the pool at the rate  $V_{\text{in}}$ . Because  $^{13}\text{C}$  has been shown to have a negligible isotope effect (Attwood *et al.*, 1986; Melzer and Schmidt, 1987; Tipton and Cleland, 1988), the rate of isotopic inflow from each source is equal to the rate of mass (labeled plus unlabeled) flow from that source, multiplied by the fraction of the flow that is  $^{13}\text{C}$ -labeled.

### 4.3.2. Constraints upon a Model

A model such as the one shown in Figure 4.3 typically has more parameters than it would be possible to evaluate in a typical set of experiments. Even if it were possible to derive some information about all of the parameters separately in the model, the ability to place constraints on the system allows one to supply more information in the model, which decreases the uncertainty in those parameters that are fitted. Therefore, it is often necessary and always desirable to constrain the values of model parameters within reasonable limits. For example, in the model of Figure 4.3, it is known that infusing  $\text{C}1$ -labeled glucose does not change the concentrations of brain glutamate or glutamine. Therefore, we can supply mass balance constraints on the flows into and out of glutamate and glutamine  $\text{C}4$  and  $\text{C}3$ . Therefore,  $V_{\text{glu}} = V_{\text{cycle}} + V_{\text{efflux}}$ , and  $V_{\text{efflux}} = V_{\text{ana}}$ .

### 4.3.3. Simplifications of a Model

The model of Figure 4.3 has been simplified in a variety of ways, and the effect of such simplifications can be calculated using the metabolic simulations. One of the simplifications was the grouping of metabolic intermediates that are in rapid equilibrium, such as glucose-6-phosphate and fructose-6-phosphate. To evaluate the effect of grouping intermediates, the time courses were simulated for several values of  $V_{\text{tca}}$ , assuming no exchange between the intermediate metabolites. Simulated labeling time courses were then used as input for the model's fitting procedure. The values of  $V_{\text{tca}}$  derived from the simulated time courses assuming no exchange among intermediates were overestimated, but the overestimate was less than 3% of the simulation value of  $V_{\text{tca}}$ . Similar procedures have been applied to evaluate the assumption of lactate–pyruvate exchange being very fast, the effects of uncertainty in glucose transport kinetics, blood–brain exchange of pyruvate and lactate, and other simplifications of metabolic models.

### 4.3.4. Isotopomer Analysis in a Model

$^{13}\text{C}$  can be incorporated not only at different positions of a molecule, but simultaneously in different combinations of positions in the molecules. The term *isotopomers* represents a single chemical species that is labeled with the same number of isotopes but at different locations within the molecule. In the analysis of metabolic NMR data, isotopomers is more loosely used to represent differently labeled moieties of the same chemical, no matter how many locations are labeled in the molecule. The evaluation of isotopomers has been used powerfully to quantify proportions of flows at junctions of different metabolic flows (den Hollander *et al.*, 1979; Sherry *et al.*, 1988). Generally, the measurements are made at an isotopic steady state and analyzed using the proportion of one isotopomer to another.

One example is the application of isotopomers to quantify the proportions of labeled and unlabeled carbon flowing to glutamate during an infusion of  $[1-^{13}\text{C}]$ glucose through the metabolic schematic shown

in Figure 4.3. Because citrate and oxaloacetate are so much smaller than the glutamate and glutamine, their kinetic effects can be neglected. Therefore, the isotope balance equations are

$$\begin{aligned}\frac{d\text{Glu}_4}{dt} &= \frac{L_3}{L} V_{\text{gly}} + \frac{G \ln_4}{G \ln} V_{\text{cycle}} + (0) V_{\text{dil}} - \frac{\text{Glu}_4}{G \ln} (V_{\text{tca}} + V_{\text{g ln}}) \\ \frac{dG \ln_4}{dt} &= \frac{\text{Glu}_4}{\text{Glu}} V_{\text{g ln}} - \frac{G \ln_4}{G \ln} (V_{\text{cycle}} + V_{\text{efflux}}) \\ \frac{d\text{Glu}_3}{dt} &= \frac{1}{2} \frac{L_3}{L} V_{\text{ana}} + \frac{1}{2} (0) V_{\text{ana}} + \frac{1}{2} \frac{\text{Glu}_4}{\text{Glu}} V_{\text{tca, net}} + \frac{1}{2} \frac{\text{Glu}_3}{\text{Glu}} V_{\text{tca, net}} + \frac{G \ln_3}{G \ln} V_{\text{cycle}} - \frac{\text{Glu}_3}{\text{Glu}} (V_{\text{tca}} + V_{\text{g ln}}) \\ \frac{dG \ln_3}{dt} &= \frac{\text{Glu}_3}{\text{Glu}} V_{\text{g ln}} - \frac{G \ln_3}{G \ln} (V_{\text{cycle}} + V_{\text{efflux}}) \\ \frac{d\text{Glu}_{3,4}}{dt} &= \frac{L_3}{L} \frac{\text{Glu}_3}{\text{Glu}} V_{\text{tca}} + \frac{G \ln_{3,4}}{G \ln} V_{\text{cycle}} - \frac{\text{Glu}_{3,4}}{\text{Glu}} (V_{\text{tca}} + V_{\text{g ln}}) \\ \frac{dG \ln_{3,4}}{dt} &= \frac{\text{Glu}_{3,4}}{\text{Glu}} V_{\text{g ln}} - \frac{G \ln_{3,4}}{G \ln} (V_{\text{cycle}} + V_{\text{efflux}})\end{aligned}$$

When the system is studied at a metabolic steady state, in which condition the concentrations of metabolites are not changing,  $V_{\text{g ln}} = V_{\text{cycle}} + V_{\text{efflux}}$ , and  $V_{\text{efflux}} = V_{\text{ana}}$ . So, at an isotopic steady state,

$$\frac{\text{Glu}_4^*}{G \ln} = \frac{G \ln_4^*}{\text{Glu}}, \quad \frac{\text{Glu}_3^*}{\text{Glu}} = \frac{G \ln_3^*}{\text{Glu}}, \quad \frac{\text{Glu}_{3,4}^*}{\text{Glu}} = \frac{G \ln_{3,4}^*}{\text{Glu}}$$

and

$$\frac{\text{Glu}_4}{\text{Glu}} = \frac{L_3}{L} \frac{V_{\text{tca}} - V_{\text{dil}}}{V_{\text{tca}}}$$

The equation for  $[3,4\text{-}^{13}\text{C}_2]\text{glutamate}$ , with substitution of  $\text{Glu}_4/\text{Glu}$ , yields

$$\frac{V_{\text{dil}}}{V_{\text{tca}}} = 1 - \frac{\text{Glu}_3 \text{Glu}_4}{\text{Glu}_{34}}$$

Therefore, from measurements of the concentration of C3-labeled glutamate, C4-labeled glutamate, and glutamate labeled at both C3 and C4, one can determine the proportion of the TCA cycle that is fueled by an unlabeled carbon source.

## 4.4. MECHANICS OF FITTING DATA

Fitting a model to experimental data is a procedure that answers two questions. (1) Can the values of parameters in this model be adjusted to provide an adequate simulation of the observations? (2) If this model were true, what values of the parameters are needed to explain the observations? In practice, the parameters are adjusted until some tolerance is attained for the proximity of the data and the simulation.

### 4.4.1. Least-squares Fitting

The most common measurement of proximity of the data and simulation is least-squares fitting. Least-squares fitting relies on the sum of the square of the difference between the data and the simulation. For a function  $f(t)$  that uses  $m$  parameters  $a_1, a_2, a_3, \dots, a_m$ ,

$$\chi^2 = \sum_{i=1}^n [f(a_{1..m}, t_i) - y_i(t_i)]^2 \quad (4.3)$$

where  $y_i(t_i)$  is the  $i$ th experimental observation, and  $f(a_{1..m}, t_i)$  is the simulated function calculated at  $t = t_i$ . The least-squares fitting is used to find the set of values of  $a_{1..m}$  that yields the minimum value of  $\chi^2$ .

For a straight line, least-squares fitting yields the values of two parameters, which are the slope  $a_1$  and intercept  $a_2$ . The purpose of the regression analysis is to find the best fit of the function  $y_i = a_1 t_i + a_2$ . The fitting is performed based on the assumption that the minimum value of  $\chi^2$  is obtained when

$$\frac{\partial \chi^2}{\partial a_1} = 2 \sum_{i=1}^n \frac{\partial f(a_1, a_2, t_i)}{\partial a_1} [f(a_1, a_2, t_i) - y_i(t_i)] = 0 \quad (4.4)$$

and

$$\frac{\partial \chi^2}{\partial a_2} = 2 \sum_{i=1}^n \frac{\partial f(a_1, a_2, t_i)}{\partial a_2} [f(a_1, a_2, t_i) - y_i(t_i)] = 0 \quad (4.5)$$

For a straight line, there are analytic expressions for the values of  $a_1$  and  $a_2$ , which are

$$a_1 = \frac{\bar{y} \sum_{i=1}^n t_i^2 - \bar{t} \sum_{i=1}^n t_i y_i}{\sum_{i=1}^n t_i^2 - n \bar{t}^2} \quad (4.6)$$

and

$$a_2 = \frac{n(\bar{t})(\bar{y}) - \sum_{i=1}^n t_i y_i}{n \bar{t}^2 - \sum_{i=1}^n t_i^2} \quad (4.7)$$

Therefore,  $a_1$  and  $a_2$  are explicitly determined and result in a straightforward solution. For most problems of metabolic modeling, however, there are no explicit expressions for the best values of the fitted parameters, so they must be evaluated iteratively. A variety of methods exist for the iterative determination of model parameters.

#### 4.4.2. Numerical Fitting Algorithms

Algorithms exist that search for the parameter set that provides the best approximation to the data, and the performance of each varies with respect to the time to complete the estimation and the likelihood of success. In general, the sum of squares of the differences, called  $\chi^2$ , can be imagined as a surface whose dimensions are the ranges of the values of the parameters in the model. The coordinates of each point on the surface are a set of values of the model parameters, and the height of the surface is the value of  $\chi^2$  that occurs for those parameter values (Figure 4.5). Because some combinations of points give a better approximation to the data than other combinations, the surface will have bumps and dips, with one dip that is deeper than any of the others. The coordinates of that deepest dip are the least-squares values of the model for the data. Fitting algorithms are assigned the task of locating that deepest dip. Examining Figure 4.5, one sees many shallow dips, which are called *false minima*, and if a search focuses quickly on one of these minima without checking for others, the conclusions will be incorrect. One can also see that if a search begins too far away from the true minimum, with a small search range, the algorithm will not find the true minimum. Search algorithms are designed to balance speed and robustness in the search.

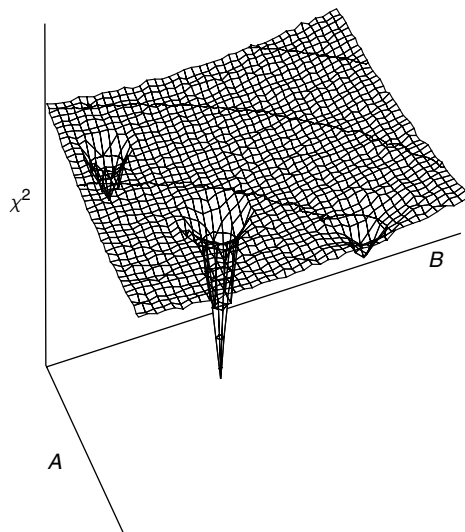


**Figure 4.5.**  $\chi^2$  surface for a model  $f(A, B)$ , which is the sum of the squares of the difference between the model prediction and the actual data for all combinations of the fitted parameters  $A$  and  $B$ . The value of  $\chi^2$  is a function of the fitted parameters in a model, which are in this case  $a_1$  and  $a_2$ . A least-squares fitting algorithm finds the combination of fitted parameters that yields the minimum value of  $\chi^2$ . The graph shows one deep minimum and two shallower minima that are called false minima. Most problems require an iterative search for the true minimum value of  $\chi^2$ . Greedy search algorithms may find only a false minimum, while a more robust method that is more likely to find the true minimum may take longer to complete the search.

An algorithm is called *greedy* if it settles quickly for the first minimum that it encounters in the  $\chi^2$  surface, but an algorithm that searches too many possibilities would be impractically slow. The *simplex* algorithm tends to be quick but greedy, by comparing the amplitudes of  $\chi^2$  at several different coordinates of the  $\chi^2$  surface. Simulated annealing, on the other hand, rarely fails but takes much longer to run. Simulated annealing can be implemented in many ways, but the common feature is the incorporation of a random alteration of the test coordinates of the  $\chi^2$  surface. In simulated annealing, the random alteration is large at the beginning, analogous to the vibrations of atoms in a crystal lattice, and as the fit progresses, the random changes become smaller and smaller until the fit is nearly identical to one of the conventional fitting methods such as simplex. A method that is faster than simulated annealing and still effective is the Levenberg–Marquardt algorithm, which uses not only the amplitude but also the slope of  $\chi^2$  at various locations. The Levenberg–Marquardt algorithm is the most common fitting algorithm in use today for the analysis of kinetic  $^{13}\text{C}$  NMR data, but when it does fail, simulated annealing has been able to fill the need.

#### 4.4.3. Effects of Scatter

When model parameters are estimated from  $^{13}\text{C}$  NMR data, there arises the question of how well the values are known, given the uncertainty in the experimental data. For the case of studies that are done *in vivo*, one wants to know not only the group mean and standard deviation, but whether the individual variability is greater than is expected given the group statistics. That is, if a study shows a twofold difference in the rate of a pathway across individuals, can that be explained on the basis of measurement error, or is there a strong inter-subject variability? On the other hand, for time courses made from tissue samples, with individual time points obtained in separate animals or groups of animals, then the group statistics must

be derived from the scatter in the time course. Such an assumption convolves the noise from the NMR measurements and differences in the tissue samples.

Most software provides an estimate in the uncertainties of parameters based on a calculation that uses the fundamental theorem of calculus, which includes an assumption of vanishingly small noise. For many NMR spectroscopic experiments, the noise is not vanishingly small and is frequently 10–30 % of the steady-state isotopic labeling, depending on how the study is done and what metabolites are measured. Having violated the assumption that underlies the manner in which most analyses determine uncertainties in fitted parameters, we are left to find an alternative and to answer the question of how small noise must be if it is to be called ‘vanishingly small’.

One solution to the problem of non-negligible noise has been the implementation of the Monte Carlo estimation of scatter. In the Monte Carlo approach, noise with the same Gaussian distribution is added randomly to the least-squares fit to create a simulated, noisy data set, and that simulated set is fed into the model to derive a simulated set of parameters (Mason *et al.*, 1995; Mason *et al.*, 1992b). The process of generating simulated sets is repeated a hundred or a thousand times to generate a list of simulated fitted parameters that are used to create a histogram of the distribution of the fitted parameters based on the scatter in the original data. The list of simulated parameters can be used to derive a standard deviation, and the histogram can be used to evaluate whether or not the parameter’s value has a normal distribution of uncertainty.

As to the size of noise that violates the assumption, it depends on the model that is evaluated. The reliability of the calculus-based determinations can be evaluated by comparison of the standard methods, which include the assumption, and the Monte Carlo approach, which does not. As shown in Figure 4.6,

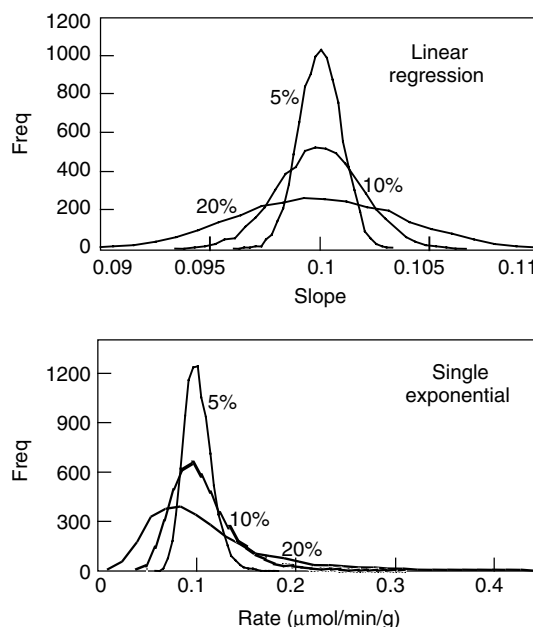


**Figure 4.6.** Relationships between the level of noise and the distribution of uncertainty for (top) the slope in linear regression analysis and (bottom) the rate constant obtained with least-squares fitting of a single-exponential function (bottom). Linear regression analysis maintains its ideal, normal distribution of uncertainty even with high levels of noise, whereas a single-exponential function rapidly deviates from the common theoretical treatment of a normal distribution of uncertainty.

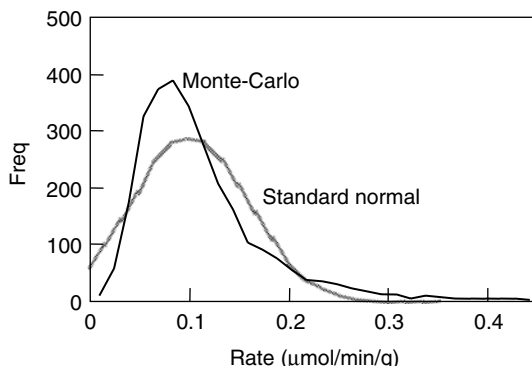


**Figure 4.7.** Comparison of distributions of normal and general Monte Carlo estimations of uncertainty for the rate determined from a single-exponential function for noise = 20 % of the steady-state value of the exponential.

the traditional error estimations from the linear regression analysis of Equations (4.1) and (4.2) track the Monte Carlo estimations indistinguishably across a wide range of noise levels. In contrast, the standard calculus-based error estimation for the rate in a single-exponential equation, which is similar to the form of the  $^{13}\text{C}$ -labeling time course of glutamate C4, deviates slightly from the ideal, normal distribution even when the noise exceeds 5 % of the steady-state signal amplitude. For a steady-state signal-to-noise level of 20 %, the deviation becomes severe.

When distributions are skewed as shown in Figure 4.6, the common estimates of noise express the uncertainty inadequately, as a standard deviation, which does not indicate the skewedness of the distribution, and that standard deviation is an underestimate of the true width of the distribution. The effects of misapplying the standard distribution estimates can yield either false positives or false negatives, depending on how the data are distributed. Figure 4.7 shows the true distribution for the rate derived using a single-exponential function together with the idealized estimate of the normal distribution. If the derived rate is compared to zero, the normal distribution leads to a false conclusion that the rate does not differ significantly from zero. In contrast, if the derived rate is compared to a value of  $0.25 \mu\text{mol}/\text{min}/\text{g}$ , the normal distribution leads to a false conclusion that the derived rate does differ significantly.

The practical reason for the skewedness is important to consider in the context of  $^{13}\text{C}$ -labeling studies. Suppose that one looks at the value of  $y = 1 - e^{-kt}$  where  $t = 20 \text{ min}$ . For  $k = 0, 0.03, 0.06, 0.09$ , and  $0.12$ , the value of  $y$  is  $0, 0.45, 0.70, 0.83$ , and  $0.91$ , which means that as the value of  $k$  rises, a given increment of noise in the data requires larger and larger values of  $k$  to achieve the same fit. So it goes in general with metabolic rate measurements, where the difference in the effects of two fast rates is not generally as great as the difference between two slower rates.

#### 4.4.4. Information Content in a $^{13}\text{C}$ -Labeling Experiment

Kinetic  $^{13}\text{C}$  MR studies are performed by observing the appearance of the  $^{13}\text{C}$  isotope over time in the sample of interest, and the entire time course is analyzed to obtain all of the information that is desired from the experiment. However, not all of the data points contain the same quantity of information about each parameter, and if an investigator knows which points are the most important in a study, it is sometimes possible to improve the experiment design. Therefore, it can be useful to understand how the information is distributed and how much information in total is obtained within the set of data. To

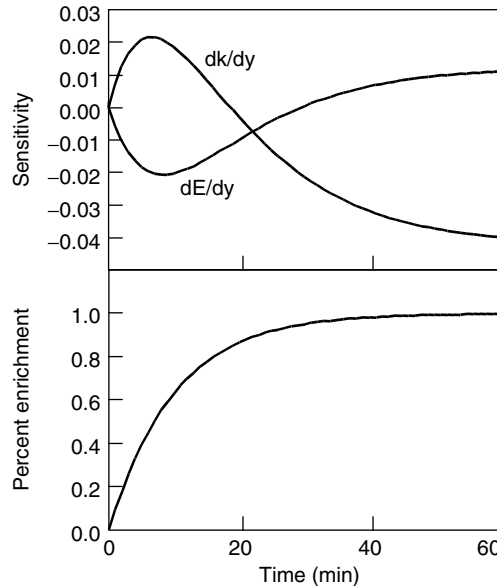


**Figure 4.8.** Sensitivities and enrichment for a single-exponential model of  $^{13}\text{C}$ -labeling. Top: sensitivities of the fitted values of the metabolic rate constant  $k$  and the source enrichment  $E$  as functions of time for a 60 min measurement of the time course of  $^{13}\text{C}$ -labeling of the product  $P$ . Bottom: time course of the percent enrichment corresponding to a single-exponential model.

arrive at a quantitative understanding of information, it is necessary to introduce the terms *sensitivity*, *data deflection*, and *relevance*.

*Sensitivity* is the influence that a data point exerts on the estimated value of a fitted parameter. That is, the sensitivity of a particular data point is the amount of change in the fitted parameter for a given change in the amplitude of the data point. Specifically, we can examine this idea with the single-exponential expression that was used for the previous example, where the respective sensitivities of the  $i$ th data point to the rate constant  $k = V/P$  and to the source enrichment  $E$  are  $dk/dy_i$  and  $dE/dy_i$ . We can estimate  $\Delta k/\Delta y_i$  and  $\Delta E/\Delta y_i$  for  $i = 1$  to  $n$  data points using values of  $\Delta y_i$  that are small enough to approximate  $dk/dy$  and  $dE/dy$ , in this case  $\Delta y = 0.01E$  (Figure 4.8).

The *noise sensitivity* is how much the parameters change with respect to the level of noise, or  $\Delta k_{\text{noise}}/\Delta y_{i,\text{noise}}$  and  $\Delta E_{\text{noise}}/\Delta y_{i,\text{noise}}$ . The *data deflection* of a data point is how much the point is moved over the ranges of possible values of the fitted parameters, which in the present example are  $V$  and  $E$ . They are approximated as  $\Delta y_{i,\text{deflection}}/\Delta E_{\text{deflection}}$  and  $\Delta y_{i,\text{deflection}}/\Delta k_{\text{deflection}}$ .

The *relevance* is defined as the reciprocal of the product of the noise sensitivity and the true deflection, minus one, or

$$R_{V,i} = \left( \frac{\Delta y_{i,\text{deflection}}}{\Delta k_{\text{deflection}}} \right) \times \left( \frac{\Delta k_{\text{noise}}}{\Delta y_{i,\text{noise}}} \right) - 1 \quad \text{and} \quad R_{E,i} = \left( \frac{\Delta y_{i,\text{deflection}}}{\Delta E_{\text{deflection}}} \right) \times \left( \frac{\Delta E_{\text{noise}}}{\Delta y_{i,\text{noise}}} \right) - 1 \quad (4.8)$$

A relevance ratio of 0 or less for  $V/P$  means that despite any sensitivity of the value of the parameter  $V$  to the amplitude of the data, the noise obscures the relevant effects and there is no information about  $V$  at that the  $i$ th data point. Besides a point-by-point analysis, the relevance ratio can be calculated for the

entire data set, as well, according to

$$R_{V,i} = \sqrt{\sum_{i=1}^n \left( \frac{\Delta y_{i,\text{deflection}}}{\Delta k_{\text{deflection}}} \right)^2 \times \sum_{i=1}^n \left( \frac{\Delta k_{\text{noise}}}{\Delta y_{i,\text{noise}}} \right)^2} - 1,$$

$$R_{E,i} = \sqrt{\sum_{i=1}^n \left( \frac{\Delta y_{i,\text{deflection}}}{\Delta E_{\text{deflection}}} \right)^2 \times \sum_{i=1}^n \left( \frac{\Delta E_{\text{noise}}}{\Delta y_{i,\text{noise}}} \right)^2} - 1 \quad (4.9)$$

The grouped approach in Equation (4.9) allows the amount of information in studies to be compared quantitatively, taking into account the sensitivity of the measurement and the level of noise in the study. The individual approach that is embodied by Equation (4.8) allows the amount of information to be compared not only across studies but among the time points in an individual experiment.

Consider, for example, the two-compartment model of Figure 4.1. Two methods to measure the rate of anaplerosis relative to the rate of glutamine synthesis are (1) the measurement of the time courses of isotopic labeling of glutamate and glutamine C4 during an infusion of  $[1-^{13}\text{C}]$ glucose (Gruetter *et al.* 2001; Shen *et al.*, 1999) and (2) the measurement of steady-state glutamate and glutamine C2 and C3 labeling while supplying  $[2-^{13}\text{C}]$ glucose (Kanamatsu and Tsukada 1999; Sibson *et al.*, 1998; Taylor *et al.*, 1996). Figures 4.9 and 4.10 show the sensitivities and time courses for the ratio of  $V_{\text{ana}}/V_{\text{gln}}$  over time for the  $[1-^{13}\text{C}]$ glucose and  $[2-^{13}\text{C}]$ glucose measurements. It is clear that most of the information sensitivity about

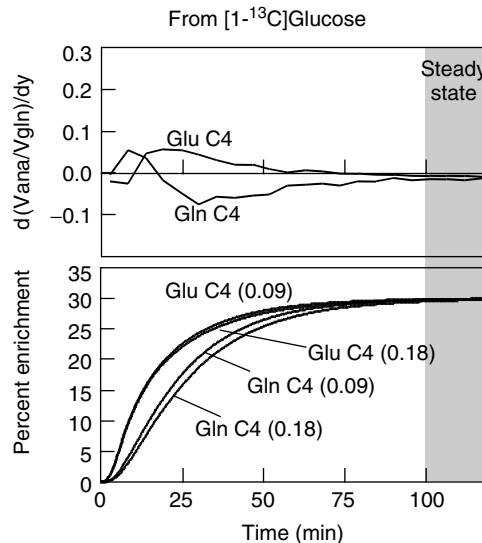


**Figure 4.9.** Time courses of  $^{13}\text{C}$ -labeling of glutamate and glutamine and the sensitivities of the ratio of  $V_{\text{ana}}/V_{\text{gln}}$  to the observed  $^{13}\text{C}$  enrichments of glutamate and glutamine during infusions of  $[1-^{13}\text{C}]$ glucose. The simulations were done for  $V_{\text{ana}}/V_{\text{gln}} = 0.09$  and  $0.18$ , and the shaded portion covers the time when the labeling approaches an isotopic steady state. Bottom: the lack of difference in labeling with the two values of  $V_{\text{ana}}/V_{\text{gln}}$  demonstrate a low sensitivity of the data to  $V_{\text{ana}}/V_{\text{gln}}$ . Top: for times less than 15 min after the start of the glucose infusion, positive deviations in the glutamine C4 enrichment lead to higher values for  $V_{\text{ana}}/V_{\text{gln}}$ , and after that, the opposite is true. The steady-state portion of the measurement shows almost no difference in the time courses, and that fact is reflected in the low steady-state sensitivity shown in the top graph.

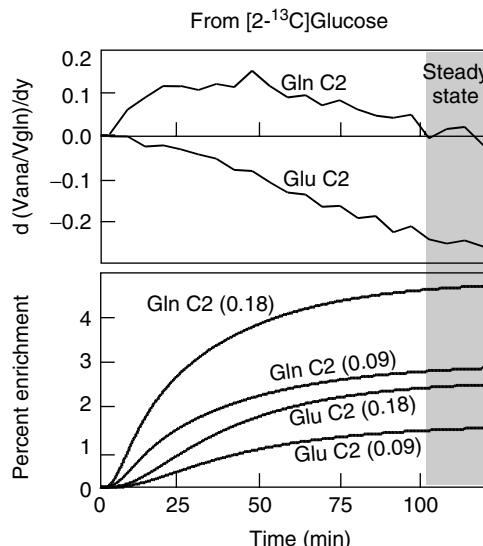


**Figure 4.10.** Time courses of  $^{13}\text{C}$ -labeling of glutamate and glutamine and the sensitivities of the ratio of  $V_{\text{ana}}/V_{\text{gln}}$  to the observed  $^{13}\text{C}$  enrichments of glutamate and glutamine during infusions of  $[2-^{13}\text{C}]$ glucose. The simulations were done for  $V_{\text{ana}}/V_{\text{gln}} = 0.09$  and  $0.18$ , and the shaded portion covers the time when the labeling approaches an isotopic steady state. Bottom: there is a marked difference in labeling with the two values of  $V_{\text{ana}}/V_{\text{gln}}$ , demonstrating a low sensitivity of the data to  $V_{\text{ana}}/V_{\text{gln}}$ . Accordingly, the sensitivity to  $V_{\text{ana}}/V_{\text{gln}}$  is high (top). The steady-state portion of the measurement shows a large difference, primarily in the C2-labeling of glutamate.

$V_{\text{ana}}/V_{\text{gln}}$  resides in the early parts of the C1-glucose study, although the sensitivity to noise is so high at that point that there is little relevance of the measurement to those parameters. In contrast, the C2-glucose study shows a distribution of sensitivity and relevance across the time course, with a large quantity of information available during the isotopic steady-state portion of the measurement. The ability to acquire the data at isotopic steady state means that a subject can be infused in relative comfort, outside the scanner, entering the magnet once an isotopic steady-state is achieved, the measurement can go on for an hour or even more, depending on how long a subject can be kept comfortably in the scanner. On an individual basis for human studies, the scatter in glutamate and glutamine C4 during are typically 1.7 and 3.8 % in 5 min of accumulation of signal, and the relevances of  $V_{\text{ana}}/V_{\text{gln}}$  for the time-dependent  $[1-^{13}\text{C}]$ glucose study and  $[2-^{13}\text{C}]$ glucose steady-state measurements are  $-0.68$  and  $+0.85$ , respectively. On a subject-by-subject basis, it should be possible to measure the value of  $V_{\text{ana}}/V_{\text{gln}}$  using the  $[2-^{13}\text{C}]$ glucose protocol. In contrast, the C1-labeled glucose protocol has no relevance for individual subjects. If the noise level were reduced by four- to five-fold, the  $[1-^{13}\text{C}]$ glucose protocol would have some relevance for measuring  $V_{\text{ana}}/V_{\text{gln}}$ .

## 4.5. CONCLUSION

In this review we have covered the basic concepts and issues in fitting  $^{13}\text{C}$  NMR data obtained from the brain *in vivo* to determine metabolic rates. The limiting factors in determining metabolic rates with  $^{13}\text{C}$  MRS are sensitivity and the deconvolution of multiple metabolic compartments. As shown above, it is useful to evaluate distributions of uncertainty in the fitted parameters. This feature is important because of effects of non-normal distributions of uncertainty when analyzing data. When working *in vivo*, it is common to obtain skewed distributions of uncertainty, which can cause a group's standard deviation to be

overestimated and obscure significant differences. By estimating the effects of noise on the distributions of uncertainty before performing most of the experiments in a set of studies, one might identify specific portions of the experimental protocol that should be improved to narrow the distribution of uncertainty to the necessary precision.

Mathematical modeling provides ways to quantify which are the most sensitive portions of a  $^{13}\text{C}$  isotopic labeling study. A fitted variable usually has unequal sensitivities to the  $^{13}\text{C}$ -labeling time courses of different metabolites throughout a kinetic labeling study, and a study may be designed to emphasize the data acquisition in the most sensitive portions of an infusion protocol, while de-emphasizing the less sensitive portions of the study.

A mathematical evaluation of the sensitivity also permits the calculation of the relevance of an experiment, where the relevance is a measurement of the ability of a study to provide a meaningful estimate of the value of a parameter from a fit to the isotopic time course data. The relevance provides an objective way to compare the effectiveness of various experimental protocols.

## REFERENCES

Attwood, P. V., Tipton, P. A., and Cleland, W. W. (1986). *Biochemistry* **25**: 8197

Badar-Goffer, R. S., Bachelard, H. S., and Morris, P. G. (1990) Cerebral metabolism of acetate and glucose studied by  $^{13}\text{C}$ -n.m.r. spectroscopy. *Biochem J* **266**: 133–139

Badar-Goffer, R. S., Ben-Yoseph, O., Bachelard, H. S., and Morris, P. G. (1992) Neuronal-glial metabolism under depolarizing conditions—a  $^{13}\text{C}$ -n.m.r. study under depolarizing conditions. *Biochem J* **282**: 225–230

Beckmann, N., Turkalj, I., Seelig, J., and Keller, U. (1991)  $^{13}\text{C}$  NMR for the assessment of human brain glucose metabolism *in vivo*. *Biochemistry* **30**: 6362–6366

Behar, K. L., Petroff, O. A. C., Prichard, J. W., Alger, J. R., and Shulman, R. G. (1986) Detection of metabolites in rabbit brain by  $^{13}\text{C}$  NMR spectroscopy following administration of [1- $^{13}\text{C}$ ]glucose. *Magn Reson Med* **3**: 911–920

Berl, S., Takagaki, G., Clarke, D. D., and Waelsch, H. (1962) Carbon dioxide fixation in the brain. *J Biol Chem* **237**: 2570–2573

Bluml, S., Moreno, A., Hwang, J. H., and Ross, B. D. (2001a) 1-(13)C glucose magnetic resonance spectroscopy of pediatric and adult brain disorders. *NMR Biomed* **14**: 19–32

Bluml, S., Moreno-Torres, A., and Ross, B. D. (2001b) [1-13C]glucose MRS in chronic hepatic encephalopathy in man. *Magn Reson Med* **45**: 981–993

den Hollander, J. A., Brown, T. R., Ugurbil, K., and Shulman, R. G. (1979)  $^{13}\text{C}$  nuclear magnetic resonance studies of anaerobic glycolysis in suspensions of yeast cells. *Proc Natl Acad Sci USA* **76**: 6096–6100

Dzubow, L., and Garfinkel, D. (1970) A simulation study of brain compartments. II. Atom-by-atom simulation of the metabolism of specifically labeled glucose and acetate. *Brain Res* **23**: 407–417

Fitzpatrick, S. M., Hetherington, H. P., Behar, K. L., and Shulman, R. G. (1990) The flux from glucose to glutamate in the rat brain *in vivo* as determined by  $^1\text{H}$ -observed/ $^{13}\text{C}$ -edited NMR spectroscopy. *J Cereb Blood Flow Metab* **10**: 170–179

Gruetter, R., Novotny, E. J., Boulware, S. D., Mason, G. F., Rothman, D. L., Shulman, G. I., Prichard, J. W., and Shulman, R. G. (1994) Localized  $^{13}\text{C}$  NMR spectroscopy in the human brain of amino acid labeling from D-[1- $^{13}\text{C}$ ]glucose. *J Neurochem* **63**: 1377–1385

Gruetter, R., Seaquist, E. R., and Ugurbil, K. (2001) A mathematical model of compartmentalized neurotransmitter metabolism in the human brain. *Am J Physiol Endocrinol Metab* **281**: E100–112

Hawkins, R. A., and Mans, A. M. (1983) Intermediary metabolism of carbohydrates and other fuels. I. In: *Biochem J* (Lajtha A, ed.), New York: Plenum Press, pp 259–294

Hawkins, R. A., Mans, A. M., Davis, D. W., Viña, J. R., and Hibbard, L. S. (1985) Cerebral glucose use measured with [ $^{14}\text{C}$ ] glucose labeled in the 1, 2, or 6 position. *Am J Physiol* **248**: C170–C176

Kanamatsu, T., and Tsukada, Y. (1999) Effects of ammonia on the anaplerotic pathway and amino acid metabolism in the brain: an ex vivo  $^{13}\text{C}$  NMR spectroscopic study of rats after administering [2- $^{13}\text{C}$ ] glucose with or without ammonium acetate. *Brain Res* **841**: 11–19

Künnecke, B., Cerdán, S., and Seelig, J. (1993) Cerebral metabolism of [1,2-<sup>13</sup>C<sub>2</sub>]glucose and [U-<sup>13</sup>C<sub>4</sub>]3-hydroxybutyrate in rat brain as detected by <sup>13</sup>C NMR spectroscopy. *NMR Biomed* **6**: 264–277

Lebon, V., Petersen, K. F., Cline, G. W., Shen, J., Mason, G. F., Dufour, S., Behar, K. L., Shulman, G. I., and Rothman, D. L. (2002) Astroglial contribution to brain energy metabolism in humans revealed by <sup>13</sup>C nuclear magnetic resonance spectroscopy: elucidation of the dominant pathway for neurotransmitter glutamate repletion and measurement of astrocytic oxidative metabolism. *J Neurosci* **22**: 1523–1531

Lewandowski, E. D., Yu, X., LaNoue, K. F., White, L. T., Doumen, C., and O'Donnell, J. M. (1997) Altered metabolite exchange between subcellular compartments in intact postischemic rabbit hearts. *Circ Res* **81**: 165–175

Mason, G. F., Behar, K. L., Rothman, D. L., and Shulman, R. G. (1992a) NMR determination of intracerebral glucose concentration and transport kinetics in rat brain *in vivo*. *J Cereb Blood Flow Metab* **12**: 448–455

Mason, G. F., Falk Petersen, K., de Graaf, R. A., Kanamatsu, T., Otsuki, T., and Rothman, D. L. (2003) A comparison of <sup>13</sup>C NMR measurements of the rates of glutamine synthesis and the tricarboxylic acid cycle during oral and intravenous administration of [1-<sup>13</sup>C]glucose. *Brain Res Protocols* **10**(3): 181–190

Mason, G. F., Gruetter, R., Rothman, D. L., Behar, K. L., Shulman, R. G., and Novotny, E. J. (1995) Simultaneous determination of the rates of the TCA cycle, glucose utilization, alpha-ketoglutarate/glutamate exchange, and glutamine synthesis in human brain by NMR. *J Cereb Blood Flow Metab* **15**: 12–25

Mason, G. F., Martin, D. L., Martin, S. B., Manor, D., Sibson, N. R., Patel, A., Rothman, D. L., and Behar, K. L. (2001) Decrease in GABA synthesis rate in rat cortex following vigabatrin administration correlates with the decrease in GAD67 protein. *Brain Res* **914**: 81–91

Mason, G. F., Rothman, D. L., Behar, K. L., and Shulman, R. G. (1992b) NMR determination of TCA cycle rate and  $\alpha$ -ketoglutarate/glutamate exchange rate in rat brain. *J Cereb Blood Flow Metab* **12**: 434–447

Melzer, E., and Schmidt, H.-L. (1987). *J Biol Chem* **262**: 8159

Moreno, A., Bluml, S., Hwang, J. H., and Ross, B. D. (2001a) Alternative 1-(13)C glucose infusion protocols for clinical (13)C MRS examinations of the brain. *Magn Reson Med* **46**: 39–48

Moreno, A., Ross, B. D., and Bluml, S. (2001b) Direct determination of the N-acetyl-L-aspartate synthesis rate in the human brain by (13)C MRS and [1-(13)C]glucose infusion. *J Neurochem* **77**: 347–350

Pardridge, W. M., and Oldendorf, W. H. (1977) Transport of metabolic substrates through the blood-brain barrier. *J Neurochem* **28**: 5–12

Rothman, D. L., Behar, K. L., Hyder, F., and Shulman, R. G. (2003) *In vivo* NMR studies of the glutamate neurotransmitter flux and neuroenergetics: implications for brain function. *Annu Rev Physiol* **65**: 401–427

Rothman, D. L., Novotny, E. J., Shulman, G. I., Howseman, A. M., Petroff, O. A. C., Mason, G., Nixon, T., Hanstock, C. C., Prichard, J. W., and Shulman, R. G. (1992) <sup>1</sup>H-[<sup>13</sup>C] NMR measurements of [4-<sup>13</sup>C]glutamate turnover in human brain. *Proc Natl Acad Sci USA* **89**: 9603–9606

Shen, J., Petersen, K. F., Behar, K. L., Brown, P., Nixon, T. W., Mason, G. F., Petroff, O. A., Shulman, G. I., Shulman, R. G., and Rothman, D. L. (1999) Determination of the rate of the glutamate/glutamine cycle in the human brain by *in vivo* <sup>13</sup>C NMR. *Proc Natl Acad Sci USA* **96**: 8235–8240

Shephard, G. M. (1994) *The Synaptic Organization of the Brain*. Oxford: Oxford University Press

Sherry, A. D., Malloy, C. R., Roby, R. E., Rajagopal, A., and Jeffrey, F. M. (1988) Propionate metabolism in the rat heart by <sup>13</sup>C n.m.r. spectroscopy. *Biochem J* **254**: 593–598

Sibson, N. R., Dhankhar, A., Mason, G. F., Rothman, D. L., Behar, K. L., and Shulman, R. G. (1998) Stoichiometric coupling of brain glucose metabolism and glutamatergic neuronal activity. *Proc Natl Acad Sci USA* **95**: 316–321

Sibson, N. R., Mason, G. F., Shen, J., Cline, G. W., Herskovits, A. Z., Wall, J. E. M., Behar, K. L., Rothman, D. L., and Shulman, R. G. (2001) *In vivo* <sup>13</sup>C NMR measurement of neurotransmitter glutamate cycling, anaplerosis and TCA cycle flux in rat brain during [2-<sup>13</sup>C]glucose infusion. *J Neurochem* **76**: 975–989

Sillerud, L. O., Alger, J. R., and Shulman, R. G. (1981) High-resolution protein NMR studies of intracellular metabolites in yeast using <sup>13</sup>C decoupling. *J Magn Reson, Ser B* **45**: 142–150

Sonnewald, U., Gribbestad, I. S., Westergaard, N., Krane, J., Unsgård, G., Petersen, S. B., and Schousboe, A. (1991) First direct demonstration of preferential release of citrate from astrocytes using [<sup>13</sup>C] NMR spectroscopy of cultured neurons and astrocytes. *Neurosci Lett* **128**: 235–239

Sonnewald, U., Westergaard, N., Jones, P., Taylor, A., Bachelard, H. S., and Schousboe, A. (1996) Metabolism of [U-<sup>13</sup>C<sub>5</sub>] glutamine in cultured astrocytes studied by NMR spectroscopy: first evidence of astrocytic pyruvate recycling. *J Neurochem* **67**: 2566–2572

Szczepaniak, L., Babcock, E. E., Malloy, C. R., and Sherry, A. D. (1996) Oxidation of acetate in rabbit skeletal muscle: detection by <sup>13</sup>C NMR spectroscopy *in vivo*. *Magn Reson Med* **36**: 451–457

Taylor, A., McLean, M., Morris, P., and Bachelard, H. S. (1996) Approaches to studies on neuronal/glial relationships by <sup>13</sup>C-MRS analysis. *Dev Neurosci* **18**: 434–442

Tipton, P. A., and Cleland, W. W. (1988). *Biochemistry* **27**: 4325

Van den Berg, C. J., and Garfinkel, C. D. (1971) A simulation study of brain compartments: metabolism of glutamate and related substances in mouse brain. *Biochem J* **123**: 211–218

Van den Berg, C. J., Krzalic, L. J., Mela, P., and H. Waelsch. (1970) Compartmentation of glutamate metabolism in brain: Evidence for the existence of two different tricarboxylic acid cycles in brain. *Biochem J* **113**: 281–290

Waagepetersen, H. S., Sonnewald, U., Larsson, O. M., and Schousboe, A. (2000) Compartmentation of TCA cycle metabolism in cultured neocortical neurons revealed by <sup>13</sup>C MR spectroscopy. *Neurochem Int* **36**: 349–358

Yu, X., White, L. T., Doumen, C., Damico, L. A., LaNoue, K. F., Alpert, N. M., and Lewandowski, E. D. (1995) Kinetic analysis of dynamic <sup>13</sup>C NMR spectra: metabolic flux, regulation, and compartmentation in hearts. *Biophys J* **69**: 2090–2102

## **Section B**

### Neuroenergetics and Activity



# 5

## Cerebral Energetics and Neurotransmitter Fluxes

**Nicola R. Sibson**

*Experimental Neuroimaging Group Department of Biochemistry, University of Oxford, South Parks Road, Oxford OX1 3QU, UK*

---

5.1	$^{13}\text{C}$ MRS Measurements of Cerebral Energy Metabolism	76
5.1.1	Neuronal Energy Metabolism	76
5.1.2	Contributions of Astrocytes and GABAergic Neurons to Cerebral Energy Metabolism	78
5.2	MRS Measurements of Neurotransmitter Fluxes	81
5.2.1	Measuring the Glutamate–Glutamine Cycle	82
5.2.2	Validating the $^{13}\text{C}$ MRS Measurement of Glutamate–Glutamine Cycling	85
5.3	Energetic Requirements of Neurotransmission	89
5.3.1	Glutamate as a Mediator of Neurometabolic Coupling	91
5.3.2	Implications for Studies of Human Brain	92
5.4	Summary	93

---

One of the major advantages of MRS is that reaction kinetics, and hence metabolic rates, can be measured noninvasively *in vivo*. This ability of MRS particularly lends it to biochemical studies of the brain which are largely inaccessible *in vivo* by other methodologies.  $^{13}\text{C}$  MRS, in particular, has been used extensively in recent years to measure the rate of cerebral oxidative glucose consumption *in vivo* and, more recently, to measure certain neurotransmitter fluxes (glutamate, GABA) that are intrinsically linked to neuronal activity. The term ‘neuronal activity’ applies to a spectrum of energy requiring processes, which include not only neurotransmitter release, uptake and recycling, but also action potential propagation, restoration

and maintenance of membrane potentials, and vesicular recycling. Consequently, it is to be expected perhaps that neuronal activity and energy metabolism should be tightly coupled in the brain, and indeed it was over a century ago that Sherrington first suggested that such a coupling exists. Nonetheless, the energetic cost of neuronal activity, and the fraction of total cerebral energy consumption that this represents, has long been debated and is only now being resolved. Furthermore, the relationship between neuronal activity and energy metabolism has implications for the interpretation of data from functional neuro-imaging studies, which mostly rely on an implied relationship between the measured parameters (glucose consumption, oxygen consumption or blood flow) and neuronal activity. The  $^{13}\text{C}$  MRS studies discussed in this chapter have begun to provide answers to some of these key biochemical questions that have remained elusive for many decades. This chapter covers recent *in vivo*  $^{13}\text{C}$  MRS studies in which measurements of cerebral energy metabolism and neurotransmitter fluxes have been made, and which address the issue of the relationship between neuronal activity and cerebral energetics. The majority of studies that are discussed have been performed in rat brain, but where analogous studies in human brain are available these are also considered.

## 5.1. $^{13}\text{C}$ MRS MEASUREMENTS OF CEREBRAL ENERGY METABOLISM

As discussed in the introductory chapter, glucose is the primary substrate for energy metabolism in the brain *in vivo* (1). Each glucose molecule undergoes nonoxidative (anaerobic) glycolysis to yield two molecules of pyruvate, which are subsequently oxidized to  $\text{CO}_2$  via the tricarboxylic acid (TCA) or Krebs cycle. The oxidative steps of glucose metabolism are generally considered to contribute  $\sim 36$  of a total of  $\sim 38$  high-energy ATP molecules generated during metabolism of a single glucose molecule, whilst just two ATP molecules are contributed by the glycolytic pathway. Approximately 15 % of glucose that undergoes glycolysis is converted to lactate and does not enter the TCA cycle, although this may be balanced by a corresponding uptake and oxidative metabolism of ketone bodies.

Techniques by which cerebral glucose metabolism ( $\text{CMR}_{\text{glc}}$ ) can be measured, either globally or regionally, have been available for some time – either by snapshot *in vivo* techniques such as autoradiography or true *in vivo* techniques such as arterio-venous difference measurements or positron emission tomography (PET). However, it is highly likely that the energetic requirements of the various cell populations of the brain will differ considerably in their energetic requirements and, hence, metabolic rates. Consequently, there is a need for measurement methods that can specifically target the different cell populations in the brain. It is at this level that *in vivo*  $^{13}\text{C}$  MRS comes into its own, primarily as a consequence of two main factors – firstly, the chemical specificity of the technique by which the chemical shift of each  $^{13}\text{C}$  peak identifies a specific carbon position within a particular molecule, and, secondly, the restricted localization of certain enzymes to specific cell types. Glutamate is the major excitatory neurotransmitter in the mammalian brain, whilst  $\gamma$ -aminobutyric acid (GABA) is the primary inhibitory transmitter. In contrast, glutamine is synaptically inert, yet plays a key role in the metabolism of both neurotransmitters. The brain pools of glutamate, GABA and glutamine have been shown to be localized within glutamatergic neurons, GABAergic neurons, and astrocytes, respectively (under nonpathological conditions), and it is the localization to specific cell types of key enzymes involved in the metabolism of these molecules that enables  $^{13}\text{C}$  MRS to separate the energetic requirements of these cell populations. In this section, we will discuss how  $^{13}\text{C}$  MRS can be used to measure pathways of energy metabolism in the cerebral cortex.

### 5.1.1. Neuronal Energy Metabolism

As explained in previous chapters, the general approach adopted to measure metabolic rates by  $^{13}\text{C}$  MRS is to intravenously infuse a  $^{13}\text{C}$ -labeled substrate (e.g. glucose, acetate) which will easily pass through the blood–brain barrier and be metabolized within the brain. Over time, a variety of metabolite pools within the brain become enriched with  $^{13}\text{C}$ , and these can be detected by  $^{13}\text{C}$  MRS. A number of studies of human

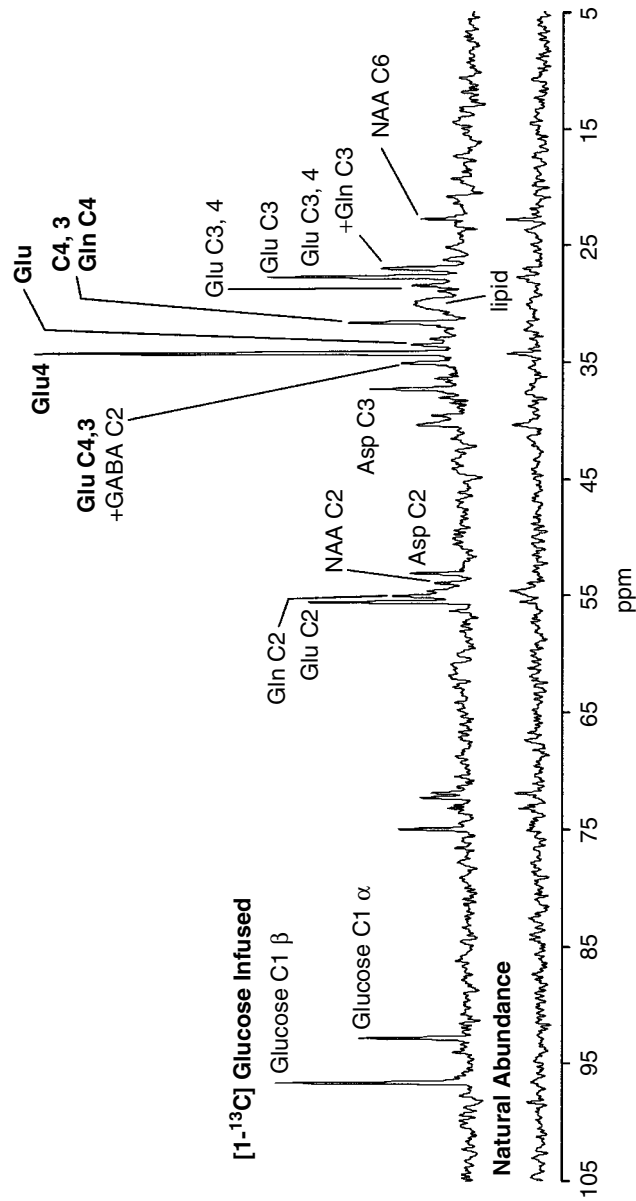


**Figure 5.1.** Example of a  $^1\text{H}$ -decoupled, NOE-enhanced  $^{13}\text{C}$  MRS spectrum acquired from human cerebral cortex over a period of  $\sim 60$  min during infusion of  $[1\text{-}^{13}\text{C}]$ glucose. Resonances from several key metabolites coupled to energy and neurotransmitter metabolism are visible including, glutamate, glutamine, GABA, aspartate and NAA.

brain (2–5) have now demonstrated that several key metabolites coupled to brain energy metabolism can be detected using  $^{13}\text{C}$  MRS, including glutamate, glutamine, GABA, aspartate and NAA (see Figure 5.1). As described in Chapter 4, the development of metabolic models has enabled determination of absolute metabolic rates from the time courses of isotopic labeling in the brain.

The most commonly used isotopic precursor for both  $^{13}\text{C}$  and  $^1\text{H}$ – $^{13}\text{C}$  MRS studies is [ $1$ – $^{13}\text{C}$ ]glucose. The original MRS measurements of metabolic fluxes in the brain *in vivo* were of the rates of the tricarboxylic acid (TCA) cycle and glucose oxidation using  $^1\text{H}$ – $^{13}\text{C}$  MRS to follow the flux of  $^{13}\text{C}$  isotope from [ $1$ – $^{13}\text{C}$ ]glucose into cerebral metabolites (6). The [ $1$ – $^{13}\text{C}$ ]glucose is initially metabolized to pyruvate via the glycolytic pathway, which results in labeling of pyruvate at C-3. The label is then transferred to the TCA cycle by the sequential actions of pyruvate dehydrogenase (PDH) and citrate synthase. When the label reaches  $\alpha$ -ketoglutarate (C-4) it is transferred to glutamate (C-4) by the high activity exchange reactions of the amino acid transaminases and mitochondrial/cytosolic transporters. Since the exchange activity of these transaminases is rapid, labeling of the  $\alpha$ -ketoglutarate and glutamate pools is in close equilibrium. Thus, the flux of  $^{13}\text{C}$  isotope from [ $1$ – $^{13}\text{C}$ ]glucose into [ $4$ – $^{13}\text{C}$ ]glutamate (shown schematically in Figure 5.2(A)) enables quantitative determination of the TCA cycle rate (2, 3, 5, 7–10). Since the TCA cycle is intrinsically linked to oxidative phosphorylation, and glucose is the primary fuel of oxidative metabolism in the brain, the measurements of the TCA cycle may be converted to measurements of glucose oxidation using known stoichiometries (7, 9).

However, we now come to the question of which specific cell type, or group of cell types, are we measuring the metabolism of? All of the different cell populations of the brain contain the necessary enzymes for glycolysis, the TCA cycle and oxidative phosphorylation. Consequently, one might assume that the rate of oxidative glucose metabolism that is obtained by this measurement is an average of the metabolic rates of all cell types. However, since the measurement is made by following the flux of  $^{13}\text{C}$  label into glutamate the weighting of this measurement to the various cell types is determined to a large extent by the relative pool sizes of glutamate in those different cell populations. The existence of more than one glutamate pool in the brain was determined several decades ago in  $^{14}\text{C}$  tracer studies (11), and initially two primary glutamate pools were identified, one large and one small. Based on kinetic and immunohistochemical staining studies the large glutamate pool is believed to correspond to the glutamate pool in glutamatergic neurons (7, 12, 13), whilst the small one has been shown to be associated with glial-specific enzymes and pathways. The difference in sizes of these pools is of the order of 100-fold, and, therefore, the glutamate pool observed by  $^{13}\text{C}$  MRS is generally attributed to the large glutamate pool within glutamatergic neurons. Consequently, the weighting of the  $^{13}\text{C}$  measurement of oxidative glucose consumption obtained by infusion of [ $1$ – $^{13}\text{C}$ ]glucose is strongly weighted towards the glutamatergic neuronal population.

The rate of glucose oxidation in glutamatergic neurons has been determined in numerous studies from both  $^{13}\text{C}$  and  $^1\text{H}$ – $^{13}\text{C}$  MRS measurements of cortical glutamate labeling during infusion of [ $1$ – $^{13}\text{C}$ ]glucose in animals (6, 9, 14–21) and humans (2–5, 7–9, 22). Comparison of the rates of neuronal glucose oxidation (0.25–0.50  $\mu\text{mol}/\text{min}/\text{g}$ ) measured in these studies with conventional arterio-venous difference and PET measurements of total glucose consumption indicates that the major fraction (60–90 %) of total glucose oxidation is associated with glutamatergic neurons in both the rat and human brain.

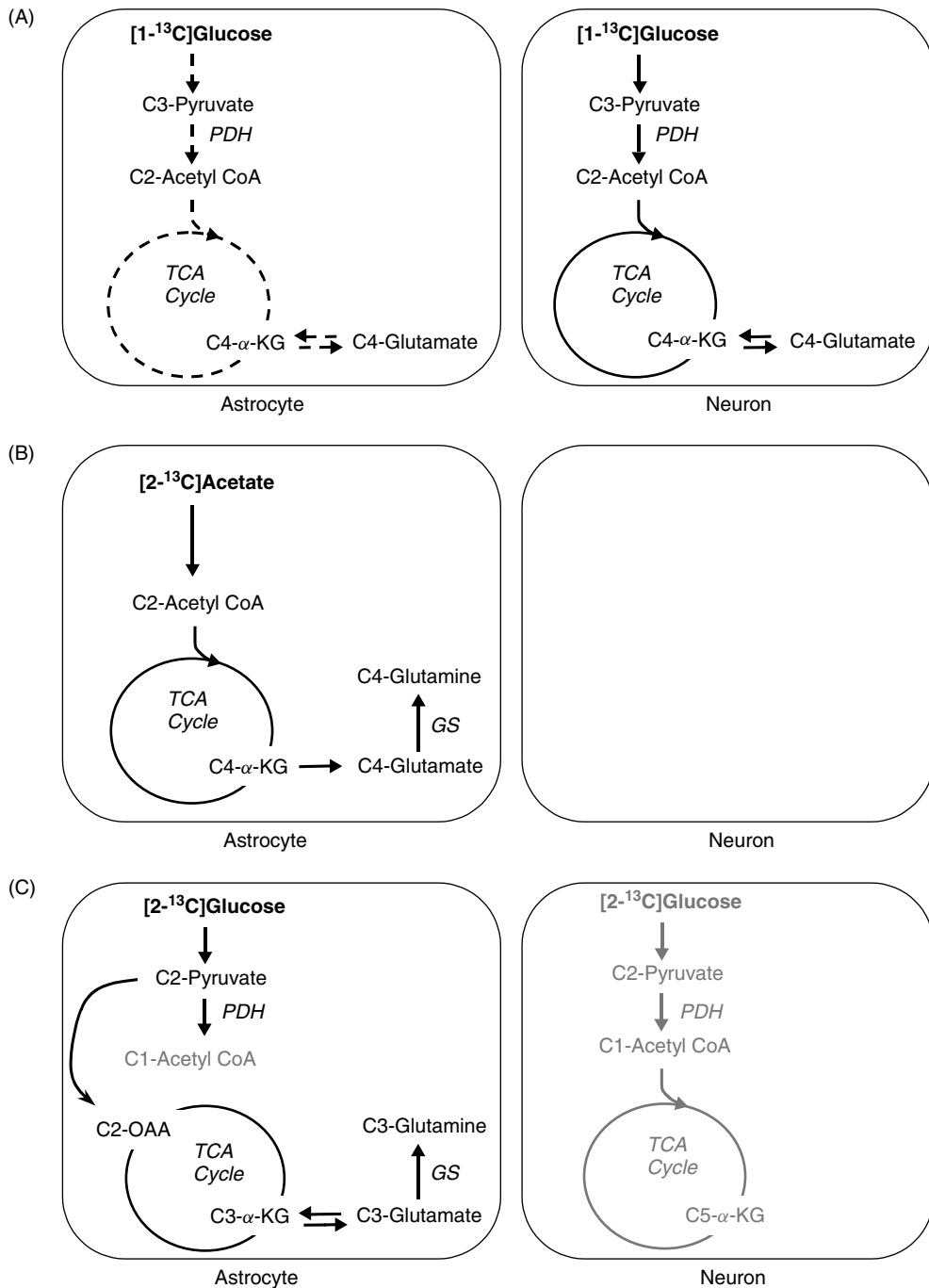
### 5.1.2. Contributions of Astrocytes and GABAergic Neurons to Cerebral Energy Metabolism

However, as mentioned above, glutamate is present in all brain cells including astrocytes, and also GABAergic neurons. Although the concentrations of glutamate in these other cell types are considerably lower than in glutamatergic neurons, the contributions of these cell populations to cerebral glucose metabolism cannot

be entirely ignored. The rate of glucose oxidation in astrocytes has long been a subject of controversy in studies of cerebral metabolism. Early estimates range from 10% to over 50% of total glucose oxidation (1).  $^{13}\text{C}$  MRS may be used to measure the rate of astrocytic glucose oxidation based on the localization of the enzyme glutamine synthetase to astrocytes (23). As a result, the rate of the astrocytic TCA cycle can be calculated based on the labeling of glutamine from astrocytic glutamate. However, it is difficult to obtain this metabolic rate with the commonly used [ $1-^{13}\text{C}$ ]glucose precursor since the label enters glutamate in both neurons and astrocytes. Consequently, owing to the differences in pool sizes (neuronal glutamate  $\approx$  10 mM, astrocytic glutamate  $< 1$  mM), as discussed above, the labeling observed *in vivo* is dominated by the neuronal compartment. As a consequence, label subsequently entering glutamine is largely derived from the neuronal glutamate pool and predominantly reflects pathways other than the astrocytic TCA cycle (see below). A solution to this problem is to use alternatively labeled isotopic precursors that yield data specific to astrocytic metabolism.

The use of alternative precursors to [ $1-^{13}\text{C}$ ]glucose in combination with  $^{13}\text{C}$  and  $^{1}\text{H}-^{13}\text{C}$  MRS has been common practice in both *in vitro* and *ex vivo* studies for over a decade (for review see Bachelard (24) and Cruz and Cerdan (25)) and provides a unique approach to the study of metabolic compartmentation. One isotopic precursor that has been used extensively, often in combination with [ $1-^{13}\text{C}$ ]glucose to investigate differences between neuronal and glial metabolism, is [ $2-^{13}\text{C}$ ]acetate. Although both neurons and astrocytes contain the enzyme for acetate catabolism, acetyl CoA synthetase, transport of acetate by astrocytes is much greater [Waniewski, 1998 #59]. Consequently, acetate is considered to be an astrocyte-specific substrate. With [ $2-^{13}\text{C}$ ]acetate the  $^{13}\text{C}$  label enters the astrocytic TCA cycle via acetyl CoA, passes into the astrocytic glutamate pool and, subsequently, into glutamine (see Figure 5.2(B)). Comparison of labeling patterns following infusion of [ $1-^{13}\text{C}$ ]glucose and [ $2-^{13}\text{C}$ ]acetate has yielded valuable information about cellular compartmentation and neuronal–glial interactions (26–33). Few measurements of absolute metabolic rates from such studies have been reported, although in a recent review the contribution of astrocytic glucose oxidation to total glucose oxidation was estimated to be 20–30% (25). Consequently, the neuronal contribution was calculated to be 70–80% of total glucose oxidation, which is similar to the findings of the *in vivo* studies described above.

Despite the longstanding use of alternative isotopic precursors *in vitro*, they have only recently begun to be utilized *in vivo*. In a recent study of human cerebral cortex, [ $2-^{13}\text{C}$ ]acetate was used to determine the rate of astrocytic glucose oxidation and it was found to account for  $\sim 15\%$  of total glucose oxidation (34). Similar *in vivo* studies in rats have recently been reported using [ $2-^{13}\text{C}$ ]glucose as the isotopic precursor (19, 35). Although [ $2-^{13}\text{C}$ ]glucose will be metabolized by both astrocytes and neurons, this precursor acts as an astrocyte-specific precursor as a consequence of the anaplerotic pyruvate carboxylase pathway, which is localized exclusively to astrocytes in the adult brain (36–38). Via this pathway, label from [ $2-^{13}\text{C}$ ]glucose is brought into the C-3 (and C-2) positions of the small astrocytic glutamate pool (19, 35, 36, 39), while label flux through either the neuronal or astrocytic PDH pathway does not contribute to labeling in these positions (see Figure 5.2(C)). In practice, the  $^{13}\text{C}$  label is first observed in glutamine (C-3 and C-2) owing to the small size, and low MRS sensitivity, of the astrocytic glutamate and TCA cycle intermediate pools, and this labeling flux can be used to obtain measurements of astrocytic metabolism. To date, absolute measurements of astrocytic metabolism have only been obtained under hyperammonemic conditions owing to the low level of isotopic labeling achieved under normoammonemic conditions (19). Hyperammonemia increases the astrocytic glutamine pool approximately threefold, and, consequently, the amount of label incorporated into brain metabolites is proportionately higher. Under hyperammonemic conditions the contribution of astrocytic glucose oxidation was found to be somewhat lower (4–7% of the total oxidative metabolic rate) than that measured in human brain with [ $2-^{13}\text{C}$ ]acetate. This difference may reflect either the different physiological conditions of these studies, or differences in the relative proportions of astrocytes and neurons in rat and human brain.



It is thought that over 30 % of the synapses in the cerebral cortex may be GABAergic (40–42), and almost all of the brain GABA pool is localized to GABAergic neurons under normal conditions. GABA is synthesized from glutamate in GABAergic neurons by the enzyme glutamic acid decarboxylase (GAD). Thus, by following the flux of  $^{13}\text{C}$  label from  $[1-^{13}\text{C}]$ glucose into the GABA pool it is possible to obtain an estimate of oxidative glucose metabolism in the GABAergic neuron (10). The time course of label flux into the GABA pool has been determined by *in vitro* MRS analysis of cortical extracts from rats infused with  $[1-^{13}\text{C}]$ glucose (43–45). Calculation of the relative rates of glucose oxidation in the glutamate and GABA pools suggests that the rate of glucose oxidation in GABAergic neurons is 10–20 % of total neuronal glucose oxidation (44). These findings and other related studies of GABA metabolism will be discussed in more detail in the following chapter.

Thus, measurements of astrocyte and GABAergic neuron metabolism indicate that these cell populations account for approximately 15 % each of total cortical glucose consumption, leaving approximately 70 % for glutamatergic neurons. Once again, this is in good agreement with the findings from the  $[1-^{13}\text{C}]$ glucose studies and their comparison with measurements of total glucose utilization. Since glutamatergic pyramidal cells exhibit a high electrical activity and a large percentage of cortical synapses are glutamatergic (42, 46), it is perhaps not surprising that the greatest fraction of total glucose oxidation is associated with glutamatergic neurons.

## 5.2. MRS MEASUREMENTS OF NEUROTRANSMITTER FLUXES

The metabolism of glutamatergic neurons, GABAergic neurons and astrocytes is coupled by neurotransmitter cycles. The concept of such a cycle between glutamatergic neurons and astrocytes was first postulated in the early 1970s by van den Berg and colleagues (11), based on data from  $^{14}\text{C}$  labeling studies (47, 48). The purpose of this cycle is to enable rapid removal of the neurotransmitter from the synaptic cleft, whilst preventing depletion of the nerve terminal glutamate pool by synaptic release. Although glutamate transporters have been found on both pre- and post-synaptic nerve terminals (see Bergles *et al.*, 1999 (49) for review), a number of studies have now demonstrated that the majority of glutamate released from nerve terminals is taken up by surrounding astrocytes (50–52). Within astrocytes glutamate is converted to glutamine, by glutamine synthetase an exclusively glial enzyme (23). Glutamine is subsequently transported into the

**Figure 5.2.** Schematic diagram illustrating flow of  $^{13}\text{C}$  label from isotopic precursors into brain amino acids in the neuronal and astrocytic compartments. (A)  $[1-^{13}\text{C}]$ glucose is metabolized to  $[3-^{13}\text{C}]$ pyruvate by the glycolytic pathway, and label is subsequently transferred to the TCA cycle by the pyruvate dehydrogenase (PDH) pathway. Label is transferred via the TCA cycle to the C-4 of  $\alpha$ -ketoglutarate ( $\alpha$ -KG). The  $\alpha$ -KG pool is in rapid exchange with the glutamate pool via the amino acid transaminases and mitochondrial/cytosolic transporters, and consequently glutamate is also labeled at C-4. Although these pathways are active in both neurons and astrocytes, the flux of label from  $[1-^{13}\text{C}]$ glucose to  $[4-^{13}\text{C}]$ glutamate measured by  $^{13}\text{C}$  MRS is taken to reflect primarily the neuronal compartment owing to the small size (and, hence, low sensitivity) of the astrocytic glutamate pool. (B)  $[2-^{13}\text{C}]$ acetate is metabolized to  $[2-^{13}\text{C}]$ acetyl CoA and enters the astrocytic TCA cycle. Label passes into the astrocytic glutamate pool at C-4 and, subsequently, into glutamine C-4 via glutamine synthetase (GS) where it is first observed by  $^{13}\text{C}$  MRS. Acetate is exclusively used in the brain by astrocytes and, consequently, this label flux reflects metabolism solely within the astrocytic compartment. (C)  $[2-^{13}\text{C}]$ glucose metabolized via the astrocytic-specific pathway of pyruvate carboxylase (PC) brings label into the C-3 position of  $\alpha$ -KG, and subsequently of the small astrocytic glutamate pool and glutamine (scrambling of label in the TCA cycle also results in C-2 enrichment of these metabolites).  $[2-^{13}\text{C}]$ glucose metabolized via the PDH pathway (in both neurons and astrocytes) results in labeling of acetyl CoA at C-1, which does not contribute to labeling in either the C-3 or C-2 positions of glutamate and glutamine. Consequently, as with  $[2-^{13}\text{C}]$ acetate, label flux into these positions reflects metabolism solely within the astrocytic compartment.

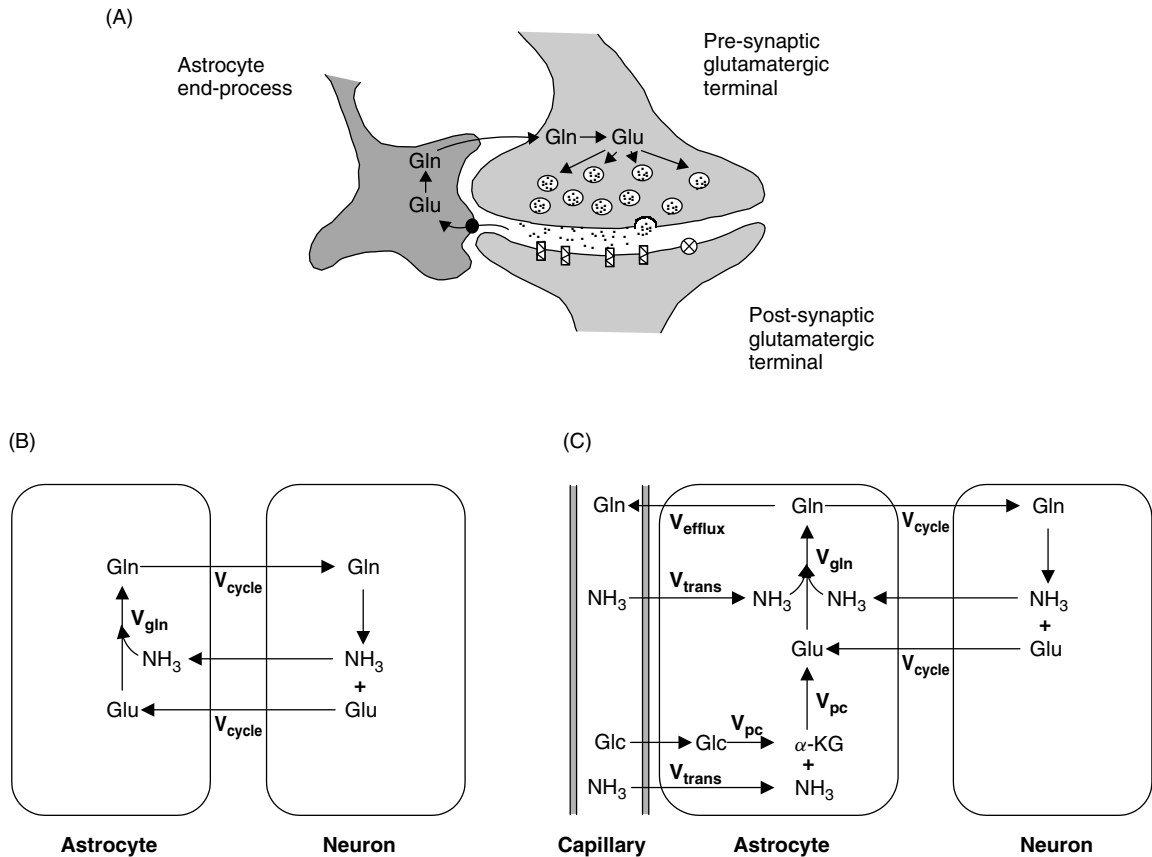


**Figure 5.3.** The glutamate–glutamine cycle. (A) Illustration of the glutamate–glutamine cycle between neurons and astrocytes. Glutamate (Glu) released from nerve terminals acts on a number of post-synaptic receptors, including ionotropic glutamate receptors, *N*-methyl-D-aspartate receptors and metabotropic glutamate receptors. Subsequently, this glutamate is taken up predominantly by surrounding astrocytes and converted to glutamine (Gln) by glutamine synthetase. Glutamine is then released for uptake by neurons, glutamate resynthesis via glutaminase, and re-packaging in vesicles. (B) Schematic diagram of the glutamate–glutamine cycle in the absence of any other contributing pathways to the glutamine synthetase flux. Under these conditions the rate of glutamine synthesis ( $V_{gln}$ ) would equal the rate of glutamate–glutamine cycling ( $V_{cycle}$ ). (C) Schematic diagram of the glutamate–glutamine cycle illustrating the contribution of ammonia detoxification to glutamine synthesis. Nitrogen influx to the brain in the form of ammonia, at a rate  $V_{trans}$ , is balanced by nitrogen efflux in glutamine, at a rate  $V_{efflux}$ . At the same time, loss of carbon skeletons from the brain in glutamine is balanced by net synthesis of carbon skeletons via the pyruvate carboxylase pathway in astrocytes, at a rate  $V_{pc}$ . Under these conditions, the total rate of glutamine synthesis can be defined as the sum of anaplerotic glutamine synthesis and glutamate neurotransmitter cycling ( $V_{gln} = V_{pc} + V_{cycle}$ ).

extracellular space, taken up by neurons and converted back to glutamate by phosphate-activated glutaminase (53). Thus, a ‘glutamate–glutamine cycle’ between neurons and astrocytes is formed (Figure 5.3(A)). Similarly, it is now thought that GABA released into the synaptic cleft participates in a neuronal–astrocytic cycle, and this will be discussed in detail in the following chapter. Since the initial proposal of a glutamate–glutamine cycle between neurons and astrocytes, this concept has gained much support from a variety of *in vitro* studies, including enzyme localization studies, isotope labeling studies in cells and brain slices,

and immunohistochemical studies of the cellular distribution of glutamate and glutamine (for review see Erecinska and Silver, 1990 (54)). However, prior to the development of *in vivo*  $^{13}\text{C}$  MRS techniques there was no methodology available by which these cycles could be demonstrated *in vivo*. Furthermore, *in vitro* measurements of the glutamate–glutamine cycle were unable to determine the magnitude of this pathway. In this section, we will discuss how MRS can be used to measure neurotransmitter cycle fluxes *in vivo*.

### 5.2.1. Measuring the Glutamate–Glutamine Cycle

As described above,  $^{13}\text{C}$  label from  $[1-^{13}\text{C}]$ glucose rapidly labels the large neuronal pool of glutamate. Thus, synaptic release of glutamate followed by uptake and conversion to glutamine in astrocytes, should result in label entering astrocytic glutamine via the glutamine synthetase pathway. Early  $^{13}\text{C}$  MRS studies of human occipital/parietal cortex showed clearly that glutamine is labeled rapidly from  $[1-^{13}\text{C}]$ glucose in the human cerebral cortex (3, 7) (Figure 5.1). Based on these data, it was suggested that the  $^{13}\text{C}$  MRS labeling time courses of glutamate and glutamine could be used to calculate the rate of glutamine synthesis, and from this the rate of the glutamate–glutamine cycle. The first measurement of glutamine synthesis from  $^{13}\text{C}$  MRS data acquired from human brain (3) was reported by Mason *et al.* in 1995 (7). At the time a relatively simplistic metabolic model was used to analyze the  $^{13}\text{C}$  MRS data, and it was concluded that the measurement contained a high degree of uncertainty. In subsequent years much work has been done to refine the metabolic model (see previous chapter) and to establish the validity of this measurement of glutamine synthesis as a measure of glutamate–glutamine cycling. A significant caveat to this approach is that the relationship between glutamine synthesis and glutamate–glutamine cycling is dependent on the contribution of any other significant fluxes through the glutamine synthetase pathway in astrocytes, which could add to the labeling observed in glutamine. Previously, it has been suggested that glutamine synthesis acts primarily as a detoxification pathway for blood-borne ammonia entering the brain (55) (Figure 5.3(C)). Consequently, in order to validate the measurements of glutamate–glutamine cycling the contribution of ammonia detoxification to the total rate of glutamine synthesis must first be determined.

The contribution of ammonia detoxification to glutamine synthesis will be determined by the rate of net ammonia transport into the brain, where this is considered to be the main source of ammonia to the brain. The issue of other sources of ammonia is reviewed in detail in Sibson *et al.*, 1998 (56), and will not be discussed here. Nitrogen influx to the brain in the form of ammonia is balanced by nitrogen efflux in glutamine (55) (Figure 5.3(C)). At the same time, loss of carbon skeletons from the brain in glutamine is balanced by net synthesis (anaplerosis) of carbon skeletons (Figure 5.3(C)), via the pyruvate carboxylase pathway in astrocytes (19, 56). Thus, the total rate of glutamine synthesis can be defined as the sum of anaplerotic glutamine synthesis and glutamate neurotransmitter cycling. The contribution of ammonia detoxification to total glutamine synthesis has been determined using  $^{13}\text{C}$  MRS in rats at two different levels of plasma ammonia–normoammonemia ( $\sim 0.05\text{ mM}$ ) and hyperammonemia ( $0.4\text{--}0.5\text{ mM}$ ). Using  $[1-^{13}\text{C}]$ glucose as the isotopic precursor, the rate of glutamine synthesis was measured at the two levels of plasma ammonia and found to increase under hyperammonemic conditions. As described above, when  $[2-^{13}\text{C}]$ glucose is used as the isotopic precursor labeling in the internal positions of glutamine arises entirely as a consequence of flux through the astrocytic pyruvate carboxylase pathway. Therefore, the rate of anaplerosis via this pathway can be determined from the flux of label from  $[2-^{13}\text{C}]$ glucose into glutamine. By this method, under similar hyperammonemic conditions to the  $[1-^{13}\text{C}]$ glucose study, an increase in anaplerotic flux was measured compared with normoammonemic conditions (19). This increase in anaplerotic flux was found to be similar in magnitude to both the increase in glutamine synthesis and the increase in net ammonia influx into the brain that has been measured by  $^{15}\text{N}$  MRS, again under similar hyperammonemic conditions (57). During infusion of  $^{15}\text{N}$ -labeled ammonia,  $^{15}\text{N}$  MRS can be used to follow fixation of the  $^{15}\text{N}$  label in the cerebral pools of glutamate and glutamine, which reflects net ammonia transport into

the brain. The good agreement of these findings lends strong support to the hypothesis that the contribution of ammonia detoxification to glutamine synthesis is determined by the rate of net ammonia transport into the brain. These experiments demonstrated that even under hyperammonemic conditions the fraction of glutamine synthesis that is attributable to detoxification is relatively small ( $\sim 30\%$ ) compared to the contribution of glutamate–glutamine cycling ( $\sim 70\%$ ). Moreover, under normoammonemic conditions the rate of ammonia transport into the brain can be calculated to be extremely low (55, 56). Consequently, the contribution of ammonia detoxification to glutamine synthesis under normal physiological conditions is very small ( $<10\%$ ), and the measurement of glutamine synthesis largely reflects glutamate–glutamine cycling (17, 56).

Thus, the studies described above provided initial support for the idea that the  $^{13}\text{C}$  MRS approach, in combination with an infusion of  $[1-^{13}\text{C}]$ glucose, is a viable means of measuring the rate of glutamate–glutamine cycling *in vivo*. Nevertheless, once this principle was established it was important to validate the  $^{13}\text{C}$  MRS measurements of the glutamate–glutamine cycle, and indeed the existence of such a cycle *in vivo*, since this single measurement is potentially open to a number of different interpretations. One of the disadvantages of using  $[1-^{13}\text{C}]$ glucose to measure the rate of the glutamate–glutamine cycle is that the  $^{13}\text{C}$  label will enter both the astrocytic and neuronal glutamate pools directly via pyruvate dehydrogenase. Thus, labeling of the astrocytic glutamine pool could occur in the absence of any neuron–astrocyte cycling, and simply reflect exchange between glutamate and glutamine within astrocytes (Figure 5.4(A)). In this situation it would have to be argued that neuronal glutamate was replenished by pre-synaptic glutamate re-uptake. A third potential model of neurotransmitter metabolism that has been proposed in recent years is one based on cycling of  $\alpha$ -ketoglutarate ( $\alpha$ -KG) rather than glutamine from astrocytes to neurons (Figure 5.4(B)) (58). In this model glutamate taken up by astrocytes is converted to  $\alpha$ -KG, by either oxidation or transamination, and this is then released for uptake and resynthesis of glutamate by neurons. With data obtained from a single experimental approach it is possible that a number of different metabolic models will equally well fit those data, and it is not possible to reliably determine which model most accurately represents the true metabolic situation. Consequently, a number of different approaches have been employed in order to validate the  $^{13}\text{C}$  MRS measurement of glutamate–glutamine cycling and to provide, thereby, support for the existence of such a cycle *in vivo*.

## 5.2.2. Validating the $^{13}\text{C}$ MRS Measurement of Glutamate–Glutamine Cycling

### 5.2.2.1. Correlation with Neuronal Activity

One approach that has been used is to measure the rate of the cycle under conditions that alter neuronal glutamate neurotransmitter release. Neuronal glutamate release increases with increased action potential propagation and neuronal depolarization. Therefore, if the rate of  $^{13}\text{C}$  flux from glutamate into glutamine measured by  $^{13}\text{C}$  MRS truly reflects synaptic glutamate release, and glutamate–glutamine cycling, then the calculated rate of this pathway should correlate with brain electrical activity. To test this prediction  $^{13}\text{C}$  MRS was used to measure the rate of glutamine synthesis in the rat cerebral cortex at three levels of electrocortical activity; isoelectric EEG induced by high dose pentobarbital anesthesia, and two milder levels of anesthesia (56). Under isoelectric conditions, at which minimal glutamate release takes place, almost no glutamine synthesis was measured ( $0.04\text{ }\mu\text{mol/min/g}$ ). Above isoelectricity, the rate of glutamine synthesis increased with higher electrical activity (Figure 5.5). These findings provide support for the hypothesis that the  $^{13}\text{C}$  MRS measurement of glutamine synthesis primarily reflects glutamate–glutamine cycling rather than internal exchange of  $^{13}\text{C}$  label within astrocytes, which would not be expected to change with the level of neuronal activity.

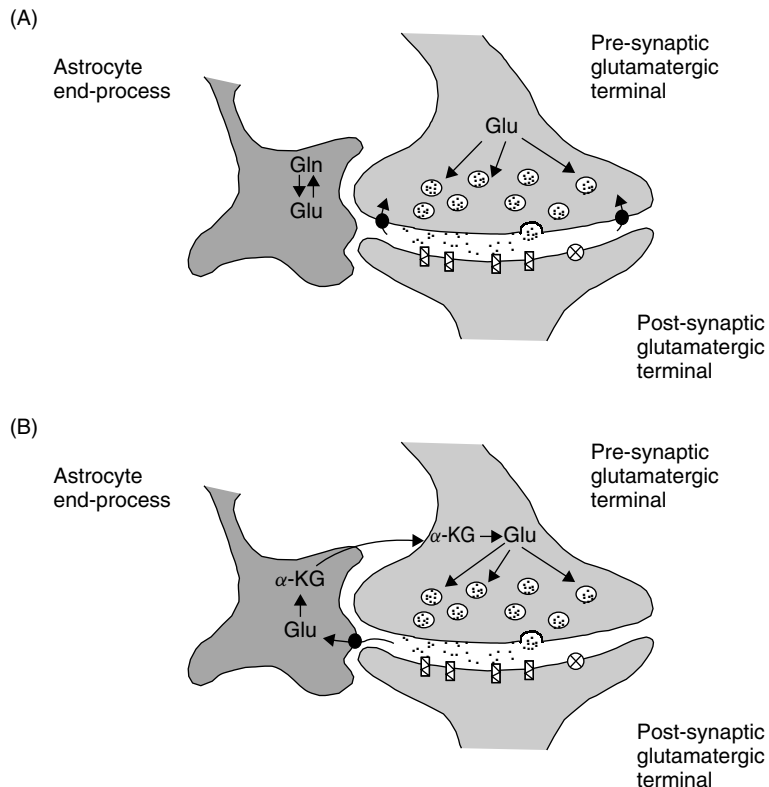


**Figure 5.4.** Alternative models of glutamate metabolism. (A) Illustration of the ‘internal exchange’ model for glutamate (Glu) and glutamine (Gln) within astrocytes. In this situation neuronal glutamate would have to be replenished by presynaptic glutamate re-uptake. (B) Illustration of the proposed glutamate- $\alpha$ -ketoglutarate cycle between neurons and astrocytes. In this model glutamate taken up by astrocytes is converted to  $\alpha$ -ketoglutarate ( $\alpha$ -KG), by either oxidation or transamination, and this is then released for uptake and resynthesis of glutamate by neurons.

#### 5.2.2.2. Alternative $^{13}\text{C}$ -labeled Precursors

A second approach to validating the  $^{13}\text{C}$  MRS measurement of glutamate–glutamine cycling is to use alternative isotopically labeled precursors, which enter the metabolic pathways of the brain specifically via different cell types and in particular astrocytes. If label is introduced specifically into astrocytic metabolite pools, then subsequent appearance of label in neuronal metabolites provides direct evidence of substrate trafficking between these cells and could not be attributed to an exchange flux within a single cell population. As discussed above,  $[2-^{13}\text{C}]$ glucose can be utilized as an astrocyte-specific precursor. Since the TCA cycle intermediate pools in astrocytes are very small, the isotopic label is first observed in glutamine. In the  $[2-^{13}\text{C}]$ glucose experiment, if there is significant cycling of labeled glutamine from the astrocyte to the neuron (as predicted by the glutamate–glutamine cycle), label would be expected to appear subsequently in neuronal glutamate. Labeling of neuronal glutamate has been demonstrated using  $[2-^{13}\text{C}]$ glucose in rat brain (19). Spectra acquired during  $[1-^{13}\text{C}]$ - and  $[2-^{13}\text{C}]$ glucose infusions, respectively, under similar physiological conditions demonstrate that in the  $[1-^{13}\text{C}]$ glucose experiment there is more rapid labeling of glutamate than glutamine, whilst in the  $[2-^{13}\text{C}]$ glucose experiment glutamine labeling precedes that of

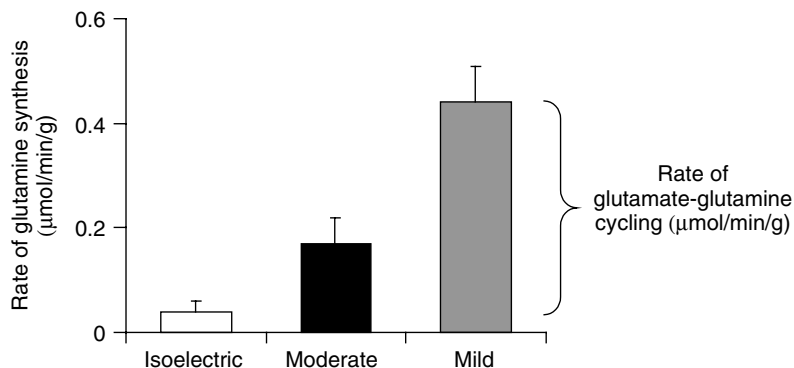


**Figure 5.5.** Graph to show relationship between different levels of neuronal activity and the rate of glutamine synthesis measured by  $^{13}\text{C}$  MRS in rat cerebral cortex (data from Sibson *et al.*, 1998). A range of neuronal activity was achieved through the use of graded levels of anesthesia, and ranged from isoelectric (as determined by EEG measurements) to mild sedation. Under isoelectric conditions minimal glutamate release occurs and the rate of glutamate–glutamine cycling is assumed to be zero. Therefore, the difference between the rate of glutamine synthesis obtained under isoelectric conditions and that obtained under each of the other anesthetic conditions yields the rate of glutamate–glutamine cycling at each level of neuronal activity (illustrated for the mild anesthesia condition).

glutamate. This reversal of the precursor–product relationship can be seen clearly in the isotopic labeling curves from the two experiments shown in Figure 5.6(A,B).

The appearance of label in the neuronal glutamate pool indicates that there is indeed substrate trafficking between astrocytes and neurons, and that labeling of glutamine in the  $[1-^{13}\text{C}]$ glucose experiment does not simply reflect intra-astrocytic exchange of label between glutamate and glutamine. However, it does not differentiate between the different substrates that may participate in the astrocyte–neuron trafficking. In order to determine which model (glutamate–glutamine cycling or glutamate– $\alpha$ -KG cycling) most accurately reflects the true metabolic situation, it is possible to apply these two different metabolic models to the data acquired from both the  $[1-^{13}\text{C}]$ glucose and  $[2-^{13}\text{C}]$ glucose experiments to see which model fits both sets of data most accurately. The assumption is that, whilst an incorrect model could fit one set of data reasonably well, it is unlikely to fit two independent sets of data accurately. When both models were used to fit the data from both  $[1-^{13}\text{C}]$ - and  $[2-^{13}\text{C}]$ glucose studies it was found that the glutamate–glutamine cycling model provided a consistently better fit to both data sets (Figure 5.6(A,B)) than the glutamate– $\alpha$ -KG cycling model (Figure 5.6(C,D)) (19).

These results indicate that the glutamate–glutamine cycle accounts for the *majority* of neuronal–astrocyte glutamate trafficking, although contributions from alternative trafficking pathways, such as the glutamate– $\alpha$ -KG cycle, cannot be excluded. Since, the  $[2-^{13}\text{C}]$ glucose experiment does not differentiate between label transferred from astrocyte to neuron in either glutamine or  $\alpha$ -KG, the flux of label into glutamate reflects the sum of *all* substrate trafficking pathways from astrocytes to neurons. In contrast, in the  $[1-^{13}\text{C}]$ glucose experiment flux of label from neuronal glutamate to astrocytic glutamine reflects glutamate–glutamine cycling alone. Consequently, comparison of the rates obtained in the two separate studies should indicate the fraction of substrate trafficking from astrocytes to neurons that can be attributed to the glutamate–glutamine cycle. The absolute rates of cycling measured using the different isotopic precursors are in close agreement ( $0.20 \pm 0.08$  versus  $0.20 \pm 0.10 \mu\text{mol}/\text{min}/\text{g}$ ), indicating that, within the standard error of the measurement, the maximum potential contribution of the  $\alpha$ -KG pathway to the total astrocyte–neuron cycling flux is  $\sim 25\%$ . These experiments were conducted under hyperammonemic conditions since, as explained in a previous section, labeling from  $[2-^{13}\text{C}]$ glucose is extremely low under

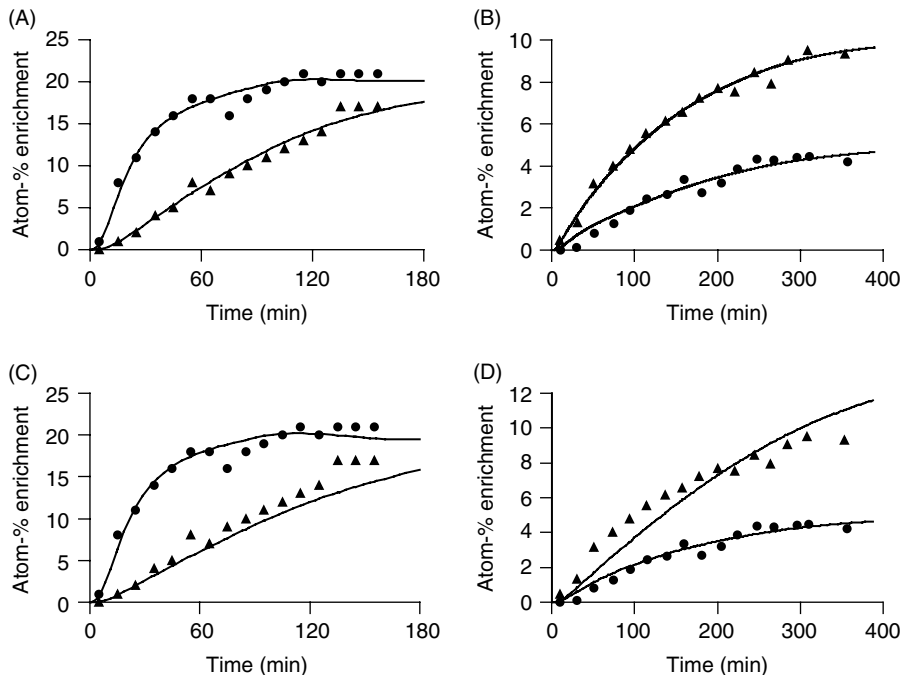


**Figure 5.6.** Graphs demonstrating  $^{13}\text{C}$  enrichment of cortical glutamate and glutamine in rat brain during infusion of different isotopic precursors, acquired under hyperammonaemic conditions (data from Sibson *et al.*, 1997, 2001). The data clearly demonstrate reversal of the precursor–product relationship between glutamate and glutamine labeling. During infusion of  $[1\text{-}^{13}\text{C}]$ glucose (A), label first appears in  $[4\text{-}^{13}\text{C}]$ glutamate (●) and, subsequently, in  $[4\text{-}^{13}\text{C}]$ glutamine (▲). In contrast, during infusion of  $[2\text{-}^{13}\text{C}]$ glucose (B), label first appears in  $[3\text{-}^{13}\text{C}]$ glutamine (▲) and, subsequently, in  $[3\text{-}^{13}\text{C}]$ glutamate (●). In (A) and (B) the solid lines indicate fits to the data obtained via metabolic modeling using the glutamate–glutamine cycling model. In (C) and (D) the solid lines indicate fits to the same data obtained using the glutamate– $\alpha$ -KG cycling model. It can be seen that the glutamate–glutamine cycling model provides a better fit to both data sets than the glutamate– $\alpha$ -KG cycling model.

normoammonemic conditions. Comparison of data from *ex vivo*  $[2\text{-}^{13}\text{C}]$ glucose experiments and *in vivo*  $[1\text{-}^{13}\text{C}]$ glucose experiments performed under normoammonemic conditions (19) also suggest that the  $\alpha$ -KG pathway could contribute 25–30 % of the total cycling flux.

Very recently, experiments in humans infused with  $[2\text{-}^{13}\text{C}]$ acetate have been performed, and these studies have yielded results that are consistent with the  $[1\text{-}^{13}\text{C}]$ - and  $[2\text{-}^{13}\text{C}]$ glucose studies in rats. As with the  $[2\text{-}^{13}\text{C}]$ glucose experiment, clear differences in labeling patterns were observed when data acquired during  $[2\text{-}^{13}\text{C}]$ acetate infusion (34) were compared with those obtained from a  $[1\text{-}^{13}\text{C}]$ glucose experiment (2) (Figure 5.7). These findings are in accord with previous findings from animal studies (*in vivo* and *ex vivo*) (24, 30), indicating that acetate and glucose are metabolized primarily in different metabolic compartments – astrocytes and neurons, respectively. The observed ratio of glutamate/glutamine labeling ( $\sim 0.63$ ) during  $[2\text{-}^{13}\text{C}]$ acetate infusion indicated that there is substantial transfer of  $^{13}\text{C}$  label from astrocytes to neurons. The rate of substrate cycling obtained from this experiment ( $0.32 \pm 0.07 \mu\text{mol}/\text{min}/\text{g}$ ) was again in close agreement with the rate of glutamate–glutamine cycling obtained from  $[1\text{-}^{13}\text{C}]$ glucose studies under identical conditions ( $0.32 \pm 0.05 \mu\text{mol}/\text{min}/\text{g}$ ). Calculations suggest that, within the error of the  $^{13}\text{C}$  measurements, a glutamate– $\alpha$ -KG cycle could account for 10 % of this substrate cycling (34).

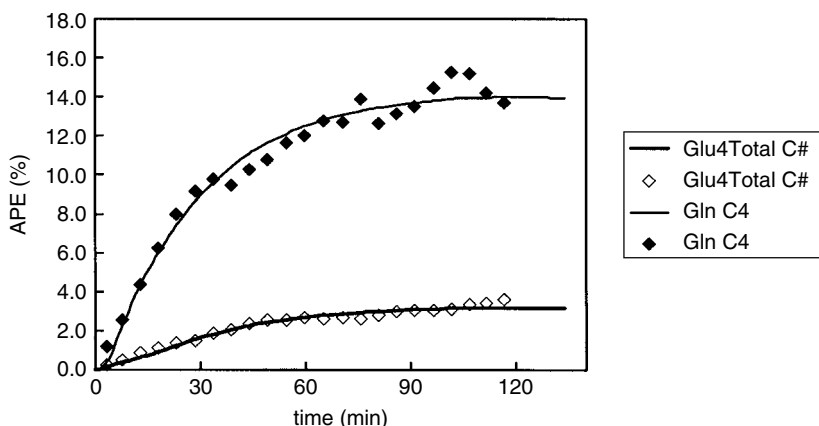


**Figure 5.7.** Time course of C4 glutamate and glutamine during  $2\text{-}^{13}\text{C}$  acetate infusion. Spectra were obtained from human occipital lobe at 2.1T. The time course clearly displays reversal of product precursor relationship relative  $1\text{-}^{13}\text{C}$  glucose.

#### 5.2.2.3. $^{15}\text{N}$ MRS Measurements

A third approach to validating the measurement of glutamate–glutamine cycling is to use  $^{15}\text{N}$  MRS to measure glutamine synthesis through label incorporation from  $^{15}\text{N}$ -labeled ammonia into the amide position of cerebral glutamine (57, 59–61). The rates of glutamine synthesis obtained in these studies have varied somewhat, but this can largely be explained by the fact that different metabolic models have been used to fit the data. It has been shown that if the same metabolic model is used to fit both  $^{13}\text{C}$  and  $^{15}\text{N}$  MRS data obtained under similar experimental conditions then the rates of glutamate–glutamine cycling obtained from both MRS studies agree closely (57). Furthermore, since  $^{15}\text{N}$ -labeled ammonia is exclusively incorporated into cerebral metabolites in astrocytes, the same hypothesis holds as with the other astrocyte-specific precursors – that label flux from glutamine into the large, neuronal glutamate pool is indicative of astrocyte–neuron substrate cycling. In these studies, it is clear from the labeling patterns in glutamine and glutamate that this is, indeed, the case and that label appears first in glutamine and only subsequently in glutamate (57, 59–61).

It is extremely unlikely that a model will accurately fit data obtained from several independent experimental approaches if it does not reasonably reflect the metabolic situation. The same metabolic model, involving a flux of glutamate from neurons to astrocytes and a reciprocal flux of glutamine from astrocytes to neurons, has now been shown to fit data obtained using  $^{13}\text{C}$  MRS and multiple different  $^{13}\text{C}$ -labeled isotopic precursors ( $[1\text{-}^{13}\text{C}]$ glucose,  $[2\text{-}^{13}\text{C}]$ glucose and  $[2\text{-}^{13}\text{C}]$ acetate), as well as data obtained from  $^{15}\text{N}$  MRS studies. These studies strongly support the existence of a glutamate–glutamine cycle between neurons and astrocytes *in vivo*, and have demonstrated that  $^{13}\text{C}$  MRS may be used *in vivo* to measure the rate of glutamatergic neuronal activity, in the form of glutamate–glutamine cycling. The rate of the glutamate–glutamine cycle found in these studies of rat cerebral cortex is of a similar order of magnitude ( $0.20\text{--}0.40\text{ }\mu\text{mol}/\text{min/g}$ ) as the rate of oxidative glucose consumption measured by  $^{13}\text{C}$  MRS. In addition, similar rates of glutamate–glutamine cycling ( $0.26\text{--}0.32\text{ }\mu\text{mol}/\text{min/g}$ ) have recently been measured in human occipital/parietal cortex (2, 4, 5) by the same methodology. These findings indicate that the glutamate–glutamine cycle is a major metabolic pathway in the mammalian cortex,

and the predominant route by which neuronal glutamate pools are replenished. The rapid incorporation of  $^{13}\text{C}$  label into glutamine via the glutamate–glutamine cycle indicates that the vesicular pool of glutamate in neurons turns over rapidly and is in dynamic equilibrium with cytosolic glutamate. This contradicts the long-standing view of functionally isolated transmitter and metabolic glutamate pools in neurons (27, 62). However, this concept had been established on the basis of *in vitro* studies of cell or tissue preparations, which exhibit little or no synaptic activity. In contrast, it has been shown more recently that inhibition of PAG (through which the neuronal glutamate pool is replenished) rapidly depletes both the synaptic and whole cell glutamate pools in rat cerebral cortex (13), in agreement with the  $^{13}\text{C}$  MRS observations of a rapid vesicular turnover. Finally, these studies highlight the importance of astrocytes in maintaining synaptic glutamate homeostasis, which has long been a source of controversy.

### 5.3. ENERGETIC REQUIREMENTS OF NEUROTRANSMISSION

Neuronal activity requires energy which is provided almost exclusively by oxidation of glucose (1). Since the brain has almost no energy reserve, a continuous vascular supply of glucose and oxygen is mandatory to sustain neuronal activity. This supply is regulated locally and dynamically to meet the increased energetic demand of functional activation. Functional imaging utilizes this association between increased neuronal activity and energetic demand, by measuring changes in either blood flow, glucose utilization or oxygen metabolism and delivery (63). The implicit assumption of functional imaging methodologies is that changes in one or more of these parameters accurately reflect changes in neuronal activity. Despite the increasing use of these imaging tools in both basic and clinical applications, the neurobiological processes responsible for the imaging signals measured are still unknown. Recent advances in the field suggest that in some brain regions glutamate release may trigger both vascular and metabolic responses via different signaling processes (for review see Bonvento *et al.*, 2002 (64)). Thus, glutamate may be a key co-coordinator of the physiological responses underlying the signal changes observed in brain imaging.

$^{13}\text{C}$  MRS has provided a means by which the relationship between glutamatergic neurotransmission and energy metabolism can be tested *in vivo*. This has been achieved in the rat brain by using  $^{13}\text{C}$  MRS to simultaneously measure the rates of glutamate–glutamine cycling and neuronal glucose oxidation in the cerebral cortex at different levels of neuronal activity (18). As described in the previous section, electrocortical activity was varied using differing levels of anesthesia, and when neuronal glucose oxidation was plotted against the rate of glutamate–glutamine cycling a linear relationship was obtained (Figure 5.8(A)). The observed relationship between oxidative glucose metabolism and glutamate–glutamine cycling demonstrates two important points – firstly, that there is a molar (1:1) stoichiometry between these two rates above a basal level of energy metabolism (isoelectric EEG), and secondly, that the basal level of glucose consumption (i.e. unrelated to synaptic activity) is only 15–20 % of resting levels. The first of these points implies that the energy requirements of pre- and post-synaptic events related to neuronal firing and synaptic transmission may be met by the oxidative metabolism of 1 mol of glucose for every mole of glutamate released synaptically. These studies are not able to assign fractions of energy utilization to each of the individual processes involved (action potential propagation, restoration and maintenance of membrane potentials, vesicle recycling and glutamate cycling), although recent theoretical calculations have begun to address this issue (65). This analysis (based on a mean neuronal action potential frequency of 4 Hz) has shown that action potentials are responsible for a large fraction (47 %) of total ATP consumption, as restoration of the sodium and potassium gradients occurs via the  $\text{Na}^+/\text{K}^+$ -ATPase. Increased activity of the  $\text{Na}^+/\text{K}^+$ -ATPase is also required to reverse ion movements evoked by the activation of post-synaptic

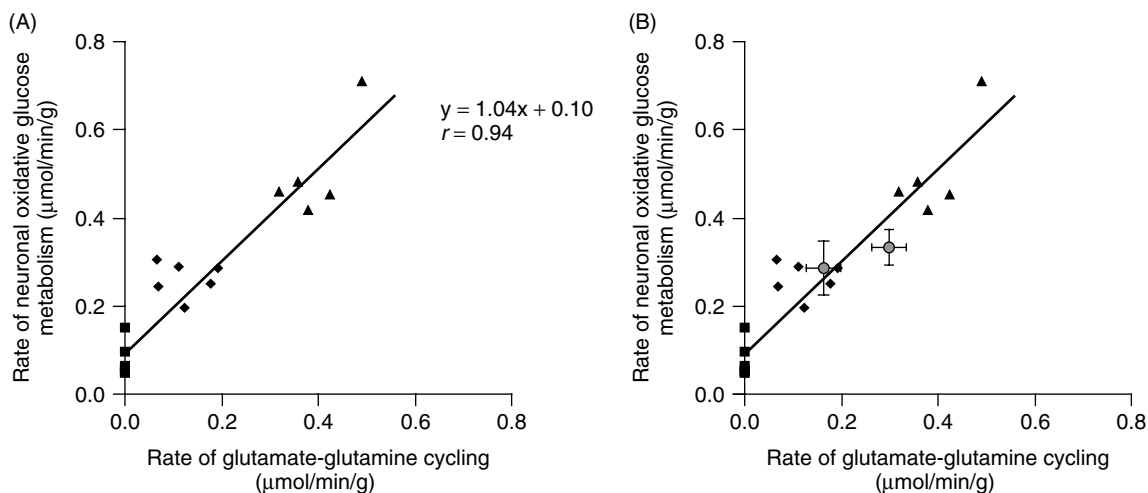


**Figure 5.8.** Graphs illustrating the relationship between oxidative glucose consumption and glutamate–glutamine cycling in the cerebral cortex. (A)  $^{13}\text{C}$  MRS data acquired from rat cerebral cortex at different levels of neuronal activity yielded rates of oxidative glucose consumption and glutamate–glutamine cycling (data from Sibson *et al.*, 1998a). Three different levels of neuronal activity were achieved through the use of graded anesthesia: isoelectric EEG (■); moderate anesthesia (●); and mild anesthesia (▲). It should be noted that the units of the  $x$  and  $y$  axes are the same and, hence, these two metabolic rates increase with a 1:1 molar stoichiometry *above* a basal level of energy consumption. The basal level of energy metabolism was measured at isoelectric EEG (i.e. no neurotransmission or glutamate–glutamine cycling) and, thus, reflects the energetic requirements of the brain that are unrelated to neuronal activity (e.g. macromolecule turnover, maintenance of membrane structure and axoplasmic transport). (B) The same data as shown in (A) are superimposed on  $^{13}\text{C}$  MRS data obtained from human cerebral cortex (○). Data are from Shen *et al.*, 1999 and Gruetter *et al.*, 2001 (mean  $\pm$  S.D. for each metabolic rate). This graph demonstrates that the measurements of oxidative glucose consumption and glutamate–glutamine cycling obtained from human cerebral cortex are entirely consistent with the rates obtained in the rat cerebral cortex. The human cortical rates appear to lie at the lower end of those obtained in the rat cortex, corresponding to a state of moderate anesthesia in the rat. The reasons for this are possibly twofold – firstly, that the human cerebral cortex has a threefold to tenfold lower density of neurons and, secondly, that in the human measurements the volume of tissue under observation contains both grey and white matter. As yet, an analogous  $^{13}\text{C}$  MRS study of human brain under different levels of neuronal activity has not been performed. Consequently, it remains to be seen whether a linear relationship between neurotransmission and energy metabolism exists in man.

NMDA and non-NMDA ionotropic glutamate receptors, and this activity has been calculated to account for as much as 34 % of total ATP usage. Therefore, the prevailing hypothesis is still that the majority ( $\sim 80\%$ ) of total cerebral energy consumption subserves restoration of the ionic gradients and resting membrane potentials that are modified during the excitation phase of neuronal activation (65). These calculations can also be expressed in terms of the pre-synaptic, post-synaptic and glial energy requirements as shown in Figure 5.9.

The second finding, of a low basal metabolic rate measured under isoelectric conditions, is in close agreement with the recent theoretical analysis of the energetic expenditure of the brain (65), and presumably supports basic cellular processes, unrelated to signaling, such as macromolecule turnover (proteins, lipids, oligonucleotides), maintenance of membrane structure, and axoplasmic transport. However, this represents a departure from the long-held view that the majority of energy consumption in the brain subserves these so-called ‘housekeeping’ functions, rather than those involved in neuronal activity and synaptic transmission.

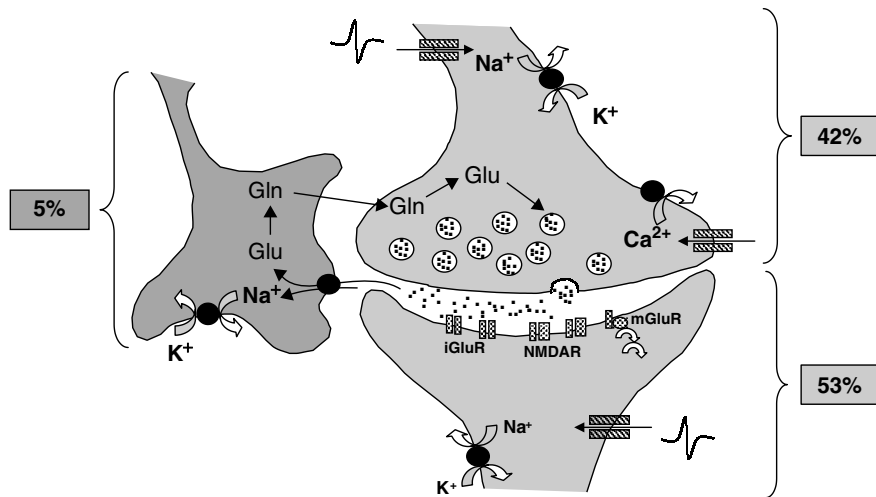


**Figure 5.9.** Glutamatergic neurotransmission involves a number of energy-requiring steps. Initially, propagation of an action potential along an axon to a pre-synaptic terminal results in changes in ionic gradients across the axonal membrane. Restoration of these ion gradients requires the activity of  $Na^{+}/K^{+}$ -ATPase pumps. Next, glutamate release is triggered by  $Ca^{2+}$  influx into the pre-synaptic terminal, which must be pumped out at the expense of ATP. Glutamate released into the synaptic cleft acts on several different post-synaptic receptors (iGluR, ionotropic glutamate receptor; NMDAR, *N*-methyl-D-aspartate receptor; mGluR, metabotropic glutamate receptor), and also on presynaptic and glial receptors (not shown). Activation of these receptors causes ion movements (mostly  $Na^{+}$ ) and second messenger cascades, and re-establishment of ion gradients is performed by the  $Na^{+}/K^{+}$ -ATPase. If enough depolarization of the post-synaptic neuron is produced, an action potential will ensue, and, once again, restoration of the ion gradients occurs via the  $Na^{+}/K^{+}$ -ATPase. Finally, glutamate recycling involves  $Na^{+}$ -dependent uptake by astrocytes and conversion to glutamine, as well as vesicular recycling in neurons, all of which consume ATP. Recent evidence suggests that astrocytes may release glutamate that participates in neuronal depolarization, although the extent of this astrocytic release remains to be determined. It has recently been calculated that in terms of the pre-synaptic, post-synaptic and glial processes, these energy requirements can be broken down to give ~42% pre-synaptic consumption (axonal action potentials, pre-synaptic  $Ca^{2+}$  entry and vesicularization of glutamate), 53% post-synaptic consumption (glutamate receptor activation, dendritic and somatic action potentials and post-synaptic resting potentials) and 5% glial consumption (resting potentials, glutamate uptake and glutamine synthesis).

On reflection, however, it is perhaps not surprising that neuronal signaling dominates the energetic cost of the brain, given that its primary functions are information processing and signaling.

### 5.3.1. Glutamate as a Mediator of Neurometabolic Coupling

The demonstrated stoichiometric relationship between oxidative glucose consumption and glutamate–glutamine cycling is supportive of the concept that glutamate release may be a means by which energy metabolism can be regulated in line with neuronal activity. This hypothesis was proposed several years ago by Pellerin and Magistretti (66) based on *in vitro* studies of cultured astrocytes. Those experiments demonstrated that glutamate induced increases in both glucose utilization and lactate production by astrocytes. These effects on glucose metabolism were not receptor mediated, but rather dependent on glutamate transport. As glutamate transport is coupled to the sodium ion gradient with a precise stoichiometry of three sodium ions for each transported glutamate molecule, glutamate uptake leads to a massive entry of sodium

ions into astrocytes (as demonstrated by fluorescence microscopy) (67). Further studies in cultured astrocytes have shown that glutamate enhances the activity of a specific glial  $\text{Na}^+/\text{K}^+$ -ATPase subunit (68), and that ouabain, a specific inhibitor of the  $\text{Na}^+/\text{K}^+$ -ATPase, prevents the enhancement of glucose utilization and lactate production by glutamate (66). Thus, the activity of this glial enzyme has been directly implicated in the metabolic response. The concept that glial glutamate transporters may play a role in neurometabolic coupling has recently received support from *in vivo* studies in glutamate transporter (GLAST and GLT-1) knockout mice (69). In these studies the metabolic response to somatosensory activation was significantly decreased compared to wild type mice, as demonstrated by 2DG autoradiography. In a second study, glucose utilization in rat brain was also found to be decreased following the downregulation of the astrocytic glutamate transporter GLAST by antisense oligonucleotides (70). Thus, these findings suggest an attractive mechanism of coupling energy metabolism to neuronal activity via astrocytic glutamate uptake, which is supported by the relationship between glucose oxidation and glutamate-glutamine cycling obtained by  $^{13}\text{C}$  MRS.

It is important to note that, although astrocytic glutamate uptake could trigger at least part of the observed changes in glucose metabolism, the energetic requirements of astrocytic glutamate uptake and recycling are small. Approximately 5% of total energy consumption is required to support glutamate uptake and recycling (65) (Figure 5.9), a percentage that would be consistent with the process being predominantly fuelled by glycolysis. This suggestion is supported to some extent by an *ex vivo*  $^{13}\text{C}$  MRS study of mice in which the astrocytic TCA cycle was inhibited with fluoroacetate (71). In this study, it was found that glutamate-glutamine cycling (as determined by  $^{13}\text{C}$  labeling of glutamine from  $[1-^{13}\text{C}]$ glucose) was maintained to a substantial degree despite an almost complete inhibition of astrocytic oxidative metabolism. One might hypothesize, therefore, that glycolytic energy might support the very rapid process ( $\sim 1\text{ ms}$  (72, 73)) of glutamate uptake by astrocytes, whilst oxidative metabolism could support those processes of synaptic activity that can occur over a longer timeframe (e.g. restoration of membrane potentials and ionic gradients, recycling of vesicles). How this last aspect is regulated and whether glucose alone or other substrates (e.g. lactate) are oxidized by active neurons remain to be determined.

### 5.3.2. Implications for Studies of Human Brain

Importantly, measurements of these metabolic rates in human cerebral cortex during infusion of either  $[1-^{13}\text{C}]$ glucose (2, 5) or, very recently,  $[2-^{13}\text{C}]$ acetate (34) are entirely consistent with the rates obtained in the rat cerebral cortex (Figure 5.8(B)). Interestingly, the human cortical rates lie at the lower end of those obtained in the rat cortex, which corresponds to a state of moderate anesthesia. The reasons for this are possibly twofold – firstly, that the human cerebral cortex has a threefold to tenfold lower density of neurons (74) and, secondly, that in the human measurements the volume of tissue under observation will contain both grey and white matter. In the first case, although the density of synapses in human cortex is no different to that in rat cortex, Attwell and Laughlin (65) calculated that a tenfold lower density of neurons per se would result in a 54% reduction in specific energy usage and oxygen consumption. In accord with this prediction, metabolic rates in neocortical grey matter of primate brain are, on average,  $\sim 50\%$  lower than in rat (75–77). With respect to the second point, we would expect the rate of glutamate-glutamine cycling to be considerably higher in grey matter, which contains large numbers of synaptic terminals, than in white matter consisting predominantly of axon bundles. Correspondingly, white matter has been shown to have a considerably lower oxidative metabolic rate than grey matter (22). Consequently, the partial volume effect of including significant fractions of white matter in the volume of tissue from which the  $^{13}\text{C}$  measurement is made will significantly reduce the measured rates of both cycling and glucose utilization.

However, it should be noted that to date an analogous  $^{13}\text{C}$  MRS study of human brain under different levels of neuronal activity has not been performed. Thus, it is not yet possible to determine whether a

linear relationship between neurotransmission and energy metabolism, similar to that found in rat cerebral cortex, exists in man.

## 5.4. SUMMARY

The application of MRS to the study of neurotransmitter and energy metabolism in the brain has provided several new insights into the relationship between brain metabolism and function. Glutamate release and recycling has been shown to be a major metabolic pathway in the cerebral cortex. Consequently, steady state measurements of neurotransmitter levels may reflect alterations in regional brain activity through feedback between neurotransmitter release and resynthesis. The glutamate–glutamine cycle appears to be the predominant route by which the neurotransmitter glutamate pool in neurons is replenished, and demonstrates the importance of astrocytes in maintaining synaptic glutamate homeostasis. Interestingly, the glutamate–glutamine cycle constitutes a significant metabolic flux in both resting, awake human brain and anesthetized rat brain, indicating that there is considerable neuronal activity even under ‘nonstimulated’ conditions. The 1:1 coupling between neurotransmission and neuroenergetics (above isoelectricity) provides a link between functional imaging and specific neuronal processes. This finding has implications for the interpretation of functional imaging signal changes, which may be most readily understood by converting the measured rates of glucose oxidation to fractions of total glucose consumption in the brain. In doing so, we find that glucose oxidation by glutamatergic neurons comprises approximately 70 % of the total energy consumption of the brain, while the astrocytic and GABAergic neuron consumptions are estimated to be approximately 15 % each. Thus, the energy requirements of glutamatergic neurons potentially explain a large fraction of the glucose consumption of the resting awake human brain. Further, these findings may provide a mechanism for converting energy changes measured in human brain activation studies into a specific neuronal process, such as excitatory glutamate release. Should an analogous study of glutamate–glutamine cycling and oxidative glucose consumption over a range brain activity in human cortex yield a similar relationship to that found in rat cortex, then this will bridge the gap that currently exists between functional activation data (based on metabolic indices) and neuronal activity. Thus, establishing the functional imaging modalities, which have the advantages of greater spatial and temporal resolution than the  $^{13}\text{C}$  MRS measurement, as true indices of neuronal activity.

## REFERENCES

- 1 Siesjo B. *Brain Energy Metabolism*. New York: John Wiley and Sons Inc., 1978
- 2 Shen J, Petersen KF, Behar KL, Brown P, Nixon TW, Mason GF, Petroff OA, Shulman GI, Shulman RG, Rothman DL. Determination of the rate of the glutamate/glutamine cycle in the human brain by *in vivo*  $^{13}\text{C}$  NMR. *Proc Natl Acad Sci U S A* 1999; **96**: 8235–40
- 3 Gruetter R, Novotny EJ, Boulware SD, Mason GF, Rothman DL, Shulman GI, Prichard JW, Shulman RG. Localized  $^{13}\text{C}$  NMR spectroscopy in the human brain of amino acid labeling from D-[1- $^{13}\text{C}$ ]glucose. *J Neurochem* 1994; **63**: 1377–85
- 4 Gruetter R, Seaquist ER, Kim S, Ugurbil K. Localized *in vivo*  $^{13}\text{C}$ -NMR of glutamate metabolism in the human brain: initial results at 4 tesla. *Dev Neurosci* 1998; **20**: 380–8
- 5 Gruetter R, Seaquist ER, Ugurbil K. A mathematical model of compartmentalized neurotransmitter metabolism in the human brain. *Am J Physiol Endocrinol Metab* 2001; **281**: E100–12.
- 6 Fitzpatrick SM, Hetherington HP, Behar KL, Shulman RG. The flux from glucose to glutamate in the rat brain *in vivo* as determined by  $^1\text{H}$ -observed,  $^{13}\text{C}$ -edited NMR spectroscopy. *J Cereb Blood Flow Metab* 1990; **10**: 170–9.

- 7 Mason GF, Gruetter R, Rothman DL, Behar KL, Shulman RG, Novotny EJ. Simultaneous determination of the rates of the TCA cycle, glucose utilization, alpha-ketoglutarate/glutamate exchange, and glutamine synthesis in human brain by NMR. *J Cereb Blood Flow Metab* 1995; **15**: 12–25
- 8 Mason GF, Pan JW, Chu WJ, Newcomer BR, Zhang Y, Orr R, Hetherington HP. Measurement of the tricarboxylic acid cycle rate in human grey and white matter *in vivo* by  $^1\text{H}-[^{13}\text{C}]$  magnetic resonance spectroscopy at 4.1 T. *J Cereb Blood Flow Metab* 1999; **19**: 1179–88.
- 9 Mason GF, Rothman DL, Behar KL, Shulman RG. NMR determination of the TCA cycle rate and alpha-ketoglutarate/glutamate exchange rate in rat brain. *J Cereb Blood Flow Metab* 1992; **12**: 434–47.
- 10 Rothman DL, Sibson NR, Hyder F, Shen J, Behar KL, Shulman RG. *in vivo* nuclear magnetic resonance spectroscopy studies of the relationship between the glutamate–glutamine neurotransmitter cycle and functional neuroenergetics. *Philos Trans R Soc London Ser B Biol Sci* 1999; **354**: 1165–77
- 11 van den Berg CJ, Garfinkel D. A stimulation study of brain compartments. Metabolism of glutamate and related substances in mouse brain. *Biochem J* 1971; **123**: 211–8.
- 12 Ottersen OP, Zhang N, Walberg F. Metabolic compartmentation of glutamate and glutamine: morphological evidence obtained by quantitative immunocytochemistry in rat cerebellum. *Neuroscience* 1992; **46**: 519–34
- 13 Conti F, Minelli A. Glutamate immunoreactivity in rat cerebral cortex is reversibly abolished by 6-diazo-5-oxo-L-norleucine (DON), an inhibitor of phosphate-activated glutaminase. *J Histochem Cytochem* 1994; **42**: 717–26.
- 14 Hyder F, Rothman DL, Mason GF, Rangarajan A, Behar KL, Shulman RG. Oxidative glucose metabolism in rat brain during single forepaw stimulation: a spatially localized  $^1\text{H}-[^{13}\text{C}]$  nuclear magnetic resonance study. *J Cereb Blood Flow Metab* 1997; **17**: 1040–7.
- 15 Hyder F, Chase JR, Behar KL, Mason GF, Siddeek M, Rothman DL, Shulman RG. Increased tricarboxylic acid cycle flux in rat brain during forepaw stimulation detected with  $^1\text{H}-[^{13}\text{C}]$ NMR. *Proc Natl Acad Sci U S A* 1996; **93**: 7612–7.
- 16 Hyder F, Renken R, Rothman DL. *In vivo* carbon-edited detection with proton echoplanar spectroscopic imaging (ICED PEPSI): [3,4-(13)CH(2)]glutamate/glutamine tomography in rat brain. *Magn Reson Med* 1999; **42**: 997–1003.
- 17 Sibson NR, Dhankhar A, Mason GF, Behar KL, Rothman DL, Shulman RG. *In vivo*  $^{13}\text{C}$  NMR measurements of cerebral glutamine synthesis as evidence for glutamate–glutamine cycling. *Proc Natl Acad Sci U S A* 1997; **94**: 2699–704
- 18 Sibson NR, Dhankhar A, Mason GF, Rothman DL, Behar KL, Shulman RG. Stoichiometric coupling of brain glucose metabolism and glutamatergic neuronal activity. *Proc Natl Acad Sci U S A* 1998; **95**: 316–21
- 19 Sibson NR, Mason GF, Shen J, Cline GW, Herskovits AZ, Wall JE, Behar KL, Rothman DL, Shulman RG. *in vivo*  $(^{13}\text{C})$  NMR measurement of neurotransmitter glutamate cycling, anaplerosis and TCA cycle flux in rat brain during [2- $^{13}\text{C}$ ]glucose infusion. *J Neurochem* 2001; **76**: 975–89.
- 20 van Zijl PC, Chesnick AS, DesPres D, Moonen CT, Ruiz-Cabello J, van Gelderen P. *in vivo* proton spectroscopy and spectroscopic imaging of [1– $^{13}\text{C}$ ]-glucose and its metabolic products. *Magn Reson Med* 1993; **30**: 544–51.
- 21 Van Zijl PC, Davis D, Eleff SM, Moonen CT, Parker RJ, Strong JM. Determination of cerebral glucose transport and metabolic kinetics by dynamic MR spectroscopy. *Am J Physiol* 1997; **273**: E1216–27.
- 22 Pan JW, Stein DT, Telang F, Lee JH, Shen J, Brown P, Cline G, Mason GF, Shulman GI, Rothman DL, Hetherington HP. Spectroscopic imaging of glutamate C4 turnover in human brain. *Magn Reson Med* 2000; **44**: 673–9.
- 23 Martinez-Hernandez A, Bell KP, Norenberg MD. Glutamine synthetase: glial localization in brain. *Science* 1977; **195**: 1356–8.
- 24 Bachelard H. Landmarks in the application of  $^{13}\text{C}$ -magnetic resonance spectroscopy to studies of neuronal/glial relationships. *Dev Neurosci* 1998; **20**: 277–88
- 25 Cruz F, Cerdan S. Quantitative  $^{13}\text{C}$  NMR studies of metabolic compartmentation in the adult mammalian brain. *NMR Biomed* 1999; **12**: 451–62.
- 26 Bachelard H, Morris P, Taylor A, Thatcher N. High-field MRS studies in brain slices. *Magn Reson Imaging* 1995; **13**: 1223–6
- 27 Badar-Goffer RS, Ben-Yoseph O, Bachelard HS, Morris PG. Neuronal–glial metabolism under depolarizing conditions, A  $^{13}\text{C}$ -n.m.r. study. *Biochem J* 1992; **282**: 225–30.

28 Brand A, Richter-Landsberg C, Leibfritz D. Metabolism of acetate in rat brain neurons, astrocytes and cocultures: metabolic interactions between neurons and glia cells, monitored by NMR spectroscopy. *Cell Mol Biol (Noisy-le-grand)* 1997; **43**: 645–57.

29 Cerdan S, Kunnecke B, Seelig J. Cerebral metabolism of [1,2-<sup>13</sup>C]acetate as detected by *in vivo* and *in vitro* <sup>13</sup>C NMR. *J Biol Chem* 1990; **265**: 12916–26.

30 Hassel B, Sonnewald U, Fonnum F. Glial-neuronal interactions as studied by cerebral metabolism of [2-<sup>13</sup>C]acetate and [1-<sup>13</sup>C]glucose: an ex vivo <sup>13</sup>C NMR spectroscopic study. *J Neurochem* 1995; **64**: 2773–82.

31 Hassel B, Sonnewald U. Glial formation of pyruvate and lactate from TCA cycle intermediates: implications for the inactivation of transmitter amino acids? *J Neurochem* 1995; **65**: 2227–34.

32 Haberg A, Qu H, Haraldseth O, Unsgard G, Sonnewald U. *in vivo* injection of [1-<sup>13</sup>C]glucose and [1,2-<sup>13</sup>C]acetate combined with ex vivo <sup>13</sup>C nuclear magnetic resonance spectroscopy: a novel approach to the study of middle cerebral artery occlusion in the rat. *Journal of Cerebral blood flow and metabolism* 1998; **18**: 1223–1232.

33 Sonnewald U, Westergaard B, Hassel B, Miller TB, Unsgard G, Fonnum F, Hertz L, Schousboe A, Petersen SB. NMR spectroscopic studies of <sup>13</sup>C acetate and <sup>13</sup>C glucose metabolism in neocortical astrocytes: evidence for mitochondrial heterogeneity. *Dev Neurosci* 1993; **15**: 351–358.

34 Lebon V, Petersen KF, Cline GW, Shen J, Mason GF, Dufour S, Behar KL, Shulman GI, Rothman DL. Astroglial contribution to brain energy metabolism in humans revealed by <sup>13</sup>C nuclear magnetic resonance spectroscopy: elucidation of the dominant pathway for neurotransmitter glutamate repletion and measurement of astrocytic oxidative metabolism. *J Neurosci* 2002; **22**: 1523–31.

35 Kanamatsu T, Tsukada Y. Effects of ammonia on the anaplerotic pathway and amino acid metabolism in the brain an ex vivo <sup>13</sup>C NMR spectroscopic study of rats after administering[2-<sup>13</sup>C]glucose with or without ammonium acetate. *Brain Res* 1999; **841**: 11–19.

36 Brand A, Richter-landsberg C, Leibfritz D. Multinuclear NMR studies on the energy metabolism of glial and neuronal cells. *Dev Neurosci* 1993; **15**: 289–298.

37 Shank RP, Bennett GS, Freytag SO, Campbell GL. Pyruvate carboxylase: an astrocyte-specific enzyme implicated in the replenishment of amino acid neurotransmitter pools. *Brain Res* 1985; **329**: 364–367.

38 Yu ACH, Drejer J, Hertz L, Schousboe A. Pyruvate carboxylase activity in primary cultures of astrocytes and neurons. *J Neurochem* 1983; **41**: 1484–1487.

39 Taylor A, Mclean M, Morris P, Bachelard H. Approaches to studies on neuronal/glial relationships by <sup>13</sup>C -MRS analysis. *Dev Neurosci* 1996; **18**: 434–442.

40 Roberts E. Failure of GABAergic inhibition: a key to local and global seizures. *Adv Neurol* 1986; **44**: 319–41.

41 Roberts E. The establishment of GABA as a neurotransmitter. In: Squires R (ed.), *GABA and Benzodiazepine Receptors*, vol. 1. Boca Raton: CRC Press, 1988; 1–21.

42 Shephard GM. *The Synaptic Organization of the Brain*. Oxford: Oxford University Press, 1994.

43 Shank RP, Leo GC, Zielke HR. Cerebral metabolic compartmentation as revealed by nuclear magnetic resonance analysis of D-[1-<sup>13</sup>C] glucose metabolism. *J Neurochem* 1993; **61**: 315–323.

44 Manor D, Rothman DL, Mason GF, Hyder F, Petroff OA, Behar KL. The rate of turnover of cortical GABA from [1-<sup>13</sup>C]glucose is reduced in rats treated with the GABA-transaminase inhibitor vigabatrin (gamma-vinyl GABA). *Neurochem Res* 1996; **21**: 1031–41.

45 Brainard JR, Kyner E, Rosenberg GA. <sup>13</sup>C Nuclear magnetic resonance evidence for  $\gamma$ -aminobutyric acid formation via pyruvate carboxylase in rat brain: A metabolic basis for compartmentation. *J Neurochem* 1989; **53**: 1285–1292.

46 Nowak LG, Sanchez-Vives MV, McCormick DA. Influence of low and high frequency inputs on spike timing in visual cortical neurons. *Cereb Cortex* 1997; **7**: 487–501.

47 Lajhta A, Berl S, Waelch H. Amino acid and protein metabolism of the brain IV. The metabolism of glutamic acid. *J Neurochem* 1959; **3**: 322–332.

48 Berl S, Lajhta A, Waelch H. Amino acid and protein metabolism VI. Cerebral compartments of glutamic acid metabolism. *J Neurochem* 1961; **7**: 186–192.

49 Bergles DE, Diamond JS, Jahr CE. Clearance of glutamate inside the synapse and beyond. *Curr Opin Neurobiol* 1999; **9**: 293–8.

50 Bergles DE, Jahr CE. Glial contribution to glutamate uptake at Schaffer collateral-commissural synapses in the hippocampus. *J Neurosci* 1998; **18**: 7709–16.

51 Bergles DE, Diamond JS, Jahr CE. Clearance of glutamate inside the synapse and beyond. *Curr Opin Neurobiol* 1999; **9**: 293–8.

52 Rothstein JD, Dykes-hoberg M, Pardo CA, Bristol LA, Jin L, Kuncl RW, Kanai Y, Hediger MA, Wang Y, SChielke JP, Welty DF. Knockout of glutamate transporters reveals a major role for astroglial transport in excitotoxicity and clearance of glutamate. *Neuron* 1996; **16**: 675–686

53 Kvamme E, Torgner IA, Svenneby G. Glutaminase from mammalian tissues. *Methods Enzymol* 1985; **113**: 241–56

54 Erecinska M, Silver IA. Metabolism and role of glutamate in mammalian brain. *Prog Neurobiol* 1990; **35**: 245–296

55 Cooper AJL, Plum F. Biochemistry and physiology of brain ammonia. *Physiological* 1987; **67**: 440–519

56 Sibson NR, Shen J, Mason GF, Rothman DL, Behar KL, Shulman RG. Functional energy metabolism: *in vivo* <sup>13</sup>C-NMR spectroscopy evidence for coupling of cerebral glucose consumption and glutamatergic neuronal activity. *Dev Neurosci* 1998; **20**: 321–30

57 Shen J, Sibson NR, Cline G, Behar KL, Rothman DL, Shulman RG. <sup>15</sup>N-NMR spectroscopy studies of ammonia transport and glutamine synthesis in the hyperammonemic rat brain. *Dev Neurosci* 1998; **20**: 434–43

58 Shank RP, Campbell GL. Alpha-ketoglutarate and malate uptake and metabolism by synaptosomes: further evidence for an astrocyte-to-neuron metabolic shuttle. *J Neurochem* 1984; **42**: 1153–61

59 Kanamori K, Ross BD. <sup>15</sup>N n.m.r. measurement of the *in vivo* rate of glutamine synthesis and utilization at steady state in the brain of the hyperammonaemic rat. *Biochem J* 1993; **293**: 461–8.

60 Kanamori K, Parivar F, Ross BD. A <sup>15</sup>N NMR study of *in vivo* cerebral glutamine synthesis in hyperammonemic rats. *NMR Biomed* 1993; **6**: 21–6.

61 Kanamori K, Ross BD, Chung JC, Kuo EL. Severity of hyperammonemic encephalopathy correlates with brain ammonia level and saturation of glutamine synthetase *in vivo*. *J Neurochem* 1996; **67**: 1584–94.

62 Nicholls D, Attwell D. The release and uptake of excitatory amino acids. *Trends Pharmacol Sci* 1990; **11**: 462–8

63 Raichle ME. Behind the scenes of functional brain imaging: a historical and physiological perspective. *Proc Natl Acad Sci U S A* 1998; **95**: 765–72

64 Bonvento G, Sibson N, Pellerin L. Does glutamate image your thoughts? *Trends Neurosci* 2002; **25**: 359–64

65 Attwell D, Laughlin SB. An energy budget for signaling in the grey matter of the brain. *J Cereb Blood Flow Metab* 2001; **21**: 1133–45

66 Pellerin L, Magistretti PJ. Glutamate uptake into astrocytes stimulates aerobic glycolysis: a mechanism coupling neuronal activity to glucose utilization. *Proc Natl Acad Sci U S A* 1994; **91**: 10625–9

67 Chatton JY, Marquet P, Magistretti PJ. A quantitative analysis of L-glutamate-regulated Na<sup>+</sup> dynamics in mouse cortical astrocytes: implications for cellular bioenergetics. *Eur J Neurosci* 2000; **12**: 3843–53

68 Pellerin L, Stolz M, Sorg O, Martin JL, Deschepper CF, Magistretti PJ. Regulation of energy metabolism by neurotransmitters in astrocytes in primary culture and in an immortalized cell line. *Glia* 1997; **21**: 74–83

69 Voutsinos-Porche B, Bonvento G, Tanaka K, Magistretti P, Pellerin L. Evidence from knockout mice for a major role of the glial glutamate transporters GLAST and GLT-1 in neurometabolic coupling. *J Cereb Blood Flow Metab* 2001; **21** (Suppl. 1): S115

70 Cholet N, Pellerin L, Welker E, Lacombe P, Seylaz J, Magistretti P, Bonvento G. Local injection of antisense oligonucleotides targeted to the glial glutamate transporter GLAST decreases the metabolic response to somatosensory activation. *J Cereb Blood Flow Metab* 2001; **21**: 404–12

71 Hassel B, Bachelard H, Jones P, Fonnum F, Sonnewald U. Trafficking of amino acids between neurons and glia *in vivo*. Effects of inhibition of glial metabolism by fluoroacetate. *J Cereb Blood Flow Metab* 1997; **17**: 1230–8.

72 Diamond JS, Jahr CE. Transporters buffer synaptically released glutamate on a submillisecond time scale. *J Neurosci* 1997; **17**: 4672–87

73 Clements JD. Transmitter timecourse in the synaptic cleft: its role in central synaptic function. *Trends Neurosci* 1996; **19**: 163–71

74 Abeles M. *Corticonics: Neural Circuits of the Cerebral Cortex*. Cambridge: Cambridge University Press, 1991

75 Clarke J, Sokoloff L. Circulation and energy metabolism of the brain. In: Siegel G, Agranoff B, Albers R, Fisher S, Uhler M (eds), *Basic Neurochemistry*, 6th edn. Philadelphia: Lippincott-Raven, 1999; 637–669

76 Kennedy C, Sakurada O, Shinohara M, Jehle J, Sokoloff L. Local cerebral glucose utilization in the normal conscious macaque monkey. *Ann Neurol* 1978; **4**: 293–301

77 Sokoloff L, Reivich M, Kennedy C, Des Rosiers MH, Patlak CS, Pettigrew KD, Sakurada O, Shinohara M. The [ $^{14}\text{C}$ ]deoxyglucose method for the measurement of local cerebral glucose utilization: theory, procedure, and normal values in the conscious and anesthetized albino rat. *J Neurochem* 1977; **28**: 897–916



# 6

## NMR Studies of the Metabolism and Energetics of GABA Neurotransmitter Pathways

**Kevin L. Behar**

*Department of Psychiatry, Yale University School of Medicine, MR Center, P.O. Box 208043, New Haven, CT 06520-8043, USA*

**Douglas L. Rothman**

*Department of Diagnostic Radiology, Yale University School of Medicine, MR Center, P.O. Box 208043, New Haven, CT 06520-8043, USA*

---

6.1	Introduction	100
6.2	Neuronal Localization of GABA	100
6.2.1	<i>In vivo</i> Detection of GABA using NMR	102
6.3	Pathways of Brain GABA Synthesis and Catabolism	102
6.3.1	GABA Metabolism in the GABA Shunt	102
6.3.2	Glutamate Decarboxylase and GABA Synthesis	103
6.3.3	Alternate Pathways of GABA Synthesis	104
6.4	Role of GABA and Glutamine Transporters in GABA Metabolism	104
6.4.1	GABA Transporters	104
6.4.2	Glutamine Transporters	104
6.5	NMR Studies of GABAergic Function	105
6.5.1	Measurements of GABA Synthesis	105
6.5.2	GABA/Glutamine Cycling	106
6.6	NMR Studies of GABA Synthesis Regulation <i>In vivo</i>	106
6.7	Conclusions	106

---

## 6.1. INTRODUCTION

Gamma-aminobutyric acid (GABA) is the major inhibitory neurotransmitter in the mature central nervous system. In the cortex, GABA may constitute as many as one-quarter of all synapses (Iversen and Schon, 1973), although such estimates are only approximate. GABA inhibition in the mature CNS involves both fast, point-to-point signaling on a timescale of milliseconds and slower tonic responses lasting seconds or longer. These responses are mediated mainly through chloride-dependent, GABA<sub>A</sub> receptors and potassium-dependent, G-protein linked, GABA<sub>B</sub> receptors, respectively (Simeone *et al.*, 2003; Owens and Kriegstein, 2002). These different GABA responses may reflect functionally distinct intracellular pools of GABA and different release mechanisms.

GABA is a product of glucose metabolism at the level of the tricarboxylic acid (TCA) cycle. GABA is synthesized from glutamate and oxidized to succinic acid in a metabolic 'shunt' that bypasses two enzymes of the TCA cycle. Whereas the enzymes of GABA synthesis are almost exclusively confined to GABAergic neurons, the enzymes of GABA catabolism are more widespread, being found in astroglia as well as neurons. GABA released from neurons is removed both by reuptake and also by astroglia through specific GABA transporters (GATs). GABA removed by astroglia must be re-supplied because mature neurons do not possess the anaplerotic enzymes (e.g., pyruvate carboxylase) needed to catalyze carbon fixation and *de novo* glutamate synthesis. In the cerebral cortex glutamine produced in astroglia provides a major fraction of the glutamate used in the re-synthesis of neurotransmitter glutamate and GABA. The cyclic flow of these neurotransmitters from their respective neurons to astroglial glutamine and back again gives rise to glutamate/glutamine and GABA/glutamine cycles (Figure 6.1). The existence of carbon cycles involving GABA, glutamate, and glutamine has been recognized for over 30 years although the magnitude of their respective flows in relation to glucose metabolism and energetics was not well known until recently.

New insights into the energetics of the GABA and glutamate neurotransmitter pathways in relation to glucose metabolism are being revealed through the tools of modern neuroimaging and NMR spectroscopy. Developments in spectroscopy and labeling techniques along with comprehensive models of metabolic networks to analyze the dynamic isotopic labeling time courses of glutamate and glutamine have permitted the pathways of glucose metabolism and glutamate/glutamine cycle to be measured. These studies have revealed that glutamatergic neuronal activity accounts for a major fraction of glucose oxidation in the cortex and is coupled to neuronal glucose oxidation in a ~ 1:1 relationship (Sibson *et al.*, 1998; Rothman *et al.*, 1999). The earliest experiments using [1-<sup>13</sup>C]glucose could not distinguish the individual contributions made by glutamate and GABA to total cycling. More recently the challenge has been to separately quantify the fluxes of these neurotransmitter pathways using astroglial targeted <sup>13</sup>C-labeled substrates (e.g., [2-<sup>13</sup>C]glucose or [2-<sup>13</sup>C]acetate) as described later in this chapter (also see Chapter 5). These studies have revealed that the GABA/glutamine cycle provides ~1/5 of the total cycling measured using [1-<sup>13</sup>C]glucose in the anesthetized rat cortex (Patel *et al.*, 2003).

In this chapter we briefly describe the major and minor metabolic pathways of GABA synthesis and catabolism, GABA transport, and the role of astroglia in the GABA/glutamine cycle. The fluxes of major and minor pathways of GABA metabolism are provided and discussed in the context of rate measurements using <sup>13</sup>C-labeled isotopes. The important role of glutamate decarboxylase in the regulation of GABA synthesis is discussed along with recent attempts using *in vivo* NMR to determine the contribution of the two brain isoforms of GAD to GABA synthesis. For a more comprehensive discussion of the NMR literature of GABA and metabolic compartmentation interested readers are encouraged to consult reviews of this subject by Bachelard (1998), Cruz and Cerdan (1999), and Waagepetersen *et al.* (1999).

## 6.2. NEURONAL LOCALIZATION OF GABA

GABA is present in brain tissue at a concentration of about 2–5  $\mu\text{mol/g}$  wet tissue weight and a large majority of this is concentrated in GABAergic neurons. In cerebellar Purkinje neurons the cellular concentration of

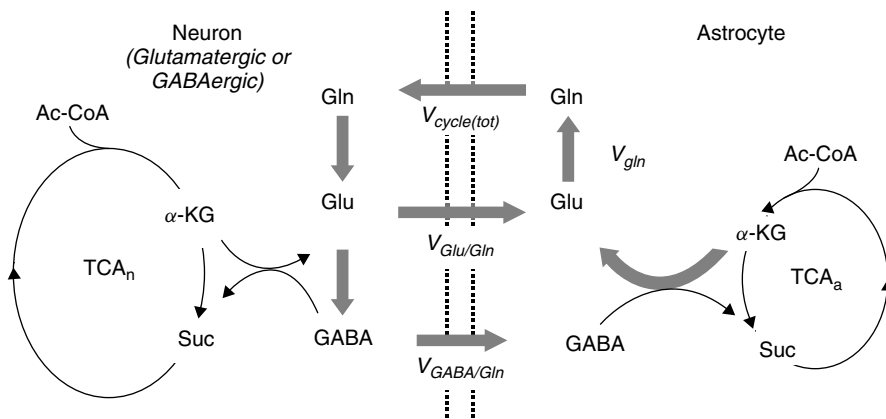


**Figure 6.1.** Schematic depiction of glutamate/glutamine and GABA/glutamine substrate cycles interconnecting glutamatergic and GABAergic neurons to astroglia. In astroglia GABA is readily metabolized through transamination and oxidation to succinic acid (Suc), which enters the astroglial TCA cycle. During transamination of GABA,  $\alpha$ -ketoglutarate ( $\alpha$ -KG) is converted to glutamate, which may then proceed to the formation of glutamine by glutamine synthetase. Thus, net uptake of GABA into astrocytes can lead indirectly to *net* glutamine formation, a process that requires a molar equivalent consumption of glucose-derived pyruvate or acetyl group donors to replace  $\alpha$ -KG consumed in the synthesis of glutamine. The carbon skeleton of GABA entering astroglia in the GABA/glutamine cycle does not contribute directly to glutamine, unlike glutamate in the glutamate/glutamine cycle. The syntheses of glutamate and GABA are depicted with a single TCA cycle to emphasize net carbon flows although glutamatergic and GABAergic neurons possess separate TCA cycles. Fluxes are depicted as follows:  $V_{\text{Glu}/\text{Gln}}$ , glutamate/glutamine cycle flux;  $V_{\text{GABA}/\text{Gln}}$ , GABA/glutamine cycle flux;  $V_{\text{cycle}(\text{tot})}$ , total (Glu + GABA) cycling flux;  $V_{\text{GAD}}$ , rate of GABA synthesis;  $V_{\text{gln}}$ , rate of glutamine synthesis. TCA<sub>n</sub> and TCA<sub>a</sub>, neuronal and astroglial tricarboxylic acid cycle fluxes, respectively. NMR measurements of neurotransmitter cycling using [ $1-^{13}\text{C}$ ]glucose reflects total (glutamate + GABA) neurotransmitter cycling. The two cycles can be separately determined using astroglia targeted  $^{13}\text{C}$ -labeled substrates (e.g., [ $2-^{13}\text{C}$ ]glucose or [ $2-^{13}\text{C}$ ]acetate).

GABA may reach 50–100 mM (Fonnum and Walberg, 1973). Based on studies of [ $^3\text{H}$ ]GABA uptake, the number of GABA nerve terminals has been estimated to range from 14 to 51 % of all terminals depending on brain region (Iversen and Schon, 1973), although actual numbers may be less because GABA transporters are expressed on glia as well as neurons. GABA neurons also tend to be smaller in size than the glutamatergic principal neurons. From a metabolic and neuroimaging viewpoint, the fractional volume of tissue occupied by GABAergic nerve terminals is of greater significance than their numbers in computations of metabolic rates.

GABA and the enzyme catalyzing its synthesis, glutamate decarboxylase (GAD), are localized to GABAergic neurons although not exclusively. Excitatory granule and mossy fiber neurons in the dentate gyrus of the hippocampus, which use glutamate as neurotransmitter, also contain GABA and GAD and their synthesis is enhanced by increasing electrical activity (Sloviter *et al.*, 1996; Cao *et al.*, 1996; Gutierrez, 2002). GABA neurons are heterogeneous as a group in that many, if not all, contain one or more neuroactive peptides, such as VIP, parvalbumin, and calbindin.

The concentration of GABA in interstitial fluid is maintained at a very low level ( $<1\text{ }\mu\text{M}$ ) by active transport and subsequent metabolism of GABA in neighboring neurons and glia. GABA catabolism in astroglia is rapid due in part to a highly active transaminase (Chan-Palay *et al.*, 1979; Larsson and Schousboe, 1990) which maintains GABA at a low level in these cells. Thus under physiologically normal conditions a large concentration gradient exists between GABA in GABAergic neurons and the surrounding transporter-rich astroglia.

### 6.2.1. *In vivo* Detection of GABA using NMR

GABA is readily detected *in vitro* using  $^1\text{H}$  and  $^{13}\text{C}$  NMR following enrichment with  $^{13}\text{C}$ -labeled isotopes (Behar *et al.*, 1983; Bachelard, 1998; Westergaard *et al.*, 1995; Patel *et al.*, 2001; Badar-Goffer *et al.*, 1992). *In vivo* detection of GABA is possible using modern NMR spectrometers although precise quantitation of GABA poses several challenges. Because the GABA concentration is low in brain,  $<1/10$  the level of major amino acids such as glutamate or *N*-acetylaspartate, NMR detection of GABA *in vivo* has most often entailed detection of the more sensitive  $^1\text{H}$  nucleus. The  $^1\text{H}$  NMR spectrum of GABA ( $\text{C}_4\text{H}_9\text{O}_2\text{N}$ ) consists of three methylene proton resonances ( $\delta$ , ppm;  $2.99_t$ ,  $2.29_t$ ,  $1.89_q$ ) and all are multiplets ( $J_{\text{HH}} \sim 7\text{ Hz}$ ), which exacerbates the extent of overlap with neighboring resonances. Macromolecules contribute to the  $^1\text{H}$  spectrum of brain and interfere specifically with quantitation of GABA (Behar and Ogino, 1993); however, these resonances can be suppressed using  $T_1$ -nulling techniques (Behar *et al.*, 1994). GABA can be quantified accurately in  $^1\text{H}$  NMR spectra of animal and human brain *in vivo* by use of *J*-editing techniques (Rothman *et al.*, 1984; 1993; Behar and Boehm, 1994; Preece *et al.*, 1994; Preece and Cerdan, 1996; Shen *et al.*, 2002; Kuzniecky *et al.*, 2002; Hetherington *et al.*, 1998; Terpstra *et al.*, 2002). As generally applied, *J*-editing is used to select H4 and H2 resonances of GABA while suppressing other metabolites and macromolecules. These methods have been adapted to the quantification of  $^{13}\text{C}$ -labeled GABA and other metabolites *in vivo* using indirect detection of the  $^1\text{H}$  nucleus (Fitzpatrick *et al.*, 1990; de Graaf *et al.*, 2003; see Chapter 3).

## 6.3. PATHWAYS OF BRAIN GABA SYNTHESIS AND CATABOLISM

### 6.3.1. GABA Metabolism in the GABA Shunt

Glutamate is the major precursor of GABA in the mature mammalian brain (Roberts and Frankel, 1950; Noto *et al.*, 1986). GABA synthesis from glutamate is catalyzed by the pyridoxal cofactor-dependent enzyme, glutamate decarboxylase (GAD) (Martin and Rimvall, 1993; Martin and Tobin, 2000), which is present in the cytoplasm of all known GABAergic neurons.

GABA is oxidized to succinic acid in mitochondria by the sequential actions of GABA-transaminase (GABA-T) and succinic semialdehyde dehydrogenase (SSADH) in a pathway known as the GABA shunt (Figure 6.2). The GABA shunt is quantitatively the major route of GABA synthesis and catabolism (Balazs *et al.*, 1970). Because the glutamate precursors used in GABA synthesis are derived from  $\alpha$ -ketoglutarate ( $\alpha\text{KG}$ ), a TCA cycle intermediate, this pathway provides an alternative route or ‘shunt’ for  $\alpha\text{-KG}$  oxidation to succinic acid around two enzymes of the TCA cycle,  $\alpha$ -ketoglutarate dehydrogenase and succinyl CoA synthetase. Oxidation of  $\alpha\text{-KG}$  through the GABA shunt is less efficient energetically than oxidation through the complete TCA cycle due to the loss of production of one molecule of GTP for each molecule of  $\alpha\text{-KG}$  (glutamate) diverted through this pathway. The enzymes of the GABA shunt are expressed in both neurons and astroglia although the fraction of GABA catabolized through the shunt in each cell type is not clear. Thus, while GABA synthesis is confined to neurons, GABA degradation can occur in both neurons and astroglia. As discussed below, results of  $^{13}\text{C}$ -isotopic labeling studies suggest that astroglia play an important role in the catabolism of GABA and the supply of glutamate precursors for GABA synthesis in the form of glutamine.

Enzymes of the GABA shunt also produce precursors for other neuroactive substances (Figure 6.3) including the psychoactive neurotransmitter/neuromodulator, gamma-hydroxybutyrate (Maitre, 1997) and GABA-conjugated peptides such as homocarnosine (Petroff *et al.*, 2001). The combined flux through these pathways, however, is small (less than a few percent) compared to the rate of GABA synthesis. These alternate pathways also appear to recycle GABA, in that GABA appears both as precursor and product, and thus are unlikely to be pathways of net GABA degradation.

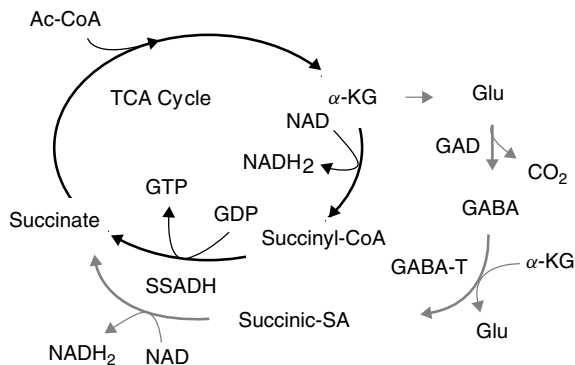


**Figure 6.2.** The GABA shunt pathway. The GABA shunt (shown in grey) bypasses two enzymatic steps of the TCA cycle resulting in the net loss of one molecule of GTP for each molecule of  $\alpha$ -ketoglutarate metabolized to succinate through the shunt. GAD, glutamate decarboxylase; GABA-T, GABA-transaminase; SSADH, succinic semialdehyde dehydrogenase.

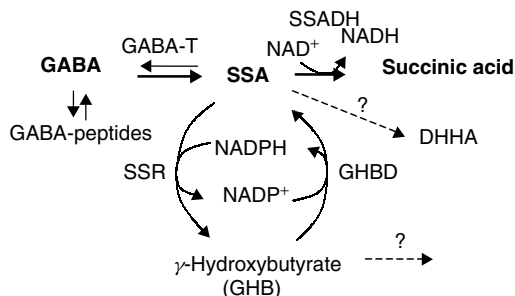


**Figure 6.3.** Pathways of brain GABA catabolism. The major pathway of GABA catabolism occurs in the GABA shunt, the enzymes for which are present in astroglia and GABAergic neurons. In this pathway GABA undergoes transamination with  $\alpha$ -ketoglutarate to produce succinic semialdehyde (SSA) and glutamate. SSA is oxidized to succinic acid which enters the TCA cycle. GABA also serves as precursor for GABA-conjugated peptides, e.g., homocarnosine. The GABA catabolite, succinic semialdehyde (SSA) is the precursor of  $\gamma$ -hydroxybutyrate (GHB). Note, however, that the alternative pathways of GABA catabolism do not result in the net loss of GABA from the main oxidative pathway of the GABA shunt. Abbreviations: GABA-T, GABA-transaminase; SSADH, succinic semialdehyde dehydrogenase; SSR, succinic semialdehyde reductase; GHBD,  $\gamma$ -hydroxybutyrate dehydrogenase; GHB,  $\gamma$ -hydroxybutyrate; DHHA, 4,5-dihydroxyhexanoic acid.

### 6.3.2. Glutamate Decarboxylase and GABA Synthesis

GABA is synthesized by  $\alpha$ -decarboxylation of glutamate via glutamate decarboxylase (GAD). GAD activity has an absolute requirement for pyridoxal-5'phosphate cofactor. The interconversion between the cofactor-bound and free forms of GAD serves as a major means of regulating GAD activity (Martin *et al.*, 1991b). GAD occurs in brain as two major isoforms of 65 and 67 kDa (Erlander and Tobin, 1991; Martin and Rimvall, 1993). In the rat cortex GAD<sub>65</sub> is the predominate form (~70%). The two forms are distributed differently within GABAergic neurons: whereas GAD<sub>67</sub> is found throughout the neuron, GAD<sub>65</sub> is highly enriched in nerve terminals and is associated with synaptic vesicles (Kaufman *et al.*, 1991; Martin and Rimvall, 1993). GAD<sub>67</sub> exists mainly as cofactor-bound active enzyme, whereas only about half of GAD<sub>65</sub> is cofactor bound (Kaufman *et al.*, 1991; Martin *et al.*, 1991a,b). The differing kinetic properties and

cellular distributions of the two GAD isoforms suggest different functional roles for cellular and vesicular GABA (Soghomonian and Martin, 1998; Belhage *et al.*, 1993). NMR studies are beginning to shed new light on the function of these two isoforms *in vivo* (Section 6.6).

### 6.3.3. Alternate Pathways of GABA Synthesis

Alternative but quantitatively minor pathways of GABA synthesis from putrescine and other polyamines have been described (Seiler, 1980). Polyamine pathways appear to play a quantitatively minor role in GABA synthesis (~1%) in the mature brain (Noto *et al.*, 1986). Polyamines, however, may have a significant role in the developing brain and retina (Yamasaki *et al.*, 1999; Zawia and Harry, 1993), or possibly in the adult hypothalamus and other neuroendocrine associated regions, where the putrescine and potential GABA precursor, agmatine (4-aminobutyryl guanidine), is concentrated in unusually high levels (Sastre *et al.*, 1996; Gorbatyuk *et al.*, 2001).

## 6.4. ROLE OF GABA AND GLUTAMINE TRANSPORTERS IN GABA METABOLISM

### 6.4.1. GABA Transporters

The flow of GABA between neurons and astroglia is critical to the operation of the GABA/glutamine cycle (Figure 6.1). GABA transport proteins in plasma membranes of neurons and astroglia serve to maintain GABA at low extracellular levels, limiting diffusion from sites of release, and effectively terminating the receptor-mediated action of GABA (Henn and Hamberger, 1971; Iversen and Kelly, 1975; Hertz *et al.*, 1977; Ryan and Roskoski, 1977). GABA transporters are  $\text{Na}^+$  and  $\text{Cl}^-$  dependent and the most highly expressed ones in brain, GAT1 and GAT3, have a stoichiometry of  $2\text{Na}^+$  and  $1\text{Cl}^-$  co-transported with each molecule of GABA (Kenyan and Kanner, 1988; Kavanaugh *et al.*, 1992). Therefore, GABA transport is electrogenic and requires ATP to maintain the  $\text{Na}^+$  ion gradient and driving force for GABA uptake. The stoichiometry of ion and substrate transport for GABA transport in astroglia is shown in Figure 6.4.

The role of the neuronal (GAT1) and astroglial (GAT1 and GAT3) GABA transporters with regard to the removal of synaptic and extra-synaptic GABA is not entirely clear. GAT1, which is the most highly expressed GAT and believed to mediate the majority of GABA transport (Schousboe, 2000; 2003), is present in high densities on axon terminals of GABA neurons and astrocytes near GABAergic synapses (Minelli *et al.*, 1995; Conti *et al.*, 1998). Inhibition of glial GAT1 results in a significant increase in extracellular GABA (Juhasz *et al.*, 1997), while inhibitors of astroglial but not neuronal GABA transporters are also effective anticonvulsants (Gadea *et al.*, 2001; Schousboe, 2000; White *et al.*, 2002). These studies suggest that astroglial transporters play an important role in the uptake and regulation of extracellular GABA. Astrocytes often show positive immunostaining with anti-GABA antibodies when GABA levels are elevated by inhibitors of GABA-transaminase (K. Behar and M. Schwartz, unpublished observations) underscoring the importance of astroglia in the removal and catabolism of GABA.

### 6.4.2. Glutamine Transporters

Although glutamine has been known to provide precursors for GABA synthesis for many years, very little was known about how glutamine actually entered the cells. Significant progress has been made recently in the characterization of glutamine transporters in both neurons and glia. Both electrogenic and electroneutral glutamine transporters are expressed in brain cells and both types involve co-transport of sodium ions. Glutamine transport into neurons involve A-type transporters (SA1 and SA2) and are electrogenic ( $\text{Gln}:\text{Na}^+ = 1:1$ ). In contrast astroglia express mainly the N-type (SN1) transporter which is electroneutral

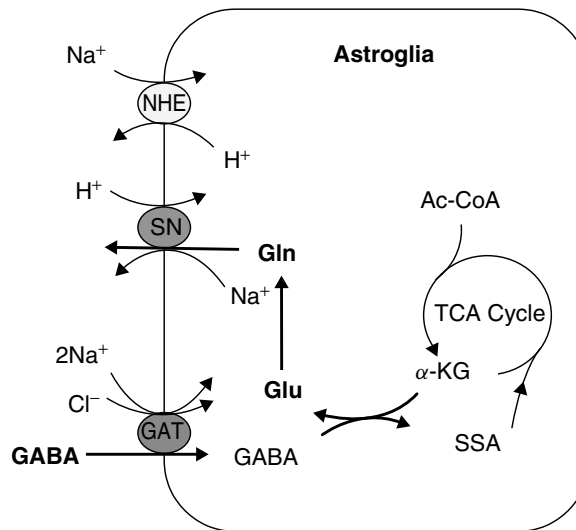


**Figure 6.4.** GABA and ion transport during GABA/glutamine cycling in astroglia. The depicted scheme shows substrate and ion flows during GABA/glutamine cycling in astroglia. GABA influx through the GABA transporter (GAT) co-transport 2  $\text{Na}^+$  and 1  $\text{Cl}^-$  into the cytoplasm. Glutamine (Gln) efflux through System-N transporters (SN) removes 1  $\text{Na}^+$  while counter-transporting 1  $\text{H}^+$  into the cytoplasm resulting in an influx of 1  $\text{Na}^+$ : 1  $\text{H}^+$ : 1  $\text{Cl}^-$  per GABA/glutamine transport cycle. Hypothetical removal of  $\text{H}^+$  by coupled  $\text{Na}^+$ / $\text{H}^+$  exchange could maintain  $\text{H}^+$  homeostasis at the expense of additional sodium loading. Thus, the degree of stimulation of  $\text{Na}^+$ / $\text{K}^+$ -ATPase by  $\text{Na}^+$  influx during the GABA/glutamine transport cycle could depend on astroglial pH regulation.

(Gln: $\text{Na}^+$  :  $\text{H}^+$  = 1:1:1) due to counter-transport of  $\text{H}^+$  (Chaudhry *et al.*, 2002). GABAergic neurons express both A-type transporters, although SA2 is particularly enriched in some interneurons. High densities of astroglial SN1 transporters surround GABAergic and glutamatergic processes (Boulland *et al.*, 2002).

## 6.5. NMR STUDIES OF GABAERGIC FUNCTION

### 6.5.1. Measurements of GABA Synthesis

Pharmacologic treatments that inhibit glutamate decarboxylase and GABA synthesis reduce GABA release and GABA-mediated inhibition (Golan *et al.*, 1996), whereas electrical stimulation increases both GABA synthesis and GABA release (Corradetti *et al.*, 1983). Thus, the rate of GABA synthesis is considered to reflect the activity of GABAergic neurons and their rate of energy utilization. The current primary methods for estimation of the GABA synthesis rate involve either administering a pharmacologic inhibitor of GABA catabolism (e.g., GABA-transaminase inhibitor) and measuring the initial rise in GABA over a defined time period (Loscher *et al.*, 1989; Behar and Boehm, 1994; Preece *et al.*, 1994) or measuring the rate of GABA turnover using isotopically  $^{13}\text{C}$  labeled precursors (Manor *et al.*, 1996; Mason *et al.*, 2001; Patel *et al.*, 2003). In general, absolute GABA synthesis rates determined with GABA-transaminase inhibitors are less than values determined by the  $^{13}\text{C}$  isotopic turnover of GABA. For example, the rate of GABA synthesis based on the initial rise of GABA in  $^1\text{H}$  NMR spectra following GABA-transaminase inhibition is 0.03–0.04  $\mu\text{mol/g}/\text{min}$ , compared to 0.10–0.15  $\mu\text{mol/g}/\text{min}$  using [1- $^{13}\text{C}$ ]glucose (Mason *et al.*, 2001). It is likely that the lower rate of GABA synthesis found when using GABA-transaminase inhibition is related to incomplete inhibition of the catabolic pathway, although feedback inhibition of GAD by rising GABA levels cannot be entirely excluded.

### 6.5.2. GABA/Glutamine Cycling

Mature neurons do not possess the necessary anaplerotic enzymes (e.g., pyruvate carboxylase) needed for net synthesis of glutamate precursors used in GABA synthesis. These precursors are derived primarily from astroglial glutamine (Paulsen *et al.*, 1988; Badar-Goffer *et al.*, 1990; 1992; Peng *et al.*, 1993; Battaglioli and Martin, 1991, 1996; Sonnewald *et al.*, 1993; Cerdan *et al.*, 1990; Patel *et al.*, 2001). While the importance of glutamine in GABA synthesis is in little doubt, quantitative information on the flux of this precursor pathway *in vivo* was lacking. A study of the role of glutamine in net GABA formation in the rat cortex was conducted using [2-<sup>13</sup>C]glucose, which labels glutamine-C3 via the astroglia-specific pyruvate carboxylase pathway (Patel *et al.*, 2001). GABA synthesized from [3-<sup>13</sup>C]glutamine precursors will lead to readily detectable <sup>13</sup>C labeling of GABA-C3. In the experiment GABA degradation and <sup>13</sup>C-isotopic label recycling was blocked by use of an inhibitor of GABA-transaminase. This study showed that ~85 % of total GABA synthesis could be attributed to glutamine precursors (Patel *et al.*, 2001). Preliminary results of an NMR study comparing GABA/glutamine and glutamate/glutamine cycling fluxes at different levels of activity suggests that GABA/glutamine cycling flux accounts for ~22 % of total (GABA + glutamate) neurotransmitter cycling (Patel *et al.*, 2003). Thus, GABA/glutamine cycling constitutes a quantitatively significant pathway of GABA neurotransmitter repletion.

## 6.6. NMR STUDIES OF GABA SYNTHESIS REGULATION *IN VIVO*

Quantitative NMR studies distinguishing contributions of the GAD isoforms to GABA synthesis have been reported recently. Manor *et al.* (1996) reported that the GABA synthesis rate was reduced when rats were treated with the GABA-T inhibitor vigabatrin, which increase GABA levels by blocking catabolism. Since GABA synthesis was reduced at 24 h but not 6 h of GABA elevation, feedback inhibition of GAD by the elevated GABA levels was unlikely. Rimvall and Martin (1994) have shown that one of the two isoforms of GAD (GAD<sub>67</sub>) is sensitive to GABA concentration and decreases as GABA levels rise. A quantitative re-analysis of the data of Manor *et al.* (1996) using a detailed metabolic model that included GABA/glutamine cycling with quantitative immunoblotting of the GAD<sub>67</sub> and GAD<sub>65</sub> isoforms from that study found that the 67–70 % reduction in  $V_{GAD}$  was associated with a selective decrease of 44 % in GAD<sub>67</sub> (Mason *et al.*, 2001). Total GAD activity was reduced by 13 %, which could be accounted for entirely by the reduction of GAD<sub>67</sub> protein. These findings provide evidence that GAD<sub>67</sub> mediates the majority of cortical GABA synthesis under anesthetized (nonactivated) conditions, even though this isoform constitutes only in ~30 % of total GAD (see Section 6.4.2). The NMR findings are supported by studies of GAD<sub>67</sub> and GAD<sub>65</sub> knockout mice, which show that the majority of brain GABA is a product of GAD<sub>67</sub> (Asada *et al.*, 1996a,b).

## 6.7. CONCLUSIONS

GABA is synthesized primarily from glutamate and degraded in the GABA shunt pathway. While GABA synthesis occurs nearly exclusively in GABAergic neurons, GABA catabolism occurs in both neurons and astroglia. *In vitro* and *in vivo* NMR findings support the role of astroglial glutamine in the synthesis of GABA. An *in vivo* NMR study of the anesthetized rat cortex using an astroglial-targeted isotope ([2-<sup>13</sup>C]glucose) indicated as much as 85 % of glutamate precursors used for net GABA synthesis arose from glutamine. Under anesthetized conditions ~1/5 of the total cycling of glutamate and GABA with glutamine is contributed by GABA. Studies of the contributions of the two GAD isoforms to GABA synthesis also show that the bulk of cortical GABA synthesis under anesthetized (nonactivated) conditions is mediated by GAD<sub>67</sub>. The combination of sophisticated NMR pulse techniques to select and localize GABA resonances with increased sensitivity and resolution provided by the new generation of high-field (>7 T) magnets and

gradients now available can be expected to provide new insights into the regulation of GABA metabolism and the GABA/glutamine cycle.

## REFERENCES

Asada H, Kawamura Y, Maruyama K, Kume H, Ding R-g, Ji FY, Kanbara N, Kuzume H, Sanbo M, Yagi T, Obata K (1996a) Mice lacking the 65 kDa isoform of glutamic acid decarboxylase (GAD65) maintain normal levels of GAD67 and GABA in their brains but are susceptible to seizures. *Biochem Biophys Res Commun* **229**: 891–895.

Asada H, Kawamura Y, Maruyama K, Kume H, Ding R-g, Kanbara N, Kuzume H, Sanbo M, Yagi T, Obata K (1996b) Cleft palate and decreased brain  $\gamma$ -aminobutyric acid in mice lacking the 67-kDa isoform of glutamic acid decarboxylase. *Proc Natl Acad Sci* **94**: 6496–6499.

Bachelard H (1998) Landmarks in the application of  $^{13}\text{C}$ -magnetic resonance spectroscopy to studies of neuronal/glial relationships. *Dev Neurosci* **20**(4–5): 277–288.

Badar-Goffer RS, Bachelard HS, Morris PG (1990) Cerebral metabolism of acetate and glucose studied by  $^{13}\text{C}$ -n.m.r. spectroscopy. A technique for investigating metabolic compartmentation in the brain. *Biochem J* **266**(1): 133–139.

Badar-Goffer RS, Ben-Yoseph O, Bachelard HS, Morris PG (1992) Neuronal–glial metabolism under depolarizing conditions. A  $^{13}\text{C}$ -n.m.r. study. *Biochem J* **282** (Pt 1): 225–230.

Balazs R, Machiyama Y, Hammond BJ, Julian T, Richter D (1970) The operation of the gamma-aminobutyrate bypass of the tricarboxylic acid cycle in brain tissue *in vitro*. *Biochem J* **116**(3): 445–461.

Battaglioli G, Martin DL (1991) GABA synthesis in brain slices is dependent on glutamine produced in astrocytes. *Neurochem Res* **16**(2): 151–156.

Battaglioli G, Martin DL (1996) Glutamine stimulates gamma-aminobutyric acid synthesis in synaptosomes but other putative astrocyte-to-neuron shuttle substrates do not. *Neurosci Lett* **209**(2): 129–133.

Behar KL, Boehm D (1994) Measurement of GABA following GABA-transaminase inhibition by gabaculine: a  $^1\text{H}$  and  $^{31}\text{P}$  NMR spectroscopic study of rat brain *in vivo*. *Magn Reson Med* **31**(6): 660–667.

Behar KL, den Hollander JA, Stromski ME, Ogino T, Shulman RG, Petroff OA, Prichard JW (1983) High-resolution  $^1\text{H}$  nuclear magnetic resonance study of cerebral hypoxia *in vivo*. *Proc Natl Acad Sci USA* **80**(16): 4945–4948.

Behar KL, Ogino T (1993) Characterization of macromolecule resonances in the  $^1\text{H}$  NMR spectrum of rat brain. *Magn Reson Med* **30**(1): 38–44.

Behar KL, Rothman DL, Spencer DD, Petroff OA (1994) Analysis of macromolecule resonances in  $^1\text{H}$  NMR spectra of human brain. *Magn Reson Med* **32**(3): 294–302.

Belhage B, Hansen GH, Schousboe A (1993) Depolarization by  $\text{K}^+$  and glutamate activates different neurotransmitter release mechanisms in GABAergic neurons: vesicular versus non-vesicular release of GABA. *Neuroscience* **54**(4): 1019–1034.

Boulland JL, Osen KK, Levy LM, Danbolt NC, Edwards RH, Storm-Mathisen J, Chaudhry FA (2002) Cell-specific expression of the glutamine transporter SN1 suggests differences in dependence on the glutamine cycle. *Eur J Neurosci* **15**(10): 1615–1631.

Cao Y, Wilcox KS, Martin CE, Rachinsky TL, Eberwine J, Dichter MA (1996) Presence of mRNA for glutamic acid decarboxylase in both excitatory and inhibitory neurons. *Proc Natl Acad Sci USA* **93**(18): 9844–9849.

Cerdan S, Kunnecke B, Seelig J (1990) Cerebral metabolism of [1,2- $^{13}\text{C}$ ]acetate as detected by *in vivo* and *in vitro*  $^{13}\text{C}$  NMR. *J Biol Chem* **265**(22): 12916–12926.

Chan-Palay V, Wu JY, Palay SL (1979) Immunocytochemical localization of gamma-aminobutyric acid transaminase at cellular and ultrastructural levels. *Proc Natl Acad Sci USA* **76**(4): 2067–2071.

Chaudhry FA, Reimer RJ, Edwards RH (2002) The glutamine commute: take the N line and transfer to the A. *J Cell Biol* **157**(3): 349–355.

Conti F, Melone M, De Biasi S, Minelli A, Brecha NC, Ducati A (1998) Neuronal and glial localization of GAT-1, a high-affinity  $\gamma$ -aminobutyric acid plasma membrane transporter, in human cerebral cortex: with a note on its distribution in monkey cortex. *J Comp Neurol* **396**(1): 51–63.

Corradetti R, Moneti G, Moroni F, Pepeu G, Wieraszko A (1983) Electrical stimulation of the stratum radiatum increases the release and neosynthesis of aspartate, glutamate, and gamma-aminobutyric acid in rat hippocampal slices. *J Neurochem* **41**(6): 1518–1525.

Cruz F, Cerdan S (1999) Quantitative  $^{13}\text{C}$  NMR studies of metabolic compartmentation in the adult mammalian brain. *NMR Biomed* **12**(7): 451–462.

de Graaf RA, Brown PB, Mason GF, Rothman DL, Behar KL (2003) Detection of [1,6- $^{13}\text{C}_2$ ]-glucose metabolism in rat brain by *in vivo*  $^1\text{H}$ - [ $^{13}\text{C}$ ]-NMR spectroscopy. *Magn Reson Med* **49**(1): 37–46.

Erlander MG, Tobin AJ (1991) The structural and functional heterogeneity of glutamic acid decarboxylase: a review. *Neurochem Res* **16**: 215–226.

Fitzpatrick SM, Hetherington HP, Behar KL, Shulman RG (1990) The flux from glucose to glutamate in the rat brain *in vivo* as determined by  $^1\text{H}$ -observed,  $^{13}\text{C}$ -edited NMR spectroscopy. *J Cereb Blood Flow Metab* **10**(2): 170–179.

Fonnum F, Walberg F (1973) An estimation of the concentration of  $\gamma$ -aminobutyric acid and glutamate decarboxylase in the inhibitory Purkinje axon terminals in the cat. *Brain Res* **54**: 115–127.

Gadea A, Lopez-Colome AM (2001) Glial transporters for glutamate, glycine, and GABA: II. GABA transporters. *J Neurosci Res* **63**(6): 461–468.

Golan H, Talpalar AE, Schleifstein-Attias D, Grossman Y (1996) GABA metabolism controls inhibition efficacy in the mammalian CNS. *Neurosci Lett* **217**(1): 25–28.

Gorbatyuk OS, Milner TA, Wang G, Regunathan S, Reis DJ (2001) Localization of agmatine in vasopressin and oxytocin neurons of the rat hypothalamic paraventricular and supraoptic nuclei. *Exp Neurol* **171**(2): 235–245.

Gutierrez R (2002) Activity-dependent expression of simultaneous glutamatergic and GABAergic neurotransmission from the mossy fibers *in vitro*. *J Neurophysiol* **87**(5): 2562–2570.

Henn FA, Hamberger A (1971) Glial cell function: uptake of transmitter substances. *Proc Natl Acad Sci* **68**(11): 2686–2690.

Hertz L, Wu PH, Schousboe A (1978) Evidence for net uptake of GABA into mouse astrocytes in primary cultures – its sodium dependence and potassium independence. *Neurochem Res* **3**(3): 313–323.

Hetherington HP, Newcomer BR, Pan JW (1998) Measurements of human cerebral GABA at 4.1 T using numerically optimized editing pulses. *Magn Reson Med* **39**(1): 6–10.

Iversen LL, Kelly JS (1975) Uptake and metabolism of gamma-aminobutyric acid by neurones and glial cells. *Biochem Pharmacol* **24**(9): 933–938.

Iversen LL, Schon FE (1973) The use of autoradiographic techniques for the identification and mapping of transmitter specific neurons in CNS. In: *New Concepts in Neurotransmitter Mechanisms*, ed. Mandell AJ. Plenum Press, New York, pp. 153–193.

Juhasz G, Kekesi KA, Nyitrai G, Dobolyi A, Krogsgaard-Larsen P, Schousboe A (1997) Differential effects of nipecotic acid and 4,5,6,7-tetrahydroisoxazolo[4,5-c]pyridin-3-ol on extracellular gamma-aminobutyrate levels in rat thalamus. *Eur J Pharmacol* **331**(2–3): 139–144.

Kaufman D, Houser CR, Tobin AJ (1991) Two forms of the  $\gamma$ -aminobutyric acid synthetic enzyme glutamic acid decarboxylase have distinct intraneuronal distributions and cofactor interactions. *J Neurochem* **56**: 20–23.

Kavanaugh MP, Arriza JL, North RA, Amara SG (1992) Electrogenic uptake of gamma-aminobutyric acid by a cloned transporter expressed in *Xenopus* oocytes. *J Biol Chem* **267**(31): 22007–22009.

Kenyan S, Kanner BI (1988) Gamma-aminobutyric acid transport in reconstituted preparations from rat brain: coupled sodium and chloride fluxes. *Biochem* **27**: 12–17.

Kuzniecky R, Ho S, Pan J, Martin R, Gilliam F, Faught E, Hetherington H (2002) Modulation of cerebral GABA by topiramate, lamotrigine, and gabapentin in healthy adults. *Neurology* **58**(3): 368–372.

Larsson OM, Schousboe A (1990) Kinetic characterization of GABA-transaminase from cultured neurons and astrocytes. *Neurochem Res* **15**(11): 1073–1077.

Loscher W, Honack D, Gramer M (1989) Use of inhibitors of gamma-aminobutyric acid (GABA) transaminase for the estimation of GABA turnover in various brain regions of rats: a re-evaluation of aminoxyacetic acid. *J Neurochem* **53**(6): 1737–1750.

Maitre M (1997) The gamma-hydroxybutyrate signalling system in brain: organization and functional implications. *Prog Neurobiol* **51**(3): 337–361.

Manor D, Rothman DL, Mason GF, Hyder F, Petroff OA, Behar KL (1996) The rate of turnover of cortical GABA from [1- $^{13}\text{C}$ ]glucose is reduced in rats treated with the GABA-transaminase inhibitor vigabatrin (gamma-vinyl GABA). *Neurochem Res* **21**(9): 1031–1041.

Martin DL, Martin SB, Wu SJ, Espina N (1991a) Regulatory properties of brain glutamate decarboxylase: the apoenzyme of GAD is present principally as one of two molecular forms of GAD in brain. *J Neurosci* **11**: 2725–2731.

Martin DL, Martin SB, Wu SJ, Espina N (1991b) Cofactor interactions and the regulation of glutamate decarboxylase activity. *Neurochem Res* **16**: 243–249.

Martin DL, Rimvall K (1993) Regulation of  $\gamma$ -aminobutyric acid synthesis in the brain. *J Neurochem* **60**: 395–407.

Martin DL, Tobin AJ (2000) Mechanisms controlling GABA synthesis and degradation in the brain. Chapter 2 in: *GABA in the Nervous System. The View at Fifty Years*, eds Martin DL, Olsen RW. Lippincott Williams & Wilkins, Philadelphia, PA, pp. 25–41.

Mason GF, Martin DL, Martin SB, Manor D, Sibson NR, Patel A, Rothman DL, Behar KL (2001) Decrease in GABA synthesis rate in rat cortex following GABA-transaminase inhibition correlates with the decrease in GAD(67) protein. *Brain Res* **914**(1–2): 81–91.

Minelli A, Brecha NC, Karschin C, DeBiasi S, Conti F (1995) GAT-1, a high-affinity GABA plasma membrane transporter, is localized to neurons and astroglia in the cerebral cortex. *J Neurosci* **15**(11): 7734–7746.

Noto T, Hashimoto H, Nakao J, Kamimura H, Nakajima T (1986) Spontaneous release of  $\gamma$ -aminobutyric acid formed from putrescine and its enhanced  $\text{Ca}^{2+}$ -dependent release by high  $\text{K}^+$  stimulation in the brains of freely moving rats. *J Neurochem* **46**: 1877–1880.

Owens DF, Kriegstein AR (2002) Is there more to GABA than synaptic inhibition? *Nat Rev Neurosci* **3**(9): 715–727.

Patel AB, Rothman DL, Cline GW, Behar KL (2001) Glutamine is the major precursor for GABA synthesis in rat neocortex *in vivo* following acute GABA-transaminase inhibition. *Brain Res* **919**(2): 207–220.

Patel AB, de Graaf RA, Mason GF, Rothman DL, Wang B, Shulman RG, Behar KB (2003) Absolute quantification of GABA/glutamine and glutamate/glutamine cycle fluxes in the rat cerebral cortex: an *in vivo*  $^{13}\text{C}$  NMR study. Abstracts, *Int Soc Magn Reson Med*, Toronto, Canada.

Paulsen RE, Odden E, Fonnum F (1988) Importance of glutamine for gamma-aminobutyric acid synthesis in rat neostriatum *in vivo*. *J Neurochem* **51**(4): 1294–1299.

Peng L, Hertz L, Huang R, Sonnewald U, Petersen SB, Westergaard N, Larsson O, Schousboe A (1993) Utilization of glutamine and of TCA cycle constituents as precursors for transmitter glutamate and GABA. *Dev Neurosci* **15**(3–5): 367–377.

Petroff OA, Hyder F, Rothman DL, Mattson RH (2001) Homocarnosine and seizure control in juvenile myoclonic epilepsy and complex partial seizures. *Neurology* **56**(6): 709–715.

Preece NE, Cerdan S (1996) Metabolic precursors and compartmentation of cerebral GABA in vigabatrin-treated rats. *J Neurochem* **67**(4): 1718–1725.

Preece NE, Jackson GD, Houseman JA, Duncan JS, Williams SR (1994) Nuclear magnetic resonance detection of increased cortical GABA in vigabatrin-treated rats *in vivo*. *Epilepsia* **35**(2): 431–436.

Rimvall K, Martin DL (1994) The level of GAD<sub>67</sub> protein is highly sensitive to small increases in intraneuronal gamma-aminobutyric acid levels. *J Neurochem* **62**(4): 1375–1381.

Roberts E, Frankel S (1950)  $\gamma$ -Aminobutyric acid in brain: its formation from glutamic acid. *J Biol Chem* **187**: 55–63.

Rothman DL, Behar KL, Hetherington HP, Shulman RG (1984) Homonuclear  $^1\text{H}$  double-resonance difference spectroscopy of the rat brain *in vivo*. *Proc Natl Acad Sci USA* **81**(20): 6330–6334.

Rothman DL, Sibson NR, Hyder F, Shen J, Behar KL, Shulman RG (1999) *in vivo* nuclear magnetic resonance spectroscopy studies of the relationship between the glutamate-glutamine neurotransmitter cycle and functional neuroenergetics. *Philos Trans R Soc London Ser B Biol Sci* **354**(1387): 1165–1177.

Ryan LD, Roskoski R (1977) Net uptake of gamma-aminobutyric acid by a high affinity synaptosomal transport system. *J Pharmacol Exp Ther* **200**(2): 285–291.

Sastre M, Regunathan S, Galea E, Reis DJ (1996) Agmatinase activity in rat brain: a metabolic pathway for the degradation of agmatine. *J Neurochem* **67**: 1761–1765.

Schousboe A (2000) Pharmacological and functional characterization of astrocytic GABA transport: a short review. *Neurochem Res* **25**(9–10): 1241–1244.

Schousboe A (2003) Role of astrocytes in the maintenance and modulation of glutamatergic and GABAergic neurotransmission. *Neurochem Res* **28**(2): 347–352.

Seiler N (1980) On the role of GABA in vertebrate polyamine metabolism. *Physiol Chem Phys* **12**(5): 411–429.

Shen J, Rothman DL, Brown P (2002) *in vivo* GABA editing using a novel doubly selective multiple quantum filter. *Magn Reson Med* **47**(3): 447–454.

Sibson NR, Dhankhar A, Mason GF, Rothman DL, Behar KL, Shulman RG (1998) Stoichiometric coupling of brain glucose metabolism and glutamatergic neuronal activity. *Proc Natl Acad Sci* **95**(1): 316–321.

Simeone TA, Donevan SD, Rho JM (2003) Molecular biology and ontogeny of gamma-aminobutyric acid (GABA) receptors in the mammalian central nervous system. *J Child Neurol* **18**(1): 39–48.

Sloviter RS, Dichter MA, Rachinsky TL, Dean E, Goodman JH, Sollas AL, Martin DL (1996) Basal expression and induction of glutamate decarboxylase and GABA in excitatory granule cells of the rat and monkey hippocampal dentate gyrus. *J Comp Neurol* **373**(4): 593–618.

Soghomonian JJ, Martin DL (1998) Two isoforms of glutamate decarboxylase: why? *Trends Pharmacol Sci* **19**(12): 500–505.

Sonnewald U, Westergaard N, Schousboe A, Svendsen JS, Unsgard G, Petersen SB (1993) Direct demonstration by  $[^{13}\text{C}]$ NMR spectroscopy that glutamine from astrocytes is a precursor for GABA synthesis in neurons. *Neurochem Int* **22**(1): 19–29.

Terpstra M, Ugurbil K, Gruetter R (2002) Direct *in vivo* measurement of human cerebral GABA concentration using MEGA-editing at 7 Tesla. *Magn Reson Med* **47**(5): 1009–1012.

Waagepetersen HS, Sonnewald U, Schousboe A (1999) The GABA paradox: multiple roles as metabolite, neurotransmitter, and neurodifferentiative agent. *J Neurochem* **73**(4): 1335–1342.

Westergaard N, Sonnewald U, Petersen SB, Schousboe A (1995) Glutamate and glutamine metabolism in cultured GABAergic neurons studied by  $^{13}\text{C}$  NMR spectroscopy may indicate compartmentation and mitochondrial heterogeneity. *Neurosci Lett* **185**(1): 24–28.

White HS, Sarup A, Bolvig T, Kristensen AS, Petersen G, Nelson N, Pickering DS, Larsson OM, Frolund B, Krosgaard-Larsen P, Schousboe A (2002) Correlation between anticonvulsant activity and inhibitory action on glial gamma-aminobutyric acid uptake of the highly selective mouse gamma-aminobutyric acid transporter 1 inhibitor 3-hydroxy-4-amino-4,5,6,7-tetrahydro-1,2-benzisoxazole and its N-alkylated analogs. *J Pharmacol Exp Ther* **302**(2): 636–644.

Yamasaki EN, Barbosa VD, De Mello FG, Hokoc JN (1999) GABAergic system in the developing mammalian retina: dual sources of GABA at early stages of postnatal development, *Int J Dev Neurosci* **17**: 201–213.

Zawia NH, Harry GJ (1993) Correlations between developmental ornithine decarboxylase gene expression and enzyme activity in the rat brain. *Brain Res Dev Brain Res* **71**(1): 53–57.

# Neural Energy Consumption and the Representation of Mental Events

**Simon B. Laughlin**

*Department of Zoology, University of Cambridge, Downing St, Cambridge CB2 3EJ, UK*

**David Attwell**

*Department of Physiology, University College London, Gower Street, London WC1E 6BT, UK*

---

7.1	Introduction	112
7.2	Constructing the Signalling Energy Budget	113
7.3	Neuronal and Glial Resting Potentials	113
7.4	The Metabolic Cost of Signalling with Glutamatergic Synapses	113
7.4.1	Neurotransmitter Recycling	113
7.4.2	Vesicle Release and Recycling	114
7.4.3	Post-synaptic Energy Consumption	114
7.4.4	The Total Energy Used by a Synapse and its Distribution Among Synaptic Mechanisms	115
7.4.5	Total Cost of Synaptic Signalling by a Single Neuron	115
7.5	The cost of Propagating Action Potentials in Grey Matter	115
7.6	The Cost of Signalling with One Neuron	116
7.7	Scaling Consumption by the Mean Firing Rate	116
7.8	The Distribution of Energy Consumption Between Signalling Mechanisms	116
7.9	The Robustness of our Estimates	117
7.10	The Distribution of Mitochondria Supports our Estimate	118
7.11	The Contribution of Neuronal Signalling to Cerebral Metabolic Rate	118
7.12	The Division of Cerebral Metabolic Rate Between Signalling and Maintenance	120

7.13 The Influence of Energy Usage on Neural Representations	120
7.14 Implications of the Energy Budget for Functional Imaging	121

---

## 7.1. INTRODUCTION

The non-invasive techniques of functional imaging monitor local changes in cerebral metabolism and blood flow. Because these local changes are associated with variations in neural signal level, functional images capture distributions of neural activity that are associated with events and actions. The brain's ability to convert events into actions resides in its ability to represent and process information in neural circuits. Thus the extent to which functional imaging reveals mental function depends upon the relationships between the metabolic and vascular signals used for imaging, and the signals in neural circuits used by the brain. To understand these relationships it is important to know the quantities of metabolic energy involved in neural signalling because these quantities determine the strength and distribution of metabolic signals, and necessitate the changes in blood flow and oxygenation that produce vascular signals.

Neural signalling consumes significant amounts of energy, consumption increases with activity and this increased demand is catered for by changes in metabolic rate and blood flow. The fast neural signals, action potentials and post-synaptic potentials, are generated by ions moving across membranes and, to maintain concentration gradients, these ions are restored by pumps, co-transporters and exchangers. These homeostatic mechanisms derive their energy, directly or indirectly, from the hydrolysis of ATP to ADP, and most of the brain's ATP is regenerated from ADP by the aerobic glycolysis of glucose. Sokoloff's application of his 6-deoxy glucose method demonstrated that the rate of glucose consumption changes locally within the brain, and increases with neural activity (Clarke and Sokoloff, 1999).

How is energy usage distributed among the many mechanisms that participate in neural activity? In 1975 Creutzfeld used biophysical data, the heat produced by action potentials in nerves, to calculate the energy required to transmit action potentials within cortex (Creutzfeld, 1975). Because of an arithmetic error, Creutzfeld's calculation indicated that action potentials only accounted for approximately 1 % of the cortical metabolic rate, leading him to suggest that synapses were primarily responsible for activity-dependent energy consumption. This conclusion placed metabolic signals at the sites at which information is processed, as opposed to transmitted, and was widely accepted. Experimental evidence supports a strong involvement of synaptic transmission in energy consumption. The density of mitochondria correlates with the density of the excitatory (glutamatergic) synapses (Wong-Riley, 1989; Wong-Riley *et al.*, 1998) and, when activity is progressively suppressed by anaesthesia, a decline in the turnover of the synaptic glutamate is accompanied by a fall in glucose consumption (Sibson *et al.*, 1998). However, changing the level of neural activity affects a wide variety of neural mechanisms, all of which use metabolic energy to a greater or lesser extent.

To resolve the distribution of energy usage among neural mechanisms we undertook a comprehensive assessment of the energy used for neural signalling in cortical grey matter. We constructed a 'bottom-up' energy budget that, like Creutzfeld's original calculation, takes biophysical and biochemical data from the literature to calculate the energy used by known signalling mechanisms as a function of action potential frequency. By multiplying these values by the numbers of sites at which they operate we estimated both the total energy requirement for neural signalling in grey matter as a function of firing rate, and the distribution of this usage among signalling mechanisms. The budget demonstrates that the ion fluxes used for electrical signalling dominate energy consumption and, contrary to Creutzfeld (1975), action potentials are as demanding as synapses. Biochemical pathways for neurotransmitter recycling are of secondary importance and, although evidence is slim, the same appears to be true of second messenger signalling.

The details of the budget, the sources of the published data and the methods used for evaluation and calculation are in Attwell and Laughlin (2001). Here we summarise our approach and our findings, draw attention to critical assumptions, identify unresolved issues, and review more recent studies. We also consider how metabolic demands influence both the structure of neural representations and the ability of functional imaging techniques to determine this structure.

Before proceeding we emphasise that the values in our budget are estimates that must be continually questioned and revised. Creutzfeld unwittingly misled the field for 25 years because his convenient conclusion that action potentials make negligible demands on cortical energy was widely accepted. The overall pattern of energy usage revealed by our budget appears to be correct because the numbers of ions and molecules involved in the different types of signalling mechanism differ by orders of magnitude, but the absolute values and percentages are estimates that must not be set in stone.

## 7.2. CONSTRUCTING THE SIGNALLING ENERGY BUDGET

We chose rodent cortex because it provides the best set of physiological and anatomical data. Much of the biophysical work on synaptic mechanisms has been carried out in rat and Braatenberg and Schüz (1998) provide unique morphometric data on the density, structure and connectivity of neurons in mouse cortex. We calculated the energy used by the average cortical neuron (taken to be a pyramidal cell) when it signals with an action potential and restricted our estimate to the dendrites, cell body, axon collaterals and synapses in grey matter. The energy consumed by myelinated axons in white matter was not considered. We calculated the energy used when a neuron's glutamatergic output synapses are stimulated by an action potential, the energy used to conduct this action potential through grey matter to the output synapses, and the energy used to maintain the resting potential, between action potentials. These values give the energy used for neural signalling as a function of action potential rate and identify the contributions made by mechanisms involved in signalling (e.g. action potentials, neurotransmitter recycling, vesicle recycling, post-synaptic currents, calcium transients in spines). Multiplying the energy consumed per neuron by the density of neurons in grey matter gives a specific metabolic rate that is comparable to measured values.

## 7.3. NEURONAL AND GLIAL RESTING POTENTIALS

We made two assumptions: the resting potential is determined by the conductances and reversal potentials for sodium and potassium ions and the electrogenic action of the Na/K pump, and the resting cell is sufficiently compact that the input conductance measured by an electrode inserted in the cell body equals the total sodium and potassium conductance of the cell. Based on these assumptions we used published measurements of resting potential and input resistance to calculate sodium and potassium currents, pumps rates and hence ATP consumption. We calculated that a neuron hydrolyses  $3.42 \times 10^8$  ATPs per second to maintain its resting potential, and a glial cell hydrolyses  $1.02 \times 10^8$  ATPs/s. With approximately as many glial cells as neurons in grey matter, the total resting consumption, neurons plus glia, is  $4.44 \times 10^8$  ATPs/neuron/s. We have classified the energy used to maintain the resting potential as a signalling activity because the resting potential fills in the gaps between action potentials. The resting potential can equally well be classified as a maintenance process that keeps a cell alive (Ames, 2000).

## 7.4. THE METABOLIC COST OF SIGNALLING WITH GLUTAMATERGIC SYNAPSES

### 7.4.1. Neurotransmitter Recycling

When an action potential reaches a synaptic bouton one synaptic vesicle of glutamate is released with a probability that depends on mean firing rate. The 4000 glutamates released from the vesicle are mainly

taken up by astrocytes. Uptake of one glutamate is driven by the co-transport of 3  $\text{Na}^+$  ions and 1  $\text{H}^+$ , and the counter-transport of 1  $\text{K}^+$  ion. The proton is restored by  $\text{Na}^+/\text{H}^+$  exchange, giving a net entry of 4  $\text{Na}^+$  ions per glutamate. These sodium ions (and the potassium ion) are restored to the extracellular space by the  $\text{Na}/\text{K}$  exchange pump with a stoichiometry of 3  $\text{Na}^+$  ions per ATP, giving an energy cost for uptake into astrocytes of 1.33 ATP per glutamate. We allowed 1 ATP per glutamate for metabolic processing in astrocytes (e.g. conversion to glutamine). The passive diffusion of processed product to neurons and the conversion back to glutamate are costless. Glutamate pumping into vesicles is powered by the vesicular proton ATPase which pumps at least one proton per glutamate at a cost of 1/3 ATP per proton (assuming that it operates like the mitochondrial F-type ATPase). Adding the costs of astrocytic uptake, metabolic processing and vesicle replenishment gave a total recycling cost of 2.66 ATP/glutamate which, with 4000 glutamates, gave a neurotransmitter recycling cost of 11 000 ATPs per released vesicle.

#### 7.4.2. Vesicle Release and Recycling

Measurements made at calyx synapses in the mammalian auditory system show that an action potential triggers a pre-synaptic influx of  $1.2 \times 10^4 \text{Ca}^{2+}$  ions per vesicle released (Helmchen *et al.*, 1997). Extruding these ions with the  $3 \text{Na}^+/\text{Ca}^{2+}$  exchanger requires  $1.2 \times 10^4$  ATPs. Thus the pre-synaptic calcium influx that stimulates vesicle release is about as costly as neurotransmitter recycling. On thermodynamic grounds the fusion of the vesicle to the membrane requires the equivalent of 10.5 ATPs (Siegel, 1993), giving an absolute requirement of 21 ATPs per cycle of fusion and endocytosis. The intricate molecular machinery used for exocytosis and endocytosis is more costly to operate. Endocytosis involves around 400 molecules per vesicle (clathrins, adaptor proteins, dynamins and hsc70s) and, if each of these molecules is phosphorylated once, the cost is 400 ATPs per vesicle. Making the generous assumption that the molecular machinery for exocytosis (triggered by calcium influx) is equally costly, the estimated cost of one cycle of exo- and endocytosis is of the order of  $10^3$  ATPs per vesicle, just 5 % of the combined cost of transmitter recycling and pre-synaptic calcium entry.

#### 7.4.3. Post-synaptic Energy Consumption

Post-synaptic energy consumption dominates the cost of synaptic transmission. The glutamate released from a vesicle binds to three types of receptors on the post-synaptic membrane, the non-NMDA and NMDA receptor channels, and G-protein coupled receptors. From measurements of channel conductance and open time and the electrochemical potential for the relevant ions,  $\text{Na}^+$  and  $\text{Ca}^{2+}$ , we calculated the numbers of ions entering the post-synaptic neuron when a channel is opened by binding glutamate, and then multiplied by the number of activated channels. Experimentally based estimates of the numbers of non-NMDA receptor channels activated by a vesicle vary from 15 to 200, giving a wide range of values of sodium influx,  $8.7 \times 10^4$  to  $1.87 \times 10^6$  per vesicle. We took a weighted mean, based on the acknowledged possibility that the upper value is an overestimate (Markram *et al.*, 1997), and calculated an influx of  $2 \times 10^5 \text{Na}^+$  ions/vesicle. 67 000 ATPs must be hydrolysed to pump these  $\text{Na}^+$  ions back. Similarly, we estimate that  $1.8 \times 10^5 \text{Na}^+$  ions and  $10 000 \text{Ca}^{2+}$  ions enter through NMDA receptor channels and 70 000 ATPs are required to return these ions. The response triggered by G-protein coupled receptors, a rise in intracellular free  $\text{Ca}^{2+}$  concentration in the post-synaptic spine, involves approximately 70  $\text{IP}_3$  molecules and 3000  $\text{Ca}^{2+}$  ions (both the spines and the intracellular calcium concentration are tiny) and the restoration of  $\text{IP}_3$  and  $\text{Ca}^{2+}$  ions gave a cost of a little over 3000 ATPs.

#### 7.4.4. The Total Energy Used by a Synapse and its Distribution Among Synaptic Mechanisms

The distribution of energy usage among synaptic mechanisms illustrates two important points. First, energy costs are roughly proportional to the numbers of ions and molecules used for signalling. Second, when a synapse is an amplifier, post-synaptic costs dominate. Releasing the vesicle involves  $12\,000\text{Ca}^{2+}$  ions, requiring 12 000 ATPs. Ejecting and retrieving the vesicle involves hundreds of molecules requiring in the order of 1000 ATPs, and recycling the 4000 glutamates released from the vesicle requires 11 000 ATPs. The post-synaptic channels opened by the pre-synaptic release of one vesicle of glutamate admit close to 400 000 ions and a total of 137 000 ATPs are needed to pump them back out. Add to this the remarkably economical second messenger response, and the total post-synaptic consumption is 140 000 ATPs. The total energy consumption associated with the release of single vesicle of glutamate is 164 000 ATPs, 85 % of which is devoted to the post-synaptic response.

#### 7.4.5. Total Cost of Synaptic Signalling by a Single Neuron

On average a mouse pyramidal cell makes 8000 output synapses. At the estimated mean firing rate in rodent cortex of 4 Hz, the probability that a spike triggers the release of a vesicle at a bouton is 0.25. On this basis the neuron releases an average of 2000 vesicles of glutamate per action potential, giving an estimated total synaptic cost of  $3.28 \times 10^8$  ATPs/neuron/action potential.

### 7.5. THE COST OF PROPAGATING ACTION POTENTIALS IN GREY MATTER

Synaptic vesicle release is stimulated by the arrival of an action potential. This electrical pulse travelled along axon collaterals in grey matter and, to make more distant connections, passed along the myelinated axon in white matter to (largely unmyelinated) terminal branches in grey matter. For statistical purposes these terminal branches are treated as collaterals (Braitenberg and Schütz, 1998). The action potential also propagated over the cell body and depolarised the dendrites. Taking data on the membrane areas of collaterals, cell body and dendrites we estimated the inward current required to charge the membrane capacitance to the peak of action potential (assumed to be a change of 100 mV). The total  $\text{Na}^+$  influx is larger than the capacitive current because  $\text{K}^+$  ions are leaving the neuron as  $\text{Na}^+$  ions enter. We multiplied the capacitive  $\text{Na}^+$  influx by 4, the factor for squid giant axon (Hodgkin, 1975). We converted this influx to energy consumption by assuming that it requires 1 ATP to pump out 3  $\text{Na}^+$  ions. Our analysis of pump kinetics showed that 3–10 % less ATP is required because the  $\text{Na}^+$  flux is influenced by changes in concentration and membrane potential, but we did not apply this small correction.

Transmission along axon collaterals accounts for 82 % of the energy used by action potentials. The average pyramidal cell makes 4 cm of axon collateral including terminal branches (Braitenberg and Schütz, 1998) with mean diameter 0.3  $\mu\text{m}$ , necessitating an influx of  $9.44 \times 10^8\text{Na}^+$  ions. Invading the 25  $\mu\text{m}$  diameter spherical cell body requires  $4.92 \times 10^7\text{Na}^+$  ions. In line with recorded responses and models of pyramidal cells we have assumed that dendrites are depolarised on average by 50 mV, consequently  $1.57 \times 10^8\text{Na}^+$  ions are needed to depolarise the 4 mm of dendrite of mean diameter 0.9  $\mu\text{m}$ . Adding these contributions (and neglecting the myelinated axon in white matter), a total of  $1.15 \times 10^9\text{Na}^+$  ions enter a neuron per action potential, and pumping them out takes  $3.84 \times 10^8$  ATPs. Any involvement of  $\text{Ca}^{2+}$  ions in dendrite depolarisation affects this total by <10 %. Thus, contrary to Creutzfeld's (1975) estimate, action potentials use slightly more energy than the synapses in rodent cortex. Our method of calculating

action potential costs was checked by A. Roth and M. Hausser, using pyramidal cell models (Vetter *et al.*, 2001) that incorporate the effects of ionic conductances and cell morphology.

## 7.6. THE COST OF SIGNALLING WITH ONE NEURON

Adding the cost of transmitting an action potential to the cost of activating output synapses, the total cost of signalling is  $7.1. \times 10^8$  ATPs/neuron/action potential. This cost per spike is equivalent to maintaining the resting potential of the neuron and associated glia for 1.6 s. Because the discharge of an action potential and the consequent activation of output synapses are metabolically significant events, neural energy consumption rises steeply in proportion to spike rate from a relatively low baseline. This approximately linear relationship between spike rate and metabolic rate is observed when electrical activity is elevated or depressed experimentally (Smith *et al.*, 2002; Clarke and Sokoloff, 1999). By coupling spike rate to neurotransmitter release, our model also predicts the linear relationship between metabolic rate and the turnover of synaptic glutamate observed in rat cortex by NMR spectroscopy (Sibson *et al.*, 1998). The stoichiometry of the relationship between glutamate turnover and metabolic rate is disputed (Choi *et al.*, 2002) and we note that a well known effect, a change in the probability of vesicle release with action potential frequency, will change the relationships between spike rate, energy consumption and the rate of turnover of synaptic glutamate.

## 7.7. SCALING CONSUMPTION BY THE MEAN FIRING RATE

Although the mean firing rate of cortical neurons is a critical parameter, both for setting the average level of usage (often called the baseline) and for interpreting the significance of fractional increases in local metabolic rate (Hyder *et al.*, 2002; Raichle and Gusnard, 2002; Smith *et al.*, 2002), there are relatively few measurements from unrestrained animals in natural surroundings. The mean firing rate in rat grey matter varies from 1.6 to 16 Hz, depending on the unit, and the means of populations vary from 1.5 to 4 Hz. Because the experiments were conducted in impoverished laboratory conditions we took the higher rate, 4 Hz, to obtain a consumption by action potentials and synapses of  $2.85 \times 10^9$  ATPs/neuron/s. Adding the consumption by resting potentials gave a total consumption by a neuron and its associated glia of  $3.29 \times 10^9$  ATPs/s.

## 7.8. THE DISTRIBUTION OF ENERGY CONSUMPTION BETWEEN SIGNALLING MECHANISMS

The relative distribution of energy usage among signalling mechanisms in rodent grey matter is plotted in Figure 7.1 for an action potential rate of 4 Hz. 81 % of signalling energy is used to restore the ions that generated fast electrical signals, 47 % to action potentials and 34 % to post-synaptic responses. The slower G-protein coupled post-synaptic responses use much less signalling energy. Only 0.7 % is required to support calcium signals in post-synaptic spines, but other second messenger responses have not been budgeted for. Neuronal and glial resting potentials come second, with 13 % of consumption, 10 % for neurons and 3 % for glia. Recycling the neurotransmitter, glutamate, takes just 3 % and this small percentage has been confirmed in conscious human brain by NMR spectroscopy (Choi *et al.*, 2002). Pre-synaptic calcium entry also requires 3 % and the mechanisms for vesicle recycling (exocytosis and endocytosis) consume less than 0.5 %.

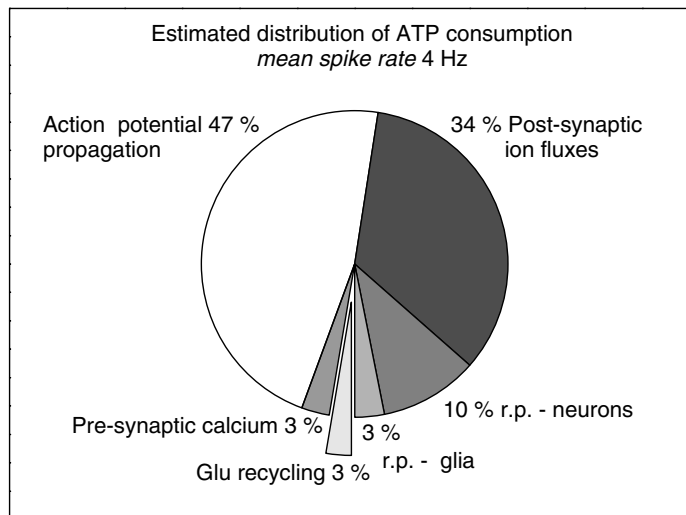


**Figure 7.1.** The distribution of ATP consumption among signalling mechanisms, calculated for grey matter of rodent cortex at a mean spike rate of 4 Hz (after Attwell and Laughlin, 2001).

## 7.9. THE ROBUSTNESS OF OUR ESTIMATES

The hierarchy of energy usage, electrical signalling >resting potentials> chemical signalling, is firmly grounded in the biophysics and biochemistry of neural information processing. Post-synaptic potentials and action potentials dominate energy usage (81 % total) because relatively large numbers of ions pass through channels to produce electrical signals that must be sufficiently large to process information in the presence of noise and to travel long distances, and sufficiently fast to provide adequate temporal resolution and reaction times. In this respect it is interesting that auditory areas of the mammalian brain have higher specific metabolic rates (Sokoloff *et al.*, 1977). One expects the restoration of pre-synaptic calcium (3 %) and the recycling of neurotransmitter (3 %) to use an order of magnitude less energy than the generation of post-synaptic responses (37 %) because the chemical synapse is an amplifier. Post-synaptic second messenger responses use almost an order of magnitude less energy (0.7 %) than pre-synaptic mechanisms because these second messenger signals are short range and relatively slow. On this basis we dispute Ames' proposal that second messenger signalling uses a significant fraction of neural energy but agree that little quantitative data is available (Ames, 2000).

Although the hierarchy of energy usage is well founded, our numbers are imprecise. Action potential usage is firmly based on the charging of the membrane capacitance and on morphometric data on membrane area (Braitenberg and Schütz, 1998). Moreover, the correct application of Creutzfeld's (1975) method of calculating cortical energy usage from measurements of the heat produced by action potentials in peripheral nerve gives similar results (Attwell and Iadecola, 2002). We have identified two uncertainties. The first is that the action potential propagates throughout the axonal arbour. Failure at branch points will reduce energy consumption. The second is the multiplication of the capacitive current by a factor of 4, to account for the shunting of inward sodium current by outward potassium current. We have assumed that this ratio applies to all excitable membrane in grey matter but the sodium and potassium conductances of the 0.3  $\mu\text{m}$  diameter axonal collaterals are unknown quantities.

Synaptic costs are subject to two uncertainties. The first is the number of post-synaptic ion channels activated by the release of a vesicle of neurotransmitter which is reported to vary over a wide range and could, in principle, vary from synapse to synapse. Better measurements of a larger number of glutamatergic pyramidal cell synapses are required. The second uncertainty is the proportion of synapses that release transmitter in response to an action potential. The probability of release varies considerably, according to the previous history of signalling. Setting a higher release probability increases both the fraction of energy consumed by synapses and the consumption per neuron per action potential (Lennie, 2003).

We have probably underestimated the energy required to maintain resting potentials. We employed resistance measurements made at or close to the cell body of an assumed isopotential neuron to estimate the resting  $\text{Na}^+$  influx. However, because a proportion of the average pyramidal cell's 4 cm of axonal arbour lies well beyond the limits of an electrically compact cell, this underestimates the energy required for neural resting potentials. A truer estimate requires data on the projection and membrane properties of axon collaterals. For glia we assumed that the lower input resistances reported in the literature result from electrical coupling and, if this is not the case, the glial contribution is underestimated. Thus estimates of resting consumption are likely to be revised upwards as better data become available. Indeed, the latest results from NMR spectroscopy suggest a more substantial contribution from glia, albeit in the deeply anaesthetised brain (Choi *et al.*, 2002).

## 7.10. THE DISTRIBUTION OF MITOCHONDRIA SUPPORTS OUR ESTIMATE

Mitochondria are located where ATP is used, and in grey matter they are concentrated around synapses, in dendrites and pre-synaptic terminals (Wong-Riley, 1989). These locations suggest that synapses use much more energy than action potentials. However, the large number of pre-synaptic mitochondria are in a position to satisfy two requirements, the modest needs of pre-synaptic mechanisms (<10 % of total) and the larger amount of energy (34 % of total) required to support action potential propagation in axon collaterals. Because the average distance between synaptic terminals along collaterals is 5  $\mu\text{m}$  (Braitenberg and Schütz, 1998), the diffusion of ATP and ions to and from the pre-synaptic terminal can provide for the axon (Attwell and Iadecola, 2002). The short length of axon and associated synapse could be a unit for energy consumption and supply in which, as in the insect photoreceptors (Stavenga and Tinbergen, 1983), the influx of  $\text{Ca}^{2+}$  ions at the pre-synaptic terminal stimulates the mitochondrion in anticipation of the demands made by ion pumps. Given that the mitochondria in pre-synaptic terminals and collaterals provide for action potential transmission through the axonal arbour, the distribution of mitochondria in grey matter agrees well with our estimate of energy usage (Figure 7.2).

## 7.11. THE CONTRIBUTION OF NEURONAL SIGNALLING TO CEREBRAL METABOLIC RATE

We converted the rate at which one neuron uses energy to signal to a specific metabolic rate (signalling usage per gram of neocortical grey matter) by multiplying by the neuronal density,  $9.2 \times 10^7$  neurons/ $\text{cm}^3$  (Braitenberg and Schütz, 1998) to give 30  $\mu\text{mol}$  ATP/g/min. This calculation assumes that all neocortical neurons are pyramidal cells—a reasonable first approximation because approximately 80 % of neurons are pyramidal cells, and 90 % are glutamatergic. The remaining 10 % of inhibitory neurons would have to have very different patterns of energy usage for this assumption to produce serious errors. Our estimate of 30  $\mu\text{mol}$  ATP/g/min is close to the range of rates measured in different areas of rat grey matter, 33–50  $\mu\text{mol}$  ATP/g/min. These rates were calculated from measurements of glucose utilization tabulated by Clarke and Sokoloff (1999) by assuming that, because of proton leak, only 31 ATPs are generated per glucose (Rolfe and Brown, 1997). The similarity between our estimates and measured usage (Figure 7.3)

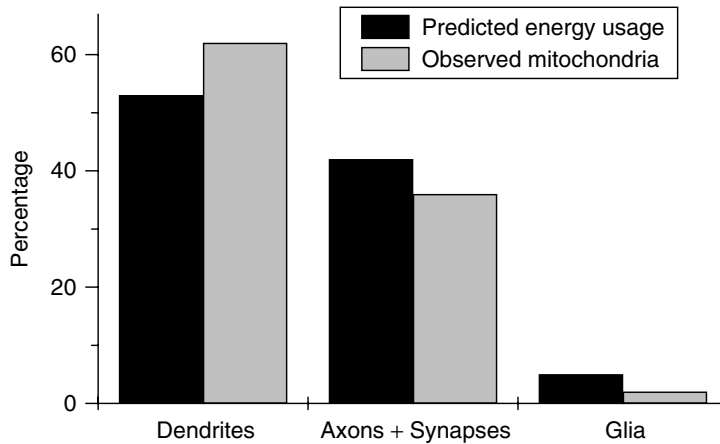


**Figure 7.2.** A comparison between the distribution of energy usage and the distribution of mitochondria among dendrites, axons plus synapses, and glia in grey matter. Energy usage is calculated for rodent grey matter spiking at 4 Hz and the mitochondrial distribution is taken from data on monkey visual cortex (Wong-Riley, 1989). The figure is replotted from Attwell and Laughlin (2001).

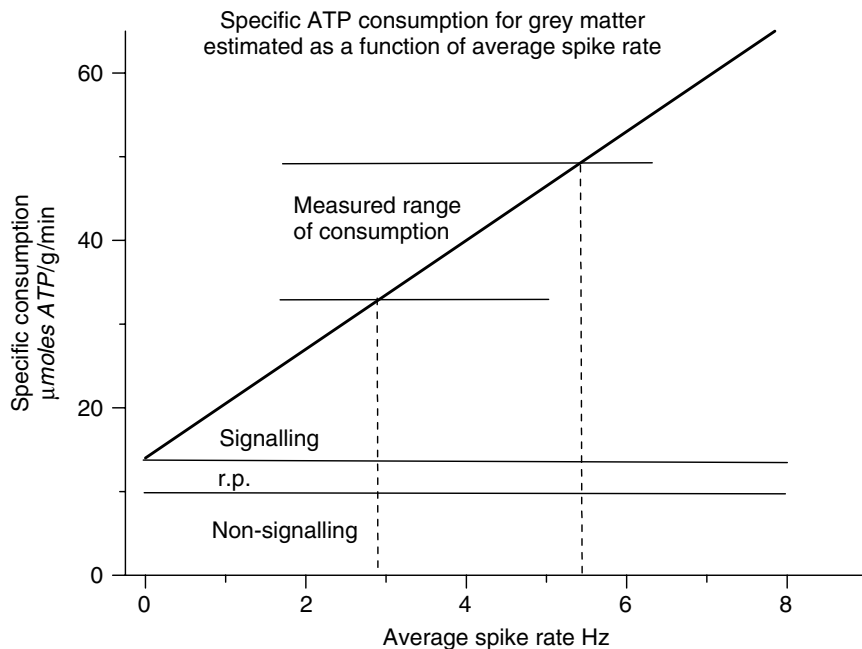


**Figure 7.3.** The specific ATP consumption of rodent grey matter estimated as a function of spike rate. The maintenance consumption is based on measurements in which all electrical activity is blocked and is assumed to be independent of spike rate (see text for further details). The contributions of neuronal plus glial resting potentials (r.p.) and signalling are from the bottom up energy budget (Attwell and Laughlin, 2001). Signalling includes both synaptic transmission and the propagation of action potentials in grey matter.

suggests that a large proportion of the energy used by grey matter goes to sustain signalling. How realistic is this suggestion?

## 7.12. THE DIVISION OF CEREBRAL METABOLIC RATE BETWEEN SIGNALLING AND MAINTENANCE

The proportion of cerebral metabolic rate devoted to signalling has been estimated by blocking neural transmission with deep anaesthesia, and by blocking the Na/K pump which uses almost all the energy required to support signalling. These manipulations reduce the energy consumption of the whole brain, or large regions of the brain, by approximately 50 % (Astrup *et al.*, 1981; Siesjö, 1978), suggesting that the energy consumption of the brain as a whole is equally divided between signalling and maintenance. This same result is obtained when NMR spectroscopy is applied to large volumes of rat brain (Choi *et al.*, 2002) but when NMR measurements are confined to cortex, blocking signalling depresses the metabolic rate by 80–90 % (Sibson *et al.*, 1998). The discrepancy between NMR measurements can be explained by attributing the higher metabolic rate in rat grey matter (30–45  $\mu\text{mol ATP/g/min}$  versus 20  $\mu\text{mol ATP/g/min}$  for the brain as a whole) to signalling. If, like the whole brain, grey matter uses 10  $\mu\text{mol ATP/g/min}$  for maintenance, the remaining 20–35  $\mu\text{mol ATP/g/min}$  is used for signalling and this range of values is in good agreement with the budget's prediction of 30  $\mu\text{mol ATP/g/min}$ . We suggest therefore that 75 % of grey matter's metabolic rate is used for signalling (Figure 7.3).

We cannot account for most of the 10  $\mu\text{mol ATP/g/min}$  that we have attributed to maintenance. Of the many processes that contribute to the viability and structural integrity of neurons, glia and blood vessels, few have been measured *in vivo*. The brain has a relatively low rate of protein turnover, and from published measurements in rat we calculated that protein synthesis uses 0.4  $\mu\text{mol ATP/g/min}$ . Ames (2000) produces a similar estimate for rabbit retina. Nucleotide turnover generally uses less energy than protein synthesis (Ames, 2000) and phospholipid metabolism could consume as much as 1  $\mu\text{mol ATP/g/min}$  (Attwell and Laughlin, 2001). These estimates suggest that macromolecular synthesis accounts for approximately 20 % of the energy used for maintenance. Actin hydrolysis has been suggested to use 50 % of the energy consumed by neurons cultured from chick ciliary ganglia (Bernstein and Bamburg, 2003), but this percentage cannot be extrapolated to intact mature brain because the technique used to measure ATP consumption involved blocking ATP production, which is known to block synaptic and action potential signalling, i.e. the major energy consuming processes in grey matter. Thus, the Bernstein and Bamburg data suggest only that the cytoskeleton uses 50 % of energy after synaptic and action potential signalling are blocked, which is about 20 % of the total energy consumption. Nonetheless, cytoskeletal maintenance and intracellular transport are good candidates for consuming a substantial fraction of the maintenance energy, and should be examined further (Ames, 2000). We calculated that the energy needed to counteract the leakage of protons from synaptic vesicles is relatively small, <0.3  $\mu\text{mol ATP/g/min}$ . Proton leakage from mitochondria should be given serious attention because in some tissues it accounts for 20 % of resting energy consumption (Rolle and Brown, 1997).

## 7.13. THE INFLUENCE OF ENERGY USAGE ON NEURAL REPRESENTATIONS

Rodent grey matter has a high specific metabolic rate, equal to that of active heart muscle (Ames, 2000) and human leg muscle running the marathon (Hochachka, 1994). The budget shows that most of this metabolic energy is used to transmit fast electrical signals relatively long distances along axon collaterals, and across large numbers of synapses. Thus the metabolic demands of grey matter are directly related to the ability of cerebral cortex to represent and associate large numbers of diverse events and actions. High metabolic

demands can profoundly influence the way in which information is represented and processed (Levy and Baxter, 1996), by limiting the number of available action potentials (Lennie, 1998). Our calculations prove that the limit is severe. The metabolic rate of rodent grey matter supports a mean firing rate of 4 Hz, and to support 18 Hz the metabolic rate equals the maximum sustainable rate of mammalian striated muscle (Attwell and Laughlin, 2001). Lennie applied our method of calculating energy usage to human brain (Lennie, 2003), and estimated that its metabolic rate can support a mean firing rate of approximately 0.16 Hz. Lennie's estimate for humans is lower than our estimate for rodent for three reasons. The human specific metabolic rate is lower than rat (as expected from the difference in body mass), Lennie's calculations assume that half the metabolic rate of cortical grey matter goes to maintenance whereas we assumed 25 %, and the proportion of synapses activated per action potential is assumed to be 0.5 in primates, compared with 0.25 in rat. Lennie (2003) predicts that approximately 50 % of signalling energy is consumed by synapses as opposed to 33 % for spike propagation. We also predicted that the proportion of energy consumed by synapses is higher in primate cortex than in rodent cortex. We based our prediction on the larger number of synapses per neuron, and noted, but did not allow for, the extension of the axonal arbour and the longer dendrites needed to connect these synapses. Allowing for longer collaterals and dendrites will increase action potential costs, and return the percentage consumption by synapses to a value closer to the rodent's. Lennie's (2003) increase in synaptic usage is largely due to the two-fold higher probability of transmitter release at boutons.

Given that metabolic costs limit signalling, brains may well have evolved to be metabolically efficient. Neurons, circuits and codes should be adjusted to reduce the costs of signal transmission and synaptic transfer, and events and actions should be represented by as few action potentials and active synapses as possible. There is *prima facie* evidence that cortex increases metabolic efficiency by these means. Fine axon collaterals (average diameter 0.3  $\mu\text{m}$ ) reduce the number of ions required to transmit an action potential by reducing membrane area. The orderly arrangement of neurons in maps has a similar effect because it reduces the distance that action potentials must travel. Sparse distributed codes reduce the numbers of action potentials required to represent events and actions, and the optimum degree of sparseness depends upon the balance between the cost of signalling and fixed costs of maintaining neurons ready to signal (Levy and Baxter, 1996; Attwell and Laughlin, 2001). For optimum efficiency <15 % of a population of cortical neurons should be activated to represent a new event or action in rodent and <4 % in human (Attwell and Laughlin, 2001; Lennie, 2003).

Reducing the probability that synapses release transmitter can save large amounts of energy. In rat, if the probability of transmitter release increased from 0.25 to 1.0, the energy used per cortical neuron per action potential would more than double and the permissible firing rate would halve. In principle, synaptic plasticity can reduce synaptic drive, and hence cost, without losing information because using 8000 synapses to drive the spike output of a single pyramidal cell is massively redundant (Levy and Baxter, 2002). A metabolically efficient cortex should use synaptic plasticity to ensure that the signal delivered by every synapse adds information that is relevant to the post-synaptic neuron's output. Cortical neurons exhibit other means of reducing redundancy, such as brief transient responses to sustained stimuli, adaptation to local signal level and subtraction of the local mean (Attwell and Laughlin, 2001). Neural mechanisms associated with attention also improve efficiency by restricting the volume of cortex in which activity is heightened (Lennie, 2003).

## 7.14. IMPLICATIONS OF THE ENERGY BUDGET FOR FUNCTIONAL IMAGING

The ability of functional imaging techniques to monitor the processing of information in neural circuits depends upon their sensitivity and resolution. Because an action potential has a significant impact on

a neuron's energy requirements and the baseline firing rate is low, metabolic measures are sensitive to small changes in neural activity. We estimated that signalling at 4 Hz accounts for 75 % of metabolic rate; consequently when 1 % of neurons increase their rate from 4 Hz to 40 Hz the energy demand increases by 7.5 %. Like the BOLD signal (Logothetis *et al.*, 2001), energy demand increases linearly with spike rate and the rate of activation of synapses but this does not necessarily mean that BOLD is a direct response to the rate at which signalling is consuming energy (Heeger and Ress, 2002). It appears that blood flow is increasing in response to neural activity in anticipation of increased energy demands. Evidence is accumulating that neurotransmitter release controls cerebral blood flow and these findings emphasise that the sensitivity and kinetics of the BOLD signal are determined by the cell signalling systems that connect neural activity to blood vessels (Zonta *et al.*, 2003; Bonvento *et al.*, 2002; Attwell and Iadecola, 2002).

Our findings are consistent with the evidence that inhibition produces a local decrease in energy demand (Shmuel *et al.*, 2002). Because most neurons are excitatory, the smaller number of inhibitory neurons are very effective at counterbalancing excitation. Consequently a small increase in the activity of inhibitory neurons can produce a larger decrease in the activity of excitatory neurons, leading to an overall reduction in energy consumption.

If the brain has compensated for the high energy demands of neural signalling by using sparse distributed codes, the neural representation of events will involve relatively small numbers of action potentials that appear transiently in a small proportion of neurons. In distributed codes, events and actions are specified by the particular combinations of neurons that are active. Thus a number of different representations will generate identical metabolic signals because they activate the same proportion of neurons in a given population. BOLD signals will be particularly badly compromised by sparse distributed coding because spatial and temporal resolution are limited by the arrangement of blood vessels (Harrison *et al.*, 2002) and the signalling mechanisms that link neural activity to vascular control (Attwell and Iadecola, 2002). Neural wiring patterns in the cortex can, in principle, limit the resolution of metabolic signals. Axon collaterals and synapses distribute approximately 80 % of a pyramidal cell's signalling consumption locally within grey matter, over distances in the order of 1 mm (Braitenberg and Schütz, 1998). Thus the neural signals that represent events and convert representation into action are not only sparse, but diffuse, and these properties make it difficult to decipher how neural circuits process signals to generate neural representations of events and actions.

If one knows how neural circuits work, one can relate changing patterns of bloodflow and energy usage to the activity of specific neurons (Lauritzen, 2001). The critical role played by a knowledge of circuitry is not obvious in our published energy budget (Attwell and Laughlin, 2001) because we considered the average distribution of signals in grey matter. Nonetheless, we followed neural signals through a defined network to determine the energy used for signalling. This network of average cortical neurons is closed (the number of intracortical connections greatly exceeds the number of fibres entering and leaving the cortex) and, by considering the average firing rate, we placed the network in a steady state. In a closed network at steady state the average number of synaptic inputs to a neuron equals the average number of its synaptic outputs and, assuming that spikes do not fail within neurons, input and output synapses are equally active. These properties of a closed steady-state system enabled us to define the pattern of energy usage without detailed descriptions of specific circuits. Detailed descriptions of specific circuits are essential for interpreting functional images, when these are images of local deviations from steady state. Under transient conditions there is no reason why the numbers of action potentials entering a voxel should equal the number leaving, and one cannot equate the number of activated input and output synapses. To infer patterns of neural activity from changes in local metabolic rate one must know which neurons are activated, how they are connected, how they drive each other and what mechanisms they use. It follows that the ability of functional imaging to reveal the neural basis of mental acts is limited by our understanding of the anatomy and physiology of neural circuits.

## Acknowledgements

Supported by the Wellcome Trust, a Wolfson–Royal Society award, and the European Union (DA), and the Rank Prize Fund and the BBSRC (SBL).

## REFERENCES

Ames, A. (2000) CNS energy metabolism as related to function. *Brain Research Reviews*, **34**, 42–68.

Astrup, J., Sorensen, P. M. and Sorensen, H. R. (1981) Oxygen and glucose consumption related to  $\text{Na}^+–\text{K}^+$  transport in canine brain. *Stroke*, **12**, 726–730.

Attwell, D. and Iadecola, C. (2002) The neural basis of functional imaging. *Trends in Neuroscience*, **25**, 621–625.

Attwell, D. and Laughlin, S. B. (2001) An energy budget for signalling in the grey matter of the brain. *Journal of Cerebral Blood Flow and Metabolism*, **21**, 1133–1145.

Bernstein, B. W. and Bamburg, J. R. (2003) Actin-ATP hydrolysis is a major energy drain for neurons. *Journal of Neuroscience*, **23**, 1–6.

Bonvento, G., Sibson, N. and Pellerin, L. (2002) Does glutamate image your thoughts? *Trends in Neurosciences*, **25**, 359–364.

Braitenberg, V. and Schütz, A. (1998) *Cortex: Statistics and Geometry of Neuronal Connectivity*, Springer, Berlin.

Choi, I.-Y., Lei, H. and Gruetter, R. (2002) Effect of deep pentobarbital anesthesia on neurotransmitter metabolism *in vivo*: on the correlation of total glucose consumption with glutamatergic action. *Journal of Cerebral Blood Flow and Metabolism*, **22**, 1343–1351.

Clarke, D. D. and Sokoloff, L. (1999) Circulation and energy metabolism of the brain. In: *Basic Neurochemistry: Molecular, Cellular and Medical Aspects* (Eds Siegel, G. J., Agranoff, B. W., Albers, R. W., Fisher, S. K. and Uhler, M. D.) Lippincott-Raven, Philadelphia, PA, pp. 637–669.

Creutzfeld, O. D. (1975) Neurophysiological correlates of different functional states of the brain. In: *Alfred Benzon Symposium VII* (Eds Ingvar, E. D. and Lassen, N. A.) Academic Press, New York, pp. 21–46.

Harrison, R. V., Harel, N., Panesar, J. and Mount, R. J. (2002) Blood capillary distribution correlates with hemodynamic-based functional imaging in cerebral cortex. *Cerebral Cortex*, **12**, 225–233.

Heeger, D. J. and Ress, D. (2002) What does fMRI tell us about neuronal activity? *Nature Reviews Neuroscience*, **3**, 142–151.

Helmchen, F., Borst, J. G. G. and Sakmann, B. (1997) Calcium dynamics associated with a single action potential in a CNS presynaptic terminal. *Biophysical Journal*, **72**, 1458–1471.

Hochachka, P. (1994) *Muscles as Molecular and Metabolic Machines*, CRC Press, Boca Raton, FL.

Hodgkin, A. L. (1975) The optimum density of sodium channels in an unmyelinated nerve. *Philosophical Transactions of the Royal Society (London) B*, **270**, 297–300.

Hyder, F., Rothman, D. L. and Shulman, R. G. (2002) Total neuroenergetics support localized brain activity: implications for the interpretation of fMRI. *Proceedings of the National Academy of Sciences of the United States of America*, **99**, 10771–10776.

Lauritzen, M. (2001) Relationship of spikes, synaptic activity and local changes in cerebral blood flow. *Journal of Cerebral Blood Flow and Metabolism*, **21**, 1367–1383.

Lennie, P. (1998) Single units and visual cortical organization. *Perception*, **27**, 889–935.

Lennie, P. (2003) The cost of cortical computation. *Current Biology*, **13**, 493–497.

Levy, W. B. and Baxter, R. A. (1996) Energy-efficient neural codes. *Neural Computation*, **8**, 531–543.

Levy, W. B. and Baxter, R. A. (2002) Energy-efficient neuronal computation via quantal synaptic failures. *Journal of Neuroscience*, **22**, 4746–4755.

Logothetis, N. K., Pauls, J., Augath, M., Trinath, T. and Oeltermann, A. (2001) Neurophysiological investigation of the basis of the fMRI signal. *Nature*, **412**, 150–157.

Markram, H., Lubke, J., Froscher, M., Roth, A. and Sakmann, B. (1997) Physiology and anatomy of synaptic connections between thick tufted pyramidal neurones in the developing rat neocortex. *Journal of Physiology–London*, **500**, 409–440.

Raichle, M. E. and Gusnard, D. A. (2002) Appraising the brain's energy budget. *Proceedings of the National Academy of Sciences of the United States of America*, **99**, 10237–10239.

Rolfe, D. F. S. and Brown, G. C. (1997) Cellular energy utilization and molecular origin of standard metabolic rate in mammals. *Physiological Reviews*, **77**, 731–758.

Shmuel, A., Yacoub, E., Pfeuffer, J., Van de Moortele, P.-F., Adriany, G., Hu, X. and Urgubil, K. (2002) Sustained negative BOLD, blood flow and oxygen consumption response and its coupling to the positive response in the human brain. *Neuron*, **36**, 1195–1210.

Sibson, N. R., Dhankar, A., Mason, G. F., Rothman, D. L., Behar, K. L. and Shulman, R. G. (1998) Stoichiometric coupling of brain glucose metabolism and glutamatergic neuronal activity. *Proceedings of the National Academy of Sciences of the United States of America*, **95**, 316–321.

Siegel, D. P. (1993) Energetics of intermediates in membrane fusion: comparisons of stalk and inverted micellar intermediate mechanisms. *Biophysics Journal*, **65**, 2124–2140.

Siesjö, B. (1978) *Brain Energy Metabolism*, Wiley, New York.

Smith, A. J., Blumenfeld, H., Behar, K. L., Rothman, D. L. and Shulman, R. G. (2002) Cerebral energetics and spiking frequency: the neurophysiological basis of fMRI. *Proceedings of the National Academy of Sciences of the United States of America*, **99**, 10765–10770.

Sokoloff, L., Reivich, M., Kennedy, C., Des Rosiers, M. H., Patlak, C. S., Pettigrew, K. D., Sakurada, O. and Shinozaki, M. (1977) The [ $^{14}\text{C}$ ]deoxyglucose method for the measurement of local cerebral glucose utilization: theory, procedure and normal values in the conscious and anesthetized albino rat. *Journal of Neurochemistry*, **28**, 897–916.

Stavenga, D. G. and Tinbergen, J. (1983) Light dependence of oxidative-metabolism in fly compound eyes studied in vivo by microspectrofluorometry. *Naturwissenschaften*, **70**, 618–620.

Vetter, P., Roth, A. and Häusser, M. (2001) Action potential propagation in dendrites depends on dendritic morphology. *Journal of Neurophysiology*, **85**, 926–937.

Wong-Riley, M. T. T. (1989) Cytochrome-oxidase - an endogenous metabolic marker for neuronal- activity. *Trends in Neurosciences*, **12**, 94–101.

Wong-Riley, M. T. T., Anderson, B., Liebl, W. and Huang, Z. (1998) Neurochemical organization of the macaque striate cortex: correlation of cytochrome oxidase with  $\text{Na}^+\text{K}^+$  ATPase, NADPH-diaphorase, nitric oxide synthetase and *N*-methyl-D-aspartate receptor subunit I. *Neuroscience*, **83**, 1025–1045.

Zonta, M., Angulo, M. C., Gobbo, S., Rosengarten, B., Hossmann, K.-A., Pozzan, T. and Carmignoto, G. (2003) Neuron-to-astrocyte signaling is central to the dynamic control of brain microcirculation. *Nature Neuroscience*, **6**, 43–50.

# Imaging Cerebral Metabolic Rate of Oxygen Consumption (CMRO<sub>2</sub>) using <sup>17</sup>O NMR Approach at Ultrahigh Field

**Wei Chen, Xiao-Hong Zhu and Kamil Ugurbil**

*Center for Magnetic Resonance Research, Department of Radiology, University of Minnesota Medical School, 2021 6th St. SE, Minneapolis, MN 55455, USA*

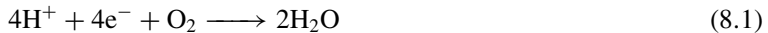
---

8.1	Central Role of Oxidative Metabolism in Brain Function and Brain Diseases	126
8.2	Existing Methodologies for Determining CMRO <sub>2</sub> <i>in vivo</i>	128
8.2.1	Positron Emission Tomography Approach	128
8.2.2	<sup>13</sup> C NMR Approach	129
8.3	<sup>17</sup> O NMR Approaches and CMRO <sub>2</sub> Measurements	129
8.3.1	Direct and Indirect <sup>17</sup> O NMR Approaches for CMRO <sub>2</sub> and CBF Measurements	129
8.4	Increased <sup>17</sup> O NMR Sensitivity at Ultrahigh Fields	130
8.4.1	<sup>17</sup> O Relaxivity and Sensitivity as a Function of Field Strength	130
8.5	Advantages of Direct <sup>17</sup> O NMR Approach for Imaging CMRO <sub>2</sub>	132
8.6	Ultrahigh Field <sup>17</sup> O NMR Approach for Imaging CMRO <sub>2</sub>	134
8.6.1	Theoretical Aspects of <sup>17</sup> O NMR Approach for Imaging CMRO <sub>2</sub>	134
8.6.2	Experimental Determination of CMRO <sub>2</sub> using <sup>17</sup> O NMR Approaches	137
8.7	Conclusions and Perspectives	141

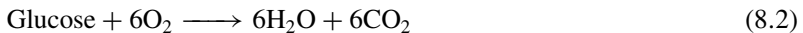
---

## 8.1. CENTRAL ROLE OF OXIDATIVE METABOLISM IN BRAIN FUNCTION AND BRAIN DISEASES

In the brain, the majority of the energy consumption occurs by neuronal activity (Attwell and Laughlin, 2001). This energy need is met predominantly through oxygen consumption mediated by the mitochondrial respiratory chain (Siesjo, 1978) which ultimately catalyzes the chemical reaction:



The energy available from this reaction is subsequently utilized to generate the high-energy phosphorous metabolite adenosine triphosphate (ATP). The oxidative energy need in the human brain to sustain neuronal activity constitutes a large fraction of the energy requirements in the entire body at basal conditions. Although the weight of the human brain is only  $\sim 2\%$  of the body weight,  $\sim 20\%$  of the body's oxygen consumption occurs in the brain. The carbon source that supports this oxidative metabolism is predominantly glucose, which is oxidized according to the chemical reaction:



A small amount of glucose can be metabolized nonoxidatively in the brain to form the lactate molecules (Figure 8.1). The oxidative process, however, provides at least 15 times more ATP than the nonoxidative pathway. Under resting conditions, the glucose metabolism is almost completely through oxidation (Siesjo, 1978, and references therein).

Basal cerebral oxygen consumption is not uniform across different regions in the brain. It is recognized that capillary density in the brain is inhomogeneous (Harrison *et al.*, 2002, and references therein), suggesting that mitochondrial density, and hence, oxygen consumption are likely to be inhomogeneous since a good correlation exists between capillarity and mitochondrial density in tissues (Hoppeler and Kayar,

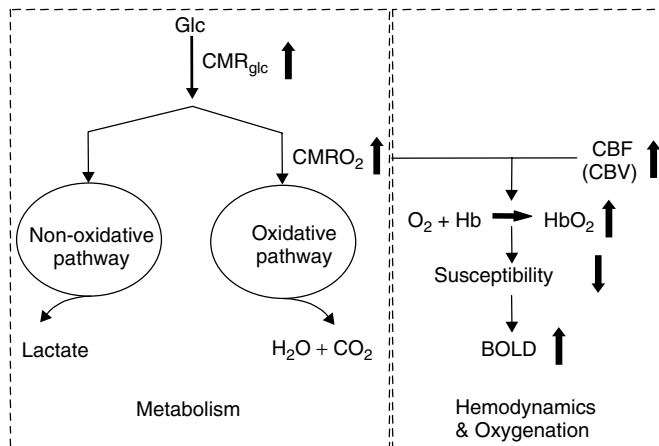


**Figure 8.1.** Schematic relationships among metabolic, hemodynamic and oxygenation responses during physiological resting and activation conditions. The glucose (Glc) compound is transported from blood plasma into the brain tissues and is consumed through two main pathways: (i) the oxidative pathway leads to the final products of  $\text{CO}_2$  and  $\text{H}_2\text{O}$  and (ii) the nonoxidative glycolysis pathway leads to the final product of lactate. The cerebral metabolic rates of glucose and oxygen are represented by  $\text{CMR}_{\text{glc}}$  and  $\text{CMRO}_2$ , respectively. Both  $\text{CMRO}_2$  and  $\text{CBF}$  (and/or  $\text{CBV}$ ) changes can affect the oxygenation level, ultimately susceptibility, and lead to BOLD contrast during neuronal activity. Zhu *et al.* (2002c). Reproduced with permission from the National Academy of Sciences, U.S.A.

1988). It is evident that there are tight correlations under basal conditions among different brain tissue compartments (e.g., gray matter versus white matter) and among different brain regions (Siesjo, 1978; Raichle, 1987) between the cerebral metabolic rates of oxygen and glucose consumption ( $CMRO_2$  and  $CMR_{glc}$ , respectively) as well as between these two metabolic rates and cerebral blood flow (CBF) (Siesjo, 1978; Raichle, 1987). Alteration in neuronal activity elevated by sensory stimulation and/or performance of a task further increases spatial nonuniformity due to *regional* changes potentially in all of these parameters (i.e.  $CMRO_2$ ,  $CMR_{glc}$  and CBF) (e.g., Fox *et al.*, 1988; Fox and Raichle, 1986; Hyder *et al.*, 1996; Chen *et al.*, 2001; Raichle, 1987).

Questions related to the oxygen consumption rate are encountered frequently in biomedical research when considering either normal tissue function or abnormalities induced by diseased states. Relevant to normal brain function, a question of particular interest is whether the alterations in  $CMRO_2$ ,  $CMR_{glc}$  and CBF induced by neuronal activity is quantitatively coupled (or matched) (Barinaga, 1997). This question is central to understanding underlying mechanisms operative in most modern neuroimaging techniques. It has been suggested that the coupling between these metabolic and hemodynamic changes during brain activation are much more complex than that under basal conditions. Based on PET measurements (Fox and Raichle, 1986; Fox *et al.*, 1988; Ribeiro *et al.*, 1993), increases in  $CMRO_2$  were reported to be considerably less than those of both CBF and  $CMR_{glc}$  during visual and somatosensory stimulations, suggesting that additional glucose utilization invoked by neuronal activity might be used nonoxidatively. This suggestion was partially supported by observations of lactate increase in the human primary visual cortex (V1) during visual stimulation (Prichard *et al.*, 1992; Sappey-Marinier *et al.*, 1992; Frahm *et al.*, 1996). However, the quantity of the increased lactate was inadequate to explain the mismatch between the  $CMRO_2$  and CBF alterations observed in the PET measurements (Fox and Raichle, 1986; Fox *et al.*, 1988; Ribeiro *et al.*, 1993; Prichard *et al.*, 1992; Shulman *et al.*, 2001b; Shulman *et al.*, 2001a). In contrast, several studies, including some that are based on the PET methodology, have provided data indicating that elevated neuronal activity could lead to a significant increase in  $CMRO_2$  in the awake human brain (e.g., Roland *et al.*, 1987; Marrett *et al.*, 1993; Chen *et al.*, 2001; Vafaei *et al.*, 1999; Davis *et al.*, 1998; Hoge *et al.*, 1999), as well as in the anesthetized rat brain (e.g., Hyder *et al.*, 1996; Kim *et al.*, 1999). The discrepancies in the literature regarding the relationship among CBF,  $CMRO_2$  and  $CMR_{glc}$  changes in response to elevated neuronal activity may have originated from differences in the nature of the stimulation employed, the cortical region involved, and the species used. In addition, however, the differences may have also arisen because of deficiencies in the neuroimaging approach used to perform the measurements.

Accurate determinations of  $CMRO_2$  and CBF changes during brain activation are also crucial for quantification of the Blood Oxygen Level Dependent (BOLD) contrast (Ogawa and Lee, 1990; Ogawa *et al.*, 1990) and understanding the mechanism underlying the functional MRI (fMRI) approach based on the BOLD contrast (Ogawa *et al.*, 1992; Blamire *et al.*, 1992; Bandettini *et al.*, 1992; Kwong *et al.*, 1992). It is generally accepted that changes in CBF and  $CMRO_2$  lead to an increase in focal blood oxygenation level, a decrease in the blood deoxyhemoglobin content and ultimately a decrease in the magnetic susceptibility gradients near the luminal boundaries of the blood vessels near the activated site as illustrated in Figure 8.1 (Ogawa *et al.*, 1998; Ugurbil *et al.*, 1999; Chen and Ogawa, 1999). In this case, a signal increase in  $T_2^*$  and/or  $T_2$ -weighted MR images defined as a positive BOLD effect can be detected. This model *qualitatively* provides a popularly accepted mechanism for interpreting the BOLD response during brain activation (Ogawa and Lee, 1990; Ogawa *et al.*, 1998). However, at a *quantitative* level, the understanding of the relationship between BOLD contrast and neuronal activity requires reliable determinations of  $CMRO_2$  and CBF changes in response to brain activation. With such reliable and independent measurements, it should be possible to interpret BOLD results of fMRI study not only in normal brain but also under diseased conditions. For example, it has been reported that the BOLD increase in the human visual cortex during visual stimulation was significantly greater in schizophrenia patients ( $4.6 \pm 1.5\%$ ) than that in normal

subjects ( $3.1 \pm 1.3\%$ ), presumably because of impaired oxidative capacity of neurons in schizophrenia patients (Renshaw *et al.*, 1994). Similarly, Huntington patients associated with mitochondrial impairment also have a greater BOLD change in response to visual stimulation (Jenkins *et al.*, 1993) as compared to normal subjects. Direct measurements of  $\text{CMRO}_2$  in these patients should explicitly test the hypothesis that the reduced oxidative metabolism in the patients is the underlying cause of these BOLD observations.

The central role of oxygen consumption is also evident in pathologies associated with the brain. Perturbations in brain oxidative metabolism have been linked to many brain diseases such as Schizophrenia, Alzheimer's disease, Huntington's disease, Parkinson's disease, mitochondrial dysfunction as well as aging problems (Maurer *et al.*, 2001; Wong-Riley *et al.*, 1997; Maurer *et al.*, 2000; Frackowiak *et al.*, 1988; Beal, 1992). One line of evidence linking these diseases and cerebral oxidative metabolism is the histopathological findings indicating that the activity of cytochrome oxidase, the key mitochondrial enzyme that catalyzes the reduction of oxygen to form water, is significantly impaired ( $>50\%$ ) in Schizophrenic (Maurer *et al.*, 2001) and Alzheimer's patients (Wong-Riley *et al.*, 1997; Maurer *et al.*, 2000) in comparison with control groups. In addition, the impairment in the cytochrome oxidase content in the diseased brain was also found to selectively affect different regions in the brain (Maurer *et al.*, 2001; Wong-Riley *et al.*, 1997; Maurer *et al.*, 2000). Therefore, the ability to *image*  $\text{CMRO}_2$  *in vivo* quantitatively is essential for efforts aimed at investigating cerebral oxidative metabolism under normal and pathological conditions as well as between basal and activation states.

## 8.2. EXISTING METHODOLOGIES FOR DETERMINING $\text{CMRO}_2$ *IN VIVO*

Due to the importance of oxidative metabolism in brain function and diseases, several methods have been developed to determine  $\text{CMRO}_2$  in the living brain. The earliest approach of  $\text{CMRO}_2$  measurement is based on the Kety–Schmidt method which relies on measuring CBF together with arteriovenous differences of oxygen content (Kety and Schmidt, 1948). This approach is relatively simple but involves substantial surgical preparations. It is thought to be the most accurate one in the literature. However, it provides global  $\text{CMRO}_2$  information without spatial differentiations within the brain.

### 8.2.1. Positron Emission Tomography Approach

Positron Emission Tomography (PET) has been established for imaging  $\text{CMRO}_2$  in humans for many years (Ter-Pogossian *et al.*, 1970; Mintun *et al.*, 1984; Lenzi *et al.*, 1981). By introducing oxygen gas enriched with the isotope  $^{15}\text{O}(\text{O}_2)$  into the human body and monitoring the spatial distribution and accumulation rate of the labeled water ( $\text{H}_2^{15}\text{O}$ ) metabolized from the inhaled  $^{15}\text{O}_2$ , PET can determine regional  $\text{CMRO}_2$ , and provide a 3D  $\text{CMRO}_2$  image. However,  $^{15}\text{O}$  PET is unable to distinguish the radioactive signals between the  $^{15}\text{O}_2$  molecule bound to hemoglobin and the  $^{15}\text{O}$  atom incorporated into  $\text{H}_2^{15}\text{O}$ . To overcome this drawback, a measurement of cerebral blood volume (CBV) using an inhalation of  $\text{C}^{15}\text{O}$  has to be performed in addition to a CBF measurement based on intravenous injection of  $\text{H}_2^{15}\text{O}$  in order to determine  $\text{CMRO}_2$  accurately (Mintun *et al.*, 1984). An alternative that eliminates a separate CBV determination has been suggested; this approach relies instead on time-weighted integration of data to estimate the vascular volume correction (Ohta *et al.*, 1992). However, the modeling used to extract this information relies on numerous assumptions. For labeled water production to attain a constant value dictated by  $\text{CMRO}_2$ , oxygen concentration in tissue has only to exceed the  $K_m$  of cytochrome oxidase; this may be attained rapidly so that even after labeled water production reaches a constant rate,  $^{15}\text{O}_2$ –hemoglobin contents in the vasculature can be changing. Thus, even if an integration time window exists where the counts reflect predominantly vascular volume, it is not clear the vascular volume estimated from that time window is applicable to the time window where data are collected on labeled water production. In addition,

utilizing this approach in CMRO<sub>2</sub> calculations requires good signal-to-noise ratio in data acquired with high temporal resolution. These requirements complicate CMRO<sub>2</sub> calculation based on PET data.

### 8.2.2. <sup>13</sup>C NMR Approach

The <sup>13</sup>C NMR approach is based on monitoring the intermediate labels incorporated from intravenously infused [1-<sup>13</sup>C] glucose and provides a useful tool for measuring CMRO<sub>2</sub> and other physiological parameters (e.g., Rothman *et al.*, 1992; Novotny *et al.*, 1990; van Zijl and Rothman, 1995; Hyder *et al.*, 1996; Gruetter *et al.*, 1998; Chen *et al.*, 1998; Chen *et al.*, 2001; Gruetter *et al.*, 2001; also see Chapters 2–4). The labeling kinetics for several intracellular metabolites, most importantly glutamate, can be unequivocally measured by direct and/or indirect <sup>13</sup>C NMR techniques. The CMRO<sub>2</sub> values can be derived based on the close correlation between the tricarboxylic acid (TCA) cycle rate and CMRO<sub>2</sub> as well as the established modeling (Hyder *et al.*, 1996; Chen *et al.*, 2001; Gruetter *et al.*, 2001; Mason *et al.*, 1992, 1995). The <sup>13</sup>C NMR approach has been applied to study the CMRO<sub>2</sub> changes in the rat somatosensory cortex during forepaw electric stimulation (Hyder *et al.*, 1996, 1997; Shulman *et al.*, 1999) and in the human visual cortex during photic stimulation (Chen *et al.*, 2001). Another unique feature of the <sup>13</sup>C NMR approach is its capability for studying the glutamate/glutamine neurotransmitter release and cycling and functional bioenergetics during brain stimulation (e.g., Shen *et al.*, 1999; Sibson *et al.*, 2001; Rothman *et al.*, 1999; Ugurbil *et al.*, 2001; Gruetter *et al.*, 2001; also see the details in Chapters 3 and 4). In general, the <sup>13</sup>C NMR approach requires a significantly long measurement time (60–120 min) due to relatively slow turnover rates of cerebral metabolites involved in <sup>13</sup>C NMR measurements. In addition, it is difficult to achieve 3D CMRO<sub>2</sub> imaging with relatively high resolution, especially in the human brain, within a short measurement period because of the relatively long repetition time required for NMR signal acquisitions and the low inherent NMR sensitivity of <sup>13</sup>C NMR.

## 8.3. <sup>17</sup>O NMR APPROACHES AND CMRO<sub>2</sub> MEASUREMENTS

### 8.3.1. Direct and Indirect <sup>17</sup>O NMR Approaches for CMRO<sub>2</sub> and CBF Measurements

In principle, NMR-detectable, magnetic isotope <sup>17</sup>O can be utilized to measure CMRO<sub>2</sub>. The concept underlying this idea is similar with that used in the <sup>15</sup>O PET approach. Explorations for monitoring labeled H<sub>2</sub><sup>17</sup>O as a tracer of oxygen utilization or tissue perfusion using NMR spectroscopy and/or imaging techniques have been initiated a decade ago (e.g., Mateescu *et al.*, 1988, 1989; Hopkins and Barr, 1987; Kwong *et al.*, 1991; Arai *et al.*, 1990; Pekar *et al.*, 1991; Fiat *et al.*, 1992; Pekar *et al.*, 1995; Ronen and Navon, 1994; Ronen *et al.*, 1998; Reddy *et al.*, 1995). These studies can be separated into two distinct groups dependent upon the types of the NMR approaches used. The first group is based on detecting H<sub>2</sub><sup>17</sup>O directly (Mateescu *et al.*, 1988, 1989; Arai *et al.*, 1990; Pekar *et al.*, 1991, 1995; Fiat *et al.*, 1992). Nonlocalized <sup>17</sup>O NMR was employed for most studies in this group to estimate CMRO<sub>2</sub> in the whole brain of experimental animals as well as in the human occipital lobe (Fiat *et al.*, 1993), following an inhalation of the oxygen gas enriched with the <sup>17</sup>O isotope (<sup>17</sup>O<sub>2</sub>). Some of these studies attempted to obtain a coarse CMRO<sub>2</sub> image (~0.8 ml voxel size) in the cat brain with a relatively long measurement time (15 min) (Pekar *et al.*, 1991; 1995). Most of these *in vivo* studies were conducted at relatively low fields compared to what is available currently. These studies demonstrated the dramatic limitations imposed by the low inherent sensitivity of <sup>17</sup>O NMR due to its low gyromagnetic ratio, which is only 14% of that of the proton nucleus. This sensitivity limitation has hindered further developments of the direct <sup>17</sup>O NMR detection approach, leading to the exploration of the second group of techniques that attempt to circumvent the sensitivity limitation by using indirect <sup>17</sup>O detection through the protons coupled to <sup>17</sup>O.

The indirect  $^{17}\text{O}$  detection approach relies on the effect of  $^1\text{H}-^{17}\text{O}$  scalar coupling on the transverse relaxation time ( $T_2$ ) or apparent  $T_2^*$  of the  $^{17}\text{O}$ -coupled water protons. The  $T_2$  of water protons are considerably shortened by the presence of the  $^{17}\text{O}$  nucleus in the water molecule (Meiboom, 1961; Hopkins and Barr, 1987). It has also been shown that the water proton  $T_2$  of  $\text{H}_2^{17}\text{O}$  can be restored to that of  $\text{H}_2^{16}\text{O}$  when  $^{17}\text{O}$  decoupling is applied; in this case, the difference between proton signals obtained with and without  $^{17}\text{O}$  decoupling is related to the  $^{17}\text{O}$  content of the water sample (Ronen and Navon, 1994; Ronen *et al.*, 1998; Reddy *et al.*, 1995). However, the indirect  $^{17}\text{O}$  measurements present difficulties for quantitatively correlating the proton signal changes to the absolute concentrations of  $\text{H}_2^{17}\text{O}$  since the water proton  $T_2$  is sensitive to many physiologic parameters, such as pH, the proton chemical exchange rate, temperature and magnetic field strength. In addition, the estimated fractional change in  $^1\text{H}$  signal induced by variations in metabolic  $\text{H}_2^{17}\text{O}$  concentration in the brain during an inhalation of  $^{17}\text{O}_2$  is small at the basal condition. This fact could significantly reduce the dynamic range of the indirect  $^{17}\text{O}$  NMR approaches for determining  $\text{CMRO}_2$ . These approaches have so far not been very successful in imaging  $\text{CMRO}_2$  quantitatively.

## 8.4. INCREASED $^{17}\text{O}$ NMR SENSITIVITY AT ULTRAHIGH FIELDS

### 8.4.1. $^{17}\text{O}$ Relaxivity and Sensitivity as a Function of Field Strength

For a spin nucleus, signal-to-noise ratio (SNR) in a given acquisition time depends on its longitudinal relaxation time ( $T_1$ ),  $T_2^*$ , and the magnetic field strength ( $B_0$ ) according to the following relationship

$$\text{SNR} \propto B_0^\beta (T_2^*/T_1)^{1/2} \quad (8.3)$$

where, based on theoretical considerations, the constant  $\beta$  was suggested to be 7/4 (Hoult and Richards, 1976; Wen *et al.*, 1994).

$^{17}\text{O}$  is the only stable oxygen isotope having a magnetic moment that can be detected by the NMR approach. It has a spin quantum number ( $I = 5/2$ ) greater than 1/2 and possesses an electric quadrupole moment. The electric quadrupole moment interacts with local electric field gradients and the temporal fluctuations in this interaction induced by molecular motion lead to  $T_1$  and  $T_2$  relaxation processes (Abragam, 1961). In the case of water molecule, for which the extreme narrowing limit (i.e.,  $\tau_c\omega \ll 1$ , where  $\tau_c$  is the rotational correlation time and  $\omega$  is Larmor frequency in radians) is applicable except for the bound water, the values of  $T_1$  and  $T_2$  can be estimated by using the following equation:

$$\frac{1}{T_2} \cong \frac{1}{T_1} = \frac{3}{40} \left( \frac{2I+3}{I^2(2I-1)} \right) \left( 1 + \frac{\eta^2}{3} \right) \left( \frac{\pi e^2 Q q}{h} \right)^2 \tau_c \quad (8.4)$$

where the term of  $(\pi e^2 Q q/h)$  is a quadrupole coupling constant and equals to 6.7 MHz (or  $4.21 \times 10^7$  rad/s) for the  $^{17}\text{O}$  nucleus, and  $\eta$  is an asymmetry parameter ( $0 \leq \eta \leq 1$ ) (Abragam, 1961). For  $^{17}\text{O}$  spins, thus,

$$\frac{1}{T_2} \cong \frac{1}{T_1} = 42.53 \times 10^{12} \left( 1 + \frac{\eta^2}{3} \right) \tau_c \quad (8.5)$$

Because both  $\eta$  and  $\tau_c$  are independent of the magnetic field strength, Equation (8.5) reveals that  $^{17}\text{O}$   $T_1$  and  $T_2$  (or  $T_2^*$ ) should be field independent. If the  $\tau_c$  value of  $8.5 \times 10^{-12}$  s is used for bulk water at 298 K (Steinhoff *et al.*, 1993), then estimated  $T_2$  and  $T_1$  according to Equation (8.5) should be between 2.8 ms (for  $\eta = 0$ ) and 2.1 ms (for  $\eta = 1$ ). This estimation dictates that the  $^{17}\text{O}$  relaxation times of water are short and in the range of several milliseconds. However, the actual  $^{17}\text{O}$   $T_2$  value should be smaller than the  $^{17}\text{O}$   $T_1$  value due to the significant contributions of the  $^{17}\text{O}-^1\text{H}$  scalar coupling and the proton chemical exchange to the  $^{17}\text{O}$   $T_2$  (or  $T_2^*$ ) relaxation processes (Meiboom, 1961).

We have experimentally and systematically investigated the longitudinal and transverse relaxation times as well as the signal-to-noise ratio (SNR) of  $^{17}\text{O}$  spins at two field strengths in both rat brain and saline solution using natural abundance water signals and  $^{17}\text{O}$  MRS imaging based on direct detection (Zhu *et al.*, 2001a). The relaxation times were found to be field independent for the rat brain ( $T_2 = 3.03 \pm 0.08$  ms,  $T_2^* = 1.79 \pm 0.04$  ms and  $T_1 = 4.47 \pm 0.14$  ms at 4.7 T; and  $T_2 = 3.03 \pm 0.09$  ms,  $T_2^* = 1.80 \pm 0.06$  ms and  $T_1 = 4.84 \pm 0.18$  ms at 9.4 T), as well as for the saline solution at the room temperature ( $T_2 = 4.28 \pm 0.08$  ms,  $T_2^* = 2.23 \pm 0.04$  ms and  $T_1 = 6.59 \pm 0.10$  ms at 4.7 T; and  $T_2 = 4.09 \pm 0.06$  ms,  $T_2^* = 2.19 \pm 0.01$  ms and  $T_1 = 6.52 \pm 0.12$  ms at 9.4 T) (Zhu *et al.*, 2001a). These results are consistent with the theoretical prediction that the dominant relaxation mechanism of  $^{17}\text{O}$  nucleus is the quadrupolar interaction and is field independent. The relaxation times measured experimentally are qualitatively in good agreement with the estimated values according to Equation (8.5).

The field independence of  $^{17}\text{O}$  relaxivity is a major advantage for  $^{17}\text{O}$  NMR at ultrahigh fields. Unlike proton spins *in vivo*, which are characterized by longer  $T_1$  and shorter  $T_2$  (or  $T_2^*$ ) with increased field strength ultimately resulting in a reduction of sensitivity gain according to Equation (8.3), the field independence of  $^{17}\text{O}$  relaxivity means that  $^{17}\text{O}$  sensitivity gain at higher fields is not compromised. Although the short  $T_2^*$  (i.e. the large linewidth) of the  $^{17}\text{O}$  resonance leads to an effective reduction in the NMR sensitivity at any magnetic field, this is compensated by the extremely short  $T_1$  value of the  $^{17}\text{O}$  spins in  $\text{H}_2^{17}\text{O}$ , especially in the brain (< 5 ms) allowing rapid signal averaging. Therefore, it is possible to achieve a large sensitivity gain of  $^{17}\text{O}$  signal at higher fields.

The  $^{17}\text{O}$  NMR sensitivity was evaluated at 9.4 T and 4.7 T in the rat brain and a saline solution (Zhu *et al.*, 2001a). Figure 8.2 shows the sensitivity comparisons obtained by a surface coil in the rat brain at the two field strengths. Figure 8.2(A) displays the localized signal profile along one dimension parallel to

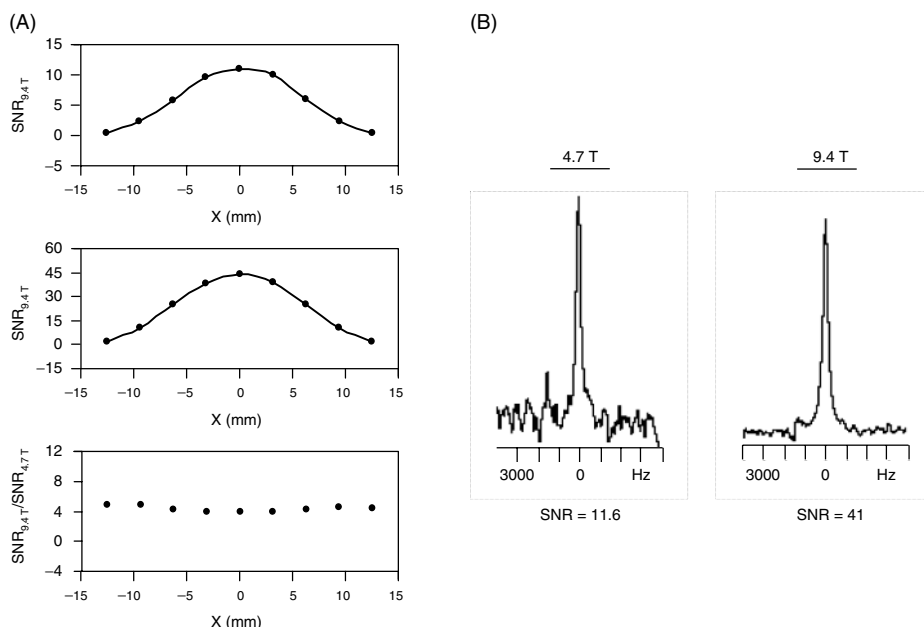


**Figure 8.2.** (A) One-dimensional SNR profiles of  $^{17}\text{O}$  MRS imaging along an axis parallel to the RF coil plane in the rat brain at 4.7 T (top) and 9.4 T (middle), and the SNR ratio between the 9.4 and 4.7 T measurements. The average SNR gain at 9.4 T is approximately 4-fold in comparison with that at 4.7 T. (B) The  $^{17}\text{O}$  NMR spectrum of natural abundance water from the central image voxel acquired from 4.7 T and 9.4 T, respectively, from the rat brain.

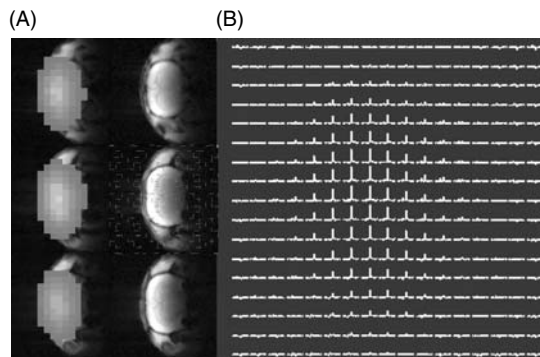


**Figure 8.3 (Plate 1).** (A) Three-dimensional  $^{17}\text{O}$  brain images of natural abundance  $\text{H}_2^{17}\text{O}$  from three adjacent slices (left color images) and corresponding anatomical images (right gray images) in the coronal orientation acquired from a representative rat. (B) Chemical shift image of natural abundance  $\text{H}_2^{17}\text{O}$  from the middle image plane as shown in (A). Zhu *et al.* (2002c). Reproduced with permission of the National Academy of Sciences, U.S.A.

the surface coil plane. Localized  $^{17}\text{O}$  spectra acquired at 9.4 T and 4.7 T from a multidimensional chemical shift image (CSI) dataset corresponding to the same location in the rat brain relative to the surface coil are illustrated in Figure 8.2(B) (Zhu *et al.*, 2001a). The striking finding from this study is the consistent SNR gain of approximately *fourfold* at 9.4 T as compared to 4.7 T indicating an approximate 7/4th power dependence of SNR on  $B_0$ . These experimental results demonstrate the significant advantage provided by high field strength for direct detection of  $^{17}\text{O}$  NMR signal. This trend for increasing  $^{17}\text{O}$  NMR sensitivity is expected to hold beyond 9.4 T.

With the dramatic sensitivity gains realized at 9.4 T, it is possible to obtain a 3D  $^{17}\text{O}$  CSI dataset (11 s of data acquisition and  $\sim 0.1$  ml voxel size) from the natural abundance water in the rat brain with good SNR despite the relatively low gyromagnetic ratio of  $^{17}\text{O}$  nucleus (Zhu *et al.*, 2002c). Figure 8.3(A) shows representative data obtained from three adjacent coronal slices in a rat brain showing anatomical images acquired by a larger  $^1\text{H}$  RF coil and the 3D  $^{17}\text{O}$  signal images of the natural abundance  $\text{H}_2^{17}\text{O}$  acquired by an  $^{17}\text{O}$  RF coil and the Fourier series window imaging technique (Hendrich *et al.*, 1994). Figure 8.3(B) displays one  $^{17}\text{O}$  chemical shift image from the middle image slice as shown in Figure 8.3(A). The spatial distributions of  $^{17}\text{O}$  signal intensity are not uniform because of the inhomogeneous  $B_1$  field of the  $^{17}\text{O}$  surface coil. Nevertheless, excellent SNR is evident with a relatively short acquisition time at 9.4 T, especially for the central voxels where SNR was optimized by the  $B_1$  profile of the  $^{17}\text{O}$  coil.

## 8.5. ADVANTAGES OF DIRECT $^{17}\text{O}$ NMR APPROACH FOR IMAGING CMRO<sub>2</sub>

There are several major advantages to using direct  $^{17}\text{O}$  spectroscopic imaging to detect the  $\text{H}_2^{17}\text{O}$  distribution and its dynamic changes in the brain tissue.

The short  $T_1$  of  $\text{H}_2^{17}\text{O}$  yields SNR gains per unit acquisition time as discussed previously. In addition, there is only a single, well-defined  $\text{H}_2^{17}\text{O}$  resonance peak, consequently, making data analysis and quantification simple and reliable.

The  $\text{H}_2^{17}\text{O}$  signal from the natural abundance (0.037 %) water, which can be accurately imaged, provides an excellent internal reference for calculating absolute  $\text{H}_2^{17}\text{O}$  concentration or the  $\text{H}_2^{17}\text{O}$  concentration change following a  $\text{H}_2^{17}\text{O}$  injection or inhalation of  $^{17}\text{O}_2$  in each CSI voxel. Such a simple quantification is crucial for determining absolute CMRO<sub>2</sub> values.

The  $^{17}\text{O}$  resonance of  $\text{H}_2\text{O}$  is relatively insensitive to  $B_0$  inhomogeneities (hence shimming performance) because of the intrinsically broad linewidth ( $>140$  Hz) and the low gyromagnetic ratio. This implies that, compared to  $^1\text{H}$  imaging, the requirements for  $B_0$  homogeneity either in the bare magnet, or together with room temperature shim compensation is considerably less stringent.

The  $^{17}\text{O}$  NMR approach for imaging CMRO<sub>2</sub> is based on measuring the spatial distribution of the dynamic changes of the water metabolized from inhaled  $^{17}\text{O}_2$ . Therefore, experimentally, the reliability and reproducibility of  $^{17}\text{O}$  NMR in consecutively acquired datasets are far more crucial than the absolute sensitivity of the  $^{17}\text{O}$  signal acquired in a single image or spectrum. In order to demonstrate this concept, we have conducted one study for comparing the signal fluctuations in repeated measurements using direct and indirect  $^{17}\text{O}$  NMR approaches. In this study, a  $^{17}\text{O}$ – $^1\text{H}$  multinuclear surface coil probe was used to collect a series of global  $^{17}\text{O}$  and  $^1\text{H}$  spectra from the natural abundance water in the rat brain in order to estimate the relative signal fluctuations (Zhu *et al.*, 2002c). Two stacked plots of 25  $^{17}\text{O}$  and  $^1\text{H}$  spectra acquired consecutively using the  $^{17}\text{O}$  coil and the  $^1\text{H}$  coil, respectively, are shown in Figure 8.4. Although the number of acquisitions (NT) for each spectrum was different for the  $^{17}\text{O}$  and  $^1\text{H}$  nuclei, the repetition time (TR) was  $\sim 3T_1$  in both cases and the total acquisition time for acquiring each spectrum was the same (6.2 s). Under this condition, we found that the signal fluctuations in the consecutively acquired spectra for the two nuclei were comparable (SD = 0.20 % for  $^1\text{H}$  spectra; SD = 0.35 % for  $^{17}\text{O}$  spectra) even though the signal-to-noise ratio of the proton spectra from water was considerably higher. This is because the signal fluctuations in the  $^1\text{H}$  data are not dominated by the inherent sensitivity of a single spectrum or image but are mainly determined by the physiological ‘noise’ caused by breathing, heart pulsation, vasomotion, and spontaneous electrical and neurotransmitter activity, as well as NMR scanner instability. The similarity in signal fluctuations in consecutively acquired  $^1\text{H}$  and  $^{17}\text{O}$  NMR spectra (Figure 8.4) indicated that, with respect to the capability for detecting *dynamic* changes in NMR signal intensity, the  $^{17}\text{O}$  NMR method is comparable to the  $^1\text{H}$  NMR method. Furthermore, these results suggested that direct  $^{17}\text{O}$  detection might be more sensitive for measuring the changes in  $\text{H}_2^{17}\text{O}$  signal caused by the cerebral oxygen consumption of inhaled  $^{17}\text{O}_2$ . This notion was based on the fact that a  $^{17}\text{O}_2$  inhalation for 2 min under basal conditions in the anesthetized rat brain was expected to result in only 0.15–0.30 % change in the water proton signal intensity detected by the indirect  $^{17}\text{O}$  detection approaches (Ronen *et al.*, 1998; Zhu *et al.*, 2002c), which is

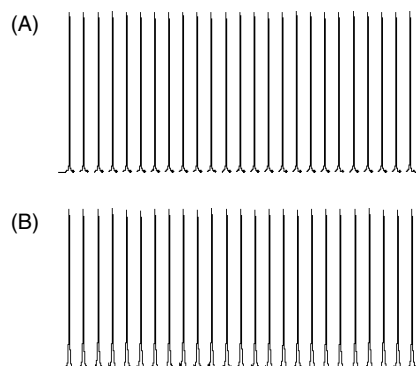


**Figure 8.4.** (A) Stacked plot of 25  $^1\text{H}$  NMR spectra of water in the rat brain acquired and processed with following parameter:  $NT = 1$ ,  $TR = 6.2$  s,  $LB = 25$  Hz ( $\sim$  half linewidth). The standard deviation of the  $^1\text{H}$  water peak height in these spectra is 0.20 %. (B) Stacked plot of 25  $^{17}\text{O}$  NMR spectra of natural abundance water in the same rat brain acquired and processed with the following parameters:  $NT = 512$ ,  $TR = 12$  ms for each scan,  $LB = 100$  Hz ( $\sim$  half linewidth), and the standard deviation of the  $^{17}\text{O}$  water peak height in these spectra is 0.35 %. The total acquisition times for each  $^1\text{H}$  and  $^{17}\text{O}$  spectra were the same (6.2 s).

comparable to signal fluctuations in consecutively acquired  $^1\text{H}$  spectra or images. In contrast, the expected  $^{17}\text{O}$  signal change for the same  $^{17}\text{O}_2$  inhalation detected by the direct  $^{17}\text{O}$  NMR approach is 20–40%. These considerations provide the major justification for pursuing the direct  $^{17}\text{O}$  NMR approach at high magnetic fields for  $\text{CMRO}_2$  imaging.

Both PET and  $^{17}\text{O}$  NMR approaches for imaging  $\text{CMRO}_2$  are based on a similar concept of detecting the labeled water formed by oxidative metabolism of labeled  $\text{O}_2$  gas. However, the  $^{17}\text{O}$  NMR approach overcomes one of the major difficulties associated with PET, namely the problem of distinguishing different forms of labeled oxygen simultaneously present in the tissue as  $\text{O}_2$  molecules bound to hemoglobin, as  $\text{O}_2$  molecules dissolved in tissue water and lipids, and as metabolically generated water. As discussed previously, in order to differentiate the radioactivity contributions from these different chemical species and precisely calculate  $\text{CMRO}_2$ , either two other PET measurements of CBF and cerebral blood volume are necessary or assumptions must be made about extracting this information from the temporal behavior of the label after a bolus inhalation. In contrast,  $^{17}\text{O}$  NMR specifically detects the metabolically generated  $\text{H}_2^{17}\text{O}$  without confounding signals from the  $^{17}\text{O}_2$  molecules bound to hemoglobin or dissolved in tissue space. When bound to hemoglobin, the  $^{17}\text{O}_2$  resonance is broadened beyond detection due to the extremely slow rotational motion of the large molecular weight oxyhemoglobin complex in comparison with water. Saturation transfer electron paramagnetic resonance studies have shown that the  $\tau_c$  value for rotational motion of the hemoglobin molecule is  $2 \times 10^{-8}$  s in solution and increases to  $8 \times 10^{-6}$  s when the hemoglobin molecule is encapsulated within the erythrocyte membrane (Cassoly, 1982). This is approximately  $10^6$  times slower than the rotational correlation time of water. Such slow rotational motion leads to extremely fast  $T_2$  relaxation according to Equation (8.5) and renders the  $^{17}\text{O}_2$  molecule bound to hemoglobin invisible in  $^{17}\text{O}$  NMR data.  $^{17}\text{O}_2$  molecule in gas phase or dissolved in water is strongly paramagnetic due to its two unpaired electrons, and hence again undetectable because of the strong dipolar coupling between the electrons and the nucleus.  $^{17}\text{O}$  signal becomes detectable *only when*  $^{17}\text{O}_2$  is incorporated into water. Because of this chemical specificity, calculation of  $\text{CMRO}_2$  from  $^{17}\text{O}$  NMR data is considerably less complicated as compared to the PET methodology (Mintun *et al.*, 1984). In addition, unlike PET, the  $^{17}\text{O}$  isotope is stable and nonradioactive. These advantages proclaim the feasibility of direct  $^{17}\text{O}$  NMR approach at ultrahigh fields for mapping the spatial distribution of metabolic  $\text{H}_2^{17}\text{O}$  dynamically, and potentially for imaging  $\text{CMRO}_2$  noninvasively.

## 8.6. ULTRAHIGH FIELD $^{17}\text{O}$ NMR APPROACH FOR IMAGING $\text{CMRO}_2$

### 8.6.1. Theoretical Aspects of $^{17}\text{O}$ NMR Approach for Imaging $\text{CMRO}_2$

The dynamic change in cerebral  $\text{H}_2^{17}\text{O}$  concentration during an inhalation of  $^{17}\text{O}_2$  is determined by three parallel processes: (i) oxygen consumption generating the metabolic  $\text{H}_2^{17}\text{O}$  in the brain, (ii) perfusion resulting in  $\text{H}_2^{17}\text{O}$  washout from the brain, and (iii) flow recirculation bringing extra  $\text{H}_2^{17}\text{O}$  into the brain. These processes are illustrated in Figure 8.5. The mass balance equation of labeled  $\text{H}_2^{17}\text{O}$  concentrations during an inhalation of  $^{17}\text{O}_2$  is given by

$$\frac{dC_b(t)}{dt} = 2\alpha f_1 \text{CMRO}_2 + \text{CBF}\{f_2[C_a(t) - C_v(t)]\} \quad (8.6)$$

where  $C_a(t)$ ,  $C_b(t)$  and  $C_v(t)$  are the time-dependent  $\text{H}_2^{17}\text{O}$  concentrations *in excess of the natural abundance  $\text{H}_2^{17}\text{O}$  concentration level* in the arterial blood, brain tissue and venous blood, respectively;  $\alpha$  is the  $^{17}\text{O}$  enrichment fraction of inhaled  $^{17}\text{O}_2$  gas. Proper use of Equation (8.6) requires consistencies of units among all terms used in this equation. The determinations of  $C_b$ ,  $C_a$  and  $C_v$  are based on the  $^{17}\text{O}$  NMR measurements and they can be calibrated using the natural abundance  $\text{H}_2^{17}\text{O}$  concentration (20.35  $\mu\text{mol}$

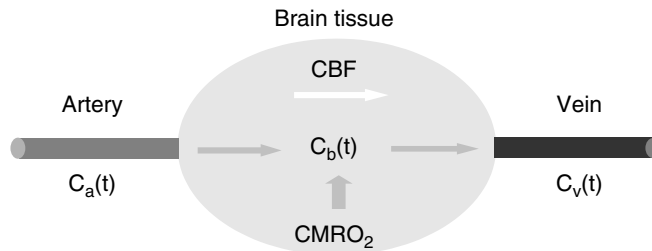


**Figure 8.5.** Schematic diagram showing the mass balance of accumulated cerebral  $\text{H}_2^{17}\text{O}$  content ( $C_b(t)$ ) contributed by oxidative metabolism of inhaled  $^{17}\text{O}_2$  ( $\text{CMRO}_2$ ), flow recirculation ( $C_a(t)$ ) through feeding arteries and perfusion washout ( $C_v(t)$ ) through veins according to Fick's equation as described by Equation (8.6).

per gram brain water for brain tissue, and  $\mu\text{mol}$  per gram blood water for blood, calculated from natural abundance  $\text{H}_2^{17}\text{O}$  enrichment of 0.037 % and the molecular weight of  $\text{H}_2^{17}\text{O} = 19.0$ ). Therefore, the preferred units are  $\mu\text{mol}/(\text{g brain water})$  for  $C_b(t)$ , and  $\mu\text{mol}/(\text{g blood water})$  for  $C_a(t)$  and  $C_v(t)$ . The unit used most commonly for  $\text{CMRO}_2$  is  $\mu\text{mol}/\text{min}/(\text{g brain tissue})$  and is retained. This dictates the use of two unit conversion factors,  $f_1 = 1.266$  and  $f_2 = 1.05$ , to achieve consistency of units among all parameters used in Equation (8.6) (Pekar *et al.*, 1995; Zhu *et al.*, 2002c). If water in the brain tissue is in equilibrium with water in the venous blood (*i.e.* fast water exchange across capillaries and membranes),  $f_2 C_v(t) = C_b(t)/\lambda$  where  $\lambda$  is the brain–blood partition coefficient ( $\approx 0.90$ ) in units of  $(\text{ml blood})/(\text{g brain tissue})$  (Herscovitch and Raichle, 1985). Substituting this relation and introducing two new correction parameters ( $n$  and  $m$ ) into Equation (8.6) leads to

$$\frac{dC_b(t)}{dt} = 2af_1\text{CMRO}_2 + m\text{CBF} \left( f_2 C_a(t) - \frac{nC_b(t)}{\lambda} \right) \quad (8.7)$$

The solution of Equation (8.7) is

$$C_b(t) = \frac{2a\lambda f_1}{mn\text{CBF}} \text{CMRO}_2 \left[ 1 - \exp \left( -\frac{mn\text{CBF}}{\lambda} t \right) \right] + f_2 m \text{CBF} \int_0^t C_a(t') \exp \left( -\frac{mn\text{CBF}}{\lambda} (t - t') \right) dt' \quad (8.8)$$

where  $m$  is a correction factor accounting for the limited permeability of water because water is not totally freely diffusible across the brain–blood barrier, and the value of  $m$  is 0.84 for the similar CBF range that we studied (Herscovitch *et al.*, 1987). The constant  $n$  is another correction factor that accounts for another type of restriction on the permeability specifically for the  $\text{H}_2^{17}\text{O}$  generated through oxidative metabolism in the mitochondria ('metabolic'  $\text{H}_2^{17}\text{O}$ ) during an inhalation of  $^{17}\text{O}_2$ . This additional restriction is included in our modeling because we have observed that the washout rate of the metabolic  $\text{H}_2^{17}\text{O}$  after the cessation of  $^{17}\text{O}_2$  inhalation was significantly slower than the washout rate of the  $\text{H}_2^{17}\text{O}$  that permeates brain tissue subsequent to a bolus injection of  $\text{H}_2^{17}\text{O}$  through the internal carotid artery in the rat (Zhu *et al.*, 2002a). The cause of this difference could be the permeability restrictions imposed by the inner and outer mitochondrial membranes that must be traversed by all water molecules generated by oxygen consumption. However, mitochondrial volume is a small fraction of the tissue volume; therefore, it is a small and likely undetectable perturbation for the washin and washout kinetics of labeled water that comes into the tissue space from the vasculature by exchange across the capillaries. Even when this exogenous labeled water equilibrates across all compartments in the tissue, extra-mitochondrial volume will contain most of that water and its washout will not be affected by the mitochondrial membranes. Irrespective of the

validity of this explanation, however, the correction factor  $n$  that is used in modeling can be experimentally determined as the ratio of the washout rate of the metabolic  $\text{H}_2^{17}\text{O}$  after the cessation of  $^{17}\text{O}_2$  inhalation versus the washout rate of the  $\text{H}_2^{17}\text{O}$  introduced after a bolus injection through the internal carotid artery ( $n < 1$ ) (Zhu *et al.*, 2002a).

The  $\text{CMRO}_2$  value can be precisely calculated using the complete model as described by Equation (8.8) if all parameters of  $C_b(t)$ , CBF,  $n$  and  $C_a(t)$  can be determined experimentally for the same animal brain. The first three parameters can be determined using the  $^{17}\text{O}$  NMR approaches. In principle, the  $C_a(t)$  function is determined by the total metabolic  $\text{H}_2^{17}\text{O}$  generated in the entire animal body.  $C_a(t)$  can be approximated as a linear function of the inhalation time (*i.e.*,  $C_a(t) \approx At$ , where  $A$  is a constant and  $t$  represents time) based on two assumptions: (i) the metabolic  $\text{H}_2^{17}\text{O}$  molecules generated in tissue space exchanges relatively rapidly with the blood compartment so that it is at or near equilibrium with the blood water<sup>1</sup>, and (ii) the oxygen consumption rate is constant (*i.e.*, time independent) in all tissues during a short  $^{17}\text{O}_2$  inhalation time. This approximation was supported by our experimental results, which will be discussed later, and the literature. Then the solution of Equation (8.8) for calculating  $\text{CMRO}_2$  is

$$\text{CMRO}_2 = \frac{\frac{C_b(t) - \frac{Af_2\lambda^2}{mn^2\text{CBF}} \left[ \frac{mn\text{CBF}}{\lambda} t \exp\left(\frac{-mn\text{CBF}}{\lambda} t\right) + \exp\left(\frac{-mn\text{CBF}}{\lambda} t\right) - 1 \right]}{1 - \exp\left(\frac{-mn\text{CBF}}{\lambda} t\right)} - \frac{Af_2\lambda t}{n}}{\frac{2a\lambda f_1}{mn\text{CBF}}} \quad (8.9)$$

Therefore, according to Equation (8.9), the  $\text{CMRO}_2$  value at *each* data point measured at different inhalation times can be calculated from experimental data of CBF,  $A$ ,  $n$ ,  $C_b(t)$  and other known constants ( $f_1$ ,  $f_2$ ,  $m$ ,  $\alpha$  and  $\lambda$ ) for each voxel. In general, the final  $\text{CMRO}_2$  value is based on the average of all  $\text{CMRO}_2$  values except the first two time points, that have been omitted because of their relatively large measurement errors and the fact that they may represent initial transient values as the  $^{17}\text{O}_2$  concentration in the tissue space increases to a value above the  $K_m$  of cytochrome oxidase. The ability to obtain  $\text{CMRO}_2$  measurements as a function of inhalation time and the use of only the time-independent  $\text{CMRO}_2$  values avoids this complication.

A fundamental limitation of spatial resolution using the  $^{17}\text{O}$  imaging approach will be water diffusion in the brain since water is usually assumed freely diffusible. The apparent diffusion constant ( $D$ ) of water in the rat brain has been measured to be  $\sim 10^{-3} \text{ mm}^2/\text{s}$  (Lee *et al.*, 1999) with small direction-dependent variations due to anisotropy. For a period of 2 min, which corresponds to the  $^{17}\text{O}_2$  inhalation time we used, this translates to an average diffusion distance of 0.35 mm. However, the more relevant parameter is the diffusion distance during the ‘lifetime’ of an  $\text{H}_2^{17}\text{O}$  molecule in the brain tissue after it is formed and before it is washed out by blood flow. This time is given by  $\lambda/\text{CBF}$ . Typically,  $\text{CBF} \sim 1 \text{ ml/g/min}$  which means  $\lambda/\text{CBF} \sim 1 \text{ min}$ . Thus, we are concerned with diffusion distances of  $\sim 0.25 \text{ mm}$ . This is much smaller than the spatial extent of brain compartments and/or the brain regions activated by most brain stimulations. In addition, the metabolic water clearly is not freely diffusible in the brain tissue, possibly because of

<sup>1</sup> When oxygen consumption rate is constant, the blood content of metabolically generated labeled water can increase linearly in time under many different kinetic scenarios only one of which is the condition of rapid exchange between the tissue and the blood compartment listed here. We have focused on this condition here only because it is generally accepted to be the case. In any case, direct experimental determinations we have performed have demonstrated that indeed the blood content of metabolically generated labeled water increases linearly in time.

permeability barriers posed by the inner and outer mitochondrial membranes (Zhu *et al.*, 2002a; Ohta *et al.*, 1992). This could further reduce the diffusion distances within the same measurement time. During brain activation, CBF increases thereby further shortening the average 'lifetime' of the water molecule in tissue. Therefore, the diffusion of  $H_2^{17}O$  in the brain tissue is unlikely to be the major factor limiting spatial resolution of  $^{17}O$  NMR imaging for determining CMRO<sub>2</sub> and/or CBF. The major limitation on spatial resolution for imaging CMRO<sub>2</sub> is still determined by the  $^{17}O$  NMR sensitivity and the allowed inhalation time of  $^{17}O_2$ . These same diffusion considerations also apply to PET measurements of CMRO<sub>2</sub> with  $^{15}O$  inhalation or even PET functional imaging using  $H_2^{15}O$  injection.

### 8.6.2. Experimental Determination of CMRO<sub>2</sub> using $^{17}O$ NMR Approaches

The complete modeling (Equation (8.9)) for accurate calculation of CMRO<sub>2</sub> requires several key parameters, which can be experimentally measured by using different methods combined with  $^{17}O$  NMR. We have recently investigated the feasibility for developing the  $^{17}O$  NMR approach for imaging CMRO<sub>2</sub> in a small animal model during a brief inhalation of  $^{17}O_2$  gas at 9.4 T. We have applied the 3D  $^{17}O$  MRS imaging method to determine CBF after a bolus injection of  $H_2^{17}O$  through an internal carotid artery and the accumulation rate of  $H_2^{17}O$  content ( $C_b(t)$ ) generated by oxidative metabolism in the rat brain during a  $^{17}O_2$  inhalation for 2 min (Zhu *et al.*, 2002c). The  $C_b(t)$  images were obtained, together with continuous experimental monitoring of the arterial input function ( $C_a(t)$ ) by using an implanted carotid artery RF coil. The parameters measured in these experiments were used to calculate CMRO<sub>2</sub> values in each voxel of the image using complete modeling that accounts for all contributions to the cerebral  $H_2^{17}O$  accumulated during an inhalation of  $^{17}O_2$ . This study demonstrates the feasibility for imaging CMRO<sub>2</sub> in the rat brain anesthetized with  $\alpha$ -chloralose (Zhu *et al.*, 2002c). The details for imaging CMRO<sub>2</sub> we have employed (Zhu *et al.*, 2002c) are the following:

#### 8.6.2.1. CBF measurements

CBF values were determined independently based on the 'washout' rate of the  $H_2^{17}O$  tracer in the brain tissue, following a rapid bolus injection of  $^{17}O$ -labeled  $H_2^{17}O$  via one feeding carotid artery (Zhu *et al.*, 2001a; Zhu *et al.*, 2002c) according to

$$C_b(t) = C_b(0) \exp[-t(mCBF/\lambda)] + B \quad (8.10)$$

where  $C_b(0)$  is the signal intensity after the first arrival of all labeled water following the bolus injection, and  $B$  is a constant. Fitting the exponential decay of the  $H_2^{17}O$  washout curve to Equation (8.10) gives the CBF value. CBF measurements can be performed by MR methods based on arterial spin tagging. However, the determination of the washout rate of exogenous (as opposed to metabolically generated)  $H_2^{17}O$  tracer in order to calculate the correction factor  $n$  requires the experiment performed with bolus injection of  $H_2^{17}O$ .

The spatial localization of  $^{17}O$  NMR was achieved by using the 3D Fourier series window technique (Hendrich *et al.*, 1994). In this imaging method, the  $k$ -space sampling is weighted according to the Fourier coefficients of a predetermined voxel shape to achieve an optimal filter applied at the acquisition stage. The short  $^{17}O$   $T_1$  value (4.5 ms) of cerebral  $H_2^{17}O$  in the rat allows rapid signal acquisition, and ultimately, more signal averages within a given sampling time (Zhu *et al.*, 2001a). Therefore, a short  $TR$  of 12 ms ( $\sim 3T_1$ ) was used for gaining SNR. A short gradient echo time ( $TE = 0.4$  ms) can be achieved by using a short phase-encoding gradient length. This short  $TE$  reduces the signal loss caused by the short  $^{17}O$   $T_2^*$  value ( $= 1.8$  ms) in the rat brain at 9.4 T (Zhu *et al.*, 2001a). The total acquisition time for acquiring each 3D image dataset was 11 s.

The same 3D  $^{17}\text{O}$  approach and acquisition parameters were used for imaging CBF and  $C_b(t)$  resulting in robust image registrations between the CBF and  $C_b(t)$  (or CMRO<sub>2</sub>) images with the same voxel size and position. For CBF measurements, one external carotid artery was catheterized for gaining access to the internal carotid artery without interrupting the blood circulation through the brain (Zhu *et al.*, 2001a). A small quantity of enriched  $\text{H}_2^{17}\text{O}$  was rapidly injected into the brain via the internal carotid artery for CBF measurements using  $^{17}\text{O}$  MRS imaging (Zhu *et al.*, 2001a). Fitting the exponential decay of the  $\text{H}_2^{17}\text{O}$  trace in each image voxel according to Equation (8.10) determined the CBF value, which can then be used to generate 3D CBF images.

#### 8.6.2.2. $C_b(t)$ measurements during an $^{17}\text{O}_2$ inhalation

It is necessary to collect 3D  $^{17}\text{O}$  MRS images of the natural abundance  $^{17}\text{O}$  labeled water before  $^{17}\text{O}_2$  inhalation as a reference for quantifying the cerebral  $\text{H}_2^{17}\text{O}$  concentration changes during and after the  $^{17}\text{O}_2$  inhalation. Figure 8.6 demonstrates stacked plots of  $^{17}\text{O}$  spectra of cerebral  $\text{H}_2^{17}\text{O}$  from one representative voxel before (natural abundance), during and after an inhalation for 2 min of  $^{17}\text{O}_2$  (72 %  $^{17}\text{O}$  enrichment) gas (Zhu *et al.*, 2002c). The  $^{17}\text{O}$  signal intensity of cerebral  $\text{H}_2^{17}\text{O}$  is characterized by three distinct phases: (i) constant before the  $^{17}\text{O}_2$  inhalation, (ii) approximately linear increase during the  $^{17}\text{O}_2$  inhalation, and (iii) approximately exponential decrease after the cessation of  $^{17}\text{O}_2$  inhalation and approaching a new steady concentration within a short recovery time (<10 min). The  $^{17}\text{O}$  NMR sensitivity achieved at 9.4 T makes it possible to distinguish the different phases and to quantify  $C_b(t)$ .

#### 8.6.2.3. $C_a(t)$ measurements during an $^{17}\text{O}_2$ inhalation

The most challenging measurement faced by the complete model for calculating CMRO<sub>2</sub> as described by Equation (8.9) is the experimental determination of  $C_a(t)$ , the concentration of  $\text{H}_2^{17}\text{O}$  in the feeding artery, especially when a small animal model is used. One of the conventional approaches for determining  $C_a(t)$  is to continuously draw arterial blood samples (e.g., Pekar *et al.*, 1995), where the  $^{17}\text{O}$  tracer concentrations in the blood samples can be analyzed independently by using *in vitro* NMR, mass spectroscopy or other methods. This approach is technically limited in studies of small experimental animals due to several factors: (i) only a small quantity of blood volume in the animal body available for blood draws, (ii) difficulty in manually drawing blood samples inside a small-bore animal magnet, (iii) the low accuracy in determining the blood sampling time and the absolute tracer concentration, thus resulting in large variations in  $C_a(t)$  measurements, and (iv) possible changes of physiological condition caused by blood removal (e.g., decrease in blood pressure). To overcome these limitations, we have designed an implanted  $^{17}\text{O}$  RF coil that permits

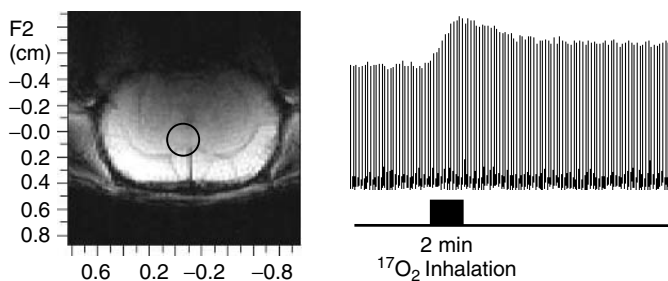


**Figure 8.6.** Stacked plots of the cerebral  $\text{H}_2^{17}\text{O}$  spectra from one representative voxel as indicated by the cycle in the anatomical image (left insert) acquired before (natural abundance), during (as indicated by the dark bar under the stacked plots) and after  $^{17}\text{O}_2$  inhalation for 2 min. Zhu *et al.* (2002c). Reproduced with permission of the National Academy of Sciences, U.S.A.

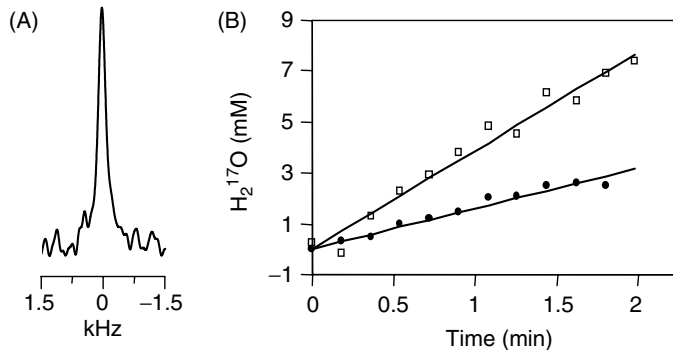


**Figure 8.7.** (A)  $^{17}\text{O}$  spectrum of natural abundance  $\text{H}_2^{17}\text{O}$  in the rat carotid artery blood ( $\sim 7 \mu\text{l}$ ) obtained using the implanted RF coil before inhalation of  $^{17}\text{O}_2$ . (B) Time course of  $^{17}\text{O}$  MR signals of  $C_a(t)$  in one carotid artery (filled circle) and  $C_b(t)$  from a representative voxel in the rat brain (open square) during inhalation of  $^{17}\text{O}_2$ .

the continuous measurement of  $C_a(t)$  in a rat carotid artery (Zhang *et al.*, 2003). This coil is based on a modified solenoid coil design combined with an RF shield. The RF shielding ensures that the NMR signal detected by the implanted coil originates only from the arterial blood ( $\sim 7 \mu\text{l}$ ) without contaminations from surrounding tissues. Therefore, additional spatial localization is not necessary for determining  $C_a(t)$ . In addition, the RF shielding minimized the electromagnetic coupling between the implanted  $^{17}\text{O}$  coil and the head  $^{17}\text{O}$  surface coil tuned at the same operating frequency (two-coil configuration); this allowed simultaneous measurements of both  $C_a(t)$  and  $C_b(t)$  using two independent receiver channels with the same temporal resolution (11 s). Figure 8.7(A) illustrates the natural abundance  $\text{H}_2^{17}\text{O}$  spectrum detected from the blood in the rat carotid artery. Figure 8.7(B) plots the results of simultaneous measurements of  $C_a(t)$  change in one carotid artery and  $C_b(t)$  change in a voxel located in the brain from the same rat during an inhalation of  $^{17}\text{O}_2$ . The results indeed demonstrate a linear relation between  $C_a(t)$  and the inhalation time  $t$ . The linear regression of  $C_a(t)$  data gives the value of the constant  $A$  used in Equation (8.9) for each  $^{17}\text{O}_2$  inhalation measurement.

#### 8.6.2.4. Calculation of $\text{CMRO}_2$ and generation of 3D $\text{CMRO}_2$ images

Finally, the values of  $C_b(t)$ , CBF and  $n$  from each voxel and the value of  $A$  measured from each  $^{17}\text{O}$  inhalation measurement in the same subject can be used to calculate  $\text{CMRO}_2$  according to Equation (8.9). Figure 8.8 demonstrates one example of  $\text{CMRO}_2$  calculation as a function of inhalation time from a *single* voxel in the rat brain. It is evident that the  $\text{CMRO}_2$  value is independent of the inhalation time if the initial two points are excluded. The typical behavior of  $\text{CMRO}_2$  versus the inhalation time as demonstrated in Figure 8.8 reveals that the calculated  $\text{CMRO}_2$  reaches a constant value during early inhalation times indicating a rapid approach of the tissue concentration of  $^{17}\text{O}$ -labeled oxygen molecule to  $K_m$  of cytochrome oxidase. On the other hand, this experimental observation also validates the accuracy of the complete model for calculating  $\text{CMRO}_2$ .

Information similar to that shown in Figure 8.8 can be obtained for all voxels in the  $^{17}\text{O}$  image and then can be used to generate 3D  $\text{CMRO}_2$  images in the rat brain. Figure 8.9 illustrates three adjacent  $\text{CMRO}_2$  images in the coronal orientation from a representative rat brain.

The averaged  $\text{CMRO}_2$  and CBF values in the rat brain from seven measurements (five rats) were  $2.19 \pm 0.14 \mu\text{mol/g}/\text{min}$  and  $0.53 \pm 0.07 \text{ ml/g}/\text{min}$ , respectively, under conditions of  $\alpha$ -chloralose anesthesia (Zhu *et al.*, 2002c).

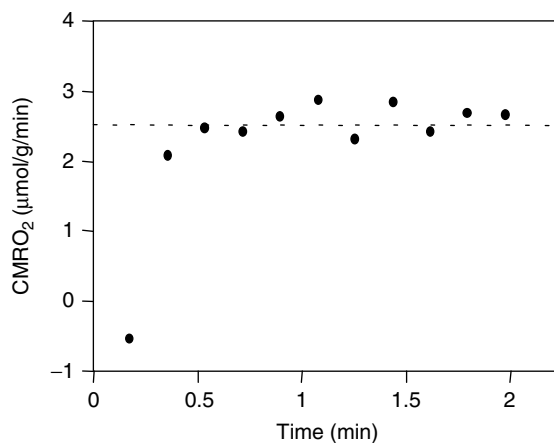


**Figure 8.8.** Plot of the calculated CMRO<sub>2</sub> values using the complete modeling as described by Equation (8.9) as a function of inhalation time.

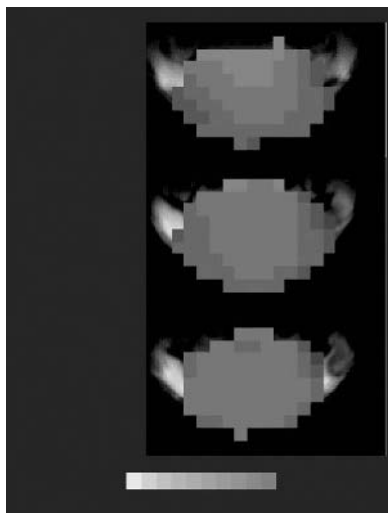


**Figure 8.9 (Plate 2).** Three-dimensional coronal CMRO<sub>2</sub> images of rat brain measured by using <sup>17</sup>O NMR approach during <sup>17</sup>O<sub>2</sub> inhalation for 2 min.

Due to the technical challenges faced by most existing CMRO<sub>2</sub> imaging methods, there is virtually no literature reporting direct measurements of 3D CMRO<sub>2</sub> image in the rat brain. Nevertheless, we compared our result of CMRO<sub>2</sub> measurements using the <sup>17</sup>O NMR approach with the literature results obtained by indirect methods under similar animal condition. Based on an autoradiographic study (Nakao *et al.*, 2001), cerebral metabolic rate of glucose (CMR<sub>glc</sub>) was estimated to be  $\sim 0.37 \mu\text{mol/g/min}$  in the somatosensory and motor cortices of rats anesthetized with  $\alpha$ -chloralose. Using the CMRO<sub>2</sub>/CMR<sub>glc</sub> ratio of 5.5–6.0 (Siesjo, 1978), CMRO<sub>2</sub> values of 2.04–2.22  $\mu\text{mol/g/min}$  are calculated from this CMR<sub>glc</sub> value. Our CMRO<sub>2</sub> result ( $2.19 \pm 0.14 \mu\text{mol/g/min}$ ) is perfectly within this range. The CBF value of 0.58–0.68  $\text{ml/g/min}$  reported in the same autoradiographic study (Nakao *et al.*, 2001) is also close to the mean CBF value of

$0.53 \pm 0.07$  ml/g/min measured in our study. The  $^{13}\text{C}$  heteronuclear editing MRS and  $^1\text{H}$  MRI methods have been used to measure  $\text{CMRO}_2$  and CBF values in the sensory motor cortex of mature rats covering a large range of cortical activity under different anesthesia conditions, and a linear correlation between  $\text{CMRO}_2$  and CBF was observed ( $\text{CMRO}_2 \approx 3.76 \times \text{CBF} + 0.18$ ,  $R^2 = 0.99$ ) (Hyder *et al.*, 2000). The estimated  $\text{CMRO}_2$  from this linear relation is  $2.16 \mu\text{mol/g/min}$  for the mean CBF value observed in our study (0.53 ml/g/min). This estimated  $\text{CMRO}_2$  value is again in agreement with our result. These comparisons provide mutual support between our direct  $\text{CMRO}_2$  measurements and other indirect measurements reported in the literature, and confirm the validity of the high-field  $^{17}\text{O}$  NMR approach for 3D  $\text{CMRO}_2$  imaging in small animal brains.

The increased  $^{17}\text{O}$  NMR sensitivity at 9.4 T has significantly improved the spatial resolution ( $\sim 0.1$  ml voxel size) for 3D  $\text{CMRO}_2$  imaging in the rat brain with a much shorter inhalation time (2 min) compared with the previous study conducted at 4.7 T (Pekar *et al.*, 1995) which reported single voxel (0.8 ml voxel size)  $\text{CMRO}_2$  results based on 2D  $^{17}\text{O}$  CSI in the cat brain with 15 min of inhalation time (Pekar *et al.*, 1995).

## 8.7. CONCLUSIONS AND PERSPECTIVES

The superior  $^{17}\text{O}$  NMR sensitivity achieved at ultrahigh fields makes it possible for detecting and imaging small dynamic changes of metabolic  $\text{H}_2^{17}\text{O}$  during a brief inhalation of  $^{17}\text{O}_2$  gas, and ultimately, for imaging  $\text{CMRO}_2$  in three dimensions in the brain. All key parameters involved in the complete model for calculating  $\text{CMRO}_2$  can be determined by independent and concurrent  $^{17}\text{O}$  NMR measurements in the same animal. The  $\text{CMRO}_2$  results obtained by the  $^{17}\text{O}$  NMR approach are consistent with the literature results for similar measurement conditions. The promising *in vivo* work conducted at ultrahigh fields provides a crucial step toward the goal for developing a robust and *noninvasive*  $^{17}\text{O}$  NMR approach for imaging  $\text{CMRO}_2$  in animal, and potentially in human brains. Meanwhile, the work also provides rich information about other interesting aspects of  $^{17}\text{O}$  NMR for  $\text{CMRO}_2$  imaging.

As demonstrated in Figure 8.6, the cerebral  $\text{H}_2^{17}\text{O}$  concentration reaches a new steady state within a short time (6–10 min) after the cessation of  $^{17}\text{O}_2$  inhalation. This fast recovery allows repeated  $\text{CMRO}_2$  measurements in the same subject and experimental session (Zhu *et al.*, 2001b). This capability is essential for studying the oxidative metabolism changes related to perturbations in physiology and function, where at least two measurements are required under control and perturbation (or stimulation) conditions. Such a capability has been demonstrated in a preliminary study conducted at 9.4 T showing a focal  $\text{CMRO}_2$  increase in the rat somatosensory areas during the forepaw electric stimulation (Zhu *et al.*, 2002b). This preliminary result indicates a great potential of high-field  $^{17}\text{O}$  NMR approach for studying the central role of oxidative metabolism in brain function, as well as for understanding the mechanisms underlying fMRI (Barinaga, 1997; Ogawa *et al.*, 1998). Furthermore, the same approach can be applied for numerous applications for addressing different physiological and pathological questions. We have recently tested this notion through the investigation of the feasibility of 3D  $^{17}\text{O}$  MRS imaging at 9.4 T for determining  $\text{CMRO}_2$  changes in the rat brain at normal and low brain temperature. The results indicate a significant decrease of  $\text{CMRO}_2$  across the entire brain when the brain temperature dropped several degrees from the normal brain temperature. The capability of  $^{17}\text{O}$  MRS imaging at ultrahigh fields for multiple measurements of 3D  $\text{CMRO}_2$  imaging is promising for measurements of  $\text{CMRO}_2$  changes elevated by perturbation of physiological condition. It should be interesting to apply the same  $^{17}\text{O}$  NMR approach to study other perturbations, such as hypoxia and ischemia, as well as brain diseases, and potentially to study other living organs beyond brain.

Another interesting finding related to Figure 8.8 is the potential of  $^{17}\text{O}$  NMR for achieving a much faster temporal resolution for  $\text{CMRO}_2$  calculation according to Equation (8.9) using a single time point

measurement (not valid for the initial points due to large calculation errors when the inhalation time is too short) if the fluctuation of the measured  $\text{CMRO}_2$  value without averaging is tolerable. The confirmation of this potential could significantly strengthen the capability of  $^{17}\text{O}$  NMR approach for achieving fastest *in vivo* 3D imaging of  $\text{CMRO}_2$ , and ultimately for studying the temporal changes of  $\text{CMRO}_2$  during physiological perturbations and/or brain stimulations. There is evidence showing that the increase of  $\text{CMRO}_2$  during a sustained stimulation might vary as a function of stimulation time (Mintun *et al.*, 2002). The high-field  $^{17}\text{O}$  NMR approach with high temporal resolution should provide a useful tool for examining this aspect.

The  $\text{CMRO}_2$  measurements described in this chapter involve two invasive procedures, one for determining  $C_a(t)$  by means of the implanted  $^{17}\text{O}$  RF coil, and the second for measuring CBF by an intra-arterial catheter and bolus injection of  $\text{H}_2^{17}\text{O}$ . The CBF measurement can be performed noninvasively using the arterial spin tagging MR approaches (Detre *et al.*, 1994; Kim, 1995; Kwong *et al.*, 1995). The use of the implanted RF coil, however, is not suitable for routine measurements of  $\text{CMRO}_2$  using small experimental animal models (e.g., rat or mouse), or for human applications. Therefore, it is important to further explore the feasibility of  $^{17}\text{O}$  NMR approach for reliably imaging  $\text{CMRO}_2$  without resorting to invasive  $C_a(t)$  and/or CBF measurements. Recently, we have investigated and showed this feasibility for imaging  $\text{CMRO}_2$  in the rat brain using simplified models, which only require noninvasive measurements of the cerebral  $\text{H}_2^{17}\text{O}$  concentration (i.e.,  $C_b(t)$ ), showing similar  $\text{CMRO}_2$  results to those obtained using the complete model accounting for all parameters (Zhang *et al.*, 2002). This work opens the possibility to establish a completely noninvasive  $^{17}\text{O}$  NMR approach for  $\text{CMRO}_2$  imaging. However, this possibility needs further validations in different physiological conditions and species. This is, in particular, interesting and important for potentially human applications, where elimination of invasive procedures is desirable if not absolutely necessary.

The success of high-field  $^{17}\text{O}$  NMR for imaging  $\text{CMRO}_2$  in the human brain again relies on the  $^{17}\text{O}$  NMR sensitivity. The sensitivity loss caused by the use of large RF coil size could be partially compensated by increasing image voxel size in the humans, which have a much large brain size in comparison with most animals. Recently, we have studied the *in vivo* NMR sensitivity for acquiring 3D  $^{17}\text{O}$  images of natural abundance  $\text{H}_2^{17}\text{O}$  in the human visual cortex at 7 T with a temporal resolution of 8.5 s and a voxel size of 6.6 ml. Figure 8.10(A) demonstrates the results obtained from a representative subject showing one coronal  $^{17}\text{O}$  CSI of natural abundance  $\text{H}_2^{17}\text{O}$  (extracted from 3D  $^{17}\text{O}$  CSI dataset). The CSI plane

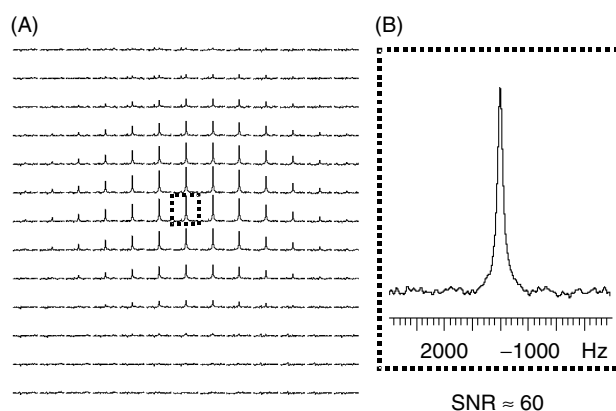


**Figure 8.10.** (A)  $^{17}\text{O}$  CSI of natural abundance  $\text{H}_2^{17}\text{O}$  in the coronal orientation acquired from the human visual cortex at 7 T. (B) One representative  $^{17}\text{O}$  spectrum from one central voxel as shown in (A) with 8.5 s of image acquisition time and 6.6 ml voxel size.

was located in the human visual cortex. Figure 8.10(B) displays a representative  $^{17}\text{O}$  spectrum from one central voxel showing the resonance peak of natural abundance  $\text{H}_2^{17}\text{O}$  in the human visual cortex with excellent SNR similar with that obtained from the rat brains at 9.4 T albeit with a smaller absolute voxel size but not relative to the size of brain (Zhu *et al.*, 2001a, 2002c). Furthermore, the dynamic concentration change of metabolic  $\text{H}_2^{17}\text{O}$  during an  $^{17}\text{O}_2$  inhalation is expected to be similar between the awake human brain and the rat brain anesthetized with  $\alpha$ -chloralose because of the similar values for both  $\text{CMRO}_2$  (2.2  $\mu\text{mol/g}/\text{min}$  in the anesthetized rat brain versus 1.7  $\mu\text{mol/g}/\text{min}$  in the awake human visual cortex) and CBF (0.53  $\text{ml/g}/\text{min}$  in the anesthetized rat brain versus 0.54  $\text{ml/g}/\text{min}$  in the awake human visual cortex) (Zhu *et al.*, 2002c; Fox *et al.*, 1988). This comparison indicates that conditions in the rat brain we studied and the awake human brain are similar relative to the parameters that impact determination of  $\text{CMRO}_2$  from the  $^{17}\text{O}$  data, and it will be possible to achieve 3D imaging of  $\text{CMRO}_2$  in the human brain at 7 T or higher magnetic fields. Realization and utilization of this potential could have an important impact on studying bioenergetics in the human brain.

The  $\text{CMRO}_2$  imaging using the  $^{17}\text{O}$  approach is expected to be more specific (*i.e.*, accurate) for functional mapping of brain activation with respect to delineation of the actual sites of evoked neuronal activity. The major reason is that a  $\text{CMRO}_2$  image can reflect the metabolic change induced by brain activation and this change is tightly coupled with the neuronal activity (Siesjo, 1978; Raichle, 1987). In principle, the  $^{17}\text{O}$  approach can circumvent many of the concerns about the specificity of currently used fMRI techniques, which are confounded by multiple contributions from different physiological changes during brain activation, and it can evolve as one of the most accurate functional imaging modalities. However, the spatial resolution of 3D  $\text{CMRO}_2$  image achieved currently is still far lower than that of BOLD-based and CBF-based fMRI as well as the  $\text{CMR}_{\text{glc}}$  imaging based on autoradiographic approach (*e.g.*, (Nakao *et al.*, 2001)). The  $^{17}\text{O}$  sensitivity gain both at 9.4 T for animal applications and at 7 T for human applications is still inadequate for functional mapping of  $\text{CMRO}_2$  changes at the spatial level of sub-cortical organizations such as the iso-orientation columns in the cat brain and the ocular dominance columns in the human brain (Bonhoeffer and Grinvald, 1993; Bonhoeffer and Grinvald, 1991; Kim *et al.*, 2000; Horton and Hedley-White, 1984; Menon *et al.*, 1997; Goodyear and Menon, 2001; Buchert *et al.*, 2002; Cheng *et al.*, 2001). It should be feasible to apply the high-field  $^{17}\text{O}$  approach for mapping and assessing  $\text{CMRO}_2$  differences between distinct brain compartments (*e.g.*, gray matter versus white matter) as well as between activated and control brain regions especially at the spatial resolution available from the  $^{17}\text{O}$  NMR approach. Furthermore, there is room for gaining more  $^{17}\text{O}$  NMR sensitivity, consequently, for going to higher spatial resolution of 3D  $\text{CMRO}_2$  imaging by improving RF coil efficacy and NMR acquisition strategies as well as NMR methodology, by averaging multiple measurements (a common strategy used for most neuroimaging modalities) and by further increasing field strength.

In conclusion, the ultrahigh-field NMR systems currently available or in development for both animals and humans provide exciting opportunities for MR applications in medicine, especially for those nuclei with low gyromagnetic ratio. One of these nuclei that benefit the most from ultrahigh field strength is  $^{17}\text{O}$  NMR, which shows great potential for *in vivo* imaging  $\text{CMRO}_2$  noninvasively in both animals and humans.

## Acknowledgments

We are grateful for the great assistance and support from Hao Lei, Nanyin Zhang, Yi Zhang, Run-Xia Tian, Xiaoliang Zhang, Hellmut Merkle, Jae-Hwan Kwag, Haiying Liu, Soeng-Gi Kim, Itamar Ronen and John Strupp. We also wish to acknowledge Gheorghe D. Mateescu, Gil Navon, Robert G. Shulman, Douglas L. Rothman, Seiji Ogawa, Joseph J.H. Ackerman and Alan C. McLaughlin for their encouragements and scientific discussions. This work was supported by NIH RO1 grants of NS41262, NS38070, NS39043, EB00329, EB00513 and P41 RR08079 (a National Research Resource grant from NIH), MIND Institute and the W.M. Keck Foundation.

## REFERENCES

Abragam, A. (1961) *The Principles of Nuclear Magnetism*, Oxford University Press, London.

Arai, T., Nakao, S., Mori, K., Ishimori, K., Morishima, I., Miyazawa, T. and Fritz-Zieroth, B. (1990) *Biochem Biophys Res Commun*, **169**, 153–158.

Attwell, D. and Laughlin, S. B. (2001) *J Cereb Blood Flow Metab*, **21**, 1133–1145.

Bandettini, P. A., Wong, E. C., Hinks, R. S., Tikofsky, R. S. and Hyde, J. S. (1992) *Magn Reson Med*, **25**, 390–397.

Barinaga, M. (1997) *Science*, **276**, 196–198.

Beal, M. F. (1992) *Ann Neurol*, **31**, 119–130.

Blamire, A. M., Ogawa, S., Ugurbil, K., Rothman, D., McCarthy, G., Ellermann, J. M., Hyder, F., Rattner, Z. and Shulman, R. G. (1992) *Proc Natl Acad Sci USA*, **89**, 11069–11073.

Bonhoeffer, T. and Grinvald, A. (1991) *Nature*, **353**, 429–431.

Bonhoeffer, T. and Grinvald, A. (1993) *J Neurosci*, **13**, 4157–4180.

Buchert, M., Greenlee, M. W., Rutschmann, R. M., Kraemer, F. M., Luo, F. and Hennig, J. (2002) *Exp Brain Res*, **145**, 334–339.

Cassoly, R. (1982) *Biochim Biophys Acta*, **689**, 203–209.

Chen, W., Adriany, G., Zhu, X. H., Gruetter, R. and Ugurbil, K. (1998) *Magn Reson Med*, **40**, 180–184.

Chen, W. and Ogawa, S. (1999). In: Moonen, C. T. W. and Bandettini, P. A. (eds), *Principle of BOLD functional MRI*, Springer, Berlin.

Chen, W., Zhu, X. H., Gruetter, R., Seaquist, E. R. and Ugurbil, K. (2001) *Magn Reson Med*, **45**, 349–355.

Cheng, K., Waggoner, R. A. and Tanaka, K. (2001) *Neuron*, **32**, 359–374.

Davis, T. L., Kwong, K. K., Weisskoff, R. M. and Rosen, B. R. (1998) *Proc. Natl. Acad. Sci. USA*, **95**, 1834–1839.

Detre, J. A., Zhang, W., Roberts, D. A., Silva, A. C., Williams, D. S., Grandis, D. J., Koretsky, A. P. and Leigh, J. S. (1994) *NMR Biomed*, **7**, 75–82.

Fiat, D., Dolinsek, J., Hankiewicz, J., Dujovny, M. and Ausman, J. (1993) *Neurol Res*, **15**, 237–248.

Fiat, D., Ligeti, L., Lyon, R. C., Ruttner, Z., Pekar, J., Moonen, C. T. and McLaughlin, A. C. (1992) *Magn Reson Med*, **24**, 370–374.

Fox, P. T. and Raichle, M. E. (1986) *Proc Natl Acad Sci USA*, **83**, 1140–1144.

Fox, P. T., Raichle, M. E., Mintun, M. A. and Dence, C. (1988) *Science*, **241**, 462–464.

Frackowiak, R. S., Herold, S., Petty, R. K. and Morgan-Hughes, J. A. (1988) *Brain*, **111** (Pt 5), 1009–1024.

Frahm, J., Kruger, G., Merboldt, K. D. and Kleinschmidt, A. (1996) *Magn Reson Med*, **35**, 143–148.

Goodyear, B. G. and Menon, R. S. (2001) *Hum Brain Mapp*, **14**, 210–217.

Gruetter, R., Seaquist, E. R., Kim, S. and Ugurbil, K. (1998) *Dev Neurosci*, **20**, 380–388.

Gruetter, R., Seaquist, E. R. and Ugurbil, K. (2001) *Am J Physiol Endocrinol Metab*, **281**, 100–112.

Harrison, R. V., Harel, N., Panesar, J. and Mount, R. J. (2002) *Cereb Cortex*, **12**, 225–233.

Hendrich, K., Hu, X., Menon, R., Merkle, H., Camarata, P., Heros, R. and Ugurbil, K. (1994) *J Magn Reson*, **105**, 225–232.

Herscovitch, A. and Raichle, M. E. (1985) *J Cereb Blood Flow Metab*, **5**, 65–69.

Herscovitch, P., Raichle, M. E., Kilbourn, M. R. and Welch, M. J. (1987) *J Cereb Blood Flow Metab*, **7**, 527–542.

Hoge, R. D., Atkinson, J., Gill, B., Crelier, G. R., Marrett, S. and Pike, G. B. (1999) *Magn Reson Med*, **42**, 849–863.

Hopkins, A. L. and Barr, R. G. (1987) *Magn Reson Med*, **4**, 399–403.

Hoppeler, H. and Kayar, S. R. (1988) *News Physiol Sci*, **3**, 113–116.

Horton, J. C. and Hedley-White, E. T. (1984) *Phil Trans R Soc London, Ser B* **304**, 255–272.

Hoult, D. I. and Richards, R. E. (1976) *J Magn Reson*, **24**, 71–85.

Hyder, F., Chase, J. R., Behar, K. L., Mason, G. F., Siddeek, M., Rothman, D. L. and Shulman, R. G. (1996) *Proc Natl Acad Sci USA*, **93**, 7612–7617.

Hyder, F., Kennan, R. P., Kida, I., Mason, G. F., Behar, K. L. and Rothman, D. (2000) *J Cereb Blood Flow Metab*, **20**, 485–498.

Hyder, F., Rothman, D. L., Mason, G. F., Rangarajan, A., Behar, K. L. and Shulman, R. G. (1997) *J Cereb Blood Flow Metab*, **17**, 1040–1047.

Jenkins, B. G., Koroshetz, W. J., Beal, M. F. and Rosen, B. R. (1993) In: *The Annual Meeting of the Society for Magnetic Resonance Imaging*, Chicago.

Kety, S. S. and Schmidt, C. F. (1948) *J Clin Invest*, **27**, 476–483.

Kim, D. S., Duong, T. Q. and Kim, S. G. (2000) *Nat Neurosci*, **3**, 164–169.

Kim, S.-G. (1995) *Magn Reson Med*, **34**, 293–301.

Kim, S. G., Rostrup, E., Larsson, H. B., Ogawa, S. and Paulson, O. B. (1999) *Magn Reson Med*, **41**, 1152–1161.

Kwong, K. K., Belliveau, J. W., Chesler, D. A., Goldberg, I. E., Weisskoff, R. M., Poncelet, B. P., Kennedy, D. N., Hoppel, B. E., Cohen, M. S., Turner, R., Cheng, H. M., Brady, T. J. and Rosen, B. R. (1992) *Proc Natl Acad Sci USA*, **89**, 5675–5679.

Kwong, K. K., Chesler, D. A., Weisskoff, R. M., Donahue, K. M., Davis, T. L., Stergaard, L., Campbell, T. A. and Rosen, B. R. (1995) *Magn Reson Med*, **34**, 878–887.

Kwong, K. K., Hopkins, A. L., Belliveau, J. W., Chesler, D. A., Porkka, L. M., McKinstry, R. C., Finelli, D. A., Hunter, G. J., Moore, J. B., Barr, R. G. and Rosen, B. R. (1991) *Magn Reson Med*, **22**, 154–8.

Lee, S. P., Silva, A. C., Ugurbil, K. and Kim, S. G. (1999) *Magn Reson Med*, **42**, 919–28.

Lenzi, G. L., Frackowiak, R. S., Jones, T., Heather, J. D., Lammertsma, A. A., Rhodes, C. G. and Pozzilli, C. (1981) *Eur Neurol*, **20**, 285–90.

Marrett, S., Fujita, H., Meyer, E., Ribeiro, L., Evans, A., Kuwabara, H. and Gjedde, A. (1993). In: Uemura, K. (ed.), *Quantification of Brain Function in Tracer Kinetics and Image Analysis in Brain PET*, Elsevier, New York, pp. 217–228.

Mason, G. F., Gruetter, R., Rothman, D. L., Behar, K. L., Shulman, R. G. and Novotny, E. J. (1995) *J Cereb Blood Flow Metab*, **15**, 12–25.

Mason, G. F., Rothman, D. L., Behar, K. L. and Shulman, R. G. (1992) *J Cereb Blood Flow Metab*, **12**, 434–447.

Mateescu, G. D., Yvars, G., Pazara, D. I., Alldridge, N. A., LaManna, J. C., Lust, D. W., Mattingly, M. and Kuhn, W. (1989). In: Baillie, T. A. and Jones, J. R. (eds), *Synthesis and Application of Isotopically Labeled Compounds* Elsevier, Amsterdam, pp. 499–508.

Mateescu, G. D., Yvars, G. M. and Dular, T. (1988) In: Lauger, P., Packer, L. and Vasilescu, V. (eds), *Water and Ions in Biological Systems*, Birkhauser, Basel, pp. 239–250.

Maurer, I., Zierz, S. and Moller, H. (2001) *Schizophr Res*, **48**, 125–136.

Maurer, I., Zierz, S. and Moller, H. J. (2000) *Neurobiol Aging*, **21**, 455–462.

Meiboom, S. (1961) *J Chem Phys*, **34**, 375–388.

Menon, R. S., Ogawa, S., Strupp, J. P. and Ugurbil, K. (1997) *J Neurophysiol*, **77**, 2780–2787.

Mintun, M. A., Raichle, M. E., Martin, W. R. and Herscovitch, P. (1984) *J Nucl Med*, **25**, 177–187.

Mintun, M. A., Vlassenko, A. G., Shulman, G. L. and Snyder, A. Z. (2002) *Neuroimage*, **16**, 531–537.

Nakao, Y., Itoh, Y., Kuang, T. Y., Cook, M., Jehle, J. and Sokoloff, L. (2001) *Proc Natl Acad Sci USA*, **98**, 7593–8.

Novotny, E. J., Ogino, T., Rothman, D. L., Petroff, O. C., Prichard, J. W. and Shulman, R. G. (1990) *Magn Reson Med*, **16**, 431–443.

Ogawa, S. and Lee, T. M. (1990) *Magn Reson Med*, **16**, 9–18.

Ogawa, S., Lee, T.-M., Kay, A. R. and Tank, D. W. (1990) *Proc Natl Acad Sci USA*, **87**, 9868–9872.

Ogawa, S., Menon, R. S., Kim, S.-G. and Ugurbil, K. (1998) *Annu Rev Biophys Biomol Struct*, **27**, 447–474.

Ogawa, S., Tank, D. W., Menon, R., Ellermann, J. M., Kim, S.-G., Merkle, H. and Ugurbil, K. (1992) *Proc Natl Acad Sci USA*, **89**, 5951–5955.

Ohta, S., Meyer, E., Thompson, C. J. and Gjedde, A. (1992) *J Cereb Blood Flow Metab*, **12**, 179–192.

Pekar, J., Ligeti, L., Ruttner, Z., Lyon, R. C., Sinnwell, T. M., van Gelderen, P., Fiat, D., Moonen, C. T. and McLaughlin, A. C. (1991) *Magn Reson Med*, **21**, 313–319.

Pekar, J., Sinnwell, T., Ligeti, L., Chesnick, A. S., Frank, J. A. and McLaughlin, A. C. (1995) *J Cereb Blood Flow Metab*, **15**, 312–320.

Prichard, J., Rothman, D., Novotny, E., Petroff, O., Kuwabara, T., Avison, M., Howseman, A., Hanstock, C. and Shulman, R. G. (1992) *Proc Natl Acad Sci (USA)*, **88**, 5829–5831.

Raichle, M. E. (1987) In: M. D. Mountcastle, V. B., Plum, F. and Geiger, S. R. (eds), *Handbook of Physiology—The Nervous System* American Physiological Society, Bethesda, pp. 643–674.

Reddy, R., Stolpen, A. H. and Leigh, J. S. (1995) *J Magn Reson B*, **108**, 276–279.

Renshaw, P. F., Yurgelun-Todd, D. A. and Cohen, B. M. (1994) *Am J Psychiatry*, **151**, 1493–1495.

Ribeiro, L., Kuwabara, H., Meyer, E., Fujita, H., Marrett, S., Evans, A. and Gjedde, A. (1993) In: Uemura, K. (ed.), *Quantification of Brain Function in Tracer Kinetics and Image Analysis in Brain PET*, Elsevier, New York, pp. 229–236.

Roland, P. E., Ericksson, L., Stone-Elander, S. and Widen, L. (1987) *J Neurosci*, **7**, 2373–2389.

Ronen, I., Merkle, H., Ugurbil, K. and Navon, G. (1998) *Proc Natl Acad Sci U S A*, **95**, 12934–12939.

Ronen, I. and Navon, G. (1994) *Magn Reson Med*, **32**, 789–93.

Rothman, D. L., Novotny, E. J., Shulman, G. I., Howseman, A. M., Petroff, O. A., Mason, G., Nixon, T., Hanstock, C. C., Prichard, J. W. and Shulman, R. G. (1992) *Proc Natl Acad Sci USA*, **89**, 9603–9606.

Rothman, D. L., Sibson, N. R., Hyder, F., Shen, J., Behar, K. L. and Shulman, R. G. (1999) *Philos Trans R Soc London, Ser B Biol Sci*, **354**, 1165–1177.

Sappey-Marinier, D., Calabrese, G., Fein, G., Hugg, J. W., Biggins, C. and Weiner, M. W. (1992) *J. Cereb. Blood Flow Metab*, **12**, 584–592.

Shen, J., Petersen, K. F., Behar, K. L., Brown, P., Nixon, T. W., Mason, G. F., Petroff, O. A., Shulman, G. I., Shulman, R. G. and Rothman, D. L. (1999) *Proc Natl Acad Sci USA*, **96**, 8235–8240.

Shulman, R. G., Hyder, F. and Rothman, D. L. (2001a) *Proc Natl Acad Sci U S A*, **98**, 6417–6422.

Shulman, R. G., Hyder, F. and Rothman, D. L. (2001b) *NMR Biomed*, **14**, 389–396.

Shulman, R. G., Rothman, D. L. and Hyder, F. (1999) *Proc Natl Acad Sci USA*, **96**, 3245–3250.

Sibson, N. R., Mason, G. F., Shen, J., Cline, G. W., Herskovits, A. Z., Wall, J. E., Behar, K. L., Rothman, D. L. and Shulman, R. G. (2001) *J Neurochem*, **76**, 975–989.

Siesjo, B. K. (1978) *Brain Energy Metabolism*, Wiley, New York.

Steinhoff, H. J., Kramm, B., Hess, G., Owerdieck, C. and Redhardt, A. (1993) *Biophys J*, **65**, 1486–1495.

Ter-Pogossian, M. M., Eichling, J. O., Davis, D. O. and Welch, M. J. (1970) *J Clin Invest*, **49**, 381–391.

Ugurbil, K., Hu, X., Chen, W., Zhu, X. H., Kim, S. G. and Georgopoulos, A. (1999) *Philos Trans R Soc London, Ser B Biol Sci*, **354**, 1195–1213.

Ugurbil, K., Kim, D. S., Duong, T., Hu, X., Ogawa, S., Gruetter, R., Chen, W., Kim, S. G., Zhu, X. H., Yacoub, E., van de Moortele, P. F., Shmuel, A., Pfeuffer, J., Merkle, H., Andersen, P. and Adriany, G. (2001) *Proc IEEE*, **89**, 1093–1106.

Vafaee, M. S., Meyer, E., Marrett, S., Paus, T., Evans, A. C. and Gjedde, A. (1999) *J Cereb Blood Flow Metab*, **19**, 272–277.

van Zijl, P. C. M. and Rothman, D. (1995) *Magn Reson Imaging*, **13**, 1213–1221.

Wen, H., Chesnick, A. S. and Balaban, R. S. (1994) *Magn Reson Med*, **32**, 492–498.

Wong-Riley, M., Antuono, P., Ho, K. C., Egan, R., Hevner, R., Liebl, W., Huang, Z., Rachel, R. and Jones, J. (1997) *Vision Res*, **37**, 3593–3608.

Zhang, N. Y., Zhu, X. H., Lei, H., Ugurbil, K. and Chen, W. (2002) In: *10th Annual Meeting of International Society for Magnetic Resonance in Medicine*, Hawaii, p. 344.

Zhang, X. L., Tain, R. X., Zhu, X. H., Zhang, Y., Merkle, H. and Chen, W. (2003) *MAGMA*, **16**, 77–85.

Zhu, X. H., Lei, H., Zhang, Y., Zhang, X. L., Zhang, N., Ugurbil, K. and Chen, W. (2002a) In: *10th Annual Meeting of International Society for Magnetic Resonance in Medicine*, Hawaii, p. 1094.

Zhu, X. H., Merkle, H., Kwag, J. H., Ugurbil, K. and Chen, W. (2001a) *Magn Reson Med*, **45**, 543–549.

Zhu, X. H., Tain, R., Ugurbil, K. and Chen, W. (2001b) In: *9th International Society for Magnetic Resonance in Medicine Annual Meeting*, Glasgow, UK, p. 649.

Zhu, X. H., Tian, R. X., Lei, H., Zhang, Y., Zhang, N., Kim, S. G., Ugurbil, K. and Chen, W. (2002b) In *10th Annual Meeting of International Society for Magnetic Resonance in Medicine*, Hawaii, p. 1368.

Zhu, X. H., Zhang, Y., Tian, R. X., Lei, H., Zhang, N., Zhang, X., Merkle, H., Ugurbil, K. and Chen, W. (2002c) *Proc Natl Acad Sci U S A*, **99**, 13194–13199.

# 9

## Deriving Changes in CMR<sub>O<sub>2</sub></sub> from Calibrated fMRI

**Fahmeed Hyder**

*Departments of Diagnostic Radiology and Biomedical Engineering, Yale University School of Medicine, MR Center, P.O. Box 208043, New Haven, CT 06510, USA*

---

9.1	Introduction	147
9.2	Physiology of Neuroimaging	148
9.3	Neuroimaging with MRI	149
9.4	Biophysics of fMRI	151
9.5	Methods for Calibrating fMRI	153
9.6	Physiological Basis of fMRI	156
9.7	Neural Basis of fMRI	161
9.8	Implications for Human fMRI	162
9.9	Future Directions	164
9.10	Conclusion	165

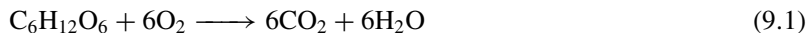
---

### 9.1. INTRODUCTION

The brain is a restless assembly of cells continuously working (i.e., receiving and routing information) to maintain its functional integrity. While advances in neuroscience (Kandel *et al.*, 1991) have revealed that variations in neuronal activity – both electrical and chemical in nature – can affect the state of mind, mood, or behavior of the person, the importance of energetics as an indicator for neural function has been less appreciated. Energy is defined as the capability of doing work and in a perfect nondissipating system the energy consumed equals the magnitude of work done (Garby and Larsen, 1995). The functioning brain is not far from equilibrium. Thus neurotransmission proceeds in a thermodynamically downhill fashion as a

consequence of transiently increased permeability of  $\text{Na}^+$  across the membrane down chemical gradients. Restoration of ionic gradients is energetically very expensive (see Chapter 7) because ions have to be transported against large chemical gradients (Creutzfeldt, 1975; Ames, 2000; Laughlin, 2001). Since most of the energy is spent to keep neurons ready to be able to work (i.e., ‘fire’) whenever called for, measuring changes in energy use of a neuronal ensemble provides a window into their grouped activity.

Under normal conditions, glucose is the main or exclusive carbon source for the adult mammalian brain and its oxidation is the main energy producing pathway (Siesjo, 1978). Glucose breakdown (through the tricarboxylic acid cycle) in the presence of oxygen generates  $\sim 36$  mol of ATP per mole of glucose, whereas in the absence of oxygen glycolysis and/or glycogenolysis generates 1–2 mol ATP per mole of glucose. Because complete glucose oxidation has a stoichiometry of



the cerebral metabolic rate of oxygen consumption ( $\text{CMR}_{\text{O}_2}$ ) is equal to six times the cerebral metabolic rate of glucose consumption ( $\text{CMR}_{\text{glc}}$ ). Since results from experiments conducted under a variety of physiological conditions reveal that glucose oxidation is nearly complete, the relationship between  $\text{CMR}_{\text{O}_2}$  and  $\text{CMR}_{\text{glc}}$  is well established (Siesjo, 1978), and therefore well accepted (Shulman *et al.*, 2001a). While small amounts of glucose can be stored as glycogen in the glia, there are no significant stores of oxygen. Furthermore the volume of blood that provides the oxygenated hemoglobin – the main oxygen carrier in the brain – is extremely small. Because the brain in the average adult human has a very high energetic demand – approximately ten times that expected simply on the basis of its weight – even transient restrictions in oxygen supply can critically harm neural function (Sokoloff, 1991). Neuronal and glial activities are tightly correlated with their energy use and the brain’s energy reserve is not very significant, so that a continuous circulation of blood – which provides nutrients and removes waste – is necessary for normal function. This phenomenon of neurovascular coupling is credited to Roy and Sherrington (1890) since they suggested, more than a century ago, a tight correlation between blood supply and cellular workload in brain tissue. Thus cerebral blood flow (CBF) can provide an indirect estimate of the ongoing neural function under most conditions. Since most modern neuroimaging methods measure some component of CBF, the experimentalist’s inherent assumption has been that these maps reflect changes in neural energy, and hence alterations in neuronal activity.

The extreme vulnerability of brain tissue to oxygen deprivation stipulates that fractional changes in CBF and  $\text{CMR}_{\text{O}_2}$  as well as regional values of CBF and  $\text{CMR}_{\text{O}_2}$  must effectively be correlated. An important point of consideration, however, is that although there is no requirement for a stoichiometric relationship between fractional changes in CBF and  $\text{CMR}_{\text{O}_2}$ , there is a prescribed stoichiometric ratio between fractional changes in  $\text{CMR}_{\text{O}_2}$  and  $\text{CMR}_{\text{glc}}$  (i.e., Equation (9.1)) if glucose oxidation is to be maintained over a wide range of activity.

## 9.2. PHYSIOLOGY OF NEUROIMAGING

The relationship between  $\text{CMR}_{\text{O}_2}$  and CBF (i.e., fractional changes or regional values), and therefore mechanisms of oxygen transport from the blood to the brain, is critical for understanding neuroimaging (Hyder *et al.*, 1998). A theory of substrate delivery from blood to tissue was formally introduced by Crone (1963). By detecting tracer amounts of an exogenous indicator’s dilution (within the blood) or diffusion (into the tissue) as a function of time, amounts of indicator permeating through the blood–brain barrier could be related to the arteriovenous concentration difference (i.e.,  $C_a - C_v$ ) in a quantitative manner. The process of oxygen extraction by cerebral tissue from capillaries can be modeled almost the same way as the exogenous indicator’s dilution or diffusion curves because the only source of oxygen is the blood (i.e.,

hemoglobin) and the major sink for oxygen is in the tissue (i.e., mitochondria). Thus a theoretical construct allowed CMRO<sub>2</sub> and CBF to be related to  $C_a$  and  $C_v$  since oxygen extraction fraction (OEF) of the tissue is equal to  $(1 - C_v/C_a)$  and to  $CMR_{O_2}/(C_a \text{ CBF})$ , according to Fick's principle (Siesjo, 1978).

$$\frac{CMR_{O_2}}{CBF} = C_a - C_v \quad (9.2)$$

The vital question about Equation (9.2) for neuroimaging is, however, what happens when there is increased neuronal activity? Two prior independent observations regarding the specifics of oxygenated blood and cerebral capillaries provided an insight. Hill (1913) identified that saturation of hemoglobin with oxygen, as reflected by the partial pressure of oxygen ( $pO_2$ ), changed the color of erythrocytes: the fully oxygenated form being bright red whereas the fully deoxygenated form being nearly black. Penfield (1933) observed that arterial ends of cerebral capillaries were almost always red whereas venous ends were purple, and veins became redder when cellular workload was regionally increased. These independent observations provided a very important contention about Equation (9.2) and changes in local neuronal activity. In an activated region, which experiences a metabolically driven increase in local perfusion due to the augmented cellular work, the difference between  $C_a$  and  $C_v$  has to become smaller. Since the blood is almost fully oxygenated at the arterial end, the arteriovenous difference in capillaries can be decreased only if venous oxygenation is increased. Thus a metabolically driven increase in local perfusion is consistent with a drop in deoxyhemoglobin concentration at the venous end of the capillary. Therefore a qualitative understanding of functional hyperemia (i.e., synonymous with higher oxygenation), which has been known for several decades, suggests raised blood oxygenation with increased neuronal activity. In other words, a larger increase in CBF than CMRO<sub>2</sub>, which in turn is commensurate with a decrease in OEF, would be expected in the activated region.

### 9.3. NEUROIMAGING WITH MRI

Pauling and Coryell (1936) showed that deoxyhemoglobin is paramagnetic. Since hemoglobin is contained in erythrocytes, there are tiny magnetic fields in and around the cells. Because water protons can sense the local field distortions around red blood cells, the changing amount of oxygen carried by hemoglobin could be sensed by NMR of water. Many decades later Ogawa *et al.* (1990) showed that a change of the venous deoxyhemoglobin concentration in brain capillaries can be detected *in vivo* with an MRI method (of water protons) which is sensitive to the microscopic magnetic susceptibility in the vasculature. Spin echo and gradient echo images are sensitive to functional hyperemia because these image contrasts can reflect physiologically induced changes in magnetic properties of blood. This new fMRI image contrast was therefore termed blood oxygenation level dependent (BOLD) by Ogawa *et al.* (1993).

While the use of NMR physics can discern the BOLD image contrast with the measurable parameters of transverse relaxation time of tissue water ( $T_2^{\text{SE}}$  and  $T_2^{\text{GE}}$  with spin echo and gradient echo image contrasts, respectively), the physiological basis of interpreting fractional changes in fMRI signal ( $\Delta S/S$ ) depends on hemodynamic and metabolic parameters because both CMRO<sub>2</sub> and CBF can directly affect  $T_2^{\text{SE}}$  or  $T_2^{\text{GE}}$  in an MRI voxel. At steady state  $\Delta S/S$  is related to the metabolically driven increase in perfusion,

$$\frac{\Delta S}{S} = M \left( \frac{\Delta CBF}{CBF} - \frac{\Delta CMR_{O_2}}{CMR_{O_2}} \right) - N \left( \frac{\Delta CBV}{CBV} \right) \quad (9.3)$$

where  $M$  and  $N$  are measurable physiologic and magnetic constants (related to  $T_2^{\text{SE}}$  or  $T_2^{\text{GE}}$ ), and  $\Delta CMR_{O_2}/CMR_{O_2}$ ,  $\Delta CBF/CBF$ , and  $\Delta CBV/CBV$  are respective changes in oxidative metabolism, blood flow and volume (for a review see Hyder *et al.*, 2001). Note that  $M$  is equal to  $N$  divided by  $(1 + \Delta CBF/CBF)$ . Obviously  $\Delta CMR_{O_2}/CMR_{O_2}$  is the most relevant of all of these physiological parameters

for studying functional activity of the brain, because it is proportional to changes in energy use associated with alterations in neuronal activity induced by the stimulation. A conventional fMRI experiment offers information about *where the neural activity has changed*; however, a calibrated fMRI experiment – meaning that  $\Delta\text{CMR}_{\text{O}_2}/\text{CMR}_{\text{O}_2}$  is extracted from Equation (9.3) using measurements of  $\Delta\text{CBF}/\text{CBF}$ ,  $\Delta\text{CBV}/\text{CBV}$ , and  $\Delta S/S$  – in addition presents valuable data about *how much the neural activity has changed by*. The main advantage of deriving  $\Delta\text{CMR}_{\text{O}_2}/\text{CMR}_{\text{O}_2}$  from calibrated fMRI, in contrast to  $^{15}\text{O}$  PET (e.g., Mintun *et al.*, 1984),  $^{13}\text{C}$  MRS (e.g., Hyder *et al.*, 1996), and  $^{17}\text{O}$  MRS (e.g., Zhu *et al.*, 2002) methods which can also measure  $\Delta\text{CMR}_{\text{O}_2}/\text{CMR}_{\text{O}_2}$ , is that the spatial and temporal resolutions are significantly higher and it is an inexpensive and effortless method without exposure to radiation that can be conducted in conventional MRI scanners.

In this chapter the energetic basis of BOLD image contrast (Figure 9.1(A)) is revealed from experiments conducted in rat brain at the high static magnetic field strength ( $B_0$ ) of 7 T. The approach used can be summarized as follows. If  $\Delta S/S$ ,  $\Delta\text{CMR}_{\text{O}_2}/\text{CMR}_{\text{O}_2}$ ,  $\Delta\text{CBF}/\text{CBF}$ , and  $\Delta\text{CBV}/\text{CBV}$  are mapped (by different NMR methods) for a range of activity levels, the combined results can then be used to calibrate the BOLD signal (at a particular magnetic field strength for a specific type of tissue) because  $\text{CBF} - \text{CMR}_{\text{O}_2}$

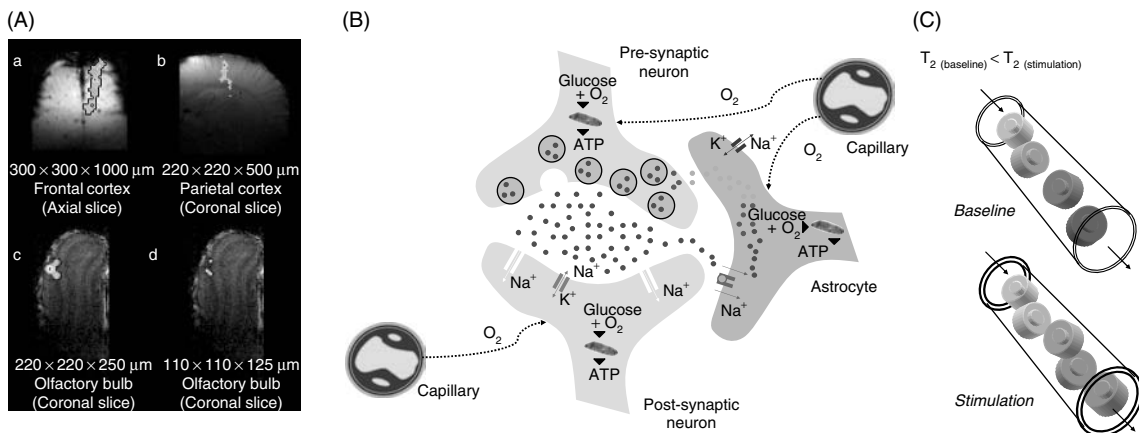


**Figure 9.1.** Neuroimaging with fMRI at 7 T. (A) Examples of localized activity detected with BOLD in anesthetized rat brain with forepaw stimulation (a, Hyder *et al.*, 1994), single whisker stimulation (b, Yang *et al.*, 1996), and olfactory stimulation (Yang *et al.* 1998) with high (c, Xu *et al.*, 2000) and ultrahigh (d, Kida *et al.*, 2002) spatial resolutions. (B) The fMRI signal changes indirectly reflect alterations in energetics of glutamatergic synapses (Shulman and Rothman, 1998; Attwell and Laughlin, 2001), where neuronal and astrocytic interactions are tightly regulated (Pellerin and Magistretti, 1994). A wide range of energy consuming processes (which include action potential propagation, maintenance of membrane potentials, vesicular recycling, neurotransmitter release and uptake) are involved in short-term neuronal information encoding, where the majority of the ATP utilized to support the cellular work is obtained from glucose oxidation. Since the only source of oxygen is hemoglobin in the blood and the major sink for oxygen is the mitochondria, a tight relationship between CBF and  $\text{CMR}_{\text{O}_2}$  is mandated. (C) Because arterial blood in cerebral capillaries is fully oxygenated (Hill, 1913; Penfield, 1933), the metabolically driven increase in local perfusion is such that the local increase in CBF is greater than the increase in  $\text{CMR}_{\text{O}_2}$  (i.e., functional hyperemia). Thus an increased blood oxygenation is expected with neuronal activation which can be detected by spin echo (or gradient echo) MRI where  $T_2$  (or  $T_2^*$ ) of tissue water protons is increased thus causing an increase in the BOLD signal during the stimulation condition in comparison to the baseline condition. Since  $T_2$  (or  $T_2^*$ ) is directly affected by local magnetic susceptibility in an MRI voxel which can attenuate the MRI signal because of intravoxel spin dephasing, an increase in  $T_2$  (or  $T_2^*$ ) is commensurate with a lesser degree of intravoxel dephasing. The more oxygenated red blood cell is shown in lighter gray, the arterial and venous ends are shown by the two arrows pointing in and out of the capillary, respectively.

and CBF–CBV relationships can be quantified to determine the constants in Equation (9.3) (i.e.,  $M$  and  $N$ ). Since a majority of energy consumed is spent in restoring ionic gradients across the cell membrane to maintain functional integrity (Figure 9.1(B)), demand and supply of nutrients are tightly correlated. Thus CMRO<sub>2</sub> values provide insight into the bioelectric work which helps sustain excitability of neurons. The obligatory dilatation of microvasculature (Figure 9.1(C)), which is the mechanical response that was noticed by Roy and Sherrington (1890), is involved in removal of waste (e.g., CO<sub>2</sub>, heat) while providing nutrients and is reflected in the CBF–CBV relationship. The type of BOLD calibration described here is unique since it adds a measure of changes in energy consumption,  $\Delta\text{CMRO}_2/\text{CMRO}_2$ , to the valuable localization results generally considered.

## 9.4. BIOPHYSICS OF fMRI

There has been great progress in the biophysical understanding of contrast enhancement with MRI contrast agents such as gadolinium (e.g., Haacke *et al.*, 2001). Thus the theory of susceptibility-based contrast mechanisms for an endogenous paramagnetic material such as deoxyhemoglobin is becoming well understood (Albert *et al.*, 1993; Kennan *et al.*, 1994; Weisskoff *et al.*, 1994). While a detailed discussion of this topic is not the objective here, some key elements are mentioned to understand the role of cerebral microvasculature in the BOLD image contrast. The presence of deoxyhemoglobin, behaving as an endogenous contrast agent, within a uniform cylinder of infinite length creates local magnetic field gradients which extend into the surrounding tissue and dephase water protons. These local gradients are a consequence of the volume magnetic susceptibility difference between tissue and the compartmentalized paramagnetic material inside the capillary. For some randomly oriented cylinders, which mimic the capillary network within tissues, the local gradients in the vicinity of proximal capillaries overlap (provided that capillaries are far enough from each other to discount diffusion of water from one vessel to another). The local gradients outside the capillaries enhance the dephasing of water protons (i.e., spins) in the tissue which can be detected by decreased signals in both  $T_2^{\text{SE}}$  and  $T_2^{\text{GE}}$  weighted images. For functional hyperemia, of course, the amount of deoxyhemoglobin is decreased and the entire argument above is reversed (Figure 9.2(A)). Since the difference between  $C_a$  and  $C_v$  becomes smaller with functional hyperemia due to increases in  $C_v$  (see Equation (9.2)), the contributions of arterial blood can be disregarded because arterial blood is almost fully oxygenated (Hill, 1913) and it is diamagnetic (Pauling and Coryell, 1936). Because studies of cerebral vascular anatomy reveal that the arteriole blood volume (as well as the surface area) is a small fraction of the entire blood volume (Craigie, 1945) in cerebral microvasculature (Figure 9.2(B)), the neglected arteriole compartment in BOLD image contrast does not present a significant bias.

How are spin echo and gradient echo image contrasts affected by local field gradients that are generated by the compartmentalized paramagnetic material inside capillaries? The diffusion of spins in the tissue space through paths that contain the perturbing fields subjects the spin ensemble to an averaged field distribution. While BOLD image contrast does not measure spin diffusion directly, a suitable choice of echo time ( $TE$ ) sensitizes the experiment to the speed of diffusion (i.e., fast, intermediate, and slow). In all regimes, the *diffusive* effects introduce a ‘dynamic’ averaging of local field gradients which causes signal decay and this loss of spin coherence is not reversible. However, in addition there are also *static* effects which introduce a ‘local’ averaging of the field gradients but this signal decay is reversible (e.g., by a refocusing pulse in a spin echo sequence). Both *static* and *diffusive* effects are present evenly in the intermediate regime (e.g., outside blood vessels, diameter 5–15  $\mu\text{m}$ ) and either image contrast is sensitive. In fMRI it is the regions with fast and intermediate diffusion that are of interest because they reflect signals from tissue outside of small blood vessels (for a recent review see Ugurbil *et al.*, 2000).

The contrast enhancement by deoxyhemoglobin for mapping neural activity should specifically respond to small vessel effects. There are two types of vascular effects, *types A* and *B*. Since the blood volume

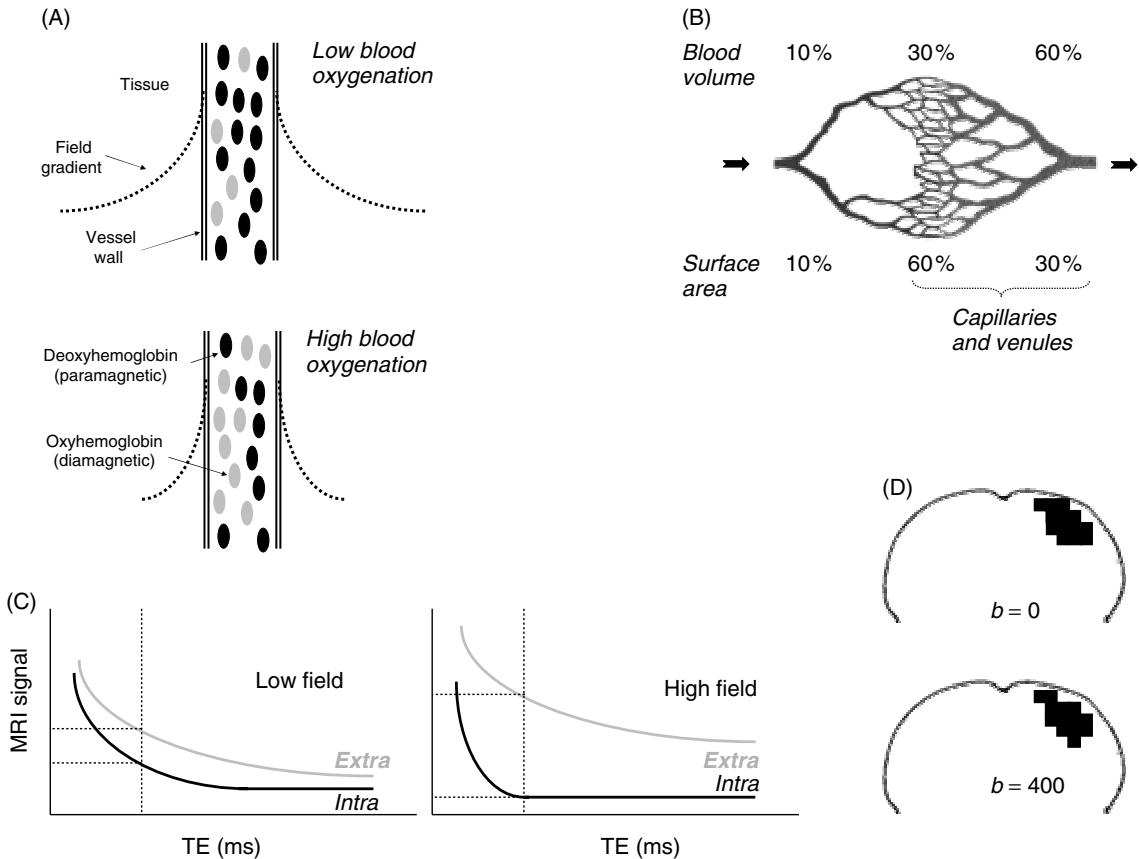


**Figure 9.2.** The biophysical basis of fMRI. (A) Since deoxyhemoglobin is paramagnetic (Pauling and Coryell, 1936), the presence of this endogenous contrast agent inside cerebral capillaries generates local magnetic field gradients which extend into the tissue (Ogawa *et al.*, 1990). The local gradients enhance dephasing of water protons in the tissue which can be detected by decreased signals in  $T_2^{\text{SE}}$  and  $T_2^{\text{GE}}$  weighted images. During activation the amount of deoxyhemoglobin is decreased in comparison to the resting condition and this difference between the stimulation-induced susceptibility difference of blood can be observed as changes in  $T_2$  (or  $T_2^*$ ) by spin echo (or gradient echo) MRI. (B) Since the arteriole blood volume and surface area are significantly smaller than other compartments of cerebral vasculature (Craigie, 1945), the neglect of the arteriole compartment in BOLD image contrast does not provide an incredible bias. (C) At any given  $B_0$ , the intravascular and extravascular weightings in BOLD data depend on the transverse relaxation times of water in blood ( $T_2^{\text{intra}}$ ; black) and tissue ( $T_2^{\text{extra}}$ ; gray). Prior studies (for a recent review see Ugurbil *et al.*, 2000) have shown that  $T_2^{\text{intra}} \approx T_2^{\text{extra}}$  at low  $B_0$  which suggests that both intravascular and extravascular compartments are equally dominant, whereas measured values show that  $T_2^{\text{intra}} < T_2^{\text{extra}}$  at high  $B_0$  which indicates that the extravascular compartment is far more dominant. In each case, the intravascular and extravascular fractions are shown by the dotted lines. (D) The contribution of the intravascular effect on BOLD can be examined by using graded diffusion-weighted spin echo MRI (e.g., Lee *et al.*, 1999) with a range of diffusion weighting factor ( $b$ ) values – the higher the  $b$  value the greater the degree of suppression of the intravascular contribution to the BOLD effect. The figure shows two spin echo fMRI maps ( $TE = 50$  ms) of the forepaw stimulation model of the same rat brain at 7T with  $b$  values of 0 and  $400 \text{ s/mm}^2$ . The high correlation between these two maps suggests negligible intravascular contamination of the BOLD effect at 7T.

fraction tends to be small (2–5 %) for a typical MRI voxel, there is an inherent partial volume bias towards signal from tissue water with either contrast. However, very large vessels (e.g., arteries and veins) can have larger partial volume and these ‘false positives’ due to *type A* vascular effect in gradient echo data can be removed by comparison with spin echo data. Furthermore it is important to realize that intravascular and extravascular weightings in BOLD data depend on the actual values of transverse relaxation times of water in blood ( $T_2^{\text{intra}}$ ) and tissue ( $T_2^{\text{extra}}$ ). Because  $T_2^{\text{intra}}$  is slightly different from  $T_2^{\text{extra}}$  at low  $B_0$  the signal is equally weighted by both compartments (Figure 9.2(C)), whereas at higher  $B_0$  the signal is more weighted by the extravascular compartment since  $T_2^{\text{intra}}$  is significantly shorter than  $T_2^{\text{extra}}$  (Figure 9.2(C)). This *type B* vascular effect can be compressed by diffusion gradients in spin echo MRI (Boxerman *et al.*, 1995; Song *et al.*, 1996; Zhong *et al.*, 1998; Lee *et al.*, 1999) to reduce signals of slow and intermediate diffusion (Figure 9.2(D)).

Although the BOLD effect at  $B_0$  of 4 T and higher depicted by spin echo and gradient echo data is predominantly associated with the small vessel effects, the gradient echo data may partly be affected by vascular artifacts (for a recent review see Ogawa *et al.*, 1998). While high  $B_0$  fMRI with diffusion-weighted spin echo is the ideal image contrast for neuroimaging (Figure 9.2(D)), the concern of enormous sensitivity losses makes this method less preferred. Instead the use of both spin echo and gradient echo image contrasts have proven to be more useful (for a recent review see Hyder *et al.*, 2001). In both image contrasts there is a relaxation term ( $T_2^0$ ) that is unrelated to susceptibility based effects (i.e., dipole–dipole),

$$\frac{1}{T_2^{\text{GE}}} = \frac{1}{T_2'} + \frac{1}{T_2^0} + \frac{1}{T_2} + \frac{1}{T_2^{\Delta B_0}} \quad (9.4a)$$

$$\frac{1}{T_2^{\text{SE}}} = \frac{1}{T_2'} + \frac{1}{T_2^0} \quad (9.4b)$$

where  $T_2^{\Delta B_0}$  is the component attributed to local  $B_0$  inhomogeneity ( $\Delta B_0$ ), and  $T_2$  and  $T_2'$  are the reversible and nonreversible terms due to blood oxygenation effects. The BOLD calibration method shown here removes the unknown component  $T_2^0$  and in addition the  $T_2^{\Delta B_0}$  term (see Equation (9.5)). The result is a term that is purely dependent on blood oxygenation effects around small blood vessels and devoid of all other relaxation terms (Equations (9.5) and (9.6)). Although the comparative sensitivity of the BOLD effect detected by this calibration approach is lower because the fraction of measured change in  $T_2^{\text{SE}}$  or  $T_2^{\text{GE}}$  that is used for localizing activated regions is smaller (see Equation (9.4)), the combined use of both  $T_2^{\text{SE}}$  and  $T_2^{\text{GE}}$  maps provides a much better statistical basis for localization of weaker activated regions.

## 9.5. METHODS FOR CALIBRATING fMRI

The approach used to calibrate BOLD as described here requires quantitative relationships between physiological parameters (CBV, CBF, and CMRO<sub>2</sub>) and BOLD signal ( $S$ ) to be established, under physiological conditions. In contrast, previous studies have measured at best two of these parameters and assumed the other parameters under conditions of nonphysiologic perturbations (e.g., hypoxia or hypercapnia). Since the physiologic perturbations used in this type of BOLD calibration (Kida *et al.*, 2000; Hyder *et al.*, 2001) were within the autoregulatory range (all of which conserved similar CBF–CMRO<sub>2</sub> and CBF–CBV relationships expected from functional hyperemia), results from the rat brain can be used for guiding comparable BOLD calibration experiments in humans. While the idea of this type of BOLD calibration is quite simple (i.e., measure changes in all parameters in Equation (9.3) induced by physiologic perturbations which are well within the autoregulatory range so that constants  $M$  and  $N$  are used without complications), implementation is quite difficult because of methodological concerns. There are two main reasons why this type

of BOLD calibration approach has not been favored in other laboratories: first, to measure quantitative changes in  $S$ , CBF, CBV, and  $\text{CMR}_{\text{O}_2}$  both high resolution MRI and MRS methods are necessary; second, only physiologic perturbations that induce simultaneous changes in all parameters in Equation (9.3) can be used because conventionally used perturbations in MRI experiments (e.g., hypoxia, hypercapnia) are inadequate since the perturbations induce different effects in comparison to functional hyperemia (e.g., 'uncoupling' of  $\text{CMR}_{\text{O}_2}$  and CBF). An additional benefit of this type of BOLD calibration is that while  $\Delta\text{CMR}_{\text{O}_2}/\text{CMR}_{\text{O}_2}$  is extracted from Equation (9.3), the prediction can be validated by comparison with measured values.

All methods described below were applied in anesthetized rats (systemic physiologic parameters were monitored and controlled) on a 7 T horizontal bore system using a radio frequency probe for both  $^1\text{H}/^{13}\text{C}$  MRS and  $^1\text{H}$  MRI experiments with an arrangement of two orthogonally oriented  $^1\text{H}$  coils (surface receiver, volume transmitter) which permitted better local shimming and higher sensitivity (via homogeneous transmission and minimum loss in surface reception). There were a total of five steady state treatment groups (i.e.,  $\alpha$  to  $\varepsilon$ ) for the multimodal measurements. The rats in group  $\alpha$  were anesthetized with morphine ( $\sim 65 \text{ mg/kg/h}$ ), whereas in groups  $\beta$  and  $\gamma$  the rats received in addition pentobarbital ( $\sim 30 \text{ mg/kg/h}$ ) and nicotine ( $\sim 10 \text{ mg/kg/h}$ ) respectively to decrease and increase global activity from baseline. The rats in group  $\delta$  were anesthetized with  $\alpha$ -chloralose ( $\sim 60 \text{ mg/kg/h}$ ), whereas the rats in group  $\varepsilon$  (i.e.,  $\alpha$ -chloralose anesthesia) received in addition electrical forepaw stimulation (3 Hz) to increase activity from the baseline. The different methods (see below) were used to obtain the multimodal data on the same rat.

Spin echo and gradient echo MRI sequences were used to measure fractional changes in BOLD signal,  $\Delta S/S$ . Since the degree of  $T_2^{\text{SE}}$  and  $T_2^{\text{GE}}$  weighting in spin echo and gradient echo data can be varied by changing  $TE$ , multiple  $TE$  values (10 – 80 ms) were used to obtain absolute  $T_2^{\text{SE}}$  and  $T_2^{\text{GE}}$  maps, respectively. The multiple  $TE$  data were rapidly acquired with echo planar imaging (EPI) and single-exponential fits were used to calculate the  $T_2^{\text{SE}}$  and  $T_2^{\text{GE}}$  maps, where the latter contained the  $T_2^{\Delta B_0}$  relaxation component (see Equation (9.4)). The  $T_2^{\Delta B_0}$  component within the region of interest is measurable with an MRI spin tagging method (Mosher and Smith, 1991), and therefore removable within a range of accuracy. The resolution of this field inhomogeneity estimate is on the order of  $1.0 \text{ mm}^2$  (i.e., coarser than the  $0.2 \text{ mm}^2$  in-plane MRI resolution). Since the biophysical basis of  $T_2^{\text{SE}}$  and  $T_2^{\text{GE}}$  shows that there are overlapping terms (see Equation (9.4)), the difference of these two relaxation terms after removal of the  $T_2^{\Delta B_0}$  component

$$\frac{1}{T_2} = \frac{1}{T_2^{\text{GE}}} - \frac{1}{T_2^{\text{SE}}} \quad (9.5)$$

exposes the  $T_2$  which is the reversible term that is due to pure blood oxygenation effects. The assumption in Equation (9.5) is that  $T_2^{\text{SE}}$  and  $T_2^{\text{GE}}$  contain the same nonreversible relaxation component, which is also dependent on blood oxygenation, and by differencing of  $1/T_2^{\text{SE}}$  and  $1/T_2^{\text{GE}}$  the remaining term is devoid of relaxation terms related to nonsusceptibility based effects. Since  $1/T_2$  was originally described by Ogawa *et al.* (1993) to be related to venous deoxyhemoglobin as well as the blood volume in the voxel, the fractional change in BOLD signal in Equation (9.3) is also given by

$$\frac{\Delta S}{S} = \exp \left( -\Delta \left( \frac{1}{T_2} \right) \times TE \right) - 1 \quad (9.6)$$

where  $\Delta(1/T_2)$  is the change in  $T_2$  due to functional hyperemia.

Changes in CBV were measured by administration of a high susceptibility (iron oxide) MRI contrast agent which has a long half-life due to an extremely slow clearance rate (Bauer and Schulten, 1992; Jung and Jacobs, 1995). Since the presence of the exogenous contrast material within the microvasculature

enhances the blood volume induced changes in  $T_2^{\text{SE}}$  or  $T_2^{\text{GE}}$ , the same MRI methods (as described above) can be used for CBV measurements. The relative changes in CBV were calculated by (Kennan *et al.* (1998))

$$\frac{\Delta \text{CBV}}{\text{CBV}} = \frac{\Delta R^w - \Delta R^{w/o}}{R^w - R^{w/o}} \quad (9.7)$$

where  $R^w$  and  $R^{w/o}$  are  $1/T_2^{\text{SE}}$  (or  $1/T_2^{\text{GE}}$ ) at baseline conditions with and without agents respectively, and  $\Delta R^w$  and  $\Delta R^{w/o}$  are absolute differences in  $1/T_2^{\text{SE}}$  (or  $1/T_2^{\text{GE}}$ ) due to the perturbation with and without the contrast agents, respectively. Equation (9.7) is based on the assumption that changes in  $T_2^{\text{SE}}$  or  $T_2^{\text{GE}}$  are separable in terms of changes in blood volume and blood oxygenation, as long as blood hematocrit effects are not significant enough to warrant inclusion (Mandeville *et al.*, 1998). Since the long half-life of the high susceptibility or super-paramagnetic MRI contrast agents arises from preferential compartmentation in the microvasculature by uniform distribution within blood plasma, the derived changes in CBV therefore mainly reflect changes in plasma volume (van Bruggen *et al.*, 1998). However, under the assumption of constant hematocrit the changes in plasma and hemoglobin in the microvasculature would be equivalent (Kennan *et al.*, 1998).

Absolute CBF maps were imaged by using magnetically labeled arterial blood water which acts as an endogenous perfusion tracer, the kinetics of which can be determined by changes in the longitudinal relaxation time of tissue water ( $T_1$ ) obtained by inversion recovery methods (Detre *et al.*, 1992; Williams *et al.*, 1992; Zhang *et al.*, 1992). The primary assumption with this MRI method (Calamante *et al.*, 1999), much like its counterpart from  $\text{H}_2^{15}\text{O}$  PET (Raichle *et al.*, 1983), is that water is a freely diffusible tracer (Eichling *et al.*, 1974; Paulson *et al.*, 1977; Silva *et al.*, 1997). Thus when water in the blood is tagged and the tracer is then followed into the tissue, water perfusion through the tissue can be inferred. The conventionally measured  $T_1$  map used for anatomical imaging, which is basically insensitive to perfusion, is obtained by global inversion recovery (i.e., both blood and tissue water are inverted nonpreferentially). Similarly, an additional  $T_1$  map can be obtained with a more localized inversion (or saturation) of spins ( $T_1^{\text{app}}$ ) that makes the contrast more sensitive to perfusion because the blood water can be selectively inverted (or saturated). The degree of loss of the tracer from the blood, the fate of which is mainly the tissue, is related to perfusion and can be inferred from comparison of the ‘unlabeled’ and ‘labeled’  $T_1$  maps, respectively, with global and local inversions,

$$\frac{1}{T_1} + \frac{\text{CBF} \times \Gamma}{\lambda} = \frac{1}{T_1^{\text{app}}} \quad (9.8)$$

where  $\lambda$  is the assumed brain–blood partition coefficient of 0.95 ml/g and  $\Gamma$  is a correction factor that accounts for the difference between relaxation of tissue water and arterial blood water (as well as units of ml/g/min for CBF). Absolute CBF maps were obtained by using combination of slice selective and global inversion recovery weighted EPI sequence and single exponential recovery fits to the multi inversion recovery data (200–2200 ms). Because the approach used here relied on comparison of  $T_1$  maps (Schwarzbauer *et al.*, 1996), arterial transit time artifacts associated with differencing ‘unlabeled’ and ‘labeled’ maps of a particular inversion recovery time could be ignored. Since a large homogenous radio frequency transmission coil (covering the rat’s torso) was used for inversions, there was negligible contamination of ‘untagged’ blood volume in the  $T_1$  maps (Hyder *et al.*, 2000a). Other artifacts were minimized with optimal choice of inversion and excitation slice thickness ratio, adiabatic inversion pulses, short inversion pulse durations, and image acquisition under fully relaxed conditions (Hyder *et al.*, 2000b).

Absolute values of CMRO<sub>2</sub> were obtained by using indirect <sup>13</sup>C MRS (i.e., detection of <sup>13</sup>C with sensitivity of <sup>1</sup>H with the proton observe carbon edit (POCE) method (Rothman *et al.*, 1985; Fitzpatrick *et al.*, 1990; Hyder *et al.*, 1996; Pfeuffer *et al.*, 1999; Henry *et al.*, 2000; Chen *et al.*, 2001; de Graaf *et al.*, 2003))

in conjunction with substrates labeled with the  $^{13}\text{C}$  isotope which have been used *in vivo* to study metabolic fluxes by detecting turnover of the  $^{13}\text{C}$  isotope into other pools (for recent reviews see Rothman *et al.*, 1999, 2002, 2003). The reader is directed towards Chapters 3 and 4 regarding the details of  $^{13}\text{C}$  MRS methods and modeling of the  $^{13}\text{C}$  turnover data. Thus  $^{13}\text{C}$  MRS provides a unique window on metabolism of  $^{13}\text{C}$ -labeled glucose which is the major energy substrate, under normal conditions (see Chapters 2 and 5). In contrast to the radioactive  $^{14}\text{C}$  isotope detected with 2-deoxyglucose autoradiography (used to measure  $\text{CMR}_{\text{glc}}$ ), the nonradioactive  $^{13}\text{C}$  isotope in conjunction with  $^{13}\text{C}$  MRS measures one or more metabolites at different carbon positions in real time. In each case, the spatial localization of each POCE study (8–48  $\mu\text{l}$ ) (Hyder *et al.*, 1996, 1997, 1999, 2000b) was guided by previously acquired CBF maps. Glutamate and  $\gamma$ -amino butyric acid (GABA) are the major excitatory and inhibitory neurotransmitters, respectively, and play dominant roles in mediating brain activity. In these POCE studies the  $^{13}\text{C}$  labeling of C4-glutamate was measured during infusion of  $[1-^{13}\text{C}]$  or  $[1,6-^{13}\text{C}]$  glucose to calculate tricarboxylic acid cycle flux ( $V_{\text{TCA}}$ ) which is stoichiometrically linked to  $\text{CMR}_{\text{O}_2}$ ,

$$\text{CMR}_{\text{O}_2} = 3V_{\text{TCA}} + \frac{3}{4}V_{\text{dil}} \quad (9.9)$$

where  $V_{\text{dil}}$  accounts for measurable  $^{12}\text{C}$  inflows from other substrates (e.g., ketone bodies) which can dilute the  $^{13}\text{C}$  fractional enrichment of the acetyl CoA pool. Thus the POCE method provides an estimate of the energetic costs associated with glutamatergic neurotransmission (see Chapter 5), with small but measurable corrections of the GABAergic system and glial oxidation (see Chapter 6). Several modeling parameters have secondary effects upon the calculated fluxes, and the magnitudes of these effects have been evaluated by sensitivity analyses and *in vivo* experiments (see Chapter 4). Since these studies reveal that these parameters have relatively small effects on  $V_{\text{TCA}} (\pm 5\%)$  for the range covered in anesthetized rat studies, the derived fluxes with  $[1-^{13}\text{C}]$  or  $[1,6-^{13}\text{C}]$  glucose provide valuable information on neuroenergetics.

## 9.6. PHYSIOLOGICAL BASIS OF fMRI

An example of the multimodal methods described above applied to rat brain imaging *in vivo* is shown in Figure 9.3 for a particular baseline condition. This type of multimodal data spanning a range of activity levels provided insight into the CBF– $\text{CMR}_{\text{O}_2}$  and CBF–CBV relationships that form the physiological basis of BOLD. For a region of interest in the somatosensory cortex, Figure 9.4(A) shows that for a specific magnitude of change in CBF from baseline, the change in  $\text{CMR}_{\text{O}_2}$  far exceeds the CBV change. This indicates that the BOLD signal is influenced strongly by the main energy consuming processes and the depiction of BOLD signal simply as mechanical events (of dilating microvessels) ignores a significant physiologic makeup of the image contrast. The constants  $M$  and  $N$  in Equation (9.3) can be estimated using the measured CBF– $\text{CMR}_{\text{O}_2}$  and CBF–CBV relationships along with commensurate changes in the BOLD signal (Figure 9.4(B)). The constants are apt for a baseline predefined by the range of activities covered and corresponding distribution of  $T_2$  values (see Figure 9.5).

Since only physiological perturbations were used for the BOLD calibration, the near-linear relationship between MRI-measured CBF and POCE-measured  $\text{CMR}_{\text{O}_2}$  over the entire range of activity covered was expected (Figure 9.5(A)). However, the range of the  $1/T_2$  values (see Equation (9.5)) was grouped over a specific range of  $\text{CMR}_{\text{O}_2}$  and CBF values, as shown in the inset to Figure 9.5(A). Thus the corresponding distributions of CBF and/or  $\text{CMR}_{\text{O}_2}$  values were used to determine the predefined baseline condition (boxed region in Figure 9.5(A)) for which the derived constants  $M$  and  $N$  were valid. Support for this type of BOLD calibration comes from comparison of NMR-measured absolute values of CBF and  $\text{CMR}_{\text{O}_2}$  values (in this laboratory) and measurements under similar conditions in rat brain by other methods (including

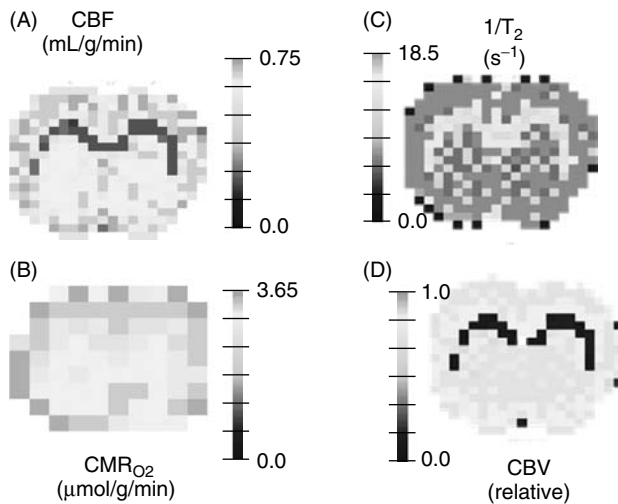


**Figure 9.3.** Multimodal MRI and MRS measurements in rat brain. The figure shows maps of (A) absolute CBF, (B) absolute  $\text{CMR}_{\text{O}_2}$ , (C) absolute  $1/T_2$ , and (D) relative CBV maps from rat brain (Hyder *et al.*, 2001). Each measurement was made under steady state metabolism and perfusion in the same rat, under morphine anesthesia (group  $\alpha$ , in Figure 9.4). The scale bars in (A) to (C) represent absolute units of CBF (ml/g/min),  $\text{CMR}_{\text{O}_2}$  ( $\mu\text{mol/g/min}$ ), and  $1/T_2$  ( $\text{s}^{-1}$ ), respectively, whereas the scale bar in (D) represents a relative scale of CBV. The spatial resolutions in (A), (C), and (D) were  $320\text{ }\mu\text{m} \times 320\text{ }\mu\text{m} \times 1000\text{ }\mu\text{m}$ , whereas in (B) the spatial resolution was  $1250\text{ }\mu\text{m} \times 1250\text{ }\mu\text{m} \times 5000\text{ }\mu\text{m}$ . Therefore the spatial resolutions in the MRI and MRS data are in the nl and  $\mu\text{l}$  ranges, respectively.

the  $^{17}\text{O}$  MRS method discussed in Chapter 8). As shown in Figure 9.5(B), the agreement from different methods for CBF and  $\text{CMR}_{\text{O}_2}$  measured in the rat brain is excellent (Table 9.1).

Using the experimentally derived CBF– $\text{CMR}_{\text{O}_2}$  and CBF–CBV relationships along with changes in the BOLD signal (Figure 9.4), the constants  $M$  and  $N$  were used with Equation (9.3) along with measured values of  $\Delta\text{CBF}/\text{CBF}$ ,  $\Delta\text{CBV}/\text{CBV}$ , and  $\Delta S/S$  to predict the changes in  $\text{CMR}_{\text{O}_2}$ , as shown in Figure 9.6(A). Because most of the data points comparing the predicted (from calibrated BOLD) and measured (from localized POCE) values of  $\Delta\text{CMR}_{\text{O}_2}/\text{CMR}_{\text{O}_2}$  fall close to the line of identity over a wide activity range, the BOLD calibration was accurate within 15 % (Kida *et al.*, 2000; Hyder *et al.*, 2001). The validation of the calibration thus allowed the prediction of  $\Delta\text{CMR}_{\text{O}_2}/\text{CMR}_{\text{O}_2}$  for functional activation studies in rat brain at 7 T, as shown in Figure 9.6(B), where changes in  $S$ , CBF, and CBV were measured in the same rat. Although the localized changes in the different parameters were quite well correlated in the example shown (Figure 9.6(B)), it is important to note that a voxel of high intensity in the BOLD map did not always correspond to a high intensity voxel in the  $\text{CMR}_{\text{O}_2}$  map (data not shown). These subtle variations arise from the activity variations of different parameters throughout the regions of interest, which when included with the calibration provides a constrained and scaled representation of  $\text{CMR}_{\text{O}_2}$  changes.

A likely source of uncertainty in comparing the MRI-predicted  $\text{CMR}_{\text{O}_2}$  data with the POCE-measured  $\text{CMR}_{\text{O}_2}$  data (Figure 9.6(A)) is that the heterogeneity in metabolism within the larger MRS voxel (in the range of  $\mu\text{l}$ ) in comparison to the multimodal MRI data (of  $\Delta\text{CBF}/\text{CBF}$ ,  $\Delta\text{CBV}/\text{CBV}$ ,  $\Delta S/S$ ), which have substantially higher spatial resolution (in the range of nl). Furthermore the degree of heterogeneity is greater under conditions of stimulation-induced activity (i.e., from group  $\delta$  to  $\varepsilon$ ) than pharmacologically induced activity (i.e., from group  $\alpha$  to  $\gamma$ ) in a particular region, based on  $\text{CMR}_{\text{glc}}$  data from  $2\text{-}^{14}\text{C}$ -deoxyglucose autoradiography studies in anesthetized rats (Ueki *et al.*, 1988). These transitions are graphically shown in

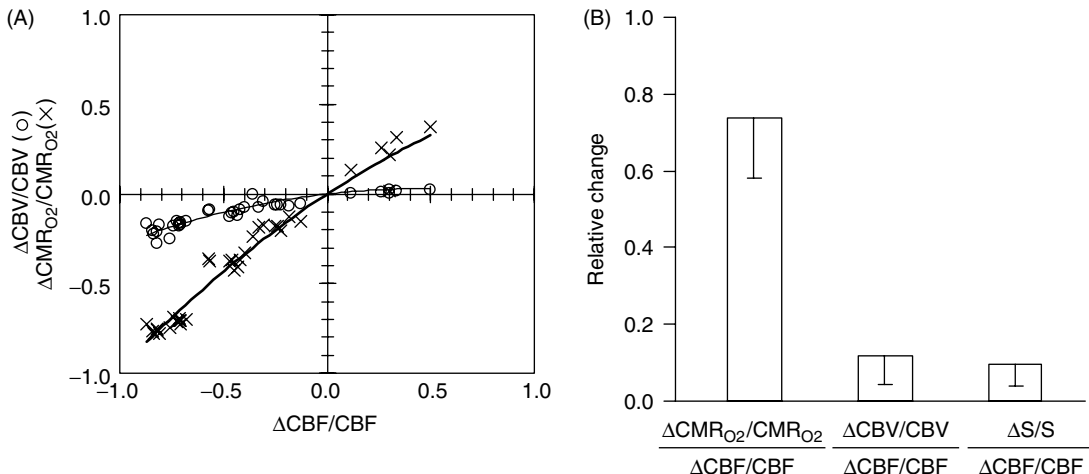


**Figure 9.4.** Summary of quantitative MRI and MRS measurements of relative changes in CBF, CMR<sub>O<sub>2</sub></sub>, CBV, and S over a wide range of neuronal activity. (A) Comparisons of  $\Delta \text{CBV}/\text{CBV}$  ( $\circ$ ) and  $\Delta \text{CMR}_{\text{O}_2}/\text{CMR}_{\text{O}_2}$  ( $\times$ ) versus  $\Delta \text{CBF}/\text{CBF}$  for the different conditions (groups  $\alpha - \varepsilon$ ). The groups  $\beta$  and  $\varepsilon$  are located at the extreme left and right corners, respectively. The group  $\delta$  is immediately next to group  $\beta$ . The group  $\gamma$  is located left of the origin, whereas the group  $\alpha$  is located left of group  $\gamma$ . The ratios of  $(\Delta \text{CMR}_{\text{O}_2}/\text{CMR}_{\text{O}_2})/(\Delta \text{CBF}/\text{CBF})$  and  $(\Delta \text{CBV}/\text{CBV})/(\Delta \text{CBF}/\text{CBF})$  are significantly different, where the slopes through the origin are  $\sim 0.7$  and  $\sim 0.1$ , respectively (Kida *et al.*, 2000; Hyder *et al.*, 2001). The origin represents the resting awake state for rat cerebral cortex (Nilsson and Siesjo, 1975). (B) The changes in CMR<sub>O<sub>2</sub></sub>, CBV, and S were normalized by changes in CBF. This normalization procedure provides a comparison of relative changes in each parameter during changes in neuronal activity. These findings show that CBF and CMR<sub>O<sub>2</sub></sub> play a more dominant role in modulation of BOLD signal at 7 T in glutamatergic neurons of rat brain. The error bars represent the standard deviation from the mean.

Figures 9.4(A) and 9.5(A). Since the CMR<sub>O<sub>2</sub></sub> measured (by localized POCE) in the larger MRS voxel is equivalent to the averaged CMR<sub>O<sub>2</sub></sub> predicted (by calibrated BOLD) from all the MRI voxels in a particular region, the voxels at the MRI spatial resolution with either very high or very low CMR<sub>O<sub>2</sub></sub> values (which cannot reliably be characterized by the current BOLD calibration) would have the greatest level of uncertainty. An important aspect of this type of BOLD calibration, however, is that both increase and decrease of activities were examined for the changes in the BOLD signal (e.g., transition from group  $\alpha$  to  $\beta$  was a decrement, whereas transition from group  $\alpha$  to  $\gamma$  was an increment, as shown in Figures 9.4(A) and 9.5(A)). Therefore, the constants  $M$  and  $N$  can be used confidently, within the experimental errors of the methods used as well as the accuracy of the BOLD calibration, to determine both decrements and increments of CMR<sub>O<sub>2</sub></sub> throughout the somatosensory cortex provided that the perturbations are physiological in nature.

Since changes in both CMR<sub>O<sub>2</sub></sub> and CBV (in relation to CBF) can affect the BOLD signal, it is important to compare the magnitudes of change in each parameter with previous measurements. However, it is known that the magnitude of  $\Delta \text{CMR}_{\text{O}_2}/\text{CMR}_{\text{O}_2}$  (or  $\Delta \text{CMR}_{\text{glc}}/\text{CMR}_{\text{glc}}$ , or  $\Delta \text{CBF}/\text{CBF}$ , or  $\Delta \text{CBV}/\text{CBV}$ ) is dependent on resting baseline values which in turn are contingent on the depth of anesthesia (for recent reviews see Shulman *et al.*, 1999, 2001b, 2002, 2003). Instead, comparing the magnitudes of  $(\Delta \text{CMR}_{\text{O}_2}/\text{CMR}_{\text{O}_2})/(\Delta \text{CBF}/\text{CBF})$ ,  $(\Delta \text{CMR}_{\text{glc}}/\text{CMR}_{\text{glc}})/(\Delta \text{CBF}/\text{CBF})$ , and  $(\Delta \text{CBV}/\text{CBV})/(\Delta \text{CBF}/\text{CBF})$  can help negate the variable effects of anesthesia for functional activation studies in animals. The values of  $\Delta \text{CMR}_{\text{O}_2}/\text{CMR}_{\text{O}_2}$  predicted by BOLD (in Figure 9.6(B)) cannot be directly compared with previous measurements of  $\Delta \text{CMR}_{\text{O}_2}/\text{CMR}_{\text{O}_2}$  (POCE) and  $\Delta \text{CMR}_{\text{glc}}/\text{CMR}_{\text{glc}}$  (<sup>2-14</sup>C-deoxyglucose) because the anesthetic dosages were different in the BOLD study. However, ratios of  $(\Delta \text{CMR}_{\text{O}_2}/\text{CMR}_{\text{O}_2})/(\Delta \text{CBF}/\text{CBF})$  and

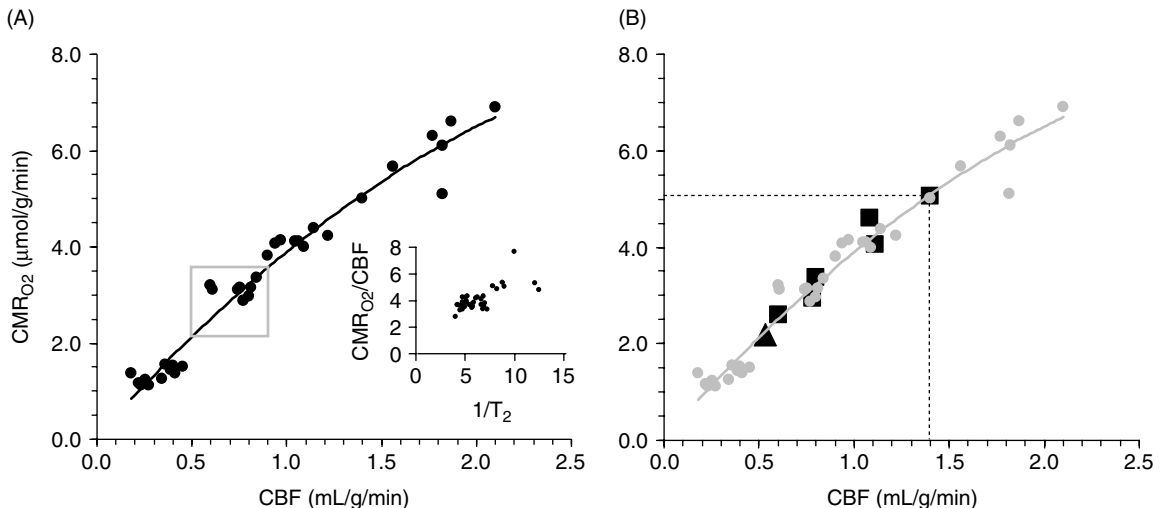


**Figure 9.5.** Absolute values of  $\text{CMR}_{\text{O}_2}$  and CBF in the rat somatosensory cortex. (A) Measurements of  $\text{CMR}_{\text{O}_2}$  and CBF in the same rat by  $^{13}\text{C}$  MRS and MRI methods for the five levels of activities (groups  $\alpha - \varepsilon$ ) measured in this laboratory (Hyder *et al.*, 2000b). The inset shows the distribution of  $1/T_2$  values for the same conditions as a function of the ratio of  $\text{CMR}_{\text{O}_2}/\text{CBF}$  values (Hyder *et al.*, 2001). Since the  $1/T_2$  values were clustered around a range of  $\text{CMR}_{\text{O}_2}/\text{CBF}$  values (shown by the gray square), the calibration of the BOLD effect is biased towards this predefined baseline condition. (B) Measurements of  $\text{CMR}_{\text{O}_2}$  and CBF in the rat from other laboratories (black symbols) are compared with measurements from this laboratory (gray circles). The dotted lines represent the nonanesthetized awake condition in rat brain (Nilsson and Siesjo, 1975). The details of the square symbols are shown in Table 9.1 whereas the triangle symbol represent measurements from Zhu *et al.* (2002) using  $^{17}\text{O}$  MRS.

**Table 9.1.** CBF and  $\text{CMR}_{\text{O}_2}$  of rat brain measured in other laboratories

Reference	Condition	CBF (mL/g/min)	$\text{CMR}_{\text{O}_2}$ ( $\mu\text{mol/g/min}$ )
Nilsson and Siesjo (1975)	Conscious (awake)	1.4	5.0
Nilsson and Siesjo (1975)	Phenobarbital (50 mg/kg)	1.1	4.1
Hagerdal <i>et al.</i> (1975)	70 % $\text{N}_2\text{O}$	1.1	4.6
Nilsson and Siesjo (1976)	70 % $\text{N}_2\text{O}^+$ 1.2 % halothane	0.8	3.4
Nilsson and Siesjo (1975)	Phenobarbital (150 mg/kg)	0.8	3.0
Nilsson and Siesjo (1975)	Phenobarbital (250 mg/kg)	0.6	2.6
Zhu <i>et al.</i> (2002)	$\alpha$ -Chloralose (45 mg/kg/h)	0.5	2.2

$(\Delta\text{CMR}_{\text{glc}}/\text{CMR}_{\text{glc}})/(\Delta\text{CBF}/\text{CBF})$  from all of these studies (Ueki *et al.*, 1988; Grunwald *et al.*, 1987, 1991; Otsuka *et al.*, 1991a,b) are reasonably comparable ( $\sim 0.7$ ), which supports the belief that oxidative glycolysis provides most of the energy during functional activation. Likewise, the ratio of  $(\Delta\text{CBV}/\text{CBV})/(\Delta\text{CBF}/\text{CBF})$  measured with superparamagnetic contrast agents is also in good agreement ( $\sim 0.1$ ) with prior results for the same rat model (van Bruggen *et al.*, 1998; Silva *et al.*, 1999). However, the  $(\Delta\text{CBV}/\text{CBV})/(\Delta\text{CBF}/\text{CBF})$  ratio may not be the same for other nonphysiologic perturbations.

Another approach that has been used for BOLD calibration studies incorporates a  $\text{CO}_2$  challenge in conjunction with the ‘normal’ experiment (i.e., a functional challenge). The first assumption in this type of BOLD calibration is that the CBF–CBV relationship is the same in both perturbations. The second

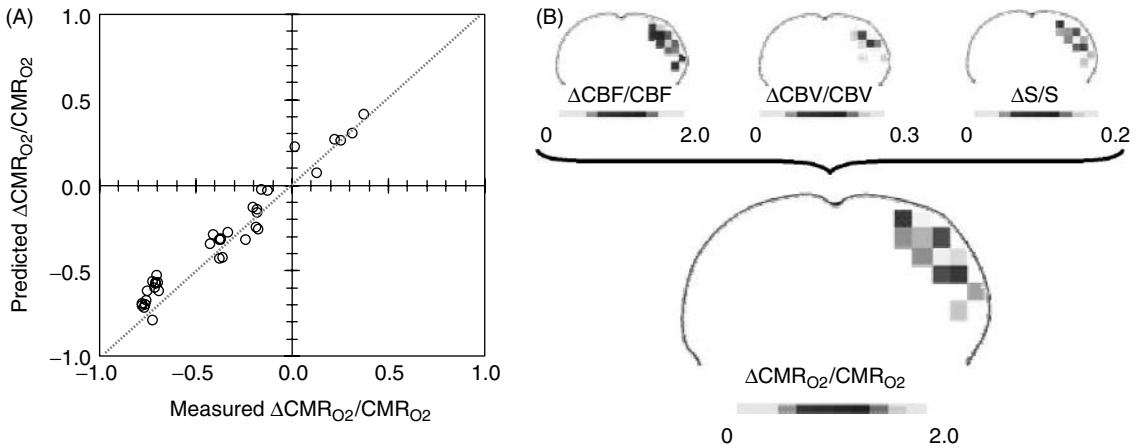


**Figure 9.6.** Validation of calibrated fMRI. (A) Comparison of predicted (by calibrated fMRI) and measured (by  $^{13}\text{C}$  MRS) values of  $\Delta\text{CMR}_{\text{O}_2}/\text{CMR}_{\text{O}_2}$  provide validation of the BOLD calibration at 7T (Kida *et al.*, 2000; Hyder *et al.*, 2001). The dotted line represents the line of identity. These results indicate that at high  $B_0$  the microscopic susceptibility effects of deoxygenated hemoglobin dominates the relaxation effects in tissue, which can be accentuated by combining the gradient echo and spin echo data (Equation (9.5)). Since the validation of BOLD calibration relies on standard errors of independent measures (for relaxation rate, blood flow, and volume), by comparing calculated and measured values of  $\Delta\text{CMR}_{\text{O}_2}/\text{CMR}_{\text{O}_2}$  it can be calculated that the validation accuracy for high resolution  $\text{CMR}_{\text{O}_2}$  mapping by multimodal MRI at 7T in rat cortex is at least 80 %. (B) Multimodal maps of localized changes in CBF, CBV, and S (Equation (9.3)) obtained during forepaw stimulation in an  $\alpha$ -chloralose-anesthetized rat which were used to calculate a relative  $\text{CMR}_{\text{O}_2}$  map. The changes in CBF, CBV, and S were  $1.17 \pm 0.41$ ,  $0.07 \pm 0.04$ , and  $0.06 \pm 0.02$ , respectively, and the localized change in  $\text{CMR}_{\text{O}_2}$  was  $0.93 \pm 0.33$ . The regional correlation observed between changes in  $\text{CMR}_{\text{O}_2}$  and CBF is very similar to regional correlation between changes in  $\text{CMR}_{\text{glc}}$  and CBF for the same rat model (Ueki *et al.*, 1988).

assumption is that changes in  $\text{CMR}_{\text{O}_2}$  (i.e., neuronal activity) during a  $\text{CO}_2$  challenge are negligible, although with prolonged exposure to high  $\text{CO}_2$  levels various pools in the tricarboxylic acid cycle become depleted (Siesjo, 1978). In most of these prior studies (van Zijl *et al.*, 1998; Davis *et al.*, 1998; Hoge *et al.*, 1999; Kim *et al.*, 1999) the changes in CBV were not measured at all and assumed a dependence on changes in CBF,

$$\frac{\Delta\text{CBV}}{\text{CBV}} = \left(1 + \frac{\Delta\text{CBF}}{\text{CBF}}\right)^\phi - 1 \quad (9.10)$$

where  $\phi$  was determined to be  $\sim 0.4$  from a PET study of hypercapnic challenge in primates (Grubb *et al.*, 1974). In contrast, the CBF–CBV relationship derived from the MRI studies (Figure 9.4(A)) shows that the value of  $\phi$  is actually closer to  $\sim 0.1$  in the rat brain. The implication of using this different value for  $\phi$  is that when this parameter is overestimated, as in some recent human fMRI studies (see below) because CBV changes cannot be measured directly due to lack of an approved MRI contrast agent, the changes in  $\text{CMR}_{\text{O}_2}$  would be underestimated (Equation (9.3)). While this discrepancy of the CBF–CBV relationship (i.e., differing values of  $\phi$ ) can be qualitatively explained by the facts that distribution spaces and half-lives of PET (Ito *et al.*, 2001, 2003) and MRI tracers (Kida *et al.*, 1999, 2000) are different, a greater concern is that a BOLD calibration experiment for a hypercapnia or a hypoxia challenge is only valid for similar perturbations because both the blood pH and hematocrit are significantly altered (Siesjo, 1978) in comparison to normal physiological conditions.

## 9.7. NEURAL BASIS OF fMRI

Recently there has been a lot of interest in exploring the neural basis of fMRI by combining electrophysiological methods (Yang *et al.*, 1997; Brinker *et al.*, 1999; Ogawa *et al.*, 2000; Rees *et al.*, 2000; Logothetis *et al.*, 2001). The correlations that have been observed between BOLD and electrical signals from neurons are based on aspects of establishing spatial overlap and matching temporal dynamics. Despite large disparities in the temporal dynamics as well as spatial responses of each signal type, these correlations are delicate at best because an experimentalist still cannot quantitatively infer from the fMRI data the degree by which the neural activity has changed in an activated focus. An unconquerable limitation of fMRI will always be that even a voxel of ultrahigh spatial resolution (e.g., 0.001  $\mu\text{l}$  voxel in the rat olfactory bulb in Figure 9.1(A)) will contain at least several thousand neurons. Thus at best a BOLD signal when calibrated may be used to reflect the energetics of an ensemble of neurons (for a recent review see Hyder *et al.*, 2002).

Since energy is defined as the capability of doing work, how efficiently do brain cells utilize energy for function? Extracellular recordings were used to measure the spiking frequency of an ensemble of neurons ( $v$ ) contained in a fraction of an fMRI voxel (Smith *et al.*, 2002). Since  $v$  is a reliable and quantifiable measure of brain work, changes in this parameter with different workloads would reflect the changing degrees of work done by the ensemble. The results show that fractional changes in energy ( $\Delta\text{CMR}_{\text{O}_2}/\text{CMR}_{\text{O}_2}$ ) were approximately equal to fractional changes in spiking rate ( $\Delta v/v$ ) during stimulations from different baseline conditions (Figure 9.7(A)), which show that particular changes in neural energy expended approximately equal percentage changes in work done in a localized region. Thus calibrated fMRI used to obtain  $\text{CMR}_{\text{O}_2}$  can provide a view of the ensemble work in a voxel. The details of the experimental approach and their implications are discussed in Chapter 10.

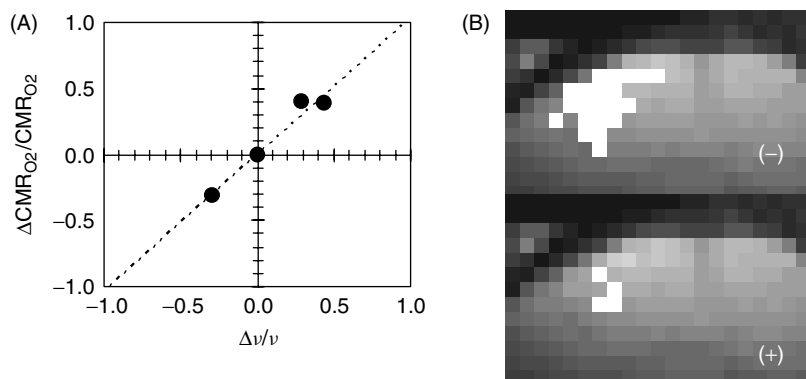


**Figure 9.7.** Neural basis of fMRI. (A) In the  $\alpha$ -chloralose-anesthetized rat, forepaw stimulation-induced changes in neuroenergetics ( $\Delta\text{CMR}_{\text{O}_2}/\text{CMR}_{\text{O}_2}$ ; by calibrated fMRI) and spiking rate of a neural ensemble ( $\Delta v/v$ ; by extracellular recordings) were measured from the somatosensory cortex (Smith *et al.*, 2002). Since  $\Delta\text{CMR}_{\text{O}_2}/\text{CMR}_{\text{O}_2} \approx \Delta v/v$  over a wide range of activity in rat brain, the changes in neural energy is commensurate with changes in neural work done in a local region (Hyder *et al.*, 2002). Thus  $\Delta\text{CMR}_{\text{O}_2}/\text{CMR}_{\text{O}_2}$  obtained from calibrated fMRI may provide insight into grouped activity a neuronal ensemble in a voxel. (B) Lamotrigine, which attenuates activity of pre-synaptic voltage-dependent  $\text{Na}^+$  channels and glutamate release (Leach *et al.*, 1986), was used to illustrate the involvement of voltage-dependent  $\text{Na}^+$  channels and glutamate release on BOLD signal. The figure shows the localized BOLD responses during forepaw stimulation in an  $\alpha$ -chloralose-anesthetized rat with (+) and without (-) lamotrigine (Kida *et al.*, 2001), at the same statistical threshold. Since only the stimulus-evoked BOLD (and CBF) responses were depressed with lamotrigine treatment, the voltage-dependent  $\text{Na}^+$  channels may play a significant role in evoked neurovascular responses, whereas under anesthesia the baseline would depend on action of voltage-independent  $\text{Na}^+$  channels.

To date much of fMRI research pertains to measurements of activity-dependent changes in physiological parameters mentioned above. It is also important to characterize the molecular mechanisms linking the BOLD signal to neurophysiological events. Under physiological conditions  $\text{Ca}^{2+}$ -dependent vesicular release of neurotransmitters (e.g., an excitatory amino acid such as glutamate) occurs in response to depolarization which results from influx of  $\text{Na}^+$  ions through pre-synaptic voltage-dependent  $\text{Na}^+$  channels. Neuronal excitability and neurotransmitter release can both be suppressed by inhibitors of these channels (e.g., lamotrigine) as well as the  $\text{Na}^+$  current that these channels mediate (Figure 9.1(B)). Is activation of voltage-dependent  $\text{Na}^+$  channels a necessary step in the neurochemical pathway leading to the BOLD signal change as well as the local CBF response during functional activation? The stimulus-evoked BOLD and CBF responses (i.e., energetics) were significantly depressed following lamotrigine treatment (Kida *et al.*, 2001).

Lamotrigine – a drug that is commonly used in treatment of epilepsy – specifically attenuates the activity of the pre-synaptically located voltage-dependent  $\text{Na}^+$  channels (Leach *et al.*, 1986). However, there is a significant fraction of  $\text{Na}^+$  channels that are voltage independent (Kandel *et al.*, 1991). In fMRI studies of animal the baseline is largely maintained by anesthesia which presumably affects all  $\text{Na}^+$  channels. Lamotrigine mainly suppresses the evoked neurovascular response, while basal activity remained unchanged (Figure 9.7(B)). This implies that the voltage-dependent  $\text{Na}^+$  channels play a major role in the evoked neurovascular response, whereas under anesthesia the baseline depends on the action of voltage-independent  $\text{Na}^+$  channels. The measured proportionality between CBF and  $\text{CMR}_{\text{O}_2}$  in anesthetized rats (Figure 9.5) supports the view that anesthetics affect the voltage-independent  $\text{Na}^+$  channels (Lees, 1972), although exact mechanisms of anesthetic action are unknown (Richard, 1998).

## 9.8. IMPLICATIONS FOR HUMAN fMRI

The results from anesthetized rats have consequences for awake human fMRI studies. Although BOLD calibration experiments of this type have not been performed in awake humans yet, some well-informed

**Table 9.2.** Changes in  $\text{CMR}_{\text{O}_2}$ ,  $\text{CMR}_{\text{glc}}$ , and CBF of awake human brain measured by PET in different laboratories for a range of sensory stimulations. Numbers in *italics* represent averaged values. See Figure 9.8 and Rothman *et al.* (2002) for implications

$\frac{\Delta \text{CBF}}{\text{CBF}}$	$\frac{\Delta \text{CMR}_{\text{O}_2}}{\text{CMR}_{\text{O}_2}}$	$\frac{\Delta \text{CMR}_{\text{glc}}}{\text{CMR}_{\text{glc}}}$	Reference
0.30	0.40	0.21	Raichle <i>et al.</i> (1976)
0.28	0.09	0.17	Fox and Raichle (1986)
0.31	0.13	0.18	Seitz and Roland (1992)
0.18	<i>–0.03</i>	0.08	Fujita <i>et al.</i> (1999)
0.18	<i>–0.01</i>	0.08	Fujita <i>et al.</i> (1999)
0.18	<i>0.13</i>	0.08	Kuwabara <i>et al.</i> (1992)
0.27	<i>0.13</i>	0.17	Ginsberg <i>et al.</i> (1988)
0.43	<i>0.13</i>	0.27	Ribeiro <i>et al.</i> (1996)
0.49	0.05	0.51	Fox <i>et al.</i> (1988)
0.25	0.28	0.28	Marrett and Gjedde (1997)
0.26	0.29	0.29	Marrett and Gjedde (1997)
0.32	0.10	0.21	Vafaee and Gjedde (2000)
0.38	0.16	0.21	Vafaee and Gjedde (2000)
0.42	0.06	0.21	Vafaee and Gjedde (2000)
0.13	0.12	0.21	Roland <i>et al.</i> (1987)
0.88	0.47	0.21	Katayama <i>et al.</i> (1986)

estimates can be made from a meta-analysis of PET results in humans (Table 9.2) that report changes in  $\text{CMR}_{\text{O}_2}$ ,  $\text{CMR}_{\text{glc}}$ , and CBF for a wide range of conditions (Figure 9.8(A)). First, there is a minor difference between fractional changes in rates of glucose and oxygen use (i.e.,  $\Delta\text{CMR}_{\text{glc}}/\text{CMR}_{\text{glc}}$  and  $\Delta\text{CMR}_{\text{O}_2}/\text{CMR}_{\text{O}_2}$  in Figure 9.8(A)) which suggests that glucose oxidation is still the major source of energy during functional activation in the awake nonanesthetized human brain (Shulman *et al.*, 2001a,b) – similar to the anesthetized rat brain (see above). Second, there is a *positive* difference between fractional changes in rates of blood flow and oxygen use (i.e.,  $\Delta\text{CBF}/\text{CBF}$  and  $\Delta\text{CMR}_{\text{O}_2}/\text{CMR}_{\text{O}_2}$  in Figure 9.8(A)) which supports a positive BOLD signal (Equation (9.3)) according to the model of functional hyperemia (Equation (9.2)), even with a significant change in oxidative metabolism.

The correlation between  $\Delta\text{CBF}/\text{CBF}$  and  $\Delta\text{CMR}_{\text{O}_2}/\text{CMR}_{\text{O}_2}$ , which is at the core of the physiological basis of BOLD, for the awake human brain has been a topic of controversy for over a decade because some PET studies (Fox and Raichle, 1986; Fox *et al.*, 1988) had shown that  $\Delta\text{CMR}_{\text{O}_2}/\text{CMR}_{\text{O}_2}$  was negligible in comparison to  $\Delta\text{CBF}/\text{CBF}$  or  $\Delta\text{CMR}_{\text{glc}}/\text{CMR}_{\text{glc}}$  during functional activation. The proposal from Raichle and coworkers was that during functional activation the brain's energy producing pathway switched from an efficient oxidative mode to a less efficient nonoxidative mode. While the small difference between values of  $\Delta\text{CMR}_{\text{glc}}/\text{CMR}_{\text{glc}}$  and  $\Delta\text{CMR}_{\text{O}_2}/\text{CMR}_{\text{O}_2}$  gathered from other laboratories (Figure 9.8(A)) qualitatively supports that  $\Delta\text{CMR}_{\text{glc}}/\text{CMR}_{\text{glc}} > \Delta\text{CMR}_{\text{O}_2}/\text{CMR}_{\text{O}_2}$ , glucose oxidation still provides more than 90 % of the ATP during functional activation at steady state (Shulman *et al.*, 2001a,b; for details see Rothman *et al.*, 2002). Therefore it is not surprising that the  $(\Delta\text{CMR}_{\text{O}_2}/\text{CMR}_{\text{O}_2})/(\Delta\text{CBF}/\text{CBF})$  ratio ( $\sim 0.6$ ) derived

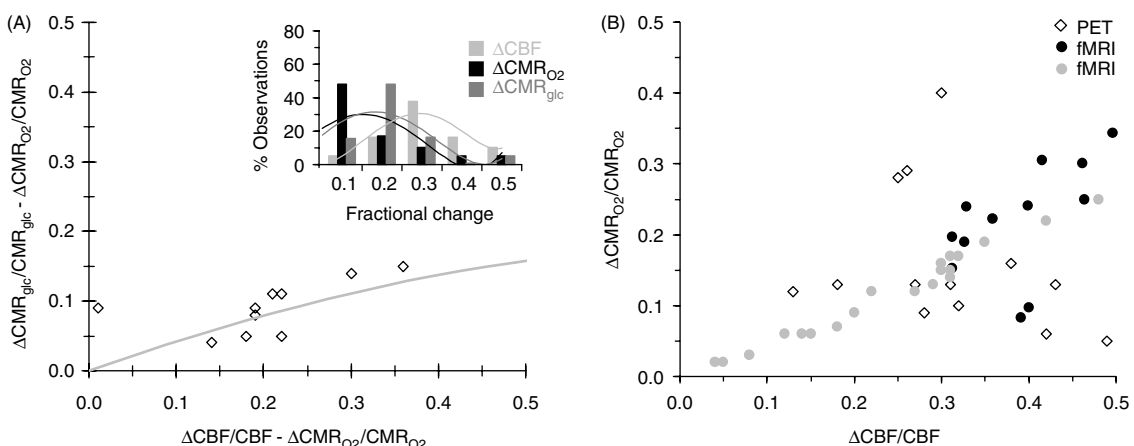


**Figure 9.8.** Stimulation-induced changes in  $\text{CMR}_{\text{O}_2}$ ,  $\text{CMR}_{\text{glc}}$ , and CBF in the awake human brain. (A) The difference between changes in  $\text{CMR}_{\text{glc}}$  and  $\text{CMR}_{\text{O}_2}$  (i.e.,  $\Delta\text{CMR}_{\text{glc}}/\text{CMR}_{\text{glc}} - \Delta\text{CMR}_{\text{O}_2}/\text{CMR}_{\text{O}_2}$  on the vertical axis) reflects the degree of glucose oxidation – the lower this value is, the greater the degree of glucose oxidation (see Equation (9.1)). The difference between fractional changes in CBF and  $\text{CMR}_{\text{O}_2}$  (i.e.,  $\Delta\text{CBF}/\text{CBF} - \Delta\text{CMR}_{\text{O}_2}/\text{CMR}_{\text{O}_2}$  on the horizontal axis) reflects the degree of blood oxygenation – the higher this values is, the greater the BOLD effect (see Equation (9.3)). The pseudo-linear relationship suggests that the BOLD signal changes are commensurate with nearly complete oxidation of glucose during functional activation. Therefore the lack of negligible increase in  $\text{CMR}_{\text{O}_2}$  during functional activation (Fox and Raichle, 1986; Fox *et al.*, 1988) is not in agreement with trends observed in literature. The inset shows the distribution of  $\Delta\text{CMR}_{\text{O}_2}/\text{CMR}_{\text{O}_2}$ ,  $\Delta\text{CMR}_{\text{glc}}/\text{CMR}_{\text{glc}}$ , and  $\Delta\text{CBF}/\text{CBF}$  values from all the PET studies, where the exact values are in Table 9.2. (B) Comparison of  $\Delta\text{CMR}_{\text{O}_2}/\text{CMR}_{\text{O}_2}$  and  $\Delta\text{CBF}/\text{CBF}$  values from PET studies ( $\diamond$ ) with calibrated fMRI studies of Hoge *et al.* (1999) and Kim *et al.* (1999) shown in grey and black circles, respectively. The data suggest that the  $(\Delta\text{CMR}_{\text{O}_2}/\text{CMR}_{\text{O}_2})/(\Delta\text{CBF}/\text{CBF})$  ratio observed in the awake human ( $\sim 0.6$ ) is approximately equal to that observed in the rat brain ( $\sim 0.7$ ). Exact values of the PET studies are in Table 9.2.

from majority of the awake human PET and fMRI data (Figure 9.8(B)) is similar to the value ( $\sim 0.7$ ) obtained from anesthetized rat data (Figure 9.5(B)). The estimates of the  $(\Delta\text{CMR}_{\text{O}_2}/\text{CMR}_{\text{O}_2})/(\Delta\text{CBF}/\text{CBF})$  ratio ( $\sim 0.6$ ) from Figure 9.8(B) are in good agreement with more recent PET studies (Mintun *et al.*, 2002). The data shown in Figure 9.8(B) are from the calibrated fMRI studies of Hoge *et al.* (1999) and Kim *et al.* (1999) as well as all of the PET studies listed in Table 9.2. As mentioned above, the BOLD calibration experiments that have been conducted until now in humans have used the relationship described by Equation (9.10) to calculate changes in CBV due to the lack of an approved MRI contrast agent that has a very long half-life for human use. But using a value for  $\phi$  of  $\sim 0.4$  in Equation (9.10), instead of  $\sim 0.1$  (see above), would underestimate the changes in  $\text{CMR}_{\text{O}_2}$  predicted by the hypercapnia BOLD calibration method (see above). Despite potential underestimation of changes in  $\text{CMR}_{\text{O}_2}$  the relationship between  $\Delta\text{CBF}/\text{CBF}$  and  $\Delta\text{CMR}_{\text{O}_2}/\text{CMR}_{\text{O}_2}$  measured by MRI in awake humans is in good agreement with the PET data (Figure 9.8(B)) and the anesthetized rat data (Figure 9.5(B)). However, both the spatial and temporal resolutions are much higher with fMRI. The calibrated fMRI data (Figure 9.6) has spatial and temporal resolutions of  $\sim 0.2\text{ }\mu\text{l}$  and  $\sim 4\text{ s}$ , respectively.

## 9.9. FUTURE DIRECTIONS

In rapidly developing fields of fMRI, where interests range from physiology to cognition, there is a fascination for measuring the stimulus-induced BOLD signal with very high temporal resolution. This experimental approach is called ‘event-related fMRI’ because the signal is measured following a very short stimulus input (i.e., an event). Although the expectation is that a temporally resolved fMRI signal will reveal new insights into brain function, the time constant of the increase in the BOLD signal cannot be modified. The slow rate of signal increase is bound by the sluggish mechanical response of the microvasculature. Since each parameter that modifies the BOLD signal (see Equation (9.3)) changes with a distinct time constant, the steady state calibration of fMRI described here cannot be readily extended to interpretation of dynamic neuroenergetic changes from ‘event-related fMRI’ data. Despite the lack of calibration of the various dynamic contributions to the fMRI signal, the ‘event-related fMRI’ data are being interpreted with these as well as other unspecified assumptions (Buxton *et al.*, 1998; Mandeville *et al.*, 1999; Friston *et al.*, 2000; Zheng *et al.*, 2002). The changes in the fMRI signal can be a delayed positive response (peaks at 4–6 s from stimulation onset; magnitude is *high*; e.g., Blamire *et al.*, 1992), or an early negative response (peaks at 1–2 s from stimulation onset; magnitude is *low*; e.g., Menon *et al.*, 1995), or a delayed negative response (peaks at 4–6 s from stimulation onset; magnitude is *intermediate*; e.g., Harel *et al.*, 2002). While each of these BOLD responses can be explained on the basis of the mechanical manifestations of the microvasculature, only the delayed positive and negative BOLD response, have been calibrated with energetic changes, as shown here. The origins of the early negative BOLD response is still unknown (Logothetis *et al.*, 1999; Buxton, 2001; Shmuel *et al.*, 2002).

Despite the lack of statistical reproducibility of event-related fMRI responses and the absence of a causative mechanism, aside from the general assumption that the energetic and hemodynamic effects change independently during the stimulation onset, interpretations of these time courses have taken a central place in the field (e.g., Buckner, 2003). Furthermore, the ‘early negative dip’ has been used to obtain columnar-like structures in the visual system (Kim *et al.*, 2000; Duong *et al.*, 2000) despite the unknown origin of the signal, the lack of statistical reproducibility, and the lower sensitivity. In contrast, the superior sensitivity of the delayed BOLD response has demonstrated an overlooked success for mapping columnar-like structures reproducibly in the cerebral cortex of animals (Yang *et al.*, 1996) and humans (Cheng *et al.*, 2001). While many cross-modal correlations (as discussed above) and expectations from psychology and neuroanatomy leave little doubt that the delayed BOLD signal is responding in some way to neuronal activity, the nature of that activity at steady state has now been revealed by calibrated fMRI experiments. Careful

fMRI calibrations with high temporal resolution are needed before the dynamic fMRI signal can be used to derive values of  $\Delta\text{CMR}_{\text{O}_2}/\text{CMR}_{\text{O}_2}$ , which provide a biophysical relationship between neuroimaging and neuronal activity.

The *in vivo* observations of tight proportionality between CBF and CMRO<sub>2</sub> measured regionally at rest and during function, both in the rat (Figure 9.5(B)) and in the human (Figure 9.8(B)), support a concept of the efficiency of oxygen transfer from the capillary bed (Hyder *et al.*, 1998, 2000b, 2001). While theories of oxygen transport have not been critical in aiding BOLD calibration at steady state, any future work leading to calibration of the BOLD signal in a time-dependent manner would need to consider distinct and competing steps involved in dynamic oxygen transport from blood to brain. Furthermore this endeavor would require combination of dynamic measurements of  $S$ , CBF, CBV,  $v$ , and  $\text{pO}_2$  in the same model, which is not trivial. However, an even bigger challenge will be to validate the predicted dynamics in CMRO<sub>2</sub>. While it is quite possible that the higher temporal resolution of <sup>17</sup>O MRS (Zhu *et al.*, 2002) may play a great role in this process, modifying the POCE method for dynamic changes in CMRO<sub>2</sub> is not completely out of the question either. Irrespective of which method is used for the validation process, until dynamic changes in CMRO<sub>2</sub> are obtained from calibrated BOLD signals, only steady state calibrated BOLD data provide meaningful neural information.

## 9.10. CONCLUSION

The conventional fMRI map offers information indirectly about localized changes in neural activity since it reliably reflects blood oxygenation changes, not alterations in neural activity. To provide neurophysiological basis of fMRI, researchers have combined electrophysiological methods to show correlations of BOLD and electrical signals. But quantitative interpretation of 'How much has the neural activity changed by?' still cannot be made from conventional fMRI data. The BOLD signal has two parts, one that describes the energetic support of the bioelectric work (CBF–CMRO<sub>2</sub> relationship) to sustain neuronal excitability and the other is the requisite dilatation of vessels (CBF–CBV relationship) presumably involved in removal of waste while providing nutrients. The BOLD signal was calibrated by quantifying these physiological parameters over a wide range of neuronal activity in the anesthetized rat brain. The end result of the BOLD calibration was the ability to calculate changes in CMRO<sub>2</sub>. This prediction of CMRO<sub>2</sub> changes were also validated with <sup>13</sup>C MRS measurements. Analysis of PET results from the awake human shows that this type of BOLD calibration may provide accurate estimates of changes in CMRO<sub>2</sub> with high temporal and spatial resolutions. Pharmacological and electrophysiological studies in the rat revealed that the changes in CMRO<sub>2</sub> derived from the BOLD calibration are closely linked with variations in neuronal glutamate release as well as the electrical workload of the neuronal ensemble in a voxel. These findings confirm the neurophysiologic makeup of BOLD and have taken the necessary steps towards mapping neuronal activity by fMRI.

## REFERENCES

Albert MS, Huang W, Lee JH, Patlak CS, Springer CS Jr (1993) Susceptibility changes following bolus injections *Magn Reson Med* **29**: 700–708

Ames III A (2000) CNS energy metabolism as related to function *Brain Res Rev* **34**: 42–68

Attwell D, Laughlin SB (2001) An energy budget for signaling in the grey matter of the brain *J Cereb Blood Flow Metab* **21**: 1133–1145

Bauer WR, Schulten K (1992) Theory of contrast agents in magnetic resonance imaging: Coupling of spin relaxation and transport *Magn Reson Med* **26**: 16–39

Blamire AM, Ogawa S, Ugurbil K, Rothman DL, McCarthy G, Ellermann JM, Hyder F, Rattner Z, Shulman RG (1992) Dynamic mapping of the human visual cortex by high-speed magnetic resonance imaging *Proc Natl Acad Sci USA* **89**: 11069–11073

Boxerman JL, Hamberg LM, Rosen BR, Weisskoff RM (1995) MR contrast due to intravascular magnetic susceptibility perturbations *Magn Reson Med* **34**: 555–566

Brinker G, Bock C, Busch E, Krep H, Hossmann KA, Hoehn-Berlage M (1999) Simultaneous recording of evoked potentials and  $T2^*$ -weighted MR images during somatosensory stimulation of rat *Magn Reson Med* **41**: 469–473

Buckner RL (2003) The hemodynamic inverse problem: Making inferences about neural activity from measured MRI signals *Proc Natl Acad Sci USA* **100**: 2177–2179

Buxton RB, Wong EC, Frank LR (1998) Dynamics of blood flow and oxygenation changes during brain activation: the balloon model *Magn Reson Med* **39**: 855–864

Buxton RB (2001) The elusive dip *Neuroimage* **13**: 953–958

Calamante F, Thomas DL, Pell GS, Wiersma J, Turner R (1999) Measuring cerebral blood flow using magnetic resonance imaging techniques *J Cereb Blood Flow Metab* **19**: 701–735

Chen W, Zhu XH, Gruetter R, Seaquist ER, Adriany G, Ugurbil (2001) Study of tricarboxylic acid cycle flux changes in human visual cortex during hemifield visual stimulation using  $^1\text{H}$ - $[^{13}\text{C}]$  MRS and fMRI *Magn Reson Med* **45**: 349–355

Cheng K, Waggoner RA, Tanaka K (2001) Human ocular dominance columns as revealed by high-field functional magnetic resonance imaging *Neuron* **32**: 359–374

Craigie EH (1945) The architecture of the cerebral capillary bed *Biol Rev* **20**: 133–146

Creutzfeldt OD (1975) Neurophysiological correlates of different functional states of the brain. In: *Alfred Benzon Symposium VII* (Ingvar DH, Lassen NA, eds), Academic Press, New York, pp 21–46

Crone C (1963) The permeability of capillaries in various organs as determined by the “indicator diffusion” method *Acta Physiol Scand* **58**: 292–305

Davis TL, Kwong KK, Weisskoff RM, Rosen BR (1998) Calibrated functional MRI: Mapping the dynamics of oxidative metabolism *Proc Natl Acad Sci USA* **95**: 1834–1839

de Graaf RA, Brown PB, Mason GF, Rothman DL, Behar KL (2003) Detection of [1,6- $^{13}\text{C}2$ ]-glucose metabolism in rat brain by *in vivo*  $^1\text{H}$ - $[^{13}\text{C}]$ -NMR spectroscopy *Magn Reson Med* **49**: 37–46

Detre JA, Leigh JS, Williams DS, Koretsky AP (1992) Perfusion imaging *Magn Reson Med* **23**: 37–45

Duong TQ, Kim DS, Ugurbil K, Kim SG (2000) Spatiotemporal dynamics of the BOLD fMRI signals: toward mapping submillimeter cortical columns using the early negative response *Magn Reson Med* **44**: 231–242

Eichling JO, Raichle ME, Grubb RL, Ter-Pogossian MM (1974) Evidence of the limitations of water as a freely diffusible tracer in brain of the Rhesus monkey *Circ Res* **35**: 358–64

Fitzpatrick SM, Hetherington HP, Behar KL, Shulman RG (1990) The flux from glucose to glutamate in the rat brain *in vivo* as determined by  $^1\text{H}$ -observed,  $^{13}\text{C}$ -edited NMR spectroscopy *J Cereb Blood Flow Metab* **10**: 170–179

Fox PT, Raichle ME (1986) Focal physiological uncoupling of cerebral blood flow and oxidative metabolism during somatosensory stimulation in human subjects *Proc Natl Acad Sci USA* **83**: 1140–1144

Fox PT, Raichle ME, Mintun MA, Dence C (1988) Nonoxidative glucose consumption during focal physiologic neural activity *Science* **241**: 462–464

Friston KJ, Mechelli A, Turner R, Price CJ (2000) Nonlinear responses in fMRI: the Balloon model, Volterra kernels, and other hemodynamics *Neuroimage* **12**: 466–77

Fujita H, Kuwabara H, Reutens DC, Gjedde A (1999) Oxygen consumption of cerebral cortex fails to increase during continued vibrotactile stimulation *J Cereb Blood Flow Metab* **19**: 266–271

Garby L, Larsen PS (1995) *Bioenergetics: Its Thermodynamic Foundations*, Cambridge University Press, Cambridge, UK

Ginsberg MD, Chang JY, Kelley RE, Yoshii F, Barker WW, Ingenito G, Boothe TE (1988) Increases in both cerebral glucose utilization and blood flow during execution of a somatosensory task *Ann Neurol* **23**: 152–160

Grubb RL, Raichle ME, Eichling JO, Ter Pogosian MM (1974) The effects of changes in  $\text{pCO}_2$  on cerebral blood volume, blood flow, and vascular mean transit time *Stroke* **5**: 630–639

Grunwald F, Schrock H, Kuschinsky W (1987) The effect of acute nicotine infusion on local cerebral glucose utilization of the awake rat *Brain Res* **400**: 232–238

Grunwald F, Schrock H, Kuschinsky W (1991) The influence of nicotine on local cerebral blood flow in rats *Neurosci Lett* **124**: 108–110

Haacke EM, Lin W, Hu X, Thulborn K (2001) A current perspective of the status of understanding BOLD imaging and its use in studying brain function: a summary of the workshop at the University of North Carolina in Chapel Hill, 26–28 October, 2000 *NMR Biomed* **14**: 384–388

Hagerdal M, Hamp JR, Nilsson L, Siesjo BK (1975) The effect of induced hypothermia upon oxygen consumption in rat brain *J Neurochem* **24**: 311–316

Harel N, Lee SP, Nagaoka T, Kim DS, Kim SG (2002) Origin of negative blood oxygenation level-dependent fMRI signals *J Cereb Blood Flow Metab* **22**: 908–917

Henry PG, Roussel R, Vaufrey F, Dautry C, Bloch G (2000) Semiselective POCE NMR spectroscopy *Magn Reson Med* **44**: 395–400

Hill (1913) The combinations of haemoglobin with oxygen and carbon monoxide *Biochem J* **7**: 471–480

Hoge RD, Atkinson J, Gill B, Crelier GR, Marrett S, Pike GB (1999) Linear coupling between cerebral blood flow and oxygen consumption in activated human cortex *Proc Natl Acad Sci USA* **96**: 9403–9408

Hyder F, Behar KL, Martin MA, Blamire AM, Shulman RG (1994) Dynamic magnetic resonance imaging of the rat brain during forepaw stimulation *J Cereb Blood Flow Metab* **14**: 649–655

Hyder F, Chase JR, Behar KL, Mason GF, Siddeek M, Rothman DL, Shulman RG (1996) Increased tri-carboxylic acid cycle flux in rat brain during forepaw stimulation detected with <sup>1</sup>H-[<sup>13</sup>C] NMR *Proc Natl Acad Sci USA* **93**: 7612–7617

Hyder F, Rothman DL, Mason GF, Rangarajan A, Behar KL, Shulman RG (1997) Oxidative glucose metabolism in rat brain during single forepaw stimulation: A spatially localized <sup>1</sup>H-[<sup>13</sup>C] NMR study *J Cereb Blood Flow Metab* **17**: 1040–1047

Hyder F, Shulman RG, Rothman DL (1998) A model for the regulation of cerebral oxygen delivery *J Appl Physiol* **85**: 554–564

Hyder F, Renken R, Rothman DL (1999) *in vivo* carbon-edited detection with proton echo-planar spectroscopic imaging (ICED PEPSI): [3,4-<sup>13</sup>CH<sub>2</sub>]glutamate/glutamine tomography in rat brain *Magn Reson Med* **42**: 997–1003

Hyder F, Renken R, Kennan RP, Rothman DL (2000a) Quantitative multi-modal functional MRI with blood oxygenation level dependent exponential decays adjusted for flow attenuated inversion recoveries (BOLDED AFFAIR) *Magn Reson Imag* **18**: 227–235

Hyder F, Kennan RP, Kida I, Mason GF, Behar KL, Rothman DL (2000b) Dependence of oxygen delivery on blood flow in rat brain: a 7 Tesla nuclear magnetic resonance study *J Cereb Blood Flow Metab* **20**: 485–498

Hyder F, Kida I, Behar KL, Kennan RP, Maciejewski PK, Rothman DL (2001) Quantitative functional imaging of the brain: Towards mapping neuronal activity by BOLD fMRI *NMR Biomed* **14**: 413–431

Hyder F, Rothman DL, Shulman RG (2002) Total neuroenergetics support localized brain activity: Implications for the interpretation of fMRI *Proc Natl Acad Sci USA* **99**: 10771–10776

Ito H, Takahashi K, Hatazawa J, Kim SG, Kanno I (2001) Changes in human regional cerebral blood flow and cerebral blood volume during visual stimulation measured by positron emission tomography *J Cereb Blood Flow Metab* **21**: 608–612

Ito H, Kanno I, Ibaraki M, Hatazawa J, Miura S (2003) Changes in human cerebral blood flow and cerebral blood volume during hypercapnia and hypocapnia measured by positron emission tomography *J Cereb Blood Flow Metab* **23**: 665–670

Jung CW, Jacobs P (1995) Physical and chemical properties of superparamagnetic iron oxide MR contrast agents: Ferumoxides, ferumoxtran, ferumoxsil *Magn Reson Imag* **13**: 661–674

Kandel ER, Schwartz JH, Jessell TM (1991) *Principles of Neural Science*, Appleton & Lange, Norwalk, CT

Katayama Y, Tsubokawa T, Hirayama T, Kido G, Tsukiyama T, Iio M (1986) Response of regional cerebral blood flow and oxygen metabolism to thalamic stimulation in humans as revealed by positron emission tomography *J Cereb Blood Flow Metab* **6**: 637–641

Kennan RP, Zhong, J, Gore JC (1994) Intravascular susceptibility contrast mechanisms in tissue *Magn Reson Med* **31**: 9–21

Kennan RP, Scanley BE, Innis RB, Gore JC (1998) Physiological basis for BOLD MR signal changes due to neuronal stimulation: separation of blood volume and magnetic susceptibility effects *Magn Reson Med* **40**: 840–846

Kida I, Hyder F, Kennan RP, Behar KL (1999) Towards absolute quantitation of BOLD functional MRI *Adv Exp Med Biol* **471**: 681–689

Kida I, Kennan RP, Rothman DL, Behar KL, Hyder F (2000) High-resolution CMR<sub>O<sub>2</sub></sub> mapping in rat cortex: a multi-parametric approach to calibration of BOLD image contrast at 7 Tesla *J Cereb Blood Flow Metab* **20**: 847–860

Kida I, Hyder F, Behar KL (2001) Inhibition of voltage-dependent sodium channels suppresses the functional MRI response to forepaw somatosensory activation in the rodent *J Cereb Blood Flow Metab* **21**: 585–591

Kida I, Xu F, Shulman RG, Hyder F (2002) Mapping at glomerular resolution: fMRI of rat olfactory bulb *Magn Reson Med* **48**: 570–576

Kim SG, Rostrup E, Larsson HB, Ogawa S, Paulson OB (1999) Determination of relative CMR<sub>O<sub>2</sub></sub> from CBF and BOLD changes: Significant increase of oxygen consumption rate during visual stimulation *Magn Reson Med* **41**: 1152–1161

Kim DS, Duong TQ, Kim SG (2000) High-resolution mapping of iso-orientation columns by fMRI *Nat Neurosci* **3**: 164–169

Kuwabara H, Ohta S, Brust P, Meyer E, Gjedde A (1992) Density of perfused capillaries in living human brain during functional activation *Prog Brain Res* **91**: 209–215

Laughlin SB (2001) Energy as a constraint on the coding and processing of sensory information *Curr Opin Neurobiol* **11**: 475–480

Leach MJ, Marden CM, Miller AA (1986) Pharmacological studies on lamotrigine, a novel potential antiepileptic drug: II. Neurochemical studies on the mechanism of action *Epilepsia* **27**: 490–497

Lee SP, Silva AC, Ugurbil K, Kim SG (1999) Diffusion-weighted spin-echo fMRI at 9.4 T: Microvascular/tissue contribution to BOLD signal changes *Magn Reson Med* **42**: 919–928

Lees P (1972) Pharmacology and toxicology of alpha chloralose: A review *Vet Rec* **91**: 330–333

Linford JH (1966) *An Introduction to Energetics*, Butterworth, London, UK

Logothetis NK, Guggenberger H, Peled S, Pauls J (1999) Functional imaging of the monkey brain *Nat Neurosci* **2**: 555–562

Logothetis NK, Pauls J, Augath M, Trinath T, Oeltermann A (2001) Neurophysiological investigation of the basis of the fMRI signal *Nature* **412**: 150–157

Mandeville JB, Marota JJ, Kosofsky BE, Keltner JR, Weissleder R, Rosen BR, Weisskoff RM (1998) Dynamic functional imaging of relative cerebral blood volume during rat forepaw stimulation *Magn Reson Med* **39**: 615–624

Mandeville JB, Marota JJ, Ayata C, Zaharchuk G, Moskowitz MA, Rosen BR, Weisskoff RM (1999) Evidence of a cerebrovascular postarteriole windkessel with delayed compliance *J Cereb Blood Flow Metab* **19**: 679–689

Marrett S, Gjedde A (1997) Changes of blood flow and oxygen consumption in visual cortex of living humans *Adv Exp Med Biol* **413**: 205–208

Menon RS, Ogawa S, Hu X, Strupp JP, Anderson P, Ugurbil K (1995) BOLD based functional MRI at 4 Tesla includes a capillary bed contribution: Echo-planar imaging correlates with previous optical imaging using intrinsic signals *Magn Reson Med* **33**: 453–459

Mosher TJ, Smith MB (1991) Mapping the static magnetic field using a double-DANTE tagging sequence *J Magn Reson* **93**: 624–629

Mintun MA, Raichle ME, Martin WR, Herscovitch P (1984) Brain oxygen utilization measured with O-15 radiotracers and positron emission tomography *J Nucl Med* **25**: 177–187

Mintun MA, Vlassenko AG, Shulman GL, Snyder AZ (2002) Time-related increase of oxygen utilization in continuously activated human visual cortex *Neuroimage* **16**: 531–537

Nilsson L, Siesjo BK (1975) The effect of phenobarbitone anaesthesia on blood flow and oxygen consumption in the rat brain *Acta Anaesth Scand Suppl* **57**: 18–24

Nilsson B, Siesjo BK (1976) A method of determining blood flow and oxygen consumption in rat brain *Acta Physiol Scand* **17**: 273–282

Ogawa S, Lee TM, Nayak AS, Glynn P (1990) Oxygenation-sensitive contrast in magnetic resonance image on rodent brain at high magnetic fields *Magn Reson Med* **14**: 68–78

Ogawa S, Menon RS, Tank DW, Kim SG, Merkle H, Ellermann JM, Ugurbil K (1993) Functional brain mapping by blood oxygenation level-dependent contrast magnetic resonance imaging *Biophys J* **64**: 803–812

Ogawa S, Menon RS, Kim SG, Ugurbil K (1998) On the characteristics of functional magnetic resonance imaging of the brain *Annu Rev Biophys Biomol Struct* **27**: 447–474

Ogawa S, Lee TM, Stepnoski R, Chen W, Zhu XH, Ugurbil K (2000) An approach to probe some neural systems interaction by functional MRI at neural time scale down to milliseconds *Proc Natl Acad Sci USA* **97**: 11026–11031

Otsuka T, Wei L, Acuff VR, Shimizu A, Pettigrew KD, Patlak CS, Fenstermacher JD (1991a) Variation in local cerebral blood flow response to high-dose pentobarbital sodium in the rat *Am J Physiol* **261**: H110–H120

Otsuka T, Wei L, Bereczki D, Acuff V, Patlak C, Fenstermacher J (1991b) Pentobarbital produces dissimilar changes in glucose influx and utilization in the brain *Am J Physiol* **261**: R265–R275

Pauling L, Coryell C (1936) The magnetic properties of and structure of hemoglobin, oxyhemoglobin and carbon-monoxyhemoglobin *Proc Natl Acad Sci USA* **22**: 210–216

Paulson OB, Hertz MM, Bolwig TG, Lassen NA (1977) Filtration and diffusion of water across the blood-brain barrier in man *Microvasc Res* **13**: 113–124

Pellerin L, Magistretti PJ (1994) Glutamate uptake into astrocytes stimulates aerobic glycolysis: A mechanism coupling neuronal activity to glucose utilization *Proc Natl Acad Sci USA* **91**: 10625–10629

Penfield W (1933) The evidence for a cerebral vascular mechanism in epilepsy *Ann Int Med* **7**: 303–310

Pfeuffer J, Tkac I, Choi IY, Merkle H, Ugurbil K, Garwood M, Gruetter R (1999) Localized *in vivo* <sup>1</sup>H NMR detection of neurotransmitter labeling in rat brain during infusion of [1-<sup>13</sup>C] D-glucose *Magn Reson Med* **41**: 1077–1083

Raichle ME, Grubb RL, Gado MH, Eichling JO, Ter-Pogossian MM (1976) Correlation between regional cerebral blood flow and oxidative metabolism *Arch Neurol* **33**: 523–526

Raichle ME, Martin WR, Herscovitch P, Mintun MA, Markham J (1983) Brain blood flow measured with intravenous H<sub>2</sub><sup>15</sup>O. II. Implementation and validation *J Nucl Med* **24**: 790–798

Rees G, Friston K, Koch C (2000) A direct quantitative relationship between the functional properties of human and macaque V5 *Nat Neurosci* **3**: 716–723

Ribeiro L, Kuwabara H, Meyer E, Fujita H, Marrett S, Evans A, Gjedde A (1993) Cerebral blood flow and metabolism during non-specific bilateral visual stimulation in normal subjects. In: *Quantification of Brain Function. Tracer Kinetics and Image Analysis in Brain PET*, Eds Uemura K, Lassen NA, Jones T, Kanno I, Elsevier, Amsterdam, pp 217–224

Richard CD (1998) What the actions of anaesthetics on fast synaptic transmission reveal about the molecular mechanism of anaesthesia *Toxicol Lett* **100–101**: 41–50

Roland PE, Eriksson L, Stone-Elander S, Widen L (1987) Does mental activity change the oxidative metabolism of the brain? *J Neurosci* **7**: 2373–2389

Rothman DL, Behar KL, Hetherington HP, den Hollander JA, Bendall MR, Petroff OAC, Shulman RG (1985) <sup>1</sup>H observed <sup>13</sup>C decoupled spectroscopic measurements of lactate and glutamate in the rat brain *in vivo* *Proc Natl Acad Sci USA* **82**: 1633–1637

Rothman DL, Sibson NR, Hyder F, Shen J, Behar KL, Shulman RG (1999) *in vivo* nuclear magnetic resonance spectroscopy studies of the relationship between the glutamate-glutamine neurotransmitter cycle and functional neuroenergetics *Philos Trans R Soc London, Ser B* **354**: 1165–1177

Rothman DL, Hyder F, Sibson NR, Behar KL, Mason GF, Shen J, Petroff OAC, Shulman RG (2002) *in vivo* magnetic resonance spectroscopy studies of the glutamate and GABA neurotransmitter cycles and functional neuroenergetics. In: *Neuropsychopharmacology: The Fifth Generation of Progress*, Eds Davis KL, Charney D, Coyle JT, Nemeroff C, Lippincott Williams & Wilkins, Philadelphia, PA, pp 315–342

Rothman DL, Behar KL, Hyder F, Shulman RG (2003) *in vivo* NMR studies of the glutamate neurotransmitter flux and neuroenergetics: Implications for brain function *Annu Rev Physiol* **65**: 401–427

Roy CS, Sherrington CS (1890) On the regulation of the blood supply of the rat brain *J Physiol (Lond)* **11**: 85–108

Schwarzbauer C, Morrissey SP, Hasse A (1996) Quantitative magnetic resonance imaging of perfusion using magnetic labeling of water proton spins within the detection slice *Magn Reson Med* **35**: 540–546

Seitz RJ, Roland PE (1992) Vibratory stimulation increases and decreases the regional cerebral blood flow and oxidative metabolism: A positron emission tomography (PET) study *Acta Neurol Scand* **86**: 60–67

Shmuel A, Yacoub E, Pfeuffer J, Van de Moortele PF, Adriany G, Hu X, Ugurbil K (2002) Sustained negative BOLD, blood flow and oxygen consumption response and its coupling to the positive response in the human brain *Neuron* **36**: 1195–1210

Shulman RG, Rothman DL (1998) Interpreting functional imaging studies in terms of neurotransmitter cycling *Proc Natl Acad Sci USA* **95**: 11993–11998

Shulman RG, Rothman DL, Hyder F (1999) Stimulated changes in localized cerebral energy consumption under anesthesia *Proc Natl Acad Sci USA* **96**: 3245–3250

Shulman RG, Hyder F, Rothman DL (2001a) Lactate efflux and the neuroenergetic basis of brain function *NMR Biomed* **14**: 389–396

Shulman RG, Hyder F, Rothman DL (2001b) Cerebral energetics and the glycogen shunt: Neurochemical basis of functional imaging *Proc Natl Acad Sci USA* **98**: 6417–6422

Shulman RG, Hyder F, Rothman DL (2002) Biophysical basis of brain activity: Implications for neuroimaging *Q Rev Biophys* **35**: 287–325

Shulman RG, Hyder F, Rothman DL (2003) Cerebral metabolism and consciousness *C R Biol* **326**: 253–273

Siesjo BK (1978) *Brain Energy Metabolism*, Wiley, New York

Silva AC, Zhang W, Williams DS, Koretsky AP (1997) Estimation of water extraction fractions in rat brain using magnetic resonance measurement of perfusion with arterial spin labeling *Magn Reson Med* **37**: 58–68

Silva AC, Lee SP, Yang G, Iadecola C, Kim SG (1999) Simultaneous blood oxygenation level-dependent and cerebral blood flow functional magnetic resonance imaging during forepaw stimulation in the rat *J Cereb Blood Flow Metab* **19**: 871–879

Smith AJ, Blumenfeld H, Behar KL, Rothman DL, Shulman RG, Hyder F (2002) Cerebral energetics and spiking frequency: The neurophysiological basis of fMRI *Proc Natl Acad Sci USA* **99**: 10765–10770

Sokoloff L (1991) Relationship between functional activity and energy metabolism in the nervous system: whether, where and why? In: *Brain Work and Mental Activity*, Eds Lassen NA, Ingvar DH, Raichle ME, Friberg L, Munksgaard, Copenhagen, pp 52–64

Song AW, Wong EC, Tan SG, Hyde JS (1996) Diffusion weighted fMRI at 1.5 T *Magn Reson Med* **35**: 155–158

Ueki M, Linn F, Hossmann KA (1988) Functional activation of cerebral blood flow and metabolism and after global ischemia of rat brain *J Cereb Blood Flow Metab* **8**: 486–494

Ugurbil K, Adriany G, Andersen P, Wei C, Gruetter R, Hu X, Merkle H, Kim DS, Kim SG, Strupp J, Hong X, Ogawa S (2000) Magnetic resonance studies of brain function and neurochemistry *Annu Rev Biomed Eng* **2**: 633–660

Vafaei MS, Gjedde A (2000) Model of blood-brain transfer of oxygen explains nonlinear flow-metabolism coupling during stimulation of visual cortex *J Cereb Blood Flow Metab* **20**: 747–754

van Bruggen N, Busch E, Palmer JT, Williams SP, de Crespigny AJ (1998) High-resolution functional magnetic resonance imaging of the rat brain: mapping changes in cerebral blood volume using iron oxide contrast media *J Cereb Blood Flow Metab* **18**: 1178–1183

van Zijl PCM, Efele SM, Ulatowski JA, Oja JME, Ulug AM, Traystman RJ, Kauppinen RA (1998) Quantitative assessment of blood flow, blood volume and blood oxygenation effects in functional magnetic resonance imaging *Nature Med* **4**: 159–167

Weisskoff RM, Zuo CS, Boxerman JL, Rosen BR (1994) Microscopic susceptibility variation and transverse relaxation: theory and experiment *Magn Reson Med* **31**: 601–610

Williams DS, Detre JA, Leigh JS, Koretsky AP (1992) Magnetic resonance imaging of perfusion using spin inversion of arterial water *Proc Natl Acad Sci USA* **89**: 212–216

Xu F, Kida I, Hyder F, Shulman RG (2000) Assessment and discrimination of odor stimuli in rat olfactory bulb by dynamic fMRI *Proc Natl Acad Sci USA* **97**: 10601–10606

Yang X, Hyder F, Shulman RG (1996) Single-whisker activation observed in rat cortex by functional magnetic resonance imaging *Proc Natl Acad Sci USA* **93**: 475–478

Yang X, Hyder F, Shulman RG (1997) Functional MRI BOLD signal coincides with electrical activity in rat whisker barrel *Magn Reson Med* **38**: 874–877

Yang X, Renken R, Hyder F, Siddeek M, Greer CA, Shepherd GM, Shulman RG (1998) Dynamic mapping at the laminar level of odor-elicited responses in rat olfactory bulb by functional MRI *Proc Natl Acad Sci USA* **95**: 7715–7720

Zhang W, Williams DS, Detre JA, Koretsky AP (1992) Measurement of brain perfusion by volume-localized NMR spectroscopy using inversion of arterial water spins: accounting for transit time and cross-relaxation *Magn Reson Med* **25**: 362–371

Zheng Y, Martindale J, Johnston D, Jones M, Berwick J, Mayhew J (2002) A model of the hemodynamic response and oxygen delivery to brain *Neuroimage* **16**: 617–637

Zhong J, Kennan RP, Fulbright RK, Gore JC (1998) Quantification of intravascular and extravascular contributions to BOLD effects induced by alteration in oxygenation or intravascular contrast agents *Magn Reson Med* **40**: 526–536

Zhu XH, Zhang Y, Tian RX, Lei H, Zhang N, Zhang X, Merkle H, Ugurbil K, Chen W (2002) Development of <sup>17</sup>O NMR approach for fast imaging of cerebral metabolic rate of oxygen in rat brain at high field *Proc Natl Acad Sci USA* **99**: 13194–13199



# 10

## Relationship between CMR<sub>O<sub>2</sub></sub> and Neuronal Activity

**Fahmeed Hyder**

*Department of Diagnostic Radiology and Biomedical Engineering, Yale University School of Medicine, MR Center, P.O. Box 208043, New Haven, CT 06510, USA*

**Hal Blumenfeld**

*Department of Neurology and Neurobiology, Yale University School of Medicine, MR Center, P.O. Box 208018, New Haven, CT 06510, USA*

---

10.1	Introduction	174
10.2	Interpretability of Neuroimaging Signals	175
10.3	Neuronal Activity and Anatomy	177
10.4	Measuring Changes in CMR <sub>O<sub>2</sub></sub> and $\nu$	179
10.5	Relationship between CMR <sub>O<sub>2</sub></sub> and $\nu$	181
10.6	Comparison with Previous Studies	184
10.7	Redeployment of Spiking Frequency Distributions	186
10.8	Implications for Interpretation of fMRI	187
10.9	Biophysical Basis of Cognitive Neuroscience	189
10.10	Future Directions	190
10.11	Conclusion	191

---

## 10.1. INTRODUCTION

Neuroimaging methods highlight specific areas of the human brain which are involved in the sensation, perception, and cognition of stimuli. Following the introduction of PET for brain mapping about two decades ago (Raichle, 1988), fMRI has come forward to play the more dominant role in both human and animal functional studies of the brain (Shulman, 2001). A modern graduate student of neuroscience would certainly have seen remarkable colored PET or fMRI images of the working human brain in text books. And why not? Both PET and fMRI methods, the former being a little more invasive than the latter, are at the forefront of cognitive and clinical neuroscience research today. The typical student's interpretation of the superb colored hues representing the activated spots would probably be that specific brain regions work when they are provoked by the stimulus. This appraisal of the active regions identifies those that survive the differencing away of the baseline, i.e., when the subject is doing 'nothing' but resting inside the scanner (Posner and Raichle, 1998). This interpretation is based on the cognitive neuroscientists' belief that doing 'nothing' during the baseline condition actually meant that the brain cells were not doing anything that was meaningful for the task in question (Shulman and Rothman, 1998). However, the results to be discussed in this chapter show that the baseline neuronal activity contains, for neuroscience and interpreting functional imaging, the most important information.

The functional integrity of the working brain is maintained by communication amongst an enormous number of neurons (Figure 10.1(A)). While neurons transmit and receive electrical signals across synapses (Kandel *et al.*, 1991), the participation of astrocytes (becoming recognized as the neurochemical collaborator in cellular activity (Pellerin and Magistretti, 1994)) in neurotransmission is an integral part of synaptic communication (Figure 10.1(B)). The communication between neurons is characterized by an electric discharge – otherwise known as an action potential (or a spike) – which is followed by a quiescent charging period (Figure 10.1(C)). At rest the cell membrane is nearly impermeable to  $\text{Na}^+$  ions, which have a greater concentration outside than inside the cell. However, during an action potential  $\text{Na}^+$  conductance rapidly increases and  $\text{Na}^+$  ions move into the cell, making the voltage inside the cell ( $V_m$ ) more positive, approaching the  $\text{Na}^+$  ion equilibrium potential ( $E_{\text{Na}}$ ). The rapid change in  $V_m$  triggers a delayed increase in  $\text{K}^+$  conductance ( $g_K$ ) as well as a delayed decrease in  $\text{Na}^+$  conductance ( $g_{\text{Na}}$ ). These conductance changes combine to cause the  $V_m$  to ultimately move back towards the resting value. Thus the action potential has a very short life time (1–2 ms), characterized by a fast depolarization ( $\text{Na}^+$  influx) phase followed by an equally rapid hyperpolarization ( $\text{K}^+$  efflux) segment (Hodgkin and Huxley, 1952).

Action potential generation is driven by gradients of  $\text{Na}^+$  and  $\text{K}^+$  ions across the cell membrane. Much like batteries powering an electric device, these gradients (high  $\text{Na}^+$  outside the cell and high  $\text{K}^+$  inside the cell) must be maintained for repeated spikes to occur. Active  $\text{Na}^+–\text{K}^+$  pumps consume large amounts of ATP to maintain these ionic gradients so that the neurons are ready to work (i.e., 'fire') whenever called for (Ritchie, 1967). The discharging and charging phases are traditionally referred to as 'firing' and 'nonfiring' periods (Figure 10.1(D)). However, these epochs are not exactly binary because cations are continuously moving across the cell membrane, either via passive diffusion or evoked by a signal from a pre-synaptic neuron, causing  $V_m$  to fluctuate. Since an action potential is generated only if  $V_m$  rises beyond a specific threshold in the post-synaptic neuron, the intermittently changing  $V_m$  creates waves of synaptic field potentials that have a longer lifetime (10–20 ms) as a consequence of failed attempts of the post-synaptic neuron at creating spikes. Thus the main difference between measures of action and field potentials is that the former is readily quantifiable because a specific rate of firing can be assigned for individual neurons, which allows for discrimination between spontaneous firing and modified intracellular potentials due to incoming signals (Gray, 1995).

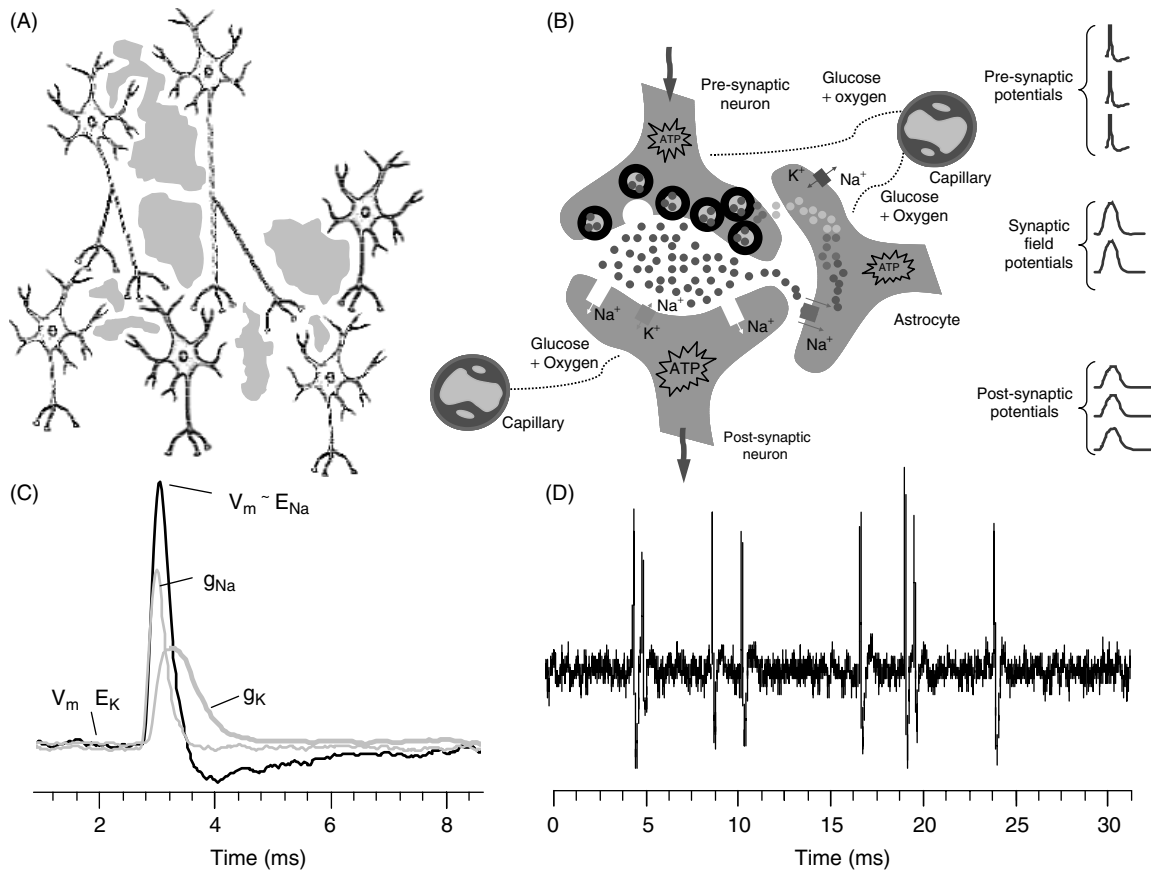


**Figure 10.1.** Neuronal activity and energetics. (A) Neurons communicate via synapses and are surrounded by astrocytes (shown in gray). (B) The electrical and chemical synapse at a magnified scale showing pre- and post-synaptic elements, along with astrocytes and capillaries. Action potentials in the pre-synaptic neuron (shown on the right inset) trigger neurotransmitter release, which in turn excite the post-synaptic neuron. This results in post-synaptic potentials which can be recorded from the post-synaptic neuron or from the extracellular space as field potentials (as shown on the right inset). Specific channels for cations allow permeability of  $Na^+$  and  $K^+$  ions across the cell membrane during action potentials.  $Na^+ - K^+$  pumps help maintain the normal ionic gradients across the cell membrane. Since ATP is consumed in neurons (and astrocytes) for maintenance of the ionic gradients, the energy pool is replenished by substrate delivery from capillaries. (C) Simulated changes in cell membrane voltage ( $V_m$ ), sodium conductance ( $g_{Na}$ ) and potassium conductance ( $g_K$ ) in a neuron during an action potential (Hodgkin and Huxley, 1952). At rest,  $V_m$  is close to the potassium equilibrium potential ( $E_K$ ), while at the peak of the action potential  $V_m$  is close to the sodium equilibrium potential ( $E_{Na}$ ). (D) A small portion of an extracellular recording demonstrating repeated firing of a single neuron from the  $\alpha$ -chloralose-anesthetized rat brain. See Smith *et al.* (2002) for details.

## 10.2. INTERPRETABILITY OF NEUROIMAGING SIGNALS

An ideal way to probe the activity of neurons would be to measure electrical signals directly with tiny electrodes. However, simultaneous measurement of a large number of neurons is limited by the number

of electrodes that can practically be implanted and recorded from the intact brain. While neuroimaging methods are obviously more practical for noninvasive experiments in humans, the techniques to localize neuronal processes are based on the assumption that local activity of a neuronal ensemble changes when a region is responding to a task. Electrical activity in the brain has significant associated energetic costs which are mainly related to ion movements across axonal and synaptic membranes (Ames, 2000). Since neuronal work requires oxidative energy and oxygen reserves in the brain are extremely low (Siesjo, 1978), supplies of nutrients (i.e., glucose and oxygen) are tightly regulated by the high energy demands of neuronal work (Figure 10.2). Thus neuronal activity is inferred from measurements of cerebral blood flow (CBF) as well as cerebral metabolic rates of glucose ( $CMR_{glc}$ ) and oxygen ( $CMR_{O_2}$ ) utilization by neuroimaging methods. Usually PET and fMRI are applied in a relative sense where the fractional signal changes in specific brain regions reveal where the neuronal activity has changed. But the degree by which neuronal activity has changed cannot be made from the differencing approach because the discard of the ‘baseline’ signal assumes the noncontributing nature of this signal for sensation, perception, and cognition. Given the widespread use of the differencing approach in cognitive neuroscience (Shulman, 1996), one might expect concerns about how the spontaneous baseline activities are related to the colored hues in the functional images. Surprisingly, however, this is far from the case.

To connect the neuroimaging signal to neuronal activity requires establishing two relationships: (i) associating the neuroimaging signal to localized neuroenergetics; (ii) establishing the connection between energy consumption and neuronal processes related to information transfer (e.g., rates of neurotransmitter release and/or action potential propagation). Recent calibration studies of fMRI in rat brain have established the first relationship (see Chapter 9), where the fMRI signal changes ( $S$ ) were correlated with alterations in energy use ( $CMR_{O_2}$ ) during glutamatergic neurotransmission. Some years ago Sokoloff and coworkers explored the second relationship in peripheral neurons with  $2-^{14}C$ -deoxyglucose autoradiography and electrophysiology (see Chapter 2) to show that energy consumption ( $CMR_{glc}$ ) associated with electrical activity is roughly proportional to spiking frequency ( $v$ ). Recent  $^{13}C$  MRS studies of anesthetized rat brain explored the

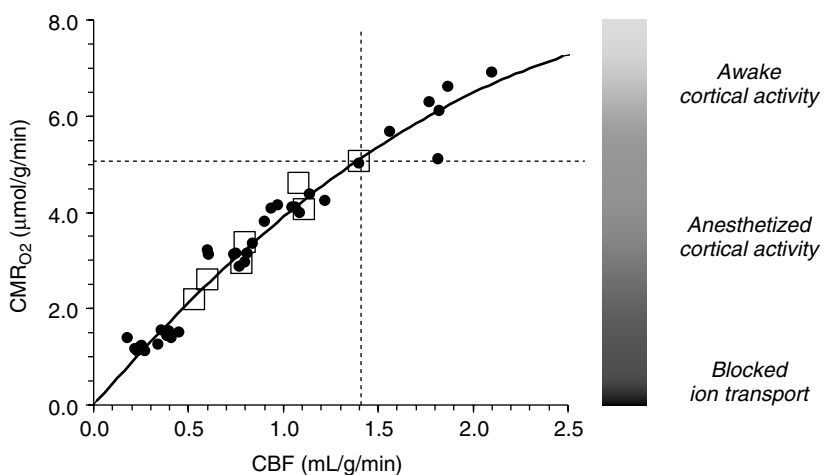


**Figure 10.2.** Relationship between CBF and  $CMR_{O_2}$ . The near-linear relationship between CBF and  $CMR_{O_2}$ , as measured by NMR (●) and non-NMR (□) methods from isoelectric conditions to awake cortical activity, allows the fMRI signal changes to be quantitatively used for neuroimaging (for a recent review see Hyder *et al.*, 2001). The scale on the right *inset* shows qualitatively the levels of cerebral activity, ranging from isoelectric conditions to awake cortical activity, where the nonanesthetized resting awake level is marked by the dotted lines. The details of the different CBF and  $CMR_{O_2}$  measurements are in Chapter 9.

second relationship further (see Chapter 5), where a stoichiometric relationship was measured between rates of neuronal energy metabolism (CMR<sub>O<sub>2</sub></sub>) and neurotransmitter cycling ( $V_{cyc}$ ). Although these combined results suggest that CMR<sub>O<sub>2</sub></sub> is related to  $v$  and  $V_{cyc}$  in glutamatergic synapses, technical limitations of studying the energetics of peripheral neurons or a heterogeneous group of cerebral neurons has limited the quantitative interpretability of these findings for neuroimaging, specially for fMRI. In this chapter the second relationship is explored further by examining the dependence of spiking frequency ( $v$ ) of a neuronal ensemble, primarily consisting of pyramidal neurons, on localized energy metabolism (CMR<sub>O<sub>2</sub></sub>) in the anesthetized rat brain. The evidence to be presented shows a positive and close to linear relationship between the functional increments in energy consumption (CMR<sub>O<sub>2</sub></sub>) and the average rate of neuronal firing ( $v$ ), which suggests that regional brain energy metabolism provides *the* most direct correlate of spiking activity of a neuronal ensemble. Furthermore the electrophysiological data of the neuronal ensemble and the distribution of spiking frequencies show that the differences induced by stimuli require deployment of most of the neurons in the nonstimulated baseline state, thereby emphasizing the importance of the total or summed activity of the ensemble.

### 10.3. NEURONAL ACTIVITY AND ANATOMY

Neuronal communication depends on electrical activity in the form of dynamic changes of  $V_m$  in massive populations of excitatory and inhibitory neurons. The changes in  $V_m$  allow signals to propagate within single neurons and to subsequently be communicated between neurons across the chemical and electrical synapses (Figures 10.1(A) and (B)). A variety of methods are available for studying the electrical signals from neurons *in vivo*. The spatial scale of the measurements range from membrane potentials of a single neuron to macroscopic potentials recorded from large regions (for a review see Kandel *et al.*, 1991). What is the most appropriate electrical measurement for determining neuronal ensemble activity in relation to energetics?

The methods for single cell recordings involve obtaining direct access into the intracellular milieu so that  $V_m$  can be measured with high impedance electrodes, which consist of fine glass capillary tubes filled with electrolytes. The disadvantage of intracellular recordings in studying populations of neurons is the difficulty of sampling large number of neurons because only one neuron can be studied with each electrode. An alternative to this approach is extracellular recordings with glass capillary or metallic electrode tips placed proximally to cell bodies so that the extracellular voltage can be measured. The action potentials from a single neuron can be resolved by adjusting the position of the electrode tip (i.e., single-unit activity (SUA) recording). An electrode with slightly lower impedance can detect action potentials from more neurons with a single penetration (i.e., multi-unit activity (MUA) recording). The neurons closest to the electrode tip generate the largest signals and these signals can be separated by spike sorting algorithms. The unresolved signals from low impedance extracellular electrodes also contain the slow waves of synaptic field potentials. The advantage of extracellular recording is that several individual neurons can be identified and therefore studied simultaneously. Other methods such as magnetoecephalography (MEG), electroencephalography (EEG), and somatosensory evoked potentials (SEP) detect summed post-synaptic potentials from cells located both near to and far from the recording elements, which are placed on the scalp and have very low impedance. These methods are less useful for quantitative measurements because the signals lack spatial specificity. Some uncertainties about the lack of spatial specificity of EEG and MEG can be diminished by using slightly higher impedance wires placed in the brain to measure local field potentials (LFP). However the LFP signals are not easily quantifiable because these signals integrate over space and time and do not have the all-or-none specificity of spikes. Thus, at the present time, the best method for measuring the activity of a population of neurons *in vivo* is extracellular unit recording, because the data can be quantified in terms of spiking rates of an ensemble of neurons and sampled continuously for variety of conditions.

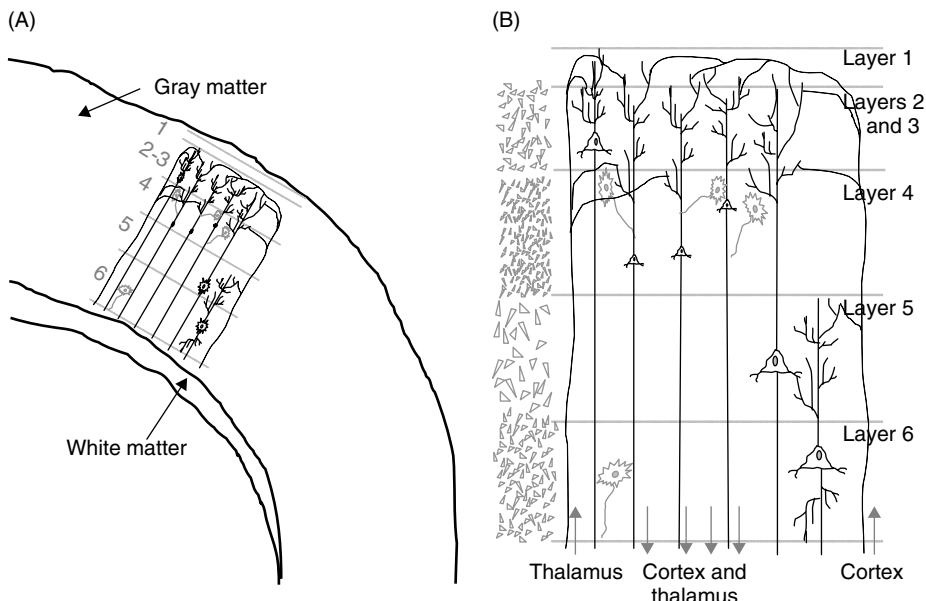


**Figure 10.3.** Cellular layers of the rat somatosensory cortex. (A) The cortical layers in gray matter are numbered 1–6 from the pial surface moving inward towards the white matter. (B) A magnified view of the cortical layers in the rat somatosensory region. The layers can be distinguished microscopically by their content of different cell density and sizes (see left inset). The small network connections across different layers vary: layer 1 composed mainly of axons and dendrites, layers 2 and 3 of small to medium pyramidal neurons with major cortical–cortical connections, layer 4 of densely packed pyramidal and nonpyramidal neurons receiving inputs from the thalamus, layer 5 of large pyramidal neurons which project to the brainstem and spinal cord, and layer 6 of modified pyramidal cells with major reciprocal projections to the thalamus.

The majority of the forebrain surface in most mammals consists of a six-layered neocortex (Figure 10.3(A)). Most neocortical regions contain laminae, which are numbered 1 through 6, progressing from the pial surface to the white matter. Layer 1, or the molecular layer, is sparsely cellular and contains mainly axons and apical dendrites of neurons from other regions. Layers 2 and 3 contain mainly small and medium sized pyramidal neurons, respectively. Layer 4, or the granular layer, consists of small densely packed pyramidal and nonpyramidal neurons. Layer 5 contains medium and large pyramidal neurons. Layer 6 consists mainly of the modified spindle-shaped pyramidal neurons. Extensive synaptic connections occur in the cortex in the vertical (radial) direction (Lorente de Nò, 1938), giving rise to functional modules or columns. In sensory systems, individual neurons oriented vertically are frequently arranged into functional units, e.g., in the cerebral cortex columns or barrels to recognize specific characteristics of stimuli (Woolsey, 1996; Mountcastle, 1997). However, horizontal connections are also prominent, and many of these are collected in plexuses of axon fibers traveling in layer 1, in layer 4, and in the deep portions of layers 5 and 6 (Nieuwenhuys, 1998). The major fraction of neocortical neurons (~80 %) consists of pyramidal neurons (Winfield *et al.*, 1980; Peters *et al.*, 1985) (Figure 10.3(B)). Their cell bodies have a pointed top, oriented towards the surface of the neocortex giving rise to a large apical dendrite, and a relatively flat bottom giving rise to a skirt of basal dendrites. The pyramidal cell axon emerges from the base of the cell and typically gives rise to extensively ramifying collateral branches which reach other cortical neurons as well as subcortical structures. The pyramidal neurons are excitatory and utilize glutamate as the neurotransmitter. Other nonpyramidal neurons (e.g., basket cells, chandelier cells, etc.) make up the

remainder of the neocortical neuronal population. Most nonpyramidal neurons form local cortical circuits and are inhibitory utilizing  $\gamma$ -aminobutyric acid (GABA) as the neurotransmitter. In addition, there are some excitatory nonpyramidal neurons which also form local cortical circuits (e.g., spiny stellate cells, bipolar cells, etc.) and are primarily found in the primary sensory areas.

The largest number of synapses in the neocortex is formed by pyramidal neurons (Thomson and Deuchars, 1997). Although the cortex has reciprocal input and output connections with subcortical structures (e.g., thalamus), the fraction of cortico-cortical connections are far greater ( $\sim 85\%$  of synapses are cortico-cortical). Axon collaterals of pyramidal neurons form a vast network interconnecting pyramidal neurons via short-range connections. Nonpyramidal local circuit neurons also contribute to the complex network of cortico-cortical connections. In addition, projecting axons from pyramidal neurons form long-range connections between cortical regions both within and across cerebral hemispheres. Although cortico-cortical connections occur between all cortical layers, they are most prominent between pyramidal neurons in the supragranular layers 2 and 3 and to a lesser extent in layer 5 (Gottlieb and Keller, 1997). Despite this massive cortical intraconnectivity, inputs from subcortical structures appear to serve as crucial 'drivers' for the information processed by many cortical regions. Information processing in primary sensory areas depends heavily on visual, auditory, or somatosensory inputs relayed to the cortex via the thalamus ( $\sim 10\%$  of synapses are thalamo-cortical). The thalamus relays input to the cortex from many subcortical sources including motor information from the basal ganglia and cerebellum, limbic pathways, arousal systems, and other higher-order processing systems. The thalamus, in turn, receives major reciprocal projections from the cortex. Various classifications have been described for the laminar distribution of thalamic inputs into nearly all cortical layers (Lorente de Nò, 1938; Macchi, 1983; Herkenham, 1986; Castro-Alamancos and Connors, 1997). However, the most prominent of these projections for primary somatosensory, visual, and auditory processing reach cortical layer 4 and lower parts of layer 3. In addition to thalamic inputs other sources of subcortical projections to the cortex include cholinergic and GABAergic inputs from the basal forebrain, histaminergic inputs from the posterior hypothalamus, dopaminergic inputs from the ventral tegmental area, serotonergic inputs from the raphe nuclei, noradrenergic inputs from the locus ceruleus, as well as various peptides and other modulators.

In summary, cortical layer 1 contains mainly axons and dendrites arising from other layers, layers 2 and 3 contain pyramidal cells projecting mainly to other cortical areas, layer 4 receives dense sensory inputs from specific thalamic relay nuclei, layer 5 projects to the spinal cord, brainstem and basal ganglia, and layer 6 projects in a reciprocal manner to thalamic relay nuclei. Intracortical connections predominate, but cortical inputs and outputs play a crucial role in signal processing. Cortical regions demonstrate different laminar organization based on their functions. Thus primary sensory regions such as the visual, auditory, or somatosensory cortex have a very prominent layer 4, which receives the majority of the sensory input from the thalamus, and a relatively thin layer 5. Primary motor cortex has a thick layer 5, and a sparse layer 4. Association cortex is intermediate in laminar organization between these two extremes.

#### 10.4. MEASURING CHANGES IN CMRO<sub>2</sub> AND $\nu$

As stated earlier, this chapter focuses on our recent studies where quantitative changes in CMRO<sub>2</sub> and  $\nu$  were measured (Smith *et al.*, 2002; Hyder *et al.*, 2002). All methods described below were applied in  $\alpha$ -chloralose-anesthetized rats (Sprague-Dawley; male) and systemic physiologic parameters were monitored and controlled. In these rats the halothane exposure during surgery was minimized ( $< 1$  h). Since halothane has a slow washout (Venkatasubramanian *et al.*, 1996), it is important to exclude the lingering effects of halothane from  $\alpha$ -chloralose (Ueki *et al.*, 1992). The *same* forepaw stimulation (2 mA; 0.3 ms duration, 3 Hz) was applied at high (condition I, light anesthesia) and low (condition II, deep anesthesia) baseline levels where the depth of anesthesia was set by  $\alpha$ -chloralose dosage. The anesthesia dosages for the high

(condition I, light anesthesia) and low (condition II, deep anesthesia) baseline levels were determined from the total amount of  $\alpha$ -chloralose given (i.e., bolus + supplemental doses) over the total time expired during measurement. The light and deep anesthesia levels (i.e., conditions I and II) were achieved with  $\alpha$ -chloralose dosages of  $36 \pm 2$  and  $46 \pm 4$  mg/kg/h, respectively. A 2–5 min stimulation protocol in a block design was repeated a few times (in each baseline condition) with  $\sim 10$  min resting periods. After a stabilization period of  $\sim 1$  h in between light and deep anesthesia levels (i.e., conditions I and II), the data for the deep anesthesia level (i.e., condition II) were collected in a similar manner as in the prior light anesthesia level (i.e., condition I) in the same rats.

The calibrated fMRI experiments, conducted on a 7 T horizontal bore system, were used to calculate  $\Delta\text{CMR}_{\text{O}_2}/\text{CMR}_{\text{O}_2}$  (see Chapter 9). Briefly the method is described as follows. At steady state the fMRI signal change ( $\Delta S/S$ ) is related to the metabolically driven increase in perfusion. Since fMRI has been calibrated over a certain dynamic range for the rat brain (see Chapter 9), multimodal measurements of changes in CBF ( $\Delta \text{CBF}/\text{CBF}$ ) and the fMRI signal ( $\Delta S/S$ ) allow changes in  $\text{CMR}_{\text{O}_2}$  ( $\Delta\text{CMR}_{\text{O}_2}/\text{CMR}_{\text{O}_2}$ ) to be calculated

$$\frac{\Delta\text{CMR}_{\text{O}_2}}{\text{CMR}_{\text{O}_2}} = \frac{\Delta\text{CBF}}{\text{CBF}} - \left( \frac{\Delta S}{S} M^{-1} + \rho \right) \quad (10.1)$$

where  $M$  is measurable physiologic and magnetic constant and  $\rho$  is a small measurable component that is related to changes in blood volume (see Chapter 9). The relationship measured between  $\text{CMR}_{\text{O}_2}$  and CBF (Figure 10.2) shows that  $\Delta\text{CMR}_{\text{O}_2}/\text{CMR}_{\text{O}_2}$  is approximately equal to  $\Delta\text{CBF}/\text{CBF}$  in the rat brain. More importantly the changes are linear over small ranges in activity. The changes in CBF generally exceed changes in  $\text{CMR}_{\text{O}_2}$  for  $\Delta S/S > 0$  (i.e., functional hyperemia, as described in Chapter 9). For both light and deep anesthesia levels (i.e., conditions I and II), activation foci (of  $\Delta\text{CMR}_{\text{O}_2}/\text{CMR}_{\text{O}_2}$ ) were obtained by using the same  $t$ -statistical threshold. A localized region of  $2 \times 2$  voxels in the somatosensory forepaw region (layer 4) was interrogated for both stimulations from light and deep anesthesia levels (i.e., conditions I and II). All electrophysiologic studies were guided by the localization of prior fMRI results (within accuracy of  $\sim 100 \mu\text{m}$ ). The rat was placed prone on a stereotaxic holder. The skull above the contralateral somatosensory forepaw region (4.4 mm lateral and 1.0 mm anterior to bregma) was opened via a small burr hole and high impedance (2–4 M $\Omega$ ) tungsten–iridium microelectrodes (tip  $< 1 \mu\text{m}$ ) were inserted to a depth of cortical layer 4 (Figure 10.3) using stereotaxic manipulators. Prior to digitization, the raw extracellular signals were amplified and filtered. Spiking activity of the neuronal ensemble was extracted from extracellular data by shape recognition of high signal-to-noise ratio (SNR) spikes using typical commercial software. Other details are in Smith *et al.* (2002).

For simplicity in describing the spike analysis procedure as well as the results, the light and deep anesthesia levels are referred to as conditions I and II, respectively, from here on. For data obtained in the baseline period of condition I (light anesthesia), spike analysis was used to create a template of single units, with a maximum of two neurons per electrode (Figure 10.4(A)). This approach allowed identification of some electrical stimulation artifacts (due to inadequate grounding in some rats) in the extracellular data (Figure 10.4(A)), which could then be easily discarded from the spiking activity data. The artifact-free template was then used to extract the spiking activity from the extracellular data (Figure 10.4(B)) such that a temporal history for each experimental run could be created. The spiking data were then converted to reflect the relative spiking frequency of the ensemble ( $\nu$ ) by analyzing consecutive 10 s bins (Figure 10.4(C)). The template created in condition I (light anesthesia) was also used to process the data collected in condition II (deep anesthesia). In all cases an additional template was created from the data in condition II. If the templates in conditions I and II (from the baseline periods only) did not match by the criteria of amplitude ( $\pm 20\%$ ) and shape ( $\pm 0.1$  ms), the data set from that rat was discarded. This approach assured, by the standards specified above, that the spiking data extracted from extracellular data were from the same neuronal ensemble in both conditions (per rat). Since  $\nu$  was measured in both conditions for

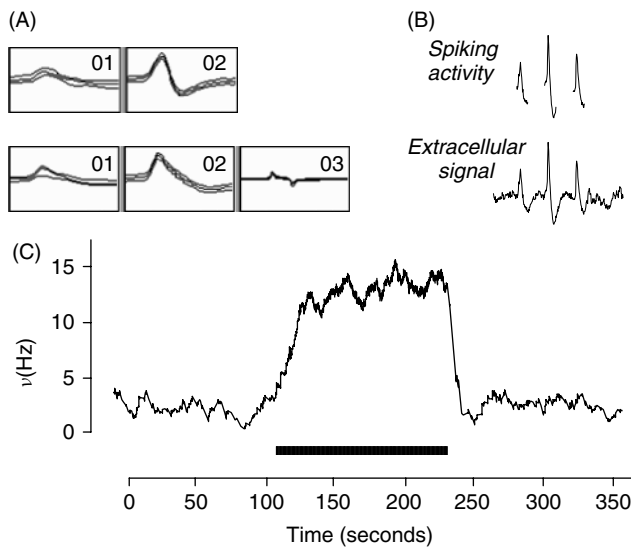


**Figure 10.4.** Measuring neuronal firing in the rat somatosensory cortex. (A) Analysis of extracellular data with commercial spike sorting software (e.g., see Zouridakis and Tam, 2000) was used to create a template of single units. This approach usually provided the recognition of two spike shapes with high SNR per electrode (top trace; spikes 01 and 02) and in some cases allowed the recognition of the stimulus artifact (bottom trace; spike 03). The time window in all spike shapes shown was 1.6 ms. The top and bottom templates were obtained from different rats. (B) The created template was then used to create a temporal history of spiking activity (top trace) extracted from the raw extracellular signal (bottom trace). (C) The spiking activity was then examined in consecutive 10 s bins to reflect the relative spiking frequency of the neuronal ensemble ( $\nu$ ) over the entire experimental run. The thick bar represents the forepaw stimulation period. All data are from rats in condition II. See Smith *et al.* (2002) and Hyder *et al.* (2002) for other details.

each rat, the changes in spiking frequency ( $\Delta\nu/\nu$ ) was used to reflect the behavior of the ensemble for all conditions.

## 10.5. RELATIONSHIP BETWEEN $\text{CMR}_{\text{O}_2}$ AND $\nu$

The stimulation-induced changes in spiking frequency of an ensemble of neurons ( $\nu$ ) were compared to changes in energy use ( $\text{CMR}_{\text{O}_2}$ ) for two different depths of  $\alpha$ -chloralose anesthesia (i.e., conditions I and II for light and deep anesthesia, respectively). Figure 10.5 shows the localized changes in  $\text{CMR}_{\text{O}_2}$  and  $\nu$  from the contralateral cortex during forepaw stimulation, whereas no significant changes were observed in the ipsilateral side (data not shown). In each baseline condition the *same* stimulation was applied, resulting in a total of four activity levels consisting of two baseline and two stimulated conditions. Thus there were three transitions: stimulation-induced increment from baseline of condition I, anesthesia-induced decrement from baseline of conditions I to baseline of condition II, and stimulation-induced increment from baseline of condition II.

In the same rat, the *same* forepaw stimulation induced different increments in  $\text{CMR}_{\text{O}_2}$  (by  $\sim 40\%$  and  $\sim 100\%$ ) from the baselines of conditions I and II (Figure 10.6). The *same* stimulation increased the contralateral values of  $\nu$  by similar magnitudes ( $\sim 30\%$  and  $\sim 100\%$ ), in good agreement with the changes in  $\text{CMR}_{\text{O}_2}$  (Figure 10.6). There was also a transition between baselines of conditions I and II, a decrement of  $\sim 30\%$  in both  $\text{CMR}_{\text{O}_2}$  and  $\nu$  (Figure 10.6). Increments in both  $\text{CMR}_{\text{O}_2}$  and  $\nu$  were greater

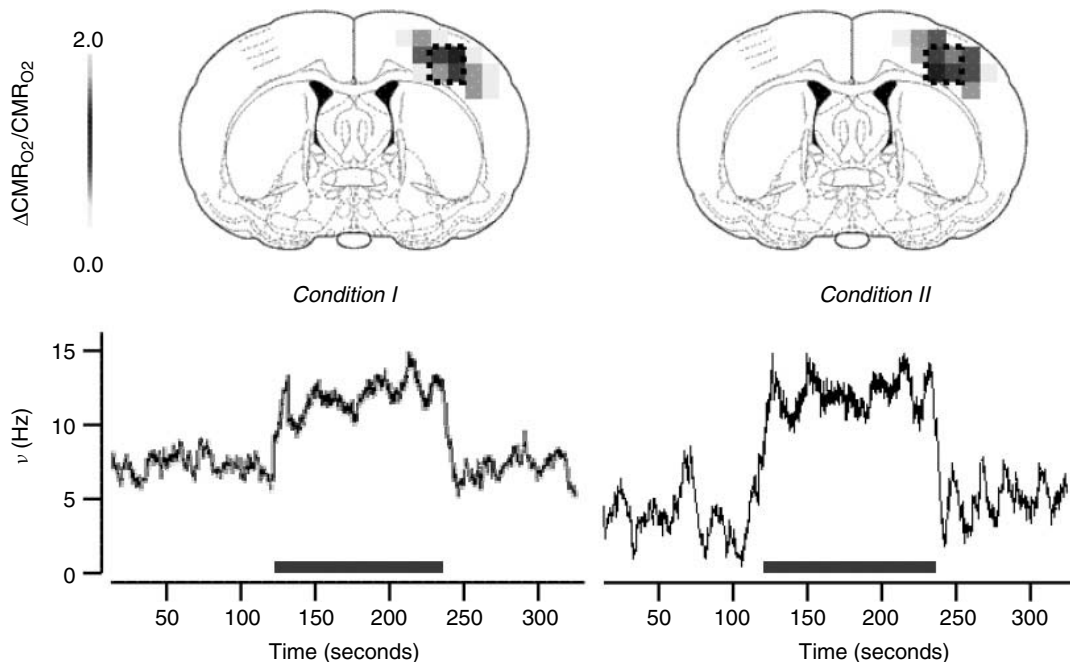


**Figure 10.5.** Localized changes in energy metabolism ( $\text{CMR}_{\text{O}_2}$ ) and spiking frequency ( $v$ ) of a neuronal ensemble. In each case, the fMRI and electrophysiology measurements were made in each rat first under high basal activity (condition I; left) then under low basal activity (condition II; right), using two different doses of  $\alpha$ -chloralose. The  $\Delta\text{CMR}_{\text{O}_2}/\text{CMR}_{\text{O}_2}$  maps (overlaid on stereotaxic coordinates from Paxinos and Watson, 1997) were determined from calibrated fMRI (see Chapter 9), whereas the  $\Delta v/v$  values were extracted from extracellular recordings (see Figure 10.4). Approximately 92 % of all microelectrode penetrations (in layer 4) identified at least two discrete neurons from the spike analysis (see Figure 10.4). No significant stimulation-induced changes in  $v$  and  $\text{CMR}_{\text{O}_2}$  were observed in the ipsilateral side (data not shown). All data adapted from Smith *et al.* (2002) and Hyder *et al.* (2002).

from baseline of condition II than from baseline of condition I. These measured changes in  $\text{CMR}_{\text{O}_2}$  and  $v$  compare well with prior studies from other laboratories. First, the localized signals detected in these anesthetized studies should not be an issue of controversy because it is accepted that the stimulation-induced increments in somatosensory cortical activity (e.g., as measured by changes in  $\text{CMR}_{\text{glc}}$  and CBF) in anesthetized animals provide localization of columnar units which agree with spatial activation patterns in nonanesthetized animals (Sokoloff, 1991). Second, it is well known that both neuronal activity and energetics are decreased with various anesthetics (e.g., halothane,  $\alpha$ -chloralose, phenobarbital) in a dose-dependent manner (Savaki *et al.*, 1981; Dudley *et al.*, 1982; Hodes *et al.*, 1985). Third, magnitudes of stimulation-induced increments are anesthesia dependent (Harding *et al.*, 1979; Bonvento *et al.*, 1994; Shulman *et al.*, 1999).

When each stimulation-induced increment (in both  $\text{CMR}_{\text{O}_2}$  and  $v$ ) from conditions I and II (i.e., light and deep anesthesia levels) was added to the respective baseline value, approximately similar total values for conditions I and II were reached (Figure 10.7(A) and (B)). The data shown in Figure 10.7(C) were normalized to the nonstimulated (values of  $\text{CMR}_{\text{O}_2}$  and  $v$  in) baseline of condition I. The increments of  $\text{CMR}_{\text{O}_2}$  and  $v$  upon forepaw stimulation elevated each signal to the same final values in both conditions, in agreement with previous suggestions from the literature (for a review see Shulman *et al.*, 1999). The current results show that  $\Delta v/v$  is approximately equal to  $\Delta\text{CMR}_{\text{O}_2}/\text{CMR}_{\text{O}_2}$ , which is in agreement with

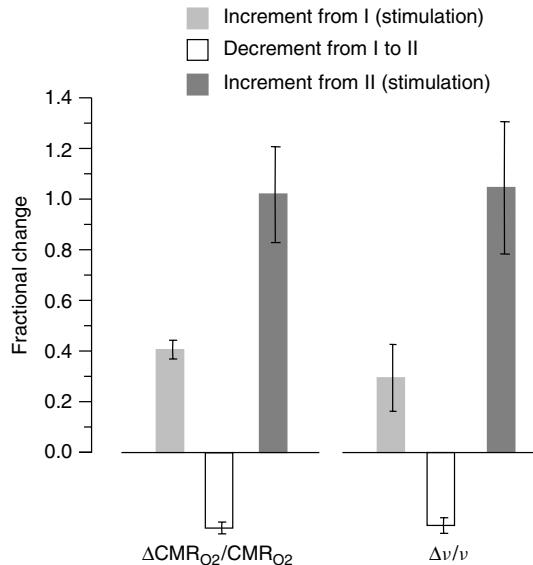


**Figure 10.6.** Relationship between energy use ( $\Delta \text{CMR}_{\text{O}_2}/\text{CMR}_{\text{O}_2}$ ) and spiking frequency ( $\Delta v/v$ ) of a neuronal ensemble. All rats were anesthetized with  $\alpha$ -chloralose, where the baseline was changed by the dosage level. The filled bars represent stimulation-induced incremental changes in  $\text{CMR}_{\text{O}_2}$  and  $v$  from baseline of condition I (light gray) and baseline of condition II (dark gray) in the same rats for each method. The open bars represent the decrement of baseline from condition I to II. The incremental change upon stimulation from baseline of condition II was larger. The  $\Delta\text{CMR}_{\text{O}_2}/\text{CMR}_{\text{O}_2}$  values were obtained from a total of 24 voxels (from all rats;  $n = 6$ ) placed over the forelimb region (other activated voxels were not analyzed). The  $\Delta v/v$  values were obtained from extracellular recordings of a total of 72 neurons in layer 4 of the forelimb region (from all rats;  $n = 36$ ). The  $\sim 1:1$  relation between  $\Delta\text{CMR}_{\text{O}_2}/\text{CMR}_{\text{O}_2}$  and  $\Delta v/v$  agrees with results from Chapter 5. All data adapted from Smith *et al.* (2002) and Hyder *et al.* (2002).

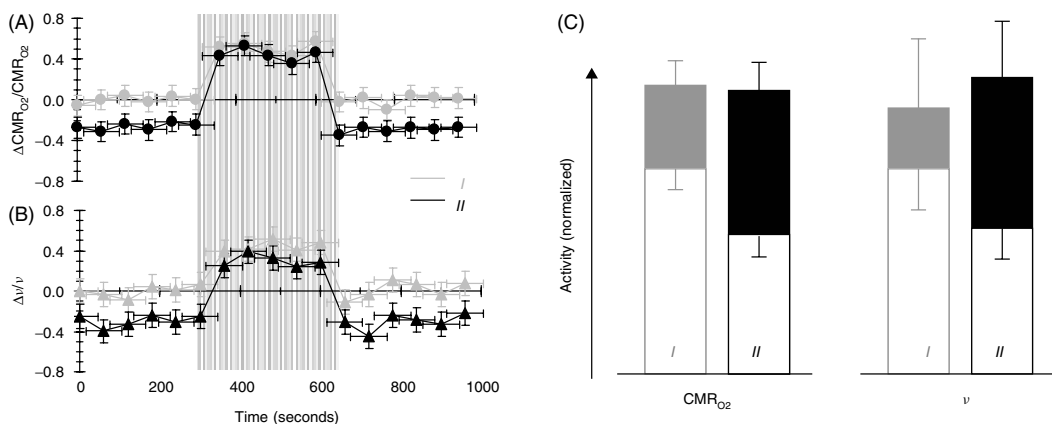


**Figure 10.7.** Absolute changes in changes in energy metabolism ( $\text{CMR}_{\text{O}_2}$ ) and spiking frequency ( $v$ ) of a neuronal ensemble. The temporal changes in (A)  $\text{CMR}_{\text{O}_2}$  and (B)  $v$  are shown relative to the baseline of condition I, where the stimulation duration is shown by the vertical lines. (C) While the increments (filled) of  $\text{CMR}_{\text{O}_2}$  and  $v$  were different in conditions I (gray) and II (black), the same total activity levels were reached upon stimulation, where the size of the increment was dependent on the baseline level (open). See Figure 10.6 for support and significance because the incremental changes (filled) can be directly compared. All data adapted from Smith *et al.* (2002) and Hyder *et al.* (2002).

linear relationships between  $\text{CMR}_{\text{glc}}$  and  $\nu$  in peripheral neurons (see Chapter 2) and  $\text{CMR}_{\text{O}_2}$  and  $V_{\text{cyc}}$  in cortical neurons (see Chapter 5). Therefore the combined results suggest

$$\frac{\Delta \text{CMR}_{\text{O}_2}}{\text{CMR}_{\text{O}_2}} \approx \frac{\Delta V_{\text{cyc}}}{V_{\text{cyc}}} \approx \frac{\Delta \nu}{\nu} \quad (10.2)$$

which means that both electrical ( $\nu$ ) and chemical ( $V_{\text{cyc}}$ ) activities of glutamatergic neurotransmission are proportional to the oxidative energy consumed ( $\text{CMR}_{\text{O}_2}$ ). Thus neurotransmission (i.e., work done) is directly coupled to neuroenergetics (i.e., energy consumed). Because the term ‘work’ is defined here as the sum of the energy consuming events associated with neuronal activity, energy connects electrical and chemical aspects of neural work (Shulman *et al.*, 2002).

## 10.6. COMPARISON WITH PREVIOUS STUDIES

An unavoidable and obvious outcome of this type of multimodal experiment with fMRI and electrophysiology is that there are consequences for the neurophysiologic interpretation of fMRI. The correlations that have been observed between fMRI and electrical signals from neurons are based on features of either matching temporal dynamics or generating spatial overlaps (Yang *et al.*, 1997; Brinker *et al.*, 1999; Ogawa *et al.*, 2000; Rees *et al.*, 2000; Logothetis *et al.*, 2001). Despite large disparities in temporal dynamics as well as the inherent ambiguities about spatial resolution of the signals, these correlations only confirm that one event is in spatial proximity with the other. Since each signal depends upon varying dynamics, any conclusion beyond the spatial anchoring of the two signals would lack biophysical foundations. The ease of finding temporal and/or spatial correlates, depending upon vague properties, in part explains why a quantitative relationship between fMRI and electrical signals (as measured by EEG, SEP, LFP, SUA, MUA, and  $\nu$ ) has been rather controversial (see below). These correlations, however, do not account for the grouped activity of an ensemble of neurons in the voxel. Why? Because an fMRI signal even from a small voxel of  $0.001 \mu\text{l}$ , which is the highest resolution achieved (see Chapter 9), contains thousands of cortical neurons. Despite these limitations of phenomenological correlations, we discuss a few studies in detail because the results which have apparently been accepted, despite the absence of convincing mechanisms, are having major impacts on the neurophysiologic basis and interpretation of fMRI.

Logothetis *et al.* (2001), working on the primary visual cortex of anesthetized primates, concluded that changes in the fMRI signal represent neuronal input because they observed a higher correlation between time courses of the fMRI signal (a response delayed response by several seconds following the stimulus onset) and the LFP signal (an almost instantaneous response following the stimulus onset). The LFP signals are believed to reflect mainly the neuronal input because they represent the weighted sum of changing membrane potentials in the dendritic branches and the soma as a consequence of spiking from neighboring neurons. Since input and output signals are not entirely distinct in a neuronal ensemble especially in layers 4 and 5 (i.e., site of the electrical measurements) where the nonpyramidal neurons form numerous cortico-cortical synapses (Figure 10.3), it seems premature to link the fMRI signal to either the input or output of the system simply due to a better temporal correlation. Furthermore the slightly worse correlation between the time courses of SUA (or MUA) and fMRI signals could in part be attributed to the higher SNR of LFP signals. Rees *et al.* (2000) tried to relate the stimulation-induced increment in the fMRI signal in humans with changes in  $\nu$  measured in non-human primates. Despite concerns about cross-species comparison of signals from two entirely different modalities, they suggested that a  $\sim 1\%$  change in the fMRI signal (at 1.5 T in humans) corresponds to  $\sim 9$  Hz change in the  $\nu$  per neuron in region V5 of the non-human primate visual cortex. Thus they concluded that the fMRI signal magnitude is better correlated with the spiking activity (i.e., the neuronal output), in direct contrast to the conclusion of Logothetis and colleagues. Similarly other studies have shown that the magnitude of the fMRI signal change correlates

well with SEP (Brinker *et al.*, 1999) and the evoked EEG (Ogawa *et al.*, 2000) signals. Since the origin of different electrical signals measured is quite varied, which correlation between the fMRI signal and neuronal activity is to be trusted? However, Ogawa *et al.* (2000) report an approach by which ‘some type of’ stimulation-induced neuronal events can be probed by fMRI signal with temporal resolution in scale of tens of ms. A dual-stimulation paradigm (e.g., bilateral forepaw stimulation separated by a delay), which generates distinct localized activations, shows that the response due to the first (contralateral forepaw) stimulation as measured by EEG or fMRI is affected by the delayed second (ipsilateral forepaw) stimulation. While a ‘refractory’ period of ~40 ms was measured for the rat forepaw stimulation model, in the human visual cortex the measured ‘refractory’ period was ~100 ms. Despite the unknown origins of this type of interaction from two neuronal events occurring at the same cortical site, this approach has received some attention perhaps due to the fact that ‘by controlling the temporal relation of input tasks it is possible to study temporal evolution of certain neural events at the time scale of their evoked electrical activity by noninvasive fMRI methodology.’ Inter-hemispheric connections (McKenna *et al.*, 1981) may in part explain this type of interaction and interactions from these dual-stimulation paradigms, which depend upon delays that reflect complex brain activity, may provide some insight into the neurophysiological basis of fMRI.

The term ‘neuronal activity’ has been applied to a host of energy requiring processes including action potential generation and propagation, maintenance of resting potentials, neurotransmitter release and uptake, vesicular recycling, and pre-synaptic Ca<sup>2+</sup> currents (see Chapter 7). All of these processes are involved in short- and long-term signal encoding. In glutamatergic synapses of the mammalian brain, an ‘excited’ neuron generates short-lived (1–2 ms) action potentials which propagate (scale of μm) down the axon to initiate Ca<sup>2+</sup>-triggered glutamate neurotransmitter release via exocytosis of vesicles from the pre-synaptic neuron. The release of glutamate into the extracellular space produces dendritic field potentials in nearby post-synaptic neurons that can integrate over time (10–20 ms) and space (scale of mm) to generate new trains of spikes. The astrocytic uptake of glutamate and its recycling to the pre-synaptic neuron is another critical energy consuming step in neurotransmission. These processes in glutamatergic neurons, as well as associated ion conductivity in glia and GABAergic neurons, all require energy because active Na<sup>+</sup>–K<sup>+</sup> pumps utilize ATP to restore Na<sup>+</sup> and K<sup>+</sup> concentrations across the cell membrane (Figure 10.1(B)).

Do brain cells utilize energy by an amount equal to the degree of work done? If so, then energy can be defined as the capability of doing work – a fundamental biophysical principle (Garby and Larsen, 1995). In our study spiking frequency of a neuronal ensemble ( $\nu$ ) was used as a reliable and quantifiable measure of brain work. Likewise, calibrated fMRI was used to measure changes in energy utilization (CMR<sub>O<sub>2</sub></sub>). The results showed that change in energy utilization ( $\Delta\text{CMR}_{\text{O}_2}/\text{CMR}_{\text{O}_2}$ ) was approximately equal to change in work done by the neuronal ensemble ( $\Delta\nu/\nu$ ). The relationship found in this study between changes in CMR<sub>O<sub>2</sub></sub> and  $\nu$  (Figures 10.5–10.7) has the advantage over previous studies of not depending upon complex electrophysiological (e.g., electrode impedance, filtering process) or fMRI (e.g., field strength, pulse sequence) parameters. These issues were effectively normalized by the fMRI calibration and validation (see Chapter 9), detecting the *same* neuronal ensemble for the entire experiment (in the same rat), and by using the *same* stimulation for both baseline conditions (in the same rat). Hence the fMRI signal change (i.e.,  $\Delta S/S$  in Equation (10.1)) when calibrated to provide  $\Delta\text{CMR}_{\text{O}_2}/\text{CMR}_{\text{O}_2}$ , allows a quantitative relationship between energy consumption and the rate of spiking activity (Figure 10.6). This offers a biophysical relation between the neuroimaging signal and a basic measurement of neuronal activity, which agrees with the relationship between CMR<sub>O<sub>2</sub></sub> and  $V_{\text{cyc}}$  obtained from <sup>13</sup>C MRS studies (Equation (10.2)).

The apparent paradox of a range of energy consuming processes being proportional to a single electrical activity may be resolved if these processes are all coupled to the averaged rate of the electrical activity, which in this case is the firing of an ensemble of pyramidal neurons. This coupling has been proposed by

Laughlin (2001) who calculated the distribution of energy amongst the different processes (see Chapter 7). The results suggest that most of the energy associated with signaling in the mammalian cortex is coupled to the ensemble firing rate of pyramidal neurons. The calculations show that at a resting spiking rate of 4 Hz (per neuron) more than 80 % of the total ATP is utilized for functional processes coupled to glutamate release, most of which is used for restoring ion gradients. While the efficient use of energy at rest is in good agreement with previous  $^{13}\text{C}$  MRS measurements (see Chapter 5), the proportionality between energy use and work done (i.e., Equation (10.2)) supports the view that the brain spends most of its resources to reestablish ionic gradients so that neurons are ready to fire whenever necessary. These energy budget estimations by Laughlin (2001), relying on morphologic and functional data of rat brain, stand in contrast to previous estimates by Creutzfeldt (1975) which were based on data obtained from the giant squid axon inappropriately extended to the mammalian brain.

## 10.7. REDEPLOYMENT OF SPIKING FREQUENCY DISTRIBUTIONS

In our study, values of  $\Delta\nu/\nu$  were determined from extracellular recordings and compared with  $\Delta\text{CMR}_{\text{O}_2}/\text{CMR}_{\text{O}_2}$  from calibrated fMRI of the same voxels (Figures 10.5–10.7). Predominantly pyramidal neurons were measured in each rat. Since more than 90 % of all microelectrode penetrations yielded at least two discrete and recognizable neurons, multiple electrode measurements provided a reasonable activity estimate of the entire neuronal ensemble ( $n = 72$ ). The histograms of  $\nu$  for all four conditions (Figure 10.8(A) and (B)) show that during stimulation the distributions became similar. Statistically significant increases and decreases in  $\nu$  were observed upon stimulation in  $\sim 60\%$  and  $\sim 10\%$  of the recordings (in condition II), respectively, whereas in the remaining population no significant changes were observed (Figure 10.8(C)). Although similar behaviors of neuronal ensembles in the cortex have been reported previously (McCasland and Woolsey, 1988; Scannell and Young, 1999), the quantitative redeployment of the *same* ensemble for different sensory workloads (i.e., stimuli) provides novel insights for understanding the relationship between neuronal activity and energetics.

The coarser spatial scale of fMRI (in sub  $\mu\text{l}$  range) relative to the electrical recordings (in sub  $\text{nl}$  range) necessitated comparison of  $\Delta\text{CMR}_{\text{O}_2}/\text{CMR}_{\text{O}_2}$  (derived from calibrated MRI) with the averaged firing rate of a neuronal ensemble. Extracellular recordings respond to the activity of a small group of neurons in the vicinity of the electrode tip. Action potentials are easily identifiable signals *in vivo* because they are short lived, have relatively high SNR, and their different spike shapes can be assigned to individual neurons. Thus spike sorting from extracellular data (Zouridakis and Tam, 2000) have regional specificity to a few spiking neurons near the microelectrode tip located at layer 4 of the rat cortex in an activated region (guided by prior fMRI results). The spiking rate did not always increase with stimulation (Figure 10.8(C)). The nature of the ‘perturb and detect’ philosophy (e.g., see Kandel *et al.*, 1991) usually biases experimentalists to focus on the population that showed an increase in  $\nu$  upon stimulation onset. The criterion that allowed the inclusion of neuronal templates into the distributions (Figure 10.8(A) and (B)) was *not* whether the neuron responded to the stimulus or not, rather the condition was high SNR spikes. This approach revealed that a significant fraction of the population (i.e.,  $\sim 30\%$  in condition II) preferentially did not respond to the stimulus. These results suggest that collaboration amongst a large number of neurons – some of which are firing faster and others slower, but *all* requiring energy – is crucial for encoding information in the cerebral cortex (for a recent review see Scannell and Young, 1999).

Since the spiking frequency distribution represents the different neurons in an ensemble, the changing of this distribution (Figure 10.8(A) and (B)) in conjunction with change in the total energy use (Figure 10.7(C)) symbolizes quantitative redeployment of the work by the ensemble. From a biophysical perspective, work is energy and *vice versa* (Garby and Larsen, 1995). Therefore the neuronal response of the ensemble at different workloads, which is depicted by the spiking frequency distributions in Figure 10.8(A)

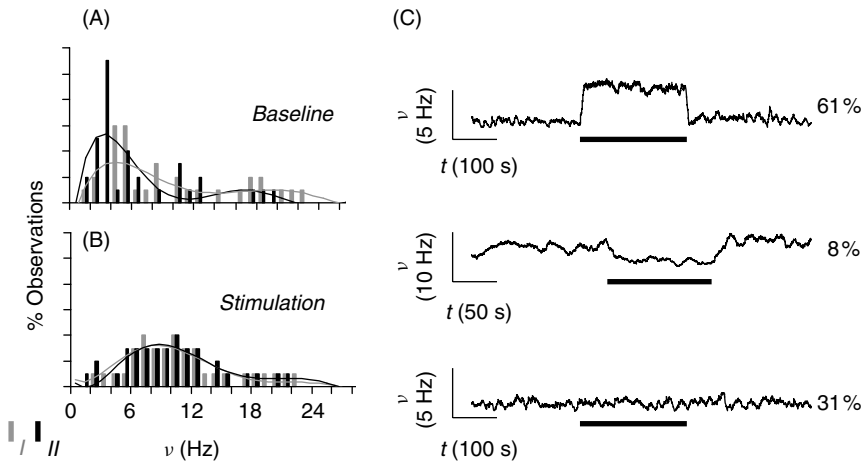


**Figure 10.8.** Neural activity patterns of an ensemble. The neuronal activity patterns, as reflected by spiking frequency ( $v$ ), of a small ensemble (72 neurons) from the rat somatosensory cortex in  $\alpha$ -chloralose-anesthetized rats for four different conditions: (A) two baseline conditions and (B) two stimulated conditions. Each bar in the histogram represents averaged value of  $v$  for the baseline and stimulated conditions. The data for conditions I and II are shown in gray and black, respectively. There is a significant difference between spiking frequency distributions in the two baseline conditions ( $p < 0.01$ ), whereas upon stimulation the spiking frequency distributions become similar ( $p > 0.25$ ). (C) Experimental variations across electrophysiological measurements (shown for condition II only) from the contralateral forelimb region. Significant increases and decreases in  $v$  were observed in 61 % and 8 % of the recordings, respectively (top and middle traces, respectively), whereas in 31 % of the recordings the stimulation did not induce any significant changes in  $v$  (bottom trace). The vertical and horizontal bars represent the scales for  $v$  (in Hz) and time (in s), respectively. The thick black horizontal black bar represents the duration of the stimulus. All data adapted from Smith *et al.* (2002) and Hyder *et al.* (2002).

and (B), is commensurate with the total energies in each case (Figure 10.7(C)). The baseline comparison in Figure 10.8(A) shows that in condition II (deep anesthesia) the frequencies are lower than in condition I (light anesthesia), with a population at very low frequencies making a significant contribution to the difference. In accordance with the similar total energies during stimulation from both baselines (Figure 10.7(C)), the histograms in Figure 10.8(B) show that not only do the average frequencies of the two states agree, but that the two distributions are very similar. This similar distribution has been reached by redeployment, not recruitment, of many neurons in the ensemble (Hyder *et al.*, 2002). As shown in Figure 10.8(C) a large majority of neurons change their firing rate upon stimulation – most increase the rate while a non-negligible minority either decrease or do not appear to change their rates. The data clearly demonstrate that the changes in total energy (Figure 10.7(C)) are affected by widespread changes in neuronal firing patterns of the ensemble (Figure 10.8(A) and (B)).

## 10.8. IMPLICATIONS FOR INTERPRETATION OF fMRI

For technical reasons neuroimaging methods generally measure increments in local brain activity (for a review see Shulman *et al.*, 2002). The ease of measuring incremental activity by functional imaging methods (with PET or fMRI) has been consonant with the widespread view in cognitive neuroscience that increments represent the modular energy required for function (Figure 10.9). Therefore the pertinent question is, does a cortical region require *total* or *incremental* neuronal activity for processing sensory information? If increments in CMRO<sub>2</sub> and  $v$  provide sufficient support for the neural activity processing the sensory

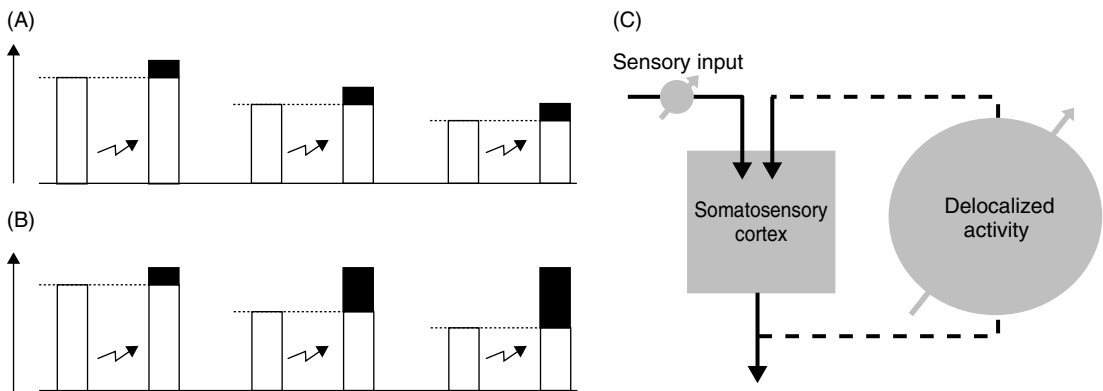


**Figure 10.9.** A model of total neural activity to support cerebral function. Two possible scenarios of nonstimulated baseline (white) and stimulation-induced incremental (black) activities are shown in (A) and (B) respectively (Shulman *et al.*, 1999; 2002). The jagged and vertical arrows represent the stimulation (same stimulus in all cases) and experimental parameters of neuronal activity are plotted vertically (same scale in all cases). (A) The stimulation induces the same increment in all cases independent of the baseline activity. In this case only the incremental activity contributes to information encoding. (B) The stimulation induces an increment which depends on the baseline, being larger from a lower baseline activity level. Here the *total* activity (i.e., baseline activity + incremental activity) is required for information encoding. (C) The microelectrode placement in layer 4 of the rat somatosensory cortex allowed measurement of the output from major excitatory efferents in the somatosensory cortex, i.e., the large pyramidal cells, which depend on connections from the thalamus (sensory input) as well as other regions of the cortex (delocalized activity). See Figure 10.3 for additional details about connections to and from layer 4. While the sensory input is the main choice of an experimental parameter to vary in neuroscientific studies, the delocalized activity can also be modified (e.g., by anesthesia dosage). The sum of the sensory and delocalized inputs, therefore, can modulate the *total* activity in a somatosensory region (Shulman *et al.*, 2003). Future experiments in measuring either or both of these connections to the activated region in the cerebral cortex in greater detail (i.e., across different layers of the cortex) will provide greater insight into the interplay of population voting amongst the neuronal ensemble in sensing a particular stimulus.

stimulation, then these increments should be independent of the basal activity level (Figure 10.9(A)). This would allow the discard of the ‘baseline’ signal because the signal would not contribute to sensing of the stimulation. Alternatively, if the neuronal activity requires particular magnitudes of  $\text{CMR}_{\text{O}_2}$  and  $\nu$ , then their increments should be larger from deeper anesthesia (Figure 10.9(B)). In this case, however, the large and important ‘baseline’ signal cannot be discarded. The current results (Figure 10.7(C)) support the view that *total* activity is required for sensory processing. These results are in agreement with a survey from the literature comprising of  $\text{CMR}_{\text{glc}}$  and spiking activity data (Shulman *et al.*, 1999; 2002), which revealed that for sensory stimulus, the deeper the anesthesia the larger the increment, leading to the suggestion that the total energy rather than the increment was needed for function. To respond to the stimulus, the energy is raised from nonstimulated anesthetized levels to a total energy above or near the nonstimulated awake levels. The high levels of activity required for function have been supported by the present results, under the more reliable conditions of same animal, same stimulation, and the same anesthetic at different doses. Using energy as the measure of neuronal activity, the size of stimulus-induced incremental activity in awake human experiments is smaller than the basal activity (Shulman *et al.*, 1999; 2002). In anesthetized animals the sizes of incremental and basal activities depend on depth of anesthesia and can be quite large (e.g., compare conditions I and II in Figure 10.7(C)). Therefore focus on only the magnitude of incremental activity neglects contributions of the basal activity, which can be misleading for interpretation of fMRI.

Since the total activity in a neuroimaging voxel represents the integrated signal from proximal and distal neurons (Braitenberg and Schuz, 1991; Shepherd, 1994), the remote or delocalized neuronal connections from the rest of the brain can contribute to measures of total activity (Figure 10.9(C)). The total neuronal activity, which arises from both local and distal neurons, is reduced by anesthesia (Ueki *et al.*, 1988; Hyder *et al.*, 1996) both inside and outside the somatosensory region. However, upon stimulation the total neuronal activity inside the region of interest becomes high, and comparable to the activity at rest in the nonanesthetized awake condition (Shulman *et al.*, 1999; 2002), whereas the total neuronal activity outside the stimulated region remains low (Ueki *et al.*, 1992; Hyder *et al.*, 1997). Thus forepaw stimulation introduces additional neuronal activity to the low baseline activity in the somatosensory cortex. However, in a nonanesthetized functional experiment the situation is slightly different. In the nonanesthetized awake brain at rest (Sokoloff *et al.*, 1977), the forepaw stimulation may introduce a smaller additional neuronal activity thereby raising the total activity only slightly above the nonanesthetized awake resting state (Shulman *et al.*, 1999; 2002). In this case, however, the fractional increase in the signal would be smaller. This type of interplay between contributions from proximal and distal neuronal connections may provide novel interpretation for fMRI as well as for brain organization (Changeux, 1985; Dehaene *et al.*, 1998; Shulman *et al.*, 2003). Although the measured neural activity in a somatosensory cortical site depends on the stimulation-induced sensory input (e.g., forepaw stimulation), the measured signal also depends on the delocalized signals from other regions of the brain (Figure 10.9(C)). Because the delocalized signals interact with the sensory input signals, the *total* measured signal in a region may potentially reveal insights into subjective experience (see Chapter 16).

Because the baseline activity measured from layer 4 in the current studies (Figure 10.8(A)) also consists of signals from proximal and distal neurons (Braitenberg and Schuz, 1991; Shepherd, 1994), the large baseline activity (Figure 10.7(C)) could therefore be identified as input from and connections to other neurons including those in regions of the ‘global workspace’ (Dehaene *et al.*, 1998). The widespread decrease of baseline activity in the anesthetized state must produce a decrease in global activity. Since anesthesia induces slow axonal conduction of most neurons (Richard, 1998), the reduction of global activity is consistent with the state of depressed activity during nonstimulated anesthetized states. Because the rest of the brain does not respond to forepaw stimulation and remains at low anesthetized activity (Ueki *et al.*, 1988, 1992; Hyder *et al.*, 1996, 1997), we propose that connections with the ‘global workspace’ are reduced during forepaw stimulation in the  $\alpha$ -chloralose-anesthetized state. Furthermore under these anesthetized conditions, the localized total neuronal activity in the somatosensory cortex must include sizeable contributions from the vigorous sensory input. Thus total activities, as measured by experiments shown in Figures 10.5–10.8, provide quantitative measures that will help separate local from global responses.

## 10.9. BIOPHYSICAL BASIS OF COGNITIVE NEUROSCIENCE

Cognitive neuroscientists use fMRI to create activation maps so that a ‘horizontal’ atlas can be created which can help locate regions of increased activity induced by specific sensory and psychological stimuli (Gazzaniga, 2000). This approach requires the subtraction of an important and required baseline activity, which as discussed above, removes an important part of the total activity that is required for cerebral function. What about the degree by which neuronal activity has changed? The current results (Figures 10.5–10.8) have allowed the quantification of ‘vertical’ maps which can help provide information about the degree of neuronal activity changes induced by the stimuli. Because calibrated fMRI derives the fundamental parameter of neural energy (i.e., CMRO<sub>2</sub>) which in turn emulates neuronal work (i.e.,  $v$ ), the total activity can be mapped noninvasively.

In cases where the baseline is well defined (e.g., sensory stimulation), differencing can localize responses with great validity and reliability based upon correlations with electrophysiological measures (e.g., SUA,

MUA, or LFP). Cognitive modalities are difficult to correlate, however, mainly due to the ambiguous definition of baseline in most tasks. There is little doubt, however, that differencing signals appropriately localize changes in some activities and the present results do not contradict these localizations (Posner and Raichle, 1998). However, meaningfulness of only using increments and discarding the important baseline signal is questioned (Shulman and Rothman, 1998) by the present results. The current findings challenge cognitive neuroscience studies, where it is generally assumed that incremental activity alone is responsible for signal processing. Therefore we propose that the goal of neuroimaging methods should be to measure *both* baseline and incremental signals in a quantitative manner (Hyder *et al.*, 2002; Shulman *et al.*, 2002). Although  $^{13}\text{C}$  MRS methods can provide quantitative estimates of both signals (see Chapters 5 and 6) which represent activities of a very large and heterogeneous population of neurons, calibrated fMRI (see Chapter 9), which represents the grouped activity of the neuronal ensemble in the voxel (Figures 10.5–10.8), can be used to provide much higher spatial and temporal resolutions.

Within the precision of the present measurements in which energy consumption and firing rates increase proportionately, there are significant contributions to the energy from quiescent neurons. Since about one third of the population (for condition II) did not respond to the stimulus (Figure 10.8(C)), the incremental energies during stimulation represent the distributed voting choices of the population of neurons (Figure 10.8(A) and (B)). The histograms of firing rates depict the redeployment of the same neurons as a function of stimulated and nonstimulated conditions. While this redistribution of the population voting is measured as an increment by neuroimaging techniques (with PET or fMRI), the *total* energies of the neuronal population (Figures 10.7(C) and 10.9(B)) in the different conditions represent integrated activities of the populations, and the increments represent their shifts. The increment is only conceptually separable from the total activity by comparing total population activities in the different conditions.

The neurons in an ensemble – with an averaged spiking frequency – when redeployed by different stimuli can be reflected by changes in the spiking frequencies (i.e., the neuroimaging signal can increase, decrease, or remain unchanged). However, at this time the variations in neuronal firing patterns upon stimulation do not provide an understanding of the single neuron's contributions to the entire ensemble, because we do not know exactly why the frequency of a specific neuron increases while for another it decreases. We can conclude, however, that the neurons that have been sampled within the somatosensory cortex are part of a local network of neurons which by anatomical necessity change their functional workload during forepaw stimulation (Harding *et al.*, 1979). While distributions of firing rates during nonstimulated conditions vary, the distributions of firing rates during a particular stimulation in these limited experiments seem to be characteristic of that state, thus allowing the possibility that a particular population is a consequence of the same total energy being required during a particular stimulation, regardless of the starting baseline activity.

## 10.10. FUTURE DIRECTIONS

While the collective activity of an ensemble of neural cells helps maintain normal cerebral function, glucose oxidation provides most of the energy needed for work (Siesjo, 1978). The term 'work' is defined here as the sum of energy consuming processes associated with neuronal activity. The energetic demands of cellular work are extremely high (Chapter 7). Furthermore the localized changes, induced by depths of anesthesia and/or stimulations, of  $\text{CMR}_{\text{O}_2}$  and  $\nu$  in layer 4 of the somatosensory cortex were proportional (Figures 10.5–10.8). The ensemble activity in layer 4 depends on both the sensory input by the thalamus and the global input from other cortical regions. If sensory and delocalized inputs to total activity are defined as task and baseline portions of the neuroimaging signal, then the current experimental results (Figures 10.5–10.8) have measured the total activity and have begun to separate sensory and delocalized contributions (Figure 10.9). Because delocalized signals (e.g., modified by anesthetic parameters) interact with the sensory inputs (e.g., modified by stimuli parameters), the *total* measured signal in a region may potentially reveal insights into the subjective experiences (Chapter 16).

Since the activities that we have measured (Figures 10.5–10.8) arise from layer 4 neurons in response to specific anesthetics and stimuli, we need far more detailed characterization of sensory and delocalized inputs of total activity from other cortical layers and regions. In the future, detailed studies of neuronal populations in nonhuman primate models (Desimone, 1996; Goldman-Rakic, 1996; Tanaka, 1996; Georgopoulos, 2000; Logothetis, 2000; Rolls, 2000) will be needed for extensions to cognitive function in the awake human brain. Additional rat experiments are also needed in the future because the contributions of individual neurons in the voting population need to be evaluated more elaborately during stimulated and nonstimulated conditions for different experimental settings and/or paradigms. There are basically three experimental parameters that are flexible in these types of anesthetized rat experiments; we can decrease the anesthesia level; we can change the stimulation; we can change the cortical depth of microelectrode penetration. By manipulation of these parameters in anesthetized rat experiments we would be able to extend the current results so that the total measured activity can be represented in terms of sensory and delocalized signaling. The first goal would be to test whether the same total activity is reached during stimulation with different anesthetics (e.g., urethane, pentobarbital, propofol, halothane) at varying doses. In addition a necessary test would be whether altering the sensory stimuli (e.g., different frequencies and amplitudes) results in similar levels of activity from different baselines. While multiple microelectrode penetrations in an array-form (e.g., 12 × 12) to probe simultaneous activity of an ensemble (Szabo *et al.*, 2001; Jog *et al.*, 2002) is an option (Chicurel, 2001) for these future studies, this approach samples too few cells (e.g., less than a hundred) across very large regions (e.g., several millimeters), and most importantly it is much more invasive a process than penetration of a single microelectrode. Instead, sampling the electrical signals from multiple layers simultaneously with tetrodes (Gray *et al.*, 1995; Hetherington and Swindale, 1999) that are vertically oriented may be a better option, although these electrodes would require careful development for these specific applications.

There is, of course, the appeal for measuring neuroimaging signals with very high temporal resolution with the expectation that the fast signals will reveal new insights into brain function (Llinas, 2002). To this end, however, new technologies combining high field fMRI with electrophysiology and/or optical imaging would play important roles. But these studies would be better suited for animal models. A much needed future research direction, however, is to test these proposals from the animal experiments on humans. Previous PET measurements in humans have reported that CMR<sub>glc</sub> decreases with depth of anesthesia (for a recent review see Heinke and Schwarzbauer, 2002). Although these reductions are global, small regional differences are also detected. Depression of glucose CMR<sub>glc</sub> (e.g., with isoflurane, halothane, and propofol) to the level of unresponsiveness (Alkire, 1998; Alkire *et al.*, 2000; Heinke and Schwarzbauer, 2002) is related to reduced synaptic activity, as judged by various EEG variables as observed in anesthetized studies in animals (Shulman *et al.*, 1999, 2002; Hyder *et al.*, 2002). However functional activation studies under awake and anesthetized conditions in the human are greatly lacking.

## 10.11. CONCLUSION

In neuroimaging (with PET or fMRI) incremental signals are generally measured. The subtraction of baseline activity removes an important part of the total activity (Shulman and Rothman, 1998) because most neurons in the ensemble contribute differently during the baseline and stimulation periods (Shulman *et al.*, 2002). Thus quantitative interpretation by which neuronal activity has changed cannot be made from differencing. Prior <sup>13</sup>C MRS measurements in mammalian brain (Rothman *et al.*, 1999) have revealed that the large energy utilization at basal conditions is almost exclusively used to support events associated with neurotransmission (Shulman and Rothman, 1998). The current results (Smith *et al.*, 2002; Hyder *et al.*, 2002) show the necessity of retaining that baseline signal in order to understand the activities of the neuronal ensemble for the different conditions. The total neuronal activity depicted by the distribution of neuronal spiking frequencies in a localized region, which is neither measured nor desired in neuroimaging,

is conveyed by measuring total energy with calibrated fMRI (Hyder *et al.*, 2001). We have integrated our results of both the incremental and baseline signals into a neuroscientific framework (Shulman *et al.*, 2003), which describes participation of large neuronal populations during function. Since the total measured activity in a small region of the cortex represents the integrated signal from proximal and distal neurons, the delocalized signals from other regions (representing the 'subjective' contributions) can also modulate the localized signals from sensory stimuli (representing the 'objective' contributions). Thus interactions between sensory cues and the high basal activity will, in the near future, allow a more comprehensive view of the functioning brain. However, to achieve that with neuroimaging methods, the cognitive neuroscience community has to acknowledge the need for both the incremental and baseline signals.

## REFERENCES

Alkire MT (1998) Quantitative EEG correlations with brain glucose metabolic rate during anesthesia in volunteers *Anesthesiology* **89**: 323–333

Alkire MT, Haier RG, Fallon JH (2000) Toward a unified theory of narcosis: Brain imaging evidence for a thalamocortical switch as the neurophysiologic basis of anesthesia – induced unconsciousness *Conscious Cogn* **9**: 370–386

Ames III A (2000) CNS energy metabolism as related to function *Brain Res Rev* **34**: 42–68

Bonvento G, Charbonne R, Correze JL, Borredon J, Seylaz J, Lacombe P (1994) Is alpha-chloralose plus halothane induction a suitable anesthetic regimen for cerebrovascular research? *Brain Res* **665**: 213–221

Braitenberg V, Schuz A (1991) *Anatomy of the Cortex: Statistics and Geometry*. Springer, New York

Brinker G, Bock C, Busch E, Krep H, Hossmann Ka, Hoehn-Berlage M (1999) Simultaneous recording of evoked potentials and T<sub>2</sub><sup>\*</sup>-weighted MR images during somatosensory stimulation of rat *Magn Reson Med* **41**: 469–473

Castro-Alamancos MA, Connors BW (1997) Thalamocortical synapses *Prog Neurobiol* **51**: 581–606

Changeux JP (1985) *Neuronal Man: The Biology of Mind*. Princeton University Press, Princeton, NJ (translated by Garcy L)

Chicurel M (2001) Windows on the brain *Nature* **412**: 266–268

Creutzfeldt OD (1975) Neurophysiological correlates of different functional states of the brain. In *Alfred Benzon Symposium VII*, Eds Ingvar DH, Lassen NA. Academic Press, New York, pp. 21–46

Dehaene S, Kerszberg M, Changeux JP (1998) A neuronal model of a global workspace in effortful cognitive tasks *Proc Natl Acad Sci USA* **95**: 14529–14534

Desimone R (1996) Neural mechanisms for visual memory and their role in attention *Proc Natl Acad Sci USA* **93**: 13494–13499

Dudley RE, Nelson SR, Samson F (1982) Influence of chloralose on brain regional glucose utilization *Brain Res* **233**: 173–180

Garby L, Larsen PS (1995) *Bioenergetics: Its Thermodynamic Foundations*. Cambridge University Press, Cambridge, UK

Gazzaniga MS (2000) *The New Cognitive Neurosciences*, 2nd edn. MIT Press, Cambridge, MA

Georgopoulos AP (2000) Neural aspects of cognitive motor control *Curr Opin Neurobiol* **10**: 238–241

Goldman-Rakic PS (1996) Regional and cellular fractionation of working memory *Proc Natl Acad Sci USA* **93**: 13473–13480

Gottlieb JP, Keller A (1997) Intrinsic circuitry and physiological properties of pyramidal neurons in rat barrel cortex *Exp Brain Res* **115**: 47–60

Gray CM (1995) Synchronous oscillations in neuronal systems: Mechanisms and functions *J Comput Neurosci* **1**: 11–38

Gray CM, Maldonado PE, Wilson M, McNaughton B (1995) Tetrodes markedly improve the reliability and yield of multiple single-unit isolation from multi-unit recordings in cat striate cortex *J Neurosci Methods* **63**: 43–54

Harding GW, Stogsdill RM, Towe AL (1979) Relative effects of pentobarbital and chloralose on the responsiveness of neurons in sensorimotor cerebral cortex of the domestic cat *Neuroscience* **4**: 369–378

Heinke W, Schwarzbauer C (2002) *In vivo* imaging of anesthetic action in humans: Approaches with position emission tomography (PET) and functional magnetic resonance imaging (fMRI) *Br J Anaesth* **89**: 112–122

Herkenham M (1986) New perspectives on the organization and evolution of nonspecific thalamocortical projections. In *Cerebral Cortex*, Eds Jones EG, Peters A. Plenum, New York, pp. 403–446

Hetherington PA, Swindale NV (1999) Receptive field and orientation scatter studied by tetrode recordings in cat area 17. *Vis Neurosci* **16**: 637–652

Hodes JE, Soncrant TT, Larson DM, Carlson SG, Rapoport SI (1985) Selective changes in local cerebral glucose utilization induced by phenobarbital in the rat. *Anesthesiology* **63**: 633–639

Hodgkin AL, Huxley AF (1952) A quantitative description of membrane current and its application to conduction and excitation in nerve. *J Physiol* **117**: 500–544

Hyder F, Chase JR, Behar KL, Mason GF, Siddeek M, Rothman DL, Shulman RG (1996) Increased tri-carboxylic acid cycle flux in rat brain during forepaw stimulation detected with <sup>1</sup>H-[<sup>13</sup>C] NMR. *Proc Natl Acad Sci USA* **93**: 7612–7617

Hyder F, Rothman DL, Mason GF, Rangarajan A, Behar KL, Shulman RG (1997) Oxidative glucose metabolism in rat brain during single forepaw stimulation: A spatially localized <sup>1</sup>H-[<sup>13</sup>C] NMR study. *J Cereb Blood Flow Metab* **17**: 1040–1047

Hyder F, Kida I, Behar KL, Kennan RP, Maciejewski PK, Rothman DL (2001) Quantitative functional imaging of the brain: Towards mapping neuronal activity by BOLD fMRI. *NMR Biomed* **14**: 413–431

Hyder F, Rothman DL, Shulman RG (2002) Total neuroenergetics support localized brain activity: Implications for the interpretation of fMRI. *Proc Natl Acad Sci USA* **99**: 10771–10776

Kandel ER, Schwartz JH, Jessell TM (1991) *Principles of Neural Science*. Appleton & Lange, Norwalk, CT

Jog MS, Connolly CI, Kubota Y, Iyengar DR, Garrido L, Harlan R, Graybiel AM (2002) Tetrode technology: Advances in implantable hardware, neuroimaging, and data analysis techniques. *J Neurosci Methods* **117**: 141–152

Laughlin SB (2001) Energy as a constraint on the coding and processing of sensory information. *Curr Opin Neurobiol* **11**: 475–480

Llinas RR (2002) *"I of the Vortex" From Neurons to Self*. MIT Press, Cambridge, MA

Logothetis NK, Pauls J, Augath M, Trinath T, Oeltermann A (2001) Neurophysiological investigation of the basis of the fMRI signal. *Nature* **412**: 150–157

Logothetis NK (2000) Object recognition: Holistic representations in the monkey brain. *Spat Vis* **13**: 165–178

Lorente de Nò R (1938) The cerebral cortex: Architecture, intracortical connections and the motor projections. In *Physiology of the Nervous System*, Ed. Fulton JF. Oxford University Press, New York, pp. 291–325

Macchi G (1983) Old and new anatomico-functional criteria in the subdivision of the thalamic nuclei. In: *Somatosensory Integration in the Thalamus*, Eds Macchi G, Rustioni A, Spreafico R. Elsevier, Amsterdam, pp. 3–16

McCasland JS, Woolsey TA (1988) High-resolution 2-deoxyglucose mapping of functional cortical columns in mouse barrel cortex. *J Comp Neurol* **278**: 555–569

McKenna TM, Whitsel BL, Dreyer DA, Metz CB (1981) Organization of cat anterior parietal cortex: Relations among cytoarchitecture, single neuron functional properties, and interhemispheric connectivity. *J Neurophys* **45**: 667–697

Mountcastle VB (1997) The columnar organization of the neocortex. *Brain* **120**: 701–722

Nieuwenhuys R (1998) Telencephalon: cerebral cortex. In *The Central Nervous System of Vertebrates*, Eds Nieuwenhuys R, ten Donkelaar HJ, Nicholson C. Springer, Berlin, pp. 1932–2023

Ogawa S, Lee TM, Stepnoski R, Chen W, Zhu XH, Ugurbil K (2000) An approach to probe some neural systems interaction by functional MRI at neural time scale down to milliseconds. *Proc Natl Acad Sci USA* **97**: 11026–11031

Paxinos G, Watson C (1997) *The Rat Brain in Stereotaxic Coordinates*. Academic Press, New York

Pellerin L, Magistretti PJ (1994) Glutamate uptake into astrocytes stimulates aerobic glycolysis: A mechanism coupling neuronal activity to glucose utilization. *Proc Natl Acad Sci USA* **91**: 10625–10629

Peters A, Kara DA, Harriman KM (1985) The neuronal composition of area 17 of rat visual cortex. III. Numerical considerations. *J Comput Neurol* **238**: 263–274

Posner MI, Raichle ME (1998) The neuroimaging of human brain function. *Proc Natl Acad Sci USA* **95**: 763–764

Raichle ME (1988) Circulatory and metabolic correlates of brain function in normal humans. In *Handbook of Physiology – The Nervous System V*. Springer, New York, pp. 633–674

Rees G, Friston K, Koch C (2000) A direct quantitative relationship between the functional properties of human and macaque V5. *Nat Neurosci* **3**: 716–723

Richard CD (1998) What the actions of anaesthetics on fast synaptic transmission reveal about the molecular mechanism of anaesthesia. *Toxicol Lett* **100–101**: 41–50

Ritchie JM (1967) The oxygen consumption of mammalian non-myelinated nerve fibres at rest and during activity *J Physiol* **188**: 309–329

Rolls ET (2000) Functions of the primate temporal lobe cortical visual areas in invariant visual object and face recognition *Neuron* **27**: 205–218

Rothman DL, Sibson NR, Hyder F, Shen J, Behar KL, Shulman RG (1999) *In vivo* nuclear magnetic resonance spectroscopy studies of the relationship between the glutamate-glutamine neurotransmitter cycle and functional neuroenergetics *Philos Trans R Soc London, Ser B* **354**: 1165–1177

Savaki HE, Desban M, Glowinski J, Besson MJ (1981) Local cerebral glucose consumption in the rat. I. Effects of halothane anesthesia *J Comput Neurol* **213**: 36–45

Scannell JW, Young MP (1999) Neuronal population activity and functional imaging *Proc R Soc London, Ser B Biol Sci* **266**: 875–881

Shepherd GM (1994) *The Synaptic Organization of the Brain*. Oxford University Press, New York

Shulman RG (1996) Interview with Robert G Shulman *J Cogn Neurosci* **8**: 474–480

Shulman RG (2001) Functional imaging studies: linking mind and basic neuroscience *Am J Psychiatry* **158**: 11–20

Shulman RG, Rothman DL (1998) Interpreting functional imaging studies in terms of neurotransmitter cycling *Proc Natl Acad Sci USA* **95**: 11993–11998

Shulman RG, Rothman DL, Hyder F (1999) Stimulated changes in localized cerebral energy consumption under anesthesia *Proc Natl Acad Sci USA* **96**: 3245–3250

Shulman RG, Hyder F, Rothman DL (2002) Biophysical basis of brain activity: Implications for neuroimaging *Q Rev Biophys* **35**: 287–325

Shulman RG, Hyder F, Rothman DL (2003) Cerebral metabolism and consciousness *C R Biol* **326**: 253–273

Siesjo BK (1978) *Brain Energy Metabolism*. Wiley, New York

Smith AJ, Blumenfeld H, Behar KL, Rothman DL, Shulman RG, Hyder F (2002) Cerebral energetics and spiking frequency: The neurophysiological basis of fMRI *Proc Natl Acad Sci USA* **99**: 10765–10770

Sokoloff L (1991) Relationship between functional activity and energy metabolism in the nervous system: Whether, where and why?. In *Brain Work and Mental Activity*, Eds Lassen NA, Ingvar DH, Raichle ME, Friberg L. Munksgaard, Copenhagen, pp. 52–64

Szabo I, Czurko A, Csicsvari J, Hirase H, Leinekugel X, Buzsaki G (2001) The application of printed circuit board technology for fabrication of multi-channel micro-drives *J Neurosci Methods* **105**: 105–110

Tanaka K (1996) Inferotemporal cortex and object vision *Annu Rev Neurosci* **19**: 109–139

Thomson AM, Deuchars J (1997) Synaptic interactions in neocortical local circuits: Dual intracellular recordings in vitro *Cerebral Cortex* **7**: 510–522

Ueki M, Linn F, Hossman KA (1988) Functional activation of cerebral blood flow and metabolism and after global ischemia of rat brain *J Cereb Blood Flow Metab* **8**: 486–494

Ueki M, Mies G, Hossmann KA (1992) Effect of  $\alpha$ -chloralose, halothane, pentobarbital and nitrous oxide anesthesia on metabolic coupling in somatosensory cortex of rat *Acta Anaesthesiol Scand* **36**: 318–322

Venkatasubramanian PN, Shen YJ, Wyrwicz AM (1996) Characterization of the cerebral distribution of general anesthetics *in vivo* by two-dimensional  $^{19}\text{F}$  chemical shift imaging *Magn Reson Med* **35**: 626–630

Winfield DA, Gatter KC, Powell TP (1980) An electron microscopic study of the types and proportions of neurons in the cortex of the motor and visual areas of the cat and rat *Brain* **103**: 245–258

Woolsey TA (1996) Barrels: 25 years later *Somatosens Mot Res* **13**: 181–186

Yang X, Hyder F, Shulman RG (1997) Functional MRI BOLD signal coincides with electrical activity in the rat whisker barrels *Magn Reson Med* **38**: 874–877

Zouridakis G, Tam DC (2000) Identification of reliable spike templates in multi-unit extracellular recordings using fuzzy clustering *Comput Methods Programs Biomed* **61**: 91–98

## **Section C**

### **Clinical Beginnings**



# 11

## NMR Studies of Bioenergetic Impairment in Human Epilepsy

**Hoby P. Hetherington**

*Department of Radiology, The Albert Einstein College of Medicine, Bronx, NY, USA*

**Jullie W. Pan**

*Department of Neurology, The Albert Einstein College of Medicine, Bronx, NY, USA*

**Dennis D. Spencer**

*Department of Neurosurgery, Yale University, New Haven, CT, USA*

---

11.1	Introduction	197
11.2	$^1\text{H}$ Spectroscopic Localization and Lateralization of Epileptogenic Regions	198
11.3	Factors Affecting Sensitivity and Specificity	199
11.4	Interpretation of Decreases in NAA Levels	202
11.5	$^{31}\text{P}$ Spectroscopic Measurements of Bioenergetics in Human Epilepsy	204
11.6	Factors Affecting the Interpretation of $^{31}\text{P}$ Data	205
11.7	Interpretation of the Bioenergetic Alterations	208
11.8	Possible Mechanism Linking Bioenergetic Impairment and Seizures	209

---

### 11.1. INTRODUCTION

Epilepsy is one of the most common neurological disorders, affecting one to two million Americans (1). For approximately 10 % of these individuals, the debilitating effects of the disease cannot be controlled

by medication. In this population surgical intervention can be highly effective, provided there is accurate lateralization and localization of the epileptogenic tissue. Over the past decade, a variety of methods for lateralizing and localizing seizure foci, MR imaging (2–5), PET (6–13), and MR spectroscopy (13,14–19) have been used. Although these measures have often been used simply as surrogate markers for the presence of disease, the alterations, when viewed in the context of the biochemical information present, provide a unique insight into the biochemical pathophysiology of the disease.

Unlike conventional MRI studies, which detect the concentration and cellular environment of tissue water, MR spectroscopy provides specific biochemical and histochemical information. For example,  $^1\text{H}$  spectroscopic measurements have utilized decreases in *N*-acetyl aspartate (NAA), a compound synthesized only in neuronal mitochondria, to identify regions of neuronal injury (13–19). Increases in total creatine (both phosphorylated and nonphosphorylated forms) and choline have been interpreted as reflecting gliosis and altered membrane turnover. In temporal lobe epilepsy, where neuronal loss and reactive gliosis is a common finding, decreases in NAA and or increases in creatine and choline have been shown to have lateralization sensitivities as high as 97 % (20). Using  $^{31}\text{P}$  spectroscopy, *in vivo* concentrations of phosphocreatine, ATP and inorganic phosphate can be imaged noninvasively along with intracellular pH to provide a measure of bioenergetic status. Interestingly, despite the reduction in metabolic rate during the interictal period commonly seen in FDG PET studies, alterations in bioenergetics (decreases in phosphocreatine/ATP (PCr/ATP) and PCr/inorganic phosphate (PCr/Pi)) have emerged as a consistent finding for a variety of epilepsies (21–26). Taken together these findings suggest a common pathophysiology of impaired neuronal bioenergetics underlying a variety of different epilepsies.

In this chapter we will review the role that MR spectroscopy has had as a clinical tool in identifying epileptic foci. As part of this discussion, we will also identify and discuss some of the technical hurdles that must be accounted for in acquiring and accurately interpreting *in vivo* MR spectroscopy data. Specifically we will discuss the effects of metabolite heterogeneity as a function of tissue type and how a failure to account for this can result in significant artifacts that degrade the interpretability of the data. As part of this discussion we will also discuss several approaches to overcome these effects. We will then discuss the biological significance of these findings and how they suggest that bioenergetic impairment occupies an important role in the pathophysiology of seizure disorders. Finally we will discuss a possible model that links the metabolic changes and energetic impairment seen by spectroscopic studies to the primary clinical manifestation of epilepsy, inappropriate spontaneous electrical activity.

## 11.2. $^1\text{H}$ SPECTROSCOPIC LOCALIZATION AND LATERALIZATION OF EPILEPTOGENIC REGIONS

During the mid 1990s a number of groups demonstrated the utility of  $^1\text{H}$  spectroscopic measurements of NAA in the lateralization of the epileptogenic region in patients with temporal lobe epilepsy (14–19). Specifically, changes in NAA content (14), NAA/Cr (17–19), NAA/CH (16) and NAA/(Cr + CH) (15) have all been used to lateralize the seizure focus in patients with intractable temporal lobe seizures. Based on the localization of NAA to neurons (8,27) and the finding that in cell cultures that Cr is higher in glial cells (28), these changes were initially interpreted as representing a combination of neuronal loss (NAA decreases) and glial proliferation (Cr increases). This interpretation was consistent with the known pathophysiology of temporal lobe epilepsy where both neuronal loss and gliosis are common.

As a lateralization and localization tool, the reported sensitivities have ranged from 60 % (15) to 97 % (20), somewhat higher than the 74 % typically reported for conventional MRI studies (29). For example Chu *et al.* (30) reported that MR spectroscopic imaging when combined with tissue segmentation correctly lateralized the epileptogenic hippocampus in patients without MRI detectable volumetric loss. This is despite the 300-fold decrease in volume resolution typical for spectroscopy studies in comparison

to conventional MRI studies. The ability of MR spectroscopy to attain higher sensitivities in comparison to standard imaging is most likely the result of the following factors: (1) that the metabolic perturbation seen in temporal lobe epilepsy is widespread, affecting not only the hippocampus (3–4 cm<sup>3</sup> in volume) but also surrounding temporal gray and white matter, and (2) that detectable decreases in hippocampal volume by conventional MRI may require neuronal losses of up to 50 %. Thus for temporal lobe epilepsy, where the effects of the disease are widespread and submillimeter spatial resolution is not required, the biochemical specificity afforded by spectroscopy provides significant advantages over higher spatial resolution measurements of tissue water.

In addition to providing a highly sensitive method for lateralizing the seizure focus, spectroscopic imaging studies may also provide some predictive insight as to surgical outcome. In these spectroscopy studies (18,20,30,31), 40–50 % of the subjects studied and diagnosed as having unilateral temporal lobe epilepsy, based on EEG studies, were found to have significant decreases in NAA in the contralateral hemisphere. These data indicated that, although the seizures were found to predominantly emanate from one hippocampus, the effects were clearly manifesting also in the contralateral hemisphere. Kuzniecky *et al.* (32) correlated the severity of NAA/Cr alterations in the ipsilateral and contralateral hippocampi with surgical outcome. Although the severity of NAA/Cr abnormality in the ipsilateral hippocampus did not appear to have a significant impact on surgical outcome, more severe alterations in the contralateral hippocampus were associated with poorer surgical outcomes, i.e. continuing seizures. Whether this finding reflected the presence of small (below the detection of MRI) but significant neuronal loss in the contralateral hippocampus or an ongoing biochemical defect could not be resolved.

The finding of decreased NAA is not solely restricted to temporal lobe epilepsy. In particular, reduced NAA levels have been reported in a variety of epileptic subtypes including frontal lobe epilepsy (33), malformations of cortical development (34,35), and Rasmussen's encephalitis (36). Thus the use of <sup>1</sup>H spectroscopic imaging for the lateralization and localization of the epileptic foci is of general use in the lateralization and localization of epileptogenic foci.

### 11.3. FACTORS AFFECTING SENSITIVITY AND SPECIFICITY

The sensitivity and specificity of these studies ranged from 60 % (15) to 97 % (20), with greater sensitivity and specificity reported from groups using higher spatial resolution spectroscopic imaging techniques. These reports suggested that metabolic heterogeneity and/or partial volume effects could play a significant role in determining the accuracy and efficacy of the measurements. Quantitative large single voxel measurements from occipital gray matter and parietal white matter (37,38) demonstrated tissue differences between white and gray matter contents of creatine (Cr) (6.3, 8.3 mM), *N*-acetyl aspartate (NAA) (10.3, 10.7 mM) and choline (1.8, 1.5 mM) (Figure 11.1). This was subsequently confirmed in spectroscopic imaging studies using 0.5 ml volumes at 4 T and image segmentation (39), reporting values for Cr (6.1, 8.2 mM), NAA (10.5, 9.7 mM) and choline (1.5, 1.5 mM). Based upon these observations it became clear that tissue heterogeneity could be a limiting factor in the identification of metabolically altered regions. Specifically, due to the lower creatine content in white matter as opposed to gray matter, inclusions of significant amounts of white matter in predominantly gray matter voxels would lower total creatine content and increase the NAA/Cr ratio, thereby mimicking more healthy tissue resulting in false negatives. Similarly, volumes with substantial gray matter, due to the higher creatine content would artificially bias the NAA/Cr ratio downwards, giving the appearance of greater damage. Additionally, it has been demonstrated that the NAA/Cr ratio in the cerebellar vermis (found medial and inferior to the hippocampus) is very low (0.72) in comparison to temporal gray and white matter (1.51, 1.79) (18). Combined, both of these effects can result in false positives and false negatives complicate the lateralization of the epileptogenic region.

To overcome the effects of tissue heterogeneity, a number of investigators in a variety of different disease states, have employed linear regression analyses to compensate for the inclusion of varying levels of gray

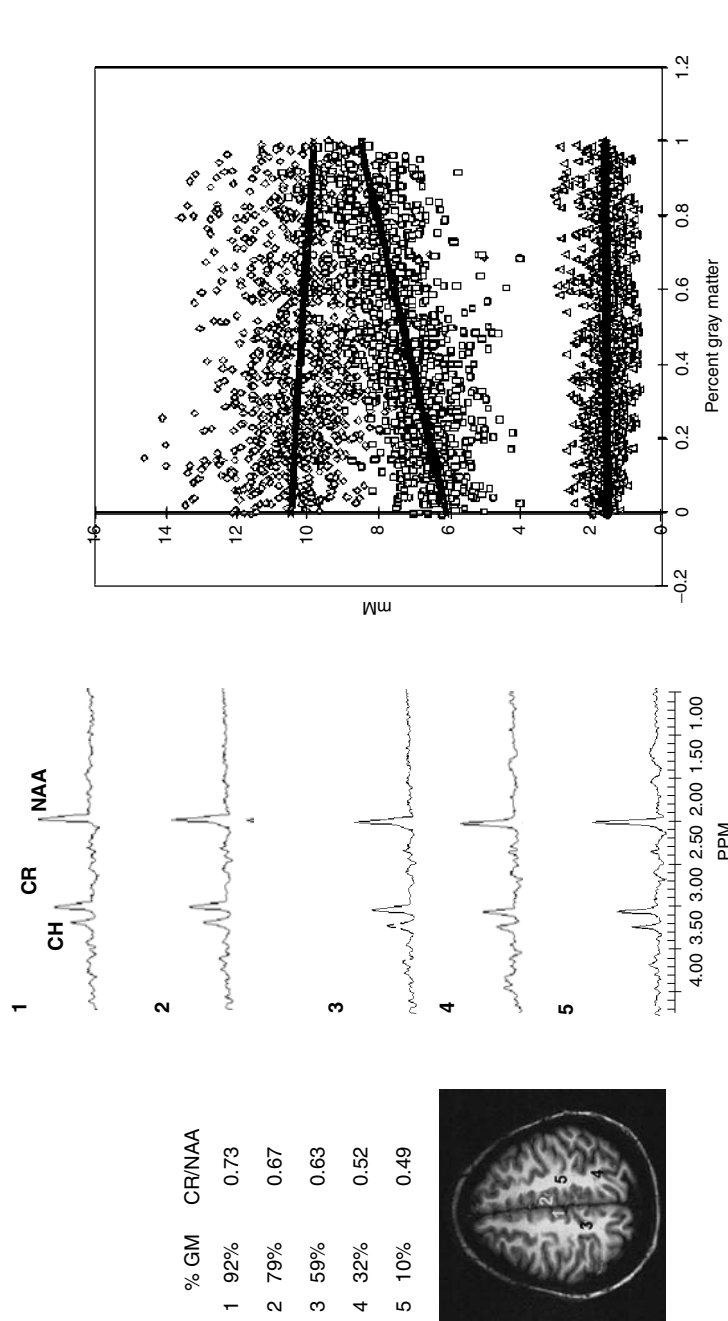
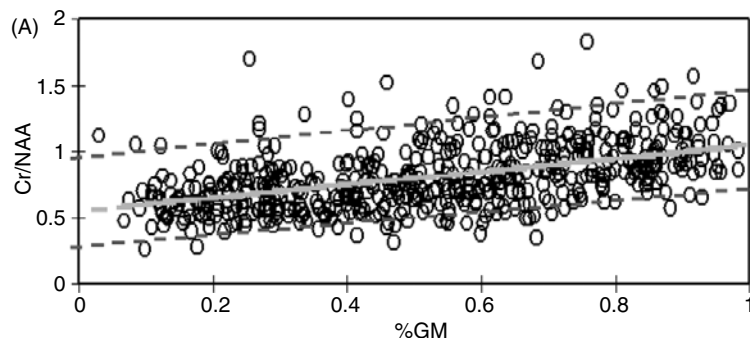


**Figure 11.1.** A scout image with five numbered locations with gray matter content varying from 92 to 10 %. The corresponding spectra are displayed in the adjacent panel to the right. The panel on the far right displays linear regression plots for the concentration of NAA (open diamonds), creatine (open squares) and choline (open triangles). The calculated regression lines are shown in solid lines.



(from Chu WJ, Kuzniecky RI, Hugg JW, Khalil BA, Gilliam F, Faught E, Hetherington HP, Evaluation of Temporal Lobe Epilepsy using  $1\text{H}$  spectroscopic imaging segmentation at 4.1T. Magn. Reson. in Med. 43:359-367, 2000)

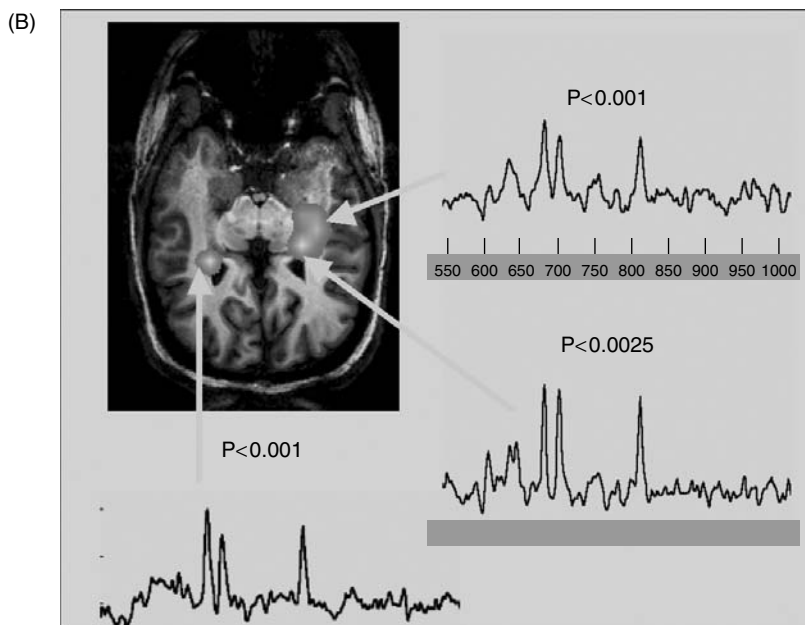


**Figure 11.2.** (A) Linear regression plot of CR/NAA as a function of percentage of gray matter. The dashed lines indicate the 95 % confidence intervals for statistical significance of an abnormal ratio from a single voxel. (B) (Plate 3) A scout spectrum with a color overlay indicating voxels with statistically significant ( $p < 0.05$ ) metabolic abnormalities. Selected spectra and the calculated  $p$  values are displayed from the ipsilateral and contralateral hippocampi.

and white matter. Although these methods are most commonly used in global pathologies to identify gray or white matter specific alterations in comparison to control subjects (40,41), they can also be employed on a voxel by voxel basis within subjects (30,39). Using segmented anatomical images, the gray and white matter content of each spectroscopic imaging voxel can be determined. From these data a regression analysis can be performed in healthy volunteers to obtain the 'pure' gray and white matter metabolite contents and ratios (Figure 11.2(A)). Using the population statistics of this data, the probability that any voxel of specific gray and white matter content in a patient study is abnormal can be calculated using

Equation (11.1) (39).

$$\text{Cr/NAA}(p \leq \alpha) = \text{Cr/NAA}_{\text{mean}} + t_{\alpha, n-2} \{ M\text{S}_{\text{E}} [1 + 1/n + (x_{\text{gm,mean}} - x_{\text{gm}})^2 / S_{\text{xx}}] \}^{1/2} \quad (11.1)$$

where

$\text{Cr/NAA}(p \leq \alpha)$ : the cutoff value corresponding to a  $p$  value  $\leq \alpha$  for Cr/NAA,

$\text{Cr/NAA}_{\text{mean}}$ : the expected value of the Cr/NAA ratio for  $x_{\text{gm,mean}}$  content of gray matter,

$t_{\alpha, n-2}$ :  $t$  value for  $p \leq \alpha$  for  $n - 2$  degrees of freedom,

$n$ : the number of pixels,

$M\text{S}_{\text{E}}$ : the residual mean square,

$x_{\text{gm}}$  is the fraction of gray matter of the voxel,

$x_{\text{gm,mean}}$  is the mean fraction of gray matter from the population.

Voxels that are statistically abnormal ( $p < 0.05$ ) can then be color coded according to  $p$  value and superimposed on the anatomical images for easy evaluation and interpretation (Figure 11.2(B)). Chu *et al.* (30) have demonstrated that when these regression-based statistical methods with image segmentation are utilized in patients with temporal lobe epilepsy, false negatives and incorrect lateralizations are reduced in comparison to simple left-right voxel comparisons. Of note in this particular patient group, fully one-half of the patients could not be lateralized by conventional MRI methods, due to either an absence of hippocampal atrophy or the presence of bilateral atrophy. Thus in these cases, MR spectroscopy provided significant new information not available in the clinical MRIs.

As described, heterogeneity due to gray and white matter mixing can be accounted for by using image segmentation schemes and linear regression-based statistical analyses. However, this assumes that there is no regional variation within the gray or white matter itself. Recently Vermathen *et al.* (42) have reported that NAA levels show an anterior-posterior bias along the hippocampal formation, with higher levels reported from more posterior locations, while choline and creatine showed the opposite trend. Thus additional corrections for local heterogeneity may also be required.

## 11.4. INTERPRETATION OF DECREASES IN NAA LEVELS

Based on the localization of NAA to neurons (27,28), the reduced NAA content found in patients with temporal lobe epilepsy was initially interpreted as being the result of neuronal loss. However, the report of Hugg *et al.* (43) of NAA recovery from the contralateral hippocampus in patients with bilateral abnormalities 1 year after successful surgery suggested that at least a portion of the observed NAA loss was not solely due to neuronal loss. This finding was confirmed by Cendes *et al.* (44) and Vermathen *et al.* (45). In a follow-up study, on average, 50% of the metabolic recovery occurred over a period of less than 6 months, demonstrating a slow but responsive nature of neuronal NAA levels (46). This indicated that alterations in NAA were not solely due to neuronal loss. In epilepsy patients with malformations of cortical development, significant reductions were also observed in NAA/Cr in the epileptogenic region (34,35). In these patients, NAA alterations were seen in the absence of neuronal loss (34). Specifically the resected tissue showed normal or elevated numbers of neurons, although morphologically they were abnormal (34). Subsequently Kuzniecky *et al.* (47) demonstrated that NAA losses in patients with temporal lobe epilepsy were also not significantly correlated with neuronal and glial densities. Thus in both temporal lobe epilepsy and malformations of cortical development, the reductions in NAA reflect a process which is not solely due to neuronal loss, but somehow reflects the functional status of the neurons themselves.

To probe the histological basis for the alterations in NAA, we correlated *in vivo* measurements of NAA from the hippocampi of patients with intractable TLE with quantitative measurement of neuronal loss and reactive astrocyte proliferation in the resected tissue. Proliferation of reactive astrocytes, as expressed by

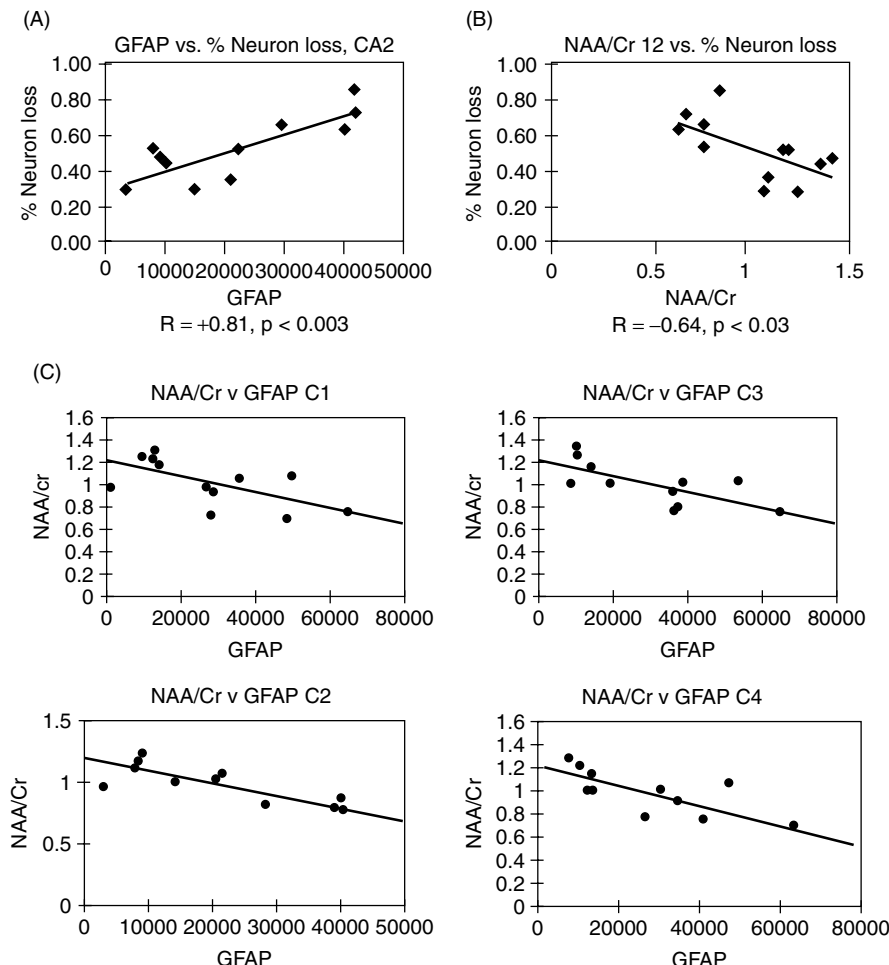


**Figure 11.3.** (A) A regression analysis of neuronal loss (vertical axis) against GFAP staining (horizontal axis) from the CA2 sector of the hippocampus,  $R = +0.81, p < 0.003$ . (B) A regression analysis of neuronal loss (vertical axis) against NAA/Cr (horizontal axis) from the CA2 sector of the hippocampus,  $R = -0.64, p < 0.03$ . (C) regression analyses for NAA/Cr (vertical axis) versus GFAP staining (horizontal axis) for CA1–CA4 sectors of the hippocampus. All four regressions were statistically significant  $p < 0.05$ .

the presence of glial fibrillary acidic protein (GFAP) has been associated with recent or ongoing neuronal injury (48). Regression analyses of NAA/Cr measured *in vivo* with quantitative neuronal counting across CA1–CA4 and the dentate gyrus revealed statistically significant correlations only in the CA2 sector (Figure 11.3(A)). Interestingly, a similar correlation between GFAP staining with neuronal number revealed statistically significant correlation again only in the CA2 sector of the hippocampus (Figure 11.3(B)). However, a statistically significant correlation was found between NAA/Cr and GFAP staining across all four sectors (Figure 11.3(C)). This suggests that in temporal lobe epilepsy, reductions in NAA/Cr more closely correlate with the presence of reactive astrocytes than alterations in neuronal density. The presence of reactive astrocytes is largely interpreted as a marker for recent or ongoing neuronal injury. Interestingly, neuronal loss in the CA1, CA3, and dentate gyrus is typically believed to be largely due to the initial

precipitating insult in temporal lobe epilepsy, while neuronal loss in the CA2 is more generally believed to correlate with the progression of the disease (49).

The reversibility of decreased NAA in the contralateral hippocampus with successful surgical outcome, i.e. cessation of seizures, suggests that the recovering NAA levels reflect a 'healing' or 'normalization' of cellular process in the contralateral hippocampus. The fact that these processes are associated with 'normalization' of neuronal function, i.e. cessation of seizures, suggests that the processes, which link the balance between NAA synthesis and degradation, may also be linked with neuronal function. Despite the extensive use of NAA as a marker for neuronal injury in a wide variety of disorders including stroke (50), multiple sclerosis (51), Alzheimer's disease (52) and AIDS dementia (53), its biological function remains controversial. NAA has been reported to act as a source of acetate transfer from the mitochondria to the cytoplasm for lipid synthesis (54). Additionally, NAA has been proposed to act as a transporter of amino nitrogen from the mitochondria to the cytoplasm (55). NAA has also been proposed to act as an osmotic agent, based on its redistribution between extracellular/intracellular compartments in response to osmotic stress (56).

Investigations of agents that perturb mitochondrial function have been demonstrated to affect NAA levels and production rates. Heales *et al.* (57) used l-buthionine sulfoximine administration to deplete glutathione resulting in cytochrome c oxidase activity decreases of 27 %, and citrate synthase activity of 18 %. Accompanying these changes, NAA levels were decreased 11 %. Bates *et al.* (58) used rotenone, cyanide and oligomycin in isolated rat brain mitochondria. In these cases ATP production, oxygen consumption and NAA production were positively correlated and decreased relative to control preparations. Thus the decreased NAA levels seen in epileptics may in fact represent alterations in the function of neuronal mitochondria and their role in modulating seizure activity. This is also consistent with the finding that in epilepsy patients with cortical malformations of development who are well controlled (less than four seizures year), NAA levels are not altered despite the presence of structural abnormalities (34). If true, this would suggest that bioenergetic deficits should be present in the hippocampi of patients with temporal lobe epilepsy and that upon successful treatment these values should normalize.

## 11.5. $^{31}\text{P}$ SPECTROSCOPIC MEASUREMENTS OF BIOENERGETICS IN HUMAN EPILEPSY

Prior to the widespread availability of  $^1\text{H}$  spectroscopy on clinical MR systems, Weiner and colleagues evaluated the use of  $^{31}\text{P}$  spectroscopy for the lateralization of epileptogenic regions. In these initial studies at 2.0 T, significant alterations in inorganic phosphate (73 % increase) and brain pH (0.17 unit increase) were reported (21,22). Although subsequent studies at 1.5 T and 4.1 T failed to reproduce the reported changes in pH, significant alterations in bioenergetic parameters were reported (23,24). At 1.5 T Kuzniecky *et al.* reported that PCr/Pi was reduced by 50 % in the ipsilateral temporal lobe whereas it was reduced by 24 % in the contralateral lobe (23). At 4.1 T, Chu *et al.* (24) later reported that PCr/Pi was significantly decreased in both the ipsilateral (32 %) and contralateral lobes (19 %). Within this group, 73 % of the patients were correctly lateralized using the PCr/Pi ratio. Despite the controversy regarding pH changes, bioenergetic impairment (increased Pi and decreased PCr/Pi) was reported by both groups. Since patients with recent seizures (less than 24 h previous) were excluded, these effects are believed not to be an acute effect of seizures, but reflect a chronic impairment of energy metabolism, consistent with a mitochondria-based deficit leading to NAA reductions.

Declines in bioenergetics are also seen in a variety of other forms of epilepsy including children with Lenox–Gasteau syndrome (25), absence seizures (25) and in adults with frontal lobe epilepsy (26). In children with Lenox–Gasteau and absence seizure, a nonfocal form of epilepsy, PCr/ATP was decreased in the cortical gray matter in comparison to control subjects. Notably, no such change was seen in white

matter, reflecting the specificity to neuronal bodies and their high energetic demands. In patients with frontal lobe epilepsy, Garcia *et al.* (26) reported elevations of inorganic phosphate, consistent with a decrease in overall energy charge. Thus the finding of bioenergetic impairment is not restricted solely to temporal lobe epilepsy, but may reflect a basic mechanism underlying epilepsy as a whole.

## 11.6. FACTORS AFFECTING THE INTERPRETATION OF $^{31}\text{P}$ DATA

Although  $^{31}\text{P}$  studies have shown that abnormalities in bioenergetics are present their use to date has been limited. Part of the limited use of  $^{31}\text{P}$  spectroscopy can be attributed to the large range of normal values for cerebral PCr (3–5 mM) and ATP (2–4 mM) in low field studies (59–62), and the resulting perception that  $^{31}\text{P}$  spectroscopy is highly inaccurate. These initial reports used large volumes of 25–100 cm<sup>3</sup> and did not attempt to account for tissue or regional heterogeneity. Although spatial resolution for  $^{31}\text{P}$  studies is limited by the SNR, recent studies even at high field have identified clear regional heterogeneities in  $^{31}\text{P}$  metabolites using regression analyses (63) (Figure 11.4). Although PCr levels are relatively uniform between cerebral gray and white matter and mixed cerebellar volumes (3.53 ± 0.33, 3.33 ± 0.37 and 3.75 ± 0.66 mM respectively), ATP levels show significant heterogeneity ranging from 1.78 ± 0.56 mM in the mixed cerebellar volumes to 2.19 ± 0.33 and 3.41 ± 0.33 mM in cerebral gray and white matter. Although skeletal muscle contributions to central volumes within the brain are negligible, due to the high concentration of PCr and ATP in temporalis muscles, (25.4 ± 2.3 and 8.5 ± 1.9 mM respectively), their contribution to the peripheral temporal regions can be substantial. The effect of this can be seen in the spectroscopic image of PCr/ATP shown in Figure 11.5. In this image we have overlaid a PCr/ATP image

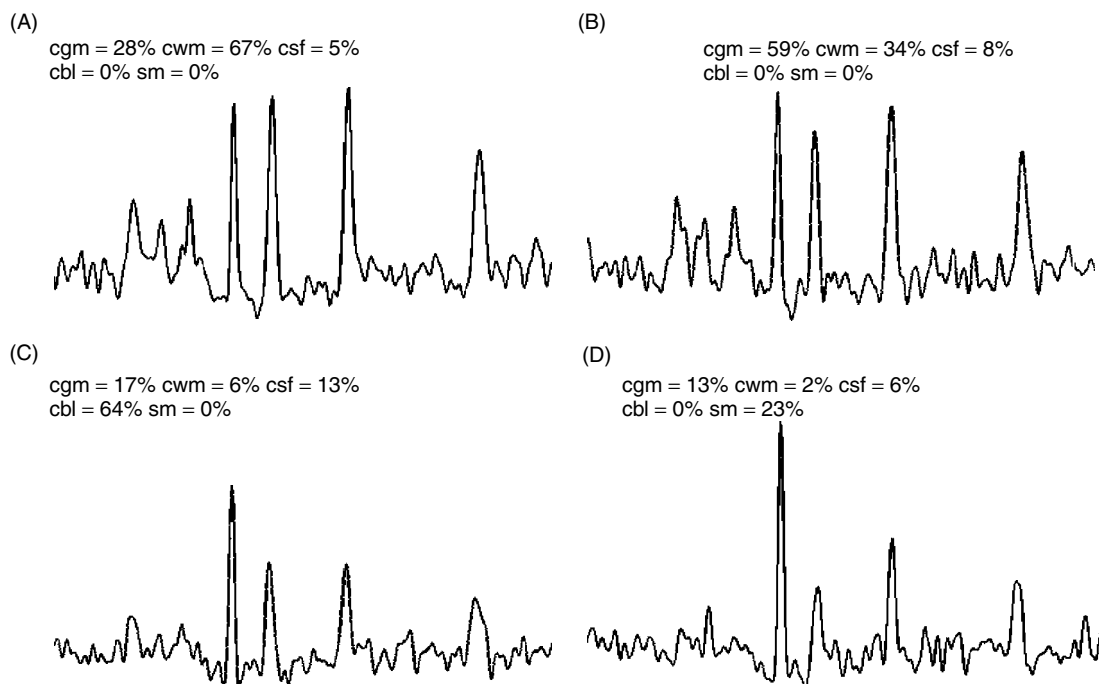


**Figure 11.4.** Spectra from predominantly (A) cortical white matter (CWM), (B) cortical gray matter (CGM), (C) the cerebellum (CBL) and (D) skeletal muscle (SM). The contribution of each tissue type, including cerebral spinal fluid (CSF) is listed above each spectrum.

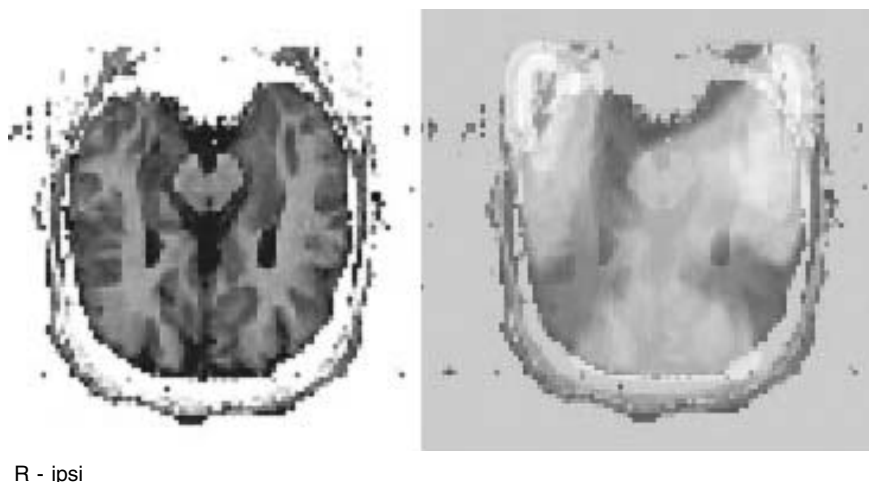


**Figure 11.5. (Plate 4).** A scout anatomical image and a composite image of the anatomical image and a color-coded overlay of PCr/ATP. The highest levels of PCr/ATP are colored red, while intermediate values are in yellow and light blue, while the lowest levels are in dark blue. The seizure focus (ipsi) was found to be on the right (left in the image) and is dark blue, while the contralateral hippocampus is light blue.

onto an anatomical image for reference. Higher PCr/ATP ratios are in red and yellow, with lower levels in blue. As can be seen the highest ratios are seen from the temporalis muscle, while the lowest values are seen in the white matter. In this case, the ipsilateral hippocampus (seizure origin) has a PCr/ATP value that is significantly lower than the contralateral hippocampus and other gray matter regions such as occipital gray matter but is similar to 'pure' white matter. Thus failure to account for these differences can result in substantial variability that is not reflective of underlying pathology, but rather normal heterogeneity based on tissue composition.

Using a five-compartment model including cerebral gray and white matter, skeletal muscle, cerebellar tissues and cerebral spinal fluid, we have demonstrated this heterogeneity can be compensated for in the regions about the hippocampus and temporal lobe. Displayed in Figure 11.6 is a plot of the predicted and measured values for PCr and ATP from 22 voxels from the temporal region. Despite the two-fold variations in measured ATP and PCr content, the predicted values based on tissue composition are in good agreement throughout the range. Using this methodology, the decrement in PCr/ATP from the epileptogenic region can be calculated, correcting for varying degrees of tissue composition. Displayed in Figure 11.7, is a scout image and spectra selected from the inferior aspect of the hippocampus. As can be seen, the largest decrements in PCr/ATP are found overlying the ipsilateral hippocampus. Thus corrections for tissue heterogeneity are essential improve our ability to interpret  $^{31}\text{P}$  spectroscopic imaging data of patients with temporal lobe epilepsy.

Even after correction for tissue content differences, the large size of the spectroscopic imaging voxels for  $^{31}\text{P}$  measurements,  $6\text{--}12\text{ cm}^3$ , can result in substantial partial volume effects with surrounding healthy tissue. This effect can be compounded when the region of interest lies at an intersection of the spectroscopic imaging grid, thereby distributing the signal arising from the affected region into as many as eight voxels for a 3D study. Although spatial interpolation of the data set by zero filling can help to offset this problem, the resulting data sets become large ( $>1\text{ GB}$  for  $1.5\text{ mm}$  spatial accuracy) resulting in significant data handling problems. To overcome this effect, the reconstruction grid can be arbitrarily shifted post-acquisition using the 3D anatomical images to calculate the necessary phase shifts to allow precise centering of the

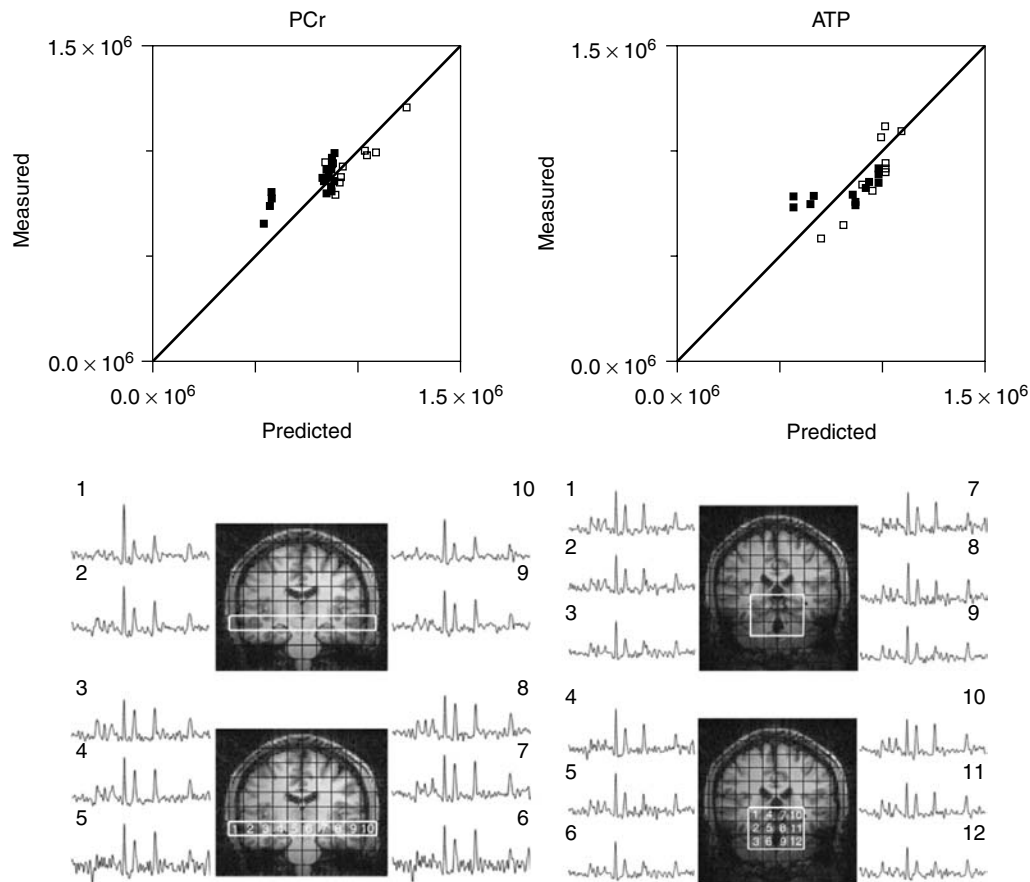


**Figure 11.6.** Plots of the predicted and measured values of PCr and ATP from 22 voxels (open squares) and (filled squares) from the region about the hippocampus. The solid line indicates values for which the measured and predicted values are identical. The locations of the 22 voxels (10 voxels spanning a row across the head at the level of the hippocampi and 12 spectra from a rectangular region about the hippocampi and superior portion of the cerebellum) are indicated on the scout images.

voxels of interest with 1.5 mm accuracy (64). Using this method, the variation in gray and white matter content of the selected voxels was dramatically reduced, also reducing the measured variation in PCr/ATP, providing for greater accuracy in comparing specific anatomical locations between subjects and controls. The fractional content of gray matter in the selected volumes was  $60 \pm 5\%$ ,  $55 \pm 4\%$  and  $47 \pm 4\%$  for the amygdala, pes and hippocampal body in controls. We then evaluated the extent of energetic impairment along the hippocampal formation (65). As shown in Figure 11.8, we observed a gradient of energetic impairment, with the greatest decline from anterior locations, and also greater declines in the ipsilateral hippocampus compared to the contralateral hippocampus. All three ipsilateral locations (body, pes and amygdala) were statistically different from normal controls, while the contralateral amygdala and pes were also statistically abnormal. Specifically, these data demonstrate that there is a clear regional heterogeneity in the impairment such that the decrement in PCr/ATP in comparison to normal controls is amygdala > pes > body and ipsi > contra. Analysis of the fractional tissue content of gray and white matter between patients and control subjects revealed no significant differences for the same locations

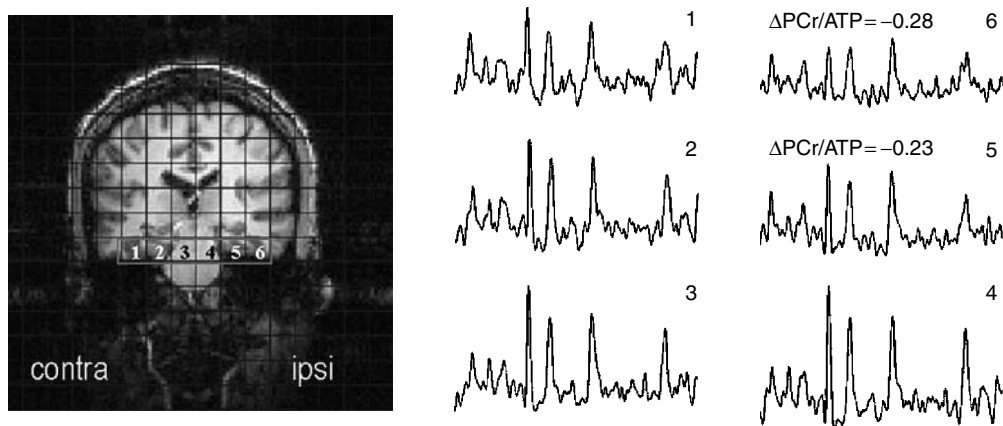


**Figure 11.7.** A scout image and spectra spanning the hippocampi in a patient with temporal lobe epilepsy. The calculated decrement in PCr/ATP is displayed above the spectra from the ipsilateral hippocampi.

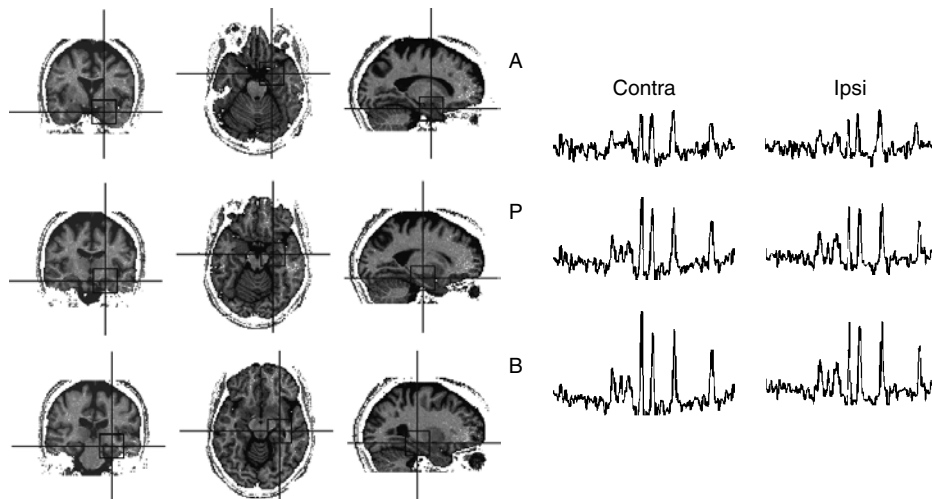


**Figure 11.8.** Orthogonal views from a 3D image set spanning the brain of a patient with temporal lobe epilepsy. The locations of the selected voxels are identified by the box and cross-hairs. The selected locations were: (A) amygdala; (P) pes, and (B) hippocampal body. The corresponding spectra from the ipsilateral and contralateral hippocampi are displayed in the spectra to the right.

allowing the locations to be directly correlated. The finding of greater energetic impairment from more anterior locations is also consistent with  $^1\text{H}$  MRSI data of Vermathen *et al.* (45) who reported that NAA declines were also more pronounced anteriorly in temporal lobe epilepsy hippocampus. This again supports the hypothesis that the reductions in NAA reflect ongoing impairment that may be mitochondrial in origin.

## 11.7. INTERPRETATION OF THE BIOENERGETIC ALTERATIONS

Similar to that seen in the  $^1\text{H}$  studies, Simor *et al.* (66) using  $^{31}\text{P}$  spectroscopic imaging reported that the energetic deficits seen in temporal lobe epilepsy patients were also reversible with successful surgery. In

this study, significant improvements in the contralateral hippocampus were observed 1 year after successful surgery. This indicated that the alterations in  $^{31}\text{P}$  metabolites were also not solely due to neuronal death, but reflected a dynamic and reversible process. Most recently, Pan *et al.* (25) have demonstrated that in pediatric epilepsy patients being treated with the ketogenic diet, bioenergetic impairments present prior to initiation of the diet are reversed as the seizures are brought under control. Specifically, after 4 months of the ketogenic diet therapy, the PCr/Pi and PCr/ATP ratios had improved by 22 and 14 % respectively. Thus both reductions in NAA and impairments in bioenergetics appear to be tightly linked with seizure activity and can be reversed with successful treatment.

Thus it appears clear that there is a significant bioenergetic component to the etiology of seizure disorders. However, it remains unclear as to whether this reflects the general damage associated with seizures or is a causative factor. If bioenergetic impairment is a causative factor, alternative treatments that modulate brain bioenergetics could provide an effective avenue for treatment. One such therapy is the use of the ketogenic diet in the treatment of nonlesional pediatric epilepsies. In this regimen, patients who are placed on a high fat, low carbohydrate diet become systemically ketotic, with elevated plasma and brain ketone levels. Although the exact mechanism for the ketogenic diet remains controversial, it is known that ketones can supplement or replace glucose as a fuel source for oxidation. In adults, ketone utilization has been reported to provide up to 25 % of total brain needs after only 3 days of fasting (67). Given that ketones are preferentially utilized by neurons as an alternate fuel source for oxidation (68), ketones can circumvent the normal mechanisms that couple glucose uptake to neuronal functional activity. Although the ketogenic diet is most commonly used in pediatric patients, recently Sirven *et al.* (69) have reported significant success in adult patients who maintain ketosis while on the diet. This finding further strengthens the general role of metabolism and bioenergetics in the pathophysiology of human epilepsy. However, this does not provide a mechanism linking the bioenergetic impairment directly to the symptoms of the disease, inappropriate electrical activity.

## 11.8. POSSIBLE MECHANISM LINKING BIOENERGETIC IMPAIRMENT AND SEIZURES

How these alterations in energetics and mitochondrial function may directly affect neurotransmission and the development of epilepsy is unknown. One possible mechanism is by modulating extracellular glutamate through alterations in  $\text{Ca}^{2+}$  sequestration in the pre-synaptic terminal. For example, Scotti *et al.* (70) have shown, in hippocampal cell cultures, that dissipation of the mitochondrial membrane potential with FCCP results in depolarization of the mitochondria and an inability of mitochondria in the pre-synaptic terminals to sequester intracellular  $\text{Ca}^{2+}$ . Elevations in  $\text{Ca}^{2+}$  in turn signal for release of synaptic vesicles and thus release the release of glutamate in glutamatergic terminals. As predicted, Scotti *et al.* (70) reported that the failure to sequester  $\text{Ca}^{2+}$  in turn led to increased spontaneous excitatory post-synaptic currents. Using the calyx of Held as a model for glutamatergic synapses, Billups *et al.* (71) reported that dissipation of the mitochondrial membrane potential with rotenone and cyanide *p*-trifluoromethoxyphenylhydrazone results in elevations of intracellular  $\text{Ca}^{2+}$ , and concluded that mitochondria are the major organelle regulating pre-synaptic calcium at central glutamatergic terminals.

Although cytoplasmic  $\text{Ca}^{2+}$  can also be cleared by the  $\text{Ca}^{2+}$  ATPase and the  $\text{Na}^+/\text{Ca}^{2+}$  exchanger, impairments in oxidative metabolism (by decreasing the availability of ATP) can also reduce flux through the  $\text{Ca}^{2+}$  ATPase. This would prolong elevations in  $\text{Ca}^{2+}$ , and thus enhance the release of glutamate. Similarly, a failure in oxidative metabolism might also reduce the efficiency of  $\text{Na}^+$  pumping and thus reduce the  $\text{Na}^+$  gradient across the terminal thereby depleting the driving force for the  $\text{Na}^+/\text{Ca}^{2+}$  exchanger. Thus in model systems (hippocampal tissue culture) neuronal mitochondrial damage and failures in neuronal bioenergetics can result in alterations in increased vesicular release of glutamate. As the primary excitatory

amino acid in mammalian brain, increased extracellular glutamate concentrations have been linked with hyper-excitability in several animal seizure models.

Thus impairments in oxidative metabolism in the neuronal mitochondria can lead to the build-up of extracellular glutamate, resulting in hyperexcitability and seizures. If true, the mitochondrial impairment would display the characteristic spectroscopic findings of decreased NAA and reduced PCr/ATP. Reversal of the mitochondrial impairment could restore extracellular glutamate homeostasis, which in principle could eliminate the inappropriate electrical activity. This too would manifest itself as an improvement in bioenergetics, as seen in the ketogenic diet work of Pan *et al.* (25), and the restoration of NAA levels as seen in temporal lobe epilepsy patients. Although the proposed mechanism is consistent with the spectroscopy data, additional investigations correlating intracellular  $\text{Ca}^{2+}$  and extracellular glutamate with  $^1\text{H}$  and  $^{31}\text{P}$  spectroscopic measures are needed to further evaluate the validity of these hypotheses.

As described, we have focused on the possible role of impairments in neuronal oxidative metabolism as leading to elevations of extracellular glutamate through enhanced glutamate release, possibly mediated by  $\text{Ca}^{2+}$ . However, extracellular glutamate levels are determined through the balance of both release and reuptake mechanisms. Thus metabolic alterations that lead to reduced astrocytic reuptake of extracellular glutamate and glutamate–glutamine cycling can also lead to increased extracellular glutamate and hyperexcitability. This possible mechanism will be the topic of the next chapter.

## REFERENCES

1. Hauser WA; Annegers JF; Kurland LT, Prevalence of epilepsy in Rochester Minnesota 1940–1980, *Epilepsia* **32**: 429–445, 1991.
2. Jack CR Jr; Sharbrough FW; Twomey CK; *et al.*, Temporal lobe seizures: lateralization with MR volume measurements of the hippocampal formation, *Radiology* **175**: 423–429, 1990.
3. Jackson GD; Connelly A; Duncan JS; Grunewald RA; Gadian DG, Detection of hippocampal pathology in intractable partial epilepsy: increased sensitivity with quantitative magnetic resonance T2 relaxometry, *Neurology* **43**: 1793–1799, 1993.
4. Spencer SS; McCarthy G; Spencer DD, Diagnosis of medial temporal lobe seizure onset: relative specificity and sensitivity of quantitative MRI, *Neurology* **43**: 2117–2124, 1993.
5. Kuzniecky RI, Magnetic resonance imaging in developmental disorders of the cerebral cortex, *Epilepsia* **35**: S44–S56, 1994.
6. Kuhl DE; Engel J Jr; Phelps ME; Selin C, Epileptic patterns of local cerebral metabolism and perfusion in humans determined by emission computed tomography of  $^{18}\text{FDG}$  and  $^{13}\text{NH}_3$ , *Ann Neurol* **8**: 348–360, 1980.
7. Engel J Jr; Kuhl DE; Phelps ME; Mazziotta JC, Interictal cerebral glucose metabolism in partial epilepsy and its relation to EEG changes, *Ann Neurol* **12**: 510–517, 1982.
8. Theodore WH; Newmark ME; Sato S; *et al.*,  $[^{18}\text{F}]$ fluorodeoxyglucose positron emission tomography in refractory complex partial seizures, *Ann Neurol* **14**: 429–437, 1983.
9. Abou-Khalil BW; Siegel GJ; Sackellares JC; Gilman S; Hichwa R; Marshall R, Positron emission tomography studies of cerebral glucose metabolism in chronic partial epilepsy, *Ann Neurol* **22**: 480–486, 1987.
10. Stefan H; Pawlik G; Bocher-Schwarz HG; *et al.*, Functional and morphological abnormalities in temporal lobe epilepsy: a comparison of interictal and ictal EEG, CT, MRI, SPECT and PET, *J Neurol* **234**: 377–384, 1987.
11. Ryvlin P; Cinotti L; Froment JC; *et al.*, Metabolic patterns associated with non-specific magnetic resonance imaging abnormalities in temporal lobe epilepsy, *Brain* **114**: 2363–83, 1991.
12. Sadzot B; Debets RM; Maquet P; *et al.*, Regional brain glucose metabolism in patients with complex partial seizures investigated by intracranial EEG, *Epilepsy Res* **12**: 121–129, 1992.
13. Duncan JS, Imaging and Epilepsy, *Brain* **120**: 339–377, 1997.
14. Hugg JW; Laxer KD; Matson GB; Maudsley AA; Weiner MW, Neuron loss localizes human temporal lobe epilepsy by *in vivo* proton magnetic resonance spectroscopic imaging, *Ann Neurol* **34**: 788–794, 1993.
15. Connelly A; Jackson GD; Duncan JS; King MD; Gadian DG, Magnetic resonance spectroscopy in temporal lobe epilepsy, *Neurology* **44**: 1411–1417, 1994.

16. Ng TC; Comair YG; Xue M; So N; Majors A; Kolem H; Luders H; Modic M, Temporal lobe epilepsy: presurgical localization with proton chemical shift imaging, *Radiology* **193**: 465–472, 1994.
17. Cendes F; Andermann F; Preul MC; Arnold DL, Lateralization of temporal lobe epilepsy based on regional metabolic abnormalities in proton magnetic resonance spectroscopic images, *Ann Neurol* **35**: 211–216, 1994.
18. Hetherington HP; Kuzniecky R; Pan JW; *et al.*, <sup>1</sup>H Spectroscopic imaging in temporal lobe epilepsy at 4.1 T, *Anal Neurol* **38**: 396–404, 1995.
19. Constantinidis I; Malko JA; Peterman SB; *et al.*, Evaluation of <sup>1</sup>H magnetic resonance spectroscopic imaging as a diagnostic tool for the lateralization of epileptogenic seizure foci, *Br J Radiol* **69**: 15–24, 1996.
20. Kuzniecky RI; Hugg JW; Hetherington HP; *et al.*, Relative Utility of <sup>1</sup>H spectroscopic imaging and hippocampal volumetry in the lateralization of mesial temporal lobe epilepsy, *Neurology* **51**: 66–71, 1998.
21. Hugg JW; Laxer KD; Matson GB; Maudsley AA; Husted CA; Weiner MW, Lateralization of human focal epilepsy by <sup>31</sup>P magnetic resonance spectroscopic imaging, *Neurology* **42**: 2011–2018, 1992.
22. Laxer KD; Hubesch B; Sappey-Marinier D; Weiner MW, Increased pH and inorganic phosphate in temporal seizure foci demonstrated by <sup>31</sup>P MRS, *Epilepsia* **33**: 618–623, 1992.
23. Kuzniecky R; Elgavish GA; Hetherington HP; Evanochko WT; Pohost GM, *In vivo* <sup>31</sup>P nuclear magnetic resonance spectroscopy of human temporal lobe epilepsy, *Neurology* **42**: 1586–1590, 1992.
24. Chu WJ; Hetherington HP; Kuzniecky RI; Simor T; Mason GF; Elgavish GA, Lateralization of human temporal lobe epilepsy by <sup>31</sup>P NMR spectroscopic imaging at 4.1 T, *Neurology* **51**: 472–479, 1998.
25. Pan JW; Bebin EM; Chu WJ; Kiel S; Hetherington HP, Ketosis and epilepsy: <sup>31</sup>P spectroscopic imaging at 4.1 T, *Epilepsia* **40**: 703–708, 1999.
26. Garcia PA; Laxer KD; van der Grond J; Hugg JW; Matson GB; Weiner MW, Phosphorous magnetic resonance spectroscopic imaging in patients with frontal lobe epilepsy, *Ann Neurol* **35**: 217–221, 1994.
27. Goldstein FB, The enzymatic synthesis of *N*-acetyl-aspartatic acid by sub-cellular preparation of rat brain, *J Biol Chem* **244**: 4257–4260, 1969.
28. Urenjack J; Williams SR; Gadian DG; Noble M, Specific expression of *N*-acetyl aspartate in neurons, oligodendrocyte type 2 astrocyte progenitors and immature oligodendrocytes *in vitro*, *J Neurochem* **59**: 55–61, 1992.
29. Spencer SS; McCarthy G; Spencer DD, Diagnosis of medial temporal lobe seizure onset: relative specificity and sensitivity of quantitative MRI, *Neurology* **43**: 2117–2124, 1993.
30. Chu WJ; Kuzniecky RI; Hugg JW; *et al.*, Evaluation of temporal lobe epilepsy using <sup>1</sup>H spectroscopic imaging segmentation at 4.1 T, *Magn Reson Med* **43**: 359–367, 2000.
31. Maton B; Gilliam F; Sawrie S; Faught E; Hugg J; Kuzniecky R, Correlation of scalp EEG and <sup>1</sup>H MRS metabolic abnormalities in temporal lobe epilepsy, *Epilepsia* **42**: 417–422, 2001.
32. Kuzniecky R; Hugg J; Hetherington H; Martin R; Faught E; Morawetz R; and Gilliam F, predictive value of <sup>1</sup>H MRSI for outcome in temporal lobectomy, *Neurology* **53**: 694–698, 1999.
33. Lundbom N; Gaily E; Vuori K; *et al.*, Proton spectroscopic imaging shows abnormalities in glial and neuronal cell pools in frontal lobe epilepsy, *Epilepsia* **42**: 1507–1514, 2001.
34. Kuzniecky RI; Hetherington HP; Pan JW; *et al.*, Proton spectroscopic imaging in patients with malformations of cortical development and epilepsy, *Neurology* **48**: 1018–1024, 1997.
35. Li LM; Cendes F; Bastos AC; Andermann F; Dubeau F; Arnold DL, Neuronal metabolic dysfunction in patients with cortical developmental malformations, *Neurology* **50**: 755–759, 1998.
36. Cendes F; Andermann F; Silver K; Arnold DL, Imaging of axonal damage *in vivo* in Rasmussen's syndrome, *Brain* **118**: 753–758, 1995.
37. Michaelis T; Merboldt KD; Bruhn H; Hänicke W; Frahm J, Absolute concentrations of metabolites in the adult human brain *in vivo*: quantification of localized proton MR spectra, *Radiology* **187**: 219–227, 1991.
38. Kreis R; Ernst T; Ross BD, Absolute quantification of water and metabolites in human brain II. Metabolite concentrations, *J Magn Res Ser B* **102**: 9–19, 1993.
39. Hetherington HP; Pan JW; Mason GF; *et al.*, Quantitative <sup>1</sup>H spectroscopic imaging of human brain at 4.1 T using image segmentation, *Magn Reson Med* **36**: 21–29, 1996.
40. Lundbom N; Barnett A; Bonavita S; *et al.*, MR image segmentation and tissue metabolite contrast in <sup>1</sup>H spectroscopic imaging of normal and aging brain, *Magn Reson Med* **41**: 841–845, 1999.
41. Lim KO; Spielman DM, Estimating NAA in cortical gray matter with applications for measuring changes due to aging, *Magn Reson Med* **37**: 372–377, 1997.

42. Vermathen P; Laxer KD; Matson GB; Weiner MW, Hippocampal structures: anteroposterior *N*-acetylaspartate differences in patients with epilepsy and control subjects as shown with proton MR spectroscopic imaging, *Radiology* **214**: 403–410, 2000.

43. Hugg JW; Kuzniecky RI; Gilliam FG; Morawetz RB; Faught RE; Hetherington HP, Normalization of contralateral metabolic function following temporal lobectomy demonstrated by <sup>1</sup>H MRSI, *Ann Neurol* **40**: 236–239, 1996.

44. Cendes F; Andermann F; Dubeau F; Matthew PM; Arnold DL, Normalization of neuronal metabolic dysfunction after surgery for temporal lobe epilepsy, *Neurology* **49**: 1525–1533, 1997.

45. Vermathen P; Ende G; Laxer KD; Walker JA; Knowlton RC; Barbaro NM; Matson GB; Weiner MW, Temporal lobectomy for epilepsy: recovery of the contralateral hippocampus measured by <sup>1</sup>H MRS, *Neurology* **59**: 633–636, 2002.

46. Serles W; Li LM; Antel SB; *et al.*, Time course of postoperative recovery of *N*-acetyl-aspartate in temporal lobe epilepsy, *Epilepsia* **42**: 190–197, 2001.

47. Kuzniecky R; Palmer C; Hugg J; Martin R; Sawrie S; Morawetz R; Faught E; Knowlton R, Magnetic Resonance spectroscopic imaging in temporal lobe epilepsy: neuronal dysfunction or cell loss?, *Arch Neurol* **58**: 2048–2053, 2001.

48. Eng LF; Ghirnikar RS; Lee YL, Glial fibrillary acidic protein: GFAP—thirty one years (1969–2000), *Neurochem Res* **25**: 1439–1451, 2000.

49. Margerison JH; Corsellis JAN, Epilepsy and the temporal lobes, *Brain* **89**: 499–503, 1966.

50. Hetherington HP; Pan JW; Mason GF; Ponder SL; Twieg DB; Deutsch G; Mountz J; Pohost G, 2D spectroscopic imaging of the human brain at 4T, *Magn Reson Med* **32**: 530–534, 1994.

51. Davie CA; Barker GJ; Thompson AJ; Tofts PS; McDonald WI; Miller DH, <sup>1</sup>H magnetic resonance spectroscopy of chronic cerebral white matter lesions and normal appearing whitematter in multiple sclerosis, *J Neurol Neurosurg Psychiatry* **63**: 736–742, 1997.

52. Schuff N; Amend DL; Meyerhoff DJ; Tanabe JL; Norman D; Fein G; Weiner MW, Alzheimer disease: quantitative H-1 MR spectroscopic imaging of frontoparietal brain, *Radiology* **207**: 91–102, 1998.

53. Salvan AM; Vion-Dury J; Confort-Gouny S; Nicoli F; Lamoureux S; Cozzzone PJ, Brain proton magnetic resonance spectroscopy in HIV-related encephalopathy: identification of evolving metabolic patterns in relation to dementia and therapy, *AIDS Res Hum Retroviruses* **10**: 1055–66, 1997.

54. Mehta V; Namboodiri MA, *N*-acetylaspartate as an acetyl source in the nervous system, *Brain Res Mol Brain Res* **31**: 151–157, 1995.

55. Miller SL; Daikhin Y; Yudkoff M, Metabolism of *N*-acetylaspartate in rat brain, *Neurochem Res* **21**: 615–618, 1996.

56. Taylor DL; Davies SEC; Onrenovitch TP; Doheny MH; Patsalos PN; Clark JB; Symon L, Investigation into the role of *N*-acetylaspartate in cerebral osmoregulation, *J Neurochem* **65**: 275–281, 1995.

57. Heales SJR; Davies SEC; Bates TE; Clark JB, Depletion of brain glutathione is accompanied by impaired mitochondrial function and decreased *N*-acetylaspartate concentration, *Neurochem Res* **20**: 31–38, 1995.

58. Bates TE; Strangward M; Keelan J; Davey GP; Munro PMG; Clark JB, Inhibition of *N*-acetylaspartate production: implications for <sup>1</sup>H MRS studies *in vivo*, *Neuroreport* **7**: 1397–1400, 1996.

59. Lara RS; Matson GB; Hugg JW; Maudsley AA; Weiner MW, Quantitation of *in vivo* phosphorus metabolites in human brain with magnetic resonance spectroscopic imaging (MRSI), *Magn Reson Imaging* **11**: 273–278, 1993.

60. Hubesch B; Sappey-Marinier D; Roth K; Meyerhoff DJ; Matson GB; Weiner MW, <sup>31</sup>P-31 MR spectroscopy of normal human brain and brain tumors, *Radiology* **174**: 401–409, 1990.

61. Hoang TQ; Bum L; Dubowitz DJ; Moats R; Kopyov O; Jacques D; Ross BD, Quantitative proton decoupled <sup>31</sup>P MRS and <sup>1</sup>H MRS in the evaluation of Huntington's and Parkinson's disease, *Neurology* **50**: 1033–1040, 1998.

62. Roth K; Hubesch B; Meyerhoff DJ; Naruse S; Gober JR; Lawry TJ; Bosk MD; Matson GB; Weiner MW, Noninvasive quantitation of phosphorus metabolites in human tissue by NMR spectroscopy, *J Magn Reson* **81**: 299–311, 1989.

63. Hetherington HP; Spencer DD; Vaughan JT and Pan JW, Quantitative <sup>31</sup>P spectroscopic imaging of human brain at 4T: assessment of gray and white matter differences of phosphocreatine and ATP, *Magn Reson Med* **45**: 46–52, 2001.

64. Twieg DB; Meyerhoff DJ; Hubesch B; Roth K; Sappey-Marinier D; Boska MD; Gober JR; Schaefer S; Weiner MW, Phosphorus-31magnetic resonance spectroscopy in humans by spectroscopic imaging: localized spectroscopy and metabolite imaging, *Magn Reson Med* **12**: 291–305, 1989.
65. Hetherington HP; Pan JW; Firlik KS; Spencer DD, Bioenergetic abnormalities in temporal lobe epilepsy, *Proc Int Soc Magn Reson Med* p 419, 2002.
66. Simor T; Chu WJ; Hetherington HP; Kuzniecky RI; Elgavish GA, Tailored temporal lobectomy induced improvements in 4.1 T 31PNMR SI generated phosphorous metabolite indices in temporal lobe epilepsy, Proceedings of the International Society of Magnetic Resonance in Medicine, p 33, Vancouver, British Columbia, Canada, April 1997.
67. Hasselbalch SG; Knudsen GM; Jakobsen J; Hageman LP; Holm S; Paulson OB, Brain metabolism during short-term starvation in humans, *J Cereb Blood Flow Metab* **14**: 125–131, 1994.
68. Pan JW; de Graaf RA; Petersen KF; Shulman GI; Hetherington HP; Rothman DL, [2,4-13C2]-b-hydroxybutyrate metabolism in human brain, *J Cereb Blood Flow Metab* **22**: 890–898, 2002.
69. Sirven J; Whedon B; Caplan D; *et al.*, The ketogenic diet for intractable epilepsy in adults: preliminary results, *Epilepsia* **40**: 1721–1726, 1999.
70. Scotti AL; Chatton JY; Reuter H, Roles of Na(+)–Ca<sup>2+</sup> exchange and of mitochondria in the regulation of presynaptic Ca<sup>2+</sup> and spontaneous glutamate release, *Philos Trans R Soc London Ser B Biol Sci* **354**(1381): 357–364, 1999.
71. Billups B; Forsythe ID, Presynaptic mitochondrial calcium sequestration influences transmission at mammalian central synapses, *J Neurosci* **22**(14): 5840–5847, 2002.



# 12

## MRS Studies of the Role of Altered Glutamate and GABA Neurotransmitter Metabolism in the Pathophysiology of Epilepsy

**Ognen A. C. Petroff and Dennis D. Spencer**

*Department of Neurology, Yale University School of Medicine, P.O. Box 208018, New Haven, CT 06520-8018, USA*

---

12.1	Introduction	216
12.2	Part I: MRS Studies of the Role of Astroglial Metabolism in Temporal Lobe Epilepsy	217
12.2.1	Glutamate Release is Increased and Clearance is Slowed in the Epileptogenic Zone	218
12.2.2	Glutamate–Glutamine Cycle	219
12.2.3	Cortical Glutamate Away From the Seizure Focus is Increased in Epilepsy Patients	220
12.2.4	Cellular Glutamate is Increased in the Epileptogenic Zone	221
12.2.5	Measuring the Glutamate–Glutamine Cycle in the Epileptogenic Hippocampus	222
12.2.6	The Glutamate–Glutamine Cycle to TCA Cycle Ratios are Markedly Reduced in the Human Epileptogenic Hippocampus with Severe Neuron Loss and Glial Proliferation	224
12.2.7	Intracellular Glutamine Content is Low in the Epileptogenic Hippocampus Despite a Major Increase in Glial Density	225
12.2.8	Proposed Metabolic Model of MTLE with Hippocampal Sclerosis	226
12.3	Part II: MRS Studies of the Role of GABA in Epilepsy	227

12.3.1 Intracellular GABA Levels Modulate the Release and Re-uptake of Extracellular GABA	227
12.3.2 Cellular GABA and Cortical Excitability	228
12.3.3 Low Cortical GABA Content is Associated with Low Rates of GABA Synthesis	230
12.3.4 Inhibition of the GABA–Glutamine or GABA–Glutamate Cycle Results in Seizures	230
12.4 Conclusion: Alteration of Metabolism in Localization Related Epilepsies and Significance for Epileptogenicity	232

---

## 12.1. INTRODUCTION

One out of every 20 Americans will suffer one or more seizures in their lifetime. The application of MRI and MRS to identify localization-related epilepsies has made a major impact on the successful treatment of the disease by surgery. Magnetic resonance methods have been in clinical use for a number of years and permit serial, noninvasive measurements of certain cerebral metabolites without discomfort or known hazards. Several recent reviews examined the value of magnetic resonance imaging (MRI) and spectroscopy (MRS) in the evaluation of the patient with epilepsy (Duncan, 1997; Cascino, 2001; Jackson and Van Paesschen, 2002; Cendes *et al.*, 2002; Hetherington *et al.*, 2002a). *N*-Acetyl aspartate levels and the ratios of *N*-acetyl aspartate to creatine (NAA/Cr) are often decreased in the epileptogenic temporal lobe. The changes are usually widespread, can affect the temporal lobe contralateral to the epileptogenic hippocampus and appear to correlate with regions of interictal hypometabolism measured using positron emission tomography. Below normal *N*-acetyl aspartate or NAA/Cr ratios can provide evidence of temporal lobe abnormalities in epilepsy patients who show no abnormality with MRI. Below normal *N*-acetyl aspartate in the temporal lobe contralateral to the epileptogenic one removed by surgery can herald a poor outcome. Despite these advances there remains a significant fraction of patients with these epilepsy syndromes who do not respond well to surgery or conventional drug treatment. The ability to diagnose patients who fall into this category has the potential of improving the quality of their medical care through both avoiding unnecessary surgery and targeting appropriate drug treatment. Furthermore better mechanistic understanding of the etiology of the disease may both further improve the ability to localize surgically treatable epilepsy, and potentially allow early intervention to prevent the progression of the disease to where surgery is required.

In order to address this challenge, we have focused on applying MRS methods for studying brain glutamate and GABA metabolism in epilepsy. Glutamate is the primary excitatory and GABA the primary inhibitory neurotransmitters. Alterations in both glutamatergic and GABAergic systems have been strongly implicated in epileptic syndromes. Continuing MRS development has resulted in techniques for the measurement of cerebral GABA and glutamate in humans, as well as the energetics and neurotransmitter fluxes associated with these compounds. The key linkage between neurotransmission and metabolism exploited by these methods is the role of the astroglia in recycling glutamate and GABA released by the neurons into the synaptic cleft. Once taken up by the astroglia the glutamate or GABA is converted to glutamine. Glutamine is then transported from the glia and taken up by the neuron for conversion to glutamate in glutamatergic neurons and GABA in GABAergic neurons. By using <sup>13</sup>C-labeled precursors the rates of glutamate and GABA neuronal release and recycling may be obtained through analysis of <sup>13</sup>C MRS time courses of glutamate, glutamine, and GABA labeling.

In this chapter, we describe some of the insights gained into the etiology and pathogenesis of epilepsy through the study of glutamate neurotransmitter cycling and neuroenergetics. The chapter is divided into two parts. The first section describes the results of studies on the role of impaired astroglial metabolism in temporal lobe epilepsy. These studies were motivated by the finding that glutamate clearance is impaired in the damaged epileptogenic hippocampus, resulting in elevated extracellular glutamate even under interictal conditions of low activity (Petroff *et al.*, 2002a). In addition to being excitotoxic, elevated extracellular glutamate leads to neuronal hyperexcitability and potentially increased susceptibility to seizure. The MRS studies have shown that the rate of the glutamate–glutamine cycle is greatly reduced in the sclerotic hippocampus, and that cellular glutamate is elevated (Petroff *et al.*, 2002b). Both of these metabolic changes may be major contributors to the epileptogenic condition. At the end of the section, we propose a model which links the elevated extracellular glutamate measured interictally to a defect in astroglial glutamine synthetase.

In Section 12.3 we describe the results of work examining the role of GABA metabolism in epilepsy and the regulation of cortical excitability. These studies stem from advances in MRS technology which have allowed the measurement of cellular GABA and its major metabolites noninvasively in the brain of healthy human subjects (Rothman *et al.*, 1993, 1997; Hyder *et al.*, 1999), and assess how it is altered in epilepsy and its role in the treatment of epilepsy. These studies have found low occipital lobe GABA concentrations in patients with poorly controlled partial seizures, mainly temporal lobe epilepsy (TLE). Raising cellular GABA levels with GABAergic drugs correlates with improvement of seizure control in partial epilepsy patients (Petroff *et al.*, 1996, 1998, 1999a). In addition, below normal cellular GABA levels are found in patients with idiopathic generalized epilepsy (Petroff *et al.*, 2001). These results support a significant role for GABA metabolism, as expressed through GABA concentration, in the hyperexcitability associated with the epileptic condition. Consistent with this hypothesis we have shown an association between increasing excitability in the visual cortex and decreasing GABA concentrations induced by light deprivation in healthy human subjects (Boroojerdi *et al.*, 2000a,b).

## 12.2. PART I: MRS STUDIES OF THE ROLE OF ASTROGLIAL METABOLISM IN TEMPORAL LOBE EPILEPSY

Temporal lobe epilepsy (TLE) is a microcosm of all localization-related epilepsies (Spencer, 2002a; de Lanerolle *et al.*, 2003). It has multiple underlying mechanisms, anatomical and molecular substrates, and presentations. Mesial temporal lobe epilepsy (MTLE) is the most common refractory partial epilepsy, and also the one most often treated surgically, because medical treatment fails in 75 % of cases. The combination of neuronal loss of at least 30 % (often greater) in the hippocampus and gliosis is called hippocampal sclerosis (HS), which is the structural correlate that underlies temporal lobe seizures of mesial temporal electrical origin, and together these features define MTLE. Neoplasms account for 10–15 % of TLE, and are commonly glial in origin. The tumors may invade the hippocampus. Mass-associated TLE (MaTLE) usually refers to non-hippocampal, most often neocortical tumors, that have not invaded the epileptogenic hippocampus. Developmental abnormalities account for another 20 % of the pathological findings in uncontrolled TLE. Developmental abnormalities are associated with mesial temporal sclerosis in 15–25 % of cases (so-called dual pathology). Conversely, 10–15 % of patients with hippocampal atrophy also have evidence of cortical developmental abnormalities. Finally, trauma accounts for 5–10 % of TLE. An altered neuron to glia ratio with decreased numbers of neurons and increase numbers of astrocytes characterizes most of these pathological states.

Astroglial uptake of glutamate plays a key role in maintaining the low extracellular levels needed for proper receptor-mediated functions. Studies of glutamatergic synapses have shown them to be closely surrounded by glial end processes possessing high densities of glutamate transporters (Danbolt, 2001).

Glutamate transporters are sodium dependent and electrogenic and have an affinity,  $K_m$ , of 1–3  $\mu\text{M}$ , which is in the range of normal estimated extracellular glutamate concentrations (Bergles *et al.*, 1999; Dzubay and Jahr, 1999). The physiological importance of astroglial glutamate transport was demonstrated in studies in which antisense oligonucleotides directed against the astrocytic glutamate and aspartate transporters GLT1 or GLAST *in vivo* result in elevated extracellular glutamate *in vivo* and excitotoxicity (Rothstein *et al.*, 1996). The large majority of cortical glutamate uptake after release is astroglial and tightly coupled to the glial sodium–potassium ATPase and therefore glial energy metabolism (Bergles and Jahr, 1997; Danbolt, 2001). Under severely depolarizing conditions of elevated extracellular potassium and glutamate, which can occur during a seizure, glutamate transporters reverse catastrophically releasing glutamate and aspartate (Rossi *et al.*, 2000; During and Spencer, 1993; Wilson *et al.*, 1996).

Compared with controls obtained at autopsy, the resected hippocampus from patients with MTLE and hippocampal sclerosis (decreased neuron densities) demonstrated altered glutamate transporter expression including increased EAAT3 on remaining granule cells and pyramidal neurons, decreased glial EAAT2 (GLT-1) in the hilus and CA1 stratum radiatum associated with neuron loss, and increased glial EAAT1 (GLAST) in CA2/3 stratum radiatum (Mathern *et al.*, 1999). Under normal conditions, GLAST and GLT-1 are located on astrocytic membranes. Glia surrounding granular and pyramidal neurons continued to express GLT-1. Glial GLAST expression was increased in 73 % of patients. These findings, combined with the finding of increased extracellular glutamate (discussed below), suggest that the increased expression of glutamate transporters were not maintaining effectively extracellular glutamate homeostasis. An increase in glial intracellular sodium, hydrogen ion (acidity) or glutamate content would contribute to glutamate transporter dysfunction by making glutamate uptake energetically more expensive. Under such conditions, failure of extracellular potassium buffering resulting in glial depolarization could be expected to result in reversal of GLAST and a catastrophic release of glutamate.

### 12.2.1. Glutamate Release is Increased and Clearance is Slowed in the Epileptogenic Zone

Dialysate glutamate was reported elevated in spiking neocortex, increasing during seizures (Sherwin, 1999; Wilson *et al.*, 1996). Increasing extracellular glutamate is associated with initiation of seizure discharges in human hippocampus measured *in vivo* by simultaneous depth electrode electroencephalography and microdialysis. The release of glutamate by the hippocampus *contralateral* to the seizure focus is less in both amplitude and duration (Figure 12.1). What is unclear is whether the excess glutamate was released by a vesicular (glutamatergic neurons) or nonvesicular (primarily glia) mechanisms. Post-ictal glutamate re-uptake is threefold slower in the epileptogenic hippocampus than the contralateral one. This suggests that glutamate uptake mechanisms, i.e., glutamate transporter function, are slowed or deficient. This finding is surprising because of severe glutamatergic neuron loss and extensive glial proliferation present in mesial temporal sclerosis resulting in a tenfold increase in the number of glia per neuron (Luby *et al.*, 1995; Spencer *et al.*, 1999; de Lanerolle *et al.*, 2003). Despite the greater density of glia in the atrophic hippocampus, the glia are less effective in clearing extracellular glutamate. Partial dysfunction of the glia slowing the glutamate–glutamine cycle could account for the findings.

Extracellular glutamate levels, measured in the interictal period more than 5 h after the last electrographic seizure, were elevated nearly fivefold in the epileptogenic hippocampus (Cavus *et al.*, 2002). Notably, while the basal extracellular glutamate levels in the non-epileptogenic hippocampi were within known normal limits (less than 5  $\mu\text{M}$ ), the levels in the epileptogenic ones were often very elevated, potentially within the neurotoxic range. Paradoxically, interictal, microdialysis glutamate levels were more elevated in those patients with a greater loss of hippocampal neurons. Neuron loss accounted for 70 % of the variance in extracellular glutamate. Raised extracellular glutamate hours into the interictal state suggest a defect in glial glutamate clearance rather than enhanced glutamate release.

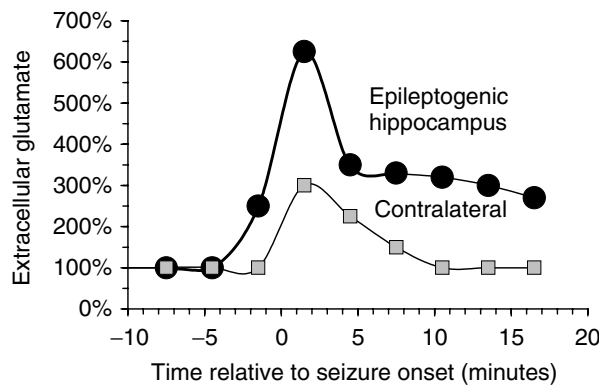


**Figure 12.1.** Microdialysis measurements from paired Spencer electrodes/catheters placed in both hippocampi of patients with MTLE. During a spontaneous seizure, the extracellular glutamate concentrations of the epileptogenic hippocampus increase more than in the contralateral one. Glutamate clearance after the seizure is threefold slower. The figure is drawn from data published by During and Spencer (1993).

Human glioma, often presenting with seizures, release large amounts of glutamate, raising extracellular glutamate to excitotoxic levels (Ye and Sontheimer, 1999). This mechanism can account for the high extracellular glutamate when epileptogenic glial tumors invade the hippocampus. Unlike normal astrocytes, glial tumors actively take up glutamine and release glutamate. Proliferating glia in the kainic acid model of MTLE also release glutamate into the extracellular space (Stein-Behrens *et al.*, 1994; Yusim *et al.*, 2000). Increased glial glutamate release is attributed to continued activity of the glutamate–cystine antiporter coupled to failure of GLAST and GLT-1. Decreased glial glucose metabolism, associated with decreased glucose transporter (GLUT1) expression and resulting decreased glial energy metabolism, appears to be responsible for decreased glutamate uptake. Glial energy failure would increase intracellular phosphate levels thereby stimulating PAG activity. The enhanced conversion of glutamine to glutamate would raise glial glutamate content.

### 12.2.2. Glutamate–Glutamine Cycle

Astroglia replete neuronal glutamate through the glutamate–glutamine cycle (Figure 12.2). Neurons lack the enzymes required for *de novo* synthesis of glutamate, and therefore depend on astroglia to provide substrates for the synthesis of glutamate lost during neurotransmission (Hertz *et al.*, 1999). The complete pathway is called the glutamate–glutamine cycle. Studies in the rat cerebral cortex have shown that the rate of the glutamate–glutamine cycle is coupled in a close to 1:1 ratio to neuronal (primarily glutamatergic) glucose oxidation above the rate measured with an isoelectric electroencephalogram (EEG) (Sibson *et al.*, 1998a,b). There is a highly significant association between electrical activity measured using EEG, the rate of glucose consumption, and glutamate–glutamine cycling.

In the normal adult brain, the glutamate concentration of gray matter primarily reflects the glutamate concentration in glutamatergic neurons, whose glutamate content is far greater than nonglutamatergic neurons or glia (Ottersen *et al.*, 1992). Neuronal glutamate is lost during glutamate transmitter release and is taken up by glia where it is recycled by glutamine synthetase (Danbolt, 2001). With increased excitatory activity, the rate of neuronal glutamate loss would be greater. Glutamate lost from the neuron is replaced through phosphate-activated glutaminase (PAG) acting upon glutamine synthesized in the glia (Fonnum, 1993; Conti and Minelli, 1994). Inhibition of PAG or blockade of glutamine transporters slows

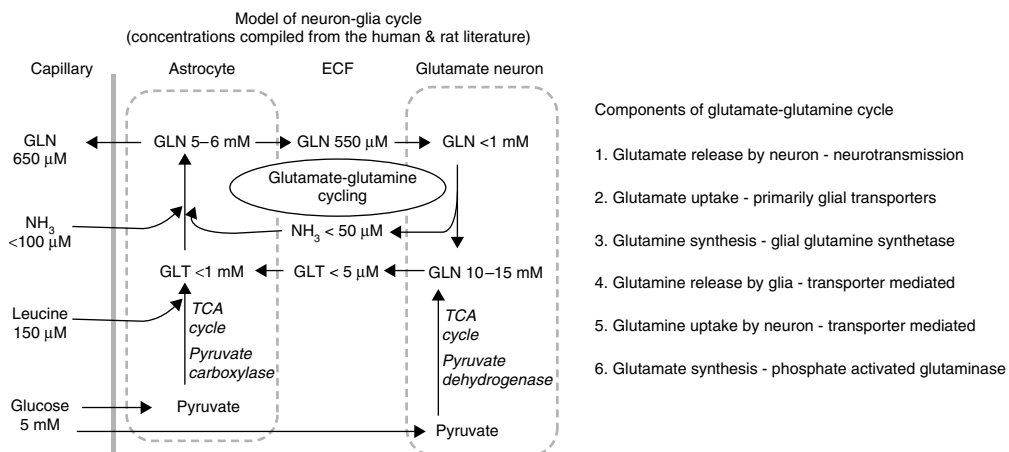


**Figure 12.2.** Schematic diagram of the glutamate–glutamine cycle between neurons and glia. The diagram is adapted from Petroff *et al.* (2002a).

the glutamate–glutamine cycle and decreases neuronal glutamate and GABA (Rae *et al.*, 2003; Chaudry *et al.*, 2002).

### 12.2.3. Cortical Glutamate Away From the Seizure Focus is Increased in Epilepsy Patients

Extensive studies in animals have shown that changes in glutamate release and metabolism may play an important role in the origin and spread of seizure activity (Bradford, 1995; Sherwin and van Gelder, 1986). Glutamate metabolism is coupled closely to mitochondrial respiration and ATP synthesis. Neurotransmitter glutamate release from synaptosomes is drastically reduced if either ATP or cytosolic glutamate concentrations are depleted, which is consistent with a critical role for cytosolic glutamate metabolism for maintaining the vesicular pool. As a result of the relationship between cytosolic and vesicular glutamate concentrations, an increase in cytosolic glutamate appears to enhance vesicular glutamate release. Glia efficiently remove glutamate released by neurons and help to terminate the action of released glutamate. *In vitro* and *in vivo* studies indicate that a major portion of glutamate transported into glia is converted to glutamine (neutral metabolite) and returned to neurons for the resynthesis of glutamate. Disturbances of the glutamate–glutamine cycle, responsible for the increased intracellular glutamate levels and impaired glutamate clearance could be an important metabolic change associated with epileptogenesis.

Neocortical intracellular glutamate levels are increased in the epileptic human brain. Biopsies of human temporal lobe cortex ipsilateral to the epileptogenic hippocampus show that glutamate is elevated by  $2.3 \mu\text{mol/g}$  in spiking cortex compared with adjacent non-spiking cortex (Sherwin, 1999). Biopsies of epileptic, but not necessarily epileptogenic, neocortex ipsilateral to the seizure focus show an increase in intracellular glutamate content of  $0.4$  to  $2.1 \mu\text{mol/g}$  compared to tissue resected from the margin of tumors of patients without seizures (reviewed in Petroff *et al.*, 1995).

Proton MRS has been used to measure intracellular glutamate levels (Petroff *et al.*, 1995, 1999a, 2000, 2002c). Occipital lobe glutamate levels of localization-related epilepsy patients with frequent seizures treated with carbamazepine or phenytoin are higher than those of epilepsy-free, drug-free volunteers (Figure 12.3). Mean glutamate content remote from the seizure focus is  $0.7 \text{ mM}$  greater in our patients with refractory complex partial seizures than control subjects. Glutamate plus glutamine (GLX) levels

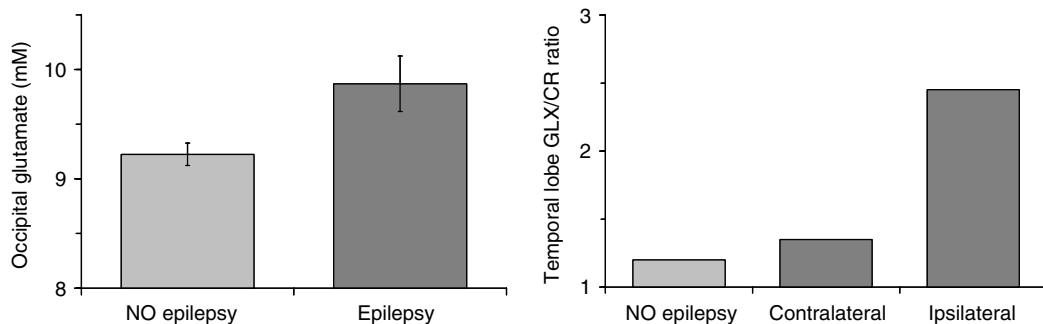


**Figure 12.3.** Graph on the left shows that mean intracellular glutamate levels ( $\pm$  standard error) measured using proton-MRS from the occipital lobe of nine patients with refractory, complex partial seizures treated with carbamazepine or phenytoin and ten drug-free, epilepsy-free volunteers. Intracellular glutamate levels remote from the seizure focus are increased, potentially contributing to the spread of seizure activity. The graph is drawn from data published by Petroff *et al.* (2000). Graph on the right shows the mean ratios of glutamate plus glutamine (GLX) to creatine plus phosphocreatine (CR) measured by *in vivo* proton MRS of the human temporal lobe. The graph is drawn from data published by Savic *et al.* (2000).

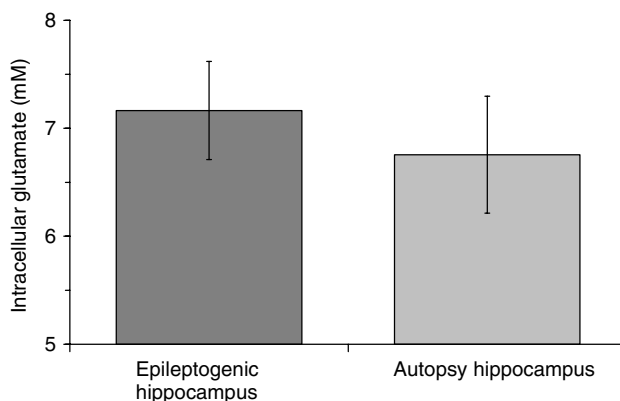


**Figure 12.4.** Mean intracellular glutamate levels ( $\pm$  standard error) of portion of the hippocampus removed at surgery for TLE compared to values reported for histologically normal hippocampi obtained at autopsy. Neuron loss is measured in an adjacent slice of the pes. Intracellular glutamate concentrations are elevated in the epileptogenic human hippocampus removed by surgery. Graph is drawn from data that includes values published by Petroff *et al.* (2002a).

appear to be increased in the temporal lobe ipsilateral to the seizure onset (Woermann *et al.*, 1999; Savic *et al.*, 2000). The increased neocortical glutamate levels ipsilateral to the epileptogenic temporal lobe suggest that increased intracellular glutamate content could contribute to the hyperexcitability of the epileptic network facilitating spread of seizure activity to brain regions outside of the ictal onset zone. Imaging glutamate may become very useful in mapping epileptic networks (Spencer, 2002b).

#### 12.2.4. Cellular Glutamate is Increased in the Epileptogenic Zone

Intracellular glutamate concentrations are elevated in the epileptogenic human hippocampus (Figure 12.4). The elevation is even more striking when hippocampal glutamate content is corrected for 60 % neuron

loss (Petroff *et al.*, 2002a). Compared with the autopsy series mean, hippocampal glutamate is elevated in MTLE patients. Elevated glutamate content is present in hippocampi with a normal clinical MRI appearance. Even higher levels are present in almost half the hippocampi with the greatest neuron loss. Intracellular glutamate concentrations must be exceedingly high in the remaining glutamatergic neurons or above normal, intracellular, glutamate concentrations must be present in the remaining non-glutamatergic neurons or glia. Brain glutamate levels should decrease in proportion to neuronal loss or simplification (loss of neuronal volume through shrinkage of dendrite, synapses, and other processes). The neuron loss, particularly of large glutamatergic neurons, and glial proliferation should decrease glutamate concentrations in the sclerotic hippocampus. Intracellular glutamate and glutamine content are the same in biopsies of epileptogenic hippocampi with the least and most severe neuron loss. Hippocampal neuron loss appeared to have little impact on the cellular content of glutamate ( $R^2 < 0.01$ ) or glutamine ( $R^2 < 0.01$ ). Our data were quite remarkable in that they failed to show any significant relationship between the degree of neuronal loss and the cellular content of glutamate (a major neuronal metabolite) and glutamine (a major glial metabolite). Rank-order regression shows that less than 2 % of the variability in cellular metabolite content is accounted for by the fourfold difference in the degree of neuron loss. Our findings suggest that there appears to be a relative increase in cellular glutamate content in the epileptogenic human hippocampus.

Under normal conditions, increased tissue glutamate would reflect increased intracellular levels in the glutamatergic neurons. However, one third of the epileptogenic HS hippocampus with more than 60 % neuron loss had the highest glutamate concentrations. The other subpopulation with clearly above normal glutamate content was those hippocampi with the least neuron loss (Ma-TLE and PTLE groups, see de Lanerolle *et al.*, 2003). The findings raise two possibilities. Either the remaining neurons, mainly 'GABAergic', have extremely high intracellular glutamate content or a subpopulation of glial cells must have high glutamate content. Cell culture studies suggest that glial precursor cells have high intracellular glutamate content (Urenjak *et al.*, 1993; Bhakoo and Pearce, 2000). Above normal intracellular glutamate concentrations could contribute to the above normal release of glutamate measured in the epileptogenic human hippocampus during spontaneous seizures. The high glutamate content would be expected to contribute to the epileptic state by increasing network excitability and promoting excitotoxicity.

### 12.2.5. Measuring the Glutamate–Glutamine Cycle in the Epileptogenic Hippocampus

In order to determine whether glutamate–glutamine cycling is impaired in MTLE we have developed a strategy for determining the ratio of the glutamate–glutamine cycle ( $V_{\text{cycle}}$ ) to the rate of the total glutamate synthesis rate, TCA cycle ( $V_{\text{TCA}}$ ) as well as the total glutamine synthesis ( $V_{\text{GS}}$ ) from steady state  $^{13}\text{C}$  labeling patterns in glutamate and glutamine (Figure 12.5). The strategy takes advantage of the label from  $2\text{-}^{13}\text{C}$ -glucose being incorporated into the internal positions of glutamate and glutamine only through the glia (Sibson *et al.*, 2001; Petroff *et al.*, 2002b). Label from  $2\text{-}^{13}\text{C}$ -glucose, which enters the TCA cycle through pyruvate dehydrogenase (PDH), is incorporated into  $5\text{-}^{13}\text{C}$ -glutamate and  $1\text{-}^{13}\text{C}$ -glutamate. It does not label the internal positions of glutamate or glutamine. In contrast,  $^{13}\text{C}$  label entering the TCA cycle from the anaplerotic pathway through pyruvate carboxylase will label glial glutamine C2 and C3 initially because both pyruvate carboxylase (PC) and glutamine synthetase (GS) are found exclusively in glia. Subsequently labeled glutamine will be taken up by the neurons to replenish released glutamate by the glutamate–glutamine cycle. The labeling in neuronal C3-glutamate is diluted relative to the precursor C3-glutamine due to unlabeled carbons entering through the neuronal TCA cycle ( $V_{\text{unlabeled}}$ ). From the ratio of C3-glutamine to C3-glutamate labeling at isotopic steady state the ratio of the rate of glutamate–glutamine cycle to neuronal TCA cycle ( $V_{\text{cycle}}/V_{\text{TCA}}$ ) may be calculated using the equations given below.

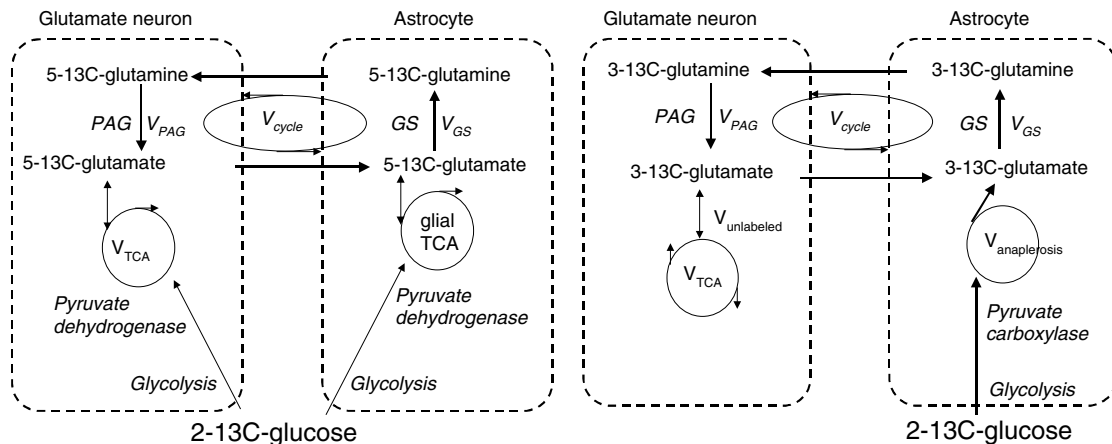


**Figure 12.5.** Schematic diagram of  $2-^{13}\text{C}$ -glucose metabolism adapted from Petroff *et al.* (2002b).

At isotopic steady state the label inflows and effluxes from the glutamate and glutamine pools must be equal and the isotopic enrichment of  $3-^{13}\text{C}$ -glutamate is determined by the following isotopic balance equation:

$$d[3-^{13}\text{C}\text{-glutamate}]/dt = 0 = \text{GN3}V_{\text{cycle}} + 0.5(\text{GT3} + \text{GT4})V_{\text{TCA}} - \text{GT3}(V_{\text{cycle}} + V_{\text{TCA}}) \quad (12.1)$$

where  $\text{GN3}$  is the isotopic enrichment of the C3 position of glutamine and  $\text{GT3}$  the isotopic enrichment of C3-glutamate. Rearrangement of the above expression and solving for the  $V_{\text{cycle}}/V_{\text{TCA}}$  ratio yields

$$V_{\text{cycle}}/V_{\text{TCA}} = 0.5(\text{GT3} - \text{GT4})/(\text{GN3} - \text{GT3}) \quad (12.2)$$

Because tissue glutamate concentrations primarily reflect the glutamate content of glutamatergic neurons, the variable  $V_{\text{TCA}}$  monitors the mitochondrial activity of the glutamatergic neuron.

We have validated this strategy of measuring the glutamate cycle/TCA cycle ratio in the rat cerebral cortex under chloralose anesthesia by comparison of the rates calculated from the steady state  $2-^{13}\text{C}$ -glucose experiment with those calculated from dynamic  $1-^{13}\text{C}$ -glucose,  $2-^{13}\text{C}$ -glucose, and  $5-^{13}\text{C}$ -glucose studies (Figure 12.6) (Sibson *et al.*, 1998a, 2001). Similar results have been obtained using  $^{14}\text{C}$ -labeled carbon dioxide, which also incorporates label through pyruvate carboxylase (Lieth *et al.*, 2001). Although the TCA cycle rate is twofold faster in the rat than in humans, the glutamate cycle/TCA cycle ratio is similar in both (Shen *et al.*, 1999; Kanamatsu and Tsukada, 1999). The glutamate cycle/TCA cycle ratio is clearly decreased by surgical-grade anesthesia. However, the effects are minor compared with the major decrease with the isoelectric EEG of pentobarbital coma. Changes in rate of glutamate turnover and thus the glutamate–glutamine cycle are proportional to EEG power and changes in the neuronal spiking frequency (Hyder *et al.*, 2001; Smith *et al.*, 2002).

The steady-state measurement has significant advantages clinically. It allows the stable isotope tracer to be administered under more flexibly controlled conditions before the MRS measurements, thereby allowing more magnet time for spectral acquisition. The signal-to-noise ratio is improved or voxel size reduced. Administering the  $^{13}\text{C}$  or  $^{15}\text{N}$  tracer before the MRS measurements facilitates infusion under a greater variety of conditions often with better control of the experimental paradigms and with greater subject comfort.

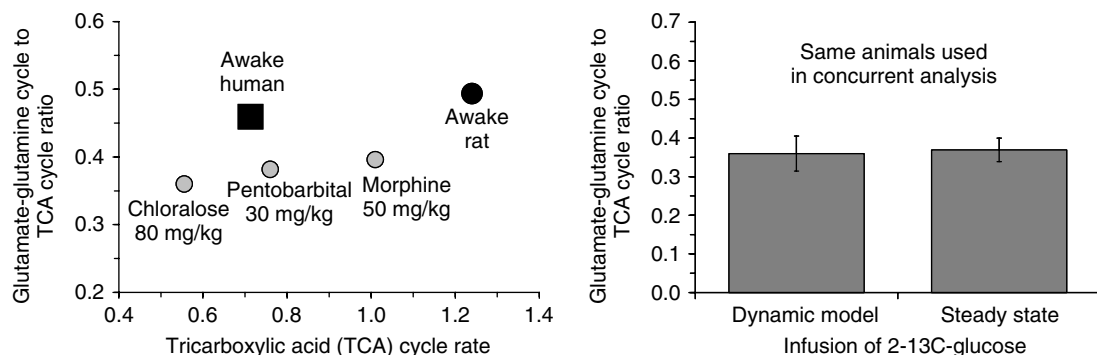


**Figure 12.6.** The graph on the left shows the ratio of the glutamate–glutamine cycle rate normalized to the TCA cycle rate plotted as a function of the rate of the TCA cycle under a variety of levels of brain activity, e.g., depth of anesthesia. The data is derived from Sibson *et al.* (1998a), Hyder *et al.* (2001), Shen *et al.* (1999), and Kanamatsu and Tsukada (1999). Graph on the right shows that the ratios of the glutamate–glutamine cycle rate to TCA cycle rate, measured using serial spectra, are the same as those measured in a single spectrum, collected after steady state is achieved. Serial spectra, collected during the dynamic phase of the experiment, and the steady-state spectrum at the end are obtained from the same animal. The graph is drawn from data published by Sibson *et al.* (2001).

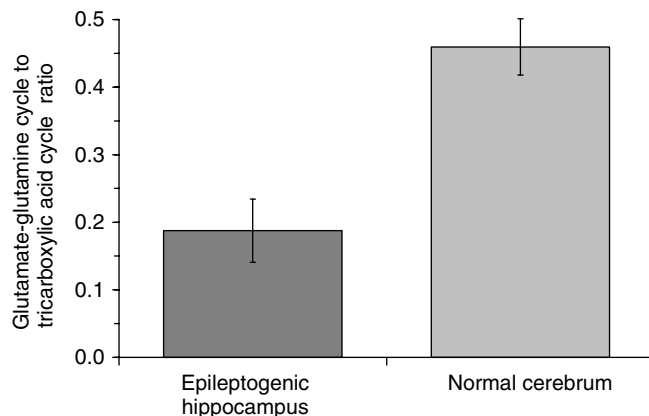


**Figure 12.7.** The ratio of the glutamate–glutamine cycle rate to TCA cycle rate ( $\pm$  standard error) of a portion of the hippocampus removed at surgery for TLE. The glutamate–glutamine cycle/TCA cycle ratio is compromised severely in almost all patients. Using the ratio normalizes for variations in the cerebral metabolic rate. The greatly reduced glutamate–glutamine cycle rate accounts for slow glutamate clearance from the synapse, increased interictal extracellular glutamate concentrations, and contributes to excitotoxicity. The graph is drawn from data that includes values published by Petroff *et al.* (2002b).

### 12.2.6. The Glutamate–Glutamine Cycle to TCA Cycle Ratios are Markedly Reduced in the Human Epileptogenic Hippocampus with Severe Neuron Loss and Glial Proliferation

Few reports address the effects of neuron loss and gliosis on the metabolite content of the epileptogenic human hippocampus. We showed that the glutamate–glutamine cycle/TCA cycle ratio is severely compromised in almost all patients (Figure 12.7) (Petroff *et al.*, 2002b). No associations with antiepileptic drugs

in use at the time of surgery, duration of the epilepsy, gender, or age were seen. There were no significant associations between glutamate–glutamine cycle to the neuronal TCA cycle ratio and hippocampal glutamate or glutamine content. Measurements of the glutamate–glutamine cycle to the neuronal TCA cycle ratio in the normal human hippocampus are not available. The closest comparisons to our results are recent measurements using *in vivo*  $^{13}\text{C}$  MRS in the human occipital–parietal lobe and the awake and lightly anesthetized rat forebrain (Shen *et al.*, 1999; Kanamatsu and Tsukada, 1999). Under low light, unstimulated conditions, values range between 0.4 to 0.5. The relative rate of the glutamate–glutamine cycle to glutamate synthesis is decreased in epileptic hippocampi that show sclerosis. The association with histopathology is striking. Neuron–glia cycling is lowest in epileptic hippocampi with significant loss of neurons and glial proliferation. Because this ratio is calculated from the relative labeling of the glutamate (primarily neuronal) and glutamine (synthesized in glia) pools, as opposed to absolute flux rates, the low ratio of the glutamate–glutamine cycle to the neuronal TCA cycle is *not* simply due to reduced cellular density or generalized hypometabolism. If the remaining neurons and glia were functioning normally the ratio of glutamate–glutamine cycle to the neuronal TCA cycle would be independent of neuronal loss.

### 12.2.7. Intracellular Glutamine Content is Low in the Epileptogenic Hippocampus Despite a Major Increase in Glial Density

Hippocampal glutamine concentrations are surprisingly low in the epileptogenic human hippocampus (Figure 12.8) (Petroff *et al.*, 2002a). Our cellular glutamine values appear to be low compared to the cellular glutamine concentration of the hippocampus obtained at autopsy from nondemented subjects (Tartib *et al.*, 1980). Brain tissue glutamine content primarily reflects glial concentrations (Ottersen *et al.*, 1992; Kvamme *et al.*, 2000). The lack of association between cellular glutamine and pathology, reflecting the degree of glial proliferation and neuron loss, suggests that glial glutamine levels are low in most cases of hippocampal sclerosis. When corrected for glial density, intracellular glutamine levels are exceedingly low (1.5 mM, SD 0.7). The lowest values are found in epileptogenic glioma involving the hippocampus with mean intracellular glutamine levels (0.7 mM) similar to values measured in the extracellular space by microdialysis.

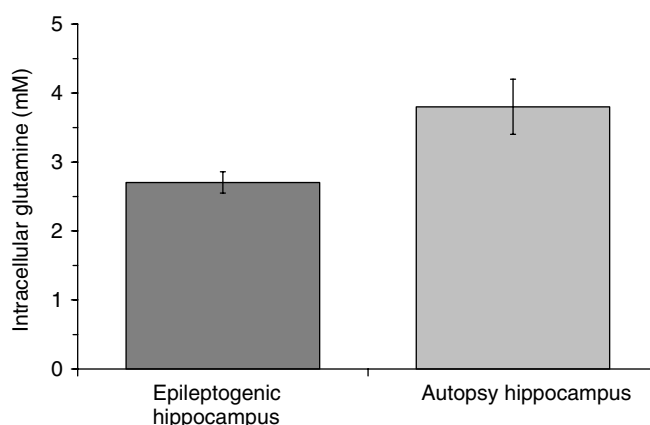


**Figure 12.8.** Mean intracellular glutamine levels ( $\pm$  standard error) of a portion of the hippocampus removed at surgery for TLE. Glial proliferation is measured in an adjacent slice of the pes. Decreased expression of glutamine synthetase, measure by quantitative electron microscopy of the resected hippocampus, can account for the low glutamine content, despite the large increase in glial density. The graph is drawn from data that includes values published by Petroff *et al.* (2002a).

The immunohistochemical distribution of GS was similar in autopsy and non-MTLE hippocampi (Eid *et al.*, 2002). In hippocampi without reactive glial proliferation, GS was strongly expressed in glial cells throughout all subfields. In contrast, in the epileptogenic and sclerotic hippocampus, a profound loss of GS-immunoreactivity was apparent, particularly in areas of peak neuronal loss and glial proliferation, such as the CA1 and CA3 regions. Western blot analysis showed that GS was down-regulated by 40 % in the MTLE hippocampus compared to surgically resected non-MTLE hippocampi. No GS-immunoreactivity was seen in neurons.

The deficiency in GS in the sclerotic regions of the MTLE hippocampus would be a sufficient mechanism for the increase in extracellular glutamate and decrease in intracellular glutamine. Glial glutamate content should be *increased*. *In vitro* experiments with organotypical hippocampal cultures have demonstrated that blocking of GS by the competitive inhibitor methionine sulfoximine (MSO) causes depletion of glutamine and accumulation of glutamate in astrocytes (Laake *et al.*, 1995). Acute administration of inhibitors of glutamine synthesis, e.g. methionine sulfoximine, results in convulsions with a lag of several hours (Sellinger *et al.*, 1986). In the ferric chloride model of focal epilepsy, glutamine synthetase activity is reduced in the seizure focus (Tiffany-Castiglioni *et al.*, 1989). Inhibition of glutamine synthesis would be expected to cause slow glutamate–glutamine cycling, to decrease tissue glutamine content and release, thereby, to raise glial glutamate content and efflux. During glial depolarization, enhanced glutamate efflux would be expected to foster spread of the seizure. Low rates of glutamate–glutamine cycling resulting from dysfunction of glutamine synthesis could contribute to the epileptic state even under conditions of severe neuron loss and gliosis.

### 12.2.8. Proposed Metabolic Model of MTLE with Hippocampal Sclerosis

Our proposed model (Figure 12.9) is based on the anatomical observation that glia to neuron ratios are increased tenfold in hippocampal sclerosis with MTLE. Neuron density is severely reduced and glial density is more than doubled. The glutamate–glutamine cycle rate is very low; reduced by a factor of four or more. Interictal extracellular glutamate concentrations are increased by a factor of three to five. Intracellular glutamate concentrations are unchanged despite the neuron loss. Intracellular glutamine concentrations are low despite an over twofold increase in glial density. Glial dysfunction would account for all these observations. Increased glutamate release from neurons would be unlikely because of the profound neuron loss. Increased neuronal release of glutamate should increase rather than decrease the rate of

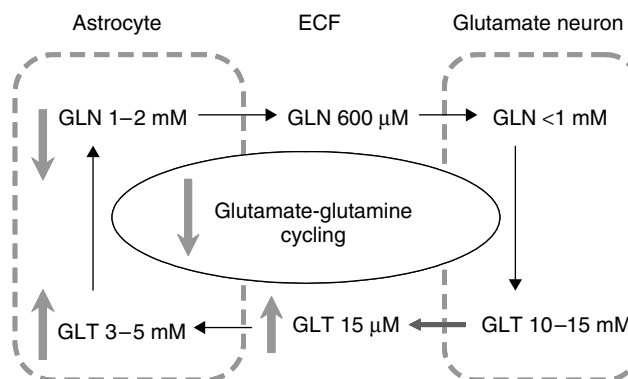


**Figure 12.9.** Schematic diagram of our hypothesis that dysfunction of the glutamate–glutamine cycle helps maintain the epileptogenic state in MTLE. Increased intracellular glutamate and decreased glial glutamate clearance maintain increased extracellular glutamate concentrations that promote spontaneous seizures.

glutamate–glutamine cycling. Furthermore, GS expression is severely reduced in hippocampal sclerosis; virtually absent from astrocytes in the most gliotic regions. Loss of this critical enzyme could account for many of our observations. Glial intracellular glutamine content should decrease. Glial glutamate content should increase. The neuron–glia, glutamate–glutamine cycling would slow. The increase in glial glutamate would make glial glutamate uptake energetically more costly and prolong clearance of glutamate from the extracellular fluid (ECF). Interictal extracellular glutamate would be chronically elevated. Glial depolarization would increase extracellular glutamate further, perhaps by reversal of GLAST or GLT-1. Hippocampal GLAST expression is increased in the majority of patients.

### **12.3. PART II: MRS STUDIES OF THE ROLE OF GABA IN EPILEPSY**

GABA plays an important role in mammalian epilepsy. GABA is the major inhibitory neurotransmitter in the mammalian brain, including humans. Reviews by several investigators have stressed the role of GABA in epilepsy and emphasized the developmental aspects of GABA physiology, with implications for childhood epilepsy (van den Pol *et al.*, 1998; Powell *et al.*, 2003; Berkovic and Scheffer, 1999; Prasad *et al.*, 1999). Animal models using advanced molecular genetic techniques such as knockout mutations have identified the role of genes affecting ion channels, the synapse (including release and uptake of neurotransmitters) synaptic receptors and the neural network that result in epilepsy. Many of these mutations result in alterations of GABA and glutamate physiology. Mutation of a nonspecific alkaline phosphatase results in markedly reduced brain GABA and intractable seizures (Waymire *et al.*, 1995). In addition, rare genetic disorders of GABA metabolism have been identified in a few hundred children (Jakobs *et al.*, 1993). These disorders include pyridoxine-dependent epilepsies, GABA-transaminase deficiency and succinic-semialdehyde-dehydrogenase deficiency (Battaglioli *et al.*, 2000; Gibson *et al.*, 1998; Medina-Kauwe *et al.*, 1999). Subjects with pyridoxine-dependent epilepsies have been observed to have extremely low CSF GABA levels, elevated glutamate, and low levels of brain GABA (Kurlemann *et al.*, 1992; Kure *et al.*, 1998; Battaglioli *et al.*, 2000). Recent reports have suggested that similar changes in CSF GABA occur in children with infantile spasms (Ohtsuka *et al.*, 2000). Despite the known role of pyridoxine (vitamin B6) as an important cofactor for glutamic acid decarboxylase (GAD), a key regulatory enzyme of GABA metabolism, characterization of the molecular defect in pyridoxine dependent epilepsies has yet to be discovered.

#### **12.3.1. Intracellular GABA Levels Modulate the Release and Re-uptake of Extracellular GABA**

Changes in cytosolic GABA concentrations alter cellular physiology in a variety of ways. Under normal conditions, the GABA content of GABAergic neurons is far greater than that of non-GABAergic neurons or glia. Neuronal GABA concentrations may influence both vesicular and non-vesicular GABA release. Vesicular uptake of GABA, thus the vesicular concentration, is dependent on cytosolic GABA concentration ( $K_m = 5\text{ mM}$ ) and energy charge (Fyske and Fonnum, 1996). An increase in cytosolic GABA will enhance vesicular GABA release (Gram *et al.*, 1989). Tonic GABA release through reversal of GAT1 is concentration dependent. Release of GABA through transporter reversal has been demonstrated with both physiological and epileptic stimuli (Gaspari *et al.*, 1998; Wu *et al.*, 2001). Tonic release of GABA increases with increasing cytosolic GABA resulting in increased basal extracellular levels. The distribution of GAD67 appears to coincide with the distribution of the neuronal GABA transporter (GAT1), suggesting that cytosolic GABA synthesized by this GAD isoform may have a significant paracrine function, perhaps through transporter reversal (Yasumi *et al.*, 1997; Gaspari *et al.*, 1998; Wu *et al.*, 2001). Thus, an increase in cytosolic GABA will enhance both vesicular and nonvesicular GABA release during seizures and slow clearance of GABA from the synaptic cleft thereby prolonging its effects (Gram *et al.*, 1989; Gaspari

*et al.*, 1998). Dynamic insertion of GABA transporters into the plasma membrane occurs in response to increased extracellular GABA. Increased transporter availability interacting with higher cytosolic GABA would act in a synergistic fashion to magnify GABAergic effects. Conversely, within the epileptogenic and sclerotic human hippocampus GABA content, release, and transporter function appear decreased (During *et al.*, 1995; Patrylo *et al.*, 2001).

### 12.3.2. Cellular GABA and Cortical Excitability

Increased cortical excitability is a hallmark of several human epileptic syndromes. Several lines of evidence support a major role for GABA levels affecting GABA release and by this mechanism having a key role in the regulation of cortical excitability. Studies in cell culture and brain slice have shown directly that increasing cellular GABA levels increases tonic GABA release in response to physiological activation (Gaspari *et al.*, 1998; Wu *et al.*, 2001). Primate models of photosensitive epilepsy have low GABA levels and improve with GABAergic drugs (Menini and Silva-Barrat, 1997; Lloyd *et al.*, 1986). Similarly, AEDs that increase GABA or enhance GABAergic inhibition block the photoparoxysmal response in photosensitivity epilepsies (Kastelein-Nolst Trenité, 1998; Rimmer *et al.*, 1987). Drug-induced enhancement of GABAergic inhibition reduces abnormal flash-evoked potentials in parallel with an improvement in the associated myoclonus (Cracco and Rossini, 1997). In normal volunteers, 1 h of low ambient lighting (darkness) increases the excitability of the visual cortex (Boroojerdi *et al.*, 2000a,b). Pretreatment with a GABA-A receptor agonist (lorazepam) abolishes the increase in excitability, measured using fMRI and transcranial magnetic stimulation. Serial MRS measurements of the visual cortex show that intracellular GABA content decreases in parallel to the enhanced cortical excitability.

Myoclonus without loss of consciousness, characteristic of JME and other myoclonic epilepsy syndromes is attributed to a defect in GABAergic inhibition (Brown *et al.*, 1996; Werhahn *et al.*, 1999). Spontaneous and photosensitive seizures are seen in alcohol and other drug withdrawal states characterized by down-regulation of the GABA-A receptors or low occipital GABA levels (Behar *et al.*, 1999). MRS-based measurements show low GABA levels in the visual cortex of patients, consistent with the enhanced cortical excitability observed in JME (Petroff *et al.*, 2001). Intracellular homocarnosine and GABA levels are often below normal in the neocortex of patients with frequent seizures. Low tissue GABA levels are associated with increased cortical excitability that would facilitate the spread of seizure activity from the epileptogenic hippocampus to the neocortex.

Studies using MRS have found reduced cellular GABA levels in the human visual cortex in localization-related epilepsies (Figure 12.10). Below normal GABA levels in the visual cortex are associated with poor seizure control in refractory localization-related epilepsy syndromes (Petroff and Rothman, 1998; Petroff *et al.*, 1996, 1998, 1999b, 2001). Whether low GABA levels are the cause or the result of frequent seizures is unknown. Both GABA concentrations and synthesis rates increase in most seizure models (Bradford, 1995). It has been proposed that enhanced glutamic acid decarboxylase (GAD67 isoform) mRNA expression, enzyme activity, and GABA levels that occur within hours in animal models of stress, seizures, and other injuries could reflect a protective response allowing the brain to heal by producing widespread inhibition (Martin and Tobin, 2000). Therefore, it is surprising that occipital GABA levels are below normal in many patients with poor seizure control (Figure 12.10), particularly in regions presumably remote from the epileptogenic areas (most often temporal and frontal lobes in our series).

Low GABA levels, measured in the occipital cortex remote from the onset of the seizure, correlate with epileptiform abnormalities seen in interictal EEG recording (Figure 12.11) (Petroff *et al.*, 1996). Some studies have shown that patients with epileptiform abnormalities on interictal EEG recorded shortly after a seizure are more likely to have another seizure within 2 years than those with normal EEGs (van Donselaar *et al.*, 1992). These interictal epileptiform abnormalities probably reflect increased cortical excitability.



**Figure 12.10.** Mean edited GABA levels ( $\pm$  standard error) measured using proton-MRS from the occipital lobe of 42 patients with localization-related epilepsy treated with carbamazepine or phenytoin. Levels are significantly lower in patients with refractory complex partial seizures. In humans, edited GABA is the sum of GABA and homocarnosine. Low cortical GABA and homocarnosine levels facilitate the spread of seizures from the epileptic focus and contribute to the cortical excitability, which characterizes the epileptic network. Data include values published by Petroff *et al.* (1996, 1999a, 2000).

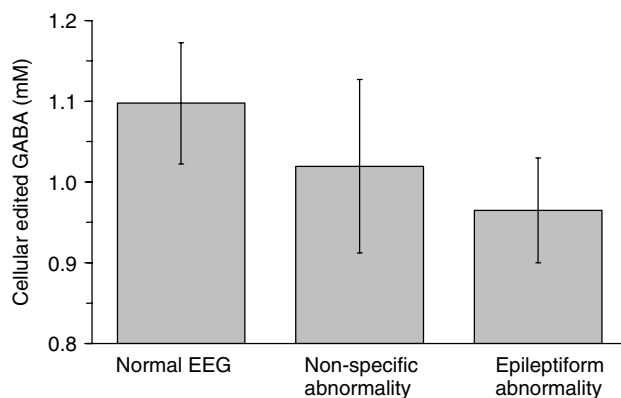


**Figure 12.11.** Mean edited GABA levels ( $\pm$  standard error) measured using proton-MRS from the occipital lobe of patients with localization related epilepsy. Levels are lowest in patients, whose interictal electroencephalogram (EEG) reveals epileptiform features that correlate with increased cortical excitability and a high risk of recurrent seizures. Measuring interictal edited GABA using proton-MRS may complement the EEG in predicting seizure recurrence. Spectroscopic imaging may define the epileptic network. The graph is drawn from data published by Petroff *et al.* (1996).

Similarly, localization of the site of termination of seizures of focal origin to cortical regions other than the onset is associated with a poorer surgical prognosis (Spencer and Spencer, 1996). This observation raises the possibility of additional abnormal epileptogenic cortical regions with impaired seizure-terminating capabilities, i.e., increased cortical excitability. The presence of interictal epileptiform discharges extending beyond the area of resection correlates with poor surgical outcome in patients with extra-hippocampal epilepsy (Bautista *et al.*, 1999). The observations are consistent with the hypothesis that increased cortical excitability beyond the epileptogenic region appears to contribute continued seizure activity. Low cellular

GABA, measured by MRS in the neocortex away from the seizure focus, reflects regions of increased excitability and may contribute to the spread of seizures.

### 12.3.3. Low Cortical GABA Content is Associated with Low Rates of GABA Synthesis

GABAergic neurons are decreased in the human epileptogenic neocortex associated with temporal lobe epilepsy (TLE), low-grade tumors, and cortical malformations (Ribak and Yan, 2000; Haglund *et al.*, 1992; Marco *et al.*, 1996; Spreafico *et al.*, 1998). Loss of GABAergic processes is seen in some cases. Low rates of GABA synthesis are measured in the occipital lobe of patients with refractory, localization-related epilepsy (Figure 12.12). These patients have normal function of the visual cortex and no anatomical lesion or atrophy of the occipital lobe.

The net rate of GABA synthesis was measured using serial MR spectra in patients following the inhibition of GABA-transaminase with vigabatrin (Petroff *et al.*, 1999c). GABA is formed from the alpha-decarboxylation of glutamate by glutamic acid decarboxylase (GAD) and is metabolized to succinate by the sequential actions of GABA transaminase (GABA-T) and succinic semi-aldehyde-dehydrogenase (SSADH). The activity of GAD is believed to be primarily responsible for regulating the steady-state concentration of GABA (Martin and Tobin, 2000; Martin and Rimvall, 1993). Low intracellular GABA content appears to be associated with low rates of GABA synthesis in human epilepsy.

### 12.3.4. Inhibition of the GABA–Glutamine or GABA–Glutamate Cycle Results in Seizures

The GABA concentration of neocortex primarily reflects the fractional volume of GABAergic neurons weighted by the GABA content of those neurons. One explanation for low intracellular GABA levels in poorly controlled epilepsy would be loss of GABA-containing neurons or a decrease in their volume (simplification of dendritic and synaptic tree or loss of axonal length and thickness). Low rates of GABA synthesis result from genetic or acquired defects in GAD expression or function (Kash *et al.*, 1997; Battaglioli *et al.*, 2000; Peltola *et al.*, 2000). Mice deficient in GAD develop seizures. Pyridoxine deficiency results

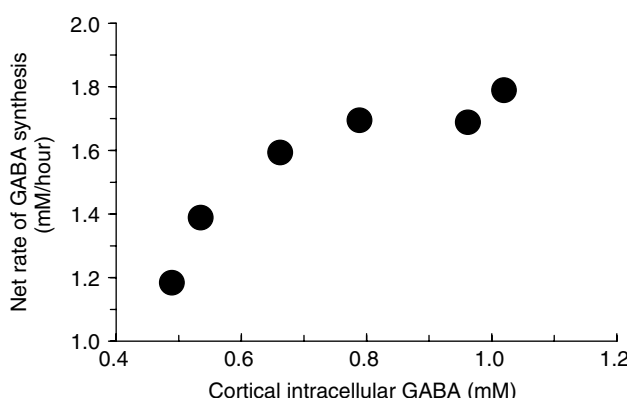


**Figure 12.12.** The net rate of GABA synthesis in six patients with refractory, localization-related epilepsy, measured using serial proton-MRS after the first dose of a GABA-transaminase inhibitor, vigabatrin. There is an association between cortical GABA content and the net rate of synthesis, suggesting that low rates of synthesis accounts for the low GABA content rather than increased catabolism. The graph is drawn from data published by Petroff *et al.* (1999c).

in epilepsy with low GABA levels. Circulating auto-antibodies against GAD occur in some patients with refractory epilepsy. Alternatively, the availability of glutamate may be rate limiting. GABAergic neurons appear to be unable to synthesize glutamate *de novo* from glucose or lactate. Glutamine, produced by glia, serves as a major precursor of the releasable pool of GABA (Kapetanovic *et al.*, 1993; Waniewski and Martin, 1998; Patel *et al.*, 2001; Rae *et al.*, 2003). Disrupting the GABA–glutamine cycle would be expected to decrease glutamine availability, reducing the glutamate content of GABAergic neurons, thereby decreasing the rate of GABA synthesis. Inhibition of neuronal glutamine uptake or inhibition of neuronal glutaminase appears to result in decreased GABAergic inhibition, before loss of glutamatergic excitation, thereby facilitating seizures. However, disruption of the glutamate–GABA cycle also results in low intracellular GABA content. A significant proportion of GABA is synthesized from glutamate transported via EAAT3 glutamate transporters. Inhibiting neuronal glutamate transporters reduced both evoked monosynaptic and miniature IPSCs with no change in the frequency of IPSCs or in the response to exogenously applied GABA, suggesting that GABA synthesis and, consequently, vesicular filling were reduced (Mathews and Diamond, 2003). Similarly, a knockdown in glutamate transporter expression was associated with a decrease in GABAergic function in mice and seizure activity (Sepkuty *et al.*, 2002). Dysfunction of the glutamate–GABA cycle (glutamatergic neurons express GABA transporters and GABA-transaminase) results in low rates of GABA synthesis and seizures. Further, labeling studies should clarify which mechanism accounts for low GABA content in an individual patient.

Occipital–posterior–temporal lobe GABA+/CR ratios are reported to be 30 % lower ipsilateral to the seizure focus (Figure 12.13) (Mueller *et al.*, 2001). The ratios are lowest ipsilateral to the seizure focus in those patients who achieved good seizure control after GABA levels are increased with vigabatrin. Vigabatrin is a GABA-transaminase inhibitor that increases intracellular and extracellular GABA and homocarnosine (Petroff and Rothman 1998, Petroff *et al.*, 1998). This suggests that increased GABA may contribute to the reduction in symptoms.

A recent review proposes that human epilepsy is a disorder of large neural networks (Spencer, 2002b). The electrical hyperexcitability associated with seizure activity reverberates within the neural structures of the network to culminate in the eventual expression of seizures. The most extensively described of these epilepsy networks, the medial temporal or limbic network, includes the hippocampi, the amygdala, the

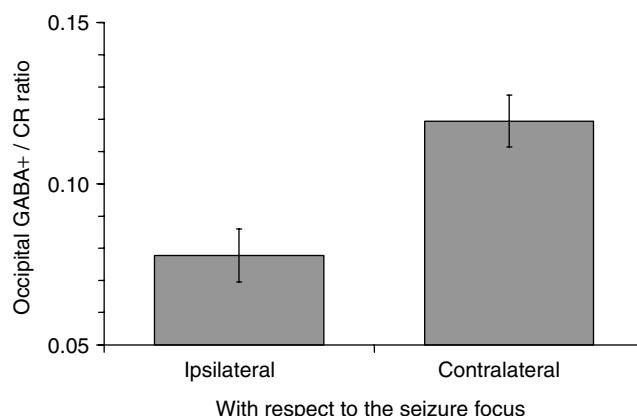


**Figure 12.13.** Proton MRS measurements of the GABA+ to creatine ratio (GABA+/CR) of the occipital lobe ipsilateral and contralateral to the seizure focus in patients with TLE. The ratio is significantly less on the ipsilateral side. Low GABA may define the epileptic network in localization-related epilepsies. The graph is drawn from data published by Mueller *et al.* (2001).

entorhinal cortices, lateral temporal neocortices, and extra-temporal components of the medial thalamus and the inferior frontal lobes. The other two networks are less commonly identified, even in their component parts: the medial occipital/lateral temporal network and the superior parietal/medial frontal network. The electrical hyperexcitability associated with seizure activity reverberates within the neural structures of the network, which operate together and inextricably to culminate in the eventual expression of seizures. Modification of network activity by electrical, biochemical, or metabolic influences in any part of the network will alter seizure expression or its occurrence. The low neocortical GABA levels ipsilateral to the epileptogenic temporal lobe suggest that low cellular GABA could contribute to the hyperexcitability of the epileptic network. Imaging GABA should become very useful in mapping epileptic networks.

## **12.4. CONCLUSION: ALTERATION OF METABOLISM IN LOCALIZATION RELATED EPILEPSIES AND SIGNIFICANCE FOR EPILEPTOGENICITY**

The studies reviewed in this chapter have focused on alterations in the metabolism, particularly astroglial neurotransmitter cycling, of glutamate and GABA in localization-related epilepsy. Based on these studies there appears to be two major alterations. In the region of the seizure focus there is a marked impairment in the glutamate–glutamine cycle and elevation of intracellular glutamate content. These alterations, the molecular basis of both of which may be reduced glutamine synthetase activity, lead to chronically elevated glutamate in the extracellular fluid (ECF). Glial dysfunction, as evidenced by low levels of glutamine synthetase, contributes to slow clearance of extracellular glutamate. Elevated extracellular levels of glutamate would enhance neuronal excitability and glial activation. It may contribute to the epileptogenicity of the seizure focus. Chronically increased extracellular glutamate would contribute to ongoing neuronal loss (excitotoxicity) and reactive glial proliferation.

Away from the focus there is a decrease in GABA concentrations, which appears to be due to a reduction in the GABA synthesis rate. One plausible hypothesis is that below normal intracellular GABA content contributes to enhanced cortical excitability and therefore to the potential for seizures. Low cellular GABA levels reflect an intrinsic alteration in GABA metabolism and may not be sufficient to serve as the sole cause of epilepsy in most patients. We hypothesize that low neocortical GABA levels contribute to the expression of seizure disorders in the localization-related epilepsies by increasing cortical excitability in a global fashion, thereby facilitating the spread of seizure to regions remote from the epileptogenic zone.

The combination of below normal cellular GABA content and above normal cellular glutamate content may act synergistically to cause epilepsy in those patients without anatomical lesions, 'MRI-negative'. Spectroscopic imaging of glutamate and GABA may delineate the epileptic networks responsible for seizures in these patients. Below normal GABA and homocarnosine content appears to contribute to the seizure diathesis of some patients with idiopathic generalized epilepsies, e.g., juvenile myoclonic epilepsy.

In addition to the alterations of the glutamate–glutamine cycle and GABA metabolism described here there is direct evidence of widespread mitochondrial dysfunction both within and remote from the sclerotic hippocampus in MTLE (see previous chapter). Phosphocreatine to ATP (PCr/ATP) ratios are reduced to the greatest extent in the amygdala ipsilateral to the seizure focus followed by the ipsilateral pes, hippocampus, and thalamus with decreasing severity. A similar pattern was seen in the contralateral hemisphere, albeit to a lesser extent (Hetherington *et al.*, 2002a,b). A similar pattern of loss is seen with respect to *N*-acetyl aspartate (NAA) levels. The NAA content of brain is controlled by the rate of synthesis in neuronal mitochondria, less the rate of neuronal release or oxidation (Petroff *et al.*, 2002a; Moreno *et al.*, 2001). Low PCr/ATP ratios and low NAA are reported also in the mitochondrial cytopathies and are associated with cortical hyperexcitability (Kunz, 2002). Hetherington and Spencer have proposed a mechanism by which impaired neuronal mitochondrial energetics could lead to increased glutamate release, due to dysregulation

of calcium metabolism. In combination with the impairment in the glutamate–glutamine cycle the increase in glutamate release (for a given degree of electrical activity) would explain the chronically elevated ECF glutamate and the hyperexcitability characteristic of the epileptogenic hippocampus.

## Acknowledgements

Grant support was provided by National Institute of Health (NINDS) PO1-NS39092. We thank our colleagues who helped design, acquired data for, and analyzed the studies including Idil Cavus, Nihal C. de Lanerolle, Tore Eid, Laura D. Errante, Hoby P. Hetherington, Fahmeed Hyder, Jung H. Kim, Richard H. Mattson, Douglas L. Rothman, and Anne Williamson. We thank the patients participating in these studies.

## REFERENCES

Battaglioli G, Rosen DR, Gospe SM, Martin DL. Glutamate decarboxylase is not genetically linked to pyridoxine-dependent seizures. *Neurology* 2000; **55**: 309–311.

Bautista RE, Cobbs MA, Spencer DD, Spencer SS. Prediction of surgical outcome by interictal epileptiform abnormalities during intracranial EEG monitoring in patients with extrahippocampal seizures. *Epilepsia* 1999; **40**(7): 880–890.

Behar KL, Rothman DL, Petersen KF, Hooten M, Delany R, Petroff OAC, Shulman GI, Navarro V, Petrakis IL, Charney DS, Krystal JH. Preliminary evidence of reduced cortical GABA levels in localized 1-H-MR spectra of alcohol-dependent and hepatic encephalopathy patients. *Am J Psychiatry* 1999; **156**: 952–954.

Bergles DE, Jahr CE. Synaptic activation of glutamate transporters in hippocampal astrocytes. *Neuron* 1997; **19**(6): 1297–1308.

Bergles DE, Diamond JS, Jahr CE. Clearance of glutamate inside the synapse and beyond. *Curr Opin Neurobiol* 1999; **9**(3): 293–298.

Berkovic SF, Scheffer IE. Genetics of the epilepsies. *Curr Opin Neurol* 1999; **12**: 177–182.

Bhakoo KK, Pearce D. *In vitro* expression of N-acetyl aspartate by oligodendrocytes: implications for proton magnetic resonance spectroscopy signal *in vivo*. *J Neurochem* 2000; **74**: 254–262.

Boroojerdi B, Bushara KO, Corwell B, Immisch I, Battaglia F, Muellbacher W, Cohen LG. Enhanced excitability of the human visual cortex induced by short-term light deprivation. *Cerebral Cortex* 2000a; **10**: 529–534.

Boroojerdi B, Cohen LG, Petroff OA, Rothman DL. Mechanisms of light deprivation-induced enhancement of visual cortex excitability (Abstract). *Soc Neurosci* 2000b; **26**: 821.

Bradford HF. Glutamate, GABA, and epilepsy. *Prog Neurobiol* 1995; **47**: 477–511.

Brown P, Ridding MC, Werhahn KJ, Rothwell JC, Marsden CD. Abnormalities of the balance between inhibition and excitation in the motor cortex of patients with cortical myoclonus. *Brain* 1996; **119**: 309–317.

Cascino GD. Advances in neuroimaging: surgical localization. *Epilepsia* 2001; **42**: 3–12.

Cavus I, Abi-Saab WM, Cassadey M, Jackob R, Sherwin RS, Krystal J, Spencer DD. Basal glutamate, GABA, glucose and lactate levels in the epileptogenic and non-epileptogenic brain sites in neurosurgery patients (Abstract). *Epilepsia* 2002; **43**: Suppl 7: 247.

Cendes F, Knowlton RC, Novotny EJ, et al. Magnetic resonance spectroscopy in epilepsy: clinical issues. *Epilepsia* 2002; **43**(suppl 1): 32–39.

Chaudhry FA, Reimer RJ, Edwards RH. The glutamine commute: take the N line and transfer to the A. *J Cell Biol* 2002; **157**: 349–55.

Conti F, Minelli A. Glutamate immunoreactivity in rat cerebral cortex is reversibly abolished by 6-diazo-5-oxo-L-norleucine (DON), an inhibitor of phosphate-activated glutaminase. *J Histochem Cytochem* 1994; **42**: 717–726.

Cracco JB, Rossini PM. Evoked responses and transcranial brain stimulation. Application to reflex epilepsy. *Adv Neurol* 1998; **75**: 49–67.

Danbolt NC. Glutamate uptake. *Prog Neurobiol* 2001; **65**: 1–105.

de Lanerolle NC, Kim JH, Williamson A, Spencer SS, Zaveri HP, Eid T, Spencer DD. A retrospective analysis of hippocampal pathology in human temporal lobe epilepsy: evidence for distinctive patient subcategories. *Epilepsia* 2003; **44**(5): 677–687.

Duncan JS. Imaging and epilepsy. *Brain* 1997; **120**: 339–377.

During MJ, Spencer DD. Extracellular hippocampal glutamate and spontaneous seizure in the conscious human brain. *Lancet* 1993; **341**: 1607–1610.

During MJ, Ryder KM, Spencer DD. Hippocampal GABA transporter function in temporal-lobe epilepsy. *Nature* 1995; **376**: 174–177.

Dzubay JA, Jahr CE. The concentration of synaptically released glutamate outside of the climbing fiber- Purkinje cell synaptic cleft. *J Neuroscience* 1999; **19**(13): 5265–5274.

Eid T, Thomas M, Spencer DD, Ottersen OP, de Lanerolle NC. Downregulation of glutamine synthetase in the human epileptogenic hippocampus despite glial proliferation: a key to sustained levels of glutamate during seizures? *Epilepsia* 2002; **43**(suppl 7): 261–262.

Fonnum F. Regulation of the synthesis of the transmitter glutamate pool. *Prog Biophys Molec Biol* 1993; **60**: 47–57.

Fyske EM, Fonnum F. Amino acid neurotransmission: dynamics of vesicular uptake. *Neurochem Res* 1996; **21**: 1053–1060.

Gaspary HL, Wang W, Richerson GB. Carrier-mediated GABA release activates GABA receptors on hippocampal neurons. *J Neurophysiol* 1998; **80**: 270–281.

Gibson KM, Hoffman GF, Hodson AK, Bottiglieri T, Jakobs C. 4-hydroxybutyric acid and the clinical phenotype of succinic semialdehyde dehydrogenase deficiency, an inborn error of GABA metabolism. *Neuropediatrics* 1998; **29**: 14–22.

Gram L, Larsson OM, Johnsen A, Schousboe A. Experimental studies of the influence of vigabatrin on the GABA system. *Br J Clin Pharmac* 1989; **27**(suppl 1): 13S–17S.

Haglund MM, Berger MS, Kunkel DD, Frank JE, Ghatan S, Ojemann GA. Changes in gamma aminobutyric acid and somatostatin in epileptic cortex associated with low-grade gliomas. *J Neurosurg* 1992; **77**: 209–216.

Hertz L, Dringen R, Schousboe A, Robinson SR. Astrocytes: Glutamate producers for neurons. *J Neurosci Res* 1999; **57**: 417–428.

Hetherington HP, Pan JW, Spencer DD. 1H and 31P spectroscopy and bioenergetics in the lateralization of seizures in temporal lobe epilepsy. *J Magn Reson Imaging* 2002a; **16**(4): 477–483.

Hetherington HP, Pan JW, Firlik K, Spencer DD. Bioenergetic impairment in the thalamus of patients with intractable temporal lobe epilepsy. *Epilepsia* 2002b; **43**(suppl 7): 306.

Hyder F, Petroff OAC, Mattson RH, Rothman DL. Localized 1H NMR measurements of 2-pyrrolidinone in human brain *in vivo*. *Magn Reson Med* 1999; **41**: 889–896.

Hyder F, Kida I, Behar KL, Kennan RP, Maciejewski PK, Rothman DL. Quantitative functional imaging of the brain: towards mapping neuronal activity by BOLD fMRI. *NMR Biomed* 2001; **14**(7–8): 413–31.

Jackson G, Van Paesschen W. Hippocampal sclerosis in the MR era. *Epilepsia* 2002; **43**(suppl 1): 4–10.

Jakobs C, Jaeken J, Gibson KM. Inherited disorders of GABA metabolism. *J Inherited Metab Dis* 1993; **16**: 704–715.

Kanamatsu T, Tsukada Y. Effects of ammonia on the anaplerotic pathway and amino acid metabolism in the brain: an ex vivo 13C NMR spectroscopic study of rats after administering [2-13C]glucose with or without ammonium acetate. *Brain Res* 1999; **841**: 11–19.

Kapetanovic IM, Yonekawa WD, Kupferberg HJ. Time-related loss of glutamine from hippocampal slices and concomitant changes in neurotransmitter amino acids. *J Neurochem* 1993; **61**: 865–872.

Kash SF, Johnson RS, Tecott LH, Noebels JL, Mayfield RD, Hanahan D, Baekkeskov S. Epilepsy in mice deficient in the 65-kDa isoform of glutamic acid decarboxylase. *Proc Natl Acad Sci USA* 1997; **94**: 14060–14065.

Kastelein-Nolst Trenité DGA. Reflex seizures induced by intermittent light stimulation. *Adv Neurol* 1997; **75**: 99–121.

Kunz WS. The role of mitochondria in epileptogenesis. *Curr Opin Neurol* 2002; **15**: 179–184.

Kure S, Sakata Y, Miyabayashi S, Takahashi K, Shinka T, Matsubara Y, Hoshino H, Narisawa K. Mutation and polymorphic marker analyses of 65K- and 67K-glutamate decarboxylase genes in two families with pyridoxine-dependent epilepsy. *J Hum Genetics* 1998; **43**: 128–131.

Kurlemann G, Ziegler R, Gruneberg M, Bommelburg T, Ullrich K, Palm DG. Disturbance of GABA metabolism in pyridoxine-dependent seizures. *Neuropediatrics* 1992; **23**: 257–259.

Kvamme E, Roberg B, Torgner IA. Phosphate-activated glutaminase and mitochondrial glutamine transport in the brain. *Neurochem Res* 2000; **25**: 1407–1419.

Kvamme E, Torgner IA, Roberg B. Kinetics and localization of brain phosphate activated glutaminase. *J Neurosci Res* 2001; **66**: 951–958.

Laake JH, Slyngstad TA, Haug FM, Ottersen OP. Glutamine from glial cells is essential for the maintenance of the nerve terminal pool of glutamate: immunogold evidence from hippocampal slice cultures. *J Neurochem* 1995; **65**(2): 871–881.

Lieth E, LaNoue KF, Berkich DA, Xu B, Ratz M, Taylor C, Hutson SM. Nitrogen shuttling between neurons and glial cells during glutamate synthesis. *J Neurochem* 2001; **76**: 1712–1723.

Lloyd KG, Scatton B, Voltz C, Bryere P, Valin A, Naquet R. Cerebrospinal fluid amino acid and monoamine metabolite levels of Papio papio: correlation with photosensitivity. *Brain Res* 1986; **363**: 390–394.

Luby M, Spencer DD, Kim JH, et al. Hippocampal MRI volumetrics and temporal lobe substrates in medial temporal lobe epilepsy. *Magn Reson Imaging* 1995; **13**: 1065–71.

Marco P, Sola RG, Pulido P, Alijarde MT, Sanchez A, Cajal SR, DeFelipe J. Inhibitory neurons in the human epileptogenic temporal neocortex: an immunocytochemical study. *Brain* 1996; **119**: 1327–1347.

Martin DL, Rimvall K. Regulation of gamma-aminobutyric acid synthesis in the brain. *J Neurochem* 1993; **60**: 395–407.

Martin DL, Tobin AJ. Mechanisms controlling GABA synthesis and degradation in the brain. In: Martin DL, Olsen RW (eds), *GABA in the Nervous System: The View at Fifty Years*. Lippincott Williams & Wilkins, Philadelphia, PA, 2000, pp 25–41.

Mather GW, Mendoza D, Lozada A, Pretorius JK, Dehnes Y, Danbolt NC, Nelson N, Leite JP, Chimelli L, Born DE, Sakamoto AC, Assirati JA, Fried I, Peacock WJ, Ojemann GA, Adelson PD. Hippocampal GABA and glutamate transporter immunoreactivity in patients with temporal lobe epilepsy. *Neurology* 1999; **52**: 453–472.

Mathews GC and Diamond JS. Neuronal glutamate uptake contributes to GABA synthesis and inhibitory synaptic strength. *J Neuroscience* 2003; **23**(6): 2040–2048.

Medina-Kauwe LK, Tobin AJ, De Meirlier L, Jaeken J, Jakobs C, Nyhan WL, Gibson KM. 4-Aminobutyrate aminotransferase (GABA-transaminase) deficiency. *J Inherited Metab Dis* 1999; **22**: 414–427.

Menini C, Silva-Barrat C. The photosensitive epilepsies of the baboon: a model of generalized reflex epilepsy. *Adv Neurol* 1997; **75**: 29–47.

Moreno A, Ross BD, Bluml S. Direct determination of the *N*-acetyl-L-aspartate synthesis rate in the human brain by <sup>13</sup>C MRS and [1-(13)C]glucose infusion. *J Neurochem* 2001; **77**: 347–350.

Mueller SG, Weber OM, Duc CO, Weber B, Meier D, Russ W, Boesiger P, Wieser HG. Effects of vigabatrin on brain GABA plus/CR signals in patients with epilepsy monitored by H-1NMR spectroscopy: responder characteristics. *Epilepsia* 2001; **42**: 29–40.

Ohtsuka Y, Ogino T, Asano T, Hattori J, Ohta H, Oka E. Long-term follow-up of vitamin B-6-responsive West syndrome. *Pediat Neurol* 2000; **23**: 202–206.

Ottersen OP, Zhang N, Walberg F. Metabolic compartmentation of glutamate and glutamine: morphological evidence obtained by quantitative immunocytochemistry in rat cerebellum. *Neuroscience* 1992; **46**: 519–534.

Patel AB, Rothman DL, Cline GW, Behar, KL. Glutamine is the major precursor for GABA synthesis in rat neocortex *in vivo* following acute GABA-transaminase inhibition. *Brain Res* 2001; **919**: 207–20.

Patrylo PR, Spencer DD, Williamson A. GABA uptake and heterotransport are impaired in the dentate gyrus of epileptic rats and humans with temporal lobe sclerosis. *J Neurophysiol* 2001; **85**: 1533–1542.

Peltola J, Kulmala P, Isojarvi J, Saiz A, Latvala K, Palmio J, Savola K, Knip M, Kieranen T, Graus F. Autoantibodies to glutamic acid decarboxylase in patients with therapy-resistant epilepsy. *Neurology* 2000; **55**: 46–50.

Petroff OAC, Rothman DL. Measuring human brain GABA *in vivo*: effects of GABA-transaminase inhibition with vigabatrin. *Mol Neurobiol*. 1998; **16**: 97–121.

Petroff OAC, Rothman DL, Behar KL, Mattson RH. Initial observations on the effect of vigabatrin on the *in vivo* 1H spectroscopic measurements of GABA, glutamate, and glutamine in human brain. *Epilepsia* 1995; **36**: 457–464.

Petroff OAC, Rothman DL, Behar KL, Mattson RH. Low brain GABA level is associated with poor seizure control. *Ann Neurol* 1996; **40**: 908–911.

Petroff OAC, Mattson RH, Behar KL, Hyder F, Rothman DL. Vigabatrin increases human brain homocarnosine and improves seizure control. *Ann Neurol* 1998; **44**: 948–952.

Petroff OAC, Rothman DL, Behar KL, Hyder F, Mattson RH. Effects of valproate and other antiepileptic drugs on brain glutamate, glutamine, and GABA in patients with refractory complex partial seizures. *Seizure* 1999a; **8**: 120–127.

Petroff OAC, Behar KL, Rothman DL. New NMR measurements in epilepsy. Measuring brain GABA in patients with complex partial seizures. *Adv Neurol* 1999b; **79**: 945–951.

Petroff OAC, Hyder F, Collins T, Mattson RH, Rothman DL. Acute effects of vigabatrin on brain GABA and homocarnosine in patients with complex partial seizures. *Epilepsia* 1999c; **40**: 958–964.

Petroff OAC, Hyder F, Rothman DL, Mattson RH. Functional imaging in the epilepsies proton MRS: GABA and glutamate. *Adv Neurol* 2000; **83**: 263–272.

Petroff OAC, Hyder F, Rothman DL, Mattson RH. Homocarnosine and seizure control in juvenile myoclonic epilepsy and complex partial seizures. *Neurology* 2001; **56**: 709–715.

Petroff OA, Errante LD, Rothman DL, Kim JH, Spencer DD. Neuronal and glial metabolite content of the epileptogenic human hippocampus. *Ann Neurol* 2002a; **52**: 635–642.

Petroff OA, Errante LD, Rothman DL, Kim JH, Spencer DD. Glutamate–glutamine cycling in the epileptic human hippocampus. *Epilepsia* 2002b; **43**: 703–710.

Petroff OAC, Pan JW, Rothman DL. Magnetic resonance spectroscopic studies of neurotransmitters and energy metabolism in epilepsy. *Epilepsia* 2002c; **43**(suppl 1): 40–50.

Powell EM, Campbell DB, Stanwood GD, Davis C, Noebels JL, Levitt P. Genetic disruption of cortical interneuron development causes region- and GABA cell type-specific deficits, epilepsy, and behavioral dysfunction. *J Neurosci* 2003; **23**(2): 622–631.

Prasad AN, Prasad C, Stafstrom CE. Recent advances in the genetics of epilepsy: insights from human and animal studies. *Epilepsia* 1999; **40**: 1329–1352.

Rae, C, Hare, N, Bubb, WA, McEwan, SR, Broer, A, McQuillan, JA, Balcar, VJ, Conigrave, AD and Broer, S. Inhibition of glutamine transport depletes glutamate and GABA neurotransmitter pools: further evidence for metabolic compartmentation. *J Neurochem* 2003; **85**: 503–14.

Ribak CE, Yan X-X. GABA neurons in the neocortex. In: Martin DL, Olsen RW (eds), *GABA in the Nervous System: The View at Fifty Years*. Lippincott Williams & Wilkins, Philadelphia, PA, 2000, pp 357–368.

Rimmer EM, Milligan NM, Richens A. A comparison of the acute effect of single doses of vigabatrin and sodium valproate on photosensitivity in epileptic patients. *Epilepsy Res*. 1987; **1**: 339–346.

Rossi DJ, Oshima T, Attwell D. Glutamate release in severe brain ischaemia is mainly by reversed uptake. *Nature* 2000; **403**: 316–321.

Rothman DL, Petroff OAC, Behar KL, Mattson RH. Localized <sup>1</sup>H NMR measurements of GABA levels in human brain *in vivo*. *Proc Natl Acad Sci (USA)* 1993; **90**: 5662–5666.

Rothman DL, Behar KL, Prichard JW, Petroff OAC. Homocarnosine and the measurement of neuronal pH in patients with epilepsy. *Magn Reson Med* 1997; **37**: 924–929.

Rothstein JD, Dykes-Hoberg M, Pardo CA, Bristol LA, Jin L, Kunci RW, Kanai Y, Hediger MA, Wang Y, Schielke JP, Welty DF. Knockout of glutamate transporters reveal a major role for astroglial transport in excitotoxicity and clearance of glutamate. *Neuron* 1996; **16**: 675–686.

Savic I, Thomas AM, Ke Y, Curran J, Fried I, Engel J. *In vivo* measurements of glutamine plus glutamate (Glx) and N-acetyl aspartate (NAA) levels in human partial epilepsy. *Acta Neurol Scand* 2000; **102**: 179–187.

Sellinger OZ, Schatz RA, Gregor P. Cerebral methylations in epileptogenesis. *Adv Neurol* 1986; **44**: 465–473.

Sepkuty JP, Cohen AS, Eccles C, Rafiq A, Behar K, Ganel R, Coulter DA, Rothstein JD. A neuronal glutamate transporter contributes to neurotransmitter GABA synthesis and epilepsy. *J Neurosci* 2002; **22**(15): 6372–6379.

Shen J, Petersen KF, Behar KL, Brown P, Nixon TW, Mason GF, Petroff OAC, Shulman GI, Shulman RG, Rothman DL. Determination of the rate of the glutamate–glutamine cycle in human brain by *in vivo* <sup>13</sup>C NMR. *Proc Natl Acad Sci USA* 1999a; **96**: 8235–8240.

Sherwin AL, van Gelder NM. Amino acid and catecholamine markers of metabolic abnormalities in human focal epilepsy. *Adv Neurol* 1986; **44**: 1011–1032.

Sherwin AL. Neuroactive amino acids in focally epileptic human brain: a review. *Neurochem Res* 1999; **24**: 1385–1395.

Sibson NR, Dhankhar A, Mason GF, Rothman DL, Behar KL, Shulman RG. Stoichiometric coupling of brain glucose metabolism and glutamatergic neuronal activity. *Proc Natl Acad Sci USA* 1998a; **95**: 316–321.

Sibson NR, Shen J, Mason GF, Rothman DL, Behar KL, Shulman RG. Functional energy metabolism: *in vivo* <sup>13</sup>C-NMR spectroscopy evidence for coupling of cerebral glucose consumption and glutamatergic neuronal activity. *Dev Neurosci* 1998b; **20**: 321–330.

Sibson NR, Mason GF, Shen J, Cline GW, Herskovits AZ, Wall JE, Behar KL, Rothman DL, Shulman RG. *In vivo* <sup>13</sup>C NMR measurement of neurotransmitter glutamate cycling, anaplerosis and TCA cycle flux in rat brain during [2-13C]glucose infusion. *J Neurochem* 2001; **76**: 975–989.

Smith AJ, Blumenfeld H, Behar KL, Rothman DL, Shulman RG, Hyder F. Cerebral energetics and spiking frequency: the neurophysiological basis of fMRI. *Proc Natl Acad Sci USA* 2002; **99**(16): 10765–70.

Spencer SS, Spencer DD. Implications of seizure termination location in temporal lobe epilepsy. *Epilepsia* 1996; **37**(5): 455–458.

Spencer SS, Kim JH, de Lanerolle NC, et al. Differential neuronal and glial relations with parameters of ictal discharge in mesial temporal lobe epilepsy. *Epilepsia* 1999; **40**: 708–12.

Spencer SS. When should temporal-lobe epilepsy be treated surgically? *Lancet Neurol* 2002a; **1**: 375–382.

Spencer SS. Neural Networks in Human Epilepsy: Evidence of and Implications for Treatment. *Epilepsia* 2002b; **43**(3): 219–227.

Spreafico R, Battaglia G, Arcelli P, Andermann F, Dubeau F, Palmini A, Olivier A, Villemure JG, Tampieri D, Avanzini G, Avoli M. Cortical dysplasia an immunocytochemical study of three patients. *Neurology* 1998; **50**: 27–36.

Stein-Behrens BA, Lin WJ, Sapolosky RM. Physiological elevations of glucocorticoids potentiate glutamate accumulation in the hippocampus. *J Neurochem* 1994; **63**(2): 596–602.

Tarbit I, Perry EK, Perry RH, Blessed G, Tomlinson BE. Hippocampal free amino acids in Alzheimer's disease. *J Neurochem* 1980; **35**: 1246–1249.

Tiffany-Castiglioni E, Roberst JA, Sheeler-Gough L. Reduction of glutamine synthetase specific activity in cultured astroglia by ferrous chloride. *J Neurosci Res* 1989; **24**: 508–516.

Urenjak J, Williams SR, Gadian DG, and Noble M. Proton nuclear magnetic resonance spectroscopy unambiguously identifies different neural cell types. *J Neurosci* 1993; **13**: 981–989.

van den Pol AN, Gao XB, Patrylo PR, Ghosh PK, Obrietan K. Glutamate inhibits GABA excitatory activity in developing neurons. *J Neurosci* 1998; **18**(24): 10749–10761.

van Donselaar CA, Schimsheimer R, Geerts AT, Declerck AC. Value of the electroencephalogram in adult patients with untreated first seizure. *Arch Neurol* 1992; **49**: 231–237.

Waniecki RA, Martin DL. Preferential utilization of acetate by astrocytes is attributable to transport. *J Neurosci* 1998; **18**(14): 5225–5233.

Waymire KG, Mahuren JD, Jaje JM, Guilarte TR, Coburn SP, MacGregor GR. Mice lacking tissue nonspecific alkaline phosphatase die from seizures due to defective metabolism of vitamin B-6. *Nature Genetics*. 1995; **11**: 45–51.

Werhahn KJ, Kunesch E, Noachtar S, Benecke R, Classen J. Differential effects on motorcortical inhibition induced by blockade of GABA uptake in humans. *J Physiol* 1999; **517**: 591–597.

Wilson CL, Maidment NT, Shomer MH, Behnke EJ, Ackerson L, Fried I, Engel J, Jr. (1996) Comparison of seizure related amino acid release in human epileptic hippocampus versus a chronic, kainate rat model of hippocampal epilepsy. *Epilepsy Res* **26**: 245–254.

Woermann FG, McLean MA, Bartlett PA, Parker GJ, Barker GJ, Duncan JS. Short echo time single-voxel <sup>1</sup>H magnetic resonance spectroscopy in magnetic resonance imaging-negative temporal lobe epilepsy: different biochemical profile compared with hippocampal sclerosis. *Ann Neurol* 1999; **45**: 369–376.

Wu Y, Wang W, Richerson GB. GABA transaminase inhibition induces spontaneous and enhances depolarization-evoked GABA efflux through reversal of the GABA transporter. *J Neurosci* 2001; **21**: 2630–2639.

Yasumi M, Sato K, Shimada S, Nishimura M, Tohyama M. Regional distribution of GABA transporter 1 (GAT1) mRNA in the rat brain: comparison with glutamic acid decarboxylase67 (GAD67) mRNA localization. *Brain Res Mol Brain Res* 1997; **44**: 205–218.

Ye Z and Sontheimer H. Glioma cells release excitotoxic concentrations of glutamate. *Cancer Res* 1999; **59**: 4383–4391.

Yusim A, Ajilore O, Bliss T, Sapolosky R. Glucocorticoids exacerbate insult-induced declines in metabolism in selectively vulnerable hippocampal cell fields. *Brain Res* 2000; **870**: 109–117.



# 13

## The Role of Altered Energetics of Neurotransmitter Systems in Psychiatric Disease

**Graeme F. Mason**

*Department of Psychiatry, Yale University School of Medicine, MR Center, P.O. Box 208043, New Haven, CT 06520-8043, USA*

---

13.1	Glial–Neuronal Interactions and Neuropsychiatric Disorders	240
13.2	$^1\text{H}$ MRS and Glial–Neuronal Interactions	241
13.2.1	<i>N</i> -Acetyl Aspartate	241
13.2.2	Glutamate, Glutamine, and GABA	243
13.3	$^{13}\text{C}$ MRS and Psychiatric Disorders	247
13.4	Future Directions	249

---

The investigation and evaluation of psychiatric disorders has for most of its history consisted largely of qualitative and subjective measurements of symptoms and behaviors. Today's views lean strongly toward the biochemical and morphological, with investigations that use the numerous brain imaging techniques, biochemical assays of body fluids and tissues, and genetic evaluations of chromosomal regions, including some specific target genes. A field long limited to subjective evaluations of disorders and the effectiveness of treatment now can avail itself of an abundance of quantitative methods. These methods are broadly used in two ways. First, investigators hoping to understand the disorders test hypotheses about brain function, shape, blood flow, genetics, or chemistry. Researchers hope that by finding alterations, such as a brain region with altered morphometry, a polymorphism of the gene for a neurotransmitter receptor, or a metabolic change, a target for rational drug design can be obtained. Second, researchers are searching for quantitative, rapidly detectable biomarkers of disease, ideally markers that are responsive to treatment.

Some potential biomarkers of disease and treatment efficacy have been reported based on studies of genetics (Del Zompo *et al.*, 1984; Hovatta *et al.*, 1991; Stine *et al.*, 1997), brain morphometry (Busatto *et al.*, 2003; Soares, 2002), receptor binding (Dean, 2003; Varrone *et al.*, 2001), and brain blood flow and metabolism (Kumar *et al.*, 1993b; Saxena *et al.*, 2002).

Nuclear magnetic resonance spectroscopy, commonly called MRS in the field of psychiatric research, can make a unique contribution because of its ability to make direct measurements of brain chemicals *in vivo* in healthy subjects and patients before and during treatments or substance withdrawal. The findings up to the present time have revealed altered functional neurochemistry in several disorders.

### 13.1. GLIAL-NEURONAL INTERACTIONS AND NEUROPSYCHIATRIC DISORDERS

Evidence has gradually accumulated for metabolic interactions between glia and neurons in the healthy brain. Erecinska and Silver (1990) reviewed evidence from a variety of experiments to present a scenario in which glutamate is released from glutamatergic neurons, taken up by astrocytes, and converted to glutamine. The glutamine is then returned to neurons, which convert the glutamine to glutamate for further neurotransmission. In the same review, a similar neurotransmitter cycle is presented for GABA and glutamine. Energetic support for such cycles could come from glial glycolysis (Magistretti and Pellerin, 1997; Sibson *et al.*, 1998).  $^{13}\text{C}$  MRS has been particularly useful for the evaluation of the glutamate–glutamine and GABA–glutamine neurotransmitter cycles, as well as for the coupling of cycling with energy metabolism (Patel *et al.*, 2001; Sibson *et al.*, 1997; Sibson *et al.*, 1998; and Chapter 5).

An interesting feature of the cycles is that the Michaelis–Menten half-saturation constants  $K_m$  for several steps in the cycle may lie in the vicinity of the concentrations of substrates for each step in the cycle (Erecinska and Silver, 1990), which opens the possibility that small changes in concentration of any of the substrates could affect the overall rate of the cycle. Glial uptake of glutamate appears to operate at high affinity (see reviews of Danbolt, 1994; Erecinska and Silver, 1990), but there are several other key steps in the process. After the astrocyte takes up glutamate, the conversion to glutamine is facilitated by glutamine synthetase, whose  $K_m$  for glutamate is 10–15 mM (Lund, 1970), which is greater than either the cortical concentration of glutamate of 9–12 mM (Hawkins and Mans, 1983; Perry *et al.*, 1987; Petroff *et al.*, 1989) or the glial concentration of less than 1 mM (Lebon *et al.*, 2002). After the glutamine is released and taken into the neuron, the conversion to glutamate occurs via phosphate-activated glutaminase, whose  $K_m$  for glutamine has been reported to lie between 1 and several millimolar in the rat brain (Dennis *et al.*, 1977; McGeer and McGeer, 1979; Weil-Malherbe, 1969), which is on the order of the brain concentration of glutamine (Hawkins and Mans, 1983). In a cycle of GABA and glutamine, the GABA-synthesizing enzyme glutamate decarboxylase lies in the range of 1 mM (Blindermann *et al.*, 1978; Maitre *et al.*, 1978; Wu *et al.*, 1978), which is similar to what is believed to be the concentration of glutamate in the GABAergic neuron (Patel *et al.*, 1974). More recently it has been shown that inhibition of glutamine transport depletes the pools of glutamate and GABA (Rae *et al.*, 2003). Taken together, the set of metabolite concentrations and enzyme kinetics are consistent with a scenario in which alternations in glial–neuronal interactions could change the concentrations of glutamate, glutamine, and GABA, and vice versa.

The comparison of substrate concentrations and  $K_m$  values for neurotransmitter cycling should be placed, however, in the context of metabolic control analysis (MCA). Presumably, the substrate concentrations and cycling rates are controlled not by individual enzymatic steps but by the neuronal firing requirements of the network of cells. The brain may be controlling the network of enzymatic steps to maintain a constant value for one or more crucial metabolic variables, such as the rate of the release of glutamate or the quantity of glutamate that is present in the extracellular space. Even with the MCA view, however, an alteration of enzyme function could be consistent with observable neurochemical changes during neuropsychiatric disorders.

There are numerous studies of FDG-PET, primarily using metabolic rates that are normalized to the whole-brain metabolic rate of each subject. Kimbrell and co-workers have demonstrated that normalization can lead to completely different conclusions about the location of cerebral abnormalities (Kimbrell *et al.*, 2002). A few studies of psychiatric disorders have reported absolute rates of glucose utilization obtained with FDG-PET, generally showing reductions in regional and global metabolic rates (Dunn *et al.*, 2002; Kumar *et al.*, 1993a). Some reductions have been shown to be proportionate to the severity of depression (Kimbrell *et al.*, 2002). Normalized metabolic rates show that, relative to the rest of the brain in depression, the subgenual prefrontal cortex and the occipital cortex have lower rates of glucose utilization than are seen in healthy controls (Drevets *et al.*, 1997, 1998). Although the occipital cortex was not evaluated further in those papers, the abnormality in the subgenual cortex was associated with a loss of volume (Botteron *et al.*, 2002; Drevets *et al.*, 1997). Reductions in glia have been reported in depressed subjects in the same brain region without apparent alteration of neurons (Öngur *et al.*, 1998). Similarly, in alcohol-dependent subjects, reduced glial density and glial nuclear size (Miguel-Hidalgo *et al.*, 2002) are associated with reductions in glucose utilization (Adams *et al.*, 1993). Abnormalities of brain volume, metabolism and cellular density and form have been reported in a variety of neuropsychiatric conditions, and these findings are consistent with altered glial–neuronal interactions.

As will be described, MRS provides a variety of tools that can be used to investigate alterations in glial–neuronal interactions in detail *in vivo*. The applications most relevant to investigations of glial–neuronal interactions are implementations of  $^1\text{H}$  MRS, and many of the resulting MRS findings are consistent with alterations in the glial–neuronal interactions and changes in NAA metabolism. Theories of altered glial–neuronal interactions are consistent with the use of MRS to investigate and monitor psychiatric diseases and their treatments. In particular,  $^1\text{H}$  MRS is particularly useful for psychiatric studies because of its high sensitivity and its safety for repeated, longitudinal studies in adults and children.

## 13.2. $^1\text{H}$ MRS AND GLIAL–NEURONAL INTERACTIONS

### 13.2.1. *N*-Acetyl Aspartate

Measurements of NAA are the most common application of  $^1\text{H}$  MRS in the brain. This application of MRS owes its widespread use to several qualities. First, the sensitivity of an MRS measurement is directly proportional to the quantity of the material present in the sample, and NAA is the most abundant neurochemical that can be detected with MRS in the brain. Furthermore, the resonance of NAA that is most often measured is that of the methyl group at 2.023 ppm, which contains three hydrogen atoms and therefore provides three times the sensitivity that would be obtained if only one hydrogen were detected.

Another helpful feature of the NAA methyl resonance is that it is composed of a single peak. Many metabolites, such as glutamate and GABA, for example, have resonances that distribute the peak intensity among two or more peaks, thereby reducing the peak height and increasing the complexity of the spectral analysis. The cause of the multiplicity is *J*-coupling, which is a form of interaction of the detected hydrogen with other nuclei in the molecule. *J*-coupling not only increases complexity in the MR spectrum but can distort peak shapes and reduce peak areas for resonance with coupling.

The last quality of NAA to make it useful for MRS studies of neuropsychiatric disorders is of biological interest. NAA is found primarily in glutamatergic neurons (Moffett *et al.*, 1991; Urenjak *et al.*, 1992) and has generally been assumed to provide a measure either of neuronal quantity or viability. Although its function is unknown, NAA is synthesized at a rate of about 1/100th the rate of glucose oxidation (Moreno *et al.*, 2001). The fact that it is synthesized by a mitochondrial enzyme (Patel and Clark, 1979) raises the possibility that its production may be related to energy metabolism or brain function. NAA does leak slowly or is released in small quantities to the extracellular space, although the release is inconsistent with a neurotransmitter function for NAA (Taylor *et al.*, 1994). Astroglia have transporters

that import NAA specifically (Sager *et al.*, 1999), and neurons take up very little (Baslow and Resnik, 1997). Aspartoacylase is expressed primarily in white matter tracts and oligodendrocytes (Bhakoo *et al.*, 2001), which is consistent with earlier reports that NAA is associated with myelination and mitochondrial membranes (Burri *et al.*, 1991; D'Adamo and Yatsu, 1966). These reports are consistent with a scenario in which NAA is synthesized in neurons in a process related to cellular energetics, released slowly to the extracellular environment, and degraded to aspartate and acetyl moieties in glia. In this scenario, disruptions in the neuronal–glial interactions or cellular energetics could alter the concentration of NAA. *In vivo*, the rate of glucose utilization and the level of NAA have been reported to be correlated (O'Neill *et al.*, 2000).

MR measurements of NAA must be evaluated with some caution because of technical complications in their interpretation. One of the most common difficulties arises from the use of echo times of 35 ms and less that are commonly used for MRS measurements. At these short echo delays, macromolecular resonances contribute significantly to the peak intensity at the spectral locations of creatine, NAA, glutamate, glutamine, and GABA (Behar and Ogino, 1993; Behar *et al.*, 1994; Hofmann *et al.*, 2001; Hwang *et al.*, 1996; Kassem and Bartha, 2003; Mader *et al.*, 2002; Rothman *et al.*, 1993), and their regular, reproducible line shapes are not properly fitted with the normal spline baseline routines that are normally employed. The macromolecular resonances decay rapidly as echo times lengthen, whereas the NAA resonance is much more resistant to lengthening echo delays. Therefore, it is advisable to use longer echo times to study NAA. A further complication is that the glutamate, glutamine, and GABA resonances appear strongly at short echo delays, and they are unresolved from one other and usually from NAA at the commonly used magnetic field strength of 1.5 T.

NAA has been evaluated in a variety of psychiatric conditions, but the most common application is to schizophrenia. Investigators have generally reported lower NAA than is seen in healthy control subjects, with the reductions localized to specific brain regions, especially the prefrontal cortex (Bertolino *et al.*, 2001; Buckley *et al.*, 1994; Ende *et al.*, 2000). One thoughtful approach combined MRS and  $^{15}\text{O}$  PET to relate NAA measurements to function in schizophrenia (Bertolino *et al.*, 2000). First, NAA was measured in different brain regions to identify the prefrontal cortical location of the abnormality in a group of patients, relative to a group of healthy control subjects. Then,  $^{15}\text{O}$  PET was used to measure cerebral blood flow at rest and during a cognitive task in the same subjects. In the patients, the region of low NAA showed a significantly smaller increase in blood flow during the functional task, compared to the healthy control subjects, thereby demonstrating the low NAA coincided with a functional abnormality.

In schizophrenia, a mutation in brain-derived neurotrophic factor (BDNF) has been identified in patients and their unaffected relatives (Egan *et al.*, 2003). BDNF is believed to be involved in the cellular processes of memory creation (Lu and Gottschalk, 2000; Poo, 2001), and so the investigators tested the working memory of carriers and non-carriers of the mutation (Egan *et al.*, 2003). Working memory is the short-term retention of information to perform cognitive tasks. Homozygous carriers of the mutation had performance scores of working memory that approached the values of schizophrenic patients. The same subjects were studied with MRS to measure NAA levels, and not only did the patients and siblings of patients have significantly reduced NAA levels, but there was a significant effect of the BDNF mutation on the NAA levels (Egan *et al.*, 2003).

NAA has not been studied as widely in mood disorders, perhaps because the disorders are less clearly diagnosed than schizophrenia or alcohol dependence. Indications are that NAA levels are not significantly altered in major depressive disorder (Farchione *et al.*, 2002; Kusumakar *et al.*, 2001). NAA may be reduced in bipolar disorder (Castillo *et al.*, 2000; Cecil *et al.*, 2002; Winsberg *et al.*, 2000), which is interesting when taken in the context of similarities to schizophrenia regarding some similarity in cognitive deficits. Lithium, which has contributed effectively to the treatment of bipolar disorder, has been reported to increase NAA concentrations (Moore *et al.*, 2000).

Some reductions of NAA levels have also been reported in alcohol dependence (Bendszus *et al.*, 2001; Jagannathan *et al.*, 1996; Parks *et al.*, 2002; Schweinsburg *et al.*, 2001). As has been discussed in this chapter, NAA appears to have a relation to neuronal function, but it may also be related to neuronal volume. In alcohol dependence, genetic factors, acute ethanol toxicity, and chronic tissue damage characterized by cortical shrinkage may all contribute to loss or shrinkage of neurons and, therefore, to reductions in NAA. The inconsistencies of the findings may result from differences in the ages, severity and duration of drinking of the subjects, nutritional state, or the presence of comorbid psychiatric disorders and other substance abuse. Perhaps more important than the discrepancies of reduction is that in at least some cases, the NAA level can increase following detoxification (Martin *et al.*, 1995; Parks *et al.*, 2002), offering hope for some degree of neuronal and functional recovery and showing a link between NAA increases and cognitive improvements that are generally observed with recovery from alcohol dependence.

The effects of other substances of abuse have not been as widely studied as those of ethanol, although results to date generally show reductions in NAA. Methamphetamine (Nordahl *et al.*, 2002) and heroin (Haselhorst *et al.*, 2002) are both associated with reductions of NAA levels, and reductions observed with ecstasy (Reneman *et al.*, 2002) are correlated with scores on working memory testing (Reneman *et al.*, 2001).

In summary, NAA is reduced in many psychiatric disorders, and it appears that NAA may be affected by either neuronal volume or function.

### 13.2.2. Glutamate, Glutamine, and GABA

Glutamate and GABA are neurotransmitters that are known to participate in functionally related cycles with glutamine, so these three neurochemicals are more directly linked to neuronal function than any other compound that is detected with MRS. They are also among the most difficult chemicals to measure with  $^1\text{H}$  MRS *in vivo*. The difficulties arise partly because *J*-coupling complicates their resonances, so that instead of well-resolved single peaks the signals are distributed among triplet resonances or in some cases even more complex patterns. Figure 13.1 shows examples of the complicated patterns for glutamate and glutamine. Furthermore, many of the resonances of glutamate, glutamine, and GABA *in vivo* overlap with one another or with other peaks. For that reason, most studies report peak areas for a single, irregular combined resonance in the vicinity of 2.4 ppm called 'Glx'. At the short echo delays normally used to detect Glx, macromolecules make a major contribution to the peak intensity at glutamate, glutamine, and GABA locations (Behar and Ogino, 1993; Behar *et al.*, 1994; Hofmann *et al.*, 2001; Hwang *et al.*, 1996; Kassem and Bartha, 2003; Mader *et al.*, 2002; Rothman *et al.*, 1993). Although the macromolecular resonances decay at long echo times, they still contribute significantly to glutamate and glutamine at the echo delay of 30 ms that is generally employed for psychiatric  $^1\text{H}$  MRS studies. Because of the issues of resolution, signal-to-noise ratios, and macromolecular contamination, many of the glutamate and glutamine measurements made in psychiatric research should be viewed with skepticism.

Before discussing psychiatric applications of MRS measurements of glutamate and GABA, it may be helpful to provide some context with regard to functional effects on neurotransmitter levels. It is thought that cortical excitability is a reflection of cortical GABAergic tone, so by modulating the GABAergic tone, one would expect to affect the ability to excite cortical neurons. Indeed, transcranial magnetic stimulation has been used to measure the voltage threshold for somatosensory excitation in the human brain before and after peripheral electrical stimulation in a nerve at the wrist. After stimulation, the voltage threshold for cortical excitation was increased (Kaelin-Lang *et al.*, 2002). The effect was blocked by lorazepam, which is a GABA<sub>A</sub> receptor agonist. With light deprivation, a similar increase in cortical excitability in the occipital lobe was observed during 45 min of darkness (Borojerdi *et al.*, 2000a), and the effect was accompanied by a 20 % drop in GABA levels over the same period (Borojerdi *et al.*, 2000b). No information about

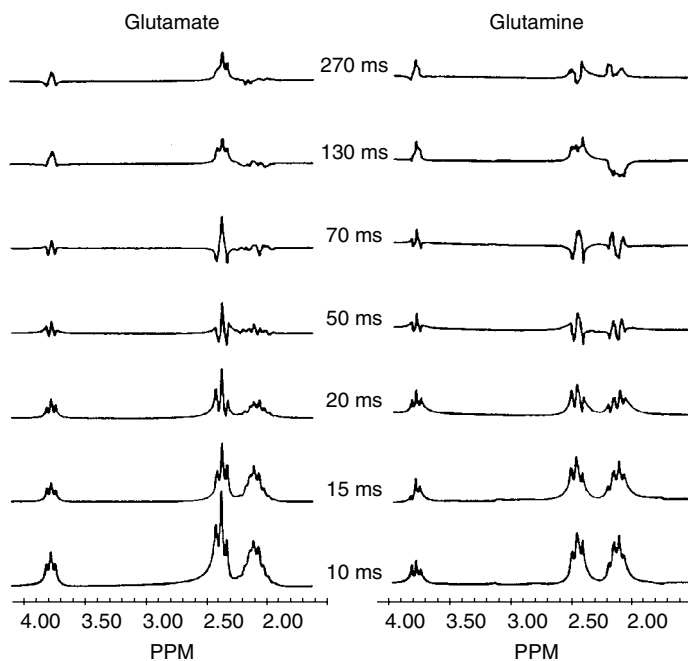


**Figure 13.1.** The effect of *J*-modulation on the resonance intensity and line shape of glutamate and glutamine at a magnetic field strength of 4.1 T. The data were acquired from a solution of 50 mM glutamate and 50 mM glutamine dissolved in distilled water, using a spin-echo sequence with a range of echo delays. As the echo time increased, the *J*-modulation reduced the resonance intensities rapidly, and although the modulation caused some return to coherence at  $TE = 130$  and 270 ms, the modulated return was incomplete. (Mason *et al.*, 1996 *Metabolic Brain Disease*. vol. 11, p. 283–313.)

the concentration of glutamate was obtained in those studies, but these studies suggest that in conditions of reduced GABA levels, one might speculate that glutamate release is reduced.

The glutamatergic and GABAergic systems have been implicated in the pathophysiology of schizophrenia from diverse lines of evidence. NMDA receptor function may be altered in schizophrenia (Javitt and Zukin, 1991; Olney and Farber, 1995). Pharmacological studies have shown that NMDA receptor antagonists can exacerbate symptoms of schizophrenia (Javitt and Zukin, 1991; Krystal *et al.*, 1994; Malhotra *et al.*, 1996), while reducing glutamate release with lamotrigine attenuates psychotic effects associated with NMDA receptor antagonism (Anand *et al.*, 2000). Examining the glutamate–glutamine and GABA–glutamine cycles from an enzymatic perspective, the prefrontal cortex of patients with schizophrenia have been shown to possess four times the activity of phosphate-activated glutaminase and twice the activity of glutamate decarboxylase (GAD-65 and GAD-67 combined) (Gluck *et al.*, 2002). Other studies showed decreased messenger RNA for GAD-67 in the prefrontal cortex of schizophrenic patients (Abkarian *et al.*, 1995; Volk *et al.*, 2000), and the loss of some cortical GABAergic neurons (Reynolds *et al.*, 2002). One possible reconciliation of the reports is that most of the increased GAD in schizophrenia is GAD-65, instead of GAD-67. GAD-67 is located primarily in the cell bodies, while GAD-65 is found in the nerve terminals, so such an explanation would suggest that in schizophrenia GABA synthesis is up-regulated in the nerve terminals. There is also a report, however, of reduced GABA release and uptake in schizophrenia (Simpson *et al.*, 1989) and a further observation of upregulated GAD-65 in association with antipsychotic treatment (Benes *et al.*, 2000). The findings of GABAergic and glutamatergic alterations have typically been

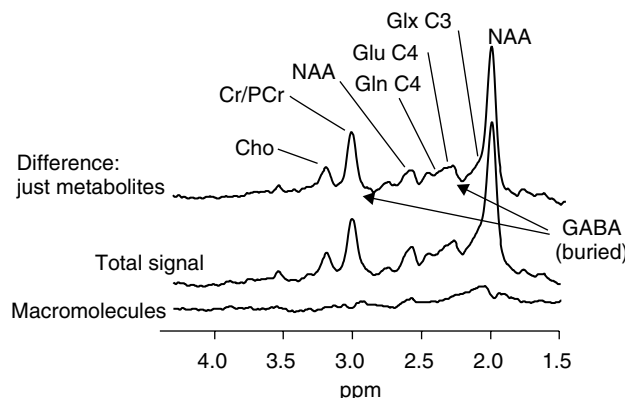


**Figure 13.2.** The overlap of GABA with glutamate, glutamine, and other resonances in spectra obtained at 2.1 T. The middle spectrum shows the spectrum obtained with the conventional spin-echo sequence using an echo delay of 12 ms. If an inversion–recovery sequence is applied to null the metabolite resonances, only the macromolecular resonances remain (bottom). When the macromolecular contribution is subtracted from the total signal, only the metabolites remain (top). The macromolecular signal can contribute significantly to the total signal amplitude and needs to be considered when quantifying glutamate and glutamine *in vivo*.

hypothesized as defects in glutamatergic and GABAergic systems (Gluck *et al.*, 2002), but it is possible that the primary defects in schizophrenia lie elsewhere, and the changes in the glutamatergic and GABAergic systems are either adaptive or maladaptive strategies by the brain to compensate for the primary defect. No matter where the defects lie, it appears likely that changes may occur in the glutamatergic and GABAergic pathways, and MRS is one tool to investigate those changes.

The technical difficulties in the measurement of glutamate, glutamine, and GABA described earlier in this section have prevented most groups from investigating these important metabolites in schizophrenia. A study at 1.5 T reported increased Glx in schizophrenic patients and speculated that Glx might be elevated due to increased glutamine as a result of above normal glutamate release (Bartha *et al.*, 1997). In a more recent study, the same group at a magnetic field strength of 4 T reported that the increase is, in fact, glutamine, without a concomitant change in glutamate (Théberge *et al.*, 2002). Little else has been reported for glutamate, glutamine, and GABA in schizophrenia with MRS. At 4 T, the spectral resolution is adequate to differentiate the glutamate and glutamine, but a cautionary note is that at the 20 ms echo delay used in this study, macromolecules are a significant contaminant of the glutamate and glutamine peaks (Figure 13.2).

GABA has been implicated strongly in mood disorders (Chang *et al.*, 2003; Sanacora *et al.*, 2000), with reported alterations in GABA receptors (Cheetham *et al.*, 1988; Gulinello *et al.*, 2003; Kaschka *et al.*, 1995), plasma GABA levels (Petty *et al.*, 1992), brain GABA levels (Baker *et al.*, 1991; Sanacora *et al.*, 1999), and beneficial effects of GABA receptor agonists (Borsini *et al.*, 1986, 1988; Delini-Stula, 1987). A study of anxiety disorder yielded a report of elevations of Glx orbitofrontal cortex, using an echo delay of 12 ms (Grachev and Apkarian, 2000). Although the spectra presented are of good quality, no macromolecular corrections were made, so some caution must be applied in the interpretation of the results. Another study using *J*-editing (Figure 13.3) to detect GABA showed that cortical GABA levels are lower in patients with panic disorder (Goddard *et al.*, 2001). This combination of studies, one of Glx, the other of GABA, suggests the possibility that the brain maintains GABA and glutamate levels in a reciprocal relationship. That is, when one increases, the other decreases.

A reciprocal relationship is also suggested by recent measurements in major depressive disorder, where the concentration of GABA has been shown to be reduced by 30–50 % (Sanacora *et al.*, 1999) and the level

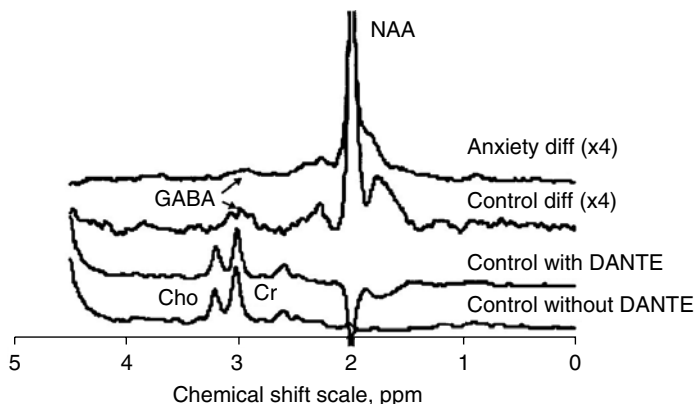


**Figure 13.3.** Representative  $\gamma$ -aminobutyric acid (GABA) spectra from a patient with panic disorder (top spectrum) and a control subject (second from top). The patient has significantly less GABA than the control subject. The bottom two spectra provide a demonstration of the *J*-editing of GABA *in vivo*. For *J*-editing, two spectra are acquired for each measurement of GABA. One spectrum has GABA, creatine, and choline in phase with one another, and the other spectrum has GABA inverted with respect to the creatine and choline, using a DANTE pulse. Upon subtraction, the creatine and choline resonances vanish, because they are identical, whereas the GABA adds to itself because its phase differs between the two spectra. (Goddard *et al.*, 2001).

of glutamate increased by 10% (Mason *et al.*, 2001a). In the context of reports of reduced glucose utilization in major depressive disorder (Dunn *et al.*, 2002; Kimbrell *et al.*, 2002; Kumar *et al.*, 1993b), it may be that the low GABA is related to chronically decreased glutamate release, just as was the case with the light deprivation (Boroojerdi *et al.*, 2000b). The reductions in GABA were normalized with electroconvulsive therapy (ECT) (Sanacora *et al.*, 2003) or treatment with selective serotonin reuptake inhibitors (Sanacora *et al.*, 2002), although the number of subjects was too small to evaluate the effects of the treatments on the level of glutamate. The increase of GABA concentration with ECT is accompanied by an increase in GABA receptor binding after ECT (Mervaala *et al.*, 2001), implying an alteration in multiple parts of the GABAergic system. In contrast to major depressive disorder, manic-depressive disorder does not show alterations in either GABA or glutamate. Although the glutamatergic system has also shown alterations in mood disorders (Krystal *et al.*, 2002), little has been reported about concentrations of glutamate, glutamine, and GABA with MRS *in vivo* in mood disorders.

Another area of investigation of  $^1\text{H}$  MRS studies of mood disorders lies with neurosteroid modulation of the GABAergic and glutamatergic systems. Neurosteroids are known to bind to the GABA receptor and potentiate the GABAergic response (Puia *et al.*, 2003; Smith *et al.*, 1998), and plasma GABA levels have been reported to vary across the menstrual cycle (Halbreich *et al.*, 1996) and to be lower in women with premenstrual dysphoric disorder (PMDD). Cortical GABA levels have also been shown to vary across the menstrual cycle but in a manner that differs in women with PMDD, relative to healthy control subjects (Epperson *et al.*, 2002). That is, in the follicular phase, during which healthy women have the highest levels of brain GABA, women with PMDD have the lowest GABA concentrations. Furthermore, glutamate levels are elevated when GABA levels are decreased (Haga *et al.*, 2001), which again raises the possibility of a reciprocal relationship of GABA and glutamate concentrations.

The GABAergic system is immediately suspected of involvement in alcoholism because of the well-known potentiation of the  $\text{GABA}_A$  receptor by the binding of ethanol. Further evidence for GABAergic involvement comes from low plasma GABA levels in alcohol-dependent subjects (Petty *et al.*, 1993) and some efficacy of the GABA receptor agonist baclofen in reducing alcohol consumption (Addolorato *et al.*,

2000, 2002; Colombo *et al.*, 2000). GABA levels in alcohol-dependent subjects after 1 month of sobriety have been shown to be reduced by ~25 % compared to healthy control subjects (Behar *et al.*, 1999). More recently, GABA levels measured by  $^1\text{H}$  MRS have been found to be normal after 1 week of detoxification but fall by approximately 20 % after 4 weeks of sobriety (Mason *et al.*, 2003a), which is in agreement with a significant decline in plasma GABA levels between 1 day and 3 weeks of sobriety (Adinoff *et al.*, 1995).

### 13.3. $^{13}\text{C}$ MRS AND PSYCHIATRIC DISORDERS

$^{13}\text{C}$  MRS studies have focused primarily on the metabolism of glutamate, glutamine, and GABA, with some attention devoted to NAA. Unlike NAA, the amino acids glutamate, glutamine and GABA are synthesized relatively rapidly in the brain, with the entire quantities turned over in about 1 h. *In vivo*, the use of glucose labeled at the C1 position has yielded the rates of glucose oxidation, glutamate–glutamine neurotransmitter cycling, GABA synthesis, neuronal  $\alpha$ -ketoglutarate–glutamate exchange, and the neuronal TCA cycle (Gruetter *et al.*, 2001; Mason *et al.*, 1992, 1995, 2001b; Sibson *et al.*, 1997, 1998). Glucose labeled at C2 has provided rates of anaplerosis and estimates of the astrocytic TCA cycle flow relative to the rate of glutamine synthesis (Kanamatsu and Tsukada, 1999; Lebon *et al.*, 2002; Tsukada *et al.*, 1998). Acetate labeled at C1 has yielded the rate of the astrocytic TCA cycle (Blüml *et al.*, 2002), while acetate labeled at C2 has provided estimates of glutamate–glutamine neurotransmitter cycling and the astrocytic glutamate pool size and astrocytic TCA cycle rate (Lebon *et al.*, 2002). In cellular preparations, even compartmentation of intermediary metabolism within glia can be evaluated (Zwingmann *et al.*, 2001). At high magnetic field strengths, the greater sensitivity allows the deconvolution of partial volume effects on metabolic rates (Mason *et al.*, 1999). The richness of the information available with  $^{13}\text{C}$  permits the study of basic mechanisms of glial–neuronal interactions and, therefore, neuropsychiatric diseases in which these may be affected.

Because  $^{13}\text{C}$  MRS is relatively new for human use, it is only now beginning to be applied to psychiatric disorders, with the first preliminary results obtained in an investigation of the low concentration of cortical GABA (Mason *et al.*, 2001c). As described earlier in this chapter, GABA has been reported to be reduced by 30–50 % in depressed subjects (Sanacora *et al.*, 1999). In light of reductions observed in glucose utilization in major depression (Dunn *et al.*, 2002; Kimbrell *et al.*, 2002; Kumar *et al.*, 1993a), at least two theories have been proposed to explain the GABA reduction: (1) the GABAergic system is more active than normal, releasing an abundance of GABA, inhibiting neuronal firing, and depleting the level of GABA to a new lower steady state, and (2) the GABAergic system has been slowed because neuronal activity is globally lower. In the first case, the rate of GABA synthesis should be elevated in depressed subjects, but in the second case, the rate of GABA synthesis should be slower (Figure 13.4). The early results obtained using infusions of  $[1-^{13}\text{C}]$ glucose in depressed patients indicate that the rate of GABA synthesis is approximately 50 % of the rate seen in healthy controls (Mason *et al.*, 2001c), which is consistent with the reported reductions in GABA concentration. The basic finding is that GABA synthesis and, presumably release, are slower in depression, and the  $^{13}\text{C}$  MRS has advanced the field to the question of why GABA and possibly glutamate release are reduced in depression.

$^{13}\text{C}$  can be used productively *in vivo* without regard to kinetics of neurotransmitter metabolism. At least three alternative applications have been achieved. The first of these is simply a measurement of the concentrations of glutamate and glutamine to overcome the technical difficulties associated with  $^1\text{H}$  MRS detection of glutamate and glutamine. The natural abundance  $^{13}\text{C}$  resonances of glutamate and glutamine C4 at 1.5 T provide more than adequate resolution to quantify glutamate and glutamine. The approach was used to compare healthy children to an infant with Canavan's disease, demonstrating reduced glutamate and increased NAA in the child with Canavan's disease (Blüml, 1999). A second approach overcomes some of the low sensitivity of  $^{13}\text{C}$  MRS while maintaining the high spectral resolution, and

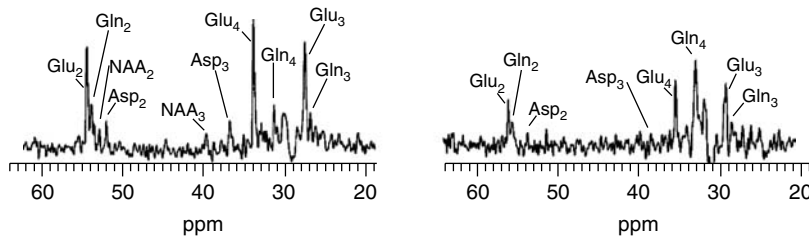


**Figure 13.4.**  $^{13}\text{C}$  label incorporation in control (left) and a representative patient with hepatic encephalopathy, grade I–II (right). The spectra were calculated from one acquisition, 80–100 min after start of an infusion of  $[1-^{13}\text{C}]$ glucose infusion. The spectra were scaled to represent absolute concentrations. Note the apparent reduction of  $^{13}\text{C}$  incorporation into glutamate C4 and C2, and aspartate C2 and C3 in CHE. Even though affected by the subtraction analysis to a larger extent in CHE than in control, the glutamine C4 resonance appears strikingly prominent in spectra of the patient. Label accumulation in NAA C2 and C3 observed in the control was not detected in CHE. (Blümli *et al.*, 2001). Reproduced with permission of John Wiley & Sons, Inc.

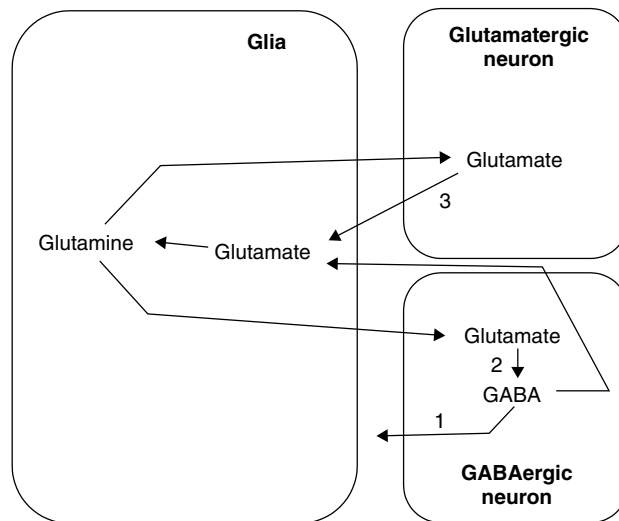


**Figure 13.5.** Cycling of glutamate, GABA, and glutamine. In depression, the concentration of cortical GABA is low. The reduction could be explained on the basis of GABA release (labeled 1) being elevated in depression and draining the GABA pool to a new steady-state level that can be sustained by glutamate conversion to GABA (labeled 2). Another possibility is that glutamate release (labeled 3) is slowed down in depression, so that less GABA is released (labeled 1), and a new higher steady-state concentration is reached. Preliminary data obtained with  $^{13}\text{C}$  indicate that the rate of GABA synthesis is reduced, which is consistent with the second scenario.

that is achieved by measuring concentrations of  $^{13}\text{C}$ -labeled glutamate and glutamine after an infusion of  $[1-^{13}\text{C}]$ glucose. This approach has been used successfully to relate labeled quantities of glutamine with disease grade in hepatic encephalopathy (Blümli *et al.*, 2001) (Figure 13.5). Of note is that NAA labeling in the patients was much lower than in the healthy controls, demonstrating that reduced NAA turnover rates can be detected in some conditions of neuronal compromise. These are two practical applications that are particularly useful for the evaluation of glutamate and glutamine at the low magnetic field strengths that are in widespread use. A third application is the measurement of the rate of synthesis of NAA (Moreno *et al.*,

2001) during an infusion of  $[1-^{13}\text{C}]$ glucose. In light of the possibility of glial–neuronal mediation of NAA turnover, measurements of the rate of NAA turnover may prove useful for studying psychiatric disorders that are associated with reduced levels of NAA and in which glial–neuronal interactions are hypothesized to be abnormal.

### 13.4. FUTURE DIRECTIONS

$^1\text{H}$  MRS studies yield measurements of the concentrations in altered disease or functional states. Those static chemical measurements are material for the development of hypotheses about neuronal viability, glial–neuronal interactions, and brain energetics. Because glutamate and GABA are the most abundant neurotransmitters in the brain, the widespread ability to make robust and accurate measurements of concentrations of glutamate, glutamine, and GABA would be of enormous benefit to research on psychiatric disorders. The rapidly spreading use of high-field magnets for MR spectroscopy will provide users with enhanced opportunities to overcome the present, serious limitations of spectral resolution, sensitivity, and macromolecular contamination. The number of groups that are eliminating the macromolecular contamination in  $^1\text{H}$  MRS is increasing, and it should soon become standard practice.

Although  $^1\text{H}$  MRS has provided abundant information about neuropsychiatric disorders, more work is required for the evaluation of neurotransmitter hypotheses that result from the MRS studies, and  $^{13}\text{C}$  MRS will play a major role. Among current hypotheses for alterations in  $^1\text{H}$  MRS concentrations of brain metabolites are alterations of energy metabolism, glutamate and GABA neurotransmitter release, glial–neuronal interactions, and the number and volume of neurons. One example of the evaluation of a hypothesis resulting from  $^1\text{H}$  MRS measurements of the lower concentration of GABA in depression is the  $^{13}\text{C}$  finding of slow GABA synthesis.

$^{13}\text{C}$  MRS studies have powerful benefits, such as a lack of radioactivity, high spectral resolution, and the ability to measure the rates of several metabolic pathways at the same time. The lack of radioactivity in particular opens the possibility of studying children, whose disorders have generally been neglected in psychiatric research. However, the disadvantages may preclude some disorders from study on the basis of practicality. The infusion times are long, typically 2 h. If absolute measurements of glucose utilization are needed, 15 min experiment times have recently been developed in animals using  $[2-^{13}\text{C}]$ deoxyglucose (Cohen *et al.*, 2002). For other rates, such as GABA synthesis or glutamate–glutamine cycling, longer infusion times are currently required. Higher-field magnets and the accompanying improvements in sensitivity will help to decrease the required experiment time and thereby expand the types of disorders and the numbers of patients who are willing and able to take part in  $^{13}\text{C}$  research projects.

A practical obstacle to patient compliance is the need for two intravenous (IV) catheters, one of which is used to infuse the  $^{13}\text{C}$ -labeled substrate and the other to draw blood samples. The greatest sensitivity is obtained when the  $^{13}\text{C}$  enrichment of the substrate in the plasma changes as rapidly as possible, and the most rapid changes available are obtained with IV infusions. One study has used a slower enrichment method, which was oral administration of  $[1-^{13}\text{C}]$ glucose to measure the rate of synthesis of NAA (Moreno *et al.*, 2001). Because the rate of synthesis of NAA is so very much slower than even the slow rate of glucose enrichment from the gut, the measurement retained practically full sensitivity. One IV catheter was eliminated by the oral administration. For measurements of more rapid processes such as glucose oxidation and glutamate–glutamine neurotransmitter cycling, however, a comparison of oral and IV administration at 2.1 T showed a major loss of sensitivity for such rapid processes when oral administration is used (Mason *et al.*, 2003b). Perhaps adequate sensitivity can be recovered by doing measurements at higher magnetic field strengths. The study of NAA synthesis also eliminated the second IV catheter by creatively using observed glutamate and glutamine labeling as input functions for the NAA synthesis determination (Moreno *et al.*, 2001), which is not feasible for studies of glutamate and glutamine neurotransmitter cycling and GABA synthesis.

Under some conditions, it may be possible to eliminate the sampling IV line, as well. For IV glucose infusions, it will continue to be necessary to maintain a sampling IV catheter to ensure that plasma glucose levels remain within safe bounds. However, it may become possible to measure the time courses of  $^{13}\text{C}$ -labeled glucose and the total glucose levels in the brain during oral administration of glucose, so that the percent enrichment could be observed simultaneously with the labeling of brain glutamate and glutamine. Then, the sampling IV line could be eliminated, which would greatly improve the appeal of the procedure to patients and control subjects alike.

In summary,  $^1\text{H}$  MRS is beginning to yield data that suggest alterations in glial-neuronal interactions through NAA and neurotransmitter metabolism. A new family of methods,  $^{13}\text{C}$  MRS, is being applied to evaluate those interactions more directly. The increasing field strengths and dissemination of methodological improvements should create an environment where widespread, good quality investigation of glial-neuronal interactions can provide biomarkers so eagerly sought by industry and yield abundant, valuable information to understand psychiatric disorders.

## REFERENCES

Abkarian, S., Kim, J. J., Potkin, S. G., Hagman, J. O., Tafazzoli, A., Bunney, W. E. J., and Jones, E. G. (1995) Gene expression for glutamic acid decarboxylase is reduced without loss of neurons in prefrontal cortex of schizophrenics. *Arch Gen Psychiatry* **52**: 258–266

Adams, K. M., Gilman, S., Koeppke, R. A., Kluin, K. J., Brunberg, J. A., Dede, D., Berent, S., and Kroll, P. D. (1993) Neuropsychological deficits are correlated with frontal hypometabolism in positron emission tomography studies of older alcoholic patients. *Alcohol Clin Exp Res* **17**: 205–210

Addolorato, G., Caputo, F., Capristo, E., Colombo, G., Gessa, G. L., and Gasbarrini, G. (2000) Ability of baclofen in reducing alcohol craving and intake: II – Preliminary clinical evidence. *Alcohol Clin Exp Res* **24**: 67–71

Addolorato, G., Caputo, F., Capristo, E., Domenicali, M., Bernardi, M., Janiri, L., Agabio, R., Colombo, G., Gessa, G. L., and Gasbarrini, G. (2002) Baclofen efficacy in reducing alcohol craving and intake: a preliminary double-blind randomized controlled study. *Alcohol Alcohol* **37**: 504–508

Adinoff, B., Kramer, G. L., and Petty, F. (1995) Levels of gamma-aminobutyric acid in cerebrospinal fluid and plasma during alcohol withdrawal. *Psychiatr Res* **59**: 137–144

Anand, A., Charney, D. S., Oren, D. A., Berman, R. M., Hu, X. S., Cappiello, A., and Krystal, J. H. (2000) Attenuation of the neuropsychiatric effects of ketamine with lamotrigine: support for hyperglutamatergic effects of *N*-methyl-*D*-aspartate receptor antagonists. *Arch Gen Psychiatr* **57**: 270–276

Baker, G. B., Wong, J. T., Yeung, J. M., and Coutts, R. T. (1991) Effects of the antidepressant phenelzine on brain levels of gamma-aminobutyric acid (GABA). *J Affect Disord* **21**: 207–211

Bartha, R., Williamson, P. C., Drost, D. J., Malla, A., Carr, T. J., Cortese, L., Canaran MacFabe, G., Rylett, R. J., and Neufeld, R. W. J. (1997) Measurement of glutamate and glutamine in the medial prefrontal cortex of never-treated schizophrenic patients and healthy controls by proton magnetic resonance spectroscopy. *Arch Gen Psychiatr* **54**: 959–965

Baslow, M. H., and Resnik, T. R. (1997) Canavan disease. Analysis of the nature of the metabolic lesions responsible for development of the observed clinical symptoms. *J Mol Neurosci* **9**: 109–125

Behar, K. L., and Ogino, T. (1993) Characterization of macromolecule resonances in the  $^1\text{H}$  NMR spectrum of rat brain. *Magn Reson Med* **30**: 38–44

Behar, K. L., Rothman, D. L., Petersen, K. F., Hooten, M., Delaney, R., Petroff, O. A., Shulman, G. I., Navarro, V., Petrakis, I. L., Charney, D. S., and Krystal, J. H. (1999) Preliminary evidence of low cortical GABA levels in localized  $^1\text{H}$ -MR spectra of alcohol-dependent and hepatic encephalopathy patients. *Am J Psychiatr* **156**: 952–954

Behar, K. L., Rothman, D. L., Spencer, D. D., and Petroff, O. A. (1994) Analysis of macromolecule resonances in  $^1\text{H}$  NMR spectra of human brain. *Magn Reson Med* **32**: 294–302

Bendszus, M., Weijers, H. G., Wiesbeck, G., Warmuth-Metz, M., Bartsch, A. J., Engels, S., Boning, J., and Sylomosi, L. (2001) Sequential MR imaging and proton MR spectroscopy in patients who underwent recent detoxification for chronic alcoholism: correlation with clinical and neuropsychological data. *Am J Neuroradiol* **22**: 1926–1932

Benes, F. M., Todtenkopf, M. S., Logiotatos, P., and Williams, M. (2000) Glutamate decarboxylase(65)-immunoreactive terminals in cingulate and prefrontal cortices of schizophrenic and bipolar brain. *J Chem Neuroanat* **20**: 259–269

Bertolino, A., Callicott, J. H., Mattay, V. S., Weidenhammer, K. M., Rakow, R., Egan, M. F., and Weinberger, D. R. (2001) The effect of treatment with antipsychotic drugs on brain N-acetylaspartate measures in patients with schizophrenia. *Biol. Psychiatr* **49**: 39–46

Bertolino, A., Esposito, G., Callicott, J. H., Mattay, V. S., Van Horn, J. D., Frank, J. A., Berman, K. F., and Weinberger, D. R. (2000) Specific relationship between prefrontal neuronal N-acetylaspartate and activation of the working memory cortical network in schizophrenia. *Am J Psychiatr* **157**: 26–33

Bhakoo, K. K., Craig, T. J., and Styles, P. (2001) Developmental and regional distribution of aspartoacylase in rat brain tissue. *J Neurochem* **79**: 211–220

Blindermann, J.-M., Maitre, M., Ossola, L., and Mandel, P. (1978) Purification and some properties of L-glutamate decarboxylase from human brain. *Eur J Biochem* **86**: 143–152

Blüml, S. (1999) *In vivo* quantitation of cerebral metabolite concentrations using natural abundance <sup>13</sup>C MRS at 1.5 T. *J Magn Reson* **136**: 219–225

Blüml, S., Moreno-Torres, A., and Ross, B. D. (2001) [1-<sup>13</sup>C]glucose MRS in chronic hepatic encephalopathy in man. *Magn Reson Med* **45**: 981–993

Blüml, S., Moreno-Torres, A., Shic, F., Nguy, C. H., and Ross, B. D. (2002) Tricarboxylic acid cycle of glia in the *in vivo* human brain. *NMR Biomed* **15**: 1–5

Borojerdi, B., Bushara, K. O., Corwell, B., Immisch, I., Battaglia, F., Muellbacher, W., and Cohen, L. G. (2000a) Enhanced excitability of the human visual cortex induced by short-term light deprivation. *Cereb Cortex* **10**: 529–534

Borojerdi, B., Cohen, L. G., Petroff, O. A., and Rothman, D. L. (2000b) Mechanisms of light deprivation-induced enhancement of visual cortical excitability. In *Society for Neuroscience*, New Orleans, LA, pp 309, 312

Borsini, F., Evangelista, S., and Meli, A. (1986) Effect of GABAergic drugs on the behavioral “despair” test in rats. *Eur J Pharmacol* **121**: 265–268

Borsini, F., Mancinelli, A., D’Aranno, V., Evangelista, S., and Meli, A. (1988) On the role of endogenous GABA in the forced swimming test in rats. *Pharmacol Biochem Behav* **29**: 275–279

Botteron, K. N., Raichle, M. E., Drevets, W. C., Heath, A. C., and Todd, R. D. (2002) Volumetric reduction in left subgenual prefrontal cortex in early onset depression. *Biol Psychiatr* **51**: 342–344

Buckley, P. F., Moore, C., Long, H., Larkin, C., Thompson, P., Mulvany, F., Redmond, O., Stack, J. P., Ennis, J. T., and Waddington, J. L. (1994) <sup>1</sup>H-Magnetic resonance spectroscopy of the left temporal and frontal lobes in schizophrenia: clinical, neurodevelopmental, and cognitive correlates. *Biol. Psychiatr* **36**: 792–800

Burri, R., Steffen, C., and Herschkowitz, N. (1991) *N*-acetyl-L-aspartate is a major source of acetyl groups for lipid synthesis during rat brain development. *Dev Neurosci* **13**: 403–411

Busatto, G. F., Garrido, G. E., Almeida, O. P., Castro, C. C., Camargo, C. H., Cid, C. G., Buchpiguel, C. A., Furui, S., and Bottino, C. M. (2003) A voxel-based morphometry study of temporal lobe gray matter reductions in Alzheimer’s disease. *Neurobiol Aging* **24**: 221–231

Castillo, M., Kwock, L., Courvoisie, H., and Hooper, S. R. (2000) Proton MR spectroscopy in children with bipolar affective disorder: preliminary observations. *Am J Neuroradiol* **21**: 832–838

Cecil, K. M., DelBello, M. P., Morey, R., and Strakowski, S. M. (2002) Frontal lobe differences in bipolar disorder as determined by proton MR spectroscopy. *Bipolar Disorders* **4**: 357–365

Chang, L., Cloak, C. C., and Ernst, T. (2003) Magnetic resonance spectroscopy studies of GABA in neuropsychiatric disorders. *J Clin Psychiatr* **64**: 7–14

Cheetham, S., Crompton, M. R., Katona, L. E., Parker, S. J., and Horten, R. W. (1988) Brain GABA/benzodiazepine binding sites and glutamic acid decarboxylase activity in depressed suicide victims. *Brain Res* **460**: 114–123

Cohen, D. M., Wei, J., O’Brian Smith, E., Gao, X., Quast, M. J., and Sokoloff, L. (2002) A method for measuring cerebral glucose metabolism *in vivo* by <sup>13</sup>C-NMR spectroscopy. *Magn Reson Med* **48**: 1063–1067

Colombo, G., Agabio, R., Carai, M. A., Lobina, C., Pani, M., Reali, R., Addolorato, G., and Gessa, G. L. (2000) Ability of baclofen in reducing alcohol intake and withdrawal severity: I – Preclinical evidence. *Alcohol Clin Exp Res* **24**: 58–66

D’Adamo, A., and Yatsu, F. (1966) Acetate metabolism in the nervous system. *N*-acetyl-L-aspartic acid and the biosynthesis of brain lipids. *J Neurochem* **13**: 961–965

Danbolt, N. C. (1994) The high affinity uptake system for excitatory amino acids in the brain. *Prog Neurobiol* **44**: 377–396

Dean, B. (2003) The cortical serotonin2A receptor and the pathology of schizophrenia: a likely accomplice. *J Neurochem* **85**: 1–13

Del Zompo, M., Bocchetta, A., Goldin, L. R., and Corsini, G. U. (1984) Linkage between X-chromosome markers and manic-depressive illness. Two Sardinian pedigrees. *Acta Psychiatr Scand* **70**: 282–287

Delini-Stula, A. V. (1987) Influence of baclofen and GABA-mimetic agents on spontaneous and olfactory-bulb-ablation-induced muricidal behavior in the rat. *Arzneim Forsch* **28**: 1508–1509

Dennis, S. C., Lai, J. C. K., and Clark, J. B. (1977) Comparative studies on glutamate metabolism in synaptic and non-synaptic rat brain mitochondria. *Biochem J* **164**: 727–736

Drevets, W. C., Öngur, D., and Price, J. L. (1998) Reduced glucose metabolism in the subgenual prefrontal cortex in unipolar depression. *Mol Psychiatr* **3**: 220–226

Drevets, W. C., Price, J. L., Simpson, J. R. J., Todd, R. D., Reich, T., Vannier, M., and Raichle, M. E. (1997) Subgenual prefrontal cortex abnormalities in mood disorders. *Nature* **386**: 824–827

Dunn, R. T., Kimbrell, T. A., Ketter, T. A., Frye, M. A., Willis, M. W., Luckenbaugh, D. A., and Post, R. M. (2002) Principal components of the Beck Depression Inventory and regional cerebral metabolism in unipolar and bipolar depression. *Biol Psychiatr* **51**: 387–399

Egan, M. F., Kojima, M., Callicott, J. H., Goldberg, T. E., Kolachana, B. S., Bertolino, A. Z. E., Gold, B., Goldman, D., Dean, M., Lu, B., and Weinberger, D. R. (2003) The BDNF val66met polymorphism affects activity-dependent secretion of BDNF and human memory and hippocampal function. *Cell* **257–269**

Ende, G., Braus, D. F., Walter, S., Weber-Fahr, W. S. B., Mauldsley, A., and Henn, F. A. (2000) Effects of age, medication, and illness duration on the *N*-acetyl aspartate signal of the anterior cingulate region in schizophrenia. *Schizophr Res* **41**: 389–395

Epperson, C. N., Haga, K., Mason, G. F., Sellers, E., Gueorguieva, R., Zhang, W., Weiss, E., Rothman, D. L., and Krystal, J. H. (2002) Cortical  $\gamma$ -aminobutyric acid levels across the menstrual cycle in healthy women and those with premenstrual dysphoric disorder. *Arch Gen Psychiatr* **59**: 851–858

Erecinska, M., and Silver, I. A. (1990) Metabolism and role of glutamate in mammalian brain. *Prog Neurobiol* **35**: 245–296

Farchione, T. R., Moore, G. J., and Rosenberg, D. R. (2002) Proton magnetic resonance spectroscopic imaging in pediatric major depression. *Biological Psychiatr* **52**: 86–92

Gluck, M. R., Thomas, R. G., Davis, K. L., and Haroutunian, V. (2002) Implications for altered glutamate and GABA metabolism in the dorsolateral prefrontal cortex of aged schizophrenic patients. *Am J Psychiatr* **159**: 1165–1173

Goddard, A. W., Mason, G. F., Almai, A., Rothman, D. L., Behar, K. L., Petroff, O. A., Charney, D. S., and Krystal, J. H. (2001) Reductions in occipital cortex GABA levels in panic disorder detected with  $^1\text{H}$ -magnetic resonance spectroscopy. *Arch Gen Psychiatr* **58**: 556–561

Grachev, I. D., and Apkarian, A. V. (2000) Anxiety in healthy humans is associated with orbital frontal chemistry. *Mol Psychiatr* **5**: 482–488

Gruetter, R., Seaquist, E. R., and Ugurbil, K. (2001) A mathematical model of compartmentalized neurotransmitter metabolism in the human brain. *American Journal of Physiol Endocrinol Metab* **281**: E100–112

Gulinello, M., Orman, R., and Smith, S. S. (2003) Sex differences in anxiety, sensorimotor gating and expression of the alpha4 subunit of the GABA<sub>A</sub> receptor in the amygdala after progesterone withdrawal. *Eur J Neurosci* **17**: 641–648

Haga, K., Epperson, N., Appel, M., Krystal, J. H., and Mason, G. F. (2001) Interactions of cortical glutamate and GABA in women with PMDD. *Biol Psychiatr* **49**: 42S

Halbreich, U., Petty, F., Yonkers, K., Kramer, G. L., Rush, A. J., and Bibi, K. W. (1996) Low plasma gamma-aminobutyric acid levels during the late luteal phase of women with premenstrual dysphoric disorder. *Am J Psychiatr* **153**: 718–719

Haselhorst, R., Dursteler-MacFarland, K. M., Scheffler, K., Ladewig, D., Muller-Spahn, F., Stohler, R., Seelig, J., and Seifritz, E. (2002) Frontocortical *N*-acetylaspartate reduction associated with long-term i.v. heroin use. *Neurology* **58**: 305–307

Hawkins, R. A., and Mans, A. M. (1983) Intermediary metabolism of carbohydrates and other fuels. In *Handbook of Neurochemistry* (Lajtha A, ed). New York: Plenum Press, pp 259–294

Hofmann, L., Slotboom, J., Boesch, C., and Kreis, R. (2001) Characterization of the macromolecule baseline in localized <sup>1</sup>H-MR spectra of human brain. *Magn Reson Med* **46**: 855–863

Hovatta, I., Varilo, T., Suvisaari, J., Terwilliger, J. D., Ollikainen, V., Arajarvi, R., Juvonen, H., Kokko-Sahin, M. L., Vaisanen, L., Mannila, H., Lonnqvist, J., and Peltonen, L. (1991) A genomewide screen for schizophrenia genes in an isolated Finnish subpopulation, suggesting multiple susceptibility loci. *Am J Hum Genet* **65**: 1114–1124

Hwang, J. H., Graham, G. D., Behar, K. L., Alger, J. R., Prichard, J. W., and Rothman, D. L. (1996) Short echo time proton magnetic resonance spectroscopic imaging of macromolecule and metabolite signal intensities in the human brain. *Magn Reson Med* **35**: 633–639

Jagannathan, N. R., Desai, N. G., and Raghunathan, P. (1996) Brain metabolite changes in alcoholism: an *in vivo* proton magnetic resonance spectroscopy (MRS) study. *Magn Reson Imaging* **14**: 553–557

Javitt, D. C., and Zukin, S. R. (1991) Recent advances in the phenylcyclidine model of schizophrenia. *Am J Psychiatr* **148**: 1301–1308

Kaelin-Lang, A., Luft, A. R., Sawaki, L., Burstein, A. H., Sohn, Y. H., and Cohen, L. G. (2002) Modulation of human corticomotor excitability by somatosensory input. *J Physiol* **540**: 623–633

Kanamatsu, T., and Tsukada, Y. (1999) Effects of ammonia on the anaplerotic pathway and amino acid metabolism in the brain: an *ex vivo* <sup>13</sup>C NMR spectroscopic study of rats after administering [2-<sup>13</sup>C]] glucose with or without ammonium acetate. *Brain Res* **841**: 11–19

Kaschka, W., Feistel, H., and Ebert, D. (1995) Reduced benzodiazepine receptor binding in panic disorders measured by iomazenil SPECT. *J Psychiatr Res* **29**: 427–434

Kassem, M. N. E., and Bartha, R. (2003) Quantitative proton short-echo-time LASER spectroscopy of normal human white matter and hippocampus at 4 Tesla incorporating macromolecule subtraction. *Magn Reson Med* **49**: 918–827

Kimbrell, T. A., Ketter, T. A., George, M. S., Little, J. T., Benson, B. E., Willis, M. W., Herscovitch, P., and Post, R. M. (2002) Regional cerebral glucose utilization in patients with a range of severities of unipolar depression. *Biol Psychiatr* **51**: 237–252

Krystal, J. H., Karper, L. P., Seibyl, J. P., Freeman, G. K., Delaney, R., Bremner, J. D., Heninger, G. R., Bowers, M. B. J., and Charney, D. S. (1994) Subanesthetic effects of the noncompetitive NMDA antagonist, ketamine, in humans: psychomimetic, perceptual, cognitive, and neuroendocrine responses. *Arch Gen Psychiatr* **51**: 199–214

Krystal, J. H., Sanacora, G., Blumberg, H., Anand, A., Charney, D. S., Marek, G., Epperson, C. N., Goddard, A., and Mason, G. F. (2002) Glutamate and GABA systems as targets for novel antidepressant and mood-stabilizing treatments. *Mol Psychiatr* **7**: S71–80

Kumar, A., Newberg, A., Abass, A., Berlin, J., Smith, R., and Reivich, M. (1993a) Regional cerebral glucose metabolism in late-life depression and Alzheimer disease: a preliminary positron emission tomography study. *Proc Natl Acad Sci USA* **90**: 7019–7023

Kumar, A., Newberg, A., Alavi, A., Berlin, J., Smith, R., and Reivich, M. (1993b) Regional cerebral glucose metabolism in late-life depression and Alzheimer disease: a preliminary positron emission tomography study. *Proc Natl Acad Sci USA* **90**: 7019–7023

Kusumakar, V., MacMaster, F. P., Gates, L., Sparkes, S. J., and Khan, S. C. (2001) Left medial temporal cytosolic choline in early onset depression. *Can J Psychiatr* **46**: 959–964

Lebon, V., Petersen, K. F., Cline, G. W., Shen, J., Mason, G. F., Dufour, S., Behar, K. L., Shulman, G. I., and Rothman, D. L. (2002) Astroglial contribution to brain energy metabolism in humans revealed by <sup>13</sup>C nuclear magnetic resonance spectroscopy: elucidation of the dominant pathway for neurotransmitter glutamate repletion and measurement of astrocytic oxidative metabolism. *J Neurosci* **22**: 1523–1531

Lu, B., and Gottschalk, W. (2000) Modulation of hippocampal synaptic transmission and plasticity by neurotrophins. *Prog Brain Res* **128**: 231–241

Lund, P. (1970) A radiochemical assay for glutamine synthetase, and activity of the enzyme in rat tissues. *Biochem J* **118**: 35–39

Mader, I., Karitzky, J., Klose, U., Seeger, U., Sperfeld, A., Naegele, T., Schick, F., Ludolph, A., and Grodd, W. (2002) Proton MRS in Kennedy disease: absolute metabolite and macromolecular concentrations. *J Magn Reson Imag* **16**: 160–167

Magistretti, P. J., and Pellerin, L. (1997) Metabolic coupling during activation. A cellular view. *Adv Exp Med Biol* **413**: 161–166

Maitre, M., Blinder, J. M., Ossola, L., and Mandel, P. (1978) Comparison of the structures of L-glutamate decarboxylases from human and rat brains. *Biochem Biophys Res Commun* **85**: 885–890

Malhotra, A. K., Pinals, D. A., Weingartner, H., Sirocco, K., Missar, C. D., Pickar, D., and Breier, A. (1996) NMDA receptor function and human cognition: the effects of ketamine in healthy volunteers. *Neuropsychopharmacol* **14**: 301–307

Martin, P. R., Gibbs, S. J., Nimmerrichter, A. A., Riddle, W. R., Welch, L. W., and Willcoft, M. R. (1995) Brain proton magnetic resonance spectroscopy studies in recently abstinent alcoholics. *Alcohol Clin Exp Res* **19**: 1078–1082

Mason, G. F., Anand, A., Sanacora, G., Epperson, N., Haga, K., Appel, M., Goddard, A. W., Charney, D. S., Rothman, D. L., and Krystal, J. H. (2001a) Different relationships among cortical amino acids in unipolar and bipolar depression. In *Int Soc Magn Reson Med*, Glasgow, UK, p 557

Mason, G. F., Appel, M., de Graaf, R. A., Ruff, E., Rothman, D. L., and Krystal, J. H. (2003a) Brain GABA falls with sobriety in alcohol-dependent subjects. In: *12th Annual Meet Int Soc Magn Reson Med*, Toronto, Canada, in press

Mason, G. F., Falk Petersen, K., de Graaf, R. A., Kanamatsu, T., Otsuki, T., and Rothman, D. L. (2003b) A comparison of (13)C NMR measurements of the rates of glutamine synthesis and the tricarboxylic acid cycle during oral and intravenous administration of [1-(13)C]glucose. *Brain Res Brain Res Protocols* **10**: 181–190

Mason, G. F., Gruetter, R., Rothman, D. L., Behar, K. L., Shulman, R. G., and Novotny, E. J. (1995) Simultaneous determination of the rates of the TCA cycle, glucose utilization, a-ketoglutarate/glutamate exchange, and glutamine synthesis in human brain by NMR. *J Cereb Blood Flow Metab* **15**: 12–25

Mason, G. F., Martin, D. L., Martin, S. B., Manor, D., Sibson, N. R., Patel, A., Rothman, D. L., and Behar, K. L. (2001b) Decrease in GABA synthesis rate in rat cortex following GABA-transaminase inhibition correlates with the decrease in GAD(67) protein. *Brain Res* **914**: 81–91

Mason, G. F., Pan, J. W., Chu, W. J., Newcomer, B. R., Zhang, Y., Orr, R., and Hetherington, H. P. (1999) Measurement of the tricarboxylic acid cycle rate in human grey and white matter *in vivo* by 1H-[13C] magnetic resonance spectroscopy at 4.1T. *J Cereb Blood Flow Metab* **19**: 1179–1188

Mason, G. F., Rothman, D. L., Behar, K. L., and Shulman, R. G. (1992) NMR determination of TCA cycle rate and a-ketoglutarate/glutamate exchange rate in rat brain. *J Cereb Blood Flow Metab* **12**: 434–447

Mason, G. F., Sanacora, G. R. H. M. A., Rothman, D. L., and Krystal, J. H. (2001c) Measurement of cortical GABA and glutamate turnover alterations *in vivo* in major depression using <sup>13</sup>C-MRS. In *Proc Am College Neuropsychopharmac*, Waikaloa Hilton, Hawaii, p 202

McGeer, E. G., and McGeer, P. L. (1979) Localization of glutaminase in the rat neostriatum. *J Neurochem* **32**: 1071–1075

Mervaala, E., Kononen, M., Fohr, J., Husso-Saastamoinen, M., Valkonen-Korhonen, M., Kuikka, J. T., Viinamaki, H., Tammi, A. K., Tiihonen, J., Partanen, J., and Lehtonen, J. (2001) SPECT and neuropsychological performance in severe depression treated with ECT. *J Affective Disorders* **66**: 47–58

Miguel-Hidalgo, J. J., Wei, J., Andrew, M., Overholser, G. J., Stockmeier, C. A., and Rajkowska, G. (2002) Glia pathology in the prefrontal cortex in alcohol dependence with and without depressive symptoms. *Biol Psychiatr* **52**: 1121–1133

Moffett, J. R., Namboodiri, M. A., Cangro, C. B., and Neale, J. H. (1991) Immunohistochemical localization of N-acetylaspartate in rat brain. *Neuroreport* **2**: 131–134

Moore, G. J., Bebchuk, J. M., Hasanat, K., Chen, G., Sarji-Bozorgzad, N., Wilds, I. B., Faulk, M. W., Koch, S., Glitz, D. A., Jolkovsky, L., and Manji, H. K. (2000) Lithium increases N-acetyl-aspartate in the human brain: *in vivo* evidence in support of bcl-2's neurotrophic effects? *Biol Psychiatr* **48**: 1–8

Moreno, A., Ross, B. D., and Blümli, S. (2001) Direct determination of the N-acetyl-L-aspartate synthesis rate in the human brain by (13)C MRS and [1-(13)C]glucose infusion. *J Neurochem* **77**: 347–350

Nordahl, T. E., Salo, R., Possin, K., Gibson, D. R., Flynn, N., Leamon, M., Galloway, G. P., Pfefferbaum, A., Spielman, D. M., Adalsteinsson, E., and Sullivan, E. V. (2002) Low N-acetyl-aspartate and high choline in the anterior cingulum of recently abstinent methamphetamine-dependent subjects: a preliminary proton MRS study. *Magnetic resonance spectroscopy*. *Psychiatr Res* **116**: 43–52

O'Neill, J., Eberling, J. L., Schuff, N., Jagust, W., Reed, B., Soto, G., Ezekiel, F., Klein, G., and Weiner, M. W. (2000) Method to correlate 1H MRSI and 18FDG-PET. *Magn Reson Med* **43**: 244–250

Olney, J. W., and Farber, N. B. (1995) Glutamate receptor dysfunction and schizophrenia. *Arch Gen Psychiatr* **52**: 998–1007

Öngür, D., Drevets, W. C., and Price, J. L. (1998) Glial reduction in the subgenual prefrontal cortex in mood disorders. *Proc Natl Acad Sci USA* **95**: 13290–13295

Parks, M. H., Dawant, B. M., Riddle, W. R., Hartmann, S. L., Dietrich, M. S., Nickel, M. K., Price, R. R., and Martin, P. R. (2002) Longitudinal brain metabolic characterization of chronic alcoholics with proton magnetic resonance spectroscopy. *Alcohol Clin Exp Res* **26**: 1368–1380

Patel, A. B., Rothman, D. L., Cline, G. W., and Behar, K. L. (2001) Glutamine is the major precursor for GABA synthesis in rat neocortex *in vivo* following acute GABA-transaminase inhibition. *Brain Res* **919**: 207–220

Patel, A. J., Johnson, A. L., and Balázs, R. (1974) Metabolic compartmentation of glutamate associated with the formation of  $\gamma$ -aminobutyrate. *J Neurochem* **23**: 1271–1279

Patel, T. B., and Clark, J. B. (1979) Synthesis of N-acetyl-L-aspartate by rat brain mitochondria and its involvement in mitochondrial/cytosolic carbon transport. *Biochem. J* **184**: 539–546

Perry, T. L., Young, V. W., Bergeron, C., Hansen, S., and Jones, K. (1987) Amino acids, glutathione, and glutathione transferase activity in the brains of patients with Alzheimer's disease. *Ann Neurol* **21**: 331–336

Petroff, O. A., Spencer, D. D., Alger, J. R., and Prichard, J. W. (1989) High-field proton magnetic resonance spectroscopy of human cerebrum obtained during surgery for epilepsy. *Neurology* **39**: 1197–1202

Petty, F., Fulton, M., Moeller, F. G., Kramer, G., Wilson, L., Fraser, K., and Isbell, P. (1993) Plasma gamma-aminobutyric acid (GABA) is low in alcoholics. *Psychopharmacol Bull* **29**: 277–281

Petty, F., Kramer, G. L., Gullion, C. M., and Rush, A. J. (1992) Low plasma gamma-aminobutyric acid levels in male patients with depression. *Biol Psychiatr* **32**: 354–363

Poo, M. M. (2001) Neurotrophins as synaptic modulators. *Nat Rev Neurosci* **2**: 24–32

Puia, G., Mienville, J. M., Matsumoto, K. T. H., Watanabe, H., Costa, E., and Guidotti, A. (2003) On the putative physiological role of allopregnanolone on GABA(A) receptor function. *Neuropharmacology* **44**: 49–55

Rae, C., Hare, N., Bubb, W. A., McEwan, S. R., Broer, A., McQuillan, J. A., Balcar, V. J., Conigrave, A. D., and Broer, S. (2003) Inhibition of glutamine transport depletes glutamate and GABA neurotransmitter pools: further evidence for metabolic compartmentation. *J Neurochem* **85**: 503–514

Reneman, L., Majolie, C. B., Flick, H., and den Heeten, G. J. (2002) Reduced N-acetylaspartate levels in the frontal cortex of 3,4-methylenedioxymethamphetamine (Ecstasy) users: preliminary results. *Am J Neuroradiol* **23**: 231–237

Reneman, L., Majolie, C. B., Schmand, B., van den Brink, W., and den Heeten, G. J. (2001) Prefrontal N-acetyl-aspartate is strongly associated with memory performance in (abstinent) ecstasy users: preliminary report. *Biol Psychiatr* **50**: 550–554

Reynolds, G. P., Beasley, C. L., and Zhang, Z. J. (2002) Understanding the neurotransmitter pathology of schizophrenia: selective deficits of subtypes of cortical GABAergic neurons. *J Neural Transm* **109**: 881–889

Rothman, D. L., Petroff, O. A., Behar, K. L., and Mattson, R. H. (1993) Localized  $^1\text{H}$  NMR measurements of  $\gamma$ -aminobutyric acid in human brain *in vivo*. *Proc Natl Acad Sci USA* **90**: 5662–5666

Sager, T. N., Thomsen, C., Valsborg, J. S., Laursen, H., and Hansen, A. J. (1999) Astroglia contain a specific transport mechanism for N-acetyl-L-aspartate. *J Neurochem* **73**: 807–811

Sanacora, G., Mason, G. F., and Krystal, J. H. (2000) Impairment of GABAergic transmission in depression: new insights from neuroimaging studies. *Crit Rev Neurobiol* **14**: 23–45

Sanacora, G., Mason, G. F., Rothman, D. L., Behar, K. L., Hyder, F., Petroff, O. A., Berman, R. M., Charney, D. S., and Krystal, J. H. (1999) Reduced cortical gamma-aminobutyric acid levels in depressed patients determined by proton magnetic resonance spectroscopy. *Arch Gen Psychiatr* **56**: 1043–1047

Sanacora, G., Mason, G. F., Rothman, D. L., Hyder, F., Ciarcia, J. J., Ostroff, R. B., Berman, R. M., and Krystal, J. H. (2003) Increased cortical GABA concentrations in depressed patients receiving ECT. *Am J Psychiatr* **160**: 577–579

Sanacora, G., Mason, G. F., Rothman, D. L., and Krystal, J. H. (2002) Increased occipital cortex GABA concentrations in depressed patients after therapy with selective serotonin reuptake inhibitors. *Am J Psychiatr* **159**: 663–665

Saxena, S., Brody, A. L., Ho, M. L., Alborzian, S., Maidment, K. M., Zohrabi, N., Ho, M. K., Huang, S. C., Wu, H. M., and Baxter, L. R. J. (2002) Differential cerebral metabolic changes with paroxetine treatment of obsessive-compulsive disorder vs major depression. *Arch Gen Psychiatr* **59**: 250–261

Schweinsburg, B. C., Taylor, M. J., Alhassoon, O. M., Videen, J. S., Brown, G. G., Patterson, T. L., Berger, F., and Grant, I. (2001) Chemical pathology in brain white matter of recently detoxified alcoholics: a  $^1\text{H}$  magnetic resonance spectroscopy investigation of alcohol-associated frontal lobe injury. *Alcohol Clin Exp Res* **25**: 924–934

Sibson, N. R., Dhankhar, A., Mason, G. F., KL, K. L. B., Rothman, D. L., and Shulman, R. G. (1997) *In vivo*  $^{13}\text{C}$  NMR measurements of cerebral glutamine synthesis as evidence for glutamate-glutamine cycling. *Proc Natl Acad Sci USA* **94**: 2699–2704

Sibson, N. R., Dhankhar, A., Mason, G. F., Rothman, D. L., Behar, K. L., and Shulman, R. G. (1998) Stoichiometric coupling of brain glucose metabolism and glutamate cycling. *Proc Natl Acad Sci USA* **95**: 316–321

Simpson, M. D., Slater, P., Deakin, J. F., Royston, M. C., and Skan, W. J. (1989) Reduced GABA uptake sites in the temporal lobe in schizophrenia. *Neurosci Lett* **107**: 211–215

Smith, S. S., Gong, Q. H., Hsu, F., Markowitz, R. S., French-Mullen, J. M., and Li, X. (1998) GABA<sub>A</sub> receptor  $\alpha$ -4 subunit suppression prevents withdrawal properties of an endogenous steroid. *Nature* **392**: 3239–3244

Soares, J. C. (2002) Can brain-imaging studies provide a 'mood stabilizer signature?' *Mol Psychiatr* **7**: S64–70

Stine, O. C., McMahon, F. J., Chen, L., Xu, J., Meyers, D. A., MacKinnon, D. F., Simpson, S., McInnis, M. G., Rice, J. P., Goate, A., Reich, T., Edenberg, H. J., Foroud, T., Nurnberger, J. I. J., Detera-Wadleigh, S. D., Goldin, L. R., Guroff, J., Gershon, E. S., Blehar, M. C., and DePaulo, J. R. (1997) Initial genome screen for bipolar disorder in the NIMH genetics initiative pedigrees: chromosomes 2, 11, 13, 14, and X. *Am J Med Genet* **74**: 263–269

Taylor, D. L., Davies, E. C., Obrenovitch, T. P., and Urenjak, J. (1994) Extracellular N-acetylaspartate in the rat brain: *in vivo* determination of basal levels and changes evoked by high  $\text{K}^+$ . *J Neurochem* **62**: 2349–2355

Théberge, J., Bartha, R., Drost, D. J., Menon, R. S., Malla, A., Takhar, J., Neufeld, R. W., Rogers, J., Pavlosky, W., Schaefer, B., Densmore, M., Al-Semaan, Y., and Williamson, P. C. (2002) Glutamate and glutamine measured with 4.0 T proton MRS in never-treated patients with schizophrenia and healthy volunteers. *Am J Psychiatr* **159**: 1944–1946

Tsukada, Y., Kanamatsu, T., Watanabe, H., and Okamoto, K. (1998) *In vivo* investigation of glutamate-glutamine metabolism in hyperammonemic monkey brain using  $^{13}\text{C}$ -magnetic resonance spectroscopy. *Dev Neurosci* **20**: 427–433

Urenjak, J., Williams, S. R., Gadian, D. G., and Noble, M. (1992) Specific expression of N-acetylaspartate in neurons, oligodendrocytes *in vitro*. *J Neurochem* **59**: 55–61

Varrone, A., Marek, K. L., Jennings, D., Innis, R. B., and Seibyl, J. P. (2001)  $[(123)\text{I}]\beta\text{-CIT}$  SPECT imaging demonstrates reduced density of striatal dopamine transporters in Parkinson's disease and multiple system atrophy. *Movement Disorders* **16**: 1023–1032

Volk, D., Austin, M. C., Pierri, J. N., Sampson, A. R., and Lewis, D. A. (2000) Decreased glutamic acid decarboxylase<sub>67</sub> messenger RNA expression in a subset of prefrontal cortical  $\gamma$ -aminobutyric acid neurons in subjects with schizophrenia. *Arch Gen Psychiatr* **57**: 237–245

Weil-Malherbe, H. (1969) Activators and inhibitors of brain glutaminase. *J Neurochem* **19**: 2257–2267

Winsberg, M. E., Sachs, N., Tate, D. L., Adalsteinsson, E., Spielman, D., and Ketter, T. A. (2000) Decreased dorsolateral prefrontal N-acetyl aspartate in bipolar disorder. *Biol Psychiatr* **47**: 475–481

Wu, J.-Y., Chude, O., Wein, J., Roberts, E., Saito, K., and Wong, E. (1978) Distribution and tissue specificity of glutamate decarboxylase (EC 4.1.1.15). *J Neurochem* **30**: 849–857

Zwingmann, C., Richter-Landsberg, C., and Leibfritz, D. (2001)  $^{13}\text{C}$  isotopomer analysis of glucose and alanine metabolism reveals cytosolic pyruvate compartmentation as part of energy metabolism in astrocytes. *Glia* **34**: 200–212

## **Section D**

### **Brain and Mind**



# Long-term Memory: Do Incremental Signals Reflect Engagement of Cognitive Processes?

**Jed A. Meltzer and R. Todd Constable**

*Department of Diagnostic Radiology, Yale University School of Medicine, MR Center, P.O. Box 208042, New Haven, CT 06520-8042, USA*

---

14.1	Introduction	259
14.2	Interpretive Methodology in Neuroimaging	260
14.3	Long-term Memory: Broad Anatomical Dissociations	262
14.4	MTL Involvement in Declarative Memory Encoding	264
14.5	Factors Related to Encoding	265
14.6	Reality of Encoding as a Cognitive Process	267
14.7	Encoding Versus Retrieval	268
14.8	Subdivisions of MTL and Long-term Memory: Correspondences	269
14.9	Imaging Studies of Episodic Recall Versus Familiarity	271
14.10	Summary	273

---

## 14.1. INTRODUCTION

Long-term memory is a general property of mammalian nervous systems that defies simple classification. Like other primary domains of cognitive science, such as attention and language, LTM has been the topic of dozens of neuroimaging studies designed to elucidate its basic neural mechanisms and their anatomical localization. Although the ability of fMRI to map physiological changes associated with cognitive activity in the awake human has proven enormously useful, controversy over the interpretation of such changes has

persisted throughout the lifetime of the field. Interpretation of neuroimaging data involves uncertainty on many levels, from the biophysical source of the signal, to the nature of the theoretical mental processes that one hopes to isolate through cognitive task design. In this chapter, we review the progress that has been made through neuroimaging studies towards an understanding of the neural basis of long-term memory. We focus on findings of activation in the medial temporal lobe (MTL), which has long been known to be necessary for certain kinds of long-term memory function. Although neural activity in the MTL undoubtedly plays a vital role in the establishment of long-term memories and their subsequent recall, neuroimaging studies have generally failed to detect any incremental signal changes in the MTL related to the performance of tasks designed to invoke mnemonic processing, in comparison to a 'baseline' state. However, significant changes have been observed in experiments that compare activity under different conditions, which, while identical in terms of the physical nature of stimulus presentation and response demands, differ with respect to incidental factors such as stimulus novelty, meaningfulness, and the extent to which the stimuli are subsequently remembered after scanning. While these various factors may reflect a common underlying process related to memory formation, the relationship between the hypothesized processes of memory encoding and retrieval on the one hand, and observable incremental signal changes on the other, has proven to be more indirect and nuanced than expected.

This pattern of findings illustrates the difficulties involved in attempts to establish direct links between the neuroenergetic changes observable in functional neuroimaging and the engagement of mental processes whose physical instantiation is largely uncertain. In reviewing neuroimaging studies that have detected activation in the MTL, we consider the extent to which the factors influencing signal levels there can be construed as reflecting differential engagement of the theoretical cognitive processes of memory encoding and retrieval. While the data are consistent with the participation of the MTL in these processes, they suggest that incremental changes in neuronal energy use, along with the associated hemodynamic changes detectable in fMRI, are not easily evoked in the MTL by the deliberate performance of a cognitive task. This does not imply that the MTL is only involved in processing the distinctions that do drive signal changes, but rather that its normal functions in memory may not require incremental increases in neural activity across different behavioral states. The subtle and intriguing factors to which MTL activation has proved sensitive might never have been discovered, if comparisons with simple baseline tasks had turned out to be effective at producing significant signal changes. Therefore, the results of long-term memory research may prove instructive for those seeking to interpret signal changes, or lack thereof, in other brain regions, as they demonstrate no straightforward relationship between a cognitive process and the presence of an incremental signal change.

## 14.2. INTERPRETIVE METHODOLOGY IN NEUROIMAGING

If the component processes that make up attention, memory, and language are to be successfully localized and distinguished using fMRI, the validity of the assumptions used must be carefully considered. The first, and most valuable, is that incremental changes in the signal (typically BOLD) reflect changes in local neural activity. Biophysical testing of this hypothesis, described fully in Chapters 9 and 16 of this volume, indicates that the magnitude of BOLD signal (expressed as percent change) can provide measures of the percent change in the cerebral metabolic rate of oxygen consumption (CMRO<sub>2</sub>), provided that measurements are available of all the other parameters that determine the BOLD signal, including cerebral blood flow, cerebral blood volume, and NMR spin relaxation parameters. As described in Chapters 5 and 10, the energy increments ( $\Delta\text{CMRO}_2$ ) are directly proportional to percent changes in neuronal firing rates and glutamate release. Hence, a BOLD signal change can be inferred to reflect a change in the level of neuronal activity. However, experiments calibrated in terms of CMRO<sub>2</sub> (Shulman *et al.*, 2002) have indicated that the increments of localized neuronal activity induced by sensory stimulation in awake

animals are small relative to a large baseline level of energy use, the function of which is poorly understood. Furthermore, the neural processing of sensory stimulation of a given magnitude requires a consistent total amount of neuronal activity, rather than a consistent increment from a variable baseline (Hyder *et al.*, 2002).

Given these findings, the comparative magnitudes of BOLD signal changes obtained under different conditions can be interpreted only in very limited circumstances. When only the magnitude of a sensory stimulus is varied, the size of the BOLD signal change within a brain area can monotonically reflect the magnitude of the difference in neuronal activity. However, comparisons of the magnitudes of signal changes across different tasks and locations cannot be considered to be meaningful, as the size of the increment is entirely dependent on the precise nature of the baseline with which it is compared. The incremental signals observed in subtractive analyses provide evidence that a given brain area is engaged in information processing induced by the task, but failure to detect such a change is by no means proof that the neural activity occurring in an area does not play a role in the task, as the baseline amount of activity may be sufficient for the region's contribution.

Consider an analogous case from the ERP literature. The ERPs to brief auditory stimuli, such as beeps, include a series of early components known to be generated by brainstem auditory structures (Rugg and Coles, 1995). The presentation of a 'rare' beep, differing slightly in frequency from the majority, gives rise to a 'P300' response – a more positive voltage level in the time-locked average response to the rare tones compared to the majority tones, occurring approximately 300 ms after the beep. This response is known to be cortical in origin (Soltani and Knight, 2000). Nonetheless, it would be absurd to conclude that the brainstem auditory components are 'not involved' in processing the difference between the rare and majority tones.

In many ERP studies, including those of the P300 effect, the finding of interest is not that a component is present in one condition and absent in another, but rather that a deflection from the prestimulus baseline occurring at a certain time is larger in one condition. Therefore, it is necessary to use conditions that are exactly matched in terms of the physical nature of the stimuli and the response, so that the appropriate 'components,' i.e. deflections with a known time course, can be reliably elicited in both conditions and their magnitude compared. In fMRI studies of long-term memory, the same technique has proven absolutely essential to elucidating the role of the medial temporal lobe, as comparisons between different task states have seldom yielded positive results. However, the use of constant task demands of visual stimulus presentation has revealed that the magnitude of activity evoked in MTL structures (such as that measured relative to an average prestimulus baseline in an event-related paradigm) is sensitive to certain cognitive factors, even though two conditions may both evoke a significant response. Therefore, the magnitude of an fMRI signal change can be extremely useful when comparisons are performed within the same voxels or ROIs under conditions that do not differ in the physical nature of the stimuli and responses involved in a given task.

The use of extrinsic sensory stimulation to evoke signal changes has been a feature of most fMRI studies, and was crucial to the validation of fMRI's ability to detect changes specifically related to localized information processing. The localization of primary sensory modalities in cortex is well known from human neuropsychology and animal experiments. For example, the occipital lobe is specialized for visual processing, whereas Heschl's gyrus is similarly dedicated to auditory processing (Gazzaniga, 1999). Furthermore, visual processing related to determining the identity of objects is anatomically dissociable from that related to monitoring their spatial locations (Ungerleider and Haxby, 1994). fMRI has confirmed and extended knowledge of the localization of primary sensory processing, and has even proven able to make fine anatomical distinctions, such as the retinotopic mapping of multiple visual processing areas (Warrington *et al.*, 2002) and the resolution of ocular dominance columns (Cheng *et al.*, 2001).

Although fMRI offers impressive spatial resolution in its detection of hemodynamic changes, considerable difficulties in interpretation of these changes arise when one moves beyond the primary sensory modalities.

Since the neural bases of higher cognitive functions are not well characterized, problems arise when one attempts to use cognitive concepts to explain signal changes. In many neuroimaging experiments, task conditions are designed deliberately to manipulate the degree to which a theoretical cognitive process is involved in the subject's performance. Brain areas that exhibit signal changes sensitive to these manipulations are then interpreted as playing a role in the cognitive process. Unfortunately, this necessitates circular reasoning, as there is little agreement among cognitive scientists about what independent cognitive subprocesses, or 'modules' (Fodor, 1983), exist. In primary sensory processing, the basic primitives are well understood: photons striking the retina trigger a well-known cascade of electrical and biochemical events in the case of vision, as do hair-cell displacements in audition and in some forms of touch (Kandel *et al.*, 2000). Unfortunately, no such body of knowledge characterizes our understanding of attention, language, and memory. Not only do we not know exactly *where* they are in the brain, we do not know *what* they are. Therefore, two scientists with diverging theoretical stances may interpret the same fMRI data differently, based on a disagreement over what cognitive processes are involved in the experimental task. This problem leads to a disappointing inconsistency in neuroimaging studies purporting to examine the same function (see e.g. Poeppel, 1996; Shulman, 1996), and encourages meta-analyses of large numbers of studies to find common ground (Cabeza and Nyberg, 2000).

Despite these difficulties of interpretation, neuroimaging studies of long-term memory have confirmed some existing theoretical concepts about the broad dissociations between multiple brain systems, which interact to give rise to the body of phenomena known collectively as memory. In part, this success is attributable to the fact that memory is expressed via a set of independent, quantifiable performance criteria, and need not be thought of as a theoretical cognitive process. Subjects can display motor learning through faster and more accurate performance of a motor task, priming through faster reaction times, and long-term declarative memory through successful recognition or recall of previously presented stimuli. In all of these cases, an independent variable is generated that can serve as a basis for analyzing signal changes. Neural signals can then be correlated with these observable *effects* of memory in order to infer the underlying *mechanisms*, freeing experimenters from the circular process of presupposing the extent to which a task engages mnemonic processing and then interpreting signal changes as indicative of such processing.

Analyses of the relationships between observable behavioral results and signal changes have, as described below, confirmed that the MTL participates in a particular form of long-term memory known as declarative memory, and is thereby distinguished from other brain structures that underlie different kinds of LTM. Beyond this broad categorization, studies have identified a number of factors related to behavioral outcomes that influence signal levels in the MTL. A primary goal of this review is to assess whether or not these factors can be considered to indicate the existence of unique cognitive processes localized to the MTL, specialized for promoting the formation and subsequent use of long-term declarative memories.

### 14.3. LONG-TERM MEMORY: BROAD ANATOMICAL DISSOCIATIONS

The phrase 'long-term memory' refers to changes in the information encoded in a nervous system that persist for an extended period, from several minutes to decades. It is distinguished from 'working memory' (WM), which refers to short-term active maintenance of information needed to perform a task, after which the information may be lost, or perhaps encoded into long-term memory as well. Long-term memory is further divided by theorists into independent forms of memory. One such form is *declarative* memory, defined as the 'acquisition, retention, and retrieval of knowledge that can be consciously and intentionally recollected' (Gabrieli, 1998). This definition is quite satisfactory in the study of humans, who can typically express the content of declarative memories verbally. Nonetheless, animals (at least mammals) are presumed to have an analogous system, although it must be tested indirectly. It is distinguished from *nondeclarative*, or *implicit* memory, defined as 'knowledge expressed through experience-induced changes in performance'

(Gabrieli, 1998). This includes such diverse phenomena as motor skill learning, probabilistic classification tasks (Knowlton *et al.*, 1994), repetition priming, and conditioning, even though, as discussed below, these different abilities are supported to some extent by separate brain systems, and are further divided into additional subsystems by some theorists.

The primary distinction between declarative and nondeclarative memory originates in the study of brain-damaged humans. Damage to certain brain structures is known to result in amnesia, a selective deficit in declarative memory with spared nondeclarative memory (Baddeley *et al.*, 2002). Amnesia frequently consists of both an *anterograde* component (failure to acquire new memories for events occurring after the lesion) and a graded *retrograde* component (failure to recall memories acquired during a variable period of time leading up to the lesion). The co-occurrence of these two deficits, along with a sparing of memories from the more distant past, has led scientists to propose that the brain structures implicated in amnesia are responsible for acquiring and retaining new memories for a limited time, but that memories are ultimately 'consolidated' in diffuse regions of the neocortex independently of these dedicated structures (Brown, 2002).

The most famous case of amnesia is the patient known as H.M., who underwent an extensive bilateral resection of brain tissue including the medial temporal lobe (MTL), an operation intended for the relief of crippling epileptic seizures. Although amnesic symptoms may also result from damage to specific regions of the thalamus and hypothalamus, it is thought that these lesions mainly exert their effect through disruption of a distributed system that depends on output from the MTL (Aggleton and Brown, 1999). Thus, the MTL remains at the forefront of research into the basis of declarative memory. Animal studies have confirmed the importance of the MTL for long-term memory, and have also characterized to some extent the unique contributions of its various substructures, including the hippocampal formation (hippocampus proper, dentate gyrus, and subiculum) and three adjacent neocortical areas: the entorhinal, perirhinal, and parahippocampal cortices (Squire, 1992; Eichenbaum *et al.*, 1994).

Although H.M. suffers from a very severe anterograde amnesia, he and other similar patients perform at normal levels on tests of nondeclarative memory. For instance, amnesics exhibit normal levels of skill acquisition through training and practice on a motor task, despite reporting no conscious recollection of ever having performed the task before (Yamashita, 1993). This suggests that nondeclarative memory is subserved by brain systems independent of those underlying declarative memory. A double dissociation between these abilities is established by complementary findings in the study of patients afflicted by diseases of the basal ganglia, including Huntington's and Parkinson's diseases. These patients sometimes show impaired acquisition of motor skills (depending on exactly which circuits are affected), with intact priming and declarative memory (Vakil and Herishanu-Naaman, 1998; Schmidtke *et al.*, 2002).

The findings of human neuropsychology regarding long-term memory have served to establish an anatomical dissociation between systems underlying implicit memory, including the basal ganglia, and systems underlying declarative memory, including the medial temporal lobe. Neuroimaging studies have largely confirmed the contrasting anatomical bases of these two major forms of long-term memory. For instance, a recent review by Doyon *et al.* (2003) reveals a complex pattern of signal increases and decreases associated with improving performance on motor skill tasks. These changes are most prevalent in the motor cortices, the striatum, and the cerebellum, all structures that were already implicated in motor learning on the basis of lesion data. Notably, effects of motor skill learning, a form of implicit memory, were not found in the MTL structures thought to be critical for declarative memory. Studies of declarative memory have instead found effects primarily in the medial temporal lobe and in several subregions of the prefrontal cortex (see below), whereas studies of priming have found effects in a broad range of neocortical areas (Schacter and Buckner, 1998). Additionally, a series of fMRI studies has examined in detail a task thought to involve both declarative and implicit learning, demonstrating that activations in medial temporal and striatal structures are anticorrelated, reflecting competitive interactions between the two systems (Poldrack

*et al.*, 1999, 2001). Therefore, fMRI results are broadly compatible with the pre-existing accounts of the major subdivisions of LTM, and have served to focus the attention of declarative memory researchers on the medial temporal lobe and the prefrontal cortex.

#### 14.4. MTL INVOLVEMENT IN DECLARATIVE MEMORY ENCODING

We will now consider studies of declarative memory in more detail, in order to illustrate how fMRI has helped to further our understanding of the nature of the mnemonic processing that occurs in the MTL. In this review, we confine our discussion to studies of *episodic* memory, the long-term retention of information stemming from individual experiences, as opposed to *semantic* memory, which pertains to general facts abstracted over many experiences and may be subserved by independent brain systems (Tulving and Markowitsch, 1998). Acquisition of semantic memories is, by definition, all but impossible to study within the time constraints of a neuroimaging experiment, but recall of semantic memories has been examined in comparison with episodic recall (Maguire *et al.*, 2000; Wiggs *et al.*, 1999).

Episodic memory is well suited for study within the common paradigm of presenting visual stimuli in the context of a classification task performed by the subject. Exposure to individual stimuli constitute individual episodes, which may be subsequently remembered or forgotten. When stimuli are presented with the intention of inducing the formation of new memory traces, tasks are considered to involve *encoding*. These are contrasted with *retrieval* tasks, in which stimuli are intended to reactivate a previously stored trace either for simple recognition of the stimulus, or for cued recall of some additional information associated with it. Encoding and retrieval are intuitively appealing as subprocesses describing the functions of the MTL, but whether they are truly dissociable and accurate depictions of what goes on in that structure must be judged on the basis of available data. They are a product of the methodology that must be used to study memory; in everyday life, experience does not come in discrete pieces. Even though it is undisputable that information is encountered for the first time at some point, and used at some later point, it is possible that there are no specific neural processes that can be construed as specifically accomplishing these tasks. An analogy to the processes of reading from and writing to a disk drive may prove to be misleading. Below, we review the specific cases in which selective activation of the MTL has been detected, and consider to what extent the pattern of results support the reality of encoding and retrieval as isolable physiological events.

Considering the critical role of intact MTL structures for episodic memory function, it was quite surprising that most early neuroimaging studies (using PET) did not report any medial temporal activation during encoding (Shallice *et al.*, 1994; Buckner *et al.*, 1995). MTL activation was detected in encoding non-verbal stimuli such as faces (Haxby *et al.*, 1996) and spatial information (Maguire *et al.*, 1996), but the failure to detect it using word stimuli was puzzling, given that the classical neuropsychological tests that established the importance of the MTL for episodic memory had relied heavily on word recall tasks (Baddeley *et al.*, 2002). In contrast, nearly all studies of episodic memory reported significant activations in prefrontal cortex (for reviews see Rugg *et al.*, 2002; Yancey and Phelps, 2001; Desgranges *et al.*, 1998), despite the fact that performance on the clinical tests is not particularly sensitive to frontal lobe damage (Shimamura, 1995). In considering the role of prefrontal regions in episodic memory, it is difficult to distinguish activity related specifically to episodic encoding and retrieval from activity involved in 'online' processing of stimuli, i.e. perception and working memory. The list of theoretical cognitive processes dependent on the prefrontal cortex is long (Miller and Cohen, 2001), and one cannot discount its importance in the performance of episodic memory tasks. As most cognitive processes not dependent on forming new memories appear to be intact in amnesics, though, we focus here on elucidating the unique contributions of the MTL, with the acknowledgement that other brain areas are critically involved in performing the same tasks.

Because researchers had every reason to expect that tasks involving encoding of words should produce hippocampal activation when compared to resting baselines, the absence of such results engendered much

speculation. A number of explanations were proposed to account for the apparent insensitivity of conventional imaging paradigms to neural activity changes in the hippocampal system. These included technical concerns such as the increased susceptibility of the MTL region to certain MRI signal acquisition artifacts (although this would apply only to fMRI, not to PET), and also partial volume effects, which may be especially pronounced in the MTL because several highly differentiated structures are typically contained within small volumes, in comparison with neocortical areas. Purely biological factors were also considered. For example, it was suggested that the particular kind of neural information processing in the MTL that leads to memory formation may simply not be characterized by the overall increases in neuronal firing that presumably drive BOLD signal changes in other brain areas (Cohen *et al.*, 1999). This idea enjoys some empirical support from the electrophysiological literature. Neighboring neurons in sensory and motor cortex tend to have very similar firing properties, leading to theoretical concepts such as columns and hypercolumns (Kandel *et al.*, 2000). In the hippocampus, when cells with specific firing properties have been discovered, such as 'place cells,' they tend not to form such tightly correlated clusters (Shen and McNaughton, 1996). Consequently, neural coding in the hippocampus is described as sparser and more distributed than in the cortex (Barnes *et al.*, 1990). Additionally, it is possible that the encoding-related activity in the MTL is nearly always engaged to a comparable degree, rendering it unsuitable for subtractive analysis methods (Haxby *et al.*, 1996; Eichenbaum, 2001).

These differences between MTL structures and neocortex should not be completely dismissed in the light of recent reports of selective MTL activation related to a variety of experimental manipulations. In general, findings of selective MTL activation have not resulted from comparisons of deliberate encoding tasks with resting states, perhaps because baseline MTL activity during commonly used resting states is actually quite high compared with several alternative baseline tasks (Stark and Squire, 2001). Therefore, it is especially important in studies of the MTL to use constant task demands. This is commonly accomplished by presenting visual stimuli to subjects, under instructions to make binary decisions about them by means of a button press. Experimental manipulations may involve the nature of the stimuli, their relative novelty, the nature of the decision made about them, and post-hoc assessment of encoding success based on subsequent memory tests for the stimuli. These practices have succeeded in eliciting selective activations in the MTL, due to incidental factors that may or may not indicate the involvement of a unitary underlying encoding process.

## 14.5. FACTORS RELATED TO ENCODING

Among the most robust findings is that presentation of novel stimuli, compared to repeated items, elicits greater activation in the MTL. This has been observed using scenes (Gabrieli *et al.*, 1997; Stern *et al.*, 1996; Constable *et al.*, 2000), words (Kirchhoff *et al.*, 2000), and faces (Stern *et al.*, 1996) in deliberate or incidental encoding tasks. Another general finding that has withstood multiple replications is that presentation of meaningful stimuli, such as words and line drawings, produces greater MTL activation than presentation of stimuli without any identifiable meaning, such as false fonts and abstract geometric patterns (Kelley *et al.*, 1998; Martin *et al.*, 1997; Golby *et al.*, 2001).

While the selective activations described above result from different stimuli over constant task demands, positive results have also come from changing task demands with constant stimulus characteristics. One such manipulation is known as 'levels of processing' (Craik, 2002). A subject's task is to make some sort of binary decision about the stimuli, not knowing that he or she is subsequently going to be tested for recognition of them. Tasks that involve identification of a stimulus, and consideration of its known properties, are considered to involve 'deeper' processing than 'shallow' tasks that only require a judgment based on the obvious physical characteristics of the stimuli. Judging whether a printed word is a concrete noun or an abstract noun is an example of a deep task, whereas judging whether or not a word contains

the letter 't' is a shallow task. Because deeper processing results in higher rates of subsequent recognition of stimuli, levels of processing manipulations provide a convenient way of influencing the extent to which memory encoding takes place while maintaining the same physical task conditions. Neuroimaging experiments have demonstrated that deeper processing induces greater MTL activation for words (Wagner *et al.*, 1998) and line drawings (Henke *et al.*, 1997).

While a general process of memory encoding in the MTL might be expected to manifest itself through effects of novelty, meaningfulness, and depth of processing, numerous alternative explanations may be proposed to account for the co-occurrence of these effects in a particular area. In each of these cases, the condition with greater MTL activity can be characterized as more arousing, engaging, or interesting. While such characteristics of experiences do correlate with their memorability, they certainly do not by themselves constitute proof of an underlying encoding process. Furthermore, as these findings are also characteristic of prefrontal areas (Lee *et al.*, 2000), they do not help to specify the role of the MTL compared to the PFC, despite the dissociations seen in the clinical neuropsychology literature. Therefore, it is necessary to consider the relationship between these findings and other physiological evidence of memory encoding within the MTL.

One of the most productive means of studying brain activity related to encoding has been made possible in fMRI only with the advent of event-related analysis procedures. Electroencephalographic studies of memory have demonstrated, using episodic encoding paradigms similar to those used in the fMRI studies discussed above, that stimuli that are subsequently recognized successfully by the subject elicit different ERPs than those that are forgotten (Rugg and Coles, 1995). This 'subsequent memory' procedure can be used to classify individual trials post-hoc in event-related fMRI, generating average hemodynamic response timecourses to remembered and forgotten stimuli. Wagner *et al.* (1998) reported that hemodynamic responses (i.e. increases from an average pre-stimulus baseline) were enhanced for subsequently remembered words in left prefrontal and parahippocampal regions. Brewer *et al.* (1998) reported a similar enhancement for complex scene pictures, in right prefrontal and bilateral parahippocampal regions. This pattern of lateralization in encoding is consistent with the other selective activations reported above: a number of studies have demonstrated that MTL selective activations for novelty (Kelley *et al.*, 1998; Golby *et al.*, 2001) and meaningfulness (Martin *et al.*, 1997) tend to be left-lateralized for words, and progressively more bilateral as verbalizability of the stimuli decreases (reviewed by Martin, 1999).

Material-specific lateralization of encoding effects is, of course, reminiscent of the general verbal/nonverbal division of labor between the two cerebral hemispheres. Several theories of hippocampal function, based on computational models (McClelland *et al.*, 1995; Gluck and Myers, 2001), posit that the MTL facilitates the long-term updating and retention of information in domain-specific regions of neocortex through establishing associative links between its inputs, and that the MTL-specific mechanisms that accomplish this feat are rather general; they establish associations between their inputs regardless of their modality. From this perspective, one would expect that similar anatomical dissociations may be found in both left and right hippocampi, but that differences between the two would be limited to the processing asymmetry that characterizes the human brain: language-related processing in the left hemisphere, and visuo-spatial processing in the right. In the next section of this chapter, we discuss a number of dissociations that have been noted regarding the differential roles of individual structures of the MTL. In the current state of the literature, however, differences between the two hemispheres have indeed been limited to the verbalization-related asymmetry, consistent with accounts of domain-general encoding mechanisms inherent in hippocampal circuitry (O'Reilly and Norman, 2002). The flexibility of these mechanisms has been uniquely demonstrated in a neuroimaging study of epilepsy patients with unilateral MTL damage. Patients with right-sided damage exhibited compensatory increases in left MTL activation for viewing novel versus repeated nonverbal stimuli, whereas patients with left-sided damage exhibited an analogous effect in the right MTL for verbalizable stimuli (Golby *et al.*, 2002).

## 14.6. REALITY OF ENCODING AS A COGNITIVE PROCESS

So far, we have discussed four separate factors that have been found to correlate with increased BOLD signal in the MTL: novelty, meaningfulness, deeper processing, and subsequent memory. We now consider whether these factors can be considered as separate reflections of an underlying unity, a physiological process of memory trace formation. Ultimately, a complete understanding of memory formation will require integration of findings on the systems and molecular levels (see e.g. Squire, 2000; Kandel, 2001). Within the domain of noninvasive study in humans, we attempt here to determine whether or not the effects delineated above do represent a homogenous physiological event, unified spatially in its extent within the MTL, and unified temporally in its post-stimulus timecourse. This question has been addressed through studies building on the initial findings already described, using the techniques of fMRI, EEG, and intracranial recordings.

An fMRI study by Otten *et al.* (2001) directly compared subsequent memory effects with depth-of-processing effects by performing the subsequent memory procedure with words presented in both a deep task (living versus nonliving classification) and a shallow task (judging whether the first and last letters are in alphabetical order). Regions in left anterior hippocampus and left ventral anterior frontal gyrus showed effects of both manipulations, as a subset of a larger group of areas showing the depth-of-processing effect. This finding suggested that the levels-of-processing manipulation caused greater engagement of neuronal processing in these two areas related to encoding. However, a subsequent experiment (Otten and Rugg, 2001b) did not support that conclusion. The use of a different shallow task (syllable counting) failed to produce subsequent memory effects in these regions, but did so instead in bilateral parietal and fusiform regions. As a follow-up, Otten and Rugg (2001a) conducted an ERP investigation of subsequent memory effects in the living/nonliving task and the alphabetical judgment task. Although both tasks produced a subsequent memory effect, the two effects were of opposite polarity, with quite different scalp distributions. These findings indicate that the effects of levels-of-processing manipulations depend on the precise nature of the tasks chosen, and therefore argue against the hypothesis that the deep/shallow distinction entails a unique underlying process related specifically to memory formation.

The relationship between novelty effects and subsequent memory effects has turned out to be rather more robust. An fMRI study directly crossed the two manipulations (Kirchhoff *et al.*, 2000) and found a number of novelty-sensitive activations in anatomically connected prefrontal and lateral temporal regions, the precise location of which varied with respect to the demands of the encoding task. Novelty effects were also seen in the MTL, mainly in the left hemisphere for word encoding, and bilaterally for pictures. Crucially, the prefrontal and medial temporal regions that were modulated by novelty on a given task were also modulated by subsequent memory, demonstrating a deep relation between these effects despite the fact that they occur in multiple parallel systems for encoding information under different task demands. However, these results do not suggest that the underlying mechanism is anything unique to the MTL.

Underlying unity for novelty and subsequent memory effects in the human hippocampus were strongly demonstrated, with high temporal resolution, by an intracranial EEG experiment in epilepsy patients undergoing presurgical electrophysiological monitoring procedures (Friedman and Sutton (1987). All patients exhibited a bilateral anterior MTL negative ERP component, known as 'AMTL-N400,' which was stronger for novel compared to repeated stimuli. The magnitude of the difference was significantly correlated with subsequent recognition performance for the stimuli, an effect that was left-lateralized for words and right-lateralized for pictures. These findings contrast with negative results of Van Petten and Senkfor (1996), and Musen and Treisman (1990), who found no subsequent memory effect in scalp ERPs for nonverbal abstract and geometrical visual stimuli, but did find such effects with verbal materials. These findings suggest that the effects of meaningfulness can also be associated with the novelty and subsequent memory effects (but see Wagner *et al.*, 1999, for discussion). This unification is concordant with the theoretical views of hippocampal function outlined above: the hippocampus establishes associations between higher-order multimodal inputs, inputs that would be greatly enriched for stimuli matching pre-existing conceptual

representations, compared with abstract patterns that evoke little higher-order processing beyond perception of physical features.

So far we have not presented evidence indicating that selective MTL activity in encoding directly reflects incidental processing inducive of lasting memory traces, as opposed to deliberate effort to memorize stimuli, nor have we dissociated the meaning of the selective activation effects in MTL from those in prefrontal cortex. Both of these points were addressed in an elegant experiment by Reber *et al.* (2002a). Words and faces were presented to subjects along with a cue to either remember the item, or to forget it deliberately. There was a significant effect of the cue on subsequent memory performance for words, but not for faces. Although subsequent memory effects for words were found in both prefrontal and MTL regions, those in prefrontal cortex were accounted for by the identity of the cue, and hence can be considered to reflect deliberate effort. The MTL effects, in contrast, were independent of the cue. This finding strengthens the conclusion, drawn from a decade of failures and successes to find encoding-related activity in the MTL, that increases in MTL activation reflect neural processes leading to memory formation that are driven mainly by incidental factors correlated with the encoding of information into LTM, but not by deliberate effort to memorize information. Neural activity within the MTL does play a specific role in the encoding of memories, but this role cannot be adequately described without specification of its interaction with other brain areas. What we do know is that the encoding-related processes leading to increased BOLD signal in the hippocampus are relatively automatic and independent of conscious manipulation, in comparison with the processing performed in prefrontal cortical regions. This distinction is completely consistent with the anatomical distinctions between these two areas. The hippocampal system is characterized by a stereotypical morphology that is extraordinarily uniform across all mammals, whereas the prefrontal cortex is one of the most greatly expanded and altered regions in the brains of humans compared with other mammals (Deacon, 1997). It is not surprising, therefore, that the functions of the hippocampus may not depend on the capacity for elaborate manipulation of information in working memory that is a characteristic of higher primates (Courtney *et al.*, 1998).

## 14.7. ENCODING VERSUS RETRIEVAL

Up until now, we have put off a discussion of the distinction between encoding and retrieval tasks. On single-item encoding and recognition tasks, 'encoding' refers to the moment a stimulus is first encountered, during which a long-term memory trace may or may not be formed, whereas 'successful retrieval' refers to the moment when a previously presented stimulus is again shown, and the subject recognizes it as old (a 'hit'). This is distinguished from 'correct rejection' of novel stimuli, and from two error outcomes: 'false alarms' (the subject wrongly indicates that a novel stimulus is old), and 'misses' (the subject wrongly indicates that an old item is novel). Assuming mostly accurate performance, successful versus unsuccessful retrieval was compared using PET by Nyberg *et al.* (1996), who presented alternating blocks of mostly new and mostly old stimuli. Greater MTL activation was detected for old stimuli, suggesting that the MTL is differentially involved in retrieval success. This contrasts with studies that have primarily implicated prefrontal regions as being involved in effort to recall information, but not specifically driven by success (Buckner *et al.*, 1998a, 1998b).

Although reports of selective activation in the MTL during successful retrieval are encouraging evidence that the same system may play a dual role in both encoding and retrieval, upon further analysis a serious problem of interpretation results. We have discussed extensively above, findings of selective activation of MTL to novel stimuli. These stimuli, if not recognized by a subject, can be expected to induce encoding-related activity. Old stimuli, in contrast, may induce retrieval of the memory trace for them, but may also induce further encoding (Buckner *et al.*, 2001), making it very difficult to separate out the processes of encoding and retrieval in a recognition paradigm. Indeed, if novel stimuli induce an encoding-specific

response, and old stimuli induce a retrieval-specific response in the same structures, then no contrast may be seen between the two conditions. It has been proposed that this conflict underlies the failure of many early retrieval studies to find effects in the MTL (Stark and Squire, 2000).

A number of strategies have been employed to overcome the confound between encoding and retrieval. Gabrieli *et al.* (1997) employed a cross-modal retrieval task with an event-related design, in which subjects encoded line drawings (unscanned) and later made recognition judgments (scanned) on written nouns that either did or did not match the drawings. Encoding novel versus repeated pictures were scanned separately. The two tasks showed peak activations in different areas: encoding pictures induced novelty-specific activation in bilateral parahippocampal cortex, consistent with the subsequent memory effect in that area described by Brewer *et al.* (1998), whereas successful retrieval gave rise to activations in an anterior MTL region centered on the subiculum. This suggests that activity within the hippocampal formation related to retrieval success may be dissociable from the decreases in hemodynamic response associated with repeated presentation of single items. Further support for this hypothesis is provided by the study of Stark and Squire (2000), who report increased activity in the hippocampus for successfully recognized words and pictures, relative to novel foils, when the very same words and pictures were used in the study phase without the cross-modal manipulation used in Gabrieli *et al.* (1997). The difference in activation between targets and foils was exacerbated on a second retrieval test, during which both types of stimuli had been previously viewed in the first retrieval test. With this manipulation, the novelty encoding effect was at least partially controlled for, allowing the experimenters to demonstrate that activity within the hippocampal formation can relate to success in recognition as well as to encoding of novel information. Below, we return to this issue of confounds inherent in dissociating encoding and retrieval, as it has been greatly clarified by further anatomical and behavioral distinctions within the medial temporal lobe declarative memory system.

#### **14.8. SUBDIVISIONS OF MTL AND LONG-TERM MEMORY: CORRESPONDENCES**

The neuroimaging studies discussed above have established that MTL activation is not easily modulated by performance of memory tasks relative to a baseline, possibly because the MTL is always engaged to a considerable degree in integrating input from the cortex. However, we have suggested that effects of novelty, encoding success, and retrieval success seen in studies with constant sensory stimulation parameters may reflect the differential engagement of an underlying physiological process with specific mnemonic functions, not directly related to conscious effort. In the following sections, we examine the extent to which these effects have localizing value as indicators of memory activity. After reviewing the internal anatomy of the medial temporal lobe, we first consider some studies that have sought to localize effects of novelty encoding to specific substructures of the MTL using strict anatomical delineation techniques. Much more informative, however, are studies that have localized effects of novelty, encoding success, and retrieval success to the hippocampal formation or extrahippocampal structures on the basis of behavioral distinctions motivated by theoretical distinctions between multiple forms of declarative memory, which have arisen from human and animal studies outside the field of neuroimaging. Although the presence of differential signal changes related to these factors may be only an indirect indicator of mnemonic function, the presence of such effects in specific structures under different conditions closely matches the roles assigned to those structures in contemporary cognitive neuroscience of memory.

In the preceding sections, we have used the term 'medial temporal lobe' to refer to a set of structures known to be critically involved in declarative memory. In fact, such a simple anatomical description belies the complexity of the brain structures that make up this region of the brain. The individual structures of the MTL differ greatly from each other in cellular organization, extrinsic and intrinsic connection patterns,

and neurophysiological characteristics (Shepherd, 1997), especially in comparison with the much larger neocortex, which displays a remarkably consistent organization throughout its extent. Given the importance of the hippocampus and associated structures in memory, an enormous amount of research effort has gone into studying the information processing that occurs there.

Whereas most cortical areas are interconnected reciprocally, neural signals are largely passed through the hippocampus in a unidirectional loop. Reciprocal inputs from higher-order sensory areas converge on the parahippocampal and perirhinal cortices, as well as the entorhinal cortex, which also receives input from the former two areas. From the entorhinal cortex, a mainly unidirectional multisynaptic circuit proceeds through the dentate gyrus, areas CA3 and CA1 of the hippocampus proper, and the subiculum, which then projects back to the entorhinal cortex (Amaral, 1999). Detailed analysis of the connectivity in this circuit has led to the suggestion that the individual areas are arranged in a 'hierarchy of associativity' (Lavenex and Amaral, 2000), in which the 'integration, complexity, or abstraction of information likely increases' as one goes through the circuit outlined above. Furthermore, the output of the MTL system projects widely and reciprocally throughout the cortex, including primary sensory areas (Lavenex and Amaral, 2000). The anatomical facts, therefore, support the emerging theoretical conception of the MTL as a system that helps to establish long-term associations between inputs whose basic representations reside in the neocortex. Nonetheless, the individual substructures may have dissociable roles, especially considering their hierarchical organization.

Severe declarative memory impairment in humans can result from hippocampal lesions of quite limited extent, such as the selective ischemia in area CA1 of patient R.B. (Zola-Morgan *et al.*, 1986), perhaps the most famous amnesia patient after H.M. However, this does not rule out critical and distinct roles for extrahippocampal structures, since they project through the hippocampus in a multisynaptic loop that can be disrupted at any point. Comparative studies of amnesics (Rempel-Clower *et al.*, 1996) combined with controlled lesion experiments in monkeys (Zola-Morgan *et al.*, 1994) have indicated that memory impairment on a variety of tasks increases as more components of the MTL are damaged. Such a general finding is of course compatible both with models that treat the MTL as an undifferentiated system and with those that assign specific functions to its components.

Several lines of animal research have focused on discovering which aspects of long-term memory are crucially dependent on the hippocampus proper as opposed to other MTL areas (Rudy and Sutherland, 1989; Eichenbaum *et al.*, 1994). Although specific accounts vary, there is much agreement that the hippocampus proper is especially necessary for '(1) strong and persistent memories for events including their constituent elements and the relationships among them, and (2) a capacity to express memories flexibly across a wide range of circumstances' (Eichenbaum *et al.*, 1994). Tasks that stress simple recognition of single items, such as the 'delayed nonmatch to sample' paradigm in monkey research, are sensitive to MTL lesions, but generally intact when the lesions are confined to the hippocampus (Squire, 1992).

Based on a variety of behavioral, neurophysiological, clinical, and genetic dissociations between the hippocampus and the extrahippocampal cortices (reviewed by Brown and Aggleton, 2001), theorists have proposed that a general dichotomy between these structures may correspond to the theoretical division of declarative memory into independent processes of 'familiarity' and 'recall.' According to theories that recognize this dissociation, recognition judgments of single items may be supported either by a rich, episodic memory of one's prior experience with that item, including contextual details, or instead, only by a more vague feeling of familiarity, in which the subject knows that a stimulus has been encountered before, but does not recall associated details. The former, but not the latter, is believed to require an intact hippocampus (Tulving and Markowitsch, 1998; Aggleton and Brown, 1999). The hippocampus has been described as necessary for binding together multiple inputs in a relational context (Eichenbaum *et al.*, 1994), for supporting the flexible use of learned information in new contexts (O'Reilly and Rudy, 2001), and for recognizing conjunctions of objects rather than individual objects (Brown and Aggleton, 2001). In

the imaging studies discussed so far, success in either encoding or retrieval has been defined as the correct discrimination of previously viewed single items from novel ones. In principle, such a judgment could be accomplished by mechanisms of either familiarity or recall. In the next section, we describe neuroimaging studies that have used novelty and success effects as a proxy for mnemonic function, but have been able to differentiate the roles of hippocampal and extrahippocampal structures through behavioral paradigms that exploit the distinction between episodic recall and 'mere' familiarity.

## 14.9. IMAGING STUDIES OF EPISODIC RECALL VERSUS FAMILIARITY

The tendency in neuroimaging studies to treat the MTL as a unitary structure derives more from technical limitations than from any theoretical rationale. It is very difficult to achieve sufficient spatial resolution to differentiate the substructures of the MTL. Although the adult human hippocampus is 4–4.5 cm in length (Duvernoy, 1998), its anatomically distinguishable substructures extend all the way along its longitudinal axis, wrapped around each other in a shape aptly described as a 'jellyroll.' As a result, many studies have reported MTL activations as taking place in the hippocampus or the parahippocampal area, without further differentiation. Fortunately, even this gross distinction is useful.

As a starting point, we consider two studies that used a simple novelty-encoding paradigm, comparing the presentation of novel visual stimuli with repeated ones, with no further manipulation. Both of these studies used special techniques designed to maximize the resolution of functional activity in the MTL by constraining the analyses to specific regions of interest (ROIs) defined by strict anatomical criteria, using co-registered high-resolution structural images for guidance in individual subjects. Zeineh *et al.* (2001) used a 'flat-mapping' technique to define six different ROIs within the MTL, each of which may be described as hippocampal or parahippocampal. This study found sustained novelty-specific activation to presentation of complex scene pictures in two parahippocampal areas, whereas two hippocampal areas exhibited activation only in the later portions of the experiment. These results are consistent with the conclusion, derived from animal studies (Squire, 1992; Brown and Aggleton, 2001) that the role of the hippocampal formation in recognition memory for single items is limited compared to that of parahippocampal structures.

Reber *et al.* (2002b) used a similar anatomically constrained analysis procedure to separate activity in anterior hippocampus, posterior hippocampus, entorhinal cortex, perirhinal cortex, and parahippocampal gyrus (the latter three being extrahippocampal cortex). Bilateral novelty-specific activity was reported in all regions for picture encoding, and in left posterior hippocampus and parahippocampal gyrus for word encoding. These two studies of anatomical specificity within MTL, taken together, suggest that novelty encoding may in fact engage the hippocampus, but they do not help much in differentiating the specific functions of the hippocampus from those of adjacent regions. One possible interpretation is that novelty encoding may involve systems responsible for familiarity as well as those that support recall. Therefore, a number of studies have attempted to distinguish, both at encoding and retrieval, neural activity specifically related to these two processes, while continuing to use novelty and success effects as the best available indicator of localized mnemonic function.

One simple way to distinguish between recall and familiarity is to have subjects make a three-way subjective judgment, as to whether single stimuli are 'new' (unrecognized), 'known' (only familiar), or 'remembered' (the subject can recall the experience of encountering it before). Such a distinction is known to elicit different ERP magnitudes for known and remembered stimuli (Rugg and Yonelinas, 2003), but whether that difference reflects a quantitative or a qualitative dissociation is not established. Eldridge *et al.* (2000) demonstrated increased activation in the hippocampus for single-item recognition trials for which subjects made a subjective judgment of 'remembered,' compared with items that were merely familiar or those that were not recognized at all. While this study supports a specific role for the hippocampus

in episodic retrieval, other studies indicate that hippocampal activation during encoding may specifically support the formation of episodic traces. Davachi *et al.* (2003) demonstrated that hippocampal activation during encoding of single words predicted a subject's ability to subsequently indicate in which of two tasks he or she had encountered the item, but did not correlate with the ability to simply identify the item as old instead of new. In contrast, the perirhinal cortex did show such a subsequent-recognition effect for encoding activation.

Other studies have demonstrated novelty (Sperling *et al.*, 2001) and subsequent-recall effects (Meltzer and Constable, *submitted*) in the hippocampus during encoding of paired associate items. During presentation of triplets of words (Davachi and Wagner 2002), hippocampal activation was greater for an encoding task emphasizing inter-item associations than for one emphasizing processing of individual items, whereas the opposite was true of entorhinal and parahippocampal cortices. Furthermore, a hippocampal subsequent-recall effect was found only for words encoded in the relational task. Montaldi *et al.* (cited in Mayes and Montaldi, 1999) found that hippocampal activation was associated with novel conjunctions between items, but not for single-item novelty, whereas varying the task instructions had no effect if the amount of encoding success was the same between tasks. Taken together, these results suggest that novelty and encoding success effects are reflective of the formation of episodic and relational memory traces in the hippocampus, in a manner analogous to the effects seen in extrahippocampal MTL structures during the encoding of single items for subsequent familiarity.

Additional evidence for such a dissociation comes from studies that have used retrieval demands other than single-item recognition. In free recall, for instance, a subject is asked to name as many items as he or she can from a previously presented set. This is much more difficult than discrimination of old versus new items, as familiarity alone is insufficient to accomplish the task, and as such it requires an intact hippocampus (Aggleton and Brown, 1999). Consistent with the lesion data, Fernandez *et al.* (1998) found, in a parametrically analyzed block design study, that activation in the posterior hippocampus correlated with the number of words presented in a given block that were subsequently recalled following a period of distraction.

Similarly, cued recall of paired associates requires relational processing beyond that necessary for familiarity judgments. Zeineh *et al.* (2003) found activation in subregions of the hippocampal formation during both encoding and cued recall of face – name associations. Meltzer and Constable (*submitted*) found that bilateral hippocampal activation was specifically enhanced during cued recall on trials in which a paired associate word was correctly recalled, compared to trials in which the subject was unable to recall the paired associate.

These fMRI studies demonstrate that, to the extent to which novelty, encoding success, and retrieval success effects can be considered as indicative of an underlying mnemonic process, effects in the hippocampal formation are specific to relational and episodic memory traces, whereas familiarity for single items are supported by an analogous process in extrahippocampal structures of the MTL. This distinction corresponds closely to the roles assigned to MTL structures by contemporary memory theorists on the basis of computational models and lesion data (Eichenbaum *et al.*, 1994; O'Reilly and Rudy, 2001; Tulving and Markowitsch, 1998). Furthermore, the hierarchical relationship between single-item and relational processing is entirely consistent with the anatomy of the medial temporal lobe, as extrahippocampal inputs converge in the hippocampus in a feedforward synaptic loop (Lavanex and Amaral, 2000). Thus, anatomical distribution of novelty and success-related activations within the MTL corresponds to the individual structures known to be necessary for item familiarity and episodic memory, and can be taken as additional support for the hypothesis that such effects reflect neural activity related to the encoding and retrieval of long-term memories.

## 14.10. SUMMARY

The search for selective activation in the medial temporal lobe began with the hypothesis, based on solid clinical and electrophysiological evidence, that neural activity in the MTL was related to the formation and recall of long-term memory traces. Cognitive tasks were designed to engage the theoretical processes of encoding and retrieval, with the expectation of producing signal increases relative to a resting baseline. Because such comparisons did not reveal selective activation in the MTL, experimental paradigms evolved to exploit an array of more subtle factors that do influence the amount of neural activity in the MTL under fairly constant task conditions. As a result, the cognitive neuroscience of memory is now faced with a complex pattern of results to evaluate, while the physiological reality of encoding and retrieval as independent processes specific to the MTL has not been proven. In particular, novelty and subsequent memory effects display a number of common characteristics, including two different anatomical distributions: lateralization effects related to verbalizability, and a hierarchical organization of sensitivity, to single-item familiarity and to associative links, in different substructures of the MTL. The fact that task-induced retrieval of recent memory traces induces activations with similar distributional characteristics suggests that both encoding and retrieval might be results of activity in the same distributed neural circuits.

Although the hippocampus and surrounding structures are undoubtedly essential for the encoding and retrieval of memories, it has been quite surprising that neuroimaging studies have highlighted its role in these functions only indirectly. The fact that comparisons between different cognitive tasks seldom elicit differential activation of the MTL, whereas incidental factors unrelated to deliberate effort often do, indicates that the reality of encoding and retrieval as independent cognitive processes is still uncertain. It is possible that the MTL is engaged in performing its memory-related functions at all times, and that the neural activity accomplishing these functions is not isolable through subtractions of different tasks. While mnemonic functions may be modulated by attention, emotion, and other factors, it is clear that the hierarchical design of cognitive tasks is not an effective means of modulating medial temporal activation levels. This situation is in contrast to neocortical higher-order association areas (including the prefrontal cortex), which typically do respond robustly to such experimental design paradigms, and also to primary sensory areas, which tend to respond to sensory stimulation regardless of cognitive task demands. These differences demonstrate that it is impossible to isolate the functions of all brain areas solely through the manipulation of performance demands. In the MTL, the existence of a physiological process for memory encoding and retrieval can only be inferred indirectly from a pattern of incidental factors, none of which seem to relate to deliberate conscious processing. This pattern constitutes a new framework within which future studies will attempt to elucidate the nature of the MTL's unique contributions to human memory.

## REFERENCES

Aggleton, J.P., and Brown, M.W. 1999. Episodic memory, amnesia, and the hippocampal–anterior thalamic axis. *Behav Brain Sci* **22**: 425–444; discussion 444–489.

Amaral, D.G. 1999. Introduction: what is where in the medial temporal lobe? *Hippocampus* **9**: 1–6.

Baddeley, A.D., Kopelman, M.D., and Wilson, B.A. 2002. *The Handbook of Memory Disorders*. John Wiley and Sons, Inc., Hoboken, NJ.

Barnes, C.A., McNaughton, B.L., Mizumori, S.J., Leonard, B.W., and Lin, L.H. 1990. Comparison of spatial and temporal characteristics of neuronal activity in sequential stages of hippocampal processing. *Prog Brain Res* **83**: 287–300.

Brewer, J.B., Zhao, Z., Desmond, J.E., Glover, G.H., and Gabrieli, J.D. 1998. Making memories: brain activity that predicts how well visual experience will be remembered. *Science* **281**: 1185–1187.

Brown, A.S. 2002. Consolidation theory and retrograde amnesia in humans. *Psychon Bull Rev* **9**: 403–425.

Brown, M.W., and Aggleton, J.P. 2001. Recognition memory: what are the roles of the perirhinal cortex and hippocampus? *Nat Rev Neurosci* **2**: 51–61.

Buckner, R.L., Koutstaal, W., Schacter, D.L., Dale, A.M., Rotte, M., and Rosen, B.R. 1998a. Functional-anatomic study of episodic retrieval. II. Selective averaging of event-related fMRI trials to test the retrieval success hypothesis. *Neuroimage* **7**: 163–175.

Buckner, R.L., Koutstaal, W., Schacter, D.L., Wagner, A.D., and Rosen, B.R. 1998b. Functional-anatomic study of episodic retrieval using fMRI. I. Retrieval effort versus retrieval success. *Neuroimage* **7**: 151–162.

Buckner, R.L., Petersen, S.E., Ojemann, J.G., Miezin, F.M., Squire, L.R., and Raichle, M.E. 1995. Functional anatomical studies of explicit and implicit memory retrieval tasks. *J Neurosci* **15**: 12–29.

Buckner, R.L., Wheeler, M.E., and Sheridan, M.A. 2001. Encoding processes during retrieval tasks. *J Cogn Neurosci* **13**: 406–415.

Cabeza, R., and Nyberg, L. 2000. Imaging cognition II: An empirical review of 275 PET and fMRI studies. *J Cogn Neurosci* **12**: 1–47.

Cheng, K., Waggoner, R.A., and Tanaka, K. 2001. Human ocular dominance columns as revealed by high-field functional magnetic resonance imaging. *Neuron* **32**: 359–374.

Cohen, N.J., Ryan, J., Hunt, C., Romine, L., Wszalek, T., and Nash, C. 1999. Hippocampal system and declarative (relational) memory: summarizing the data from functional neuroimaging studies. *Hippocampus* **9**: 83–98.

Constable, R.T., Carpentier, A., Pugh, K., Westerveld, M., Oszunar, Y., and Spencer, D.D. 2000. Investigation of the human hippocampal formation using a randomized event-related paradigm and Z-shimmed functional MRI. *Neuroimage* **12**: 55–62.

Courtney, S.M., Petit, L., Haxby, J.V., and Ungerleider, L.G. 1998. The role of prefrontal cortex in working memory: examining the contents of consciousness. *Philos Trans R Soc London, Ser B Biol Sci* **353**: 1819–1828.

Craik, F.I. 2002. Levels of processing: past, present, and future? *Memory* **10**: 305–318.

Davachi, L., Mitchell, J.P., and Wagner, A.D. 2003. Multiple routes to memory: distinct medial temporal lobe processes build item and source memories. *Proc Natl Acad Sci U S A* **100**: 2157–2162.

Davachi, L., and Wagner, A.D. 2002. Hippocampal contributions to episodic encoding: insights from relational and item-based learning. *J Neurophysiol* **88**: 982–990.

Deacon, T.W. 1997. *The Symbolic Species*. W.W. Norton, London.

Desgranges, B., Baron, J.C., and Eustache, F. 1998. The functional neuroanatomy of episodic memory: the role of the frontal lobes, the hippocampal formation, and other areas. *Neuroimage* **8**: 198–213.

Doyon, J., Penhune, V., and Ungerleider, L.G. 2003. Distinct contribution of the cortico-striatal and cortico-cerebellar systems to motor skill learning. *Neuropsychologia* **41**: 252–262.

Duvernoy, H.M. 1998. *The Human Hippocampus*. Springer, Berlin.

Eichenbaum, H. 2001. The hippocampus and declarative memory: cognitive mechanisms and neural codes. *Behav Brain Res* **127**: 199–207.

Eichenbaum, H., Otto, T., Cohen, N.J. 1994. Two functional components of the hippocampal memory system. *Behav Brain Sci* **17**: 449–518.

Eldridge, L.L., Knowlton, B.J., Furmanski, C.S., Bookheimer, S.Y., and Engel, S.A. 2000. Remembering episodes: a selective role for the hippocampus during retrieval. *Nat Neurosci* **3**: 1149–1152.

Fernandez, G., Weyerts, H., Schrader-Bolsche, M., Tendolkar, I., Smid, H.G., Tempelmann, C., Hinrichs, H., Scheich, H., Elger, C.E., Mangun, G.R., *et al.* 1998. Successful verbal encoding into episodic memory engages the posterior hippocampus: a parametrically analyzed functional magnetic resonance imaging study. *J Neurosci* **18**: 1841–1847.

Fodor, J.A. 1983. *Modularity of Mind*. MIT Press, Cambridge, MA.

Friedman, D., and Sutton, S. 1987. Event-related potentials during continuous recognition memory. *Electroencephalogr Clin Neurophysiol Suppl* **40**: 316–321.

Gabrieli, J.D. 1998. Cognitive neuroscience of human memory. *Annu Rev Psychol* **49**: 87–115.

Gabrieli, J.D., Brewer, J.B., Desmond, J.E., and Glover, G.H. 1997. Separate neural bases of two fundamental memory processes in the human medial temporal lobe. *Science* **276**: 264–266.

Gazzaniga, M.S. 1999. *The New Cognitive Neurosciences*. MIT Press, Cambridge, MA.

Gluck, M.A., and Meyers, C.E. 2001. *Gateway to Memory*. MIT Press, Cambridge, MA.

Golby, A.J., Poldrack, R.A., Brewer, J.B., Spencer, D., Desmond, J.E., Aron, A.P., and Gabrieli, J.D. 2001. Material-specific lateralization in the medial temporal lobe and prefrontal cortex during memory encoding. *Brain* **124**: 1841–1854.

Golby, A.J., Poldrack, R.A., Illes, J., Chen, D., Desmond, J.E., and Gabrieli, J.D. 2002. Memory lateralization in medial temporal lobe epilepsy assessed by functional MRI. *Epilepsia* **43**: 855–863.

Haxby, J.V., Ungerleider, L.G., Horwitz, B., Maisog, J.M., Rapoport, S.I., and Grady, C.L. 1996. Face encoding and recognition in the human brain. *Proc Natl Acad Sci U S A* **93**: 922–927.

Henke, K., Buck, A., Weber, B., and Wieser, H.G. 1997. Human hippocampus establishes associations in memory. *Hippocampus* **7**: 249–256.

Hyder, F., Rothman, D.L., and Shulman, R.G. 2002. Total neuroenergetics support localized brain activity: implications for the interpretation of fMRI. *Proc Natl Acad Sci U S A* **99**: 10771–10776.

Kandel, E.R. 2001. The molecular biology of memory storage: a dialogue between genes and synapses. *Science* **294**: 1030–1038.

Kandel, E.R., Schwartz, J.H., and Jessell, T.M. 2000. *Principles of Neural Science*. McGraw-Hill, New York.

Kelley, W.M., Miezin, F.M., McDermott, K.B., Buckner, R.L., Raichle, M.E., Cohen, N.J., Ollinger, J.M., Akbudak, E., Conturo, T.E., Snyder, A.Z., et al. 1998. Hemispheric specialization in human dorsal frontal cortex and medial temporal lobe for verbal and nonverbal memory encoding. *Neuron* **20**: 927–936.

Kirchhoff, B.A., Wagner, A.D., Maril, A., and Stern, C.E. 2000. Prefrontal-temporal circuitry for episodic encoding and subsequent memory. *J Neurosci* **20**: 6173–6180.

Knowlton, B.J., Squire, L.R., and Gluck, M.A. 1994. Probabilistic classification learning in amnesia. *Learn Mem* **1**: 106–120.

Lavenex, P., and Amaral, D.G. 2000. Hippocampal-neocortical interaction: a hierarchy of associativity. *Hippocampus* **10**: 420–430.

Lee, A.C., Robbins, T.W., and Owen, A.M. 2000. Episodic memory meets working memory in the frontal lobe: functional neuroimaging studies of encoding and retrieval. *Crit Rev Neurobiol* **14**: 165–197.

Maguire, E.A., Frackowiak, R.S., and Frith, C.D. 1996. Learning to find your way: a role for the human hippocampal formation. *Proc R Soc London, Ser B Biol Sci* **263**: 1745–1750.

Maguire, E.A., Mummery, C.J., and Buchel, C. 2000. Patterns of hippocampal-cortical interaction dissociate temporal lobe memory subsystems. *Hippocampus* **10**: 475–482.

Martin, A. 1999. Automatic activation of the medial temporal lobe during encoding: lateralized influences of meaning and novelty. *Hippocampus* **9**: 62–70.

Martin, A., Wiggs, C.L., and Weisberg, J. 1997. Modulation of human medial temporal lobe activity by form, meaning, and experience. *Hippocampus* **7**: 587–593.

Mayes, A.R., and Montaldi, D. 2001. Exploring the neural bases of episodic and semantic memory: the role of structural and functional neuroimaging. *Neurosci Biobehav Rev* **25**: 555–573.

McClelland, J.L., McNaughton, B.L., and O'Reilly, R.C. 1995. Why there are complementary learning systems in the hippocampus and neocortex: insights from the successes and failures of connectionist models of learning and memory. *Psychol Rev* **102**: 419–457.

Meltzer, J.A. and Constable, R.T. Activation of human hippocampal formation reflects success in both encoding and cued recall of paired associates. *Submitted*.

Miller, E.K., and Cohen, J.D. 2001. An integrative theory of prefrontal cortex function. *Annu Rev Neurosci* **24**: 167–202.

Musen, G., and Treisman, A. 1990. Implicit and explicit memory for visual patterns. *J Exp Psychol Learn Mem Cogn* **16**: 127–137.

Nyberg, L., McIntosh, A.R., Houle, S., Nilsson, L.G., and Tulving, E. 1996. Activation of medial temporal structures during episodic memory retrieval. *Nature* **380**: 715–717.

O'Reilly, R.C., and Norman, K.A. 2002. Hippocampal and neocortical contributions to memory: advances in the complementary learning systems framework. *Trends Cogn Sci* **6**: 505–510.

O'Reilly, R.C., and Rudy, J.W. 2001. Conjunctive representations in learning and memory: principles of cortical and hippocampal function. *Psychol Rev* **108**: 311–345.

Otten, L.J., Henson, R.N., and Rugg, M.D. 2001. Depth of processing effects on neural correlates of memory encoding: relationship between findings from across- and within-task comparisons. *Brain* **124**: 399–412.

Otten, L.J., and Rugg, M.D. 2001a. Electrophysiological correlates of memory encoding are task-dependent. *Brain Res Cogn Brain Res* **12**: 11–18.

Otten, L.J., and Rugg, M.D. 2001b. Task-dependency of the neural correlates of episodic encoding as measured by fMRI. *Cereb Cortex* **11**: 1150–1160.

Poeppel, D. 1996. A critical review of PET studies of phonological processing. *Brain Lang* **55**: 317–351; discussion 352–385.

Poldrack, R.A., Clark, J., Pare-Blagoev, E.J., Shohamy, D., Crespo Moyano, J., Myers, C., and Gluck, M.A. 2001. Interactive memory systems in the human brain. *Nature* **414**: 546–550.

Poldrack, R.A., Prabhakaran, V., Seger, C.A., and Gabrieli, J.D. 1999. Striatal activation during acquisition of a cognitive skill. *Neuropsychology* **13**: 564–574.

Reber, P.J., Siwiec, R.M., Gitelman, D.R., Parrish, T.B., Mesulam, M.M., Paller, K.A., and Gittleman, D.R. 2002a. Neural correlates of successful encoding identified using functional magnetic resonance imaging. *J Neurosci* **22**: 9541–9548.

Reber, P.J., Wong, E.C., and Buxton, R.B. 2002b. Encoding activity in the medial temporal lobe examined with anatomically constrained fMRI analysis. *Hippocampus* **12**: 363–376.

Rempel-Clower, N.L., Zola, S.M., Squire, L.R., and Amaral, D.G. 1996. Three cases of enduring memory impairment after bilateral damage limited to the hippocampal formation. *J Neurosci* **16**: 5233–5255.

Rudy, J.W., and Sutherland, R.J. 1989. The hippocampal formation is necessary for rats to learn and remember configural discriminations. *Behav Brain Res* **34**: 97–109.

Rugg, M.D., and Coles, M.G.H. 1995. *Electrophysiology of Mind: Event-related Brain Potentials and Cognition*. Oxford University Press, Oxford.

Rugg, M.D., Otten, L.J., and Henson, R.N. 2002. The neural basis of episodic memory: evidence from functional neuroimaging. *Philos Trans R Soc London, Ser B Biol Sci* **357**: 1097–1110.

Rugg, M.D., and Yonelinas, A.P. 2003. Human recognition memory: a cognitive neuroscience perspective. *Trends Cogn Sci* **7**: 313–319.

Schacter, D.L., and Buckner, R.L. 1998. On the relations among priming, conscious recollection, and intentional retrieval: evidence from neuroimaging research. *Neurobiol Learn Mem* **70**: 284–303.

Schmidtke, K., Manner, H., Kaufmann, R., and Schmolck, H. 2002. Cognitive procedural learning in patients with fronto-striatal lesions. *Learn Mem* **9**: 419–429.

Shallice, T., Fletcher, P., Frith, C.D., Grasby, P., Frackowiak, R.S., and Dolan, R.J. 1994. Brain regions associated with acquisition and retrieval of verbal episodic memory. *Nature* **368**: 633–635.

Shen, B., and McNaughton, B.L. 1996. Modeling the spontaneous reactivation of experience-specific hippocampal cell assemblies during sleep. *Hippocampus* **6**: 685–692.

Shepherd, G.M. 1997. *The Synaptic Organization of the Brain*. Oxford University Press, Oxford.

Shimamura, A.P. 1995. Memory and the prefrontal cortex. *Ann N Y Acad Sci* **769**: 151–159.

Shulman, R.G. 1996. Interview with Robert G. Shulman. *J Cogn Neurosci* **8**: 474–477.

Shulman, R.G., Hyder, F., and Rothman, D.L. 2002. Biophysical basis of brain activity: implications for neuroimaging. *Q Rev Biophys* **35**: 287–325.

Soltani, M., and Knight, R.T. 2000. Neural origins of the P300. *Crit Rev Neurobiol* **14**: 199–224.

Sperling, R.A., Bates, J.F., Cocchiarella, A.J., Schacter, D.L., Rosen, B.R., and Albert, M.S. 2001. Encoding novel face-name associations: a functional MRI study. *Hum Brain Mapp* **14**: 129–139.

Squire, L.R. 1992. Memory and the hippocampus: a synthesis from findings with rats, monkeys, and humans. *Psychol Rev* **99**: 195–231.

Squire, L.R. 2000. *Memory: From Mind to Molecules*. W.H. Freeman, New York.

Stark, C.E., and Squire, L.R. 2000. Functional magnetic resonance imaging (fMRI) activity in the hippocampal region during recognition memory. *J Neurosci* **20**: 7776–7781.

Stark, C.E., and Squire, L.R. 2001. When zero is not zero: the problem of ambiguous baseline conditions in fMRI. *Proc Natl Acad Sci U S A* **98**: 12760–12766.

Stern, C.E., Corkin, S., Gonzalez, R.G., Guimaraes, A.R., Baker, J.R., Jennings, P.J., Carr, C.A., Sugiura, R.M., Vedantham, V., and Rosen, B.R. 1996. The hippocampal formation participates in novel picture encoding: evidence from functional magnetic resonance imaging. *Proc Natl Acad Sci U S A* **93**: 8660–8665.

Tulving, E., and Markowitsch, H.J. 1998. Episodic and declarative memory: role of the hippocampus. *Hippocampus* **8**: 198–204.

Ungerleider, L.G., and Haxby, J.V. 1994. ‘What’ and ‘where’ in the human brain. *Curr Opin Neurobiol* **4**: 157–165.

Vakil, E., and Herishanu-Naaman, S. 1998. Declarative and procedural learning in Parkinson’s disease patients having tremor or bradykinesia as the predominant symptom. *Cortex* **34**: 611–620.

Van Petten, C., and Senkfor, A.J. 1996. Memory for words and novel visual patterns: repetition, recognition, and encoding effects in the event-related brain potential. *Psychophysiology* **33**: 491–506.

Wagner, A.D., Koutstaal, W., and Schacter, D.L. 1999. When encoding yields remembering: insights from event-related neuroimaging. *Philos Trans R Soc London, Ser B Biol Sci* **354**: 1307–1324.

Wagner, A.D., Schacter, D.L., Rotte, M., Koutstaal, W., Maril, A., Dale, A.M., Rosen, B.R., and Buckner, R.L. 1998. Building memories: remembering and forgetting of verbal experiences as predicted by brain activity. *Science* **281**: 1188–1191.

Warnking, J., Dojat, M., Guerin-Dugue, A., Delon-Martin, C., Olympieff, S., Richard, N., Chehikian, A., and Segebarth, C. 2002. fMRI retinotopic mapping – step by step. *Neuroimage* **17**: 1665–1683.

Wiggs, C.L., Weisberg, J., and Martin, A. 1999. Neural correlates of semantic and episodic memory retrieval. *Neuropsychologia* **37**: 103–118.

Yamashita, H. 1993. Perceptual-motor learning in amnesic patients with medial temporal lobe lesions. *Percept Mot Skills* **77**: 1311–1314.

Yancey, S.W., and Phelps, E.A. 2001. Functional neuroimaging and episodic memory: a perspective. *J Clin Exp Neuropsychol* **23**: 32–48.

Zeineh, M.M., Engel, S.A., Thompson, P.M., and Bookheimer, S.Y. 2001. Unfolding the human hippocampus with high resolution structural and functional MRI. *Anat Rec* **265**: 111–120.

Zeineh, M.M., Engel, S.A., Thompson, P.M., and Bookheimer, S.Y. 2003. Dynamics of the hippocampus during encoding and retrieval of face-name pairs. *Science* **299**: 577–580.

Zola-Morgan, S., Squire, L.R., and Amaral, D.G. 1986. Human amnesia and the medial temporal region: enduring memory impairment following a bilateral lesion limited to field CA1 of the hippocampus. *J Neurosci* **6**: 2950–2967.

Zola-Morgan, S., Squire, L.R., and Ramus, S.J. 1994. Severity of memory impairment in monkeys as a function of locus and extent of damage within the medial temporal lobe memory system. *Hippocampus* **4**: 483–495.



# 15

## Using fMRI to Study the Mind and Brain

**Bruce E. Wexler**

*Department of Psychiatry, Yale University School of Medicine, MR Center, P.O. Box 208068, New Haven, CT 06520-8068, USA*

---

15.1	Studies Assuming Localized and (often) Fixed Relationships between Cognitive and Brain Functions	280
15.1.1	Examples	280
15.1.2	Problems	281
15.2	Studies of Changing Relationships between Brain Function and Cognition	286
15.2.1	Changes in Activation with Task Repetition and Learning	286
15.2.2	Changes in Activation with Age	288
15.2.3	Changes in Activation with Changes in Physiological State	289
15.2.4	Effects of Shifting Attention on Activation	290
15.2.5	Impact of Brain Injury or Disease on Functional Activation	291
15.3	Summary	292

---

In science our theories constrain both the way we conceive and the way we interpret experiments. The more limited our understanding of a field of inquiry, the greater the gap between theory and reality, the more limiting are these constraints. Consequently, theories about how the brain works, even nascent and implicit, have major effects on how we design and interpret brain-imaging experiments.

Brain-imaging research is immersed in the confusion of the mind–brain conundrum. Mind and brain are generally considered two sides of the same coin; moreover, we think, with some justification, that we are chipping away at the mind–brain problem with each experiment. A major difficulty, however, is that there is no well-developed solution to the problem. Research often slips back and forth between mind and brain perspectives and loses focus on the question being addressed. Not infrequently we pose experimental

questions in psychological terms, collect and present data in brain terms, and do little more than wave hands when discussing what the experiment had to say about the initial questions.

These are very difficult problems. In this chapter, I will discuss them in the context provided by the intersection of two theoretical dimensions: (1) localizationist versus distributed models of brain function, and (2) fixed versus changing relationships between brain structure and function. Localizationist models equate specific cognitive functions with specific brain locations; a particular cognitive operation is carried out by brain tissue at a particular location, and the functional property of that brain tissue is that particular cognitive operation. Distributed models, in contrast, postulate that even basic cognitive operations emerge from the integrated action of brain tissue at several locations, and that the functional properties of specific brain regions cannot be characterized as a cognitive operation.

Models with fixed relationships between brain structure and function assume that a particular cognitive operation is carried out by the brain in the same way at all times. Models with changing relationships between structure and function assume that a particular cognitive operation may be carried out by the brain in a different location, or by a different collection of regional activations, at different times. The time scale may be anywhere from seconds to years. The nature of the assumed relationship between structure and function in localizationist models often also leads to the assumption that the relationship between structure and cognitive function is fixed or constant across time. I will provide examples of studies based on these different theoretical assumptions, and discuss some of their relative strengths and weaknesses.

## **15.1. STUDIES ASSUMING LOCALIZED AND (OFTEN) FIXED RELATIONSHIPS BETWEEN COGNITIVE AND BRAIN FUNCTIONS**

The great majority of early functional imaging studies, both with PET and with fMRI, were of this type, and essentially all established imaging programs include a number of such studies in their portfolios. These 'where is it done' studies are the easiest to conceive and analyze. It can be argued with some justification that results of those studies provide a skeleton of cerebral functional organization upon which to hang the complexities of inter- and intra-personal variability. However, problems with this approach are significant enough to raise the possibility that they are fundamentally misleading.

### **15.1.1. Examples**

In their 1988 *Science* paper 'Localization of cognitive operations in the human brain', Posner *et al.* (1988) articulated a guiding rationale for studies of fixed, localized aspects of brain function, and described the 'subtraction' method central to their design. As they state, 'The hypothesis is that elementary operations forming the basis of cognitive analysis of human tasks are strictly localized.' They described earlier experiments in which subjects were asked to determine whether two uppercase (AA) letters were the same, whether an upper and a lower case letter (Aa) were the same, or whether two letters belonged to the same category (Ac). The dependent measure, reaction time, increased during this task progression. They suggested that the differences in reaction times indicated that different cognitive operations were involved in each task variant, and that each operation is related to a *separate* neural system. In their studies of language operations, they constructed a series of progressively more complex activation tasks. Each task served as a 'control' for the next more complex task. Activations associated with the 'control' task were subtracted from activations associated with the more complex task in order to identify the brain regions associated with the cognitive operations present only in the more complex task. For example, activations associated with viewing a simple fixation cross were subtracted from activations associated with passively viewing a series of words. All areas showing significantly greater activity during word viewing were in the occipital lobe. The authors 'conclude that visual word forms are developed in the occipital lobe'. They suggested

that particular areas are specific to visual words since they are activated neither by auditory words nor visual checkerboards nor dot patterns. They next subtracted the activations associated with passive viewing of words from those seen when subjects are asked to mentally note the names of dangerous animals in the series of visual words. Two areas survived this subtraction, one in the anterior left frontal lobe and one in the anterior cingulate gyrus. Based on results of other studies, the authors concluded that the left frontal activation is 'specific to semantic language tasks' while the cingulate activation is 'identified' with attention.

Multiple studies, including many from our imaging center at Yale also fall into the category of assuming localized relationships between cognitive and brain function. In one, activations in English-only speaking subjects listening to sentences spoken in Turkish were subtracted from activations in the same subjects listening to the same sentences spoken by the same speaker in English (Schlosser *et al.*, 1998). Activations related to listening to the English but not the Turkish sentences were found in the left posterior temporal and the left inferior frontal lobes. The authors 'conclude that the activation pattern evoked by the English sentences reflects auditory comprehension.' They note that another study found much more extensive activations associated with an auditory semantic judgment task when a baseline without auditory stimulation was used for subtraction, but 'assert that the more local focal activations in the present study likely reflect the isolation of language comprehension from lower-level auditory processing.' Other studies have compared: object and spatial memory tasks to each other and to perceptual tasks in order to identify specific areas associated with specific types of memory (McCarthy *et al.*, 1996); orthographic, rhyming, and semantic matching tasks to identify regions associated with specific components of reading (Pugh *et al.*, 1997); and re-reading and immediately recalling of words to identify regions associated with component stages of working memory (Raye *et al.*, 2002). There are probably over a thousand reports in the literature of studies conceived and interpreted in this manner.

## 15.1.2. Problems

### 15.1.2.1. *Thresholds for significance*

The problem here is that there is no agreed-upon, and probably no fully satisfactory, way to select a probability threshold for statistical significance of differences between experimental and baseline conditions. At a scientific meeting 8 years ago, a group of Russian scientists complained to me that Americans used too restrictive thresholds, thereby creating a false sense of very few and highly localized activation differences between experimental and baseline conditions. If less restrictive thresholds are used, the same experimental conditions appear to be associated with more widely distributed activations of multiple brain areas. Shulman and colleagues have looked at this issue experimentally in high field imaging of rat olfactory cortex (Figure 15.1). If the significance threshold is held constant but the concentration of odorant is increased (columns 1–3), there is a progressive increase in areas activated. Thus there seems to be a widely distributed potential response system that becomes more activated as stimulus intensity increases. When the activation with the lowest level of odorant is evaluated at a more relaxed threshold (column 4), more areas appear activated and the expanded activation image matches that seen with the highest concentration of odorant at the more restrictive threshold. In other words, when the threshold is relaxed, the newly appreciated activations appear to be meaningful (signal) rather than artifactual (noise). The Russians may have had a point!

### 15.1.2.2. *Matching experimental and baseline tasks for difficulty and interest*

One of the most difficult problems in choosing experimental and baseline tasks for a subtraction paradigm is matching them for difficulty and interest. Both increased task difficulty and increased interest of a task can increase task-associated brain activation. Thus, an experimental task may generate greater brain

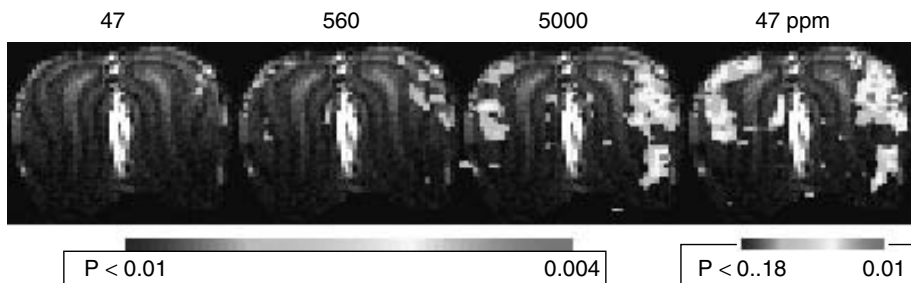


**Figure 15.1.** Evidence that activations evident at less restrictive thresholds are meaningful. The activation intensity increases with increasing odorant concentration (left three panels). However, when the pattern elicited at low concentration (left panel) is normalized to the pattern at high concentration by lowering the threshold for display, the topography of the patterns at different concentrations is similar (third and right panels). This suggests that the activations evident at the less restrictive thresholds (right panel) are meaningful and not noise.

activation than a baseline task because it is more interesting or more difficult rather than because of the differences between experimental and baseline tasks designated by the researchers. In the Posner *et al.* study, for example, monitoring a list of words for dangerous animals may be more difficult and more interesting than passive viewing of words, and passive viewing of words may be more interesting than looking at a fixation cross. Hence, the experiment might be exploring the brain activations associated more generally with 'interest'. McCarthy *et al.* have data on this issue. In an initial study, they reported memory-related activations in the middle frontal gyrus based on differences between their memory task and a perceptual baseline task (McCarthy *et al.*, 1994). In a subsequent study they found that a more difficult perceptual task produced a significantly smaller difference signal than the original perceptual task in this same region. By subtraction in the first study, the area was identified as a memory and not a perceptual area. However, in the second study, using a 'parametric' design (Friston *et al.*, 1996) the same area could be identified as showing activity related to the difficulty of perception without a memory component.

#### 15.1.2.3. Problems intrinsic to the subtraction concept itself

Vygotsky, writing in 1960, summarized and critiqued the subtraction design as it had been applied in experimental psychology with reaction time as the dependent measure (Vygotsky, 1978). In those experiments, the simplest baseline condition consisted of having the subject respond to the appearance of a single, repeating stimulus (simple recognition reaction time,  $R_S$ ). In the next more complex condition, subjects were required to discriminate between a specific target stimulus and other stimuli. Total reaction time ( $R_T$ ) was then assumed to reflect  $R_S + R_D$ , with  $R_D$  being the time required for discrimination. In some experiments, the situation was then further complicated by asking the subject to respond to stimulus A with their right hand and stimulus B with their left hand.  $R_T$  was then assumed to consist of  $R_S + R_D + R_C$ , with  $R_C$  being the time required to choose the correct movement. As Vygotsky summarized the idea, '...the discrimination response is a simple reaction plus discrimination; the choice reaction is a simple reaction plus discrimination plus choice. The higher, more complex response is seen as the arithmetic sum of its elementary components.' He cited studies that assumed that 'by subtracting the time needed to comprehend and name a word from the time needed to comprehend, translate a word into a different language, and name it, we can obtain a pure measure of the translation process. In short, even higher processes such as speech comprehension and production can be analyzed by these methods. A more mechanical notion of the complex, higher forms of behavior would be hard to imagine.... In our view, the basic premise

underlying this entire line of analysis is incorrect. It is not true that a complex reaction consists of a chain of separate processes which may be arbitrarily added and subtracted. Any such reaction reflects processes that depend upon the entire process of learning at every level of practice.'

Friston *et al.* (1996) offered a critique of cognitive subtraction designs in brain imaging conceptually similar to Vygotsky's, and followed with an empirical demonstration of its limitations. They write that the subtraction 'approach, predicated on a pure insertion, assumes that each cognitive component evokes an 'extra' physiological activation that is the same irrespective of the cognitive or physiological context.' They 'suggest that nonlinear systems like the brain do not behave in a fashion that is consistent with cognitive subtraction.' They argue that factorial designs that allow for interaction effects provide more appropriate conceptual and experimental approaches. In an experimental demonstration, Friston *et al.* evaluated activations apparently associated with object recognition by comparing cognitive subtraction and factorial approaches. They hypothesized that inferotemporal activation associated with object recognition would change as a function of whether or not phonological reference was also required. If so, assumptions of additive linearity and pure insertion would be violated. To test this, Friston *et al.* first created two different subtractions that should each isolate activity associated with object recognition. The first compared activation when subjects simply said yes when presented with any colored shape to activation when they said yes only when the colored shape was an object (e.g., a tree) rather than an abstract form; only the latter condition required object recognition. The second subtraction compared activation when subjects named the color of a presented shape to activation when they named a visually presented colored object. In this contrast both conditions required phonological retrieval but only the latter required object recognition. As hypothesized, inferotemporal activation associated with object recognition was very different in the two cognitive contexts; it was almost 10-fold higher in the presence of concurrent phonological retrieval. Friston and colleagues then applied a factorial analysis to the four experimental conditions. This analysis identified a robust area of interaction between object recognition and phonological retrieval in the inferotemporal cortex as well as in the angular gyrus. They conclude that 'pure insertion disallows any interactions and yet these interactions are evident, even in the simplest experiments.' Identification of the interactions still derives from a subtraction process, but by comparing incremental changes in activity across regions and conditions it identifies changing interactive processes among neural and cognitive processes (see discussion below of studies of aspects of brain structure–function relationships.) It may be tempting to interpret the main effect of object recognition and phonological retrieval that are also identified in the factorial analyses as primary locations of these functions (i.e., areas active in association with these cognitive functions in both experimental contexts), but the general difficulty of assigning meaning to main effects in the presence of significant interactions certainly applies here as well as in other types of research. At the least, it would require creating a large number of cognitive contexts in which to embed a particular function, i.e., many factors, to feel confident of the stability of the main effect.

Finally, Shulman and colleagues have done a series of MRS, fMRI and single-cell electrical recordings which together make a powerful argument for the functional importance of what is subtracted away in subtraction paradigms, even for the specific cognitive activity putatively isolated by the subtraction. By quantitatively measuring rates of metabolism of glutamate to glutamine and rates of glucose oxidation, they determined that close to 75 % of brain energy consumption supports neurotransmission (see Chapter 5). By relating BOLD-derived changes in cerebral oxygen consumption to changes in electrical physiological measures of neuronal spiking, they demonstrated a stoichiometric relationship between the two that was in close agreement with the measured relationship between glutamate metabolism and glucose oxidation. Conservatively, they estimate that 75 % of brain oxygen metabolism is associated with neural activity. The problem this creates for the subtraction paradigm is that differences in the fMRI BOLD signal between the baseline and cognitive tasks are typically only a few percent of the energy. Since 75 % of brain oxygen consumption is linked to neuronal activity, this difference in bold signal represents a difference in neuronal

activity only on the scale of approximately 2 %. If we march around the brain associating different cognitive operations each with 2 % of neuronal activity at different brain locations, what are we going to do with the unassigned majority of activity? And how are we going to study it with a paradigm that eliminates it? In accord with the experimental results described in the other chapters on brain activity, we argue that a 2 % increase in neuronal activity in an area is a marker that that area is associated in some way with the added task activity. However, the idea that absence of a small activity increase in an area means that it is not involved in the task is immediately problematic. This idea has no more a priori validity than saying that if a Beethoven symphony calls for 100 instruments, and a Brahms symphony those same 100 and three more, then the difference between the Brahms and the Beethoven is located exclusively in those three added instruments.

Hyder *et al.* (Chapter 10) have also demonstrated experimentally that the large amount of neuronal activity eliminated by subtraction procedures is essential for task performance, at least for the particular case they studied of anesthetized rats. They measured oxygen consumption and neuronal firing in the somatosensory area during forepaw stimulation of rats under varying depths of anesthesia. They reasoned that if, as the subtraction paradigms suggest, increments in oxygen consumption and neuronal firing are sufficient to support the somatosensory processing, then incremental changes following stimulation should be the same regardless of the depth of anesthesia. They found instead that both oxygen consumption and neuronal firing reached approximately the same total level during stimulation no matter how deep the anesthesia and how low the baseline metabolic and firing rates. When the baseline starting point was lower, the task-related increments were greater. Rather than finding fixed increments across anesthesia levels, they found fixed activity end points reached by increments that were greater with lower baseline states. Apparently, then, most or all activity in the region is necessary to support the somatosensory processing. This fact underlines the problems for the subtraction paradigm that arose from the earlier work on brain energetics by Shulman *et al.* First, if most or all of the neuronal activity in a region is needed when that region is functionally active, how can it be adequately studied if the experimental design subtracts away 95 % of the activity? It is a bit like trying to learn about dogs by looking only at how their tails wag. Second, if functional engagement of a brain region involves activity of all or most of the neurons in the region, how can we be at all confident that if a region is only 97 % active (i.e., fails to show a 3 % increase in activity) it is not engaged by the task?

#### *15.1.2.4. What is localized, anyway?*

Perhaps the most fundamental question to be asked about localizationist models and studies is ‘what is localized?’. One way to appreciate this question is to do a computer literature search of functional imaging papers sorted by a particular brain region. Most research reports are organized around the activation task rather than the brain region or regions activated, as evidenced for example in paper titles (e.g., ‘fMRI study of working memory’). In discussing their findings, most researchers compare their results with those of other studies using similar or related activation tasks. This can create the impression that the areas activated are associated primarily with the particular activation task and others very similar to it. If, however, the literature is searched by brain region, it is quickly apparent that individual regions (albeit coarsely defined) are associated with a quite wide-ranging collection of functions. The facts that researchers tend to sort themselves into groups based on type of activation task rather than particular brain regions, and tend not to discuss the work of other groups using different types of activation tasks, contribute further to the sense that regions are specialized for cognitive tasks.

A.R. Luria drew two general conclusions from examination of soldiers with localized brain injuries incurred during World Wars I and II (Luria, 1973). First, even highly localized lesions affect many different behaviors and functions, thus seeming to ‘locate’ multiple functions in the same area. Second, lesions in different places interfere with the same apparent behavior or function, seeming to ‘locate’ the same behavior

in multiple areas. Luria concluded that cognitive functions result from the integrated action of multiple brain areas. The defining characteristic of those 'cerebral functional systems' was production of an invariant outcome by variable means. Moreover, not only were behaviors as simple as breathing or as complex as memory not located in a single region, the distributed network of regions that generated the behavior varied from time to time. This was not as holistic a view as offered by Lashley, because only some regions were potentially involved in any given task, and whereas a specific region could contribute to multiple functions, it would not contribute to all functions. However, if we accept Luria's view, the types of cognitive function often studied with brain imaging are not located in a specific region, and cannot even be said to be located in a specific set of regions, since the regions that come together to create the function change from time to time. Friston and colleagues suggested a similar view: 'Cognitive processes themselves may only express themselves at the level of interaction.' In both these views, the cognitive function is an emergent property of the interaction among multiple brain regions, and does not reside in any one.

These views, then, argue that functions like those often studied with brain imaging methods are not localized in specific areas of the brain. This does not imply that all brain areas are functionally equivalent. It says only that their functional differences do not correspond to specific cognitive functions. The question of how to characterize the functional characteristics of specific brain regions, the question of what is localized, remains open. Patricia Churchland develops this openness more fully in *Neurophilosophy* (Churchland, 1986). She suggests that new knowledge about the functional organization of the brain may lead to new ways to think about psychological operations. The current concepts of psychology, she argues, may eventually be seen as a 'folk psychology' and replaced by a true neuropsychology. The same argument can be made in regard to cognitive psychology, since despite its laboratory rigor it has little more of a neurological base than do the psychological concepts Churchland critiques. From this position, starting with concepts of cognitive psychology may be a misleading way to approach the task of studying brain organization and function, since there is little reason to believe that component cognitive processes as we have defined them are homologous to component brain processes.

In a 1985 article I discussed these issues by comparison of pictographic and alphabetic systems of writing (Wexler, 1986). In pictographic writing, each symbol represents a single thing, action, or idea. A thousand pictographs are needed to represent a thousand things, actions, or ideas. In an alphabetic language, individual symbols or letters do not have representational value; it is combinations of letters that represent things, actions, or ideas. Webster's Dictionary has over 460 000 entries based on the 26 letters of the Roman alphabet! Words, the functional units of alphabetic languages, emerge from the combination of letters. This creates much greater functional capacity than is possible with a pictographic language. The functional organization of the brain, I suggested, is more like an alphabetic than a pictographic language; functionally differentiated regions serve as letters in a neuropsychological alphabet, and represent cognitive functions in combination but not in isolation. A cognitive localizationist view of brain function, on the other hand, is more like a pictographic language. The task, in order to move beyond the localizationist view that equates specific brain regions with specific cognitive operations, is to discover the letters of the brain's alphabet and how they are combined into words and sentences that correspond to recognizable components of cognition. The analogy breaks down, however, and the complexity of the conceptual challenge increases, when we appreciate that the letters or components themselves can change when in combination and that the processes of combination can be nonlinear.

## 15.2. STUDIES OF CHANGING RELATIONSHIPS BETWEEN BRAIN FUNCTION AND COGNITION

The limitations of simple subtraction/localizationist experiments have been increasingly appreciated by the imaging community, and newer approaches have focused on changing and distributed aspects of the

relationship between brain function and cognition. Changes with time in the relationship between brain function and cognition have been studied with a variety of approaches. Studies have compared regional activation associated with the same experimental task when the task is simply repeated, when the subject is in different baseline physiological states, after practice and learning, in young and old subjects, and in people with and without the effects of neurologic illness or injury. Others have looked at the effects of other cognitive activity, preceding or concurrent with the index task, on activity associated with the index task. A third set of studies has demonstrated changes in activity as a function of the direction of attention. I will describe examples of studies focusing on each of these types of changes in the brain activation correlates of cognitive activity, and discuss what types of things we can learn and have learned from them about distributed as well as changing aspects of the relationship between cognitive activity and brain function. I will conclude by considering which of the problems identified in reference to static localizationist studies are also problematic in these studies.

### **15.2.1. Changes in Activation with Task Repetition and Learning**

In the most basic of these studies, subjects did the same simple repetitive motor movements during multiple imaging sessions. In one, the same subject was imaged on nine occasions over six weeks while tapping with his right index finger (Wexler *et al.*, 1997). A device constructed for the study ensured that the force and range of motion were constant throughout. The rate of tapping was paced by an auditory signal and confirmed by observation. A highly similar area of the left sensorimotor cortex was activated in all sessions. What was of interest was that on one occasion, but not others, activation was also evident in the supplementary motor area at an intensity comparable to that in the sensorimotor cortex, and on another day activity of similar intensity was evident in parietal cortex. Activity in all these areas was evident during more complex motor tasks such as tapping according to a patterned sequence of different finger movements, indicating that they are part of a distributed motor system. Even such a basic task as single finger tapping may be associated with different activation patterns in the same individual on different occasions. A second, similar study, looked at activation associated with opening and closing of the fist paced at 1 Hz by an auditory cue, in a group of 12 subjects scanned in an initial session and then in two follow-up sessions, one 5 h later and another 49 days later (Loubinoux *et al.*, 2001). When this simple task was repeated after 5 h, task-related activation was greater in the contralateral premotor cortex and in a small area of the cerebellar cortex, and lesser in the contralateral sensorimotor and supplementary motor areas, and the parietal cortex and posterior cingulate. Most of these changes were diminished at 49 day follow-up. In the contralateral sensorimotor area, for example, the area of activation was reduced nearly 20 % at 5 h retest and actually was greater than the original response at 49 day follow-up. So here again we see multiple distributed and significant changes in task-related activation when a very simple motor task is performed a second time 5 h after having first done the task.

Studies like these leave us with the unsettling question of which activation pattern is the real one? Understanding these results is complicated by the fact that similar tasks are done repeatedly throughout one's life. Despite this, though, reconfiguration of activation after a single session of opening and closing one's fist is similar enough across subjects to show significant group effects, and durable enough to last at least 5 h. One must wonder, though, whether the major change from session 1 to session 2 is accommodation to the setting and experience of fMRI itself. It is true that the motor task is always differenced from the baseline activity associated with the general fMRI experience, but as we have seen when discussing static localizationist studies, changes in this baseline activity can alter task-related increments. Indeed, if one's goal was to identify changes in brain activation associated with increasing familiarity with the fMRI environment, one might see the resting period as the active or experimental condition, and use a simple motor task as a baseline condition in which brain activation is relatively constant. In this case, the difference

in difference scores between sessions 1 and 2 would be seen as changes in activity patterns associated with resting quietly in the magnet. These considerations demonstrate the difficulty of interpreting studies of even simple changes in the relationship between cognitive functions and brain activation; the multiple degrees of freedom require systematic experimental manipulation of multiple components of the situation and tasks before conclusions can be formulated. Studies like these, though, demonstrate how richly dynamic a system we seek to understand, and in their aggregate hold the promise of revealing some principles that govern these dynamics.

Other studies have done repeated imaging while subjects learned to improve their performance on difficult motor tasks. In one, for example, the investigators compared regional cerebral blood flow measured with positron emission tomography early in an initial session when errors were high to later in that same session when errors were low (Shadmehr and Holcomb, 1997). Values at each voxel were normalized for overall brain blood flow, and these relative flow values during a resting baseline were then subtracted from values during the motor task. Changes in these incremental difference scores were limited to blood flow decreases in the sensorimotor cortex and putamen, suggesting less neuronal activity as performance became more efficient. More extensive changes were noted when comparisons were made between the later part of the initial session and a follow-up session 5.5 h later, even though performance was not significantly different at these two time points. At follow-up, blood flow was greater in the left posterior parietal cortex and the left dorsal premotor cortex, and lesser in the left and right middle frontal gyri within the prefrontal cortex. The authors attribute these changes to the heretofore hidden process of consolidation of learning that stabilizes mnemonic representations. Although we don't see the process actually in action, we get clues as to what areas of the brain are more and less involved after consolidation. Moreover, it appears that consolidation involves decreases in activity in some regions and increases elsewhere.

Efforts have also been made to study changes in activation related to learning cognitive tasks. For example, in one study subjects pushed a button when they thought stimulus cards signified rain (Poldrack *et al.*, 1999). They were not told which combination of cards signified rain, but figured this out based on feedback throughout the imaging session. For subtraction purposes, a control task consisted of simply indicating when two, rather than one or three stimulus cards were present. Voxels showing changes in signal over the course of the imaging session while doing the rain prediction task but not while doing the control task were assumed to show learning-related changes in activation. Activity increased with learning in the right inferior prefrontal cortex, right and left inferior parietal cortex, posterior cingulate and right insula. Learning-related decreases in activity were seen in the medial prefrontal cortex, orbitofrontal cortex, left dorsolateral prefrontal cortex, and the right occipital cortex. In other words, more cortical areas showed activation changes over the course of learning than not; only the temporal lobes seemed unchanged.

As discussed in other chapters, it is reasonable to conclude that if activity in a region changes when a task is done repeatedly, or under different conditions, it is evidence that the region is somehow involved with the task, at least at one or the other times or under one or the other experimental condition. Results like those just cited demonstrate that many widely distributed brain areas are involved in even simple tasks in controlled laboratory settings. A hope of studies like these is that the experimental findings will reveal principles and processes of dynamic change in the brain, and provide a foundation for understanding the interaction and integration of the distributed areas of activity. The large number of brain areas in which apparent task-related activity changes over time or under different conditions, however, makes this a daunting task. Moreover, it is even more complex than it looks, since brain regions may function at times by changes in firing patterns within and across neurons that do not lead to overall changes in regional metabolic activity, and because the anatomic resolution of our imaging methods may be insufficient to resolve distinct functional components. As a result, the conclusions we are able to draw from studies like these, while a valuable beginning, remain very general. For example, the very competent team of investigators who conducted the aforementioned study of the weather prediction task began the

discussion of their findings by stating 'The present findings are consistent with a number of other recent studies suggesting that skill learning involves changes in which neural networks are involved in performance (Poldrack *et al.*, 1999).' Even conclusions like this, however, must be qualified by the fact that the absence of activity differences in a region between task and control conditions, or the absence of changes in the difference before and after learning, to do not prove that the regions is not active during task performance.

### 15.2.2. Changes in Activation with Age

Changes with age take place too slowly to be measured in within-subject designs that test the same individuals repeatedly. Instead, groups of younger and older subjects are compared with the assumption that differences represent changes that occur within individuals over time. For example, covert word generation in response to letter cues has been compared in children (mean age 10.7 years) and young adults (mean age 28.7 years) (Gaillard *et al.*, 2000), and semantic encoding studied in young adults (mean age 25 years) and elderly adults (mean age 77 years) (Stebbins *et al.*, 2002). Task performance was not monitored during imaging in the first study, but in the second, younger and older subjects performed at similar levels. In both studies, activation was apparent in the inferior frontal cortex (Brodmann areas 44/45), the middle frontal gyrus (BA 46) and the superior frontal gyrus, facilitating comparison across studies. Children showed significantly more extensive activation overall than young adults, with the differences greatest in the right hemisphere. While the activation task produced greater left than right hemisphere activation in nearly all subjects, this laterality was decreased in the children due to the more extensive right hemisphere activation. PET studies indicate that resting glucose metabolism and cerebral blood flow in the frontal lobes are more than 50 % higher in 8- to 12-year-old children than in adults (Chugani *et al.*, 1987; Chiron *et al.*, 1992). Therefore, greater task-related increases in activity in children can *not* be explained by lower baseline levels. Moreover, the lateralized nature of the differences between children and young adults also makes a general metabolic explanation less likely. Older adults also show less strongly lateralized activity than young adults, but here the primary effect is lesser left hemisphere activation rather than greater right hemisphere activation, as seen in children. The extent of left hemisphere activation was significantly greater in the younger than the older adults in the inferior, middle and superior frontal gyri while intergroup differences in corresponding right hemisphere structures did not approach significance. Here again, the laterality of the group differences, together with the fact that older adults showed marginally greater activation than younger adults in the cingulate, make it unlikely that the findings are due to a general metabolic or vascular effect of aging. In this particular study, however, activation during a control task in which subjects decided whether letters were upper or lower case, was subtracted from activation during the semantic encoding task. This leaves open the possibility that older subjects actually had greater left hemisphere activation than younger subjects on the control task, rather than lesser left hemisphere activation on the experimental task.

Despite this problem, it seems that a number of things can be learned from studies like these. First, here is still more evidence that the brain can do the same cognitive task with varying configurations of neural resources. Beyond this, some things are suggested about functional development and aging of the brain. The adult pattern of functional lateralization for language-related tasks is not yet developed in 10- to 12-year-old children. Children appear to activate their brains more extensively than young adults. This is similar, at least in a superficial way, to the fact that activation is often more extensive when young adults do a task for the first time than when they repeat it. With aging, lateralization of functional activation is altered again, this time perhaps with loss of the selective left hemisphere activation during language-related tasks. These observations may add to our understanding of normal neural development and aging when considered along with other types of information. Experimental paradigms like these may also be useful in studying abnormal development and aging.

### 15.2.3. Changes in Activation with Changes in Physiological State

Here the same activation task is given to the same individuals when they are in different general physiological states. The degree of hunger and the degree of sleep deprivation provide examples. It is common sense that when one is hungry, food-related stimuli become more salient. Imaging studies, though, can identify some of the ways that neural correlates of information processing change in association with this increased salience. In one study the signal associated with looking at pictures of tools was subtracted from signals associated with looking at pictures of food (LeBar *et al.*, 2001). One group of subjects was scanned 8 h after having last eaten and then again 1 h later with a different stimulus set. A second group was scanned twice, each time just after having eaten, to control for retesting effects. The double subtraction of food items – tools in the hungry versus satiated state identified many regions that showed a greater response to food than to tools in the hungry than in the satiated state: the amygdala, parahippocampal gyrus, and anterior fusiform gyrus. Given that the physiological manipulation is known to increase perceptual and subjective sensitivity to food stimuli, it is reasonable to conclude that the findings are due to changes in the neural response to food stimuli, rather than to changes in the neural response to tools. It is not as clear, however, whether it is more useful to think that food-related activation decreased in these areas during the satiated state or increased in these areas during the hungry state. A paradigm like this might be useful in studying individuals with eating disorders, and evaluating treatments for these problems, but it is less clear what has been learned about the brain, or what the next step would be in this investigation of normal function.

In a study of sleep deprivation, subjects were scanned after 30 h without sleep or after a normal night's sleep (Drummond *et al.*, 2000). During the experimental task, subjects read and attempted to memorize 20 words presented in blocks of five words. Between blocks, subjects did a control or baseline task in which they were asked to determine whether words were in upper or lower case letters. In the double subtraction of memory minus control task and sleep-deprived versus rested states, multiple changes were noted. Memory-related activation present during the rested state in the left prefrontal cortex increased following sleep deprivation while that in the temporal cortex decreased. Additional activations were noted following sleep deprivation in the parietal lobes bilaterally, in the right inferior frontal gyrus, and in the left middle frontal gyrus. Despite, or perhaps because of, these generally increased activations, performance was worse in the sleep-deprived condition. The increased activations might be seen as the greater effort one must make to do something when fatigued, effort to compensate for dysfunction or inefficiency in processing systems. Alternately, the greater activations might be the problem itself; an unruly and therefore a less focused and a less efficient brain. Again we see evidence that the brain performs the same task in quite different ways at different times. The complex relationships between activity and performance are also evident; both increased and decreased activity can apparently be seen with either increased or decreased performance. And then there is the issue that we are never either fully rested or fully fatigued, but are often somewhere in between.

### 15.2.4. Effects of Shifting Attention on Activation

The ability of self-directed attention to increase activations related to sensory processing has been demonstrated repeatedly. For example, in one study we presented auditory and visual stimuli to subjects simultaneously, with instructions to attend to the visual stimuli at some times and to the auditory stimuli at other times. Although the visual and auditory stimuli were received by peripheral sensory receptors throughout the experiment, voluntarily directing attention to one or the other increased the degree of activation in the respective sensory receptive areas. A recent study was able to evaluate this attentional amplification further by having subjects attend selectively to one visual field that contained upward and downward moving dots (Saenz *et al.*, 2002). They were then instructed to alternately track either the upward or downward stream.

All dots in the unattended visual field moved in the same direction. Activation to the dots in the unattended visual field (i.e., in the contralateral visual cortex) increased when subjects were tracking the stream in the attended field that moved in the same direction as the dots in the unattended field. Here, then, was evidence that this attentional modulation of brain response to a stimulus feature extended throughout visual processing systems in both hemispheres and to aspects of the visual field to which conscious attention itself was not directed. This may seem only a small gain in knowledge about the brain and mind, but it is steps like these that our current methods allow.

Another set of studies has examined changes in activation that result when subjects do and do not attend to simple motor tasks. These are in effect dual task experiments as described earlier by Kinsbourne and Cook (1971), since in the conditions when subjects are not attending to the motor task they are instead attending to a second task. In one study, for example, subjects moved their right index finger back and forth in the form of a 'U' at a constant frequency paced by a metronome (Binkofski *et al.*, 2002). In one condition they looked at a screen on which green flashes appeared intermittently but were told to attend only to their finger movements. In a second condition they were asked to attend to the green flashes while moving their finger, and in a third to count the flashes while moving their finger. For a baseline condition, they were asked to look at the screen and flashes but not to move their finger. One area of the left motor cortex showed the same activation relative to the baseline in all three conditions. A second nonoverlapping area showed greater activation when attention was directed to the movement itself. When the motor attention condition was compared directly to the two visual attention conditions, differences associated with the direction of attention were evident in prefrontal cortex, premotor, superior and posterior parietal, extrastriatal, fusiform, precuneate and primary visual cortices.

In a similar study, the motor task was to push a button with the right index finger at 1 Hz paced by a flashing green light (Indovina and Sanes, 2001). In the visual attention-low movement condition, subjects pushed the button in response to a blue flash at 0.2 Hz but not in response to a red flash at 1 Hz. In the movement and attention condition, subjects again pushed one button when the green light flashed at 1 Hz, and another when the blue light flashed at 0.2 Hz. For a baseline, subjects viewed a red cross flashing at 1 Hz. The authors introduce their study with an explicit discussion of distributed and changing aspects of brain function. They saw themselves as testing the rather general hypotheses 'that visual attention performed concurrently with a simple repetitive finger movement would reveal novel brain representations.' The results indicated complex interactions. When the attention task was added to the movement task, there was an increase in activity in the left superior parietal lobule and in the precuneus. However, when the attention task alone was compared to the baseline, activity in these same areas was decreased. In addition, when the attention task was added to the movement task, there were also decreases in activity in the left insula and right fusiform areas. These same areas showed increases in activity when the attention task itself was compared to the baseline. Overall, the movement plus attention condition, when compared to the baseline, showed multiple activations not apparent (or below threshold) in either the movement versus baseline or attention versus baseline comparisons. These included the superior and inferior parietal lobules and the orbitofrontal cortex. The authors drew three very general conclusions from the data. First, the movement and attention condition 'activated a widespread brain network.' Second, 'collectively these data indicate that visual attention during movement modifies movement-related activation patterns in the human brain.' And third, 'attention can suppress or facilitate movement-related activation.'

These two studies illustrate changes in brain activation when the same task is performed in a different overall functional context. Interpretation is confounded, however, by some of the difficulties noted in discussion of the static – localizationist studies. Even interaction analyses rest on a subtraction foundation. Post-hoc efforts to understand interactions have to deal with the arbitrariness of thresholds. Combining tasks (e.g., motor and visual attention) raises issues of overall task difficulty, and requires comparison to single tasks of greater difficulty. But perhaps most problematic are the wide-ranging changes in activation

in multiple brain regions from relatively simple experimental manipulations. Nobody seems able to do any more than catalog the results. At this point, the complexity is overwhelming rather than informative.

### 15.2.5. Impact of Brain Injury or Disease on Functional Activation

Finally, I will mention in passing the now thousands of functional imaging studies of patients with a wide variety of brain injuries or illnesses. While these studies are primarily for the purpose of learning more about the clinical condition, the way the brain functions when compromised by injury or disease can potentially provide additional information about principles and processes of normal function. Like the studies of aging, these studies compare different groups of subjects rather than comparing the same individuals under different conditions. The cross subject comparisons, however, serve as a standin for comparing individuals before and after the onset of illness, and thus provide a wealth of information about possibilities and principles of changing relationships between cognitive function and brain activation. Here again the number of clinical conditions studied and the extent and variety of reported changes in brain activation, overwhelms current ability to interpret and integrate the observations. But here again there are also tantalizing bits of information that suggest the potential of this information to increase our understanding of the brain and mind. I will describe briefly several of the most interesting of these bits of information.

Following traumatic brain injury, patients showed right lateralized activation asymmetries on a task that healthy controls showed left lateralized activity (Christodoulo *et al.*, 2001), and generally showed more widely distributed activity than did the healthy subjects (McAllister *et al.*, 1999; Christodoulo *et al.*, 2001). Like elderly adults, these brain-injured young adults lost the normal laterality of activation that develops between childhood and adulthood. Several lines of imaging data thus converge in pointing to the importance of laterality of functional organization. The data from brain injured patients suggests that focal gray matter lesions and/or the disruption of white matter tracts interferes with maintenance of this higher-order lateralized functional organization.

Patients with HIV infection show somewhat different results, preserving the general pattern of activation seen in healthy subjects, but showing more extensive activation despite slower task performance (Chang *et al.*, 2001). This is similar to the load-related increases in activation seen in healthy subjects when task difficulty is increased. Perhaps things are more difficult for the HIV-infected brain. If so, knowledge of the brain pathology associated with HIV infection may shed light on aspects of normal function. Studies of patients recovering from strokes that affect motor function have demonstrated that components of the normal, distributed motor system that are unaffected by the stroke become more active as patients recover movement. In one sense this is an unsurprising recovery mechanism, but in another it reveals a functional interchangeability among components that is contrary to the assumption that each of these distinct but interconnected regions must have their own special functional contribution even if we have not yet figured out the functional alphabet.

Finally, a whole series of studies in psychiatric patients, as well as some in normal aging and other illnesses, have found that patients or older individuals activate the same regions as do healthy or younger subjects but to a lesser degree. This is particularly interesting because the patients and older individuals often show this underactivation despite performing as well as healthy and younger subjects on the activation task. What does it mean that patients do the tasks as well as controls but with less brain activation? Perhaps the brains of healthy subjects activate more than is necessary to do the task. This 'elaborative activation' could be an important aspect of normal brain function that is lost in illness (Wexler, 1991).

## 15.3. SUMMARY

Functional imaging studies have now established beyond question that cognitive and motor functions depend upon the integrated action of many regions distributed throughout the brain. Moreover, the particular

constellation of regions involved in any particular function changes throughout the life span, after simple repetition of the task, and after systematic learning and practice. The activation of specific components in these distributed functional systems is responsive to the direction of attention, as well as to the physiological and cognitive context in which the particular task is being executed. Together these observations indicate that the simple concepts and experiments that sought to determine the location of cognitive functions, and which were the foundation for most early functional imaging studies, have limited value. Questions remain as to how to define the characteristics and boundaries of functionally distinct brain regions, because all of the brain is not the same, how these regional components are integrated, and to what degree even these structure–function associations are stable.

Imaging studies of the distributed aspects of brain function, and of the ways in which the relationship between cognitive function and brain activation changes, have the potential to continue providing new information about how the mind and brain work. However, serious difficulties continue to limit such studies. One is the fact that with fMRI, in many ways the most versatile of imaging methods, signals from two conditions must be compared which necessitates a subtraction of one from the other thereby hiding approximately 90 % of neuronal activity from view. Still, important aspects of brain function have been revealed. For example things that we think about as psychological or cognitive functions such as attention, perception or memory emerge from the interaction among brain regions, and different configurations of regional activation can support the same function, functional synonyms in the brain functional alphabet. The changes in functional activation patterns, however, are routinely so extensive as to overwhelm our current ability to understand the observations we make. There is great need for new concepts to integrate our findings and guide future work. Generative, nonlinear and combinatorial models may prove useful in this regard (Friston, 2002), but problems related to functional subtraction, threshold setting and task difficulty still persist.

## REFERENCES

Binkofski, F., Fink, G. R., Geyer, S., Buccino, G., Gruber, O., Shah, N. J., Taylor, J. G., Seitz, R. J., Zilles, K., Freund, H.-J., Neural activity in human primary motor cortex areas 4a and 4p is modulated differentially by attention to action, *The Journal of Neurophysiology* **88**(1) (2002) 514–519.

Chang, L., Speck, O., Miller, E. N., Braun, J., Jovicich, J., Koch, C., Itti, L., Ernst, T., Neural correlates of attention and working memory deficits in HIV patients, *Neurology* **57**(6) (2001) 1001–1007.

Chiron, C., Raynaud, C., Maziere, B., *et al.*, Changes in regional cerebral blood flow during brain maturation in children and adolescents, *The Journal of Nuclear Medicine* **33** (1992) 696–703.

Christodoulou, C., DeLuca, J., Ricker, J. H., Madigan, N. K., Bly, B. M., Lange, G., Kalnin, A. J., Liu, W. C., Steffener, J., Diamond, B. J., Ni, A. C., Functional magnetic resonance imaging of working memory impairment after traumatic brain injury, *Journal of Neurology, Neurosurgery, and Psychiatry* **71**(2) (2001) 161–168.

Chugani, H. T., Phelps, M. E., Mazziotta, J. C., Positron emission tomography study of human brain functional development, *Annals of Neurology* **22**(4) (1987) 487–497.

Churchland, P. S., Neurophilosophy, *Toward a Unified Science of the Mind–Brain*, MIT Press, Cambridge, MA, 1986.

Drummond, S. P. A., Brown, G. G., Gillin, J. C., Stricker, J. L., Wong, E. C., Buxton, R. B., Altered brain response to verbal learning following sleep deprivation, *Nature* **403**(6770) (2000) 655–657.

Friston, K., Beyond Phrenology: What can neuroimaging tell us about distributed circuitry? *Annual Review of Neuroscience* **25** (2002) 221–250.

Friston, K. J., Price, C. J., Fletcher, P., Moore, C., Frackowiak, R. S. J., Dolan, R. J., The trouble with cognitive subtraction, *Neuroimage* **4** (1996) 97–104.

Gaillard, W. D., Hertz-Pannier, L., Mott, S. H., Barnett, A. S., LeBihan, D., Theodore, W. H., Functional anatomy of cognitive development: fMRI of verbal fluency in children and adults, *Neurology* **54**(1) (2000) 180.

Indovina, I., Sanes, J. N., Combined visual attention and finger movement effects on human brain representations, *Experimental Brain Research* **140** (2001) 265–279.

Kinsbourne, M., Cook, J., Generalized and lateralized effect of concurrent verbalization on a unimanual skill, *Quarterly Journal of Experimental Psychology* **23** (1971) 341–345.

LeBar, K. S., Gitelman, D. R., Parrish, T. B., Kim, Y. H., Nobre, A. C., Mesulam, M.-M., Hunger selectively modulates corticolimbic activation to food stimuli in humans, *Behavioral Neuroscience* **115**(2) (2001) 493–500.

Loubinoux, I., Carel, C., Alary, F., Boulanger, K., Viallard, G., Manelfe, C., Rascol, O., Celsis, P., Chollet, F., Within-session and between-session reproducibility of cerebral sensorimotor activation: a test-retest effect evidenced with functional magnetic resonance imaging, *Journal of Cerebral Blood Flow and Metabolism* **21**(5) (2001) 595–607.

Luria, A. R., *The Working Brain*, Ed. Pribram, K. H., Basic Books, New York, (1973).

McAllister, T. W., Saykin, A. J., Flashman, L. A., Sparling, M. B., Johnson, S. C., Guerin, S. J., Mamourian, A. C., Weaver, J. B., Yanofsky, N., Brain activation during working memory 1 month after mild traumatic brain injury: a functional MRI study, *Neurology* **53**(6) (1999) 1300–1308.

McCarthy, G., Blamire, A. M., Puce, A., Nobre, A. C., Bloch, G., Hyder, F., Goldman-Rakic, P., Shulman, R. G., Functional magnetic resonance imaging of human prefrontal cortex activation during a spatial working memory task, *Proceedings of the National Academy of Sciences of the United States of America* **91**(18) (1994) 8690–4.

McCarthy, G., Puce, A., Constable, R. T., Krystal, J. H., Gore, J. C., Goldman-Rakic, P., Activation of human prefrontal cortex during spatial and non-spatial working memory tasks measured by functional MRI, *Cerebral Cortex* **6** (1996) 600–611.

Poldrack, R. A., Prabhakaran, V., Seger, C. A., Gabrielli, J. D. E., Striatal activation during acquisition of a cognitive skill, *Neuropsychology* **13**(4) (1999) 564–574.

Posner, M. I., Petersen, S. E., Fox, P. T., Raichle, M. E., Localization of cognitive operations in the human brain, *Science* **240** (1988) 1627–1631.

Pugh, K. R., Shaywitz, B. A., Shaywitz, S. E., Shankweiler, D. P., Katz, L., Fletcher, J. M., Skudlarski, P., Fulbright, R. K., Constable, R. T., Bronen, R. A., Lacadie, C., Gore, J. C., Predicting reading performance from neuroimaging profiles: the cerebral basis of phonological effects in printed word identification, *Journal of Experimental Psychology: Human Perception and Performance* **23**(3) (1997) 299–318.

Raye, C. L., Johnson, M. K., Mitchell, K. J., Reeder, J. A., Greene, E. J., Neuroimaging a single thought: dorsolateral PFC activity associated with refreshing just-activated information, *Neuroimage* **15**(2) (2002) 447–53.

Saenz, M., Buracas, G. T., Boynton, G. M., Global effects of feature-based attention in human visual cortex, *Nature Neuroscience* **5**(7) (2002) 631–632.

Schlosser, M. J., Aoyagi, N., Fulbright, R. K., Gore, J. C., McCarthy, G., Functional MRI studies of auditory comprehension, *Human Brain Mapping* **6** (1998) 1–13.

Shadmehr, R., Holcomb, H. H., Neural correlates of motor memory consolidation, *Science* **277** (1997) 821–825.

Shulman, R. G., Interview with Robert G. Shulman, *Journal of Cognitive Neuroscience* **8**(5) (1996) 474–480.

Stebbins, G. T., Carrillo, M. C., Dorfman, J., Dirksen, C., Desmond, J. E., Turner, D. A., Bennett, D. A., Wilson, R. S., Glover, G., Gabrielli, J. D. E., Aging effects on memory encoding in the frontal lobes, *Psychology and Aging* **17**(1) (2002) 44–55.

Vygotsky, L. S. *Mind In Society*, Ed. Cole, M., John-Steiner, V., Scrubner, S., Souberman, E., Harvard University Press, Cambridge, (1978).

Wexler, B. E., A model of brain function: its implications for psychiatric research, *British Journal of Psychiatry* **148** (1986) 357–362.

Wexler, B. E., Failure at task-specific regional brain activation: new conceptualization of a disease entity, *Neuropsychiatric Practice and Opinion* **3**(1) (1991) 94–98.

Wexler, B. E., Fulbright R. K., Lacadie, C. M., Skudlarski, P., Kelz, M. G. Constable R. T., Gore, J. C., An fMRI study of the human cortical motor system response to increasing functional demands, *Magnetic Resonance Imaging* **15** (1997) 385–396.



# 16

## Brain and Mind: an NMR Perspective

**Robert G. Shulman**

*Yale University School of Medicine, MR Center, P.O. Box 208043, New Haven, CT 06520-8043, USA*

**Fahmeed Hyder**

*Department of Diagnostic Radiology, Yale University School of Medicine, MR Center, P.O. Box 208043, New Haven, CT 06520-8043, USA*

---

16.1 $^{13}\text{C}$ MRS	297
16.2 The Restless Brain	299
16.3 Implications for Functional Imaging	299
16.4 Neuronal Basis of Baseline and Incremental Signals	301
16.5 Consciousness and Baseline Activity	302
16.6 Neurophysiological Structures	303
16.7 Neuroscientific Measures of Baseline Activities	304
16.8 Need for Philosophy	305

---

‘The fascination of a growing science lies in the work of the pioneers at the very borderland of the unknown, but to reach this frontier one must pass over well traveled roads; of these one of the safest and surest is the broad highway of thermodynamics.’

Lewis, G.N. and Randall, M. (1923) *Thermodynamics and the Free Energy of Chemical Substances*, McGraw-Hill, New York and London.

‘physiology traces . . . the results of mental processes which do not fall within the sphere of consciousness, and must therefore have remained inaccessible to us’

Herman von Helmholtz. *Academical Discourse at Heidelberg, November 22, 1862*, published in *Science and Culture: Popular and Philosophical Essays* (1995) Ed. David Cahan, University of Chicago Press, Chicago, IL, p. 95.

Neuroscience generally consists of bottom-up approaches that seek scientific answers to larger questions of brain function. However, upon a close examination of the scientific directions that are lumped together as neuroscience considerable diversity becomes apparent. Francis Crick proposed that an understanding of brain–mind can be found in terms of the constituent molecules (Crick, 1991). Although this proposal would be accepted by many neuroscientists it is not obvious that this commonality overcomes the differences between the subfields of neuroscience. Very different questions are asked about molecules and cells in the studies of cellular axonal connections, genetic development and neurotransmission to mention just some of the many faces of neuroscience. Different methods are used and more importantly, different assumptions, with different worldviews, form these investigations' starting points in the world of neuroscience.

In the physical sciences understanding is based upon micro explanations of macro phenomena, which forms the generalized basis of Crick's proposal. The systematic understanding reached by atomic physics, the physics of matter, represents for many the scientific paradigm. Its micro explanations of macro phenomena have created our technological world and it has given us control of many natural forces. To 'understand' heat is to know how it depends upon the energies of particles and while water has long been known as  $H_2O$  such understanding is improved by quantum and statistical explanations. The goal of understanding complex matter, which is particularly acute for living organisms, brings into question the most reliable and informative ways to generate these explanations. Varied criteria are chosen as the starting points for different physical explanations of brain matter. The choices made of these criteria, of the starting assumption as to what the problem is and what the answer might be, distinguishes the various scientific disciplines lumped together as neuroscience.

The hopes of neuroscience derive from the bottom-up successes of physics which is the study of energy and matter. When applied to the molecules and structures of life which exist in aqueous solutions, physics is most directly formulated as thermodynamics. The laws of classical, nonquantum physics as applied to the solutions of molecules found in biology are codified as Gibbs free energy, which is the ability to do work. This explanatory level is intermediate between the too diffuse, as for example laminar and turbulent flow would be, or too microscopic, as it would be if we started from the fundamental particles. The success of thermodynamics in explaining the work of skeletal muscle, a functional organ of life, in which energy consumption and work done have been clearly defined, exemplifies the achievements of this level of explanation in biological science.

Neuroscience research described in this book has been based upon experimentally relating brain energy consumption (in the form of oxygen usage) to brain work done (in the form of neuronal firing). From the relations established between brain energy consumption and neuronal activity, we have addressed the more complex questions of brain function. This approach is a unique starting point for bottom-up studies because for modern science it is the ultimate bottom. A work–energy relationship is more directly based upon physics than are the molecular, genetic, or psychological assumptions postulated in other subfields of neuroscience. Although thermodynamical explorations of brain function may at first seem unacceptably distant from the qualities of mind which form the ultimate goals of neuroscientific enquiry, we propose to show that, because of their reliability, they form a particularly valuable methodology. Further by starting with these thermodynamical assumptions we are unequivocally considering the brain to be subject to the laws of physics concerning energy–work. Our assumptions are that the brain–mind in this respect is not different from any other material, whose thermodynamical properties have been elucidated in the past four centuries by empirical physical studies of matter.

By adopting an empirical research program based upon this intrinsic view of brain, we hope that firmly based physical studies of the brain's organic matter will lead to a novel vantage point for understanding

its more complex properties. We do not undervalue the qualities of mind that are the essence of human life. On the contrary we think they are too important to be assumed in order to study the brain. Qualities of mind are the ultimate, although, in our opinion, the distant goals of brain studies. Our approach differs from many neuroscientific studies which, starting from a presumed understanding of how the brain works, strive to understand how the brain subserves these assumptions.

### 16.1. $^{13}\text{C}$ MRS

Nuclear magnetic resonance studies of the brain have delineated the coupling between brain energy consumption and work. Magnetic resonance spectroscopy (MRS) has non-invasively measured *in vivo* concentrations and kinetics of molecular metabolites. These small molecules, e.g. glutamate, glutamine, lactate, glucose, etc. are studied as the components of the energetic and neurotransmitter pathways (for reviews see Shulman *et al.*, 2002, 2003; Rothman *et al.*, 1999).

The understanding that glucose oxidation provides the brain energy was continued by  $^{13}\text{C}$  MRS measurements of the flux from labeled substrates like  $1\text{-}^{13}\text{C}$  glucose through the tricarboxylic acid (TCA) cycle. Numerical values of the neuronal metabolic rate of oxygen consumption obtained from this measure of TCA cycle flux agreed with measurements by other methods described in Chapter 2.

The second thermodynamic measurement was of the neuronal work done by the brain. This work is coupled to the release of the neurotransmitter glutamate upon neuronal firing and its subsequent recycling through glutamine (Figure 16.1). Glutamate is the major cortical neurotransmitter serving that function in

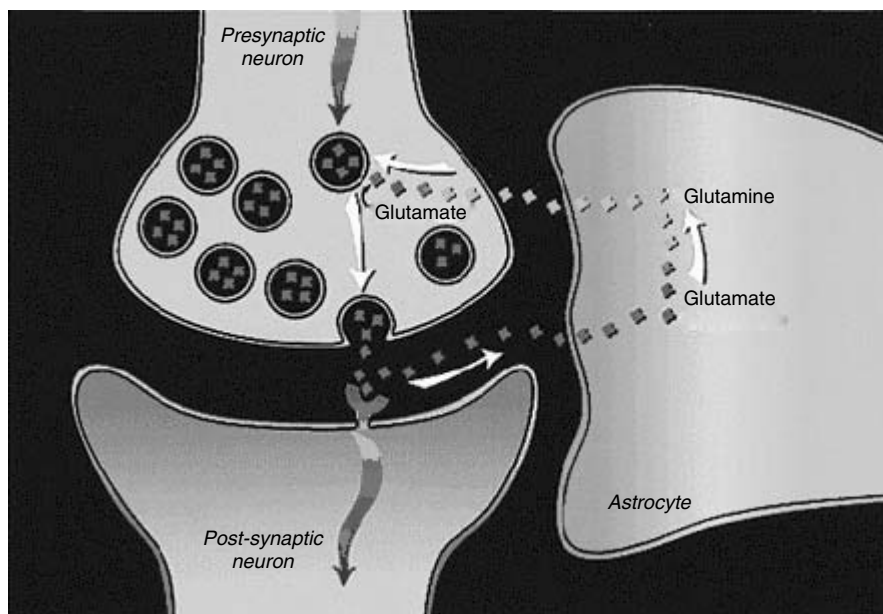


**Figure 16.1.** A model of glutamate–glutamine neurotransmitter cycling between neurons and astrocytes (for a review see Magistretti *et al.*, 1999). The rate of the glutamate-to-glutamine cycle ( $V_{\text{cyc}}$ ) has been quantitated by  $^{13}\text{C}$  MRS (for reviews see Rothman *et al.* 1999, 2002). Action potentials or spikes (shown by curved arrows) reach the pre-synaptic terminal to initiate the release of vesicular glutamate into the synaptic cleft. This activates the glutamate receptors in the post-synaptic neuron, which is a step required in the propagation of spiking activity to the adjacent neuron (in an all-or-none manner). The extracellular glutamate is removed rapidly by  $\text{Na}^+$ -coupled transport into astrocytes, where it is converted into glutamine. The synthesized glutamine then passively diffuses back to the neuron, and after re-conversion to glutamate, is repackaged into vesicles. (Modified from Shulman and Rothman, 2001).

~80 % of the neurons. The ability of  $^{13}\text{C}$  NMR to follow the time course of  $^{13}\text{C}$  label flow into glutamate and subsequently into glutamine in the human brain has opened glutamate neurotransmitter cycling to quantitation.

Soon after these first experiments on human subjects, the easily manipulated rat model was exploited to expand the understanding of the interactions of the different rates *in vivo* (for a review see Rothman *et al.*, 1999). The relative rates of neuronal oxidation ( $\text{CMR}_{\text{glu}(\text{ox})}^{\text{N}}$ ) and glutamate cycling ( $V_{\text{cyc}}$ ) were measured over a wide range anesthesia in the rat (Sibson *et al.*, 1998; Chapter 5). Simultaneous measurements of the  $^{13}\text{C}$  flow into glutamate and its subsequent flow into glutamine were converted into  $\text{CMR}_{\text{glu}(\text{ox})}^{\text{N}}$  and  $V_{\text{cyc}}$ , respectively. Figure 16.2 and Equation (16.1) summarize the results

$$\text{CMR}_{\text{glu}(\text{ox})}^{\text{N}} = V_{\text{cyc}} + 0.1 \quad (16.1)$$

in units of  $\mu\text{mol/g/min}$ . The results are significant for understanding brain activity in several respects. First, a quantitative relationship between neurotransmission (i.e., neurotransmitter flux) and neuroenergetics (i.e., neuronal oxidation) quantified the model in Figure 16.1. Second, at the intercept of Figure 16.2 as  $V_{\text{cyc}}$  approached zero, which corresponds to no neuronal firing,  $\text{CMR}_{\text{glu}(\text{ox})}^{\text{N}}$  falls to 20 % of the value at the nonstimulated awake condition. Hence in the nonstimulated awake condition ~80 % of the energy supports events associated with neurotransmission. Third the slope of the  $\text{CMR}_{\text{glu}(\text{ox})}^{\text{N}}$  and  $V_{\text{cyc}}$  curve is ~1 (Figure 16.2 and Equation (16.1)), hence for every additional glucose molecule oxidized neuronally, one glutamate is released as a neurotransmitter and cycled through glutamine. This stoichiometry allows changes in glutamate neurotransmitter flux to be determined from measured changes in oxygen consumption. The observed stoichiometry provides strong support for an advanced model of glial–neuronal coordination, linking glucose consumption and glutamate neurotransmitter cycling, which was originally proposed from research on cellular suspensions (Pellerin and Magistretti, 1994), and has been shown to be the major pathway *in vivo* (Magistretti *et al.*, 1999).

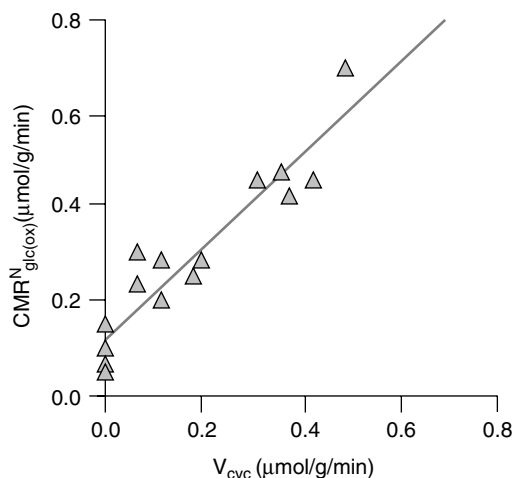


**Figure 16.2.** Relationship between  $V_{\text{cyc}}$  and  $\text{CMR}_{\text{glc}(\text{ox})}^{\text{N}}$  established from experimental results of  $^{13}\text{C}$  MRS experiments at 7T (Sibson *et al.*, 1998) where rats were moderately anesthetized (with morphine and  $\alpha$ -chloralose) to isoelectric conditions (high-dose pentobarbital). The best-fit line is given by Equation (16.1) (in units of  $\mu\text{mol/g/min}$ ), which suggests that each mole of neurotransmitter glutamate cycling requires the oxidation of 1 mol of glucose. The awake, resting state has  $\text{CMR}_{\text{glc}(\text{ox})}^{\text{N}}$  of approximately  $0.8 \mu\text{mol/g/min}$ , which means that under this condition ~80 % of the resting energy consumption is dedicated to events associated with  $V_{\text{cyc}}$ . (Modified from Sibson *et al.*, 1998).

## 16.2. THE RESTLESS BRAIN

The functional integrity of the brain depends on a collection of active cells which are continuously transferring and processing information. Our studies have established the relationship between neuroenergetics and neurotransmission most quantitatively in animal models and similar results fit the available human data (Rothman *et al.*, 1999, 2002). Our major findings can be summarized as follows:

1. Changes in energy consumed are coupled to the flux of glutamate neurotransmission (Chapter 5) and neuronal firing (Chapter 10) over a wide range of cortical activity (see Equation (16.2)).
2. In the awake condition (i.e., baseline activity), more than three-quarters of the brain energy is efficiently devoted to neuronal activity in the absence of external stimulation (Chapter 5). Cognitive or sensory stimulation can change this activity slightly.
3. A specific level of neuronal activity is required to perform a task. Increments detected by functional imaging do not measure the energy supporting the task but only the difference from baseline (Shulman *et al.*, 1999; Hyder *et al.*, 2002: Chapter 9).
4. The incremental functional imaging signal upon stimulation can localize regional changes in activity. However, the absence of an incremental signal does not mean the region does not participate in the function, rather that the activity does not differ from the baseline state.
5. Based upon these results we propose in this chapter that consciousness, defined as the individual's awareness of the world and of his subjective experience, tracks the degree of total brain activity. Most of the activity responsible for consciousness is discarded in a conventional functional imaging experiment.

## 16.3. IMPLICATIONS FOR FUNCTIONAL IMAGING

These results allow new neurophysiological and neuronal interpretations of contemporary functional imaging experiments. Two possible interpretative pathways of functional imaging protocols are shown in a schematic presentation (Figure 16.3) taken from an earlier study (Shulman and Rothman, 1998). As indicated by the top line, the signal S, measured in a functional imaging experiment can be interpreted to provide insight into brain functioning M. The signals may derive from sensory experiments, or from more psychologically based protocols, but in either case they are interpreted in terms of a psychological model to elucidate brain function directly. The insights provided by this upper pathway are responsible for the popularity of functional imaging experiments.

However, from our viewpoint the main explanatory pathway is diagrammed in the lower lines. In that approach, the fMRI or PET functional imaging experiments can be interpreted, usually in conjunction with ancillary data, to determine the neurophysiological parameters (NP) of brain energy consumption, most conveniently expressed as  $CMR_{O_2}$ . Our results have shown that the values of  $CMR_{O_2}$  determine neuronal activity, (N) expressed either as neurotransmitter cycling,  $V_{cycle}$ , (Chapter 5) or neuronal spiking frequencies (see Equation (2) of Smith *et al.*, 2002 and Chapter 10). This explanatory pathway provides thermodynamic approaches to the questions of brain function M and reach different conclusion about the brain than those used in the psychological approach represented by S–M.

The ease of measuring incremental activity by functional imaging has been consonant with the widespread view that increments localize the modular energy required for functional activity (Posner and Raichle, 1998). Our findings (Chapter 10) show that these increments arise from changes across the total neuronal populations whose sum changes the localized activity. The magnitude of stimulus-induced incremental activity in awake human experiments is much smaller than the basal activity. In anesthetized animals the size of incremental activities depend on depth of anesthesia and can be larger (Shulman *et al.*, 1999) but

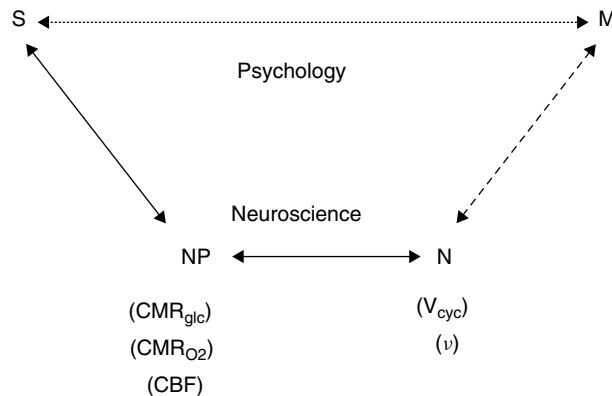


**Figure 16.3.** Schematic relationship between the neuroimaging signal (S) and mental processes (M). In the usual experimental plan and interpretation, which is influenced by psychology and cognitive neuroscience, a direct relationship between S and M is assumed, as represented by the upper Psychology pathway (dotted line). While the definition of M is based on psychology, the experimentally derived S serves to localize and quantitate the brain activity identified with the process. The lower Neuroscience pathway, assumes that M has a molecular and cellular basis, which is broken into three steps leading to S. The signal, S, in fMRI or PET experiments, is primarily a measure of the neurophysiological parameters (NP) of CMR<sub>glc</sub>, CMR<sub>O<sub>2</sub></sub>, or CBF, as shown by the gray line. The relation between (NP) the neurophysiological measure of energy consumption and neuronal activity (N), which is shown by the dark line, has been clarified by the <sup>13</sup>C MRS (Sibson *et al.*, 1998) and electrophysiology (Smith *et al.*, 2002) experiments. These recent findings allow measurements of S to be converted into measures of N, which places us squarely facing the unsolved 'hard' problem of neuroscience, i.e., what is the relationship between M and N (dashed line)? (Adapted from Shulman and Rothman, 1998).

are still generally smaller than the baseline. Considering that a specified task is supported by the magnitude of incremental activity neglects contributions of basal activity and is misleading for two reasons (Shulman and Rothman, 1998). First, for example, if  $\Delta\text{CMR}_{O_2}/\text{CMR}_{O_2}$  in a localized region for one cognitive task is 1% (a typical value) and for another task it is 2%, it would be misleading to conclude that twice the neuronal activity is required in the second task. Since approximately 75% of CMR<sub>O<sub>2</sub></sub> is associated with neuronal activity in humans (Shen *et al.*, 1999; Lebon *et al.*, 2001), a more accurate conclusion would be an increase in neuronal activity from 76% to 77% of the total energy consumed. Second, differencing discards high regional activity which is required in response to a stimulus (Hyder *et al.*, 2002). This required activity includes, in our interpretation, subjective contributions, which invalidate the starting assumptions. The subjective contributions including, for example, emotions, associations and experience, play the role in cognitive experiments that the 'Moose' fulfills in business. The 'Moose' is the widely acknowledged big problem that is not discussed (McNeil, 2003). Some executives show leadership qualities by 'putting the Moose on the table' and discussing the big problem, but very few cognitive psychologists have analogously acknowledged these confounding contributions to cognitive tasks (Fodor, 2000).

Consequences of the large baseline activity determined by <sup>13</sup>C MRS studies (Sibson *et al.*, 1997, 1998) for interpreting neuroimaging data have been discussed previously (Shulman and Rothman, 1998). This interpretation provided a simple explanation of the negative difference signals, observed with fMRI and PET, which at that time had been considered an anomaly, (Raichle, 1998), from the assumption that baseline activity was negligible. On the basis of high baseline brain activity negative signals in a localized region were interpreted as a stimulated reduction in regional activity (Shulman and Rothman, 1998). More recently, the existence and the importance of significant neuronal activity during nonstimulated conditions as a special property of certain brain regions (based on a meta-analysis of neuroimaging data) has been

recognized by Gusnard and Raichle (2001). However, in contrast to the  $^{13}\text{C}$  MRS measurements of a ubiquitous high resting brain activity, efficiently supporting neuronal activity, Gusnard and Raichle have proposed the existence of specific localized activities at rest in limited cortical regions. Their assignment follows from their finding that negative difference signals occur in certain regions to which they accordingly attribute high cognitive activities at rest. Their postulated 'baseline' activity also differs in kind from the widespread high activities determined from the  $^{13}\text{C}$  experiments in that they claim a psychological basis (the difference observed between two psychological states) rather than a quantitative neuroenergetic basis for the existence and identification of baseline activity (they have named the Moose). We now discuss how the high baseline activity provides an approach to brain function that goes beyond the Posner and Raichle (1998) interpretation of fMRI, to uncovering previously inaccessible brain activities.

#### 16.4. NEURONAL BASIS OF BASELINE AND INCREMENTAL SIGNALS

The  $^{13}\text{C}$  MRS experiments (as well as fluorodeoxyglucose (FDG) experiments by PET) can separately measure either baseline or incremental signals, which represent activities of a very large population of neurons. Electrophysiological brain studies have suggested that the collaboration amongst a large number of neurons, firing at different frequencies, is crucial for encoding information in the brain (for a review see Scannell and Young, 1999). The idea that a certain number of neurons in a cortical region respond to a given stimulus (i.e., population voting) is not new. It was suggested long ago by E.D. Adrian who observed that touch causes discharges in several nerve fibers, with relative intensities that map the stimulus onto the cortex (for a review Kandel *et al.*, 1991). Information is more likely to be encoded in the brain by neuronal populations than by actions of individual neurons (for a review see Kristan and Shaw, 1997) because typically each cell responds to more than one stimulus variable (e.g., intensity, frequency, etc.), and an individual cell cannot distinguish amongst these different stimulus variables. Since the response profiles of neurons are different, and a single neuron does not participate in just one type of function, the firing of a single cell by itself does not provide a meaningful basic code for information processing (for a review see Chapin and Nicolelis, 1999).

The  $^{13}\text{C}$  MRS measurements of high resting baseline activity are the sum of energy consuming connections measured in the voxel between neurons of different types (Chapter 10). In addition to local interneurons the synaptic activity in a voxel responds to connections with the rest of the brain (Braitenberg and Schuz, 1991). These remote neuronal connections, which support the delocalized aspects of brain activity, contribute to the total activity. Finally the somatosensory cortex has direct input from the sensory neurons via the thalamus – an input that is measured in the experiment. The resting unstimulated neuronal activity, which arises from local and distal neurons, is reduced by anesthesia *both* inside and outside of the somatosensory region. Upon stimulation of the anesthetized rat, the total neuronal activity inside the somatosensory voxels increased whereas total neuronal activity outside the stimulated region remained low (Ueki *et al.*, 1988, 1992; Hyder *et al.*, 1997). Thus the forepaw stimulation increased neuronal activity in the somatosensory cortex, but since the rest of the brain continues to show low activity its transmission to the somatosensory region remains low. This conforms to our observation that under strong stimulation the somatosensory firing, seen in the neuronal histograms, is the same at our two levels of anesthesia so that it responds mainly to the sensory input (Smith *et al.*, 2002; Shulman *et al.*, 2002; 2003). In a nonanesthetized experiment the situation seems different. In the nonanesthetized awake brain at rest, the forepaw stimulation raises the total neuronal activity only slightly (Shulman *et al.*, 1999; Hyder *et al.*, 2002). Preliminary results, extending the  $\alpha$ -chloralose experiments of Smith *et al.*, using a lighter level of anesthesia, have shown departures from the histograms of populations with and without sensory stimulation (Hyder, Chapter 10) suggesting that the remainder of the brain is beginning to contribute significantly. The interplay between contributions from localized and delocalized neuronal connections is measured by these

experiments, with the promise that experiments varying the parameters of sensory input, anesthesia depth and the cortical level probed will provide additional insight to important questions of brain organization.

The pattern of neuronal firing, specific down to the level of individual neurons, is created, in these deeply anesthetized stimulated conditions, by the stimulus. The change in total energy upon a stimulus, detected as the difference signal,  $S$ , is a determinant of the signal usually reported in an fMRI experiment. The usual assumption of an fMRI experiment, i.e., that  $S$  reflects an involvement of that localized activity, is consistent with these neuronal results and is the basis of the usefulness of the differencing signals. Difference signals reflect an integrated, localized change in neuronal activity caused by the stimulus. However, the magnitude of the increment depends upon the relative activities in baseline and stimulated states, so that it does not measure brain activity needed to support the stimulus. Furthermore, neglect of the large baseline activity additionally invalidates the magnitude of the increment as a measure of brain activity.

This kind of differencing, which is the basis of cognitive functional imaging experiments, has the form of a paradigmatic scientific experiment (Shulman, 1996). From a psychological or cognitive basis, a hypothesis is proposed that a task will change brain activity in a localized region and an experiment is performed to see if this is observed. In contrast, when considering the total or baseline brain activity such a formal structure of cause and effect is not available. The total level at rest, being identified as the baseline level – without any specific controlled sensory input – we consider to have no objective cause. There are no psychological or cognitive concepts that we would postulate to cause this activity, since there is no identified stimulation. We would not consider it scientifically valid, for example, to hypothesize that the brain, in this kind of unstimulated resting state, was engaged in or dedicated to a particular, identifiable activity, e.g., memory, love or computing. Without a causal claim, the baseline activity contrasts with the difference activity in a cognitive experiment, where an orchestrated event is postulated to cause the difference signals measured.

## 16.5. CONSCIOUSNESS AND BASELINE ACTIVITY

In agreement with many efforts to review and define consciousness we have no exact definition to propose. Zeman has reviewed a wide range of the concepts of consciousness and found that two definitions dominate the usage. To be conscious in the first condition is taken to be awake, aroused, alert or vigilant (Zeman, 2001). This aspect of consciousness describes how we communicate with our environment including others. The second concept emphasizes the 'qualitative subjective dimension of experience'. We do not try to distinguish a priori between these two conceptualizations and for the moment identify both of these activities of mind with neuronal responses. Our question is how does the high neuronal activity, measured in the absence of specified external stimuli, relate to consciousness? In a start to answer this question we consider the quantitative relations between, and empirical definitions of, the degree of brain activities and the degree of consciousness used clinically by anesthesiologists. Our biophysical results measure the rate of energy consumption evaluated by  $CMR_{O_2}$ , the rate of neuronal signalling measured by neuronal firing,  $v$ , and the rate of neurotransmitter release  $V_{cycle}$ .

PET measurements have reported that glucose metabolism decreases with deepening anesthesia for several anesthetics (for a review see Heinke and Schwartzbauer, 2002). These reductions are generally global although small regional differences are found. Titrating human glucose consumption with isoflurane, halothane and propofol anesthetics 'to the point of unresponsiveness', the whole brain rates of glucose metabolism measured by PET were decreased by 40 %, 46 % and 55 % respectively (Heinke and Schwartzbauer 2002; Alkire, 1998; Alkire *et al.*, 2000). These decreases in metabolic activity were 'believed to reflect the reduced synaptic activity', as judged by EEG variables.

Our relationships (Equations (16.1) and (16.2)) now establish this connection with great certainty, since the available measurements of glucose metabolism are now quantitatively linked to neuronal firing (Chapter 10). Along the pathway of deepening anesthesia, upon reaching about one half the normal brain firing rates,

the subjects reached 'the point of unresponsiveness', where they have, by these criteria, lost consciousness. This clinical definition includes both of Zeman's concepts of consciousness as subjects were no longer aware nor did they report subjective experience. Therefore there is a quantitative correlation between both commonly accepted qualities used to describe consciousness and the magnitude of neuronal firing. While these correlations may be further refined by taking advantage of the spatial resolution of functional imaging methods (Alkire *et al.*, 2000), we emphasize here the first order correlation between the averaged level of brain activity and the degree of consciousness. This correlation could be expanded by associating intermediate levels of neuronal activity with varying degrees of consciousness. Decrease of the baseline activity with deepening anesthesia and the accompanying loss of consciousness establishes the importance of high baseline activity. It is connected, in ways that we are only now able to start exploring, with both aspects of consciousness.

In the differencing methods of functional imaging the baseline activities are discarded, only the differences between two cognitive states being retained. In this respect the differencing imaging methodology parallels the assumptions of cognitive psychology, in which, as has been shown (Searle, 1992; Fodor, 2000), subjective aspects of consciousness are neglected.

## 16.6. NEUROPHYSIOLOGICAL STRUCTURES

Our experimental results have measured two kinds of neuronal activity. One, arising from a specific sensory stimulation, causes a redeployment of neuronal firing, which changes the total energy consumption of a localized brain region. This energy difference can be detected in a functional imaging experiment as an incremental change. The other kind of neuronal activity takes place in the rest of the brain, outside of the sensory cortex that responds to the stimulus. This delocalized outside activity is strongly reduced in the anesthetized state, and it is not increased during stimulation of the anesthetized animal. A relevant neuroscientific framework for relating localized and widespread activities has been offered and developed by Dehaene and colleagues (Dehaene *et al.*, 1998; Dehaene, 2001). They assumed the participation of large neuronal populations in brain function from measurements of electrical activity in awake and asleep humans (Changeux, 1985). They have conceptually divided neuronal activity into a specific localized response to brain tasks (in our experiments this would be to forepaw stimulation) which interacts with a more delocalized response that modulates and controls the specific response. They define the delocalized activity as a *global workspace* that can 'potentially interconnect multiple distributed and specialized brain areas in a coordinated, though variable manner, and whose intense mobilization might be associated with a subjective feeling of conscious effort.' (Dehaene *et al.*, 1998). They propose the global workspace to be active when, in addition to the specific modules, a stimulus interacts with other brain regions (Figure 16.4).

The baseline activity measured from layer 4 in the absence of stimulation is identified as input from, and connections to, other neurons including from those in regions of the *global workspace* (Shepherd, 1994). The widespread decrease of baseline activity by anesthesia reflects a decrease in global activity, while the similar low baseline activity in the sensory cortex shows low input from the global workspace in the absence of peripheral stimulation. Outside the somatosensory cortex the brain remains at the low anesthetized level of activity during stimulation. Therefore input from the *global workspace* to the sensory cortex, should be reduced during stimulation in the anesthetized state compared to the non-anesthetized state. Consequently the high neuronal activity observed in the anesthetized somatosensory cortex during stimulation presumably is caused primarily by sensory input. This interpretation is supported by the almost identical histograms of neuronal firing in the stimulated state at both levels of anesthesia (Smith *et al.*, 2002; Shulman *et al.*, 2003). By placing the electrodes in layer 4 of the somatosensory cortex the responses are weighted heavily towards the sensory input arriving via thalamo-cortical axons. The nearly identical histograms at two levels of rather deep anesthesia are in accord therefore, with expectations that the neuronal population is responding primarily to the sensory stimulation. The entire population of neurons selected

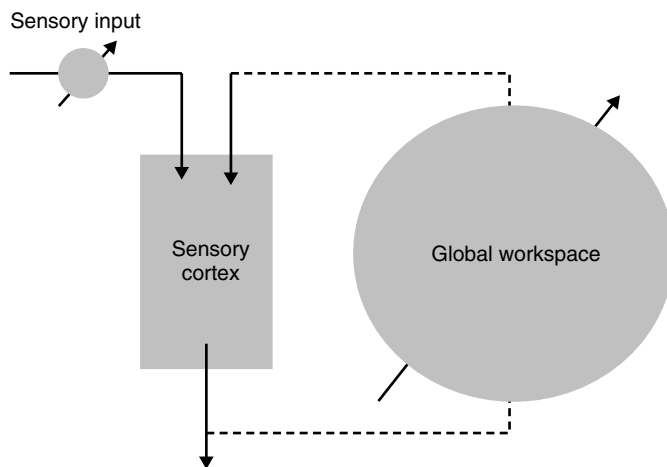


**Figure 16.4.** Schematic confluence of local and global firings in the sensory cortex.

responds to the stimulus in a fixed way at these deep levels of anesthesia where there is essentially no input from the global workspace. Early results from lighter levels of anesthesia, halothane, do not give the same histogram of firing (Hyder, personal communication). These results are consistent with a very specific neuronal deployment responding to sensory stimulation and suggest that the firing pattern is a response to some integration of inputs from sensory and global firing. The nature of this integration, and the assessment of the components, can be examined by varying the experimental parameters of (1) amplitude of stimulus, (2) global activity and (3) somatosensory cortical layer probed. These opportunities encourage us to expect progress in understanding some aspects of the interaction between the objective sensory task and the intrinsically subjective global interactions. In these assignments of total energetics and activities, the experiments described in this paper can provide quantitative measures to help separate contributions from local and global responses.

## 16.7. NEUROSCIENTIFIC MEASURES OF BASELINE ACTIVITIES

Differencing methods in functional imaging are consistent with psychological views of brain in which undefined baseline activities can be neglected. The differencing methods proving so useful in functional imaging, both fMRI and PET, have obtained results that are fitted comfortably into psychologies that neglect baseline activity and have thereby strengthened their objectifying concepts of brain activity. However, the ranks of psychologists and brain scientists with more inclusive views of brain, have also been swelling recently. These researchers are of the opinion that cognition considers only a small fraction of brain activity. The high level of brain activity in the absence of any conscious stimulus shown by our results is consistent with those psychologies which include these kinds of activity.

Gerald Edelman has written and experimented extensively in support of his views of the brain–mind relationship. In a brilliant, scholarly postscript he has criticized views that claim mind can be fully described by the representations of cognitive psychology. Framed by his view that cognitive psychologists have disregarded ‘a large body of evidence that undermines the view that the brain is a kind of computer’, he has delineated the nature of interactions between neurons, which he characterizes as re-entrant pathways. Without summarizing his broad studies we only note that the magnitude of baseline activities which we measure and attribute, in large part, to subjective experiencing would accommodate the continuous deep neuronal interactions that Edelman has proposed (Edelman, 1992).

Damasio in a series of books (Damasio, 1999) has also concluded that cognition must be considered as only part of the far reaches of the brain that includes emotions and extends to interactions with the body that are inseparable from brain activities. It is also clear that criticisms claiming Freud's work has been contradicted by modern brain research in cognitive neuroscience (Kitcher, 1995) are not supported by our findings. Rather, Freud's work, based upon the existence of high levels of brain activity, operating dynamically with much of it unconscious, would be consistent with our high baseline activities in contrast to more recent theories where subjective activity is discounted.

In addition to these claims for broader views of brain including, in some guise or other, high unstimulated brain activities, several neuroscientists have developed models of brain activity from observed baseline activities that are consistent with the high activities we have quantitatively measured. The need for substantial unfocussed neuronal activity for the service of even sensory responses was suggested by the brilliant experiment of Grinvald and colleagues (Tsodyks *et al.*, 1999). Starting with the recognition that 'cortical neurons are spontaneously active in the absence of external input even in primary sensory areas,' they studied the correlations between single-unit recordings and real-time optical imaging. While interpreting their data, they concluded by suggesting that 'in the absence of stimulation the cortical network wanders through various states represented by coherent firing of different neuronal assemblies' and that a stimulus pushes the network into a particular activated assembly. Analogously, the elegant temporal synchronization of neuronal responses on which Singer's conclusion are based has led to the conclusion, 'Of the many responses of VI those that become synchronized best will be particularly effective in influencing neurons in higher areas (Singer, 1994).' This hypothesis recognizes the large neuronal activity in the absence of stimulation and includes that activity in proposals about brain function.

In a similar vein also emphasizing the importance of neuronal oscillations, Llinas (2002) starts from the view, 'that nervous system function may actually operate on its own, intrinsically, and that sensory input modulates rather than informs this intrinsic system'. The interaction between sensory cues and the high existing brain activity allows a larger view of brain function. In contrast to localized computer-like modules, Llinas has proposed that synchronized firing of thalamo-cortical connections form the content of a highly active brain and play an important role in defining the subjective self. Our  $^{13}\text{C}$  NMR results, measuring high baseline activities can provide a basis for the assumptions made by these other brain studies, and offer a measure of their magnitudes.

## 16.8. NEED FOR PHILOSOPHY

We have touched upon differences between the interpretation of functional imaging experiments in terms of cognitive psychology and the interpretations of the same experiments to explore the neuronal activities responsible for the signals. While these extremely different approaches are readily recognized as reflecting different perspectives, less dissimilar scientific positions also differ more than are commonly recognized. In neuroscience, different subfields of science provide methods and approaches that require different starting assumptions and seek different types of understanding. In order to distinguish these diverse approaches it is necessary to examine their origins closely to see what their results mean, and upon what assumptions they depend. In contrast to many physicists who find no need for philosophy in a science where epistemological methods and metaphysical assumptions are generally accepted, in neuroscience philosophical analysis is necessary in order to distinguish the differing basis of starting assumptions, methodology, and epistemological goals.

Our separation of brain activities into a differencing activity and a baseline or total activity, where the former arises from a cognitive task and the latter from wide unspecified internal brain connections, finds a parallel in David Chalmers' philosophical analysis of brain activity or consciousness. Chalmers has suggested that consciousness could profitably be divided into 'easy' and 'hard' problems (Chalmers, 1996). Easy problems would be those that can be addressed objectively, such as the studies of sensory or cognitive

tasks which are evaluated in functional imaging experiments by the difference signal. Hard problems that would help to explain subjective experience, he suggests are beyond our present ability to formulate. These subjective experiences, we suggest, are expressed in the totality of neuronal activity, whose connections, at present, cannot be formulated in causal terms. We propose that the present approach, which does not claim to explain subjectivity, still does offer an experimental entry for exploring these unknown areas of subjective brain activity, and for measuring their magnitude.

Can philosophers not only help us to understand what scientists are doing but also provide useful advice? Chalmers has suggested that scientists might do well to look for an understanding of the hard problem by starting with cognitive studies of related qualities such as awareness. He says (Chalmers, 1996), 'consciousness and cognition do not float free of one another but cohere in an intimate way'. This direction has been followed by many respected cognitive scientists. Starting with difference signals, they have looked for interactions between the signals found from the effects in the visual response of attention being paid to nearby stimuli (Kastner *et al.*, 1998) while others have taken correlations between difference signals in different brain regions (Friston, 2002). These attempts to extend the meaningfulness of fMRI beyond the objective assumptions of cognitive psychology are in accord with Chalmers' suggestion that cognitive conceptualizations can provide a good starting point for studying related subjectivities. But we have chosen a different direction to study the 'hard' problem, a direction which starts with hard, reliable assumptions based on physical knowledge. We have measured the relationship between energy consumption and the activity of local and distributed neurons. Our starting points have been quantitative and unambiguous and the questions they ask have been answered with 'hard' data. From the secure position these results have generated, we have proposed to advance slowly, but sure-footedly, towards the exploration of previously inaccessible neuronal functions.

Thomas Nagel (1986) has focussed philosophical studies upon 'how to combine the perspective of a single person with an objective view of that same world.' Because of the pervasiveness of the two different views any reconciliation or accommodation would form the core of a worldview. He disavows the aim of unification being unwilling to settle for its simplifications, and he prefers the perplexities generated by a frontal juxtaposition of subjective and objective. If developed separately into a worldview he discusses how each would suffer from incompleteness. He claims, for example, that existing objective studies must leave the subjective human perspective behind. Physics, he continues, where we have achieved 'our greatest detachment from a specifically human perspective' for that reason 'is bound to leave undescribed the irreducible subjective character of conscious mental processes'.

This limitation has been countered by many and most directly by John Searle (1982) who argued that just because the mind is intrinsically or ontologically subjective does not mean that objective study is incapable of understanding its subjectivity. Difficult and complicated but not impossible. Nagel brings us close to the present scientific problem when he suggests that the modern acceptance of physicalist reduction has not been the answer since 'a less impoverished and reductive idea of objectivity has not been available' to provide the understanding he seeks.

This brings us to the present study. We do not, of course, find physics a burden to understanding but quite the opposite, it is the very basis we are celebrating. In agreement with Searle we find the early steps in the road the most challenging and feel that, as described above, we are on a path towards some objective measures of subjectivity. How far it will go we have no idea. But if we wish to compare the present state of neuroscientists with a similar moment in history we could do worse than to reflect upon the Scientific Revolution of the 17th century. To provide a perspective on the varieties of options available for modern neuroscientific research we select a few features of the innovations introduced by Renee Descartes in the early years of modern physical science. Those issues focussed the state of physical science during the Scientific Revolution of the 17th century. With its exciting hopes for future understanding, and with

its nascent methodologies Descartes's time has many similarities with the conditions prevailing in today's neuroscience. Changing methods went hand in hand with philosophical re-evaluations to give birth to physical science. Descartes, whose life spanned the first half of the century played a pivotal role in the transition from the older ways of scholasticism, where novelty was expressly forbidden, to the empirically testable hypotheses of modern science. In 1637 Descartes published his *Discourse on the Method of Properly Conducting One's Reason and of Seeking the Truth in the Sciences* (Descartes, 1637), which started with his disappointment, in finding after much study, 'that there was no body of knowledge in the world such as I had been led previously to believe existed'. Philosophy was useless since it contained nothing that was not still in dispute. 'As for the other sciences, in so far as they borrow their principles from philosophy, I consider that nothing solid could have been built on such shifting foundations'. He thereby abandoned two millennia of Aristotelian science, incorporated into theology as Scholasticism, and risked being condemned for heresy, as Galileo had suffered 4 years earlier.

In this skeptical state, Descartes confidently resolved to ignore available knowledge completely and to start fresh. He proposed rules for arriving at knowledge. The method started by assuming that which is 'clear and distinct' and the questions raised by this individualistic vision are then reduced, by Descartes' method, to their components so as to understand the original whole. Attention is more usually paid to Descartes' method of analysis, which was, in fact his subject, and particularly to its concluding dualism, which bears directly upon neuroscience. However, we suggest that those particular consequences of Descartes' method are of minor interest for the modern neuroscientist, who generally uses both Descartes' methods and assumes that physical studies of brain will help to explain features of mind. Instead we wish to emphasize the revolutionary nature of his starting assumptions, which opened the way for modern physical science, and provide the kind of fresh start which, we suggest, we need in neuroscience today.

In rejecting the existing scholastic view of nature, Descartes introduced a scientific worldview that became the method of physical science. [The rapid replacement of 'clear and distinct' by modern scientific hypothesis, susceptible to empirical disproof has been traced by many (see Clarke, 1992)].

Neuroscience has been created in the expectation that scientific methods can help to explain the qualities of mind, thereby extending the successes of physical science. We are not at a loss for the methods of analysis and experimentation, but in seeking scientific approaches we are struggling with conflicting starting assumptions. As summarized above, while studies of the brain-mind problem start from the objectivity of physical science, they must include subjectivity, which has been the purview of literature, psychology and other characteristically human concerns. Existing physical science does not provide a worldview that includes these opposites. We have not found the answer, but we feel that by quantitatively measuring the extent of brain activity that supports subjectivity, we are measuring the existence and magnitude of a physical parameter that is devoted to the complexities of subjective experience whose fine structure cannot be presently separated.

By considering that the brain is subject to the physical laws concerning energy and work, our assumptions are that the brain-mind is not different from any other material and that subjectivity is an intrinsic property of brain that cannot be neglected but whose magnitude can be explored objectively. We hope that an empirical research program based upon this intrinsic view of matter will make progress, and that, as empirical studies have expanded our physical understanding, firmly based physical studies of the organic matter that constitutes the body-brain-mind will continue to make novel understanding.

## REFERENCES

Alkire M.T. Quantitative EEG correlations with brain glucose metabolic rate during anesthesia in volunteers, *Anesthesiology* **89** (1998) 323–333.

Alkire M.T., Haier R.G., Fallon J.H. Toward a unified theory of narcosis: brain imaging evidence for a thalamocortical switch as the neurophysiologic basis of anesthesia-induced unconsciousness, *Conscious Cogn* **9** (2000) 370–386.

Braitenberg V., Schuz A. *Anatomy of the Cortex: Statistics and Geometry*, Springer, Berlin, 1991.

Chalmers D. Facing up to the problem of consciousness. In *Toward a Science of Consciousness, The First Tucson Discussions and Debates*, Ed. Hameroff S.R., Kazniak A.W. and Scott A.C. 1996 pp. 5–28.

Changeux J.P. *Neuronal man: The Biology of Mind*, translated by Garcy L., Princeton University Press, Princeton, NJ, 1985.

Chapin J.K., Nicolelis M.A. Principal component analysis of neuronal ensemble activity reveals multidimensional somatosensory representations, *J Neurosci Methods* **94** (1999) 121–140.

Clarke D.M. *The Cambridge Companion to Descartes*, Ed. Cottingham J., Cambridge University Press, Cambridge, 1992, pp. 258–285.

Crick F.H.C. *The Astonishing Hypothesis: The Scientific Search for the Soul*, Touchstone Books, New York, 1991.

Damasio A. *The Feeling of What Happens*, Harcourt Brace, New York, 1999.

Dehaene S., Kerszberg M., Changeux J.P. A neuronal model of a global workspace in effortful cognitive tasks, *Proc Natl Acad Sci USA* **95** (1998) 14529–14534.

Dehaene S. *The Cognitive Neuroscience of Consciousness*, Ed. Dehaene S., MIT Press, Cambridge, MA, 2001.

Descartes, R. (1637) *Discourse on Method*

Edelman G.M. *Bright Air, brilliant Fire: On the Matter of the Mind*, Basic Books, New York, 1992. p. 14.

Fodor J. *The Mind Doesn't Work that Way: The Scope and Limits of Computational Psychology*, A Bradford Book, MIT Press Cambridge, MA, 2000.

Friston K. Functional integration and inference in the brain, *Prog Neurobiol* **68** (2002) 113–143.

Gusnard D.A., Raichle M.E. Searching for a baseline: functional imaging and the resting human brain, *Nat Rev Neurosci* **2** (2001) 685–694.

Heinke W., Schwarzbauer C. *in vivo* imaging of anesthetic action in humans: approaches with positron emission tomography (PET) and functional magnetic resonance imaging (fMRI), *Br J Anaesth* **89** (2002) 112–122.

Hyder F., Rothman D.L., Mason G.F., Rangarajan A., Behar K.L., Shulman R.G. Oxidative glucose metabolism in rat brain during single forepaw stimulation: a spatially localized  $^1\text{H}$ [ $^{13}\text{C}$ ]NMR study, *J Cereb Blood Flow Metab* **17** (1997) 1040–1047.

Hyder F., Rothman D.L., Shulman R.G. Total neuroenergetics support localized brain activity: Implications for the interpretation of fMRI, *Proc Natl Acad Sci USA* **99** (2002) 10771–10776.

Kandel E.R., Schwartz Z.J.H., Jessell T.M. *Principles of Neural Science*, Appleton & Lange, Norwalk, CT, 1991.

Kastner S., Deweerd P., Desimone R., Ungerleider L.G. Mechanisms of directed attention in the human extrastriate cortex as revealed by functional MRI, *Science* **282** (1998) 108–111.

Kitcher P. *Freud's Dream*, MIT Press, Cambridge, MA, 1992.

Kristan Jr W.B., Shaw B.K. Population coding and behavioral choice, *Curr Opin Neurobiol* **7** (1997) 826–831.

Lebon V., Petersen K.F., Cline G.W., Shen J., Mason G.F., Dufour S., Behar K.L., Shulman G.I., Rothman D.L. Astroglial contribution to brain energy metabolism in humans revealed by  $^{13}\text{C}$  nuclear magnetic resonance spectroscopy: Elucidation of the dominant pathway for neurotransmitter glutamate repletion and measurement of astrocytic oxidative metabolism, *J Neurosci* **22** (2001) 1523–1531.

Llinas R.R. “*I of the Vortex*” *From Neurons to Self*, MIT Press, Cambridge, MA, 2002.

Magistris P., Pellerin L., Rothman D.L., Shulman R.G. Perspective: neuroscience “energy on demand”, *Science* **283** (1999) 496–497.

McNeil, P.G. *New York Times*, July 29, 2003, p. F1.

Nagel T. *The View from Nowhere*, Oxford University Press, Oxford, 1986.

Pellerin L., Magistretti P.J. Glutamate uptake into astrocytes stimulates aerobic glycolysis: a mechanism coupling neuronal activity to glucose utilization, *Proc Natl Acad Sci USA* **91** (1994) 10625–10629.

Posner M.I., Raichle M.E. The neuroimaging of human brain function, *Proc Natl Acad Sci USA* **95** (1998) 763–764.

Rothman D.L., Hyder F., Sibson N., Behar K.L., Mason G.F., Shen J., Petroff O.A.C., Shulman R.G. *in vivo* magnetic resonance spectroscopy studies of the glutamate and GABA neurotransmitter cycles and functional neuroenergetics. In *Neuropsychopharmacology: The Fifth Generation of Progress*, Eds Davis K.L., Charney D., Coyle J.T., Nemeroff C., Lippincott Williams & Wilkins, Philadelphia, PA, 2002, Chapter 25, pp. 315–342.

Rothman D.L., Sibson N.R., Hyder F., Shen J., Behar K.L., Shulman R.G. *in vivo* nuclear magnetic resonance spectroscopy studies of the relationship between the glutamate–glutamine neurotransmitter cycle and functional neuroenergetics, *Phil Trans R Soc London Ser B* **354** (1999) 1165–1177.

Scannell J.W., Young M.P. Neuronal population activity and functional imaging, *Proc R Soc London, Ser B* **266** (1999) 875–881.

Searle J. *The Rediscovery of the Mind*, MIT Press, Cambridge, MA, 1992.

Shen J., Petersen K.F., Behar K.L., Brown P., Nixon T.W., Mason G.F., Petroff O.A.C., Shulman G.I., Shulman R.G. Determination of the rate of the glutamate–glutamine cycle in the human brain by *in vivo*  $^{13}\text{C}$  NMR, *Proc Natl Acad Sci USA* **96** (1999) 8235–8240.

Shepherd G.M. *The Synaptic Organization of the Brain*, Oxford University Press, New York, 1994.

Shulman R.G. Interview with Robert G. Shulman, *J Cong Neurosci* **8** (1996) 474–480.

Shulman R.G., Hyder F., Rothman D.L. Biophysical basis of brain activity: implications for imaging, *Q Rev Biophys* **35** (2002) 287–325.

Shulman R.G., Hyder F., Rothman D.L. Cerebral metabolism and consciousness, *CR Biol* (2003) in press.

Shulman R.G., Rothman D.L. Interpreting functional imaging studies in terms of neurotransmitter cycling, *Proc Natl Acad Sci USA* **95** (1998) 11993–11998.

Shulman R.G., Rothman D.L., Hyder F. Stimulated changes in localized cerebral energy consumption under anesthesia, *Proc Natl Acad Sci USA* **96** (1999) 3245–3250.

Sibson N.R., Dhankhar A., Mason G.F., Rothman D.L., Behar K.L., Shulman R.G. Stoichiometric coupling of brain glucose metabolism and glutamatergic neuronal activity, *Proc Natl Acad Sci USA* **95** (1998) 316–321.

Sibson N.R., Dhankhar A., Mason G.F., Behar K.L., Rothman D.L., Shulman R.G. *In vivo*  $^{13}\text{C}$  NMR measurements of cerebral glutamine synthesis as evidence for glutamate–glutamine cycling, *Proc Natl Acad Sci USA* **94** (1997) 2699–2704.

Singer W. Putative functions of temporal correlations in neocortical processing. In *Large-scale Neuronal Theories of the Brain*, Ed. Koch C., Davis J.L., MIT Press, Cambridge, MA, 1994, pp. 201–238.

Smith A.J., Blumenfeld H., Behar K.L., Rothman D.L., Shulman R.G., Hyder F. Cerebral energetics and spiking frequency: The neurophysiological basis of fMRI, *Proc Natl Acad Sci USA* **99**(16) (2002) 10765–10770.

Tsodyks M., Kenet T., Grinvald A., Arieli A. Linking spontaneous activity of single cortical neurons and the underlying functional architecture, *Science* **286** (1999) 1943–1946.

Ueki M., Linn F., Hossman K.A. Functional activation of cerebral blood flow and metabolism and after global ischemia of rat brain, *J Cereb Blood Flow Metab*, **8** (1988) 486–494.

Ueki M., Mies G., Hossmann K.A. Effect of  $\alpha$ -chloralose, halothane, pentobarbital and nitrous oxide anesthesia on metabolic coupling in somatosensory cortex of rat, *Acta Anaesthesiol Scand* **36** (1992) 318–322.

Zeman A. Consciousness, *Brain* **24** (2001) 1263–1289.



# The Role of the NMR Baseline Signal in the Study of Consciousness: the Restless Brain

**Robert G. Shulman**

*Yale University School of Medicine, MR Center, P.O. Box 208043, New Haven, CT 06520-8043, USA*

The research directions summarized in this book have converged to create an understanding of the brain's baseline activity. Baseline is the awake activity that goes on in the absence of objective stimulation. When we require a subject to do a task involving memory or perception or understanding, any change in activity measured is relative to the activity that goes on in the brain in the absence of such stimulation. Two scientific directions, MRS and the calibrated fMRI data accompanied by spiking activity, provide a scientific understanding of the baseline which has consequences for activity of brain and mind. The results describe a high amount of brain activity in the absence of external stimulation. As shown in Chapters 5 and 10, the baseline activity is decreased with depth of anesthesia as the amount of energy consumed and the neuronal firing rates decrease. From the MRS experiments this activity accounts for the majority of the energy consumption of the brain. The brain in this sense is very efficient, making good use of its energy consumption for its function, namely to fire neurons and to handle information. We have named the brain exhibiting this baseline activity the restless brain.

The second important attribute of baseline activity, shown in Chapter 5 and extended in Chapter 10, is that high baseline activity is needed for the performance of a task. During stimulation of the animal from two different levels of anesthesia the energy consumed and the neuronal firing rate reached the same total levels during stimulation regardless of the depth of anesthesia. Hence the total activity, of the order of the resting baseline activity, is needed for the animal to respond to a sensory stimulus. Not only is the baseline activity high but a similar level of high activity is needed for the animal to respond to a stimulation.

Psychological concepts, particularly from cognitive neuroscience, have played a major role in the formulation and interpretation of functional imaging experiments. The major operative concept for image interpretation is that the functional localization of the brain can be mapped based upon regional changes in brain activity. The many images obtained have been considered affirmation of the valuable nature of the starting hypothesis. However, as indicated in Chapter 10, a different approach to functional imaging

experiments is suggested by our present understanding of baseline activity. First the baseline contains valuable information which is ignored or discarded in a functional imaging differencing experiment. Second the baseline activity which is discarded is of the same nature – namely neuronal – as all the increments which are retained. Third the difference signal in a functional imaging experiment represents not the energy needed for the brain to perform a task but the difference in energy and activity between the conditions of that task and the baseline. The magnitude of this difference is not the magnitude of the brain activity needed to perform the task. Finally the localization of energy differences in a BOLD signal does represent a difference in brain activity between the baseline and stimulated conditions. Therefore, as so many functional imaging experiments have found, localization of a change is indicative of the participation of that brain region in the task. However, the absence of a change does not mean the region is not participating in the function. Differences of incremental signals in different regions of the brain do not measure their relative degree of participation in the task at hand. A larger incremental signal does not indicate a larger degree of activity being required for the task when the baselines may differ. In experiments starting from the same baseline magnitude differences do have meaning, but the role of total regional energy cannot be neglected.

These findings logically need to lead to a re-evaluation of functional imaging experiments. Two chapters in the book have surveyed recent functional imaging experiments in the context of the other chapters of this book. In Chapter 14, Meltzer and Constable have surveyed the literature on declarative memory systems. Meltzer and Constable provide an updated search of experimental and conceptual studies of long-term declarative (LTD) memory – focused on the role of the hippocampus as found by functional imaging. The early fMRI studies failed to see incremental signals in that regional although the necessity of hippocampal function for LTD had been established by lesion studies. The authors acknowledge that a high baseline activity which did not increase significantly would explain these results, an explanation quite consistent with the proposals in Chapter 16. Subsequent enrichments of the episodic declarative memory tasks in several ways such as by novelty and by the success of encoding did show incremental fMRI signals. A search to find a unifying concept to conceptualize the incidental but often necessary additional task components was not successful in cognitive terms.

Another example of where the standard functional imaging paradigm has led to paradoxical results, in which baseline activity is neglected, has been the reports of negative fMRI (and PET) difference signals during tasks. Negative signals were considered paradoxical because the activity during a task was implicitly assumed to be many fold higher than baseline. Our finding of a high baseline activity provided the obvious explanation of this phenomenon that had puzzled many. Gusnard and Raichle have recently explained the high baseline activity leading to negative signals using standard cognitive psychological concepts. Their explanation of the baseline activity is that it is caused by specific mental functions, related to awareness. In this way they have assumed an objective understanding both of the baseline condition and of the stimulated condition. On the other hand, we have offered a quite different explanation of the negative signals and of the high baseline activity. When a subject, in the magnet with eyes closed and the ears plugged, has no input from the experimentalist she is in a state that can only be described in subjective terms. We do not know by any objective criteria what that subject is thinking at that time. We prefer to lump all baseline activity together as not being objectively knowable for these reasons.

In Chapter 15 Bruce Wexler has taken a broad view of functional imaging not only with respect to the recommendations of this book but also from the viewpoint of a practitioner who has reservations about some of the concepts being followed. His view is that there are limitations of the methods, which come not specifically from the neglect of baseline, nor from the use of differencing, but which come from the very nature of the objective knowledge being sought. To what extent, he asks, is the concept of localized brain activities really experimentally valid? He readily accepts the prevailing view that there are necessary interactions between regions that form a thought or a response, but he enquires about the experimental

nature of the localization. Is the idea of localized function actually driving data interpretation, and possibly leading to unsubstantiated claims. Furthermore he goes on to examine the meaningfulness of brain responses in view of the changing brain activities with time, e.g. the time of the experiment, the conditions of the subject at the time, the changes within the subject in short times, with familiarity of the protocols, and the contents. Furthermore subjects also change with time, with growth, with aging, with development. All these considerations lead to an acknowledgement of the complexity of brain function which is consistent with the argument, made in Chapter 15 that we should be less confident of our psychological starting points for brain studies.

The high baseline activity in the absence of stimulation and its requirements during stimulation have great consequences for an understanding of the brain–mind relationship. The relation of brain and mind is the traditional subject of psychology. It is our contention that these neuroscientific measurements of baseline provide constraints for what a proper approach to psychology should be. In looking for explanations of the higher activities of brain–mind from scientific results the most successful ventures in the past have shown how particular activities, considered to be those of mind, can be explained scientifically. The results of neurotransmitter receptor agonists, the consequences of hormonal release and the suggested explanations of long-term potentiation are but a few of the many scientific results that have been shown to have a bearing on the more complex activities of mind. However, this aspect of our approach is more metaphysical and directed to the level of what a valid explanation would be rather than to specific features of brain activity. We have proposed that scientific results require a proper framework for the study of mind, and that this framework should acknowledge the importance of subjectivity at the outset of the experiments, such subjectivity being supported by the high, unassigned brain activity measured at baseline.

A clear separation between the subjective and object of aspects of brain–mind was made by Francis Crick in his book *The Astonishing Hypothesis*, which reinvigorated the scientific investigation of consciousness. Crick proposed that we should study the brain objectively and postpone any considerations of the subjective, which he lumped as Qualia. This reasonable traditional scientific approach, of selecting parameters, has been followed by many psychologies. However, it is our position that ignoring subjective aspects of brain–mind activity is first of all misleading as a beginning and second, in light of our present scientific results, is no longer necessary. It would take us too far afield at this point to categorize different psychological approaches by their attitude towards objective/subjective. We have found that, as a working hypothesis, the concept of a global workspace to include subjective experiencing is extremely useful. Chapter 10 indicates how future experiments can continue to explore particular aspects of subjectivity in a quantitative neuroscientific fashion.

At present these different assumptions about the nature of baseline activity are a matter of opinion. It is perfectly valid, as represented by Crick's stand and by Gusnard and Raichle's approach, to expect that unexplained areas of brain will be explained successfully by objective hypotheses that can be proposed now and be tested. However, the ability to explore and to measure the contents of resting baseline activity without postulates as to the specific meaning of their contents is a promising approach not previously available. NMR makes it possible to begin exploring these unknown areas without postulating in advance what they may be. Rather we can now measure their magnitudes and the pathways they follow, e.g., cortical thalamic pathway versus cortical, and see if by these explorations of the unknown areas of brain activity we can come to unexpected exploratory hypothesis. In this way hypotheses will be guided more by the neuroscientific findings than by the psychological concept of how the brain works.

Zeman in a recent review concluded that consciousness is generally used in two ways. In one it is used as synonymous with awareness. A person is aware of bright lights, of noises and these enter into one's performance of other activities. This is an objective aspect of awareness and an objective aspect of consciousness and the word is often used in this meaning. The second meaning of consciousness is

of subjective experiencing. This would include for example the inputs that the body is experiencing at any time but where the response of the body is below the level of conscious awareness. This is, in these respects, the unconscious aspect of consciousness. We propose that the total baseline activity supports both these aspects of consciousness. This is illustrated in Chapter 10 where Hyder and Blumenfeld present a neuronal response in the somatosensory cortex to a forepaw stimulation in the rat. The response at deep anesthesia, where only the sensory input is acknowledged by the neuronal firing pattern, contrasts with the response at lighter anesthesia where additional input from the global workspace is seen. In these experiments, as described in Chapter 10, many empirical parameters can be varied in order to explore the interplay of conscious sensory input and the more global subjective response of the animal. In human experiments, the results of anesthesia show that at the point of nonresponsiveness, corresponding to the loss of consciousness, the human brain energy consumption has decreased by about 50 %. In the rat, of course, we do not have the subjective accounting that the anesthesiologist relies upon for the description of consciousness. However, anesthesia is used in the rat for the same reason that it is used in humans, namely to protect the animals from being conscious of pain. The dependence of subjective response upon the level of baseline activity allows the neuroscientific results to be extended into psychological considerations. These approaches provide an experimental opportunity to study the over-reaching interactions of brain and mind.

# Index

3D imaging, CMRO<sub>2</sub> 139–141, 143  
acetate 79, 87  
action potentials  
  biochemical mechanisms 17, 174, 175  
  cortical metabolic rate 112, 113  
  energy metabolism relationship 17–19, 27–28  
  glucose utilization relationship 16–17  
  grey matter propagation cost 115–116  
  spiking frequency 179–184, 186–187  
activation maps 189  
adenosine triphosphate (ATP)  
  energy consumption distribution between signalling mechanisms 116–117  
  glutaminergic synapse metabolic cost 114  
  ion pumps 17, 19  
  phosphorus NMR measurement 37  
  total resting consumption 113  
age effects on brain activation 288  
alcoholism 246–247  
Alzheimer's disease 128  
ammonia 83–84, 88  
amnesia 263, 270  
anaplerosis 79, 82, 83  
anesthesia  
  brain activity effects 302  
  CMRO<sub>2</sub> and spiking frequency 179–184  
  glucose utilization effects 15  
  neurotransmission effects 298  
  stimulation response effects 179–184, 284, 301–302  
astrocytes  
  cerebral energy metabolism 78–81  
  functional activity–energy metabolism relationship 24, 28  
  glutamate effects on glucose utilization 25–27  
  glutamate–glutamine cycle 55, 81–93  
astroglia (macroglia) 217–227  
ATP *see* adenosine triphosphate  
attention shifting 289–291

autoradiography 13–14, 18  
awareness/consciousness relationship 313  
  
baseline neuronal activity  
  consciousness 311–314  
  functional imaging 174, 188, 191–192  
  importance 304–305, 312  
  stimulus induced incremental activity comparison 299–301  
blood oxygenation level dependent (BOLD) contrast  
  CMRO<sub>2</sub> and cerebral blood flow 127–128  
  event-related fMRI 164  
  fMRI biophysics 151–153  
  fMRI calibration 153–156  
  MRI neuroimaging 149–151, 260–261  
  physiological basis 122, 156–160  
brain cell types 54  
brain damage 263, 270, 284–285, 291  
brain function  
  baseline activity 301–307, 311–314  
  changing cognition relationship 285–291  
  incremental signals 301–302  
  localized/fixed models 280–285  
  oxidative metabolism role 126–128  
  subtraction study method 280–284  
brainwork 4–5, 185, 186–7, 190  
  
2-[<sup>14</sup>C] deoxyglucose 13–14, 18  
1-[<sup>13</sup>C] glucose NMR  
  compartment models 54–57, 68–69  
  data modeling 54–70  
  *in vivo* techniques 37–39  
  metabolic pools 57–60  
  model creation 60–62  
  model data fitting 62–66  
  MR information content 66–69

<sup>13</sup>C MRS  
 cerebral energy metabolism 76–81  
 CMRO<sub>2</sub> measurement 155–156  
 glucose oxidation 297  
 glutamate–glutamine cycle 83–89  
 intravenous catheters 249–250  
 neurotransmission energy requirements 89–93  
 neurotransmitter systems 297–298  
 psychiatric disorders 247–250  
<sup>13</sup>C NMR 37–39, 49–50, 67, 100–107, 129  
 Ca<sup>2+</sup> sequestration 209–210  
 calibrated fMRI *see* functional magnetic resonance imaging  
 CBF *see* cerebral blood flow  
 cell bodies 20–21  
 cell types 54  
 cerebral blood flow (CBF)  
   early *in vivo* metabolism studies xi, 12–13  
   imaging cerebral metabolic rate of oxygen consumption 127, 137–138, 139–141  
   imaging using magnetically labeled arterial blood water 155  
   positron emission tomography studies 162–164  
     relationship to CMRO<sub>2</sub> 148–149, 150, 159, 165, 176  
   cerebral blood volume (CBV) 128, 154–155  
   cerebral energy metabolism 75–93, 118–120  
   cerebral metabolic rate of glucose consumption (CMR<sub>glc</sub>) 13–17, 148, 162–163  
 cerebral metabolic rate of oxygen consumption (CMRO<sub>2</sub>)  
<sup>13</sup>C NMR approach 129  
 calibrated fMRI derived changes 147–165  
 cerebral blood flow relationship 176  
 change measurement 179–181  
 early *in vivo* metabolism studies xi, 12–13  
 imaging using <sup>17</sup>O NMR approach at ultrahigh field 125–143  
 neuronal activity relationship 173–192, 260–262  
 positron emission tomography studies 128–129, 162–164  
 relationship to cerebral blood flow 148–149, 150, 159, 165  
 relationship to CMR<sub>glc</sub> 148  
   spiking frequency relationship 181–184  
 chemical shift data 35, 36, 39  
 CHEmical Shift Selective (CHESS) 43  
 childhood epilepsy 204, 209, 227  
 children 204, 209, 227, 288  
 chloralose anesthesia 179–184  
 choline 198, 199, 200  
 clinical MRI applications 7–8

CMR<sub>glc</sub> *see* cerebral metabolic rate of glucose consumption  
 CMRO<sub>2</sub> *see* cerebral metabolic rate of oxygen consumption  
 cognitive neuroscience 189–190  
 cognitive processes  
   brain structure/function relationship 280–292  
   deep versus shallow tasks 265–266  
   fMRI interpretation 262  
     long term memory 259–277  
   cognitive psychology, criticism 304–305  
   cognitive subtraction approach 280–284  
   coils, <sup>17</sup>O RF 132, 138–139, 142  
   combination pools 60  
   condition I *see* light anesthesia  
   condition II *see* deep anesthesia  
   consciousness  
     baseline activity 311–314  
     brain activity 299, 302–303  
     concept 302, 313–314  
     unconscious aspects 305, 314  
   consumption of energy 111–122, 283  
   correlation NMR spectroscopy *see* two-dimensional NMR spectroscopy  
   cortical depression 17–18  
   cortical excitability 228–230, 243–244  
   creatine 198, 199, 200–202  
   creatine kinase (CK) reaction 37

data deflection 67  
 data fitting  
<sup>13</sup>C NMR modeling 62–69  
 least-squares 62–63  
 numerical algorithms 63–64  
 scatter effects 64–66  
 declarative memory 262–264  
 deep anesthesia 179–184  
 deoxyglucose tracer molecule 5  
 deoxyhemoglobin 149, 151, 152  
 depolarization (Na<sup>+</sup> influx) 174  
 depressive disorder 245–246, 247–248  
 depth-of-processing effects 265–266, 267  
 Descartes, René 306–307  
 detoxification, ammonia 83–84  
 differencing methods  
   *see also* subtraction method  
   baseline neuronal activity 176, 189–190  
   drawbacks 311–312  
   functional image interpretation 304  
   negative signals 312  
   stimulation versus baseline 302

disease 126–128, 291  
*see also* brain damage; childhood epilepsy; epilepsy; psychiatric disorders

electrodes 177, 191  
electroencephalography (EEG) 177  
encoding in long term memory 264–269  
endocytosis 114  
energy consumption 111–122, 283  
energy metabolism 76–81  
epilepsy  
  astroglial metabolism 215–237  
  GABA role 227–232  
  glutamate metabolism 217–227  
  glutamate–glutamine cycle 219–220, 222–225  
  glutamine levels 225–226  
  healing process 204, 208–209  
  ketogenic diet 209  
  magnetic resonance spectroscopy 197–213, 215–237  
  astroglial metabolism 217–227  
  GABA role 227–232  
   $^1\text{H}$  techniques 198–204  
  *N*-acetyl aspartate/creatinine levels 198, 199–204, 208  
   $^{31}\text{P}$  techniques 198–204  
  tissue heterogeneity 199, 201–202, 205–208  
neuronal injury 202–204  
seizure foci localization 198–199  
seizure mechanisms 209–210, 232–233  
episodic memory 264–265, 271–272  
event-related fMRI 164  
exocytosis 114

familiarity, memory studies 271–272  
2-[ $^{18}\text{F}$ ]deoxy-D-glucose ( $^{18}\text{FDG}$ ) 14–15  
Fick's equation 134–135  
field potentials 174  
firing rate of grey matter 116, 121  
fixed brain structure/function relationship 280  
fluoroacetate 92  
fMRI *see* functional magnetic resonance imaging  
forepaw stimulation 179, 181, 185, 189  
Fourier transform NMR 32  
fuel sources, monocarboxylic acids 54  
functional magnetic resonance imaging (fMRI)  
  biophysics 151–153  
  BOLD signals 260–261  
  calibration methods 153–156  
  CMRO<sub>2</sub> change measurement 147–165, 180  
  development x–xii, 4

event-related 164, 266  
human 162–164  
interpretation 187–189, 299–301  
long term memory 259–277  
medial temporal lobe subdivisions 271–272  
memory encoding 264–265  
mind–brain studies 279–293, 299–301  
neural basis 161–162  
neural energy consumption 112, 121–122  
neuroimaging 149–151  
neurotransmission energy requirements 89  
physiological basis 156–160

GABA (gamma-aminobutyric acid)  
  catabolism 101, 102–103  
  cortical excitability 228–230  
  epilepsy role 216–217, 227–232  
  *in vivo* NMR studies 102, 106  
  neuronal localization 100–101  
  regulation 227–228  
  synthesis 102–104, 105–106  
GABA shunt 102–103  
GABA transporters (GATs) 104  
GABA–glutamine cycle  
   $^{13}\text{C}$  MRS 247–250  
  GABA neurotransmitter repletion 106  
  glial–neuronal interactions 240  
  glutamate/glutamine cycling 100, 101, 106  
   $^1\text{H}$  MRS 241–247, 249  
  psychiatric disorders 243–248  
GABAergic neurons 78–79, 81  
GABAergic tone 243–244  
GAD *see* glutamate decarboxylase  
gamma-aminobutyric acid *see* GABA  
GATs *see* GABA transporters  
GLAST (glutamate transporter) 92  
glial cells  
  *see also* astrocytes; astroglia  
  function 54, 55  
  glial-specific enzymes 78  
  neuronal interactions 240–250  
  proliferation in epilepsy 224–225, 226  
  resting potential 113  
  tumors 219  
global workspace 189, 303–304  
glucose  
  *see also* 1-[ $^{13}\text{C}$ ] glucose; 2-[ $^{13}\text{C}$ ] glucose;  
  2-[ $^{14}\text{C}$ ]deoxyglucose; 2-[ $^{18}\text{F}$ ]deoxy-D-glucose  
deoxyglucose tracer molecule 5  
isotopic precursors 76, 78, 85–87  
neurotransmission energy requirements 89, 90

glucose metabolism  
<sup>13</sup>C MRS measurements 76–78, 79  
<sup>13</sup>C NMR modeling 53–72  
 astrocytic oxidation 79  
 importance in brain metabolism 12–13  
 oxidative 126–128  
 psychiatric disorders 241  
 glucose utilization  
   action potential relationship 16–17, 27  
 glutamate effects in astrocytes 25–27  
   local measurement methods 13–17  
   neuronal inhibition 23  
 glutamate  
   *see also* glutamate–glutamine cycle  
   clearance rates, epilepsy 218–219  
   effects on glucose utilization in astrocytes 25–27  
   epilepsy mechanisms 216–227  
   extracellular levels in epilepsy 209–210, 217–227  
   GABA cycle in epilepsy 230–232  
   intracellular levels in epilepsy 221–222  
   neurometabolic coupling 91–92  
   recycling 113–114  
   release, epilepsy 218–219, 220  
 glutamate decarboxylase (GAD) 102, 103–104, 106  
 glutamate pools 78  
 glutamate transporter (GLAST) 92  
 glutamate–glutamine cycle  
   <sup>13</sup>C MRS 247–250  
   epilepsy 219–220, 222–225  
   GABA/glutamine cycling 100, 101, 106  
   glial–neuronal interactions 240  
   <sup>1</sup>H MRS 241–247, 249  
   modeling 54–57  
   MRS measurements 81–93  
   neurone–astrocyte interaction 297–298  
   one-compartment model 56  
   psychiatric disorders 243–248  
   quantitation 297–298  
   two-compartment model 55, 68–69  
 glutamatergic synapses 113–115  
 glutamine  
   *see also* glutamate–glutamine cycle  
   GABA cycle in epilepsy 230–232  
   GABA synthesis 106  
   intracellular levels in epilepsy 225–226  
   neurotransmission 78, 89–91  
   transporters 104–105  
 grey matter  
   <sup>1</sup>H MRS measurements 199–202  
   action potential propagation cost 115–116  
   cortical layers 178  
   energy consumption 112, 120–121  
   mean firing rate 116  
   metabolic rate 92  
<sup>1</sup>H MRS studies *see* proton MRS  
 hemoglobin 128, 134  
 heteronuclear spectral editing 49–50  
 hippocampal sclerosis *see* epilepsy  
 hippocampus 265, 266, 270–272, 273  
 homonuclear spectral editing 46–49  
 human animal comparison techniques x  
 hunger 289  
 Huntington's disease 128  
 hyperammonemia 79, 83–84  
 hyperpolarization (K<sup>+</sup> efflux) 174  
 hypothalamo-neurohypophyseal pathway 20, 22  
 implicit memory 262–264  
*in vivo* techniques  
   2-[<sup>14</sup>C]deoxyglucose 13–14, 18  
   cerebral blood sampling 12–13  
   development x–xii  
   2-[<sup>18</sup>F]deoxy-D-glucose 14–15  
   local glucose metabolism 13–17  
   NMR suitability 32, 33  
   incremental signals 259–277, 299–301  
   information processing 179  
   information representation 120–121  
   inhibition of neurons 23  
   inorganic phosphate 204–205  
   interactive processes 283  
   intracellular pH 37  
   intravenous catheters 249–250  
   ionic gradients 17–19, 27  
   isotope balance equations 60–61  
   isotopic labeling 12–15, 18, 53–72  
   isotopic precursors 76, 78, 79, 85–87  
   isotopomer analysis 61–62  
<sup>J</sup> scalar coupling constant 45–49  
 K<sup>+</sup> efflux 174  
 K<sup>+</sup> extracellular concentration 17, 19, 24–25  
 $\alpha$ -ketoglutarate ( $\alpha$ -KG) 84, 85, 86, 87, 102  
 Krebs cycle *see* tricarboxylic acid cycle  
 lamotrigine 162  
 language 280–281  
 lateralization 266, 288, 291

LCmodel signal quantification algorithm 43–45  
learning 286–288  
least-squares fitting 62–63  
'levels of processing' (Craik) 265–266, 267  
LFP *see* local field potentials  
light anesthesia 179–184  
local cerebral energy metabolism 13–17  
local field potentials (LFP) 177, 184  
localization 280–285, 301, 313  
long term memory (LTM)  
  anatomical dissociations 262–264  
  depth-of-processing relationship 266, 267  
  encoding and retrieval 264–269  
  incremental signals 259–277  
  medial temporal lobe subdivisions 269–272

macroglia *see* astroglia  
magnetic field homogeneity 40–42  
magnetic resonance imaging (MRI) 4, 32, 149–151, 198–199  
  *see also* functional magnetic resonance imaging  
magnetic resonance spectroscopy (MRS)  
  *see also*  $^{13}\text{C}$  MRS;  $^{15}\text{N}$  MRS; proton MRS  
  cerebral energetics and neurotransmitter fluxes 75–93  
  data modeling 54  
  development 32  
  epilepsy 215–237  
  epileptogenic tissue 198–213  
     $^1\text{H}$  techniques 198–204  
    interpretation 202–204, 208–209  
     $^{31}\text{P}$  techniques 204–209  
    sensitivity/selectivity 199–202, 205–208  
  importance xi–xii, 4  
magnetoencephalography (MEG) 177  
maintenance function (energy consumption) 120  
mass balance equations 60–61  
mean firing rate of grey matter 116, 121  
medial temporal lobe (MTL)  
  declarative memory role 263, 264–265  
  incidental versus deliberate memorizing 268  
  long term memory 260  
  memory encoding 264–268  
  memory retrieval 268–269  
  subdivisions 269–272  
MEG *see* magnetoencephalography  
memory  
  *see also* long term memory  
  cognitive processes 259–277  
  declarative 262–264  
  encoding 264–269

episodic 264–265, 271–272  
types 262–263, 264  
mental event representation 120–122  
metabolism  
  *see also* glucose metabolism  
   $^{13}\text{C}$  MRS measurements 76–81  
  glutamate release regulation of energy 91–92  
  importance ix–xii  
  rates modeling 59, 69–70  
metabolite pools  
   $^{13}\text{C}$  NMR modeling 57–60  
  brain cell types 54  
  NMR chemical shift data 35, 36, 39  
  NMR signal quantification techniques 43–45  
mind–brain relationship 8–9, 279–293, 295–309  
mitochondria  
  distribution and neural energy consumption 118, 119  
  dysfunction in epilepsy 204, 209–210, 232  
  metabolic  $\text{H}_2^{17}\text{O}$  135  
modeling analysis  
   $^{13}\text{C}$  NMR studies 53–72  
  constraints and simplification 61  
  data deflection 67  
  data fitting 62–69  
  isotopomer analysis 61–62  
  mass and isotope balance equations 60–61  
  metabolite pools 57–60  
  relevance ratio 67–68  
  sensitivity 67  
  target data 60  
monocarboxylic acids 54  
mood disorders 245–246, 247–248  
MRI *see* magnetic resonance imaging  
MRS *see* magnetic resonance spectroscopy  
MUA *see* multi-unit activity recording  
multi-compartmental models of metabolism 54, 55, 68–69  
multi-unit activity (MUA) recording 177, 184

$^{15}\text{N}$  MRS 88  
*N*-acetyl aspartate (NAA)  
   $^1\text{H}$  MRS measurements 198–204  
   $^{13}\text{C}$  MRS psychiatric disorder studies 247–249  
  epileptogenic tissue 198–199, 200  
   $^1\text{H}$  MRS psychiatric disorder studies 241–243  
 $\text{Na}^+$  influx, depolarization 174  
 $\text{Na}^+$  intracellular concentration 17, 19, 24–25  
NAA *see* *N*-acetyl aspartate (NAA)  
negative signals, high baseline relationship 312  
neocortex anatomy 178–179  
neural circuits 112, 122

neural energy consumption 111–122  
 neuroimaging  
*see also* functional magnetic resonance imaging  
 interpretability of signals 175–177  
 MRI 4, 32, 149–151, 247–248  
 physiology 148–149  
 neurons  
 activity  
   brain structure/function studies 283–284  
   energy requirement 283  
 inhibition 23  
 injury/*N*-acetyl aspartate level relationship 202–204  
 loss in epilepsy 224–225, 226  
 oxidative metabolism in epilepsy 210  
 resting potential 113  
 types 54  
 neuropil 20–21, 23, 24, 27–28  
 neuroscience approach 295–297  
 neurotransmitters  
   <sup>13</sup>C MRS flux measurements 81–89  
   energetic requirements 89–93  
   functional activity–energy metabolism relationship  
     19, 25–27, 28  
   glucose metabolism relationship 298  
   glutamate–glutamine flux studies 6–7  
   psychiatric disorders 239–251  
     recycling 113–114  
 neurovascular coupling 148–149  
 nitrous oxide method 12–13  
 NMR *see* nuclear magnetic resonance  
 novelty 265, 267, 268  
 nuclear magnetic resonance (NMR)  
*see also* 1-<sup>13</sup>C glucose NMR  
<sup>13</sup>C techniques 37–39  
 GABA neurotransmitter pathways 100–107  
 heteronuclear spectral editing 49–50  
 homonuclear spectral editing 46–49  
 importance ix–xii, 3–4  
*in vivo* techniques 33–50  
 phosphorus techniques 34–37  
 proton techniques 33–34, 35  
 pulsed 32  
 scalar coupling 45–46, 47  
 shimming techniques 40–42  
 signal quantification techniques 43–45  
 spatial localization techniques 39–40  
 spectral editing techniques 45–50  
 technique development 31–33  
 two-dimensional 45  
 water suppression techniques 42–43  
 numerical fitting algorithms 63–64

<sup>17</sup>O NMR 129–143  
 object recognition 283  
 older adults 288  
 one-dimensional NMR spectroscopy 45  
 osmotic stimulation 20, 22  
 ouabain 92  
 oxidative metabolism 126–128  
 oxygen 12, 129–143  
*see also* cerebral metabolic rate for oxygen

<sup>31</sup>P MRS 204–209  
 paramagnetism of deoxyhemoglobin 149, 151, 152  
 Parkinson's disease 128  
 PCr/Pi ratio 204–205  
 'perturb and detect' philosophy 186  
 PET *see* positron emission tomography  
 pH effects 37  
 philosophy 305–307  
 phosphate, inorganic 204–205  
 phosphorus MRS 204–209  
 phosphorus NMR 34–37  
 physiological states 289  
 POCE (Proton-Observed, Carbon-Edited) NMR  
   spectroscopy 49, 155–156  
 polyamines 104  
 positron emission tomography (PET)  
   CMRO<sub>2</sub>, (CMR<sub>glc</sub>) and CBF changes in awake  
     human brain 162–164  
   CMRO<sub>2</sub> *in vivo* determination 128–129, 134  
   development x, 4  
   2-[<sup>18</sup>F]deoxy-D-glucose method 15  
   functional imaging 299–301  
   medial temporal lobe memory role 264–265  
   post-synaptic energy consumption 114, 115, 117  
 potassium ions *see* K<sup>+</sup>  
 prefrontal cortex 264  
 proton (<sup>1</sup>H) MRS studies  
   epileptogenic tissue 198–199  
   glutamate role in epilepsy 220–221  
   glutamate–glutamine–GABA cycles 243–247, 249  
     *in vivo* techniques 33–34, 35  
     *N*-acetyl aspartate 241–243  
     psychiatric disorders 241–247  
     signal quantification techniques 43–45  
     water suppression techniques 42–43  
 proton leakage 120  
 proton observe carbon edit (POCE) method 49,  
   155–156  
 psychiatric disorders  
   <sup>13</sup>C MRS 247–250  
   glutamate–glutamine–GABA cycles 243–248

<sup>1</sup>H MRS 241–247, 249  
*N*-acetyl aspartate levels 242–243  
neurotransmitter systems 239–251  
pulsed NMR 32  
pyramidal neurons 178–179  
pyridoxine 227  
pyruvate carboxylase 79, 82, 83

quantification of brainwork 4–5

radioactive tracers  
2-[<sup>14</sup>C]deoxyglucose method 13–14, 18  
cerebral blood flow and metabolism studies 12  
2-[<sup>18</sup>F]deoxy-D-glucose method 14–15  
isotope labelling data 53–72  
PET study limitations x  
rats, anesthesia studies 15, 179–184, 284, 298, 301–302  
relaxivity 130–131  
relevance ratio 67–68  
repetitive tasks 286–287  
resting potential 113, 118  
restless brain concept 299, 311  
retrieval, long term memory 264, 268–269

scalar coupling 45–46, 47  
scatter effects 64–66  
schizophrenia 128, 244–245  
sciatic nerve 20–21, 23  
sensory cortex 303–304  
shimming techniques 40–42  
shunts, GABA 102–103  
signal-to-noise ratio (SNR) 130–132  
signalling 112–122  
significance thresholds 281  
single cell recordings 177  
single-unit activity (SUA) recording 177, 184  
sleep deprivation 289  
SNR *see* signal-to-noise ratio  
sodium ions *see* Na<sup>+</sup>  
somatosensory cortex 178–179, 180–181  
somatosensory processing 179–184, 284, 301–302  
spatial localization techniques 39–40  
spectral editing techniques 45–50  
spiking frequency ( $v$ )  
*see also* action potentials  
measuring changes 179–181

redeployment of distributions 186–187  
relationship to CMRO<sub>2</sub> 181–184  
stimulus induced incremental activity 299–301  
striate cortex 20, 21  
structure/function relationship (brain) 280  
SUA *see* single-unit activity recording  
substrate sources 59  
subtraction method 280–284  
*see also* differencing methods  
synapses 20–21, 24, 113–115, 121

target data 60  
TCA cycle *see* tricarboxylic acid cycle  
techniques in NMR 31–52  
temporal lobe epilepsy (TLE) 198–199, 217–227, 230  
tetrodes 191  
thalamus 179  
thermodynamic approach 295–297  
tissue heterogeneity 199, 201–202, 205–208  
TLE *see* temporal lobe epilepsy  
total brain activity 299, 303–306  
*see also* baseline activity  
tracers *see* radioactive tracers  
tricarboxylic acid (TCA) cycle  
<sup>13</sup>C MRS measurements of cerebral energy metabolism 76, 78  
fluoroacetate inhibition 92  
GABA synthesis 100, 102  
glutamate–glutamine cycle rate ratios 222–225  
modeling 54  
tumors, glutamate release 219  
two-compartment model 55, 68–69  
two-dimensional NMR spectroscopy 45

ultrahigh field <sup>17</sup>O NMR 130–132, 134–143  
unconscious activity 305, 314

VAPRO signal quantification algorithm 43  
verbalization 266  
vesicle release, glutamatergic synapses 114  
visual occlusion 20, 21  
voltage inside cells 174, 177

water 132–134  
suppression 33, 42–43  
white matter 92, 199–202  
work (brainwork) 4–5, 185, 186–187, 190  
writing systems 285